Total Synthesis and Biology of Antiparasitic Natural Products



Yasmine Biddick

Keble College, University of Oxford

Supervisor: Prof. Edward A. Anderson

2025

A thesis submitted in partial fulfilment of the requirements for the degree of Doctor of Philosophy

“Remember that the bad days are not for ever, and the trouble which seems so terrible will disappear at last.”

George Orwell, Down and Out in Paris and London (1933)

Abstract

This thesis is focused on evaluating the antiparasitic activity of marine natural products. Within this, there are two main objectives: (1) elucidation of the mechanism-of-action of the potent antileishmanial natural product ascididemin (**I**), and (2) development of a novel total synthesis of thiaplakortone A (**II**).

Chapter 1 provides a general introduction to neglected tropical diseases and the use of natural products as treatments.

Chapter 2 describes the total synthesis and biological activity of ascididemin (**I**) and ten analogues, and mechanism-of-action studies of ascididemin (**I**).

Chapter 3 details the total synthesis and biological activity of thiaplakortone A (**II**) and B (**III**).

Chapter 4 outlines studies towards related natural product families, ascidiathiazones and macrophilones.

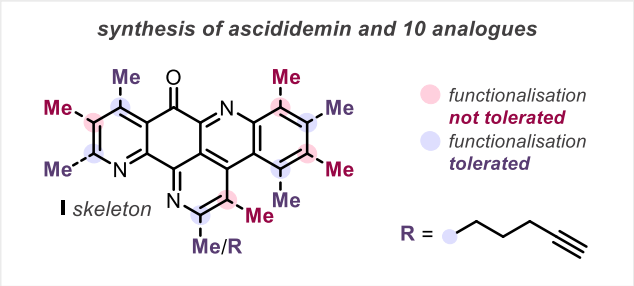

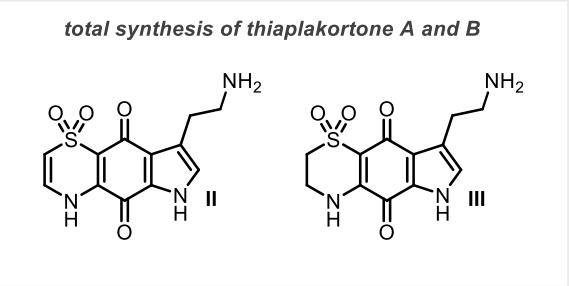

Declaration

Due to the nature of the project, it has required the collaboration of many different research groups: Professor Edward Anderson (EAA, University of Oxford), Dr Richard Wheeler (RW, University of Oxford), Dr André Gustavo Tempone (AGT, Instituto Butantan) and Dr Susan Wyllie (SW, University of Dundee). The contribution of each person will be explicitly stated here.

As part of the analogue synthesis of ascididemin, Oscar Poll (EAA) conducted the synthesis and collected data for compounds: **2.100**, **2.101**, **2.103**, **2.105**, **2.106**, **2.108**, **2.110**, **2.111**, **2.113**, **2.119** and **2.121**. For completeness, the synthesis and experimental details for preparing **2.119** and **2.121** are included in this thesis with permission from Oscar Poll. The synthesis of the aforementioned compounds is discussed in **Section 2.3.4.1**, pages 52–58. The experimental details for the aforementioned compounds are detailed in **Section 5.2.1**, pages 209–233.

Dr Maiara Amaral (AGT) and Vanessa Albuquerque (AGT) measured IC_{50} for *L. infantum* promastigotes, *T. cruzi* trypomastigotes and amastigotes, and mammalian cells. Dr Hannah Asiki (EAA & RW) performed the light microscopy and image analysis to monitor cell morphology and cell cycle analysis in *L. mexicana*. Dr Hannah Asiki determined the maximum dose concentration for divalent metal ions. Dr Hannah Asiki and Dr Marta Lopes Lima (SW) performed the DNA intercalation studies. Dr Hannah Asiki performed the knockout library study with *T. b. brucei*, data analysis was carried out by Dr Sandra Carvalho (SW) and Dr Michele Tinti (SW).

All other experiments, data analysis and interpretation described in this thesis is entirely the work of the author.

This thesis has not been previously submitted for a degree, diploma or any other qualification at the University of Oxford or elsewhere.

Yasmine Biddick

September 2025

Acknowledgements

First and foremost, I would like to express my deepest gratitude to Professor Ed Anderson for the opportunity to join your group. I am truly thankful that you believed in me and gave me this chance. These past four years have been filled with learning, laughter and friendship, and I have loved every moment. Thank you for everything you have taught me – I will miss working with you enormously!

Thank you to Academic Futures for funding my DPhil and making this all possible, and to Vertex for the industrial placement opportunity.

I would like to thank the following people from the group who have been far more than fellow group members – they have become true friends. Special thanks go to Ryan McNamee for taking me under your wing at the start of my DPhil. To the Antiparasitic Natural Products subgroup: Ana Sozanschi, whose early guidance I remain deeply grateful for, and Hannah Asiki, without whose help much of the biology in this project would not have been possible. To my wonderful summer student, Oscar Poll, thank you for your dedication, enthusiasm, and invaluable contributions to the project. To Pavle Kravljanac, I will always treasure our time breaking bonds together and proudly representing SynCity in the National Retrosynthesis Competition. To the best postdoc ever, Jisook Park – I miss you and I hope we are reunited soon! And finally, to Nandini Guzman – although our time together in the group was brief, it was a pleasure working with you. I wish you the very best for the remainder of your DPhil! Additionally, I am grateful to both past and present group members, each of whom has contributed to making this an incredible experience. As well as my friends outside of the group, within the department, your company has made my time here even more enjoyable.

To my non-chemistry friends, thank you for your patience and for sticking with me despite four years of near-total absence!

To my partner Harry, thank you for believing in me, especially in the moments when I did not believe in myself. Thank you to my parents Paul and Sarah for your unwavering support throughout the entirety of my studies. And to my late-mother Christine who suggested that I should become an accountant, I hope you can see how happy chemistry has made me.

Selected abbreviations

°C	degrees Celsius
Ac	acetyl
acac	acetylacetonate
aq.	aqueous
b.p.	boiling point
BEMP	*tert*-butylimino-2-diethylamino-1,3-dimethylperhydro-1,3,2-diazaphosphorine
Bn	benzyl
Boc	*tert*-butyloxycarbonyl
brsm	based on recovered starting material
BTMA	benzyltrimethylammonium
^{n}Bu	*n*-butyl
^{s}Bu	*sec*-butyl
^{t}Bu	*tert*-butyl
CAN	ceric ammonium nitrate
CC_{50}	50% cytotoxicity concentration
Cleland's reagent	dithiothreitol
conc.	concentrated
COSY	correlation spectroscopy

CV	column volume
d	day
DABCO	1,4-diazabicyclo[2.2.2]octane
DBAB	di-*tert*-butyl azodicarboxylate
DBN	1,5-diazabicyclo[4.3.0]non-5-ene
DBU	1,8-diazabicyclo[5.4.0]undec-7-ene
DCE	dichloroethane
DCM	dichloromethane
DFT	density functional theory
DIAD	diisopropyl azodicarboxylate
DIBAL	diisobutylaluminium hydride
DMAP	4-dimethylaminopyridine
DMA	dimethylacetamide
DMDO	dimethyldioxirane
DMF	dimethylformamide
DMF-DMA	dimethyl formamide dimethyl acetal
DMP	Dess–Martin periodinane
DMSO	dimethylsulfoxide
DND*i*	Drugs for Neglected Diseases initative
DOM	directed *ortho*-metallation
dppe	1,2-bis(diphenylphosphino)ethane

DPPF	1,1'-bis(diphenylphosphino)ferrocene
DPPP	1,3-bis(diphenylphosphino)propane
EI	electron impact
eq.	equivalent
ES	electrospray
ESI	electrospray ionisation
Et	ethyl
FCC	flash column chromatography
Frémy's salt	potassium nitrosodisulfonate
h	hour
HFIP	hexafluoroisopropanol
HMBC	hetero nuclear multiple bond correlation
HMDS	hexamethyldisilazide
HPLC	high performance liquid chromatography
HRMS	high resolution mass spectroscopy
HSQC	heteronuclear single quantum coherence spectroscopy
HTE	high-throughput experimentation
Hz	Hertz
IC_{50}	half-maximal inhibitory concentration
Im	imidazole
IPA	isopropyl alcohol

IR	infrared
J	coupling constant
lit.	literature
LRMS	low-resolution mass spectrometry
M	molar
m.p.	melting point
m/z	mass/charge ratio
Magic Blue	tris(4-bromophenyl)ammoniumyl hexachloroantimonate
*m*CPBA	*meta*-chloroperoxybenzoic acid
Me	methyl
min	minute
MKP	monopotassium phosphate
MOA	Mechanism-of-action
Ms	mesyl
NBP	*N*-butyl-2-pyrrolidone
NBS	*N*-bromosuccinimide
NCS	*N*-chlorosuccinimide
NIS	*N*-iodosuccinimide
NMM	*N*-methyl morpholine
NMP	*N*-methyl-2-pyrrolidone
NMR	nuclear magnetic resonance

NOE	nuclear Overhauser effect
NOESY	nuclear Overhauser effect spectroscopy
Nuc	nucleophile
OXONE®	potassium peroxymonosulfate
P	product
PFA	paraformaldehyde
Ph	phenyl
PIDA	(diacetoxyiodo)benzene
PIFA	bis(trifluoroacetoxy)iodobenzene
PMB	*para*-methoxybenzyl
ppm	parts per million
rr	regioisomeric ratio
r.t.	room temperature
R	generic group
R_f	retention factor
Rongalite®	sodium hydroxymethanesulfinate
ROS	reactive oxygen species
SAR	Structure activity relationship
sat.	saturated
SFC	supercritical fluid chromatography
SI	selectivity index

SM	starting material
STAB	sodium triacetoxyborohydride
TAA	*tert*-amyl alcohol
TBA	tetrabutylammonium
$TBABr_3$	tetrabutylammonium tribromide
TBACl	tetrabutylammonium chloride
TBAI	tetrabutylammonium iodide
$TBAI_3$	tetrabutylammonium triiodide
TBME	*tert*-butyl methyl ether
TBS	*tert*-butyldimethylsilyl
TEA	triethylamine
Tf	triflate
TFA	trifluoroacetic acid
TFAA	trifluoroacetic anhydride
THF	tetrahydrofuran
TKP	tripotassium phosphate
TLC	thin layer chromatography
TMEDA	tetramethylethylenediamine
TMG	tetramethylguanidine
TMP	tetramethylpiperidide
TMS	trimethylsilyl

TOF	time-of-flight

Table of Contents

1. Introduction **1**

1.1. Neglected tropical diseases 1

1.2. Leishmaniasis 1

1.2.1. Life cycle 1

1.3. Trypanosomiasis 2

1.4. Current treatments 3

1.5. Natural products 4

1.5.1. Natural product selection 5

1.6. Mechanism–of–action determination 6

2. Ascididemin **8**

2.1. Total synthesis employing an oxidative amination strategy 9

2.1.1. *ortho*-Aminoacetophenone-derived anilines 9

2.1.2. Other anilines 11

2.1.3. Total synthesis employing other strategies 13

2.2. Biological activity 18

2.2.1. DNA intercalation and cleavage 18

2.2.2. Reactive oxygen species 20

2.2.3. Antiparasitic activity of ascididemin 1.11 20

2.2.4. Structure–activity relationship studies 22

2.2.5. Zinc(II) homeostasis 25

2.2.6. Iron(II) homeostasis 26

2.2.7. Metal binding 27

2.3. Research and discussion 28

2.3.1. Synthesis of ascididemin 28

2.3.2. Antiparasitic activity of ascididemin 1.11 30

2.3.3. Mechanism-of-action studies 31

2.3.3.1. Morphology changes and cell cycle analysis 31

2.3.3.2. Metal binding 34

2.3.3.3. DNA intercalation 39

2.3.3.4. Knockdown libraries 42

2.3.3.4.1. Knockdown of an RNA helicase 43

2.3.3.4.2. Knockdown of nitroreductases 43

2.3.3.5. First attempt at visualising the localisation of ascididemin 1.11 47

2.3.4. Structure–activity relationship studies 51

2.3.4.1. Functionalisation via the synthetic route developed by Wang *et al.* 52

2.3.4.1.1. *A*-Ring substitution 52

2.3.4.1.2. *D*-Ring substitution 56

2.3.4.1.3. *E*-Ring substitution 58

2.3.4.2. Functionalisation via the synthetic route developed by Bracher 59

2.3.4.2.1. *E*-Ring substitution 60

2.3.4.2.2. *D*-Ring substitution 62

2.3.5. Antiparasitic activity of methyl analogues 63

2.3.6. Second generation analogue 67

2.3.6.1 Synthesis of alkyne-ascididemin 2.165 67

2.3.6.2. Activity of alkyne-ascididemin 2.165 69

2.3.6.2. Summary and future work 70

3. Thiaplakortone A 72

3.1. Biosynthesis of the thiaplakortones 72

3.2. Total synthesis of thiaplakortone A 1.12 75

3.3. Antiparasitic activity of the thiaplakortones 77

3.3.1. Structure–activity relationship studies 79

3.4. Project aims 81

3.5. Research and discussion 82

3.5.1. Total synthesis of thiaplakortone B 3.1 and A 1.12 – initial considerations 82

3.5.2. *De novo* construction of substituted tryptamine 82

3.5.2.1. Fischer indole synthesis 82

3.5.2.2. Larock indole synthesis 86

3.5.3. Connecting the *S*-atom first 93

3.5.3.1. Electrophilic halogenation 93

3.5.3.2. Directed *ortho*-metallation 96

3.5.3.3. Bartoli indole synthesis 98

3.5.3.4. Nucleophilic aromatic substitution 99

3.5.4. Synthesis of trimethoxytryptamine 101

3.5.4.1. Attempted synthesis of trimethoxyindole 3.125 as a model substrate 102

3.5.4.2. Continued synthesis of trimethoxytryptamine 3.135 104

3.5.5. Oxidation of trimethoxytryptamine 3.135 to indolequinone 3.89 106

3.5.6. Thiazine 1,1-dioxide formation 108

3.5.6.1. Thiazine 1,1-dioxide formation on a model substrate 109

3.5.6.2. Addition–elimination with cystamine 3.156 113

3.5.6.3. Dihydrothiazine formation on indolequinone 3.89 114

3.5.6.4. Other amine nucleophiles 117

3.5.6.5. Base-induced cyclisation 120

3.5.6.6. Optimising dihydrothiazine formation 122

3.5.6.6.1. Use of cystamine 3.153 122

3.5.6.6.2. High-throughput experimentation 125

3.5.6.7. Oxidation of sulfide 3.166 to sulfone 3.190 141

3.5.6.7.1. The unexpected side-product 145

3.5.6.7.2. Oxidation of sulfide 3.166 to sulfone 3.190 (continued) 151

3.5.6.8. Endgame 155

3.5.6.8.1. Oxidation strategies 155

3.5.6.8.2. Deprotection to thiaplakortone B 3.1 and A 1.12 162

3.5.6.9. Antiparasitic activity of thiaplakortone A 1.12, B 3.1 and sulfide 3.247 164

4. Attempted synthesis of related natural products 166

4.1. Macrophilone F and G 166

4.2. Macrophilone E 176

4.3. Ascidiathiazone B 178

4.4. Future work 186

5. Supporting information 191

5.1. Experimental details 191

5.1.1. Chemistry 191

5.1.2. Biology 194

5.1.3. Analytical 194

5.1.4. Crystallography 195

5.2. Experimental procedures 196

5.2.1. Chapter 2 196

5.2.2. Chapter 3 251

5.2.3. Chapter 4 308

5.3. Spectroscopic data 318

5.4. Crystallographic data 321

6. References 322

1. Introduction

1.1. Neglected tropical diseases

Neglected tropical diseases (NTDs) are a diverse collection of diseases which are prevalent in the most impoverished rural and urban communities, within tropic and subtropic regions across the world.[1] As of 2020, the World Health Organisation (WHO) has identified 20 NTDs, including leishmaniasis and trypanosomiasis.

1.2. Leishmaniasis

Leishmaniasis is a vector-borne parasitic disease transmitted predominantly through the bite of infected female Phlebotomine sandflies when taking a blood meal from human or animal.[2] It is estimated that 12 million people are currently affected worldwide. The most severe clinical form of the disease is visceral leishmaniasis, caused by *Leishmania infantum* and *Leishmania donovani*, which is fatal in approximately 95% of untreated cases. The most common form of the disease is cutaneous leishmaniasis, typically caused by *Leishmania mexicana*, and is characterised by disfiguring lesions.

1.2.1. Life cycle

Leishmania parasites exhibit two distinct life cycle stages, each morphologically adapted to their respective environments (**Figure 1.1**). The flagellated and motile promastigote form resides within the sandfly vector, while the non-flagellated amastigote form persists intracellularly within the mammalian host.[3] Differentiation between these forms is triggered by environmental cues, including a rise in temperature from 26–28 °C in the sandfly midgut to 37 °C in the mammalian

host, as well as pH changes. To facilitate morphological transformation and enhance survival within the new host environment, this transition is accompanied by shifts in gene expression.

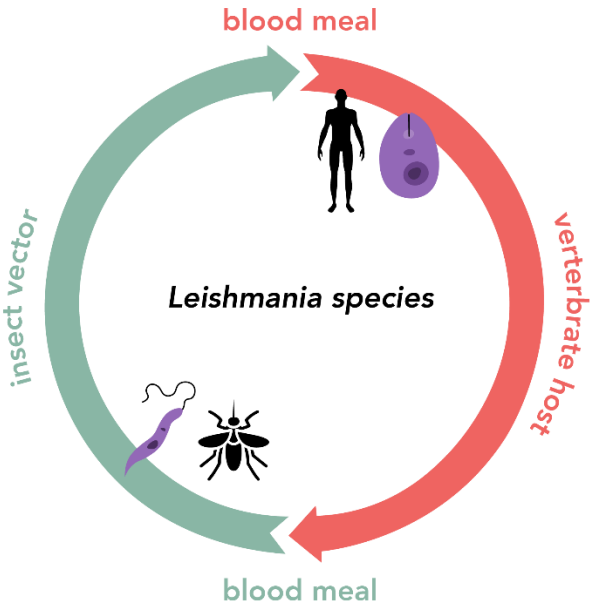

Figure 1.1. *Life cycle of Leishmania, differentiating between the promastigote form in the sandfly and amastigote form in mammalian cells.*

1.3. Trypanosomiasis

The *Trypanosoma* genus is closely related to *Leishmania*, with both belonging to the order *Trypanosomatida* within the class *Kinetoplastea*.[4] These protozoan parasites share several biological features, including the presence of a kinetoplast – a unique mitochondrial organelle containing circular DNA. Unlike *Leishmania*, which causes leishmaniasis, *Trypanosoma* species such as *T. b. brucei* and *T. cruzi* are responsible for African trypanosomiasis (sleeping sickness) and American trypanosomiasis (Chagas disease), respectively.

1.4. Current treatments

Despite ongoing efforts, leishmaniasis remains a NTD, with current treatment strategies relying exclusively on a small repertoire of chemotherapeutic agents (**1.1–1.5**, **Figure 1.2**).[5] These drugs, while clinically effective, are associated with notable limitations, including severe toxicity, prolonged treatment duration, invasive administration routes, specific storage requirements, high production costs, and the recent emergence of resistance. Given these drawbacks, there is an urgent need for new, effective, safer, cheaper and more practical antileishmanial therapeutic agents that operate through novel mechanisms-of-action distinct from those of existing treatments.

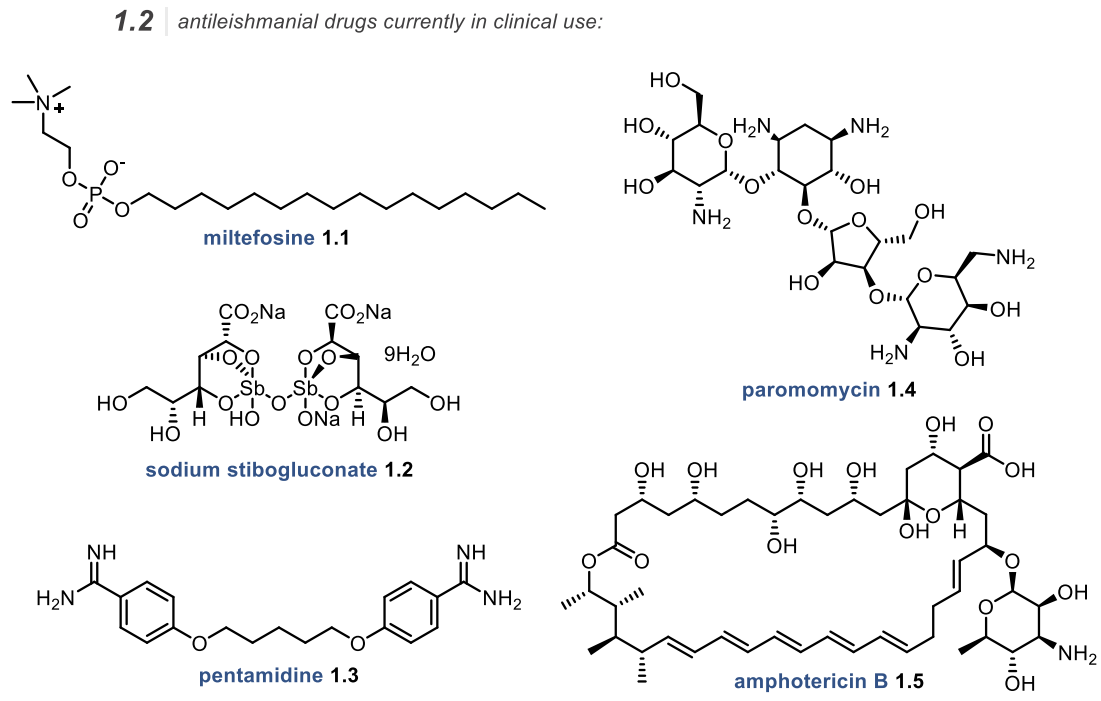

Figure 1.2. *Structures of antileishmanial drugs currently in clinical use.*

1.5. Natural products

Since plants and marine invertebrates produce metabolites as part of their defence mechanism against environmental stressors, such as infection, these natural products have long served as a source of structurally diverse, biologically active starting points for drug discovery programmes. Several natural products have led to the development of FDA-approved therapeutics, particularly for parasitic diseases. Among the earliest examples is quinine **1.6** (**Figure 1.3**), a cinchona alkaloid, used for the treatment of malaria.[6] Documented as early as 1630 by Jesuit missionaries in South America, quinine represents one of the first antiparasitic agents derived from a natural source. Amphotericin B **1.5** (**Figure 1.2**), a polyene macrolide isolated from *Streptomyces nodosus* in 1955 and approved by the FDA in 1958, was originally introduced as an antifungal agent but later found clinical utility in the treatment of visceral leishmaniasis.[7]

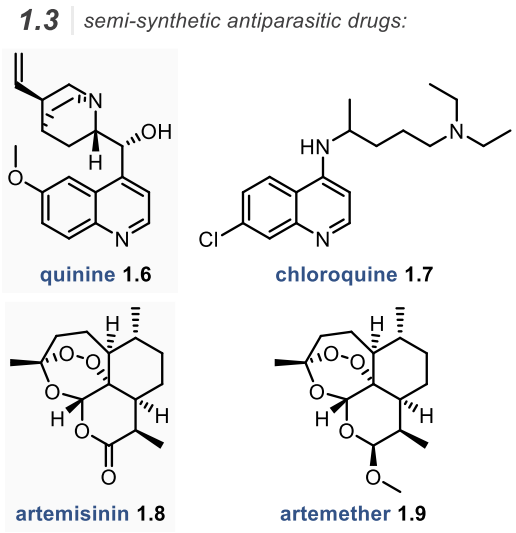

Figure 1.3. *Structures of semi-synthetic antiparasitic drugs.*

While relatively few natural products have advanced as direct therapeutics, many have provided privileged scaffolds for the development of analogues with enhanced pharmacological properties, including improved oral bioavailability, metabolic stability, and target selectivity. For example, chloroquine **1.7** (**Figure 1.3**) was developed as a safer and more efficacious alternative to quinine, while preserving the parent natural product scaffold.[8] Similarly, artemisinin **1.8**, a sesquiterpene lactone endoperoxide, isolated in 1972 from *Artemisia annua*,[9] exhibited potent antimalarial

activity which eventually led to the development of semi-synthetic derivatives such as artemether **1.9**, which was FDA-approved in 2009 (in combination with lumefantrine).[10]

Beyond these examples, numerous semi-synthetic analogues and derivatives inspired by natural products are either FDA-approved or currently in various stages of clinical development, further underscoring the enduring value of natural products in the search for novel antiparasitic agents.

1.5.1. Natural product selection

Many natural products have been reported to exhibit potent activity against *Leishmania* species; however, not all represent viable starting points for drug development. In many cases, limitations such as structural complexity and synthetic intractability or cost hinder further studies of these natural products. For example, although manzamine A **1.10** (**Figure 1.4**) demonstrates submicromolar antiparasitic activity, with an IC_{50} = 1.76 nM against *L. donovani* promastigotes,[11] its highly complex polycyclic structure poses significant challenges for analogue synthesis and scalable production.[12]

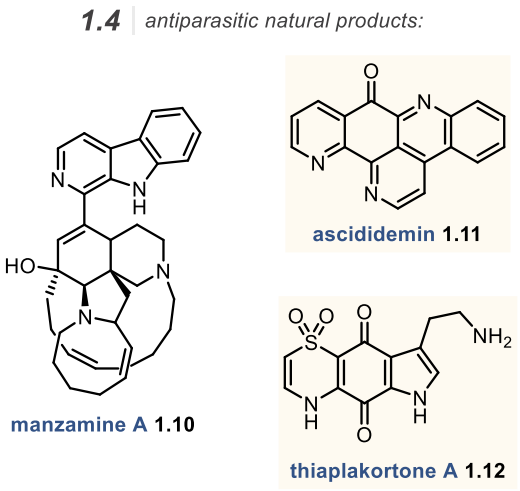

Figure 1.4. *Structures of antiparasitic natural products.*

General hit selection criteria have been proposed by the Drugs for Neglected Diseases initiative (DND*i*) to aid in prioritising leads, which can thus be applied to the selection of natural products

for study.[13] For visceral leishmaniasis, compounds should exhibit an IC_{50} < 10 μM against intracellular *Leishmania* amastigotes, with a selectivity index (SI = CC_{50}/ IC_{50}) > 10 versus mammalian cells. In addition, synthetic accessibility is a key consideration, with a preference for structures that can be synthesised in fewer than five steps and in good overall yield – primarily to enable cost-effective development, which is paramount for novel treatments against NTDs. Preliminary structure–activity relationship (SAR) data is also considered advantageous. Notable examples of promising natural product scaffolds meeting several of these criteria include ascididemin **1.11** and thiaplakortone A **1.12** (**Figure 1.4**), both of which have demonstrated potent antiparasitic activity.[13]

1.6. Mechanism–of–action determination

Biological activity alone is insufficient to justify the progression of a compound as a drug candidate; an understanding of the mechanism–of–action (MOA) is also essential. Several techniques have been developed to aid in elucidating a compound's molecular target and mechanism-of-action. These include the installation of photoaffinity probes to visualise compound localisation, selection of resistant cell lines followed by whole-genome sequencing, identification of resistance-conferring genes from overexpression libraries, and transcriptomic profiling to analyse mRNA expression changes upon compound treatment.[14] Although not a direct method for determining mechanism-of-action, structure–activity relationship (SAR) analysis remains a closely related and complementary approach. In SAR studies, specific structural modifications are systematically introduced or removed to assess their impact on biological activity. When integrated with preliminary mechanistic data, SAR trends can help identify critical pharmacophores and suggest potential interactions with the molecular target.

MOA studies not only enable the identification of key drug–target interactions that can be exploited with analogue design to enhance potency and selectivity, but also help determine

whether the biological target is appropriate. In cases where the target lacks sufficient differentiation from mammalian homologs, early MOA insights can enable the deprioritisation of certain natural product scaffolds.

2. Ascididemin

Ascididemin **1.11** is a pentacyclic marine alkaloid member of the pyridoacridine family (**Figure 2.1**), which was first isolated in low abundance in 1988 off the coast of the Kerama Islands, Japan from the Okinawan tunicate *Didemnum* sp. (0.006%, wet weight).[15] The natural product 2-bromoleptoclinidinone **2.1** was isolated a year prior, but the relationship with ascididemin **1.11** was only recognised in 1989 when hydrogenation of 2-bromoleptoclinidinone **2.1** with palladium on carbon in ethanol yielded ascididemin **1.11**.[16] Structurally related natural products have been additionally isolated, such as calliactine **2.2** (isolated in 1940) and 11-hydroxyascididemin **2.3** (isolated in 1991).[17] Although pyridoacridines are now a large family of over one hundred known natural products, they were still emerging as a novel class at the time of ascididemin **1.11**'s discovery. Their unique polycyclic framework quickly captured the attention of the synthetic community. As a result, numerous total syntheses of ascididemin **1.11** and related natural products have since been reported.

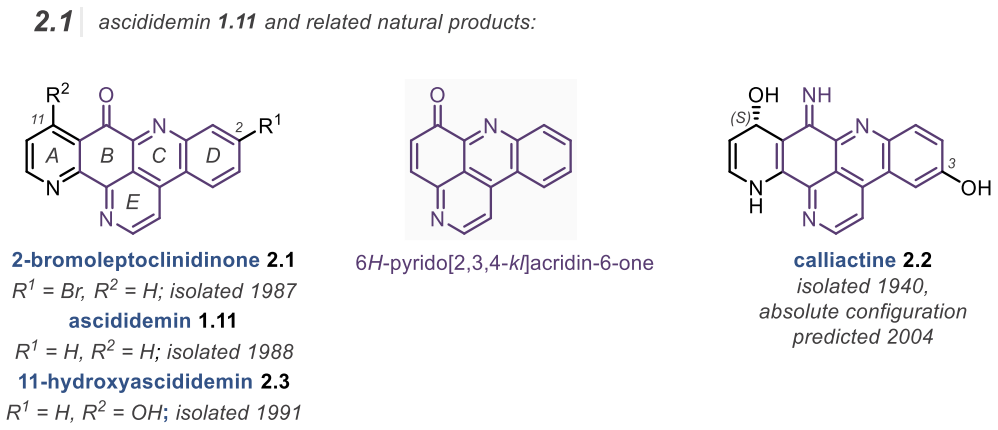

Figure 2.1. *The isolation of ascididemin* ***1.11*** *(1988) and related natural products in the 6H-pyrido[2,3,4-kl]acridin-6-one family. Ring labelling system for ascididemin* ***1.11*** *included.*

2.1. Total synthesis employing an oxidative amination strategy

2.1.1. *ortho*-Aminoacetophenone-derived anilines

Bracher published the first total synthesis of ascididemin **1.11** in 1989,[18] a year after the compound was first isolated (**Scheme 2.1**). Oxidative amination of quinoline-5,8-dione **2.4** with *ortho*-aminoacetophenone **2.5** and cerium(III) chloride under air led to enamine **2.6** in 78% yield. The desired regioselectivity was achieved by increasing the electrophilicity of the C6-position of the quinone via chelation of cerium between the pyridine nitrogen and carbonyl. Brønsted acid-promoted cyclisation via attack of the enamine on the aryl ketone followed by aromatisation yielded tetracycle **2.7** in 94% yield. The final ring was synthesised by a two-step procedure in which the activated methyl substituent, *para* to the pyridine, was alkylated with *N*,*N*-dimethylformamide dimethyl acetal (DMF-DMA) **2.8** forming enamine **2.9** in 64% yield. Finally, intramolecular cyclisation under acidic conditions led to ascididemin **1.11** in 59% yield. This strategy commenced the development of a series of alternative routes all employing quinone-5,8-dione **2.4** but differing in the choice of aniline partner.

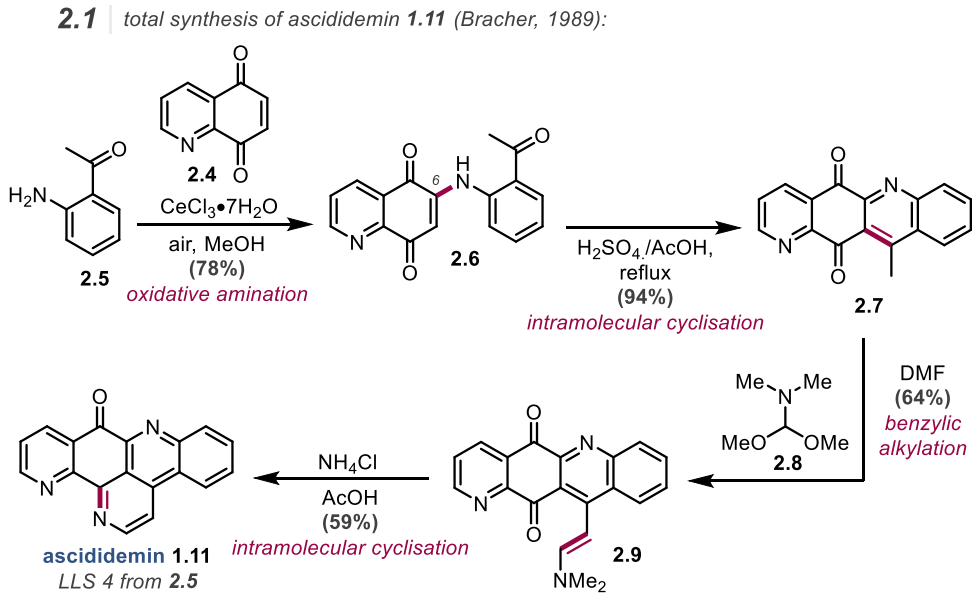

Scheme 2.1. *First total synthesis of ascididemin* ***1.11*** *(Bracher, 1989), employing quinoline-5,8-dione* ***2.4*** *with ortho-aminoacetophenone* ***2.5****.*

Kashman *et al.* developed a three-step biomimetic synthesis of ascididemin **1.11** from the natural product kynuramine **2.10** (**Scheme 2.2**).[19] Initially, the primary amine was protected as trifluoroacetamide **2.12** in 95% yield. Oxidative amination of quinoline-5,8-dione **2.4** with *ortho*-aminoacetophenone **2.12** and cerium(III) chloride under air then led to enamine **2.13** in 15% yield. Treatment with either acid (hydrochloric acid, HCl) or base (ammonium hydroxide) activated the carbonyl by protonation, or the enamine by deprotonation, respectively. In the absence of air, intermediate **2.14** could be obtained in 65% yield (reported for both conditions). Upon aerobic oxidation, ascididemin **1.11** could be directly accessed in 95% yield (reported for both conditions).

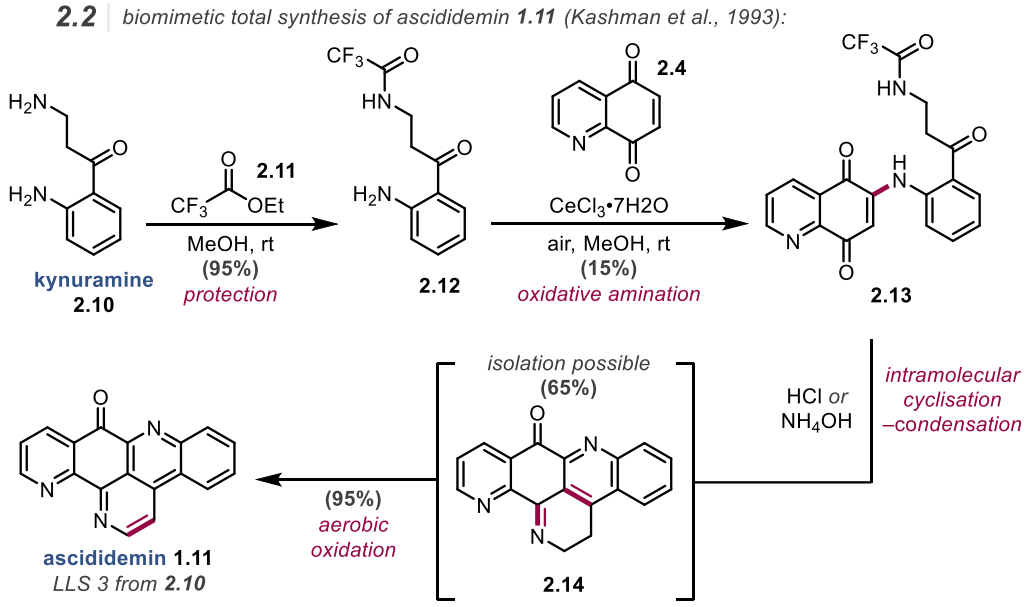

Scheme 2.2. *Biomimetic total synthesis of ascididemin* ***1.11*** *(Kashman et al., 1993). Starting from natural product kynuramine* ***2.10****. Employs quinoline-5,8-dione* ***2.4*** *with ortho-aminoacetophenone-derived aniline.*

2.1.2. Other anilines

Taking inspiration from the enamine intermediate **2.9** reported by Bracher (refer back to **Scheme 2.1**), Echavarren *et al.* synthesised ascididemin **1.11** via the cyclisation of enamine **2.18** in 64% yield (**Scheme 2.3**).[20] Instead of using an *ortho*-aminoacetophenone-derived aniline for the oxidative amination of quinoline-5,8-dione **2.4**, α,β-unsaturated hydrazone **2.16** (which was synthesised in two steps from cinnamaldehyde **2.15**) was employed with cerium(III) chloride under an oxygen atmosphere yielding enamine **2.17** in 52%. No additive was required for the activation of enamine **2.17**; refluxing in xylene was sufficient to obtain enamine **2.18**.

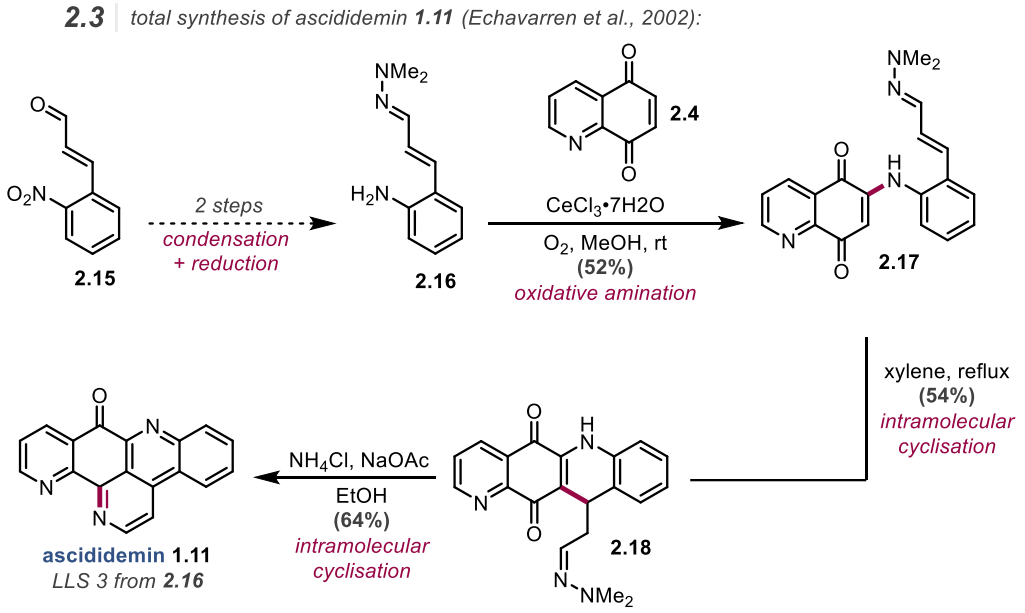

Scheme 2.3. *Total synthesis of ascididemin* ***1.11*** *(Echavarren et al., 2002). Employs quinoline-5,8-dione* ***2.4*** *with aniline* ***2.16****.*

The most recent total synthesis of ascididemin was described by Wang *et al.* in 2014 (**Scheme 2.4**),[21] 25 years after the first was reported by Bracher. Instead of a ketone or an α,β-unsaturated hydrazone as the electrophilic functional group for attack by the enamine, an alkyne was used. Enamine **2.22** could be constructed by a Sonogashira cross-coupling of *N*-Boc propargyl amine **2.20** with *ortho*-iodoaniline **2.19** at room temperature to afford aniline **2.21** in 91% yield. Oxidative amination of quinoline-5,8-dione **2.4** with aniline **2.21** under an atmosphere of oxygen furnished enamine **2.22** in 75% yield; Wang *et al.* were the first to demonstrate that complete

regioselectivity could be achieved in this reaction using cerium(III) chloride in catalytic amounts (10 mol%).

Initially, a gold(I) catalyst was employed as a soft and carbophilic Lewis acid, in combination with stoichiometric sulfuric acid in acetic acid, to activate the alkyne in **2.22** towards nucleophilic attack, forming a tetracyclic intermediate. Additionally, *in situ* deprotection of the *N*-Boc group allowed the primary amine to cyclise onto the ketone, furnishing ascididemin **1.11** in 40% yield after aerobic oxidation (**Scheme 2.4** table, entry 1). However, the yield was found to be comparable in the absence of the gold(I) catalyst; when sulfuric acid was used as a co-solvent and the gold(I) complex was omitted the yield was similar (**Scheme 2.4** table, entry 2; 45% yield), suggesting the cyclisation was Brønsted acid-catalysed. Iron(III) sulfate was added to facilitate the aromatisation step to ascididemin **1.11**, delivering an improved yield of 75% (**Scheme 2.4** table, entry 3).

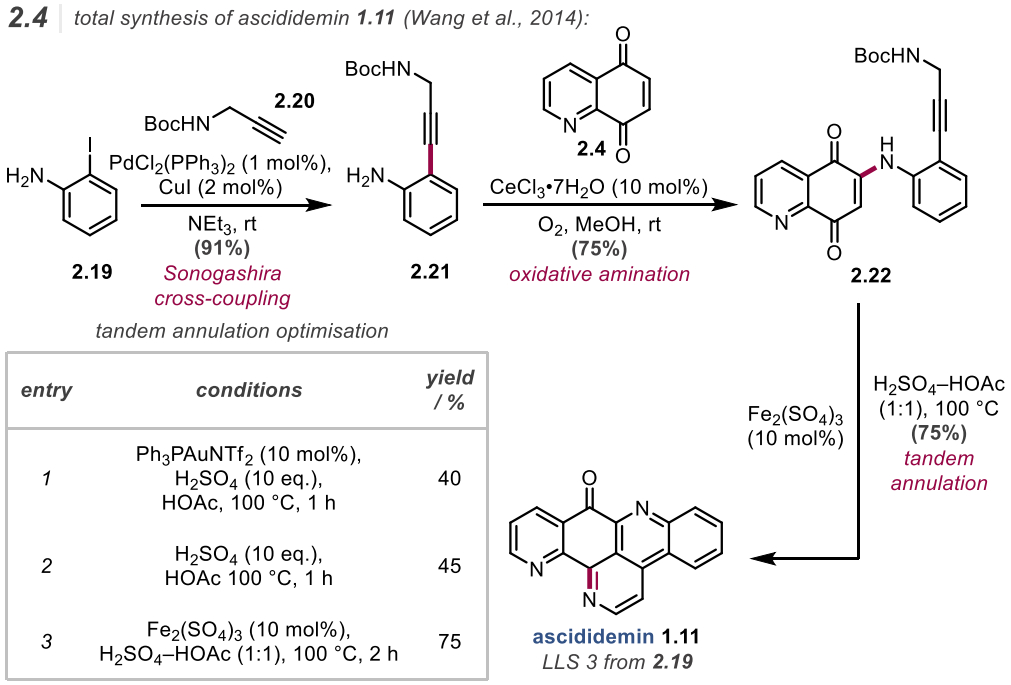

Scheme 2.4. *Total synthesis of ascididemin* ***1.11*** *(Wang et al., 2014). Employs quinoline-5,8-dione* ***2.4*** *with aniline* ***2.21****. Selected optimisation conditions for the tandem annulation key step of enamine* ***2.22*** *to ascididemin* ***1.11****.*

2.1.3. Total synthesis employing other strategies

In 1990, Moody *et al.* reported a novel strategy for the synthesis of ascididemin **1.11** (**Scheme 2.5**),[22] which differed significantly from the oxidative amination strategy initiated by Bracher. An *aza*-Horner–Wadsworth–Emmons (HWE) reaction was employed using phosphonamide **2.25** and *ortho*-quinone **2.24** to form quinoneimine **2.26**, albeit in a poor yield of 10%. Alternatively, quinoneimine **2.26** could be synthesised by a two-step procedure; activation of epoxide **2.27** with triethylaluminium enabled epoxide-opening with *ortho*-iodoaniline **2.19** to furnish amino alcohol **2.28** in 79% yield. Oxidation of both the alcohol and amine with barium manganate led to quinoneimine **2.26** in 83% yield (66% yield over two steps versus 10% for quinone **2.24**). **2.26** underwent a photocyclisation when exposed to a high-pressure mercury lamp in concentrated sulfuric acid to afford ascididemin **1.11** in 32% yield.

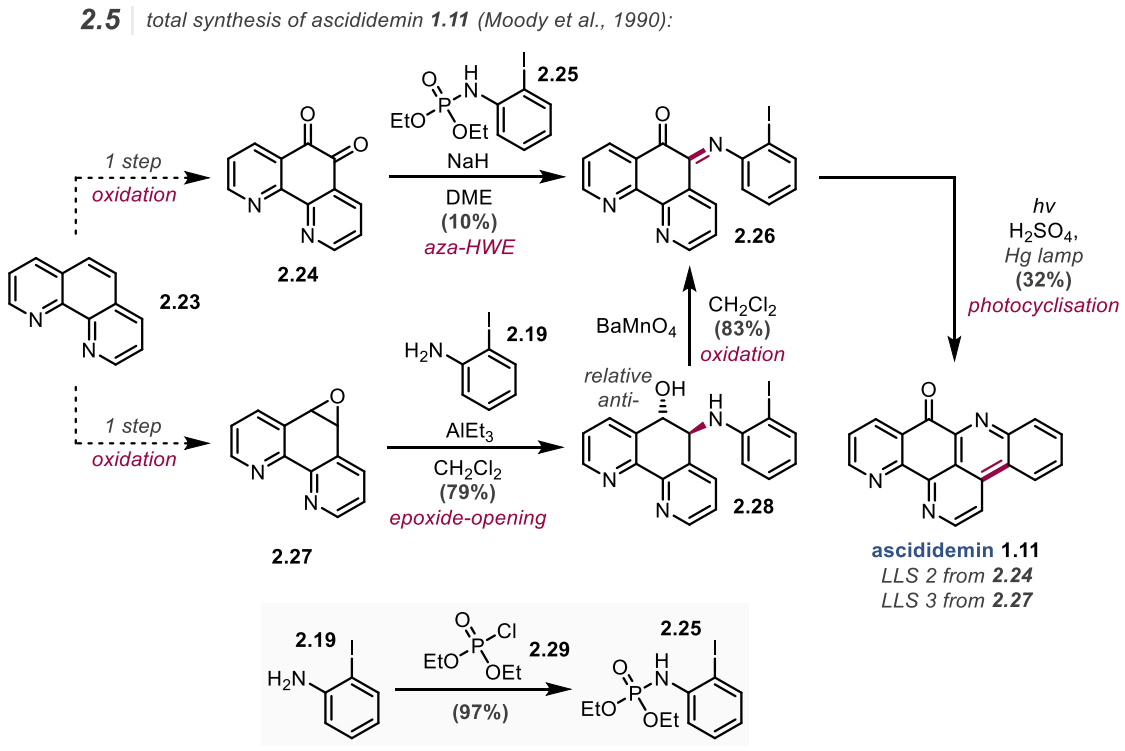

Scheme 2.5. *Total synthesis of ascididemin* ***1.11*** *(Moody et al., 1990). Featuring a photocyclisation of quinoneimine* ***2.26*** *as the key step. Quinoneimine* ***2.26*** *could be synthesised from either quinone* ***2.24*** *or epoxide* ***2.27****.*

Later, Joule *et al.* developed an *aza*-Diels–Alder strategy for the synthesis of ascididemin **1.11** (**Scheme 2.6**). Using bromoquinone **2.37** and α,β-unsaturated hydrazone **2.38** under high pressure and temperature, this cycloaddition proceeded in a low yield of 21%.[23]

2.6 *total synthesis of ascididemin* ***1.11*** *(Joule et al., 2000):*

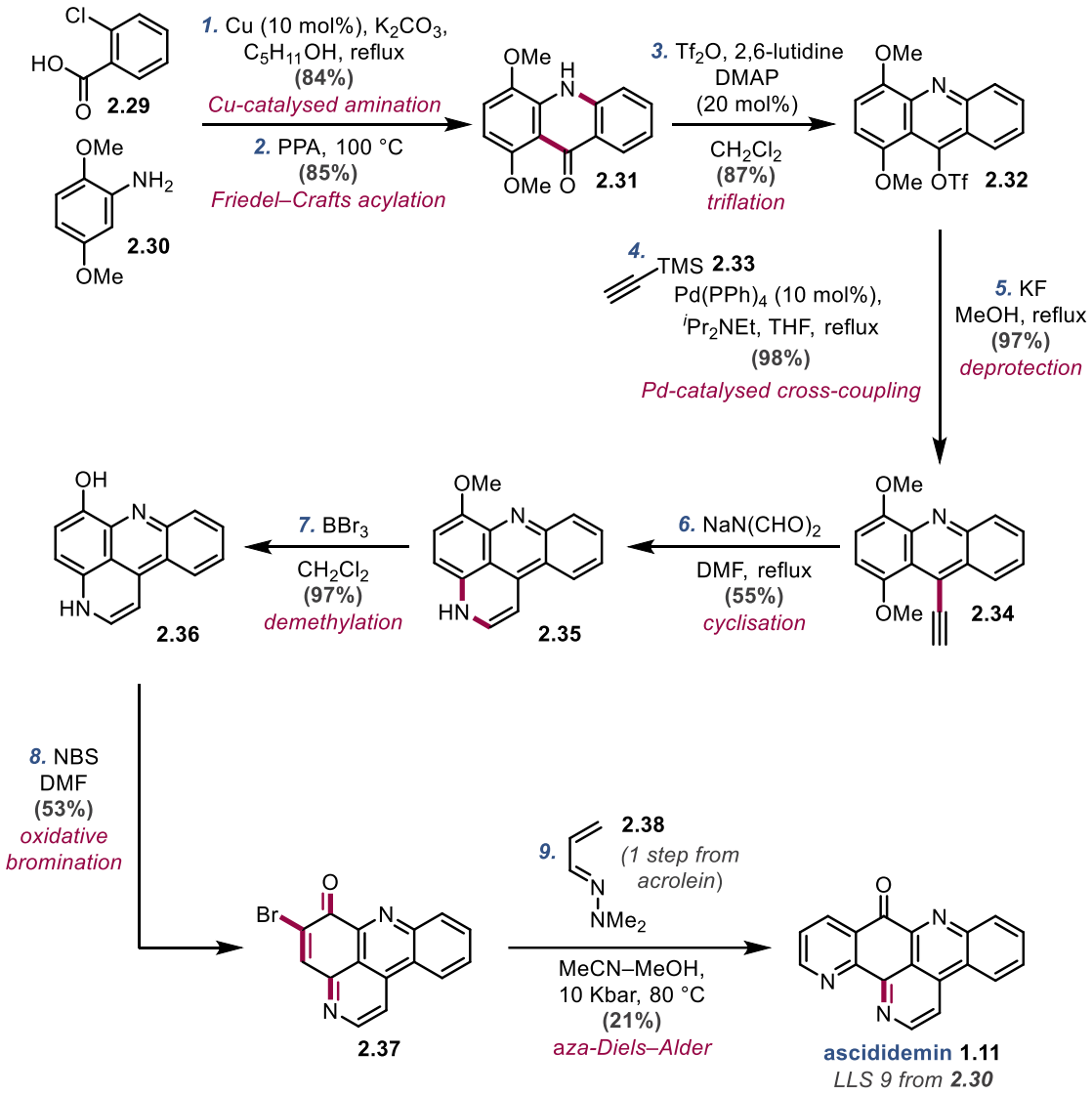

Scheme 2.6. *Total synthesis of ascididemin* ***1.11*** *(Joule et al., 2000), featuring a regioselective aza-Diels–Alder of bromoquinone* ***2.37****.*

When the bromide substituent was not present, as in quinone **2.39**, the opposite regioselectivity was observed, yielding *iso*-ascididemin **2.40** (**Scheme 2.7A**; 40% yield). A similar α,β-unsaturated hydrazone fragment was used by Echavarren *et al.* (refer back to **Scheme 2.3**; α,β-unsaturated hydrazone **2.16**); however, an *aza*-Diels–Alder was not observed with quinoline-5,8-

dione **2.4**. Bromoquinone **2.37** was synthesised beginning from tricycle **2.31**. Initially, the tricycle core underwent triflation in 87% yield (**Scheme 2.6**). Palladium-catalysed cross-coupling with trimethylsilyl-acetylene **2.33** proceeded in 98% yield, and fluoride deprotection yielded terminal alkyne **2.34** in 97% yield. Treatment of terminal alkyne **2.34** with sodium diformylamide in DMF at reflux led to tetracycle **2.35** in 55% yield.

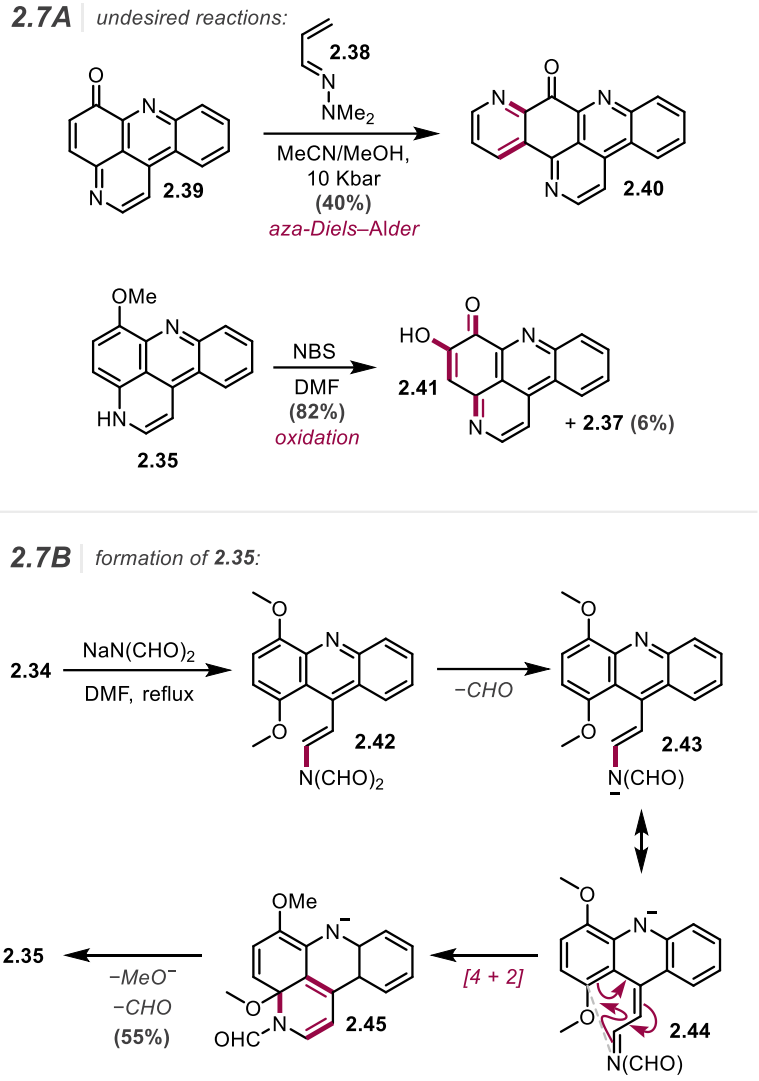

Scheme 2.7. ***(A)*** *Undesired reactions observed during the total synthesis of ascididemin* ***1.11*** *.* ***(B)*** *Proposed mechanism for the formation of tetracycle* ***2.35*** *from alkyne* ***2.34****.*

The formation of enamine **2.35** proceeds by an interesting mechanism: it was proposed that alkenyl imide **2.42** was formed in the reaction (**Scheme 2.7B**) which subsequently underwent a base-induced deformylation to intermediate **2.43**. Tautomerisation to α,β-unsaturated imine

2.44 then enabled a 6π-electrocyclisation reaction to form intermediate **2.45**, which rearomatised and underwent a second deformylation to afford tetracycle **2.35**.

Returning to the synthesis of bromoquinone **2.37** (**Scheme 2.6**), demethylation with boron tribromide, then bromination with *N*-bromosuccinimide (NBS) yielded **2.37** in 53% yield over two steps, setting the stage for the key *aza*-Diels–Alder reaction. When NBS was used with tetracycle **2.35** bromoquinone was achieved in low yield (**Scheme 2.7A**; 6% yield), with primarily hydroxyquinone **2.41** formed instead in a yield of 82%. Tricycle **2.31** could itself be synthesised by the copper-catalysed amination of *ortho*-chlorobenzoic acid **2.29** with 2,5-dimethoxyaniline **2.30** and a subsequent intramolecular Friedel–Crafts acylation.

Kristensen *et al.* synthesised ascididemin **1.11** via an anionic cascade ring closure strategy (**Scheme 2.8**).[24] Deprotonation at the benzylic position of tricycle **2.52** by sodium hydride in DMF at 90 °C under microwave irradiation generated a benzylic anion **2.54** which could undergo a 6-*exo*-*dig* cyclisation onto the nitrile group. The resulting imine anion (**2.55**) then underwent a nucleophilic aromatic substitution (S_NAr) of the proximal fluoride substituent, yielding the natural product 12-deoxyascididemin **2.53** as a transient intermediate. Sparging the reaction mixture with oxygen then gave ascididemin **1.11** in 69% yield. The synthesis of tricycle **2.52** began with *ortho*-fluoroacetophenone **2.46**, Knoevenagel condensation of which with malononitrile **2.47** led to bis-nitrile **2.48**. Alkylation of the acidic methyl group using DMF-DMA **2.8** led to enamine **2.49** which could be converted to pyridine **2.50** on treatment with HCl in 81% yield over three steps. Negishi cross-coupling with 3-methylpyridylzinc bromide **2.51** under microwave irradiation completed the synthesis of tricycle **2.52** in 80% yield.

2.8 | *total synthesis of ascididemin* ***1.11*** *(Kristensen et al., 2012):*

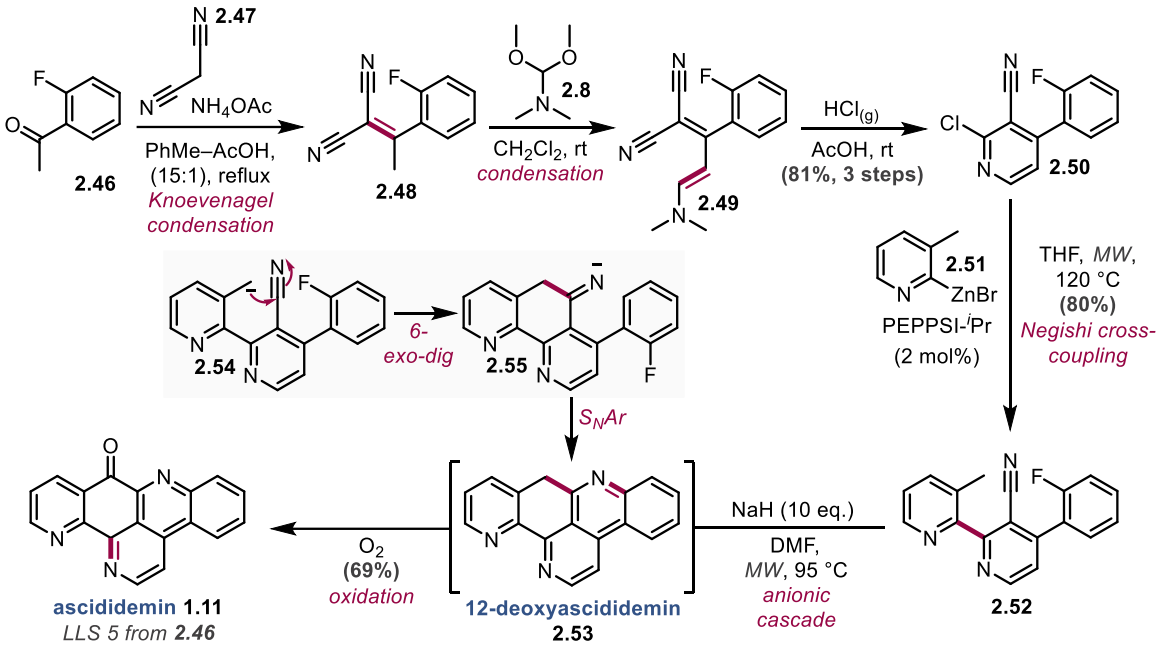

Scheme 2.8. *Total synthesis of ascididemin* ***1.11*** *(Kristensen et al., 2012). Featuring an anionic cascade ring closure as a key step. Where PEPPSI-^{i}Pr = [1,3-bis(2,6-diisopropylphenyl)imidazol-2-ylidene](3-chloropyridyl)palladium(II) dichloride.*

2.2. Biological activity

The antitumour activity of ascididemin **1.11** was first investigated by Kobayashi *et al.*.[15] This study was driven by a growing interest in the discovery of novel anticancer agents that act via DNA intercalation – a widely pursued strategy at the time, as small, planar aromatic compounds had already demonstrated promise as potential therapeutics. Since then, the pyridoacridine family of natural products has been extensively studied for its potent antitumor properties.

2.2.1. DNA intercalation and cleavage

The potent bioactivity of ascididemin **1.11** (**Figure 2.2**) and related pyridoacridine natural products has prompted investigation into their antitumour mechanisms-of-action, with DNA widely regarded as the primary cellular target.[25] Both DNA intercalation[26] and cleavage have been reported for ascididemin **1.11**.[27,28] Bonnard *et al*. demonstrated that ascididemin **1.11** can intercalate between base-pairs, with a preference for CG-rich sequences.[26] Additionally, Mergny *et al*. further observed a preference of ascididemin **1.11** for higher-order DNA structures, such as triplexes and quadraplexes.[29] Notably, ascididemin **1.11** exhibited high affinity for guanine-rich G-quadruplexes, which are considered attractive targets in oncology due to their involvement in gene expression. In contrast, only moderate affinity was observed for DNA duplexes, while single-stranded DNA showed weak binding. Schmitz *et al*. observed that an octahedral ruthenium(II) complex **2.56** containing the natural product 2-bromoleptoclinidinone **2.1** (**Figure 2.2**) [30] – C2-brominated ascididemin **1.11** – could also intercalate with double-stranded DNA, however no direct comparison between the intercalation abilities of 2-bromoleptoclinidinone **2.1** and ruthenium(II) complex **2.56** was conducted.

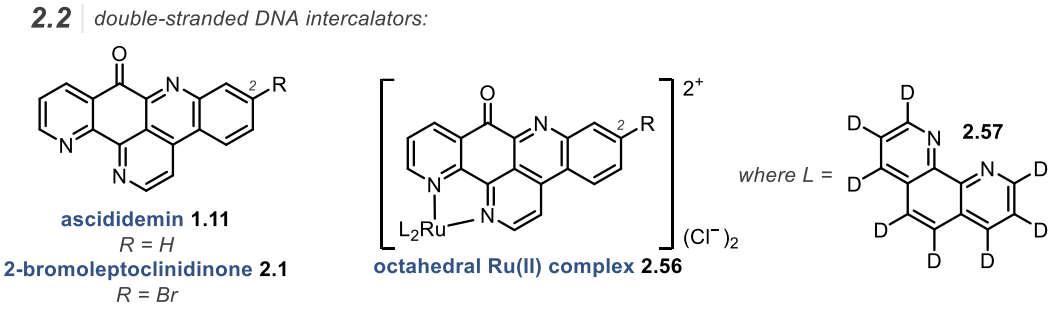

Figure 2.2. *Compounds shown to intercalate to double-stranded DNA.*

DNA cleavage has been proposed to occur either through inhibition of topoisomerase enzymes that regulate DNA topology,[31] or via the generation of reactive oxygen species induced by cellular reductants, such as thiols.[27,28] Supporting a DNA cleavage-based mechanism-of-action, cells deficient in a DNA repair protein exhibited increased sensitivity to ascididemin **1.11**.

2.2.2. Reactive oxygen species

When evaluating the antitumour activity, Copp *et al.* proposed that ascididemin **1.11** was capable of generating reactive oxygen species from direct reduction of the iminoquinone moiety, leading to DNA cleavage. Since cleavage was not enhanced in the presence of iron(II) or decreased in the presence of iron(II)-chelators this refuted the theory of trace iron(II)-catalysed Fenton-like generation of reactive oxygen species. The redox potential of ascididemin **1.11** (−226 mV) was comparable with NADPH (−280 mV), thus within the minimum threshold for bioreduction with cells.[27] Additionally, hyper-fine splitting was observed by electron paramagnetic resonance spectroscopy, suggesting ascididemin **1.11** was capable of generating radical species in the presence of the reducing agent dithiothreitol. To further support a mechanism-of-action via oxidative damage, supplementing with the antioxidant enzyme catalase provided strong protection, while moderate protection was provided by antioxidant- or radical scavenger-supplementation. Moreover, the upregulation of antioxidant enzymes heme oxygenase-1 and glutathione transferases was observed in mammalian cells treated with ascididemin **1.11**.

2.2.3. Antiparasitic activity of ascididemin 1.11

In addition to antitumour activity, ascididemin **1.11** has demonstrated antiviral, antifungal, antibacterial[32,33] and antiparasitic activity.[34] Ascididemin **1.11** has shown to exhibit potent activity against a range of different parasites (**Table 2.1**). Feng *et al.* tested ascididemin **1.11** against *T. b. brucei* trypomastigotes which gave an IC_{50} of 0.032 μM ± 0.004.[35] The activity was comparable with known treatments, such as pentamidine (IC_{50} = 0.028 μM ± 0.012), diminazene (IC_{50} = 0.094 μM ± 0.011) and puromycin (IC_{50} = 0.069 μM ± 5.40). Copp *et al.* observed 1000-fold less potent activity against *T. cruzi* (IC_{50} = 68.5 μM versus 1.61 μM for known treatment benznidazole **2.58**) and *T. b. rhodesiense* promastigotes (IC_{50} = 14.1 μM versus 0.003 μM for known treatment melarsoprol).[34] The activity against *L. donovani* promastigotes (IC_{50} = 30.7 μM

versus 0.027 μM for known treatment amphotericin B **1.5**) was similar to that against *Trypanosoma* reported by Copp *et al.*. Ascididemin **1.11** showed similar potency to known treatment chloroquine **1.7** against the chloroquine-sensitive (NF54) *P. falciparum* strain (IC_{50} = 0.071 μM versus 0.016 μM for chloroquine **1.7**). Similar potency was observed against the chloroquine-resistant (K1) *P. falciparum* strain (IC_{50} = 0.078 μM versus 0.138 μM for chloroquine **1.7**) suggesting ascididemin **1.11** has a different mechanism-of-action.

2.1 | *antiparasitic activity of ascididemin **1.11**:*

species	*associated disease*	*IC_{50} / μM*	*SI*
T. b. brucei trypomastigotes	HAT	0.032 ± 0.004	47
T. cruzi trypomastigotes	Chagas disease	68.5	*ND*
T. b. rhodesiense trypomastigotes	HAT	14.1	*ND*
P. falciparum NF54	malaria	0.071	*ND*
P. falciparum *K1*	malaria	0.078	*ND*
L. donovani promastigotes	visceral leishmaniasis	30.7	*ND*

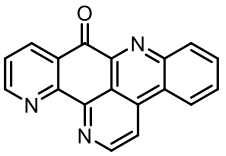

ascididemin 1.11

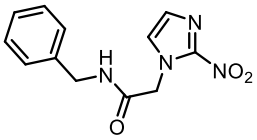

benznidazole 2.58
trypanocidal agent

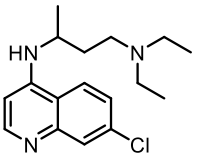

chloroquine 1.7
active treatment against P. falciparum

Table 2.1. *Reported antiparasitic activity of ascididemin **1.11**. Converted to μM. Associated disease for each species displayed. Where HAT = human African trypanosomiasis.*

2.2.4. Structure–activity relationship studies

Analogues of ascididemin **1.11** have been isolated or synthesised, featuring modifications such as heteroatom translocation, heteroatom deletion, ring deletion and ring functionalisation. However, only some of these compounds have been tested for biological activity, and a limited number of these have had their antiparasitic activity evaluated (**Table 2.2**). Copp *et al.* synthesised ascididemin **1.11**, along with *D*-ring functionalised analogue 2-bromoleptoclinidinone **2.1**, *A*-ring heteroatom deletion analogue **2.59**, *D*-ring deletion analogue **2.60**, *D*-ring deletion and *A*-ring heteroatom deletion analogue sampangine **2.61**, and *D*-ring deletion and *A*-ring heteroatom translocation analogue **2.62**.[34] Such structural changes had a more significant impact on the biological activity against *L. donovai* promastigotes than *T. cruzi* and *T. b. rhodesiense* trypomastigotes. Deletion (analogues **2.60**–**2.62**) or functionalisation (analogue **2.1**) of the *D*-ring of ascididemin **1.11** was detrimental to activity against *L. donovai* promastigotes, whereas the deletion of the *A*-ring heteroatom (analogue **2.59**) was tolerated.

2.2 | *antiparasitic acitivity of ascididemin **1.11** and analogues:*

compound	IC_{50} / μM		
	L. donovani promastigotes	*T. cruzi* trypomastigotes	*T. b. rhodesiense* trypomastigotes
1.11	30.7	68.5	14.1
2.1	>276	0.607	4.86
2.59	24.1	2.41	0.007
2.60	>429	0.103	0.064
2.61	207	0.990	8.61
2.62	>429	0.240	0.064

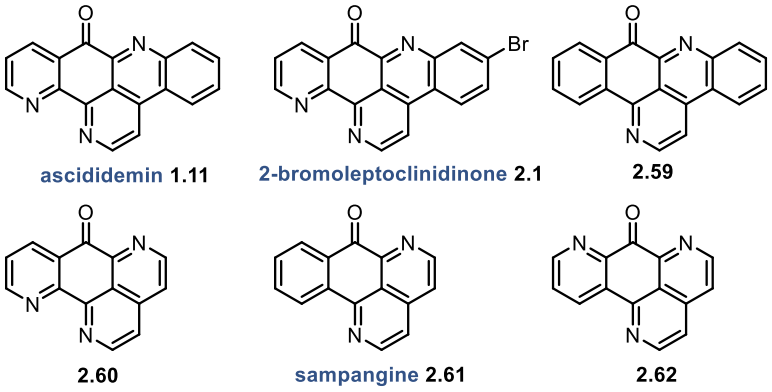

Table 2.2. *Reported antiparasitic activity of ascididemin **1.11** and analogues. Biological data reported in μg mL^{-1} and converted to μM, 100 μg mL^{-1} was the experimental limit.*

Additionally, 12-deoxyascididemin **2.53**, isolated by Quinn *et al.*, possessed similar activity against *T. b. brucei* as ascididemin **1.11** (**Table 2.3**),[35] even in the absence of the iminoquinone moiety.

2.3 | *antiparasitic acitivity of ascididemin **1.11** and analogues:*

compound	IC_{50} / μM
	T. b. brucei
1.11	0.032 ± 0.004
2.53	0.077 ± 0.005

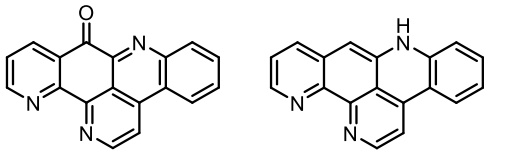

Table 2.3. *Reported antiparasitic activity of ascididemin **1.11** and analogues, continued.*

In the context of this project, no other *A*-, *D*- or *E*-ring functionalisation analogues have to date been synthesised for testing against *Leishmania* or *Trypanosoma* species. Moreover, the mechanism-of-action for ascididemin's antiparasitic activity has yet to be elucidated. However, it has been speculated to involve DNA intercalation and DNA oxidative damage, as has been proposed for its antitumor activity.[34] This work aimed to either validate this assumption or provide insight into an additional mechanism-of-action of ascididemin **1.11** in trypanosomatids.

2.2.5. Zinc(II) homeostasis

Zinc(II) is an essential metal ion within *Leishmania* possessing both catalytic and structural roles within proteins. Due to being the active metal in DNA binding transcriptors and DNA/RNA polymerases, zinc(II) is required for the synthesis of DNA and RNA, thus enabling cell growth, repair and differentiation.[36] Zinc(II) is present in two forms in cells, either: (1) tightly-bound to proteins (non-exchangeable pool of zinc); or (2) loosely- or un-bound to proteins (labile intracellular pool of zinc). The latter has more metabolic significance with lower abundance of zinc(II) within the labile intracellular pool associated with a reduction in DNA synthesis and cell proliferation, and an increase in cell death. Lal *et al.* observed that the apoptosis-like cell death of *L. donovani* promastigotes was triggered by the known membrane-permeable metal ion chelator tetrakis-(2-pyridylmethyl)ethylenediamine (TPEN) **2.64** (**Figure 2.3A**), likely due to altered levels of zinc(II) present within the labile intracellular pool.[36] A less pronounced effect on cell viability was observed for disturbances to extracellular zinc(II) levels when using the known membrane-impermeable metal ion chelator pentetic acid **2.66**. Branquinha *et al*. reported that the antileishmanial activity of 1,10-phenanthroline **2.63** was due to the conversion of a zinc-dependent metalloprotease, involved in *Leishmania* virulence, to the inactive apoenzyme in *L. amazonensis*, by removal of the active metal ion via chelation of 1,10-phenanthroline **2.63**.[37] Similarly, zinc(II)-supplementation restored growth in 1,10-phenanthroline **2.63** treated cells.

Proteins, such as cysteine-rich metallothioneins, which are capable of binding up to seven zinc(II) ions in their fully reduced state, are tasked with maintaining cellular metal homeostasis, since this is paramount for *Leishmania* survival.[38] Additionally, although zinc(II) is redox-inactive within biological systems, it is also important for cellular antioxidant defence. Partial oxidation of metallothioneins, due to cellular redox signalling in response to oxidative stress, translates into the release of bound zinc(II) and an increase in the abundance of the labile intracellular pool zinc(II).

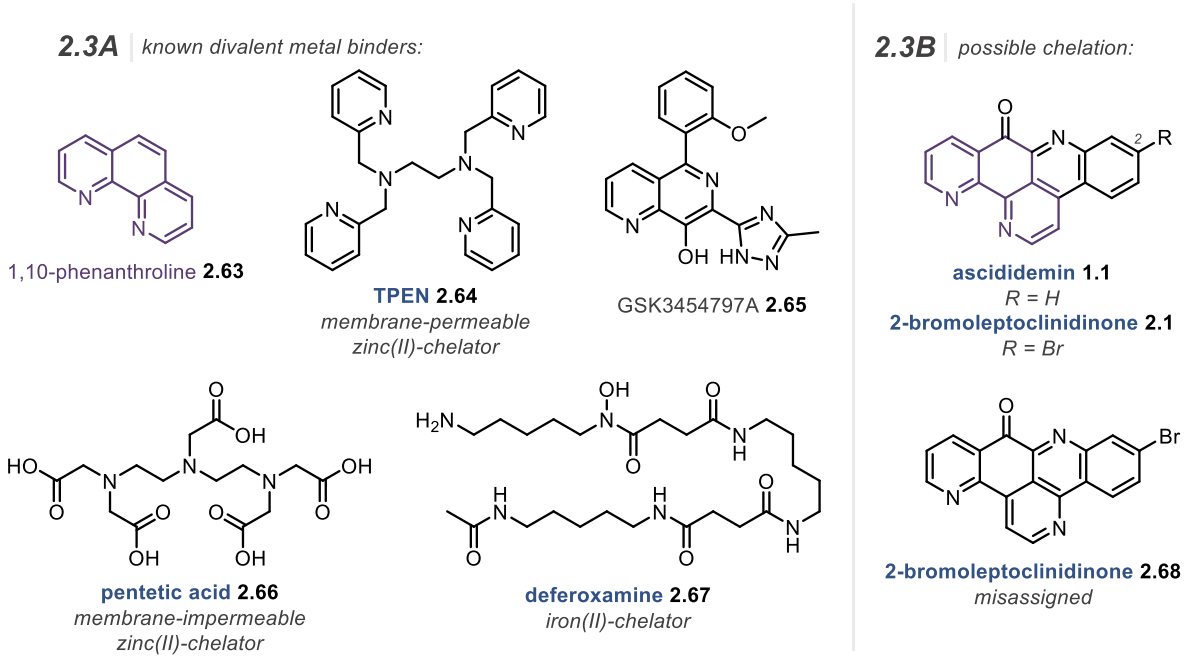

Figure 2.3. (A) *Known divalent metal binders.* ***(B)*** *Potential metal chelators: ascididemin* ***1.11*** *and 2-bromoleptoclinidinone* ***2.1****. Both possess phenanthroline motif. 2-Bromoleptoclinidinone* ***2.1*** *originally misassigned as* ***2.68*** *since a red-coloured complex with iron(II) was not observed.*

2.2.6. Iron(II) homeostasis

Iron is likewise essential to *Leishmania* for cellular growth and differentiation, and like zinc(II) plays key structural and catalytic roles within enzymes, alongside being involved in cellular signalling processes.[39] Iron has an important antioxidant role within *Leishmania*. For example, iron is the active metal within superoxide dismutase enzymes, which convert superoxide radicals to hydrogen peroxide and water. However – unlike zinc(II) – iron(II) is redox-active and is capable of generating reactive oxygen species, leading to cellular toxicity through the iron(II)-catalysed reduction of hydrogen peroxide via the Fenton reaction ($Fe^{2+} + H_2O_2 \rightarrow Fe^{3+} + HO^{\bullet} + HO^-$). As a consequence, iron homeostasis is crucial, with iron either incorporated into proteins or stored as the less toxic iron(III).[40] Mukhopadhyay *et al.* noted treatment of *L. donovani* amastigotes with known iron chelator deferoxamine **2.67** (**Figure 2.3A**) led to approximately 75% inhibition of cell growth after 12 hours.[41]

2.2.7. Metal binding

The metal binding ability of ascididemin **1.11** had been investigated as early as 1988 during its initial isolation to aid structural determination of the novel natural product (**Figure 2.3B**).[15] Colorimetric tests were considered an effective method for structural determination since "1,10-phenanthrolines with the nitrogen atoms correctly situated for bidentate coordination are excellent ligands for chelating metal ions".[25,42] However, unlike 1,10-phenanthroline **2.63** (**Figure 2.3A**), the formation of red-coloured complexes with iron(II) salts was not observed for ascididemin **1.11**. Although this observation did not lead to the mischaracterisation of ascididemin **1.11**, Schmitz *et al.* had previously misassigned the skeleton of 2-bromoleptoclinidinone **2.1** (2-bromoleptoclinidinone-misassigned **2.68**, **Figure 2.3B**)[43] due to a similar observation of no apparent chelation.[44]

Wyllie *et al*. identified that depletion of the divalent metal ions zinc(II) and iron(II) through chelation, was the mechanism-of-action of 8-hydroxy-naphthyridine GSK3454797A **2.65** against *L. donovani* and *T. b. brucei* (**Figure 2.3A**).[45] Whilst metal chelation by ascididemin **1.11** has never explicitly been demonstrated, Copp *et al.* noted that a reduction of DNA cleavage was observed in the presence of nickel(II) salts (nickel(II) chloride), due to a possible ascididemin **1.11**–nickel(II) interaction reducing the concentration of unbound ascididemin **1.11**.[27] Additionally, the natural product 12-deoxyascididemin **2.53**, like ascididemin **1.11**, possesses a phenanthroline motif and is highly active against *T. b. brucei* trypomastigotes even with the absence of the iminoquinone moiety.[35] Accordingly, it was planned by us to investigate the metal-chelating properties of ascididemin **1.11** as a potential contributor to its mechanism-of-action, possibly resulting to the disruption of zinc(II) and iron(II) homeostasis.

2.3. Research and discussion

2.3.1. Synthesis of ascididemin

As well as elucidating the mechanism-of-action of ascididemin **1.11**, we sought to expand the range of different *Leishmania* or *Trypanosoma* species which ascididemin **1.11** has been tested against. For this, the synthesis of ascididemin **1.11** was required. Upon review of the total syntheses reported, that of Wang *et al.* was deemed the most appealing due to its short length, high yield, operational simplicity, and potential to modify the skeleton of the natural product (refer back to **Scheme 2.4**).

Hence, *N*-Boc-protected propargylamine **2.20** was synthesised in an excellent yield of 91% from propargylamine **2.69** (**Scheme 2.9A**). In our hands, the reported conditions for the Sonogashira cross-coupling reaction of *N*-Boc-protected propargylamine **2.20** and *ortho*-iodoaniline **2.19** yielded only trace aniline **2.21**;[21] primarily unreacted starting material was observed. The catalyst loading of both the palladium and copper catalyst was increased 5-fold, however still only trace aniline **2.21** was observed. However, upon increasing the temperature to 60 °C, the desired reactivity was restored, and aniline **2.21** was obtained in a good yield of 61%.

With **2.21** in hand, our attention turned towards the synthesis of the quinoline-5,8-dione **2.4** fragment. This was accessible via the oxidation of 8-hydroxyquinoline **2.70** with bis(trifluoroacetoxy)iodo benzene (PIFA, **Scheme 2.9B**). Unfortunately, purification by flash column chromatography (FCC) to remove the iodobenzene **2.71** by-product revealed quinoline-5,8-dione **2.4** was unstable on silica, as the ^{1}H NMR spectrum of the "purified" product indicated significant decomposition had occurred. It was hoped that crude quinoline-5,8-dione **2.4**, contaminated with the iodobenzene **2.71** by-product, could be used directly in the oxidative amination reaction with aniline **2.21**. However, the quality of quinoline-5,8-dione **2.4** was found to be paramount for the success of the subsequent oxidative amination reaction. Poor quality quinoline-5,8-dione **2.4** displayed the characteristics of near-black colour and poor solubility in

dichloromethane, chloroform and methanol. Alternative purification strategies for quinoline-5,8-dione **2.4** were attempted, such as trituration with diethyl ether or dissolving in dichloromethane or methanol and filtering, however this did not bring about success in oxidative amination with aniline **2.21**. Purification by rapid FCC using a plug of silica enabled the isolation of quinoline-5,8-dione **2.4** in a moderate yield of 43%, but of sufficient quality for the next reaction; pleasingly, oxidative amination with aniline **2.21** and catalytic cerium(III) chloride in methanol furnished enamine **2.22** in good yield of 77% (**Scheme 2.9A**). Finally, enamine **2.22** could be transformed to ascididemin **1.11** via a double annulation in a moderate 44% yield upon treatment with catalytic iron(III) sulfate in sulfuric acid–acetic acid at 100 °C.

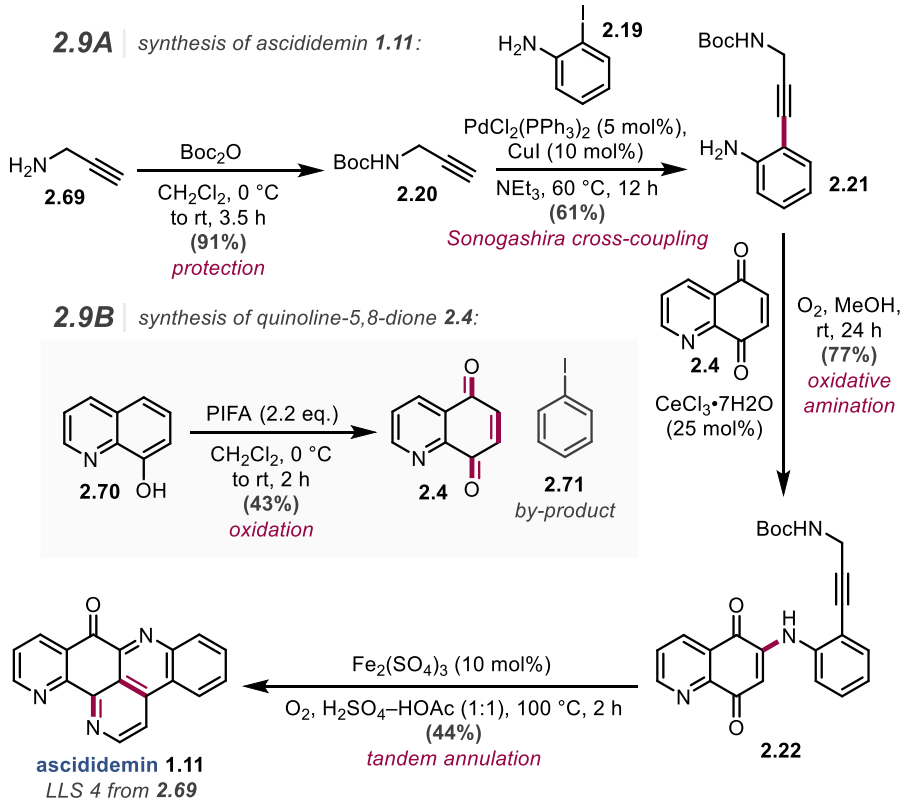

Scheme 2.9. (A) *Synthesis of ascididemin* ***1.11*** *via the route developed by Wang et al.* ***(B)*** *Synthesis of quinoline-5,8-dione* ***2.4****.*

2.3.2. Antiparasitic activity of ascididemin 1.11

Ascididemin **1.11** was found to be similarly active (**Table 2.4**) against *L. infantum* promastigotes (IC_{50} = 0.50 ± 0.35 μM) and *T. cruzi* trypomastigotes (IC_{50} = 0.34 ± 0.34 μM) and amastigotes (IC_{50} = 0.29 ± 0.01 μM). Ascididemin **1.11** displayed greater potency against *T. b. brucei* trypomastigotes (IC_{50} = 1.6 ± 0.1 nM) and *L. donovani* promastigotes (IC_{50} = 19.6 ± 1.3 nM); this was 200-fold and 1,500-fold greater, respectively, than what Copp *et al.* reported.[34] It should be noted that the IC_{50} against *T. b. brucei* trypomastigotes is the most potent antiparasitic activity of ascididemin **1.11** recorded to date. Additionally, ascididemin **1.11** demonstrated high potency against *L. mexicana* promastigotes (IC_{50} = 69 nM ± 17 nM).

2.4 | *antiparasitic activity of ascididemin **1.11**:*

	species	IC_{50} / μM	SI
previously reported	*T. cruzi* trypomastigotes	68.5	*ND*
	T. b. brucei trypomastigotes	0.032 ± 0.004	47
	T. b. rhodesiense trypomastigotes	14.1	*ND*
	P. falciparum NF54	0.071	*ND*
	P. falciparum *K1*	0.078	*ND*
	L. donovani promastigotes	30.7	*ND*
this work	*T. cruzi* trypomastigotes	0.34 ± 0.34	*ND*
	T. cruzi amastigotes	0.29 ± 0.01	9.89
	T. b. brucei trypomastigotes	0.0016 ± 0.0001	*ND*
	L. donovani promastigotes	0.0196 ± 0.0013	*ND*
	L. infantum promastigotes	0.50 ± 0.35	*ND*
	L. mexicana promastigotes	0.069 ± 0.017	*ND*

Table 2.4. *Reported antiparasitic activity of ascididemin **1.11** and this work.*

2.3.3. Mechanism-of-action studies

2.3.3.1. Morphology changes and cell cycle analysis

Within *Leishmania*, the cellular shape and size, and the organelle shape, size, orientation, and the per-cell organelle number are well defined for the promastigote, amastigote, and transitional phases within their life cycle.[46] Light microscopy facilitates the detection of micrometre-scale phenotype changes within drug treated cells. For example, Lal *et al.* reported that *L. donovani* promastigotes treated with known zinc(II) chelator TPEN **2.64** were ovoid-shaped, and of significantly smaller size with shortened flagella compared with the untreated control cells.[36] Conversely, when additional zinc(II) was supplemented, no morphology change was observed for TPEN **2.64** treated cells, suggesting the morphology change observed stemmed from factors caused by the reduction of intracellular zinc(II).

Healthy *Leishmania* promastigotes are spindle-shaped and contain a single nucleus (1N), which is posterior to, a single kinetoplast (1K, a DNA-containing organelle within the cell's single mitochondrion), and a long motile flagellum (**Figure 2.4A**).[47] However, upon treatment with ascididemin **1.11** (250 nM) for 6 hours, shortened ovoid-shaped cells with shortened flagella and abnormal nucleus- and kinetoplast-positioning were observed in 97% of the population (n = 200). Only 3% of the population had morphologies similar to the untreated control cells.

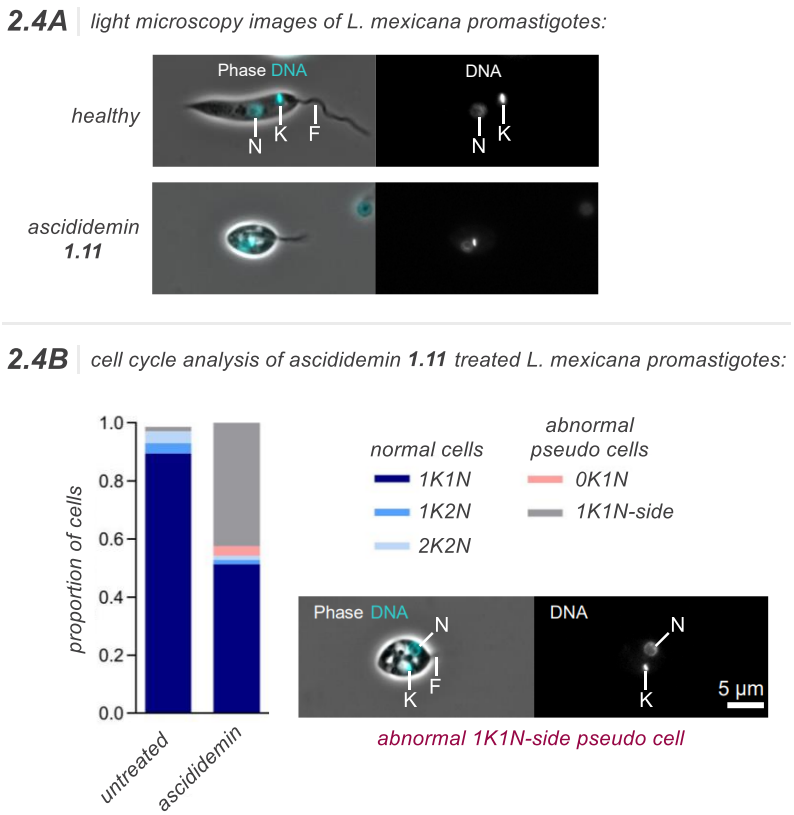

Figure 2.4. (A) *Light microscopy images of healthy versus ascididemin **1.1**-treated L. mexicana promastigotes.* ***(B)*** *Cell cycle analysis of L. mexicana promastigotes 6 hours after treatment with ascididemin **1.11** versus untreated cells. Reduction in cells in 1K1N, 1K2N and 2K2N suggesting a disruption of normal cell cycle progression for ascididemin **1.11** treated cells. Abnormal pseudo cells 0K1N and 1K1N-side observed. Light microscopy image of 1K1N-side abnormal morphology.*

Like the cellular morphology of *Leishmania,* the cell cycle progression – characterised by the number of kinetoplasts and nuclei – is well defined.[46] *Leishmania* populations are heterogeneous and are primarily expected to have the 1K1N (one kinetoplast and one nucleus) morphotype. Cells undergoing cellular division will be present with a 1K2N (one kinetoplast and two nuclei) or 2K2N (two kinetoplasts and two nuclei) morphotype before dividing to two 1K1N daughter cells. Abnormalities in the cell cycle of drug treated cells can sometimes provide information on the mechanism-of-action.

After cells were treated with ascididemin **1.11** (250 nM) for 6 hours, a large reduction in the number of *L. mexicana* promastigotes with a 1K1N morphotype, and a reduction in cells with a 1K2N and 2K2N morphotype indicated a disruption of normal cell cycle progression (**Figure 2.4B**).[48] Additionally, an increase in the number of abnormal pseudo-cells was also observed. A large proportion (42%, n = 540) of the ascididemin **1.11** treated cells had an abnormal

morphotype where the orientation of the kinetoplast relative to the nucleus had changed (1K1N-side). The second largest proportion of the population had an abnormal morphotype where the cell did not possess a kinetoplast (0K1N). This could possibly stem from the inappropriate orientation of the kinetoplast relative to the nucleus found in 1K1N-side cells, resulting in the failure of kinetoplast duplication and the production of 0K1N cells. However, the exact reason for these abnormalities remains unknown.

2.3.3.2. Metal binding

It was hypothesised that the divalent metal chelation ability of ascididemin may alter the intracellular or extracellular metal ion levels within *Leishmania* species leading to toxicity. Moreover, an ovoid-shaped phenotype with shortened flagella was observed for ascididemin **1.11** treated cells, which is a characteristic morphotype change for zinc(II)-depletion. Thus, chelation may play a key role in its mechanism-of-action.

The ability of ascididemin **1.11** to bind zinc(II) and iron(II) extracellularly was evaluated by performing a ultraviolet–visible (UV–vis) spectrophotometric titration for each divalent metal ion. Upon the addition of either zinc(II) chloride (**Figure 2.5A**) or iron(II) chloride (**Figure 2.5B**), a change in the absorbance spectrum was observed suggesting chelation was occurring, with the most significant change occurring at λ = 284 nm. Thus, in latter experiments, the absorbance intensity at 284 nm (A_{284}) was monitored during sequential addition of either zinc(II) or iron(II).

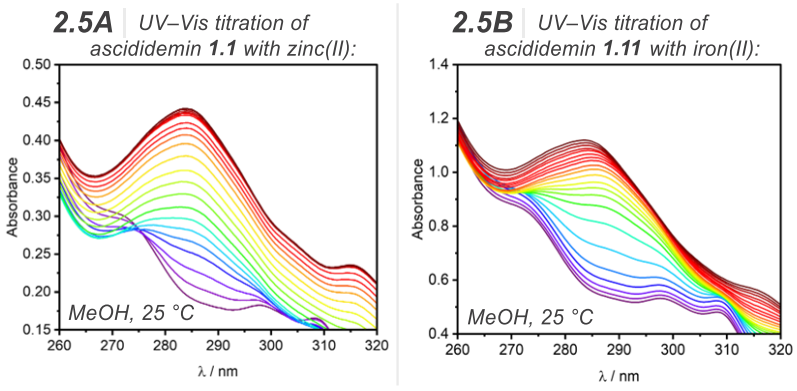

Figure 2.5. (A) *UV–Vis titration of ascididemin* ***1.11*** *with zinc(II) chloride at 25 °C in methanol.* ***(B)*** *UV–Vis titration of ascididemin* ***1.11*** *with iron(II) chloride at 25 °C in methanol. Each line represents a different titration. The bottom purple curve is for 0 eq. of M(II) added, and the colour becomes more red-shifted as the eq. of M(II) added increases. M(II) was sequentially added in non-integer equivalents.*

The binding stoichiometry and binding constants for ascididemin **1.11** with zinc(II) were obtained after comparison of the data to different models (using BindFit) and selecting the most appropriate.[49] A model was rejected if the calculated association constant (K_a) was negative. The remaining models were assessed based on the: (1) percentage error – ideally close to zero; (2) ratio between covariances (Cov_{fit} ratio) – ideally being 5–8-fold times the value of the statistical

model to justify a higher order model with a greater number of parameters; (3) isotherm – ideally a similar number of experimental data points above and below the model; (4) chemical intuition – does it make chemical-sense.[50] It was determined that ascididemin **1.11** non-cooperatively binds zinc(II) in a 2:1 binding stoichiometry (**Figure 2.6A**) – thus the association constants were determined as K_{11} = 3807 M^{-1} and K_{21} = 952 M^{-1} (it is assumed that K_{11}= 4 K_{21}, since statistically fewer bindings sites are available and less unbound zinc(II) is available after the first binding event). This is further supported by the observation that 1,10-phenanthroline **2.63** binds zinc(II) in a 2:1 binding stoichiometry forming an overall octahedral complex **2.72** by the coordination of two molecules of water (**Figure 2.7**). Due to the high dilution-nature of the UV–vis spectrophotometric titration experiment, higher order ascididemin **1.11** complexes with zinc(II) (and for iron(II), also) were not considered since aggregation is less likely.

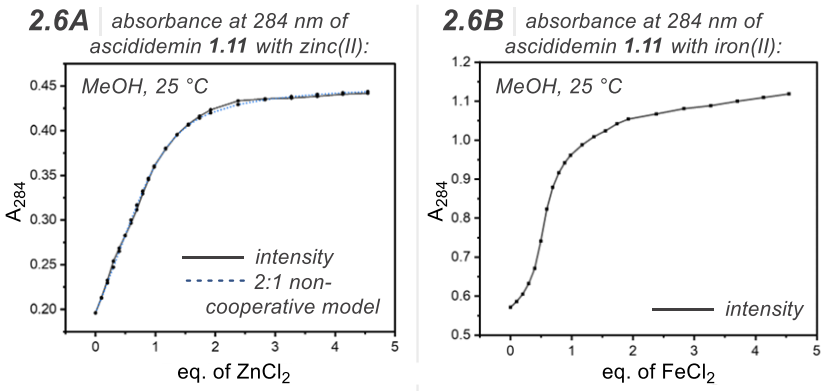

Figure 2.6. (A) *Absorbance at 284 nm of ascididemin **1.11** with zinc(II) chloride. The 2:1 non-cooperative model fitted the UV–Vis titration data well.* ***(B)*** *Absorbance at 284 nm of ascididemin **1.11** with iron(II) chloride. No model fitted the UV–Vis titration data well. BindFit cannot model for anything other than 1:2, 1:1 and 2:1.*

The determination of the binding stoichiometry of ascididemin **1.11** with iron(II) was unsuccessful as the data did not fit to any of the models for 1:2, 1:1 or 2:1 binding stoichiometries (**Figure 2.6B**). This result could be explained by the observation that 1,10-phenanthroline **2.63** binds iron(II) in a 3:1 binding stoichiometry forming an octahedral complex **2.73** (**Figure 2.7**),[51] which cannot be modelled using BindFit.

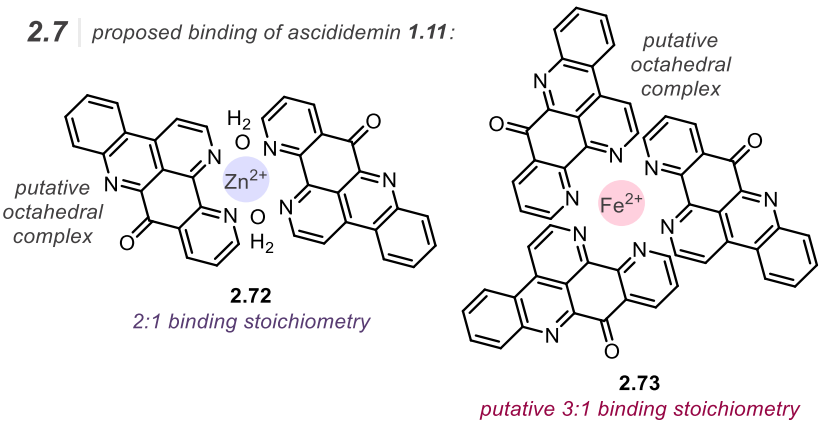

Figure 2.7. *Proposed 2:1 binding for ascididemin* ***1.11*** *with zinc(II) (overall octahedral complex with two water molecules) and 3:1 binding for ascididemin* ***1.11*** *with iron(II). Suggested by UV–Vis titrations and experimental data of 1,10-phenanthroline* ***2.63****.*

With the divalent metal ion chelation abilities of ascididemin **1.11** confirmed, we sought to evaluate whether ascididemin was capable of disturbing metal homeostasis within *Leishmania* through altering of the intracellular or extracellular metal levels.

Before investigating the effect of divalent metal ion-supplementation on ascididemin-treated cells, dose–response curves were obtained to establish the maximum tolerated dose for *L. mexicana* promastigotes.[48] Only for zinc(II) and iron(II) could a maximum tolerated dose be determined. The maximum tolerated dose for zinc(II) (800 μM) was significantly higher than that of iron(II) (1.5 μM). The lower tolerated value for iron(II) may be a consequence of its ability to generate toxic reactive oxygen species through iron(II)-catalysed intracellular reduction of hydrogen peroxide. In *L. mexicana* promastigotes a 4.8-fold increase in IC_{50} was observed for ascididemin after zinc(II)-supplementation (IC_{50} = 330.8 ± 60.9 nM) suggesting decreased sensitivity of the cells towards ascididemin (**Figure 2.8**). A smaller increase in IC_{50} (1.8-fold) was observed for zinc(II)-supplementation in ascididemin treated *L. donovani* promastigotes versus without supplementation. In contrast, no significant change in IC_{50} was observed after iron(II)-supplementation in either *L. mexicana* or *L. donovani* promastigotes. Since we have already demonstrated that ascididemin can chelate both zinc(II) and iron(II), a possible explanation for not observing reduced sensitivity of *Leishmania* towards ascididemin with iron(II)-

supplementation is, compared to zinc(II), the maximum tolerated dose (1.5 μM) was insufficient to counteract the effect of ascididemin on the extracellular or intracellular iron(II) levels.

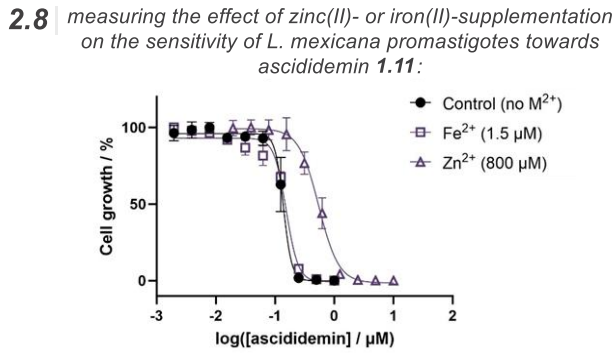

Figure 2.8. *Measuring the effect of zinc(II)- or iron(II)-supplementation on the sensitivity of L. mexicana promastigotes towards ascididemin* ***1.11****. Maximum tolerated doses for zinc(II) and iron(II) established first (800 μM and 1.5 μM, respectively). A 4.8-fold increase in* IC_{50} *was observed for ascididemin* ***1.11*** *after zinc(II)-supplementation. No change to* IC_{50} *after iron(II)-supplementation. Where, n = 3 biological replicates each with 6 technical replicates. The mean is plotted with error bars representing standard deviation. Statistical significance derived from a two-tailed t-test had P-value < 0.05 for zinc(II) when compared with the control.*

Since zinc(II)-supplementation provided protection to both *L. mexicana* and *L. donovani* promastigotes, this suggested a mechanism-of-action either directly linked to zinc(II), through disturbing zinc(II) homeostasis via chelation, or indirectly, serving as a pro-antioxidant and contributing to cellular protection against oxidative stress. To attempt to decipher the mechanism-of-action of ascididemin we sought to quantify the ascididemin-induced depletion or accumulation of the labile intracellular pool of zinc(II) in *Leishmania*. Membrane-permeable fluorescent reporter FluoZin-3 **2.74** binds intracellular zinc(II) with a 1:1 binding stoichiometry (**Figure 2.9**).[52] An increase in the fluorescence signal is observed during an enhancement of intracellular zinc(II) versus a decrease in the fluorescence signal during intracellular zinc(II) deprivation, relative to normal homeostasis. We hypothesised we would observe a decrease in the concentration of intracellular zinc(II) if disruption of zinc(II) homeostasis via chelation was the mechanism-of-action, as was observed by Wyllie *et al.* for GSK3454797A **2.65**.[45]

In *L. mexicana* promastigotes, a significant increase in the abundance of zinc(II) within the labile intracellular pool was observed for ascididemin-treated cells after 5 minutes, versus the dimethyl sulfoxide treated negative control cells representing homeostasis (**Figure 2.9**). The direction of

disruption to homeostasis was identical to when exogeneous zinc(II) was provided to *L. mexicana* promastigotes – *i.e.* an increase in intracellular zinc(II) – but opposite to when cells were treated with membrane-permeable zinc(II)-chelator TPEN **2.64** – *i.e.* a decrease in intracellular zinc(II). This suggested depletion of the labile intracellular pool of zinc(II) is not the mechanism-of-action of ascididemin **1.11** in *Leishmania*.

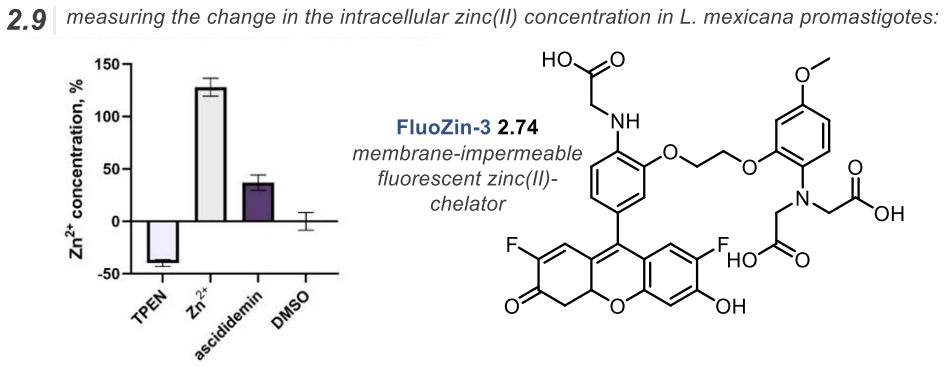

Figure 2.9. *Measuring the change in the intracellular zinc(II) concentration in L. mexicana promastigotes after 5 mins of treatment. Membrane-impermeable fluorescent reporter FluoZin-3* ***2.74*** *localises within Leishmania cells. Increase in fluorescence is caused by an in increase in intracellular zinc(II) levels. FluorZin-3 fluorescence readout is normalised to 0.1% DMSO treatment and the zinc(II) concentration plotted relative to 0.1% DMSO of 0%. Where n = 3 replicates, the mean is plotted with error bars representing standard deviation and statistical significance was derived from a two-tailed t-test versus DMSO; only P < 0.05 are shown. Ascididemin* ***1.11*** *causes an increase in the intracellular zinc(II) concentration. An increase in fluorescence was also observed when zinc(II) was supplemented. Known zinc(II)-chelator TPEN* ***2.64*** *caused a reduction in the intracellular zinc(II) concentration.*

Lal *et al.* reported a time-dependent fluctuation in the direction of change of the labile intracellular pool of zinc(II) with TPEN **2.64**, with depletion or accumulation observed at different time-points. It was observed that initially zinc(II) abundance decreased for 0–3 hours after treatment, then increased to give a large abundance up until 16 hours, finally decreasing again after 24 hours.[36] It has been suggested the increase in abundance of zinc(II) between 3–16 hours is due to upregulation of a zinc transporter to overcome intracellular zinc(II) deprivation,[53] or by release of protein bound zinc(II) due to oxidation state changes of proteins resulting from oxidative stress.[54] Similarly, for ascididemin **1.11** treated cells, the increase in the concentration of intracellular zinc(II) after 5 minutes could be the result of the release of protein bound zinc(II) in response to increased oxidative stress (refer back to **Section 2.2.5.** Zinc(II) homeostasis).

2.3.3.3. DNA intercalation

Given the consensus that DNA is the primary cellular target of ascididemin **1.11** in mammalian cells, contributing to its antitumor activity, it was postulated that DNA may likewise serve as the main cellular target in *Leishmania*.

The proposed DNA intercalation ability of ascididemin **1.11** was initially evaluated through a displacement assay using the fluorescent reporter acridine orange **2.75** (**Figure 2.10**), prebound to double-stranded DNA. Intercalation was quantitatively evaluated by monitoring the change in fluorescence polarisation when acridine orange was displaced from the double-stranded DNA. Ascididemin **1.11** successfully displaced acridine orange **2.75**, achieving 50% intercalation at 50 µM, compared to 1 µM observed for the positive control – the known DNA intercalator daunorubicin**.** Copp *et al.* observed complete displacement with ascididemin **1.11** at 10 µM when using ethidium bromide **2.76** (**Figure 2.10**) as the fluorescent reporter.[27] Discrepancies in the values may be a result of the different binding affinities of acridine orange **2.75** versus ethidium bromide **2.76** with double-stranded DNA.

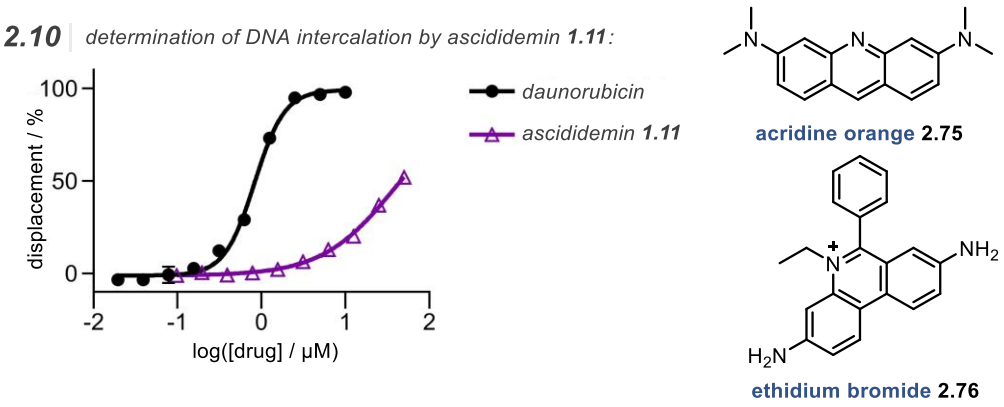

Figure 2.10. *Determination of DNA intercalation by ascididemin* ***1.11****. Ascididemin* ***1.11*** *was capable of displacing acridine orange* ***2.75*** *from DNA. Representative dose-response curves for the displacement of acridine orange* ***2.75****, n = 3. The mean is plotted with error bars representing standard deviation.*

The relatively weak binding affinity of ascididemin **1.11** for double-stranded DNA observed by Mergny *et al*. would suggest reversible DNA-binding, resulting in an equilibrium between the bound and unbound state. As a consequence, high concentrations of ascididemin **1.11** may have

been required to achieve 50% DNA intercalation. Therefore, one reason for why the concentration in which ascididemin achieves 50% inhibition (50 μM) is 700-fold the IC_{50} value (68.6 nM in *L. mexicana*) could be because of its moderate affinity towards double-stranded DNA. Another possible explanation could be that DNA intercalation itself is not the main source of cytotoxicity. Additionally, the assay does not accurately replicate cellular conditions. Previously, we have demonstrated the ability of ascididemin **1.11** to bind to the divalent metal ions zinc(II) and iron(II) thus making it possible that the active compound *in vivo* is not the monomer ascididemin **1.11**.

With the modest DNA intercalation ability of ascididemin **1.11** confirmed, we hoped to demonstrate a link between DNA intercalation and DNA damage in *Leishmania*. Although nuclear DNA (located in the nucleus) accounts for the largest proportion of cellular DNA, *Leishmania* also possesses kinetoplast DNA (10–30% of cellular DNA, located in the kinetoplast situated within the mitochondrion).[55] We believe it unlikely that kinetoplast DNA is the major cellular target of ascididemin **1.11** since this would require dual barrier entry across both the mitochondrial and kinetoplast membranes, requiring either passively-driven diffusion to occur or a mechanism to allow active transport. In contrast, nuclear pores provide a facile route to compound accumulation in the nucleus. Additionally, kinetoplast DNA is AT-rich, whereas ascididemin has shown a preference for CG-rich sequences.[26] Copp *et al*. observed only minor double-stranded DNA breakages *in vitro*, with ascididemin primarily breaking single-stranded DNA.[27] However, in a different study Copp *et al.* observed increased sensitivity of cancer cells deficient of double-stranded DNA repair proteins towards ascididemin suggesting double-stranded DNA breakages were also part of its mechanism-of-action.[56]

We aimed to indirectly monitor DNA breakages by fluorescent light microscopy by fluorescent tagging of a nuclear DNA repair protein – the upregulation of the tagged nuclear DNA repair protein, shown by the formation of fluorescent foci in the nucleus, would suggest nuclear DNA damage. A prevalent double-stranded DNA recombinase repair protein, RAD51, was fluorescently

tagged in *L. mexicana* promastigotes using CRISPR/Cas9 machinery to introduce an mNeonGreen fluorescent protein. After a period of 24 hours, no fluorescent foci were observed in cells treated with ascididemin **1.11** (250 nM) suggesting no upregulation of the fluorescently tagged-RAD51 protein (**Figure 2.11**). This indicated that ascididemin **1.11** was not capable of causing nuclear double-stranded DNA breakages.[27] In contrast, fluorescent foci were observed 24 hours after treatment with a known nuclear double-stranded DNA breaker, phleomycin.

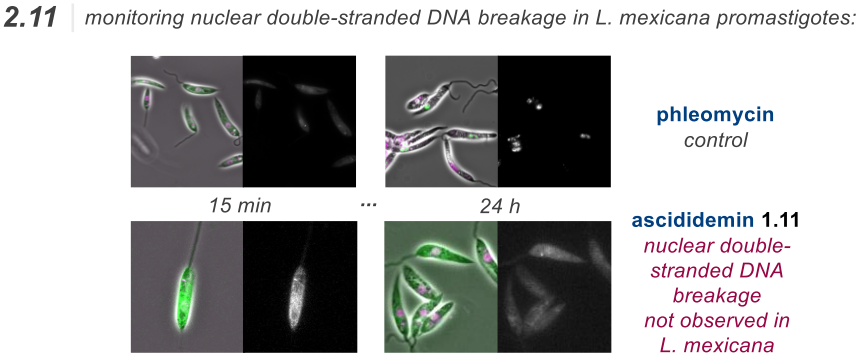

Figure 2.11. *Monitoring nuclear double-stranded DNA breakage in L. mexicana promastigotes. Upregulation of fluorescently tagged RAD51 (nuclear double-stranded DNA repair protein) indicates nuclear double-stranded DNA breakages. No fluorescent foci observed 24 hours after Leishmania cells treated with ascididemin* ***1.11****. DNA was stained with Hoechst 33342 (magenta), all mNeonGreen images are shown with equivalent contrast. n > 100 cells for each condition.*

In summary, ascididemin **1.11** was shown to displace DNA-bound acridine orange **2.75**, indicating its ability to intercalate into DNA and supporting the widely held view that DNA is the primary cellular target of pyridoacridine natural products. However, the observed cytotoxicity of ascididemin **1.11** does not appear to attributed to nuclear double-stranded DNA breakages.

2.3.3.4. Knockdown libraries

Gene knockdown is a technique used to reduce the expression of a specific gene in an organism. This process can confer a selective advantage to the organism in the presence of an active compound if the targeted gene plays a role in the compound's mechanism-of-action – such as encoding proteins responsible for its uptake or for its activation within the organism. Researchers at the University of Dundee have developed a genome-wide knockdown library for *T. b. brucei* covering greater than 99% of non-redundant genes.[57] Although the same genome-wide knockdown library cannot be created for *Leishmania* species since they lack the molecular machinery required for the process, results from the *T. b. brucei* library can be translated to *Leishmania* using genome databases, such as TriTrypDB,[58] to identify orthologs – genes separated by species which are assumed to have retained function.

For the knockdown experiment, the cell library was cultured in the presence of ascididemin **1.11** in duplicate parallel runs. While the majority of cells were nonviable, surviving cells were presumed to exhibit a fitness advantage conferred by specific gene knockdowns. DNA from the surviving populations was extracted and sequenced. Results were quantified as reads per kilobase per million mapped reads (RPKM), with genes showing the highest RPKM values highlighted. Genes identified across both runs were considered to more likely represent true positives.

2.5 | *T. b. brucei genome-wide knockout library hits for ascididemin **1.11**:*

gene ID	gene name	RPKM	total reads
7.3020	nitroreductase family (putative)	60253	8644
7.2980	nitroreductase family (putative)	51824	7452
7.2970	ATP-dependant DEAD/H RNA helicase (putative)	9726	4046

Table 2.5. *Hits from genome-wide knockout library of T. brucei for ascididemin **1.11**. Tb927 gene IDs RPKM = reads per kilobase per million mapped reads.*

2.3.3.4.1. Knockdown of an RNA helicase

For the *T. b. brucei* genome-wide knockout library, the downregulation of a putative ATP-dependent DEAD/H RNA helicase was shown to provide a selective advantage against ascididemin **1.11** (**Table 2.5**). Helicases are a class of motor proteins that unwind double stranded DNA (DNA helicase) or RNA (RNA helicase) using energy derived from the hydrolysis of ATP. However, this signal was detected in only one of the two parallel runs and exhibited the lowest RPKM values recorded, suggesting it is unlikely to represent a true positive. As such, it was not considered further.

2.3.3.4.2. Knockdown of nitroreductases

More significantly, a selective advantage against ascididemin was observed from both of the two parallel runs when two putative nitroreductase enzymes were downregulated. Nitroreductases are enzymes which catalyse the reduction of nitro-substituents and are categorised based on oxygen sensitivity. Both drug compounds nifurtimox **2.77** and benznidazole **2.58** take advantage of nitroreductases in *T. b. brucei* to generate reactive oxygen species as part of their mechanism-of-action (**Figure 2.12A**). The apparent selectivity of these drugs comes from the lower abundance of nitroreductases in mammalian cells versus bacteria and trypanosomatids. Type I nitroreductases are oxygen-insensitive and perform two-electron reductions of nitro-groups to amines, accompanied with the formation of by-products capable of damaging DNA.[59] Type II nitroreductases are oxygen-sensitive and perform one-electron reductions of nitro-groups to the corresponding nitro-radical anion. This reactive species can react with oxygen to produce superoxide and regenerate the nitro-group. Although more commonly found in bacteria, type I nitroreductases in trypanosomatids, such as *T. b. brucei* and *T. cruzi*, exhibit low substrate specificity, catalysing the two-electron reduction of quinones to hydroquinones, as well as nitroaromatics. Notably, Wilkinson *et al.* reported a preference of type I nitroreductases for quinones, such as ubiquinone 5 **2.78** (**Figure 2.12B**), over the nitroaromatic drugs nifurtimox

2.77 and benznidazole **2.58**.[60] Futhermore, it was observed that compounds which were shown to be effective substrates for *T. b. brucei* type I nitroreductase were also potent trypanocidal agents, such as quinone **2.79** (**Figure 2.12B**; IC_{50} = 21 nM). A modified *T. b. brucei* cell line with nitroreductase overexpressed was 7-fold more sensitive to quinone **2.79** (IC_{50} = 3 nM).

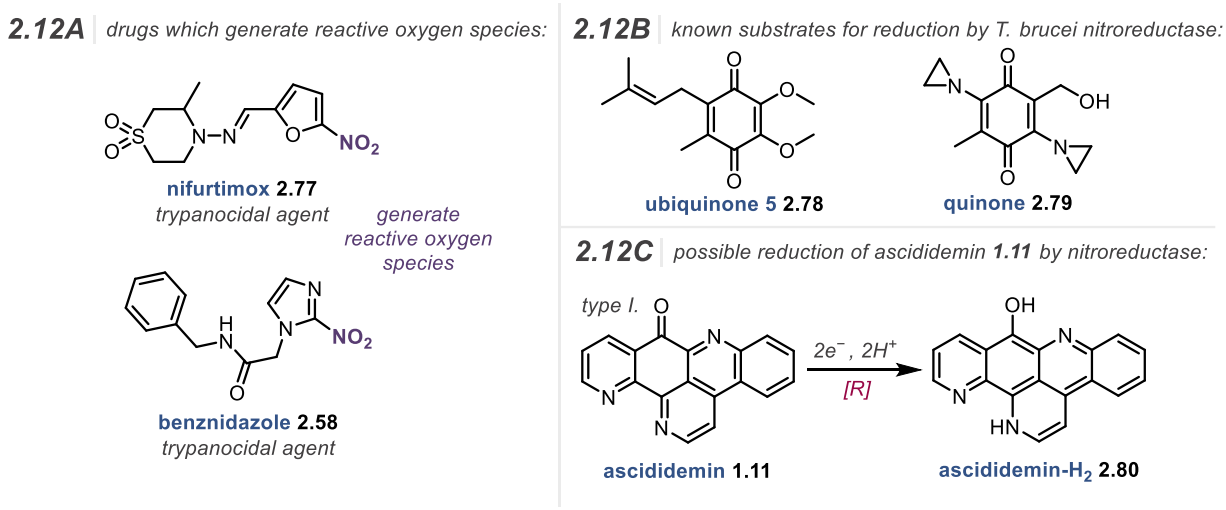

Figure 2.12. (A) *Trypanocidal agents which generate reactive oxygen species as part of their mechanism-of-action.* ***(B)*** *Quinones which have been shown to be reducible by T. b. brucei nitroreductase.* ***(C)*** *Possible reduction of ascididemin* ***1.11*** *to ascididemin-H_2* ***2.80*** *by a type I nitroreductase – accompanied by the generation of reactive oxygen species.*

Type II nitroreductase reduction of quinones or iminoquinones has not been reported in the literature for trypanosomatids to date. Although Wilkinson *et al.* have only identified a type I nitroreductase in *T. b. brucei* and *T. cruzi*,[60] Fairlamb *et al.* recently discovered a type II nitroreductase in *L. donovani* which activates bicyclic nitro-drugs.[61] It is plausible that nitroreductases would also be capable of reducing the iminoquinone moiety of ascididemin to the hydroiminoquinone (**2.80**) and generating reactive oxygen species within *Leishmania* (**Figure 2.12C**). Moreover, the antitumor activity of ascididemin **1.11** may also be driven by nitroreductase-catalysed reduction leading to the generation of reactive oxygen species, particularly since tumour cells have been reported to overexpress nitroreductase-encoding genes.[62]

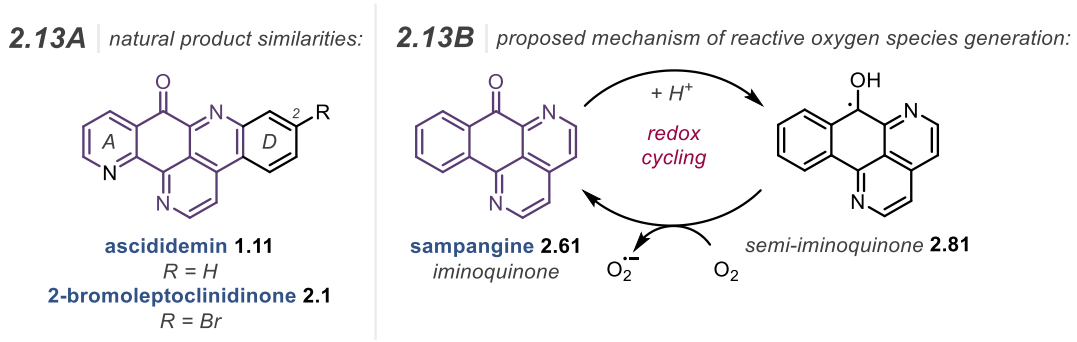

Figure 2.13. (A) *Similarities of ascididemin* ***1.11*** *and 2-bromoleptoclinidinone* ***2.1*** *with sampangine* ***2.61****.* ***(B)*** *Proposed redox cycling mechanism of sampangine* ***2.61*** *which generates reactive oxygen species.*

Zhou and Nagle *et al.* reported that the mechanism-of-action of the closely related natural product sampangine **2.61** (**Figure 2.13B**) – differentiated from ascididemin (**Figure 2.13A**) by the lack of heteroatom in the *A*-ring and complete lack of *D*-ring – for its antimicrobial and antitumour activity was the generation of reactive oxygen species.[63] A single-electron reduction of the iminoquinone moiety to a reactive semi-iminoquinone **2.81** was proposed. This reactive semi-iminoquinone **2.81** readily reacts with oxygen to produce superoxide and regenerate the iminoquinone functionality. An oxygen-sensitive reduction was proposed due to an increase in cellular oxygen consumption – potentially this could be facilitated by a type II nitroreductase, which as previously mentioned are prevalent in bacteria and upregulated in tumour cells.[62,64] Although sampangine **2.61** displayed antileishmanial activity against *L. donovani* promastigotes (IC_{50} = 206.7 μM), the activity was significantly less than that of ascididemin **1.11** (IC_{50} = 30.7 μM).[34] This reduced activity may be attributed to its higher redox potential (−318 mV versus −226 mV for ascididemin **1.11**) and weaker DNA intercalation, as indicated by the higher concentration required for complete ethidium bromide displacement observed (20 μM versus 10 μM for ascididemin **1.11**). However, conversely, Schwalbe *et al.* reported that sampangine **2.61** did not intercalate DNA.[65]

Future studies would aim to validate nitroreductase-mediated reduction of ascididemin **1.11** as the mechanism responsible for reactive oxygen species (ROS) generation in *Leishmania*. This would involve targeted knockout of *Leishmania* orthologs encoding nitroreductases, followed by assessment of changes in sensitivity to ascididemin **1.11** treatment. Additionally, future studies

could involve metabolite profiling following incubation of ascididemin **1.11** with purified nitroreductases to detect the formation of ascididemin-H_2 **2.80**, thereby confirming enzymatic reduction by nitroreductases. Experiments to detect ROS in *Leishmania* would be conducted using the membrane-impermeable, nonfluorescent probe dihydrodichlorofluorescein.[36] Upon oxidation by ROS, dihydrodichlorofluorescein is converted to the fluorescent species dichlorofluorescein, with fluorescence intensity directly correlating with intracellular ROS levels. This approach would support validation of ROS-mediated damage as the primary mechanism-of-action of ascididemin **1.11**.

2.3.3.5. First attempt at visualising the localisation of ascididemin 1.11

Pyrido[2,3,4-*kl*]acridine natural products (**Figure 2.14**) and their derivatives have shown promise for bioimaging and theranostic applications due to their unique combination of spectroscopic and biological properties.[66] Although many ultraviolet–visible spectra have been reported for pyrido[2,3,4-*kl*]acridine natural products, including ascididemin **1.11**,[67] the only reported fluorescence spectrum is of the natural product kuanoniamine D **2.82** (**Figure 2.14**; λ_{ex} = 350 nm, λ_{em} = 524 nm in 4:1 methanol–water at pH = 8.5).[68] However, it was hypothesised that the highly conjugated structure of ascididemin **1.11** may impart fluorescence capabilities which could be harnessed to visualise compound localisation in treated *Leishmania* cells. This could be informative to the MOA, particularly if ascididemin **1.11** could be visualised in the nucleus to confirm DNA intercalation.

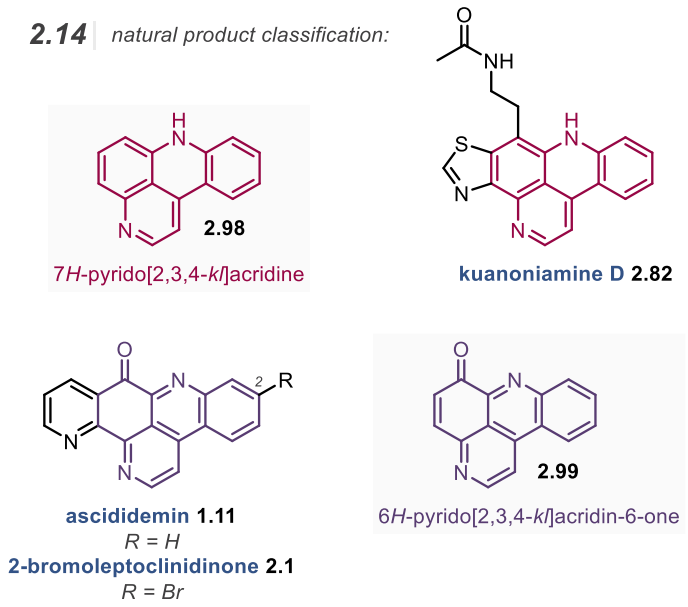

Figure 2.14. *Natural product classification. Kuanoniamine D* ***2.82*** *is a 7H-pyrido[2,3,4-kl]acridine natural product. Ascididemin* ***1.11*** *and 2-bromoleptoclinidinone* ***2.1*** *are 6H-pyrido[2,3,4-kl]acridin-6-one natural products.*

For ascididemin **1.11**, excitation–emission matrix (EEM) fluorescence spectroscopy revealed two distinct fluorescence emissions corresponding to two different excitation wavelengths in dimethyl sulfoxide at 25 °C (**Figure 2.15**): (1) λ_{ex} = 345 nm, λ_{em} = 542 nm, and (2) λ_{ex} = 425 nm,

λ_{em} = 533 nm. These appear as two separate resonances in the three-dimensional contour plot. The second excitation event produced a fluorescence emission of greater intensity therefore demonstrated more promise in succeeding with compound visualisation.

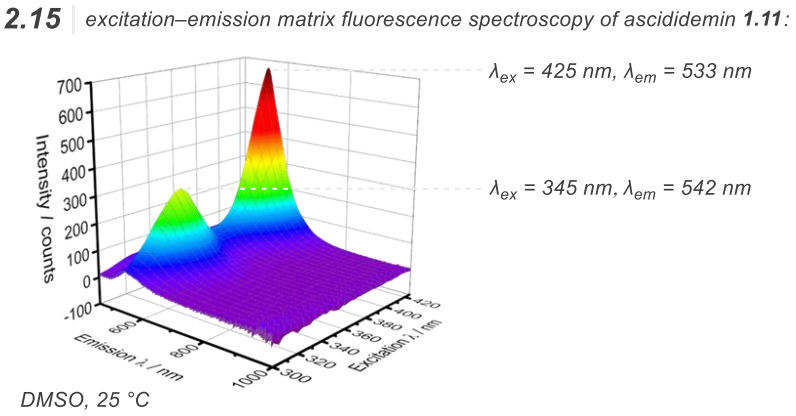

Figure 2.15. *Excitation–emission matrix fluorescence spectroscopy of ascididemin in DMSO at 25 °C. Two fluorescence wavelengths observed.*

L. mexicana promastigotes were treated with ascididemin for 24 hours, followed by fluorescence microscopy using an optimised filter (λ_{ex} = 430/24 nm, λ_{em} = 515–565 nm) to match the most intense fluorescence of ascididemin. When fluorescence microscopy was performed (**Figure 2.16**) no significant difference in fluorescence emission was observed for ascididemin-treated (0.175 μM) *L. mexicana* promastigotes versus the control (dimethyl sulfoxide-treated *L*. mexicana promastigotes). This may have been because the fluorescence intensity was insufficient, or because other important factors such as fluorescence lifetimes and quantum yields were not considered. Additionally, Faulkner *et al*. observed partial quenching of the fluorescence of kuanoniamine D **2.82** coupled with a shift in the emission wavelength upon the addition of the divalent metal ions zinc(II), iron(II), and copper(II) ($ZnCl_2$, $FeSO_4$ and $Cu(OAc)_2$, respectively) – with complete quenching of the signal by addition of cobalt(II) ($CoCl_2$).[68] Moreover, a large shift in the emission wavelength from 524 nm to 593 nm, along with significant fluorescence quenching, was observed upon the addition of calf thymus DNA. Since it has been demonstrated that ascididemin **1.11** forms complexes with divalent metal ions (refer back to **Figure 2.8**) and intercalates with DNA (refer back to **Figure 2.10**), it was plausible that the emission wavelength

was shifted outside of the monitored range (515–565 nm) and/or the fluorescence signal was partially or fully quenched *in vivo*.

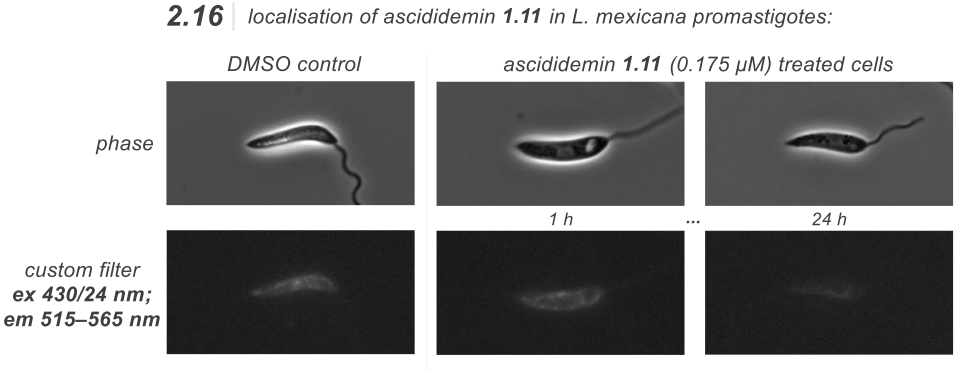

Figure 2.16. *Fluorescence microscopy of ascididemin* ***1.11*** *treated L. mexicana promastigotes. No significant increase in fluorescence observed versus the DMSO control. The localisation of ascididemin* ***1.11*** *inside Leishmania cells not observed.*

To continue to investigate the hypothesis that ascididemin **1.11** localises within the nucleus, alternative strategies were considered. A possible solution was to tune the fluorescence spectroscopic properties to fit our desired function through the design of an ascididemin analogue to facilitate compound visualisation. Colinet *et al*. established a quantitative relationship between the molecular structure and spectroscopic properties of pyrido[2,3,4-*kl*]acridines to allow predictions to be made for this exact purpose.[66] The largest variations in the computationally calculated electron density between the ground state and first excited state of each position around the pyrido[2,3,4-*kl*]acridine-core indicates the positions most sensitive to substitution, with substitution at these sites most significantly affecting the transition energy between the two states. For example, sites which gain electron density in the first excited state benefit from stabilisation by electron-withdrawing substituents, thus lowering the transition energy and increasing the wavelength of emission – therefore the shift in the fluorescence absorption and emission wavelengths can be quantitatively determined using the Hammett (σ_p) and Remya (ΔV_C) parameters for a given substituent. However, shifting of the emission wavelength and/or partial or full quenching of the fluorescence signal may have still been an issue *in vivo* when ascididemin **1.11** bound to its biological target. Additionally, modification of the (stereo)electronic properties of the ascididemin core carried the risk of altering its potency,

biological target, and mechanism-of-action. For example, substitution with a bromine atom at the C2-position – as in the natural product 2-bromoleptoclinidinone **2.1** – resulted in a marked loss of activity, with the IC_{50} against *L. donovani* amastigotes increasing from 31 μM (ascididemin **1.11**) to >276 μM (values converted from μg/mL).[34]

An alternative, and more attractive, approach was the introduction of a linker between ascididemin **1.11** and a fluorescent probe to preserve the electronics properties of the core. It was hypothesised that this design would minimise interference with the parent compound's binding interactions, enabling the cellular localisation of ascididemin to be visualised via fluorescence microscopy, without compromising bioactivity. Implementation of this strategy first required substitution-tolerant positions on the ascididemin scaffold to be identified.

2.3.4. Structure–activity relationship studies

As the intrinsic fluorescence of ascididemin **1.11** could not be directly exploited for visualisation within *Leishmania mexicana* promastigotes, it was planned to install a fluorescent probe distally to the core to preserve the interaction between ascididemin **1.11** and its cellular target. Given the presence of nine potential sites for probe attachment, each position required evaluation to determine the impact of functionalisation on biological activity. The primary objective was not to identify more potent antileishmanial analogues but to retain activity comparable to that of ascididemin **1.11**. Nonetheless, a significant loss of activity was also of interest, as it could indicate disruption of the compound's antiparasitic mechanism-of-action. Additionally, identification of substitution-tolerant sites would allow functionalisation of the ascididemin-core to enhance its drug-like properties, should this natural product scaffold be advanced as a lead for further development in the future.

A methyl substituent was chosen as a model substituent for representing a longer alkyl chain tether. This substituent was considered optimal because it is sterically relatively unencumbered, and was expected to have a negligible influence on the electronics of the ring system; therefore, a lack of tolerance for a methyl group would suggest that a more significant modification would unlikely to be accommodated. Additionally, it is accompanied with minimal changes in lipophilicity ($\Delta c\text{Log}P \approx 0.5$) and molecular weight ($\Delta M_W = 14$ g mol^{-1}).[69] Furthermore, methylated precursors were readily available, and the synthetic strategies previously employed for ascididemin **1.11** were anticipated to be applicable. If multiple positions on the ascididemin scaffold proved tolerant to substitution, the preferred site would be chosen based on synthetic accessibility.

As with the synthesis of ascididemin **1.11**, the route developed by Wang *et al*. was employed to access the target methylated ascididemin-analogues. However, an alternative route was required for functionalisation of the C5-position, as the position of the triple bond (**Scheme 2.10**, **2.83**) used for *E*-ring construction precluded further functionalisation (**2.84**). In this case, an

alternative approach employing quinoline-5,8-dione **2.4** was sought; the route reported by Bracher was identified as the most suitable option.

2.10 *functionalisation via the synthetic route developed by Wang et al, 2014:*

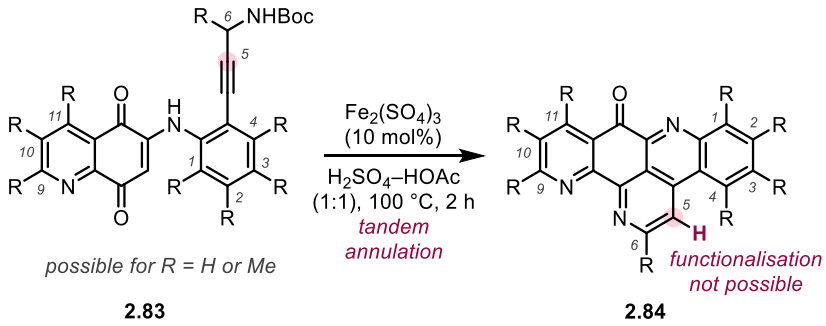

2.83 **2.84**

Scheme 2.10. *The C5-position of ascididemin* ***1.11*** *cannot be functionalised using the synthetic route developed by Wang et al.*[21]

2.3.4.1. Functionalisation via the synthetic route developed by Wang *et al.*

2.3.4.1.1. *A*-Ring substitution

For functionalisation of the C9-position of ascididemin **1.11** (**Scheme 2.10**, **2.84**), methylquinanol **2.85** was oxidised to methylquinoline-5,8-dione **2.86** in a moderate 45% yield using PIFA (**Scheme 2.11A**). It should be noted that quinoline-5,8-diones displayed poor stability on silica gel. For functionalisation of the C10- and C11-positions (**Scheme 2.10**, **2.84**), methylquinanol **2.87** and **2.91** were not commercially available (**Scheme 2.11A**). The desired methylquinanols were synthesised using the Doeber–von Miller quinoline synthesis of *ortho*-aminophenol **2.88** with either methacrolein **2.89**, for methylquinanol **2.87**, or methyl vinyl ketone **2.92**, for methylquinanol **2.91**. When using methacrolein **2.89**, a low isolated yield of 22% was obtained – it was believed this was due to competing polymerisation of methacrolein **2.89**. For the reaction with methyl vinyl ketone **2.92** the number of equivalents and duration of addition

was increased to counter possible polymerisation issues – methylquinanol **2.91** was isolated in excellent yield of 75%. However, unlike for methylquinanol **2.85**, the oxidation of both methylquinanol **2.87** and **2.91** was unsuccessful.

As ceric ammonium nitrate (CAN) is a powerful oxidant capable of performing oxidative demethylation reactions of *para*-dimethoxy compounds,[70] we wanted to explore the use of methyl-substituted *para*-dimethoxyquinolines as precursors for quinoline-5,8-diones. For the synthesis of methylquinoline-5,8-dione **2.93**, when using methyl vinyl ketone **2.92** with 2,5-dimethoxyaniline **2.30** (**Scheme 2.11B**) instead of *ortho*-aminophenol **2.88**, the Doeber–von Miller quinoline synthesis occurred in lower isolated yield of 36%. However, methyl-*para*-dimethoxyquinoline **2.95** could be successfully converted to methylquinoline-5,8-dione **2.93** in an excellent yield of 78% without the need of FCC purification. Additionally, methyl-*para*-dimethoxyquinoline **2.94** was synthesised in a similar yield of 34% and converted to methylquinoline-5,8-dione **2.90**, again, in an excellent 86% yield without the need for further purification. This was later employed in the synthesis of quinoline-5,8-dione **2.4**. 5,8-Dimethoxyquinoline **2.97** was synthesised from the Doeber–von Miller quinoline synthesis of 2,5-dimethoxyaniline **2.30** with acrolein **2.96** in 22% yield. Oxidative demethylation with CAN yielded quinoline-5,8-dione **2.4** in quantitative yield without FCC purification.

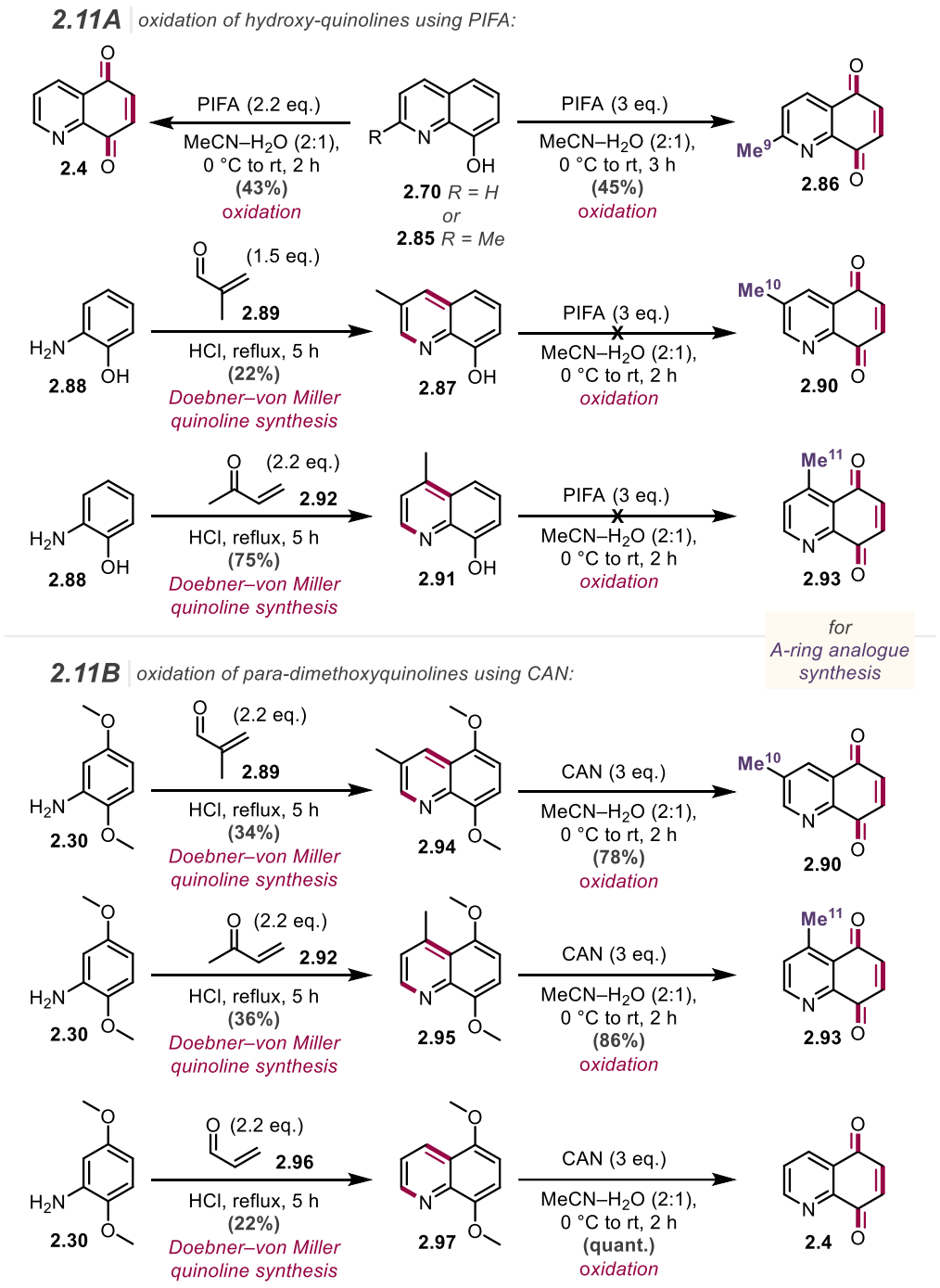

Scheme 2.11. (A) *Oxidation of hydroxyquinolines using PIFA.* ***(B)*** *Oxidation of para-dimethoxyquinolines using CAN. Synthesis of quinolines achieved by a Doebner–von Miller quinoline synthesis from given aniline.*

With methylquinoline-5,8-dione **2.86**, **2.90** and **2.93** in hand, each was reacted with aniline **2.21** (**Scheme 2.12A**) to furnish enamine **2.115** (**Scheme 2.12B** table, entry 6; 79% yield), **2.116** (entry 7; 72% yield), and **2.117** (entry 8; 58% yield), respectively. Finally, the tandem annulation of all three yielded the desired 9-methyl ascididemin **2.123** (**Scheme 2.12B** table, entry 6; 53%

yield), 10-methyl ascididemin **2.124** (entry 7; 48% yield), and 11-methyl ascididemin **2.125** (entry 8; 53% yield) analogues for biological testing.

2.12A | *methyl ascididemin analogue synthesis – via route one (Wang et al., 2014):*

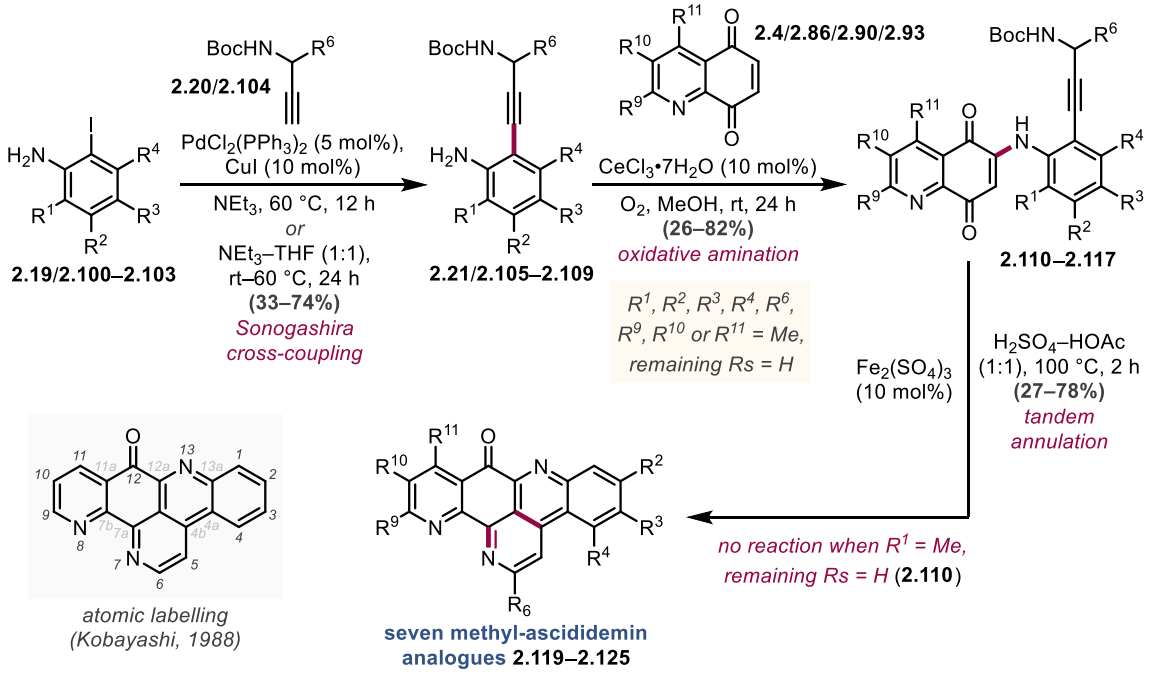

2.12B | *yields for methyl ascididemin analogye synthesis via route one*

entry	R^1	R^2	R^3	R^4	R^6	R^9	R^{10}	R^{11}	*Sonogashira cross-coupling / %*	*oxidative amination / %*	*tandem annulation / %*
1	**Me**	H	H	H	H	H	H	H	74	60	*NR*
2	H	**Me**	H	H	H	H	H	H	74	82	36
3	H	H	**Me**	H	H	H	H	H	71	34	78
4	H	H	H	**Me**	H	H	H	H	33	26	27
5	H	H	H	H	**Me**	H	H	H	73	54	53
6	H	H	H	H	H	**Me**	H	H	61	79	53
7	H	H	H	H	H	H	**Me**	H	61	72	48
8	H	H	H	H	H	H	H	**Me**	61	58	53

Scheme 2.12. (A) *The synthesis of methylascididemin analogues via the route developed by Wang et al.* ***(B)*** *Table summary of the yields for each step. Seven methylascididemin analogues were synthesised for biological testing. When R^1= Me and all remaining Rs = H (**2.110**) the tandem annulation reaction was unsuccessful.*

A single crystal could be obtained for 9-methylascididemin **2.123** by dissolving the sample in a minimum volume of chloroform-d_1 and then layering on top an equal volume of cold hexane. The crystal structure obtained by single crystal X-ray diffraction (XRD) exemplified the ability of the

ascididemin-core to act as a hydrogen bond acceptor, with hydrogen bonding to two molecules of chloroform-d_1 (**Figure 2.16**). A crystal structure could not be obtained for ascididemin **1.11** itself.

2.16 | *crystal structure of 9-methylascididemin* ***2.123****:*

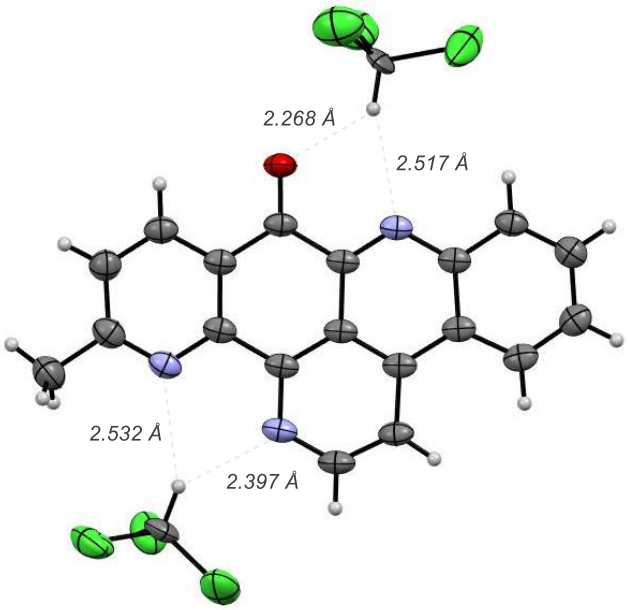

Figure 2.16. *Crystal structure of 9-methylascididemin* ***2.123.*** *Displacement ellipsoid plots are drawn at 50% probability.*

2.3.4.1.2. *D*-Ring substitution

For *D*-ring substitution, the synthetic route developed by Wang *et al.* required methyl-substituted *ortho*-iodoanilines for Sonogashira cross-coupling to propargylamine **2.20**. Some were commercial (**Scheme 2.13A**, *ortho*-iodoanilines **2.102**), while others were synthesised either by Béchamp reduction of the corresponding *ortho*-iodonitrobenzenes (**Scheme 2.13B**, *ortho*-iodoaniline **2.103**; 63% yield and *ortho*-iodoaniline **2.101**; 78% yield) or iodination of a pre-existing aniline (**Scheme 2.13C**, *ortho*-iodoanilines **2.100**; 67% yield).

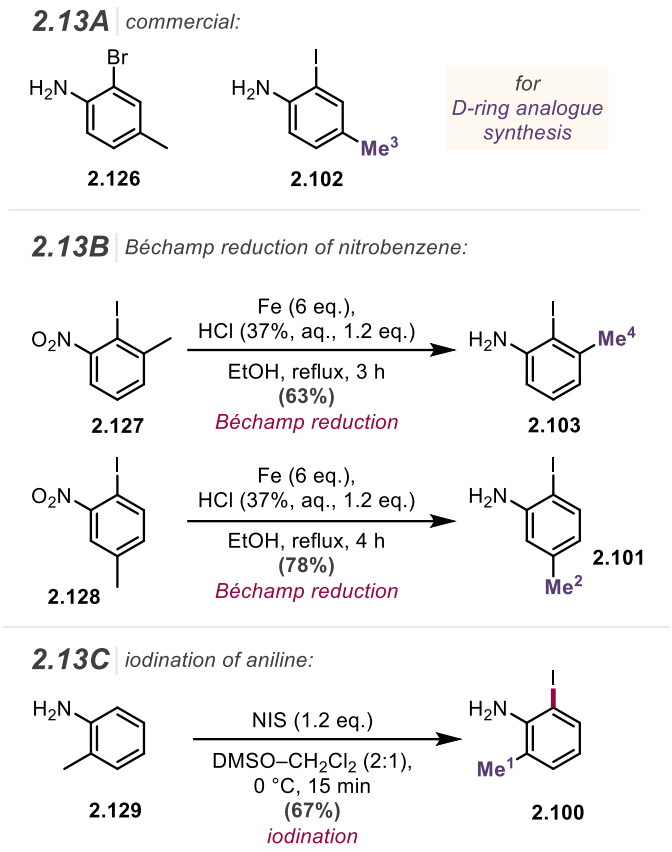

Scheme 2.13. (A) *Commercially available ortho-haloanilines.* ***(B)*** *Synthesis of ortho-iodoanilines via a Béchamp reduction of the corresponding nitrobenzene.* ***(C)*** *Synthesis of ortho-iodoanilines via iodination of the corresponding aniline.*

Sonogashira cross-coupling of propargylamine **2.20** with *ortho*-bromoaniline **2.126** (**Scheme 2.13A**) was initially attempted for the synthesis of aniline **2.107**; however, mainly starting material remained. On the other hand, the equivalent reaction occurred in good yield for *ortho*-iodoaniline **2.100** (**Scheme 2.12B** table, entry 1; 74% yield), *ortho*-iodoaniline **2.101** (entry 2; 74% yield), and *ortho*-iodoaniline **2.102** (3; 71% yield). Conditions were modified to include tetrahydrofuran (THF) as a co-solvent with triethylamine (NEt_3). In some cases, elevated temperatures were required (see **Section 5.2.1.** Chapter 2). However, for *ortho*-iodoaniline **2.103** (**Scheme 2.12B** table, entry 4; 33% yield) the yield was significantly lower – presumably due to steric encumbrance caused by the bis-*ortho*-substitution of the iodide. Oxidative amination with quinoline-5,8-dione **2.4** was achieved for aniline **2.106** (**Scheme 2.12B** table, entry 2; 82% yield), **2.107** (entry 3; 34% yield), and **2.108** (entry 4; 26% yield). Even for aniline **2.105** – with steric encumbrance from bis-*ortho*-flanking of the aniline – the yield of the oxidative amination reaction

was good (entry 1; 60% yield). However only enamines **2.111**, **2.112**, and **2.113** were successful in the final tandem annulation, yielding the desired 2-methyl ascididemin **2.119** (**Scheme 2.12B** table, entry 2; 36% yield), 3-methyl ascididemin **2.120** (entry 3; 78% yield), and 4-methyl ascididemin **2.121** (entry 4; 27% yield) analogues, respectively, for biological testing. Enamine **2.110**, on the other hand, could not be converted to 1-methyl ascididemin **2.118** (**Scheme 2.12B** table, entry 1). This was surprising since we predicted that the flanking methyl would be more problematic for the oxidative amination reaction than the final tandem annulation. Therefore, 1-methylascididemin **2.118** needed to be synthesised by other means.

2.3.4.1.3. *E*-Ring substitution

For the synthesis of the *E*-ring substituted analogue, 6-methylascididemin **2.122**, propargylamine **2.104** was required and was synthesised via the route depicted in **Scheme 14**. A Mitsunobu reaction of propargyl alcohol **2.130** with di-*tert*-butyl-iminodicarboxylate **2.131**, diisopropyl azodicarboxylate (DIAD) and triphenylphosphine (PPh_3) delivered propargylamine **2.132** in a low 21% yield, although this was comparable with literature reports of 13%.[71] While, mechanistically, the di-*N*-Boc protected amine was expected to behave the same as the mono-protected amine – and undergo global deprotection – under the Brønsted acid-catalysed tandem annulation, the protecting group was kept the same for each substrate to increase the likelihood of reaction success. Mono-*N*-Boc-deprotection was initially attempted using catalytic bismuth(III) bromide however the rate of reaction, and yield, was low (**Scheme 2.14**; 32%). The yield improved greatly to 64% under alternative conditions of trifluoroacetic acid (TFA) in dichloromethane at room temperature, with quenching of the reaction after 5 minutes.

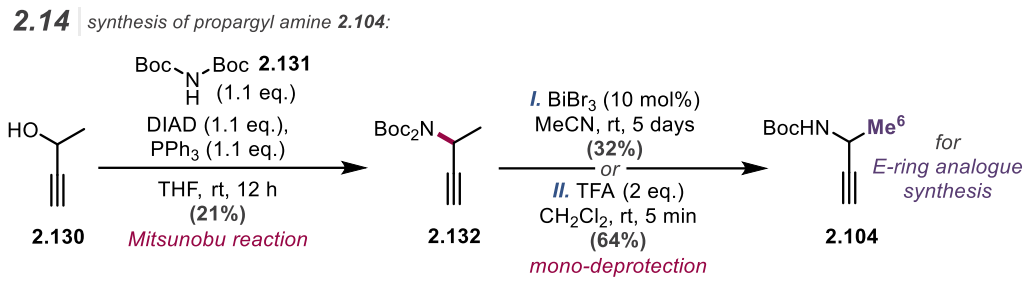

Scheme 2.14. *Synthesis of propargylamine* ***2.104*** *via a Mitsunobu reaction from methyl propargylalcohol* ***2.130*** *and mono-Boc-deprotection.*

Propargylamine **2.104** then cleanly underwent Sonogashira cross-coupling with *ortho*-iodoaniline **2.19** (Scheme 11B table, entry 5; 73% yield), and the resultant aniline **2.109** underwent an oxidative amination reaction with quinoline-5,8-dione **2.4** (Scheme 11B table; 54% yield). Finally, enamine **2.114** was converted to the desired 6-methylascididemin **2.122** (Scheme 11B table, entry 5; 53% yield) in readiness for biological testing.

2.3.4.2. Functionalisation via the synthetic route developed by Bracher

Since 1-methylascididemin **2.118** and 5-methylascididemin **2.136** were inaccessible via the synthetic route developed by Wang *et al.*, an alternative route was required. The route reported by Bracher (**Scheme 2.15**) seemed the most promising option as it was short and high-yielding. Similar to the route developed by Wang *et al.* it also involved the amination of quinoline-5,8-dione **2.4** with an aniline, in this case *ortho*-aminoacetophenones.

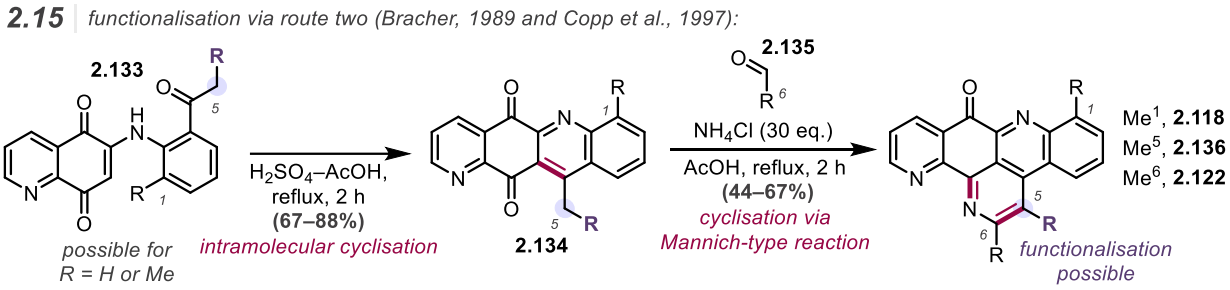

Scheme 2.15. *Utilisation of the route developed by Bracher and Copp et al. to synthesise the remaining methylascididemin analogues.*

2.3.4.2.1. *E*-Ring substitution

To complete the collection of *E*-ring analogues, 5-methylascididemin **2.136** was the final compound to synthesise – synthesis via the route of Wang *et al.* was not possible but was hoped to be achievable by Bracher's route by replacing *ortho*-aminoacetophenone **2.5** with **2.137**. *ortho*-Aminoacetophenone **2.137** was synthesised in 32% yield by the addition of ethylmagnesium bromide to *ortho*-aminobenzonitrile **2.138** (**Scheme 2.16A**).

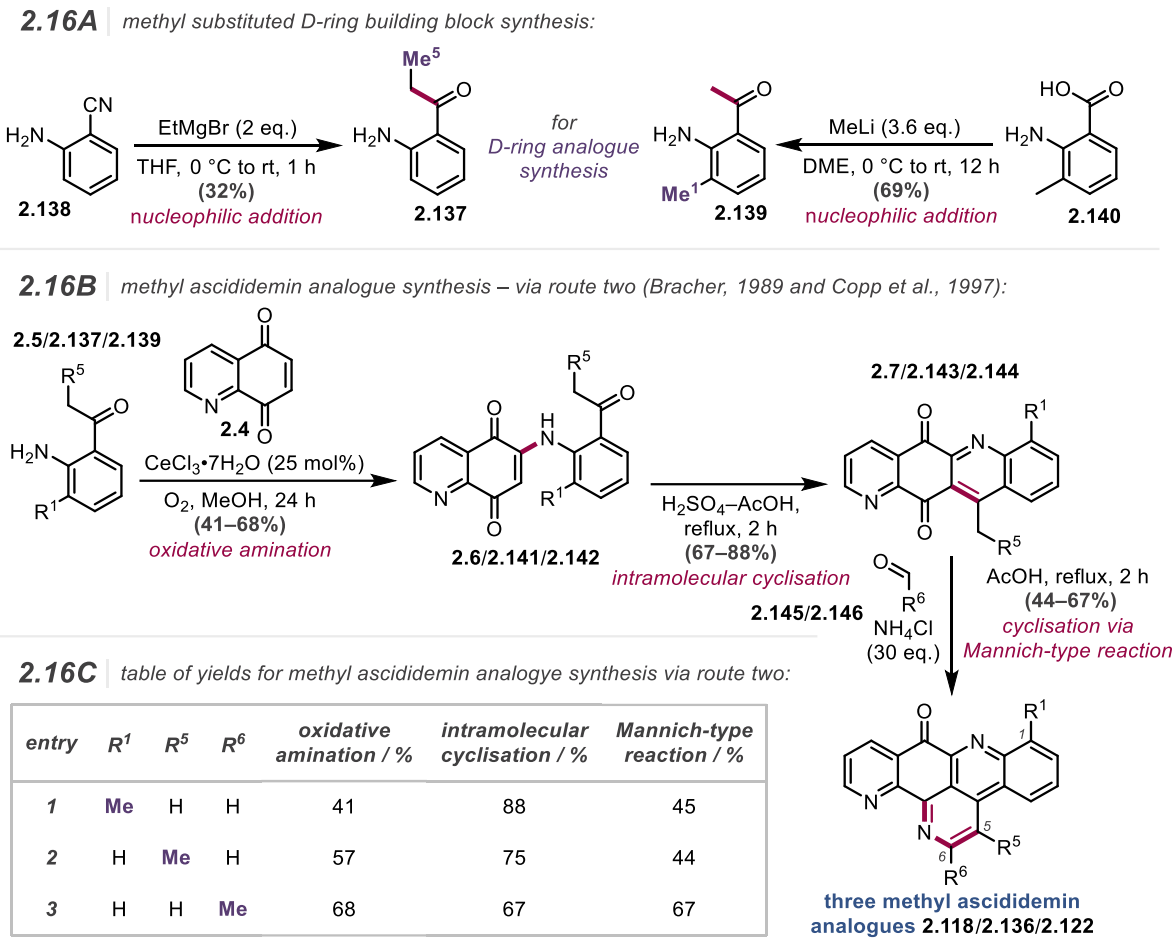

entry	R^1	R^5	R^6	oxidative amination / %	intramolecular cyclisation / %	Mannich-type reaction / %
1	Me	H	H	41	88	45
2	H	Me	H	57	75	44
3	H	H	Me	68	67	67

Scheme 2.16. (A) *Synthesis of the methyl substituted building blocks using organometallics.* ***(B)*** *Synthesis of three methylascididemin analogues using the route developed by Bracher and Copp et al.* ***(C)*** *Summary of yields for each step.*

Oxidative amination of *ortho*-aminoacetophenone **2.137** with quinoline-5,8-dione **2.4** (**Scheme 2.16B**) delivered enamine **2.142** in good yield (**Scheme 2.16C** table, entry 2; 57% yield), which underwent a Brønsted acid-promoted intramolecular condensation to furnish tetracycle **2.144** (**Scheme 2.16C** table, entry 2; 74% yield). However, attempts to perform the final two-step enamine formation at the activated benzylic *para*-position of the pyridine ring followed by intramolecular cyclisation were unsuccessful (refer back to **Scheme 2.1**). Fortunately, Copp *et al*. developed a complementary procedure for the total synthesis of ascididemin **1.11** from tetracycle **2.7** which enabled a one-pot condensation–cyclisation with paraformaldehyde and ammonium chloride in acetic acid via a Mannich-type reaction.[72] This approach was successfully applied to tetracycle **2.144**, affording 5-methylascididemin **2.136** (**Scheme 2.16C** table, entry 2) in 44% yield.

The attractiveness of the Copp *et al*. modification is that it enabled late-stage diversification at the C6-position. The reaction had previously been demonstrated with acetaldehyde **2.146**, benzaldehyde and cinnamaldehyde with tetracycle **2.7**,[33] as well as on other substrates.[73,74] Therefore, this route provided a more convenient synthesis of 6-methylascididemin **2.122**. Rather than requiring aniline **2.109** (synthesised in three steps from propargylalcohol **2.130**) for oxidative amination of quinoline-5,8-dione **2.4**, commercially available *ortho*-aminoacetophenone **2.5** was used (**Scheme 2.16C** table, entry 3; 68% yield). After intramolecular condensation (**Scheme 2.16C** table, entry 3; 67% yield), the subsequent tetracycle **2.7** was treated with acetaldehyde **2.146** and ammonium chloride in acetic acid to achieve 6-methylascididemin **2.122** (**Scheme 2.16C** table, entry 3; 67% yield).

2.3.4.2.2. *D*-Ring substitution

Since 1-methylascididemin **2.118** could not be synthesised by the route developed by Wang *et al.*, it was hoped that we would have more success using that of Bracher coupled with the Copp modification. Aniline **2.139** was synthesised in 69% yield by the addition of methyllithium to *ortho*-aminobenzoic acid **2.140** (**Scheme 2.16A**). Oxidative amination with quinoline-5,8-dione **2.4** yielded enamine **2.141** (**Scheme 2.16C** table, entry 1; 41% yield), which could undergo Brønsted acid-promoted intramolecular condensation to form tetracycle **2.143** (**Scheme 2.16C** table, entry 1; 88% yield). The final condensation–cyclisation with paraformaldehyde and ammonium chloride in acetic acid successfully yielded 1-methylascididemin **2.118** (**Scheme 2.16C** table, entry 1; 45% yield) – completing the collection of nine methyl-ascididemin analogues.

2.3.5. Antiparasitic activity of methyl analogues

The methyl analogues performed similarly against *L. infantum* promastigotes to ascididemin **1.11** (**Table 2.6**) suggesting the additional steric encumbrance did not hinder the ascididemin-core from binding to its molecular target, such as intercalating with DNA, and causing cellular damage. Due to unforeseen circumstances the compounds were not tested on the clinically more relevant intracellular amastigote form of the parasite.[75] Intracellular amastigotes are more heavily guarded than extracellular promastigotes; in order for an active compound to accumulate within *Leishmania* amastigotes it must cross three membranes:[76] (1) the host cell membrane; (2) the parasitophorous vacuole membrane – a defence membrane formed around the *Leishmania* cell using the host's cell membrane; and (3) the amastigote membrane. Additionally, the active compound is subjected to detoxification mechanisms in both the host and amastigote cells. Moreover, due to differences in gene regulation between *Leishmania* promastigotes and amastigotes, their metabolisms also differ. Selitewnnikoff *et al.* observed that some compounds which were active against *L. major* promastigotes were completely inactivate against *L. major* amastigotes, likely due to poorer membrane permeability limiting compound accumulation intracellularly or increased metabolism within the cell.[76]

The analogues were however screened against both the extracellular (trypomastigote) and intracellular (amastigote) form of the protozoan parasite *T. cruzi*. All methyl analogues, apart from 1-methylascididemin **2.118** and 4-methylascididemin **2.121**, possessed similar activity to ascididemin against *T. cruzi* trypomastigotes (**Table 2.6**), again implying minimal impact on the ability of the ascididemin core from binding to its molecular target and causing cellular damage. However, 1-methylascididemin **2.118**, 3-methylascididemin **2.120**, 5-methylascididemin **2.136** and 10-methylascididemin **2.124** did not retain this activity when tested against the intracellular form, becoming completely inactivated. Similar observations were observed by Anderson *et al*. when studying analogues of (bis)benzyltetrahydroisoquinoline alkaloids.[75] An attempt was made

to rationalise the inactivity of methylascididemin **2.118**, **2.120**, **2.136** and **2.124** by permeability and metabolism considerations.

2.6 *antiparasitic activity of ascididemin **1.11** and analogues:*

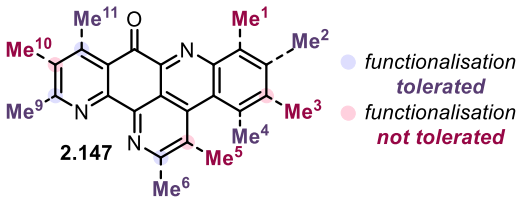

	L. infantum / μM	*T. cruzi / μM*		
compound	***promastigotes***	***trypomastigotes***	***amastigotes***	***SI***
ascididemin	0.50 ± 0.35	0.34 ± 0.34	0.29 ± 0.01	9.89
Me^{1a}	1.29 ± 0.31	3.20 ± 0.30	***not active***	*ND*
Me^{2a}	0.20 ± 0.06	0.50 ± 0.01	0.16 ± 0.04	5.00
Me^{3}	0.32 ± 0.10	0.34 ± 0.13	***not active***	*ND*
Me^{4a}	0.41 ± 0.27	7.90 ± 5.50	0.30 ± 0.20	1.33
Me^{5}	0.32 ± 0.10	0.56 ± 0.05	***not active***	*ND*
Me^{6}	0.27 ± 0.04	0.18 ± 0.05	0.22 ± 0.11	21.6
Me^{9}	0.30 ± 0.08	0.75 ± 0.11	1.26 ± 0.74	3.58
Me^{10}	0.32 ± 0.10	0.72 ± 0.19	***not active***	*ND*
Me^{11}	0.75 ± 0.00	0.34 ± 0.11	0.82 ± 0.75	1.95
miltefosine	6.5 ± 3.0	*ND*	*ND*	*ND*
benznidazole	*ND*	12.81 ± 0.74	5.00 ± 1.53	>40.0

SI = selectivity index, ND = not determined, a = HCl salt

Table 2.6. *Antiparasitic activity of ascididemin **1.11** and methylascididemin analogues against L. infantum promastigotes and T. cruzi trypomastigotes and amastigotes. For compounds active against T. cruzi amastigotes, a selectivity index (SI = CC_{50}/IC_{50}) was calculated using NCTC mammalian cells. Where a = HCl salt.*

Increased basicity is observed for pyridines with *ortho*- or *para*-electron donating groups (**Figure 2.17A**); therefore it might be expected that the equilibrium for methylascididemin **2.122**, **2.123** and **2.125** would be shifted towards the less membrane-permeable protonated form.[77] Additionally, each analogue has identical lipophilicities. This suggests permeability differences between the analogues is unlikely the cause of the inactivity of some compounds when evaluating against the intracellular *T. cruzi* amastigotes.

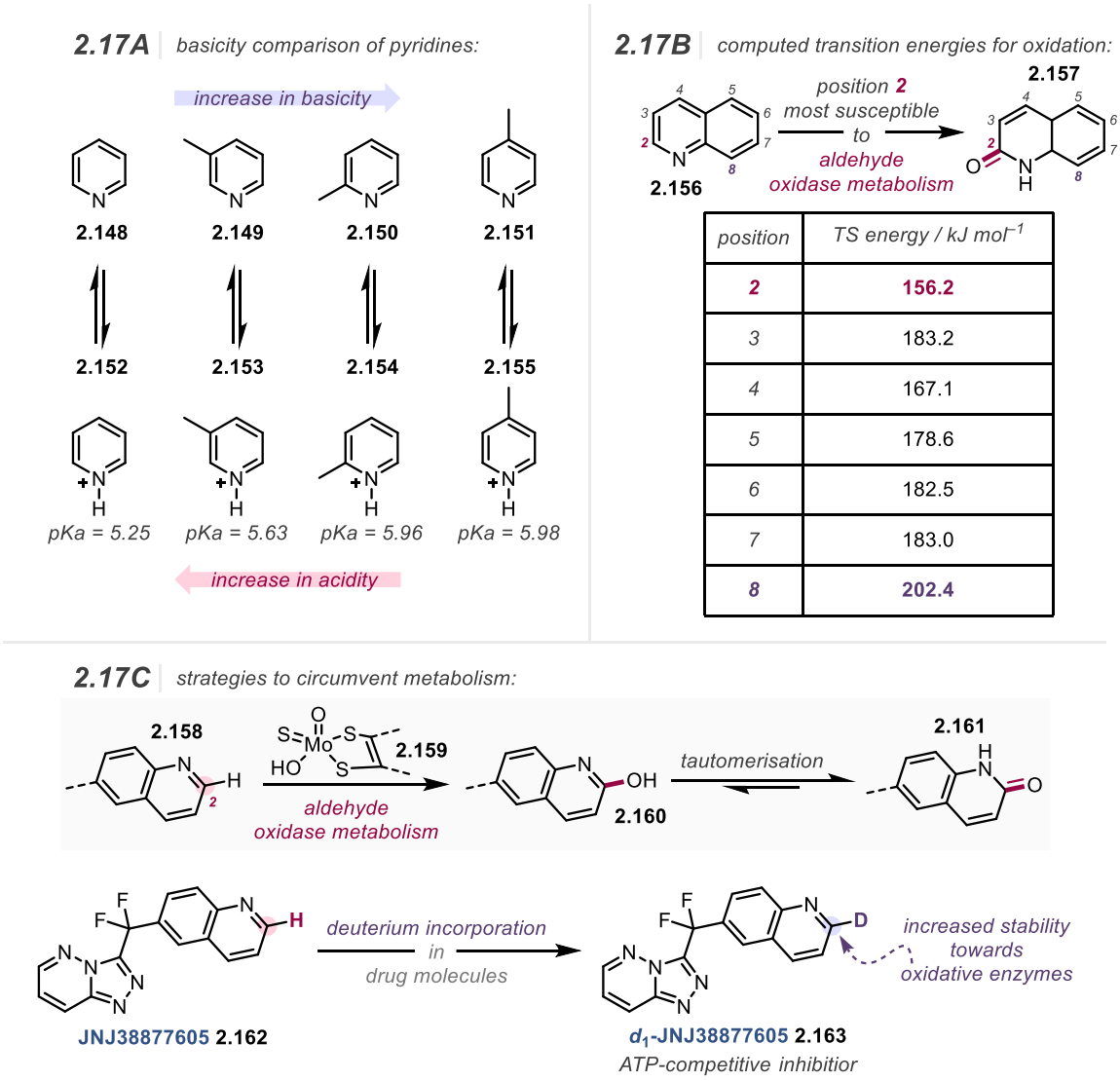

Figure 2.17. (A) *Basicity comparison of pyridines.* ***(B)*** *Computed transition energies for oxidation at each side of quinoline by aldehyde oxidase.* ***(C)*** *Replacing a proton with a deuterium at susceptible sites towards oxidation to circumvent metabolism.*

Oxidation of active compounds by enzymes such as aldehyde oxidases has been shown to lead to increased clearance. For pyridines, the *ortho*-positions have been identified as the most susceptible, however other sites can be targeted by aldehyde oxidases as well, such as the *para*-position. Olsen *et al.* calculated that the C2-position of quinoline **2.156** had the lowest transition state energy for oxidation (**Scheme 2.17B**) by aldehyde oxidase (156.2 kJ mol^{-1}) –[78] this has been experimentally validated in the literature by the formation of lactam oxidation metabolite **2.157**. The C4-position had the second lowest transition state energy (167.1 kJ mol^{-1}). The remaining positions, apart from the C8-position, had transition state energies between 175–185 kJ mol^{-1}.

The least susceptible position towards aldehyde oxidase was calculated to be the C8-position, with a transition state energy of 202.4 kJ mol^{-1}. Strategies have been developed to reduce the metabolism by enzymes like aldehyde oxidases. For example, isotopic replacement of the *ortho*-proton in JNJ38877605 **2.162** with deuterium increased the energy of cleavage of the bond and reduced metabolism (**Scheme 2.17C**, **2.163**).[79] Similarly, replacement of a proton with a methyl substituent has been shown to provide protection of susceptible metabolic sites.[69] However a wrongly placed methyl substituent can have a detrimental effect as non-sterically hindered 'benzylic' sites are susceptible to oxidation by cytochrome P450 enzymes.[80] A possible rationale for the observed inactivity of 1-methylascididemin **2.118**, 3-methylascididemin **2.120**, 5-methylascididemin **2.136** and 10-methylascididemin **2.124** could be that the installation of a methyl substituent at a less susceptible site, to enzymes such as aldehyde oxidases, increases their susceptibility to enzymes like cytochrome P450. Although Lago *et al.* noted *T. cruzi* amastigotes downregulated genes encoding aldehyde oxidases compared to their trypomastigotes, the host cell metabolism must also be considered.[81] However, this rationale cannot be used to explain the activity of 2-methylascididemin **2.119** and the inactivity of 3-methylascididemin **2.120** in *T. cruzi* amastigotes.

2.3.6. Second generation analogue

The discovery of sites on the ascididemin-core which did not tolerate functionalisation validated our decision to perform an initial SAR study around the ascididemin-core before committing to a specific attachment site for the external fluorescent probe. The C2-, C4-, C6-, C9-, and C11-positions demonstrated their tolerance to functionalisation, with methylascididemin **2.119**, **2.121**, **2.122**, **2.123** and **2.125** retaining activity in *T. cruzi* amastigotes. Therefore, it was hoped that further functionalisation at one of these sites could be achieved to instal a linker for the probe.

2.3.6.1 Synthesis of alkyne-ascididemin 2.165

Previously, the synthesis of 6-methylascididemin **2.122** was enabled by the Copp *et al*. modification, using acetaldehyde **2.146** with tetracycle **2.7** (refer back to **Scheme 2.16**).[72] It was envisioned that any aldehyde could be incorporated late-stage. Aldehyde **2.164** was selected as the alkyne would enable a fluorescent probe (**2.166**) to be attached using Click chemistry (**Scheme 2.17**, **2.167**),[82] and the length of the alkyl chain would position the fluorescent probe distal from the ascididemin-core. Aldehyde **2.164** was prepared from alcohol **2.168** via oxidation with Dess–Martin periodinane (DMP) in 30% yield based on purity (**Scheme 2.17**). Subsequent treatment of tetracycle **2.7** with aldehyde **2.164** and ammonium chloride in acetic acid furnished alkyne-ascididemin **2.165** in 26% yield.

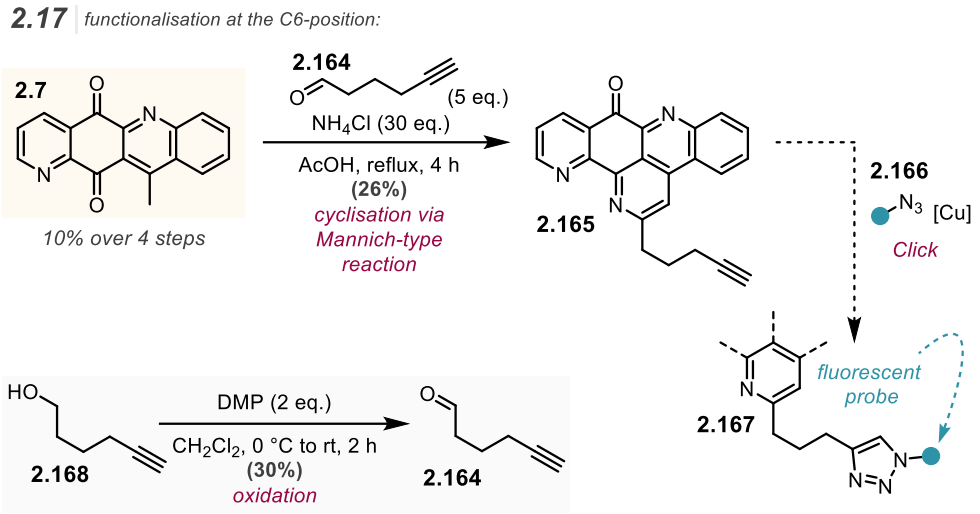

Scheme 2.17. *The Copp et al. modification enables late-stage functionalisation at the C6-position. Installation of a tethered alkyne achieved which could be used to attach a fluorescent probe. A fluorescent probe would enable compound localisation to be visualised.*

2.3.6.2. Activity of alkyne-ascididemin 2.165

The length and nature of the linker can have a significant effect on compound activity.[83] Gratifyingly, alkyne-ascididemin **2.165•**HCl retained activity against *L. donovani* promastigotes (IC_{50} = 6.0 ± 0.8 nM) to ascididemin **1.11** (IC_{50} = 19.6 ± 1.3 nM).

In future studies, alkyne-ascididemin **2.165** would be employed to test the hypothesis that ascididemin **1.11** accumulates in the nucleus of *Leishmania*, thereby supporting DNA as the primary cellular target underlying its antiparasitic mechanism-of-action. This would be assessed by fluorescence microscopy following attachment of a fluorescent probe (**2.166**) via Click chemistry (**Scheme 2.17**, analogue **2.167**).

2.3.6.2. Summary and future work

In summary, it was hypothesised that the potent antiparasitic natural product ascididemin **1.11** exerts its activity in *Leishmania* through interaction with DNA, analogous to its proposed antitumor mechanism-of-action. Initial studies confirmed the DNA intercalation ability of ascididemin **1.11**; however, the concentration required to achieve 50% DNA binding was substantially higher than its *in vitro* IC_{50} value in *L. mexicana*, suggesting that DNA binding alone may not account for its cytotoxicity. Furthermore, ascididemin **1.11** did not induce nuclear double-stranded DNA breaks, indicating that this is unlikely part of its antiparasitic activity. To investigate the cellular localisation of ascididemin **1.11** in *Leishmania* and assess the hypothesis that it accumulates in the nucleus, fluorescence microscopy was pursued. Given the planar, highly conjugated structure of ascididemin **1.11**, it was speculated to exhibit intrinsic fluorescence, analogous to that reported for the natural product kuanoniamine D **2.82**. Excitation–emission matrix (EEM) fluorescence spectroscopy revealed two distinct fluorescence signals, with one of notably higher intensity. However, when these more favourable excitation/emission parameters were utilised for cellular imaging, no significant fluorescence signal was observed in *Leishmania* cells. This lack of visualisation was attributed to potential *in vivo* effects, such as wavelength shifts and partial fluorescence quenching due to target binding, or due to a lack of consideration of factors, like the fluorescence lifetime and quantum yield. To overcome this set-back, an analogue was designed to allow the distal attachment of a fluorescent probe. A complete series of methyl-analogues were synthesised at each position of the ascididemin-core, with the biological activity of each evaluated against *T. cruzi* amastigotes to identify positions amenable to functionalisation. The C6-position emerged as functionalisation-tolerant and the most synthetically accessible site. An alkyne-appended analogue, alkyne-ascididemin **2.165**•HCl, was subsequently synthesised at this position, and was found to retain comparable potency to the parent compound in *L. donovani* promastigotes, suggesting its suitability for future fluorescent tagging and imaging studies.

Interestingly, the structurally related natural product 12-deoxyascididemin **2.53**, lacking the iminoquinone moiety, also displayed high potency against *Leishmania*, suggesting an alternative or additional mechanism-of-action. Given that both compounds share a conserved phenanthroline bay, it was proposed that metal ion chelation, particularly of zinc(II) and iron(II), may contribute to their antiparasitic activity. Metal binding was confirmed for both ions; however, only zinc(II) supplementation at its maximum tolerated dose had an effect on the IC_{50} of ascididemin **1.11** in *L. mexicana* promastigotes, supporting a potential role of ascididemin **1.11** in zinc(II)-homeostasis disruption. To further explore this mechanism, the effect of ascididemin **1.11** on intracellular labile zinc(II) levels was assessed. Unexpectedly, treatment led to an increase in the labile zinc pool, contrasting with the depletion observed for known chelator TPEN **2.64**. This paradoxical increase may reflect the release of protein-bound zinc as a cellular response to oxidative stress, consistent with previous reports of reactive oxygen species generation associated with this natural product.

The potent activity of 12-deoxyascididemin **2.53**, despite the absence of the redox-active iminoquinone, could be explained by its possible oxidation *in vivo*. Kristensen *et al.* noted during their total synthesis of ascididemin **1.11**, that direct oxidation of the formed intermediate 12-deoxyascididemin **2.53** under an oxygen atmosphere was better than after isolation.

Finally, gene knockdown studies in *T. b. brucei* revealed that reduced expression of two nitroreductases conferred resistance to cells against ascididemin **1.11**. These findings suggest a novel mechanism for ROS generation, involving nitroreductase-reduction of ascididemin **1.11**, a mechanism-of-action not previously described for this compound.

Future studies would focus on genetic knockout of nitroreductases in *Leishmania* to validate this mechanism, as well as direct measurement of ROS levels and DNA damage, for example nuclear single-stranded DNA breakages, following treatment using ascididemin **1.11** and alkyne-ascididemin **2.165**.

3. Thiaplakortone A

Thiaplakortone A **1.12** (**Figure 3.1**) is a member of a novel class of thiazinoquinone natural products that was isolated from an Australian marine sponge, *Plakortis lita*, in 2013.[84] Its discovery was part of high-throughput screening (HTS) of a library containing 18453 plant and marine invertebrate extracts, during an initiative to identify novel antimalarial lead compounds. Three additional thiaplakortone natural products, thiaplakortone B–D **3.1**–**3.3** (**Figure 3.1**), were isolated alongside thiaplakortone A **1.12**. These members differ only by the oxidation state and orientation of the thiazine 1,1-dioxide ring, or the presence of a carboxylic acid and *N*-methyl group on the tryptamine side-chain.

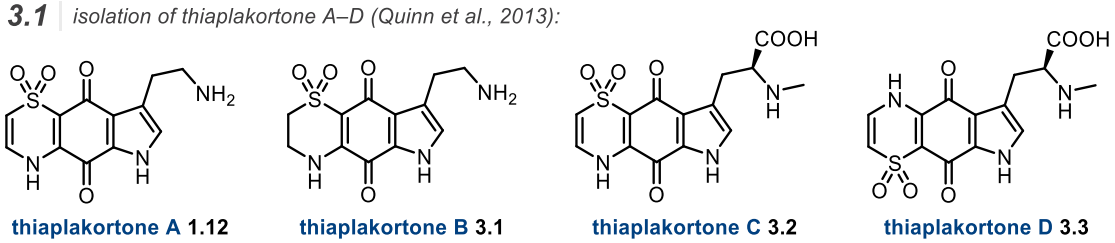

Figure 3.1. *Chemical structures of thiaplakortone A* ***1.12*** *and B–D* ***3.1–3.3*** *(Quinn et al., 2013) from Plakortis lita. All isolated as the trifluoroacetate salt.*

3.1. Biosynthesis of the thiaplakortones

Quinn *et al.* proposed a biosynthetic pathway for thiaplakortones A **1.12**, B **3.1** and C **3.2** (**Scheme 3.1A**), suggesting that the process begins with the successive oxidation of *L*-tryptophan **3.4** to form indolequinone **3.5**.[84] Subsequent addition of cysteine **3.6**, followed by oxidation, leads to the formation of enamine **3.7**. Oxidation of the thiol group in this intermediate mediated by cysteine dioxygenase generates sulfinate **3.8**, which then undergoes decarboxylation from the cysteine framework facilitated by a decarboxylase. Cyclisation–oxidation then yields sulfone **3.9**, which serves as a common precursor for thiaplakortones A **1.12**, B **3.1** and C **3.2**. From this point, decarboxylation of sulfone **3.9** leads to thiaplakortone B **3.1**, which can be further oxidised to

produce thiaplakortone A **1.12**. Alternatively, oxidation followed by *N*-methylation of the tryptamine primary amine yields thiaplakortone C **3.2**.

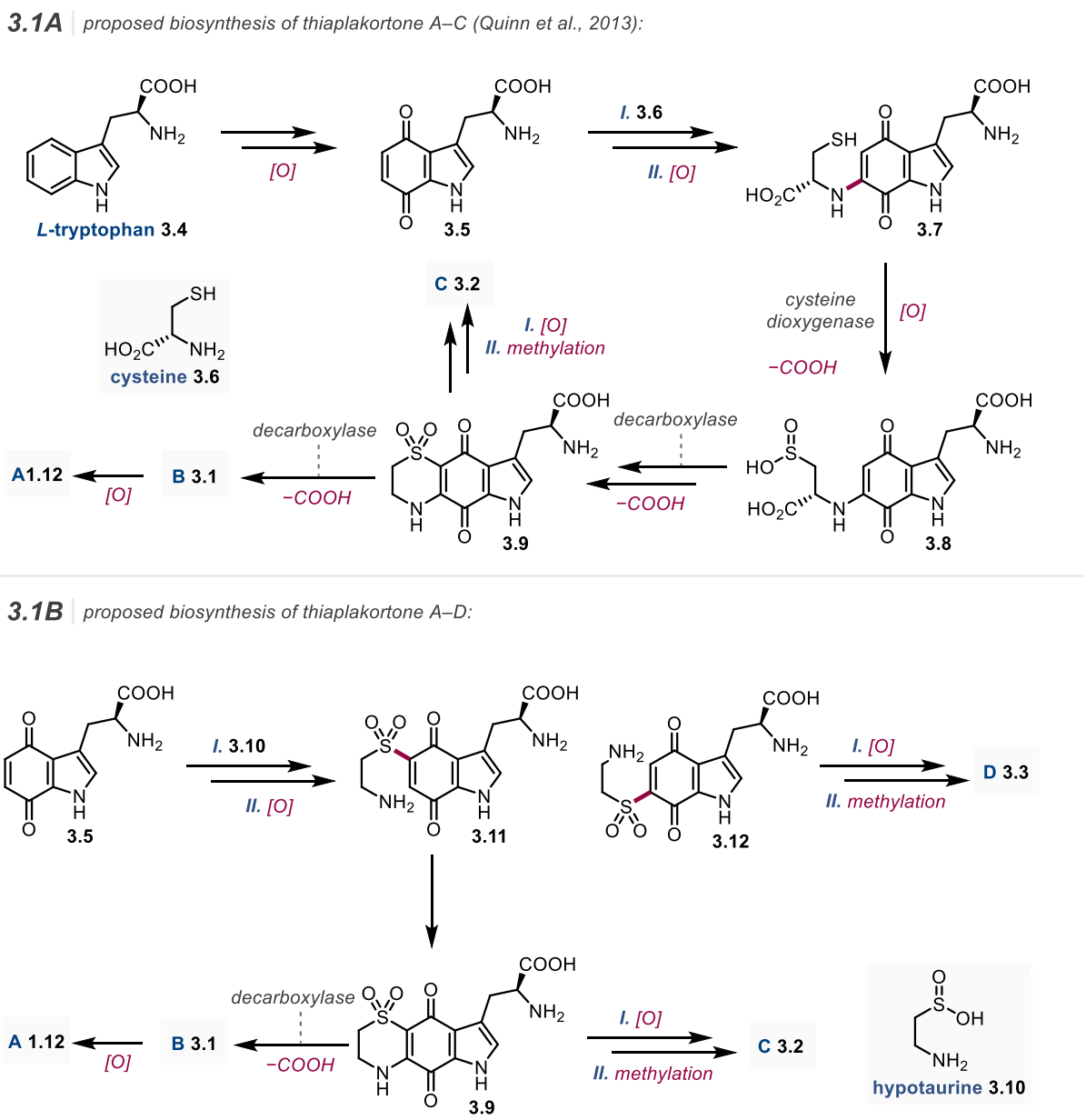

Scheme 3.1. (A) *Proposed biosynthesis of thiaplakortone A* ***1.12,*** *B* ***3.1*** *and C* ***3.2*** *(Davis et al., 2013). Installation of the thiazine 1,1-dioxide ring using cysteine* ***3.6****.* ***(B)*** *Proposed biosynthesis of thiaplakortone A* ***1.12*** *and B–D* ***3.1–3.3*** *(Anderson et al., 2025). Installation of the thiazine 1,1-dioxide ring using hypotaurine* ***3.10*** *in a non-regioselective manner.*

In contrast to this pathway, we question whether hypotaurine **3.10** could also serve as the source of the thiazine 1,1-dioxide ring instead of cysteine **3.6** (**Scheme 3.1B**), as indeed has been demonstrated chemically by Quinn *et al.* (see below, **Scheme 3.2A**).[85] Although not explicitly considered by Quinn *et al.*, we further hypothesise that the non-regioselective addition of either

cysteine **3.6** or hypotaurine **3.10** to indolequinone **3.5** could account for the formation of thiaplakortone D **3.3**.

3.2. Total synthesis of thiaplakortone A 1.12

The following year, Quinn *et al.* disclosed the first – and to date, only – total synthesis of thiaplakortone A **1.12** (**Scheme 3.2A**).[85] The synthesis commenced from commercially available 4-hydroxyindole **3.13**, which was protected using benzyl bromide to afford *O*-benzyl indole **3.14** (yield not reported). Subsequent Vilsmeier–Haack formylation with phosphoryl chloride in DMF introduced an aldehyde at the C3-position, furnishing formylindole **3.15** in 68% yield. A Henry reaction between the aldehyde and nitromethane anion provided nitroalkene **3.16**. Reduction of the nitroalkene with lithium aluminium hydride delivered the corresponding tryptamine, *O*-benzyl tryptamine **3.17**. *N*-Boc protection of the primary amine using Boc anhydride furnished *N*-Boc tryptamine **3.18** in 80% yield over three steps. Hydrogenation using hydrogen with palladium on carbon in methanol removed the *O*-benzyl protecting group to yield hydroxytryptamine **3.19**. Oxidation of the hydroxyindole was achieved using Frémy's salt (potassium nitrosodisulfonate), affording the key indolequinone **3.20**. Installation of the thiazine 1,1-dioxide core was effected via a non-regioselective addition of hypotaurine **3.10**, providing sulfone **3.22** along with its regioisomer, sulfone **3.21**, in 45% yield over three steps; the regioisomeric ratio was not given.

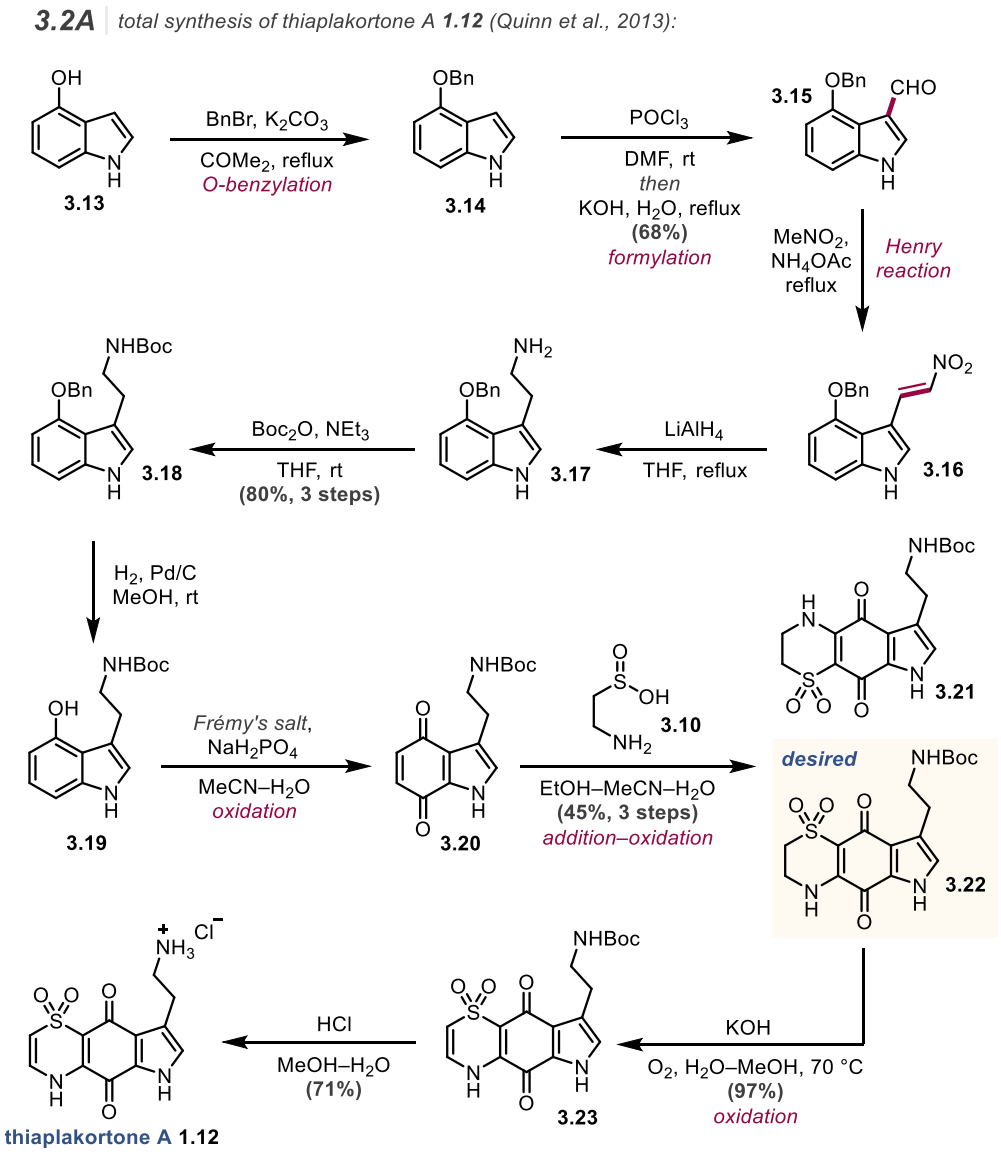

Scheme 3.2. (A) *Total synthesis of thiaplakortone A* ***1.12*** *(Quinn et al., 2014). Addition of hypotaurine* ***3.10*** *to indolequinone* ***3.20*** *led to a mixture of sulfone* ***3.21*** *and sulfone* ***3.22****, however the regioisomeric ratio was not revealed.* ***(B)*** *Regioselectivity of hypotaurine* ***3.10*** *addition to indolequinone* ***3.24****.*

However, in an analogous system, indolequinone **3.24** – lacking the tryptamine side-chain – underwent reaction with hypotaurine **3.10** to afford sulfone regioisomers **3.25** and **3.26** in a 3.3:1 ratio, respectively, with a combined yield of 36% (**Scheme 3.2B**).[86] Subsequent base-promoted

oxidation of sulfone **3.22** using KOH under an oxygen atmosphere introduced unsaturation within the thiazine ring, affording vinyl sulfone **3.23** in a 97% yield (**Scheme 3.2A**). Finally, *N*-Boc deprotection using aqueous HCl in methanol delivered thiaplakortone A **1.12** as the hydrochloride salt in 71% yield, completing the synthesis.

3.3. Antiparasitic activity of the thiaplakortones

Thiaplakortone A **1.12** (**Table 3.1**) was identified during HTS to be potent against both the *P. falciparum*, chloroquine-sensitive strain, *3D7* (IC_{50} = 0.051 μM) and the multidrug-resistant strain, *Dd2* (IC_{50} = 0.0066 μM). Although thiaplakortone A has not been evaluated against *Leishmania* or *Trypanosoma* species, precedent suggests that antiparasitic activity often translates across related protozoan parasities.[13] The mechanism-of-action of the antimalarial activity of thiaplakortone A remains unknown, but related thiazinoquinone natural products have been reported to exert anticancer activity through the generation of reactive oxygen species, a mechanism that may plausibly contribute to the observed antiparasitic effects.[87] Additionally, this is similar to what has been suggested for ascididemin **1.11** as a result of the iminoquinone moiety present (refer back to **Section 2.2.2.** Reactive oxygen species).

In addition to possessing potent antiparasitic activity, thiaplakortone A **1.12** also satisfies the general hit selection criteria by possessing preliminary structure–activity relationship (SAR) data, which is advantageous for insights into target engagement and the elucidation of the mechanism-of-action. For example, this could enable identification of key structural features for activity and potential sites for derivatisation, enabling the incorporation of photoaffinity probes.

3.1 *structure–activity relationship of thiaplakortone A* ***1.12****:*

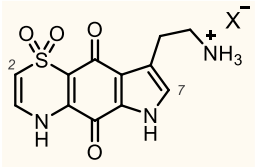

thiaplakortone A 1.12

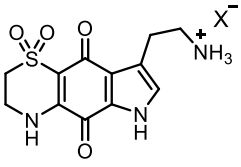

thiaplakortone B 3.1

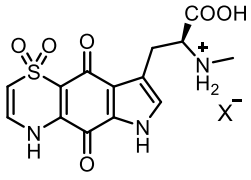

thiaplakortone C 3.2

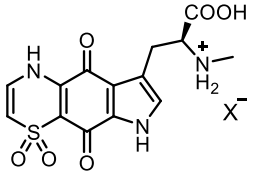

thiaplakortone D 3.3

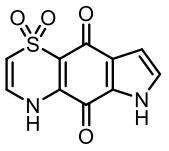

3.27

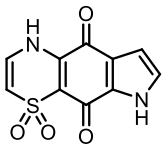

3.28

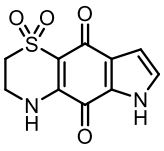

3.25

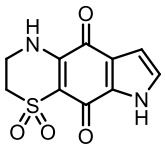

3.26

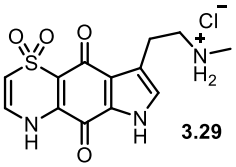

3.29

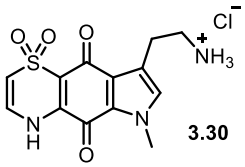

3.30

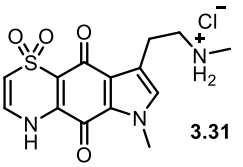

3.31

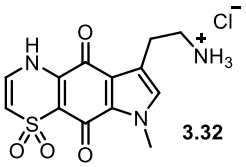

3.32

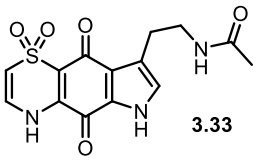

3.33

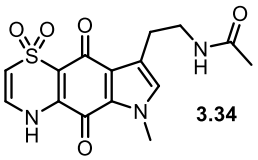

3.34

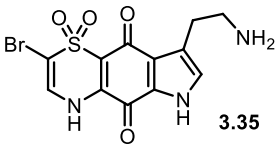

3.35

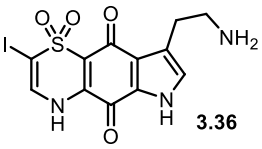

3.36

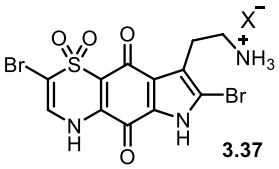

3.37

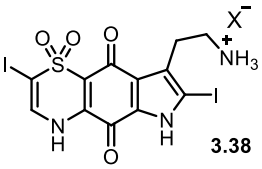

3.38

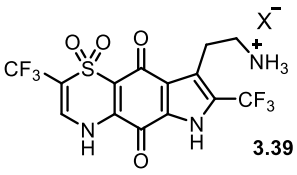

3.39

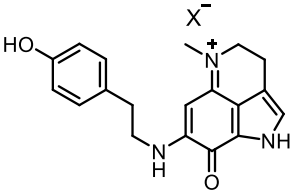

makaluvamine J 3.40

where X = CF_3COO

compound	*3D7 / μM*	*Dd2 / μM*
1.12	0.051	0.0066
3.1	0.650	0.092
3.2	0.309	0.171
3.3	0.279	0.159
3.27	0.252	0.127
3.28	0.313	0.129
3.25	6.90	3.70
3.26	7.50	3.80
3.29	0.160	0.047
3.30	0.128	0.057

compound	*3D7 / μM*	*Dd2 / μM*
3.31	0.137	0.079
3.32	0.416	0.162
3.33	0.472	0.182
3.34	0.684	0.706
3.35	0.559	0.058
3.36	2.22	0.317
3.37	1.65	0.487
3.38	1.69	0.725
3.39	6.80	4.55
3.40	0.0188	0.0283

Table 3.1. *Antimalarial activity of thiaplakortone A* ***1.12*** *and isolated or synthesised analogues.*

3.3.1. Structure–activity relationship studies

The potent antimalarial activity of thiaplakortone A **1.12**, along with the moderate activity exhibited by other members of the thiaplakortone family, has prompted extensive analogue synthesis by multiple research groups. As a result, several structure–activity relationship (SAR) trends have emerged among both natural and synthetic thiaplakortone A **1.12** analogues (**Table 3.1**).

The olefinic bond within the thiazine 1,1-dioxide ring is a critical structural feature, as its removal resulted in approximately a 10-fold reduction in antimalarial potency (**Table 3.1**, **3.1**),[84] with a greater than 100-fold reduction when combined with truncation of the tryptamine side chain (**3.25**).[86] In analogues retaining the olefin, modifications to the tryptamine moiety, such as truncation (**Table 3.1**, **3.27**), *N*-methylation with (**3.2**)[85] or without a carboxylic acid group present (**3.29**), or amide coupling (**3.33**),[88] also led to substantial decreases in activity. Similarly, methylation at the indole *N*-atom (**Table 3.1**, **3.30**) resulted in reduced potency. While the regioisomeric orientation of the thiazine 1,1-dioxide ring generally had minimal effect (**Table 3.1**, **3.2**/**3.3**, **3.25**/**3.26**, **3.27**/**3.28**), a notable exception was observed for *N*-methylated indole analogues (**3.31**/**3.32**), where a 2- to 3-fold loss in activity was recorded. Minimal functionalisation has been reported directly on the thiaplakortone A **1.12** carbocyclic core. However, substitution at the C2- and/or C7-positions with halogens was detrimental to activity (**Table 3.1**, **3.35**–**3.39**);[89] this is possibly due to altered physicochemical properties (such as increased lipophilicity) affecting solubility, and/or metabolic stability.

Certain modifications, including removal of the thiazine olefin, functionalisation of the carbocyclic core, and indole *N*-methylation, likely influence the electronic properties of the quinone system. The effect of these structural changes supports the hypothesis that reactive oxygen species generation may contribute to the mechanism-of-action, given that such electronic changes modulate the quinone redox potential. This hypothesis is further supported by the comparable antimalarial activity observed for iminoquinone natural products such as makaluvamine J **3.40**,[90]

which lacks the thiazine 1,1-dioxide ring altogether. In contrast, structural changes to the tryptamine side chain would not be expected to significantly influence the electronics, suggesting this structural unit may additionally serve a distinct role in the mechanism-of-action.

Photoaffinity probe incorporation typically relies on functional groups for derivatisation at positions distal to the natural product core to preserve biological activity and mechanism-of-action. However, in the thiaplakortone series, functionalisation of the amine using amide (**Table 3.1**, **3.33**) and urea couplings led to diminished antimalarial activity.[88] Additionally, to date, no site has been identified that permits modification without compromising potency. Also, no analogue has demonstrated improved activity over the parent compound. Moreover, the synthetic route developed by Quinn and co-workers restricts modification at several positions, limiting opportunities for late-stage diversification and further SAR exploration.

3.4. Project aims

Although numerous analogues of thiaplakortone A **1.12** have been synthesised, none have demonstrated conserved or enhanced potency to date. The development of an alternative synthetic strategy may provide access to previously inaccessible modification sites on the skeleton, thereby enabling exploration of novel vectors for functionalisation to enhance antimalarial activity (**Figure 3.2**). Furthermore, for elucidating the mechanism-of-action of thiaplakortone A **1.12**, it is essential to identify sites amenable to structural modification. This would enable the incorporation of functional groups which could be utilised for the attachment of fluorescent probes distal to the core scaffold for imaging studies.

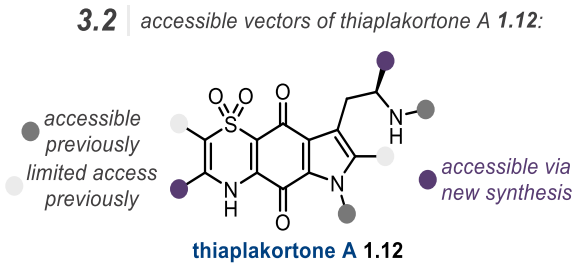

Figure 3.2. *Accessible vectors of thiaplakortone A* ***1.12*** *previously versus the route developed in this work.*

The aim of this project is to design a novel synthetic route for the total synthesis of thiaplakortone A **1.12**, to be used alongside the one developed by Quinn *et al.* to further expand the library of analogues for biological testing. An additional aim is for thiaplakortone A **1.12** to be evaluated against *Leishmania* and *Trypanosoma* parasities, to explore its broader antiparasitic profile.

3.5. Research and discussion

3.5.1. Total synthesis of thiaplakortone B 3.1 and A 1.12 – initial considerations

The previous total synthesis of thiaplakortone A **1.12** started from indole **3.13** and required four steps to install the tryptamine side-chain to convert it to tryptamine **3.17** (refer back to **Scheme 3.2**). Additionally, the unsubstituted quinone **3.20** generated after oxidation of tryptamine **3.19** with Frémy's salt lacked regiocontrol towards the addition of hypotaurine **3.10**. We envisioned a *de novo* synthesis of a tryptamine which would have substituents correctly positioned for subsequent transformations. This includes, *para*-dimethoxy substituents for facile oxidation to the quinone and, to improve the regiocontrol in the construction of the thiazine 1,1-dioxide ring, a leaving group substituent was hoped to be introduced to enable an addition–elimination pathway. Given the prohibitively high cost of hypotaurine **3.10**, the development of a more accessible alternative reagent was also planned to be pursued.

3.5.2. *De novo* construction of substituted tryptamine

3.5.2.1. Fischer indole synthesis

The Fischer indole synthesis remains one of the most widely employed methods for the *de novo* construction of indole scaffolds, involving the condensation of a phenylhydrazine with an aldehyde or ketone. Numerous adaptations have extended its utility to the synthesis of tryptamines, wherein an aldehyde or ketone bearing an appropriate tether is required. Because of the inherent reactivity of aldehydes, latent aldehyde equivalents are often used since controlled unmasking under the acidic reaction conditions is possible. We sought to assess the feasibility of

employing a Fischer indole approach for the synthesis of a synthetically useful tryptamine derivative for the synthesis of thiaplakortone A **1.12**.

Given the oxidative benefits conferred by a *para*-dimethoxy substitution pattern, 2,5-dimethoxyphenylhydrazine **3.43** was selected as a model substrate for the Fischer indole synthesis (**Scheme 3.3A**) – simply lacking additional functionality for regiocontrol of the thiazine 1,1-dioxide ring installation. An initial approach involving metal–halogen exchange of 2,5-dimethoxybromobenzene **3.41** followed by trapping with di-*tert*-butyl azodicarboxylate (DBAD) was unsuccessful, possibly due to competitive benzyne formation under the reaction conditions. Alternatively, 2,5-dimethoxyaniline **2.30** was diazotized with sodium nitrite and HCl, and the resulting transient diazonium intermediate was reduced with stannous chloride to furnish 2,5-dimethoxyphenylhydrazine **3.43** in 29% yield over two steps.

2-Methoxypyrrolidine **3.45** was selected as the latent aldehyde partner for coupling with 2,5-dimethoxyphenylhydrazine **3.43** (**Scheme 3.3B**). Synthesis of 2-methoxypyrrolidine **3.45** was accomplished in 87% yield over two steps via oxidative decarboxylation of pyrrolidine-2-carboxylic acid **3.44**, followed by methanol addition to the resulting intermediate.

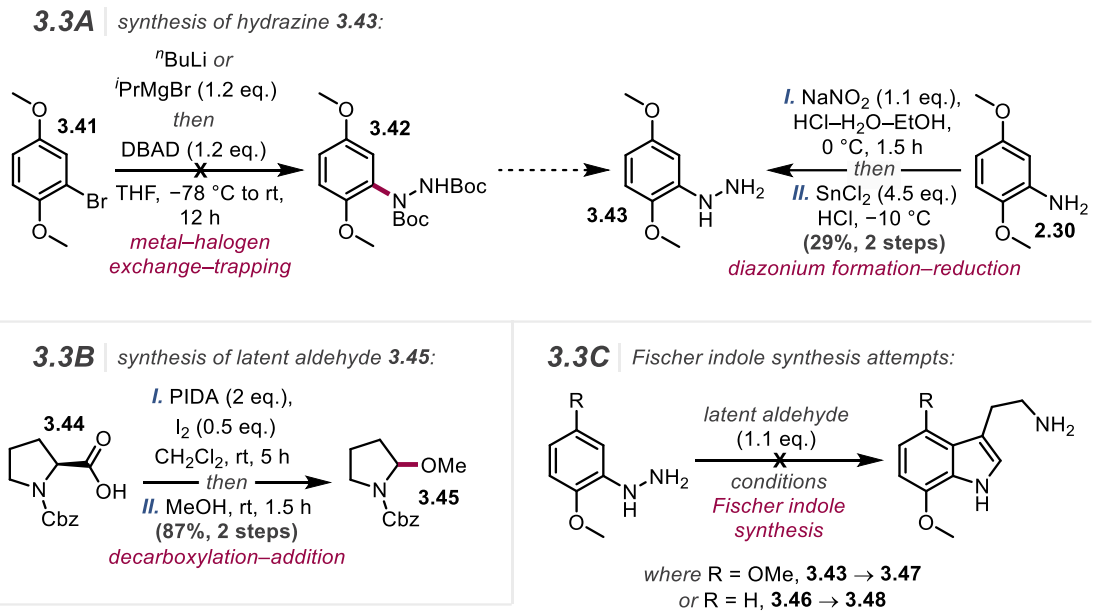

entry	phenylhydrazine	latent aldehyde	conditions
1	3.43	3.45	AcOH, 100 °C, 1.5 h
2	3.43	3.45	H_2O–EtOH–AcOH (40:35:25), 100 °C, 1.5 h
3	3.46	3.45	AcOH, 100 °C, 1.5 h
4	3.46	3.45	H_2O–EtOH–AcOH (40:35:25), 100 °C, 1.5 h
5	3.46	3.45	0.1 M HCl, 100 °C, 1.5 h
6	3.46	3.45	H_2O–AcOH (3:1), 100 °C, 1.5 h
7	3.46	3.49	5% HCl–MeOH (1:1), 40 °C, 12 h
8	3.46	3.50	5% HCl–EtOH (1:1), 40 °C, 12 h
9	3.46	3.51	MeOH–H_2O (5:1), 100 °C, 1.5 h
10	3.46	3.52	EtOH–H_2O (5:1), 100 °C, 1.5 h

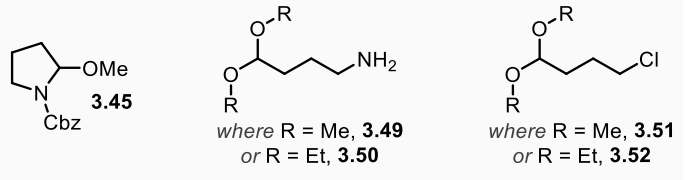

Scheme 3.3. (A) *Synthesis of phenylhydrazine* ***3.43****.* ***(B)*** *Synthesis of latent aldehyde* ***3.45****.* ***(C)*** *Attempted Fischer indole synthesis. Table of conditions tried.*

However, attempted Fischer indole synthesis using 2,5-dimethoxyphenylhydrazine **3.43** and 2-methoxypyrrolidine **3.45** under either acetic acid (**Scheme 3.3C** table, entry 1) or an acetic acid–ethanol–water mixture (entry 2) at 100 °C resulted in only decomposition products. To simplify

the system, 2,5-dimethoxyphenylhydrazine **3.43** was replaced with 2-methoxyphenylhydrazine **3.46** hydrochloride; nonetheless, similar decomposition was observed when the reaction was conducted in acetic acid (**Scheme 3.3C** table, entry 3), acetic acid–ethanol–water (entry 4), 0.1 M aqueous HCl (entry 5), or acetic acid–water (entry 6). Substitution of the latent aldehyde from 2-methoxypyrrolidine **3.45** to acetal derivatives **3.49** or **3.50** and lowering the temperature to 40 °C in either 5% HCl–methanol (**Scheme 3.3C** table, entry 7) or 5% HCl–ethanol (entry 8), respectively, also failed to suppress decomposition.

The Grandberg reaction represents a notable example of an interrupted Fischer indole synthesis, wherein a γ-leaving group is employed in place of the conventional amino substituent.[91] Rather than undergoing elimination of ammonia, the nitrogen centre ultimately gives rise to the primary amine of the tryptamine scaffold. The lone pair of imine **3.53** instead participates in a 5-*exo*-*tet* cyclisation (Scheme **3.4A**). Tautomerisation of the generated iminium forms five-membered cyclic enamine **3.55** which then resumes the usual Fischer indole mechanism. To probe this strategy, acetals **3.51** and **3.52** were evaluated under aqueous methanol (**Scheme 3.3C** table, entry 9) and aqueous ethanol (entry 10) conditions, respectively; however, these attempts again resulted in decomposition and no desired product formation.

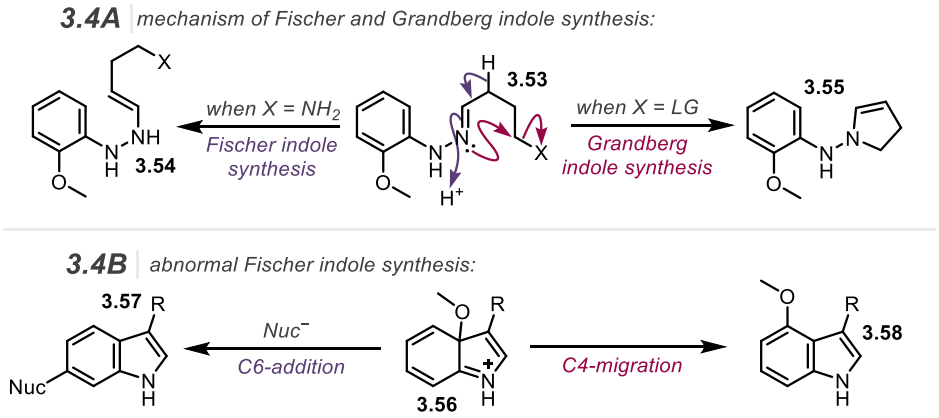

Scheme 3.4. (A) *Fischer indole synthesis mechanism versus the Grandberg indole synthesis, an example of an interrupted-Fischer indole synthesis.* ***(B)*** *Abnormal Fischer indole synthesis.*

An abnormal Fischer indole reaction has been reported for systems with unsymmetrical phenylhydrazines bearing an *ortho*-methoxy substituent.[92] In such systems, cyclisation

preferentially occurs at the *ipso*-position of the methoxy substituent rather than at the usual unsubstituted *ortho*-position to the hydrazine (**Scheme 3.4B**). Depending on the reaction conditions, the resulting cationic intermediate **3.56** may undergo nucleophilic attack at the C6-position, for example with chloride (**3.57**) with subsequent ejection of the methoxy group and rearomatisation; or, the methoxy substituent migrates to the C4-position (**3.58**).[93] It was proposed that analogous reactivity may be operative in our system, contributing to undesired side reactions and decomposition.

Given the lack of success with the Fischer indole strategy, we redirected our efforts toward alternative indole-forming methodologies that could incorporate strategically positioned substituents to facilitate the synthesis of thiaplakortone A **1.12**.

3.5.2.2. Larock indole synthesis

The Larock indole synthesis is a modern approach for the construction of indole scaffolds (**Scheme 3.5A**), coupling together an *ortho*-iodoaniline (**2.19**) and an alkyne (**3.59**).[94] Following oxidative addition of the *ortho*-iodoaniline to palladium(0), unsymmetrical alkynes undergo regioselective carbopalladation such that the more sterically demanding substituent is positioned furthest away from the aryl ring. This orientation minimises steric strain in the developing C–C bond (**3.60**), ultimately placing the bulky group at the C2-position of the resulting indole (**3.63**). As a result of this, silyl-substituted alkynes have been widely explored in this reaction, as the silyl group provides effective regiocontrol during carbopalladation and can be readily removed post-cyclisation to yield C2-unsubstituted indoles (**Scheme 3.5B**, **3.67**). In addition, Larock *et al.* demonstrated that C2-silyl indoles could undergo further functionalisation at the C2-position via Heck cross-coupling coupling with alkenes (**3.68**). As with the Fischer indole synthesis, this methodology can be adapted for tryptamine synthesis, in this case using homopropargyl amine-derived alkynes (**Scheme 3.5A**, **3.66**).

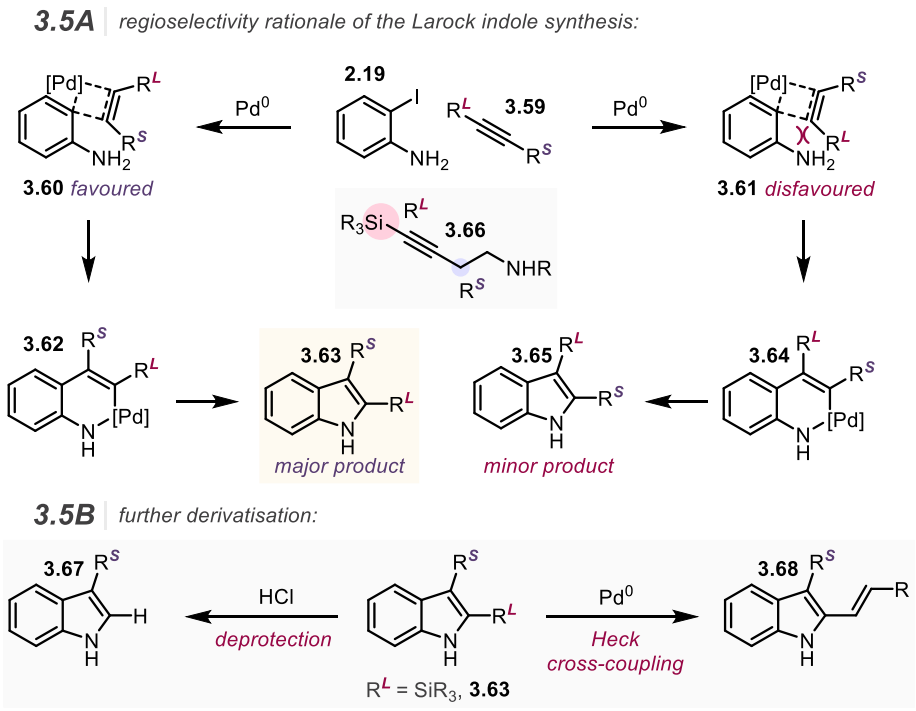

Scheme 3.5. (A) *Regioselectivity rationale for the Larock indole synthesis.* ***(B)*** *Further derivatisation of a C2-silyl group.*

Although the *para*-dimethoxy relationship explored so far would have been ideal, the incorporation of a leaving group adjacent to this 1,4-oxygenation as well as a halide electrophile for the Larock synthesis would require a pentasubstituted aryl, which would likely require numerous steps for its preparation. With the overall step count to thiaplakortone A **1.12** in mind, it was hoped that a tetrasubstituted arene would be sufficient (lacking one methoxy group), since there have been some reports of oxidations to quinones in such systems.[95–102] It was hypothesised that *ortho*-iodoaniline **3.70** (**Scheme 3.6A**) would be an ideal substrate, since 3,5-dimethoxyaniline **3.69** is symmetrical for iodination purposes. One methoxy group of this system would ultimately be oxidised to provide the quinone, and the other would provide regiocontrol (as a leaving group) for thiazine 1,1-dioxide ring installation.

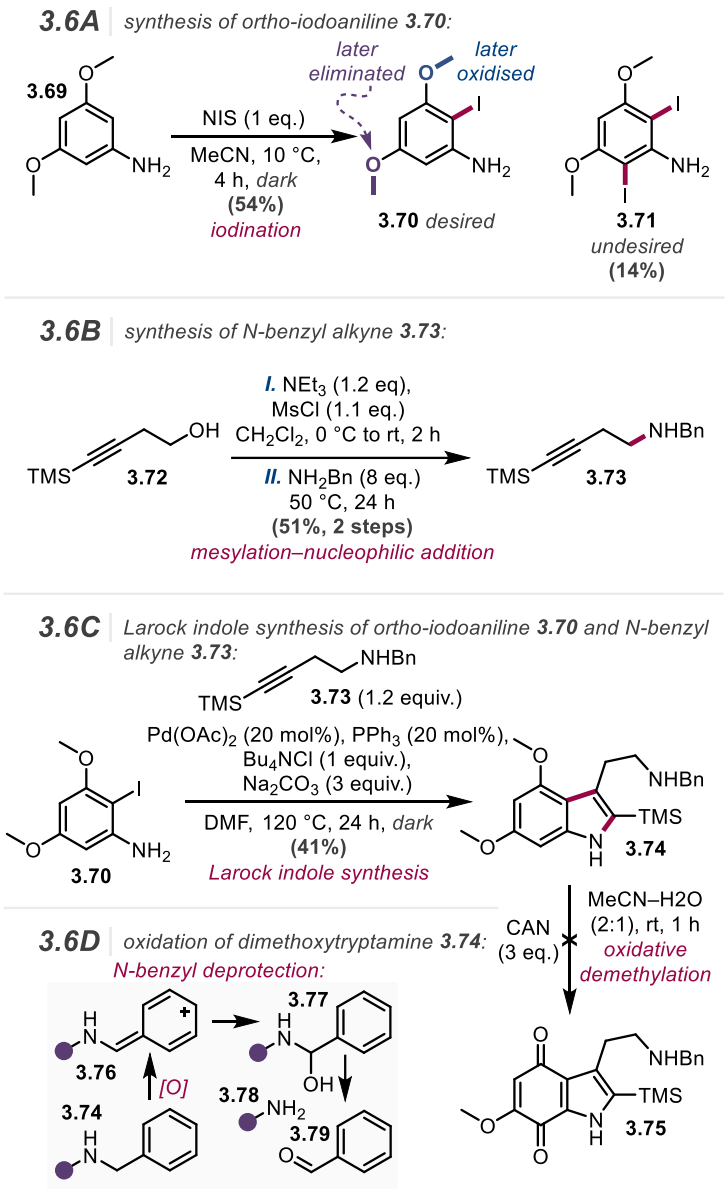

Scheme 3.6. (A) *Synthesis of ortho-iodoaniline* ***3.70****.* ***(B)*** *Synthesis of N-benzyl alkyne* ***3.73****.* ***(C)*** *Coupling of ortho-iodoaniline* ***3.70*** *and N-benzyl alkyne* ***3.73*** *to furnish dimethoxytryptamine* ***3.74****.* ***(D)*** *Failed oxidation of dimethoxytryptamine* ***3.74****.*

Iodination of dimethoxyaniline **3.69** with *N*-iodosuccinimide (NIS) afforded *ortho*-iodoaniline **3.70** as the major product in a moderate 54% yield (**Scheme 3.6A**). A minor product, diiodinated product **3.71**, was also isolated in 14% yield. For the alkyne coupling partner, homopropargyl amine **3.73** was envisioned as a suitable substrate (**Scheme 3.6B**). This compound was readily prepared from homopropargyl alcohol **3.72** via mesylation followed by nucleophilic displacement with benzylamine, affording the desired alkyne in 51% yield over two steps. Coupling of *ortho*-iodoaniline **3.70** with homopropargyl amine **3.73** under Larock indole synthesis conditions

(**Scheme 3.6C**) – using catalytic palladium(II) acetate and PPh_3, tetrabutylammonium chloride (TBACl) and sodium carbonate – furnished dimethoxytryptamine **3.74** in 41% yield. The regioisomer arising from carbopalladation at the other end of the alkyne was not detected by ^1H NMR analysis of the crude mixture prior to FCC.

Attempts to oxidise dimethoxytryptamine **3.74** using CAN were unsuccessful (**Scheme 3.6D**). Oxidants such as CAN and 2,3-dichloro-5,6-dicyano-1,4-benzoquinone (DDQ) are known to cleave *para*-methoxybenzyl (PMB) and related electron-rich benzyl protecting groups. It was hypothesised that under these oxidative conditions, deprotection of the *N*-benzyl group may have occurred, leading to undesired side reactions and decomposition (**3.78**). To circumvent this issue, the *N*-benzyl protecting group was replaced with an oxidatively-robust *N*-Boc group to prevent deprotection and hopefully improve reaction outcome.

Homopropargyl amine **3.84** was accessible via multiple synthetic routes (**Scheme 3.7A**). In one approach, treatment of *N*-Boc ethanolamine **3.80** with thionyl chloride, followed by oxidation with *in situ* generated ruthenium tetroxide, furnished cyclic sulfamidate **3.81** in 77% yield over two steps. However, cyclic sulfamidate **3.81** could also be obtained commercially. Nucleophilic attack of cyclic sulfamidate **3.81** with TMS-acetylide, with extrusion of SO_2, afforded homopropargyl amine **3.84** in 61% yield. In a separate route to **3.84**, homopropargylamine **3.86** was doubly deprotonated and subsequently treated with trimethylsilyl chloride (TMSCl). Following acidic workup, homopropargylamine **3.84** was obtained in 84% yield.

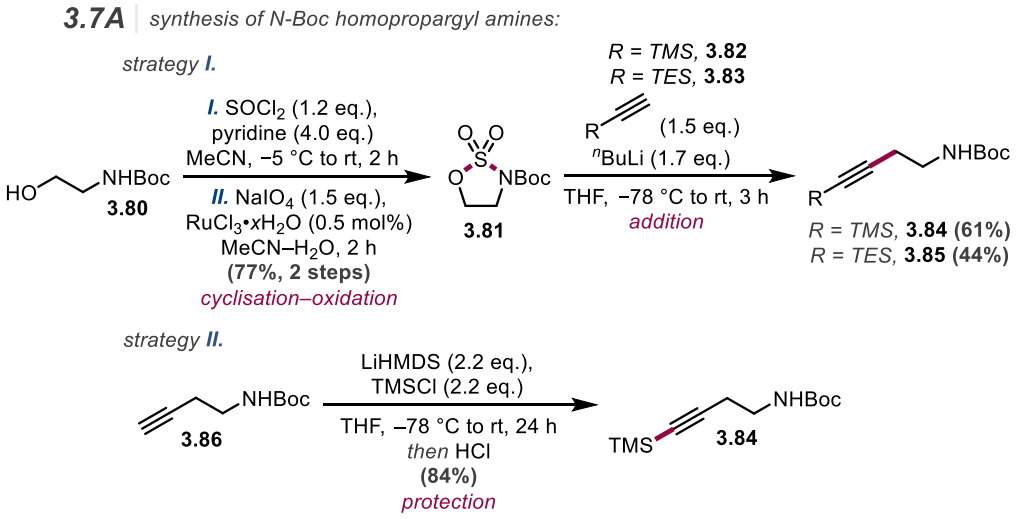

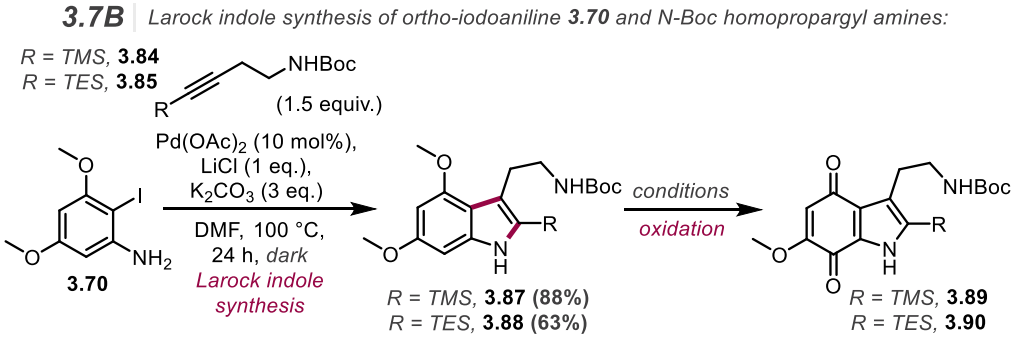

3.7C *dimethoxytryptamine oxidation to indolequinone:*

entry	*R*	*conditions*	*yield / %*
1	TMS	CAN (3 eq.) MeCN–H_2O (2:1), 0 °C, 0.5 h	0
2	TES	CAN (3 eq.), NaOAc (6 eq.) MeCN–H_2O (2:1), 0 °C, 0.5 h	0
3	TES	CAN (3 eq.), *buffer* (pH 7) MeCN–H_2O (2:1), 0 °C, 0.5 h	0
4	TMS	$K_2S_2O_8$ (2 eq.) $^nBu_4NBF_4$ [0.1 M], MeCN–H_2O (5:1), rt, Pt(+)–Pt(−), 10 mA, 1 h	0
5	TMS	*Frémy's salt* (6 eq.) Me_2CO–buffer (pH 6) [0.025 M], rt, 12 h	8

Scheme 3.7. (A) *Preparation of N-Boc homopropargyl amines.* ***(B)*** *Coupling of N-Boc homopropargylamines with ortho-iodoaniline* ***3.70*** *for the synthesis of dimethoxytryptamines.* ***(C)*** *Table summarising optimisation attempts of dimethoxytryptamines to the corresponding indolequinone.*

Larock indole synthesis between *ortho*-iodoaniline **3.70** and homopropargyl amine **3.84** proceeded smoothly to furnish dimethoxytryptamine **3.87** in an excellent yield of 88% (**Scheme 3.7B**) – surpassing the yield previously obtained for the analogous *N*-benzyl derivative. This

improved outcome was attributed to several modifications to the original conditions, including: (1) replacement of TBAC with lithium chloride as the chloride source, (2) substitution of sodium carbonate with potassium carbonate as the base, and (3) omission of the PPh_3 ligand. Once again, the other regioisomer was not detected by ^1H NMR analysis of the crude mixture prior to FCC.

However, subsequent attempts to oxidise dimethoxytryptamine **3.87** with CAN again resulted in decomposition (**Scheme 3.7C** table, entry 1). It was hypothesised that the acidic nature of CAN may cause undesired *in situ* deprotection of the trimethylsilyl group under the reaction conditions with subsequent degradation. To mitigate this, a more robust C2-TES dimethoxytryptamine **3.88** was employed with buffered oxidation conditions (**Scheme 3.7C** table, entry 2 & 3); however, the reaction outcome remained the same. Returning back to C2-TMS dimethoxytrymptamine **3.87**, an alternative electrochemical–chemical oxidation strategy was then explored involving hydroxylation at the C7-position using platinum electrodes, followed by oxidation with potassium persulfate (**Scheme 3.7C** table, entry 4). This approach likewise led to decomposition. Of the methods evaluated, only Frémy's salt was able to effect oxidation of dimethoxytryptamine **3.87** to the corresponding indolequinone **3.89** (**Scheme 3.7C** table, entry 5), albeit in low yield of 8%.

It was hypothesised that the failure of dimethoxytryptamine **3.87** and **3.88** to undergo oxidation to indolequinone **3.89** and **3.90** respectively using CAN might be attributed to undesired reactivity of the unprotected indole moiety. To mitigate this, protection of the indole nitrogen was pursued (**Scheme 3.8A**). Initial efforts for *N*-Boc protection of dimethoxytryptamine **3.88** using Boc anhydride and catalytic DMAP were unsuccessful, likely due to steric hindrance imposed by the C2-TES substituent. Pleasingly, removal of the TES group by refluxing in dichloromethane with acetic acid enabled subsequent *N*-Boc protection, affording dimethoxytryptamine **3.91** in 34% yield over two steps. Despite successful protection, oxidation of dimethoxytryptamine **3.92** with CAN again led to decomposition. To access an indolequinone, efforts were made to convert dimethoxytryptamine **3.88** into an intermediate which could more readily be oxidised (**Scheme**

3.8B). However, attempts at C7-functionalisation via (1) bromination using NBS (**3.93**) and (2) iridium-catalysed borylation with pinacolborane (**3.94**) proved unsuccessful.

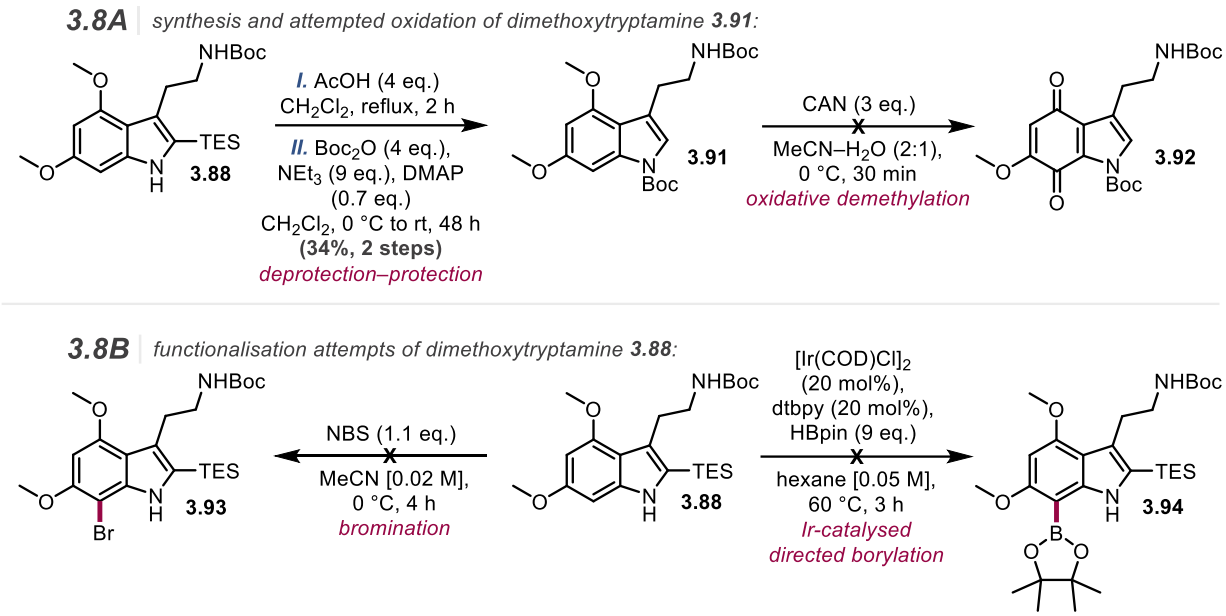

Scheme 3.8. (A) *Synthesis and attempted oxidation of dimethoxytryptamine* ***3.91****.* ***(B)*** *Functionalisation attempts of dimethoxytryptamine* ***3.88****.*

In summary, while dimethoxytryptamine **3.74**, **3.87** and **3.88** were efficiently accessed via the Larock indole synthesis, only dimethoxytryptamine **3.87** could be oxidised to the corresponding indolequinone (**3.89**), and only in poor yield. Efforts to mask the enamine functionality of the indole moiety through *N*-protection did not improve the oxidation outcome. Furthermore, all attempts to derivatise dimethoxytryptamine **3.88** into a more readily oxidisable intermediate were unsuccessful. Consequently, this prompted the exploration of alternative synthetic strategies for the synthesis of thiaplakortone A **1.12**.

3.5.3. Connecting the *S*-atom first

3.5.3.1. Electrophilic halogenation

We turned our attention to construction of the thiazine 1,1-dioxide ring via introduction of the sulfur functionality first (**Scheme 3.9A**). This approach again necessitated an appropriate leaving group at the target site to enable regioselective installation of the ring. Given the emphasis on step economy and cost-effectiveness in the context of NTD drug discovery, careful consideration was given to the selection of starting materials.

2,5-Dimethoxy-4-chloroaniline **3.95** was identified as a promising precursor for the synthesis of an *ortho*-iodoaniline (**3.96**) for the Larock indole synthesis, as it contains a suitable leaving group (chloride) for later regiocontrol. However, extensive screening of iodination conditions proved unsuccessful (**Scheme 3.9A** table). For example, treatment with NIS in acetonitrile at 0 °C (**Scheme 3.9A** table, entry 1) resulted in apparent oligomerisation or non-selective reactions; ^{1}H NMR analysis of the crude reaction mixture revealed ten distinct methyl resonances in the 3.70–4.15 ppm region, characteristic of methoxy substituents. Lowering the reaction temperature to −40 °C (**Scheme 3.9A** table, entry 2) or −78 °C (entry 3) failed to suppress this issue. Similarly, attempts using *N*-chlorosuccinimide (NCS) and sodium iodide in acetic acid (**Scheme 3.9A** table, entry 4), and benzyltrimethylammonium dichloroiodate (BTMA–ICl_2) and calcium carbonate in dichloromethane–methanol (entry 5) led to decomposition. Additionally, BTMA–ICl_2 and zinc(II) chloride in acetic acid (**Scheme 3.9A** table, entry 6) led to an intractable mixture.

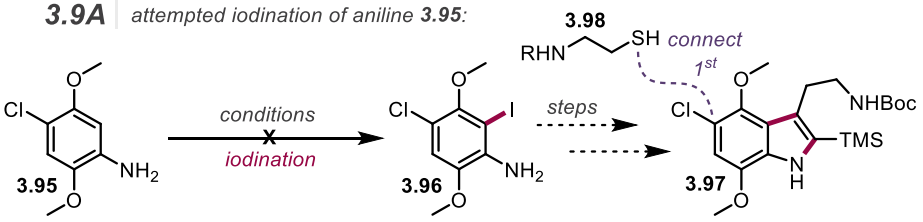

entry	conditions
1	NIS (1 eq.), MeCN, 0 °C, 2 h
2	NIS (1 eq.), MeCN, −40 °C, 2 h
3	NIS (1 eq.), MeCN, −78 °C, 2 h
4	NCS (1 eq.), NaI (1 eq.), AcOH, rt, 2 h
5	BTMA–ICl_2 (1 eq.), $CaCO_3$ (5 eq.), CH_2Cl_2–MeOH (2:1), rt, 1 h
6	BTMA–ICl_2 (1 eq.), ZnCl (1 eq.) AcOH, rt, 12 h
7	TBATI (1 eq.), CH_2Cl_2–MeOH (3:2), 70 °C, 24 h

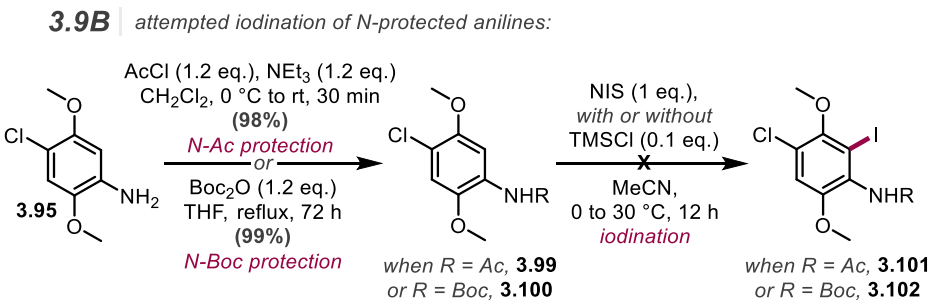

Scheme 3.9. (A) *Attempted iodination of aniline* ***3.95****.* ***(B)*** *Attempted iodination of N-protected anilines.*

In contrast, regioselective bromination was successfully achieved using tetrabutylammonium tribromide ($TBABr_3$), affording the corresponding *ortho*-bromoaniline **3.103** in 79% yield (**Scheme 3.10**). This substrate was evaluated in the Larock indole synthesis, as *ortho*-bromoanilines can be effective coupling partners, but often require the presence of suitable ligands.[103] We therefore screened the use of 1,1'-bis(diphenylphosphino)ferrocene (DPPF) and 1,3-bis(diphenylphosphino)propane (DPPP) as ligands. However, under both conditions, the major product was aniline **3.95**, arising from oxidative addition–protodebromination. Minor products included desilylated alkyne **3.86** and putative styrene **3.104**, arising from carbopalladation across alkyne **3.86**. The presence of this styrene side-product was supported by

diagnostic ^{1}H NMR signals at δ 6.00 (dt, *J* = 15.8, 7.3 Hz) and 5.51 (dt, *J* = 15.8, 1.5 Hz), consistent with an (*E*)-olefin. Thus, our attention returned to the iodination of aniline **3.95**.

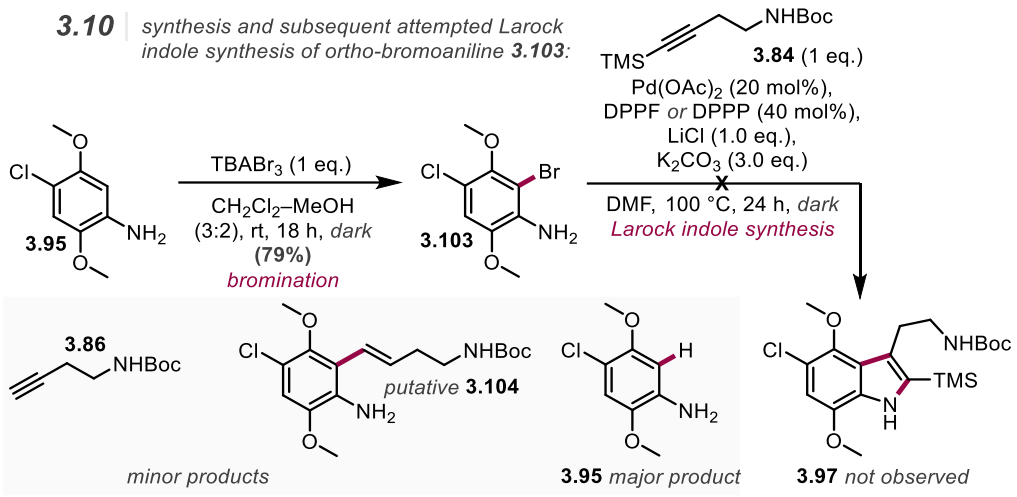

Scheme 3.10. *Synthesis and subsequent attempted Larock indole synthesis of ortho-bromoaniline* ***3.103****.*

As an alternative iodination strategy, tetrabutylammonium triiodide ($TBAI_3$) was synthesised from tetrabutylammonium iodide (TBAI) and iodine in 50% yield (assuming desired product). However, treatment aniline **3.95** with $TBAI_3$ in a dichloromethane–methanol mixture at 70 °C (**Scheme 3.9A** table, entry 7) failed to induce iodination, and only starting material was recovered.

To attenuate the reactivity of the aniline moiety and facilitate iodination, protection as either the *N*-acetyl **3.99** or *N*-Boc derivative **3.100** was explored (**Scheme 3.9B**). Acetylation of aniline **3.95** proceeded in 98% yield, but no reaction was observed with NIS, even upon heating to 30 °C or with TMSCl as a Lewis acid additive. Similarly, the *N*-Boc–protected derivative **3.100** was obtained in 99% yield but likewise remained inert to iodination under analogous conditions.

3.5.3.2. Directed *ortho*-metallation

To overcome the limitations encountered with electrophilic aromatic substitution (S_EAr), we turned our attention to a directed *ortho*-metalation (DOM)–electrophile trapping strategy. We hypothesised that *N*-Boc aniline **3.100** could undergo deprotonation *ortho* to the Boc group using a strong base (**Scheme 3.11**).

Initial attempts employing *n*-butyllithium (^{n}BuLi) and tetramethylethylenediamine (TMEDA) (**Scheme 3.11** table, entry 1) or lithium tetramethylpiperidide (LiTMP) (entry 2) in THF, followed by the addition of 1,2-diiodoethane led primarily to the recovery of unreacted starting material. When *sec*-butyllithium (^{s}BuLi) and TMEDA were used under similar conditions (**Scheme 3.11** table, entry 3), *N*-Boc aniline **3.100** was observed alongside protodechlorinated byproduct **3.106** in an approximate 1:0.2 ratio. Use of *tert*-butyllithium (^{t}BuLi) in diethyl ether (**Scheme 3.11** table, entry 4) followed by electrophilic trapping resulted in a mixture, including the starting material, of lithium–halogen exchange product **3.107**, and protodechlorinated product **3.106** in an approximate 1:1:0.5 ratio, respectively.

3.11 | *directed ortho-metallation–iodination of* ***3.100****:*

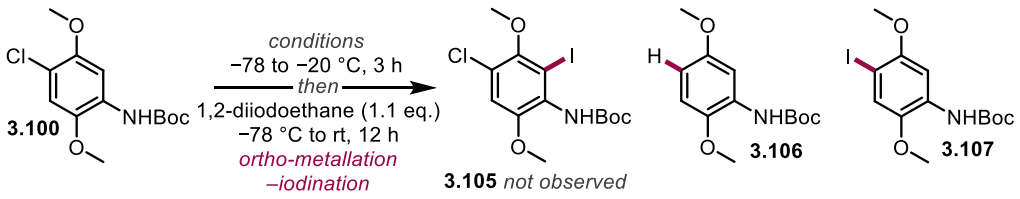

entry	*conditions*	*3.100 : 3.106 : 3.107 ratio*
1	^{n}BuLi (2.2 eq.), TMEDA (2.2 eq.) THF	1 : 0 : 0
2	^{n}BuLi (2.2 eq.), TMP (2.2 eq.) THF	1 : 0 : 0
3	^{s}BuLi (2.2 eq.), TMEDA (2.2 eq.) THF	1 : 0.2 : 0
4	^{t}BuLi (2.2 eq.) Et_2O	1 : 0.5 : 1

Scheme 3.11. *Attempted directed ortho-metallation–iodination of N-Boc aniline* ***3.100****. Table of conditions explored.*

These outcomes suggested that the chloro substituent was incompatible with the DOM conditions, prompting its replacement with a fluoride. The synthesis of *N*-Boc aniline **3.110** was achieved by treatment of 2-fluoro-1,4-dimethoxybenzene **3.108** with concentrated nitric acid, affording nitrobenzene **3.109** as a single regioisomer in 76% yield (**Scheme 3.12**).[104] One-pot reduction of the nitro group and *in situ* Boc protection was accomplished using hydrogen and palladium on carbon in the presence of Boc anhydride and triethylamine in THF, affording *N*-Boc aniline **3.110** in 74% yield. To assess the efficiency of the DOM step independently of electrophilic trapping, deuterium incorporation was examined. Treatment of *N*-Boc aniline **3.110** with ^{t}BuLi followed by quenching with methanol-d_4 at −40 °C resulted in less than 20% deuterium incorporation (**3.111**). Increasing the reaction temperature to −20 °C led to incorporation levels of 70%. These results suggested that an *ortho*-iodoaniline for Larock indole synthesis could likely be accessed efficiently through screening of electrophilic iodine sources and electrophile stoichiometry.

3.12 | *synthesis and directed ortho-metallation–deuteration of* ***3.110****:*

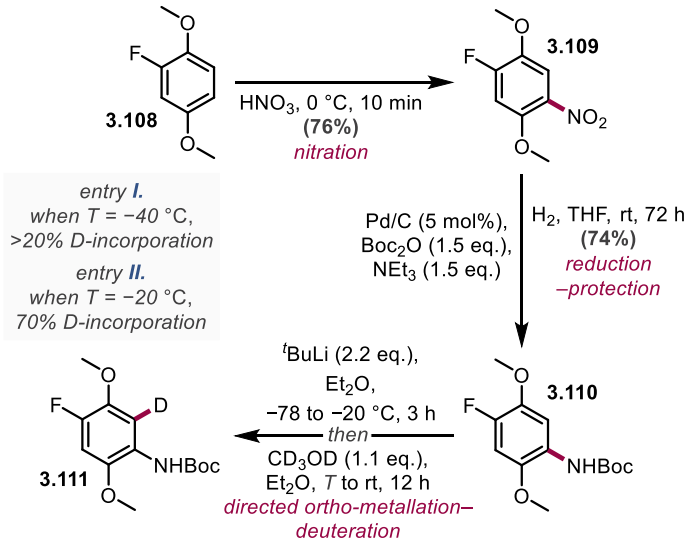

Scheme 3.12. *Synthesis and directed ortho-metallation–deuteration of N-Boc aniline* ***3.110****.*

3.5.3.3. Bartoli indole synthesis

In parallel, we investigated alternative strategies starting from nitrobenzene **3.109** (**Scheme 3.13A**). Specifically, the Bartoli indole synthesis was considered for the direct construction of indole **3.112**. This indole could serve as a precursor for the corresponding tryptamine since methodologies have been developed to instal the tryptamine side-chain from cyclic sulfamidate **3.81** in one step. However, attempts to effect the Bartoli reaction with vinylmagnesium bromide **3.113** failed to yield the desired indole **3.112**. Instead, the starting material was consumed, and ^{1}H NMR analysis showed the disappearance of two doublets, observed previously due to coupling to fluorine, and the appearance of two singlets in the aromatic region (δ 6.65 and 5.83 ppm). This suggested nucleophilic aromatic substitution (S_NAr) of the fluorine, although no evidence of the corresponding styrene was observed. Lowering the reaction temperature from −40 to −78 °C entirely suppressed the reactivity of nitrobenzene **3.109**.

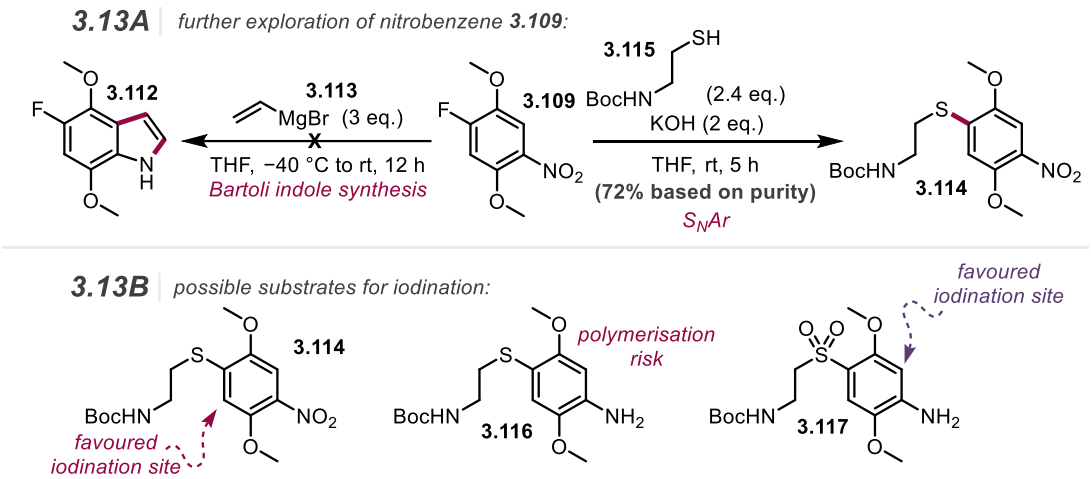

Scheme 3.13. (A) *Further exploration of nitrobenzene* ***3.109****. (B) Possible substrates for iodination.*

3.5.3.4. Nucleophilic aromatic substitution

Given that nitrobenzene **3.109** was predisposed toward S_NAr, we aimed to exploit this reactivity (**Scheme 3.13A**). Treatment of **3.109** with *N*-Boc mercaptamine **3.115** and potassium hydroxide in THF afforded the aryl sulfide **3.114** in 72% yield (based on crude purity without FCC). However, further elaboration of this intermediate seemed challenging (**Scheme 3.13B**). While the desired *ortho*-iodoaniline could, in principle, be accessed via iodination, concerns arose regarding regioselectivity. Initial reduction of the nitro group to the aniline intermediate (**3.116**) was not advised, as the increased aryl-electron density was anticipated to lead to undesired oligomerisation under iodinating conditions (refer back to **Scheme 3.9A** table, iodination of aniline **3.95**). An alternative strategy was proposed in which the sulfur atom could be oxidised to a sulfone (**3.117**) to enable regioselective iodination and reduce aryl electron density. Nonetheless, uncertainty surrounding the compatibility of *S*-containing substrates in the Larock indole synthesis, since sulfur is a known poison to palladium, discouraged further pursuit of this route.[105]

In summary, a range of synthetic strategies were investigated to enable construction of the thiazine 1,1-dioxide ring via early stage incorporation of the *S*-atom. Initial efforts employed a chloride as the eventual leaving group to direct regioselective installation. However, direct iodination of aniline **3.95** proved unsuccessful in the absence or presence of *N*-protection. Although bromination proceeded smoothly, the resulting *ortho*-bromoaniline failed to deliver tryptamine **3.97** via the Larock indole synthesis. Consequently, the approach shifted to DOM–iodination, although this strategy was found to be incompatible with the aryl chloride. Replacing the chloride with a fluoride revived the feasibility of the DOM strategy, potentially enabling access to an *ortho*-iodoaniline for the Larock indole synthesis. In parallel, an alternative route attempting to leverage an earlier nitrobenzene intermediate **3.109** via a Bartoli indole synthesis revealed the substrates' predisposal to undergo S_NAr. Capitalising on this reactivity, early incorporation of the thiazine framework via S_NAr using *N*-Boc mercaptamine **3.115** was achieved. However, the

optimal strategy to convert this aryl sulfide intermediate to thiaplakortone A **1.12** remained unclear. As such, alternative synthetic approaches toward thiaplakortone A **1.12** were subsequently pursued.

3.5.4. Synthesis of trimethoxytryptamine

While efforts were underway toward the synthesis and oxidation of dimethoxytryptamine **3.74**, **3.87** and **3.88**, Wood *et al.* reported the total synthesis of makaluvamines A **3.121** and K **3.120** (**Scheme 3.14A**), structurally related indolequinone natural products to thiaplakortones A **1.12** and B **3.1**. [106] Indolequinone **3.119** was accessed via oxidative demethylation of trimethoxytryptamine **3.118** using CAN. Notably, a Larock indole synthesis was used to construct the electron-rich tryptamine – mirroring our approach. We sought to adopt portions of their strategy for the preparation of a trimethoxytryptamine towards the thiaplakortone framework.

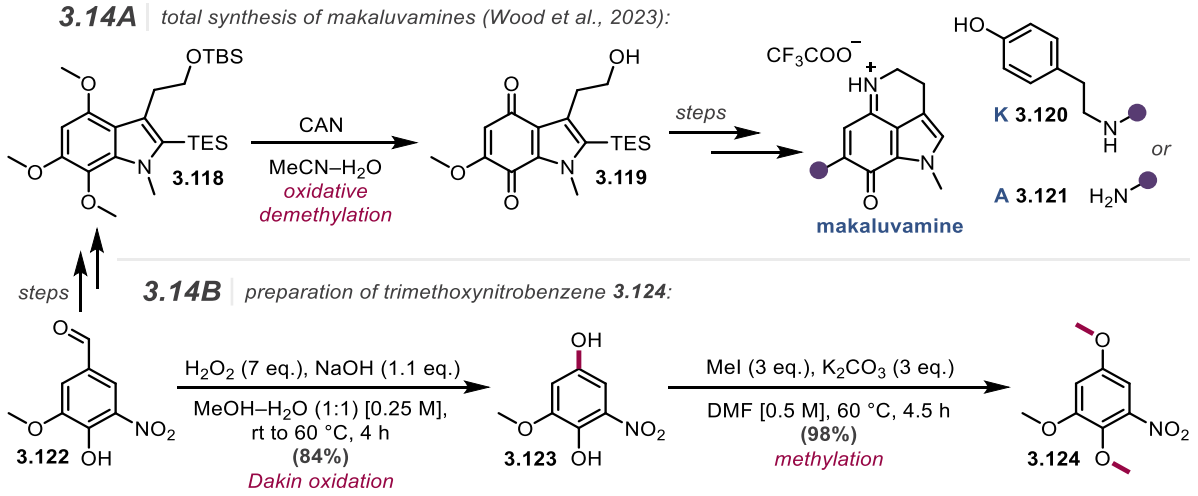

***Scheme 3.14**. **(A)** Total synthesis of makaluvamine K **3.120** and A **3.121** (Wood et al., 2023). **(B)** Preparation of trimethoxynitrobenzene **3.124**.*

Beginning from 5-nitrovanilin **3.122**, Dakin oxidation of the aromatic aldehyde with hydrogen peroxide and sodium hydroxide provided phenol **3.123** in an excellent yield of 84% (**Scheme 3.14B**). Subsequent methylation of the resulting hydroquinone using methyl iodide afforded trimethoxynitrobenzene **3.124** in a, near quantitative, 98% yield.

3.5.4.1. Attempted synthesis of trimethoxyindole 3.125 as a model substrate

With trimethoxynitrobenzene **3.124** in hand, we sought its conversion to trimethoxyindole **3.125** (**Scheme 3.15A**), a model compound designed to probe two key transformations: (1) oxidation to the corresponding quinone and (2) construction of the thiazine 1,1-dioxide ring. Omission of the tryptamine side-chain was intended to simplify the system. Initial attempts to effect a Bartoli indole synthesis by treating trimethoxynitrobenzene **3.124** with vinylmagnesium bromide **3.113** failed to yield the desired trimethoxyindole **3.125**. Instead, ^{1}H NMR analysis of the crude reaction mixture revealed a single indole species, which was isolated and identified as dimethoxyindole **3.126** in a low yield of 9% (**Scheme 3.15A**). Although this outcome was not synthetically useful – given the previously demonstrated challenges associated with the absence of *para*-dimethoxy substitution (refer back to **Scheme 3.6C** & **3.7C**) – it was nevertheless mechanistically intriguing.

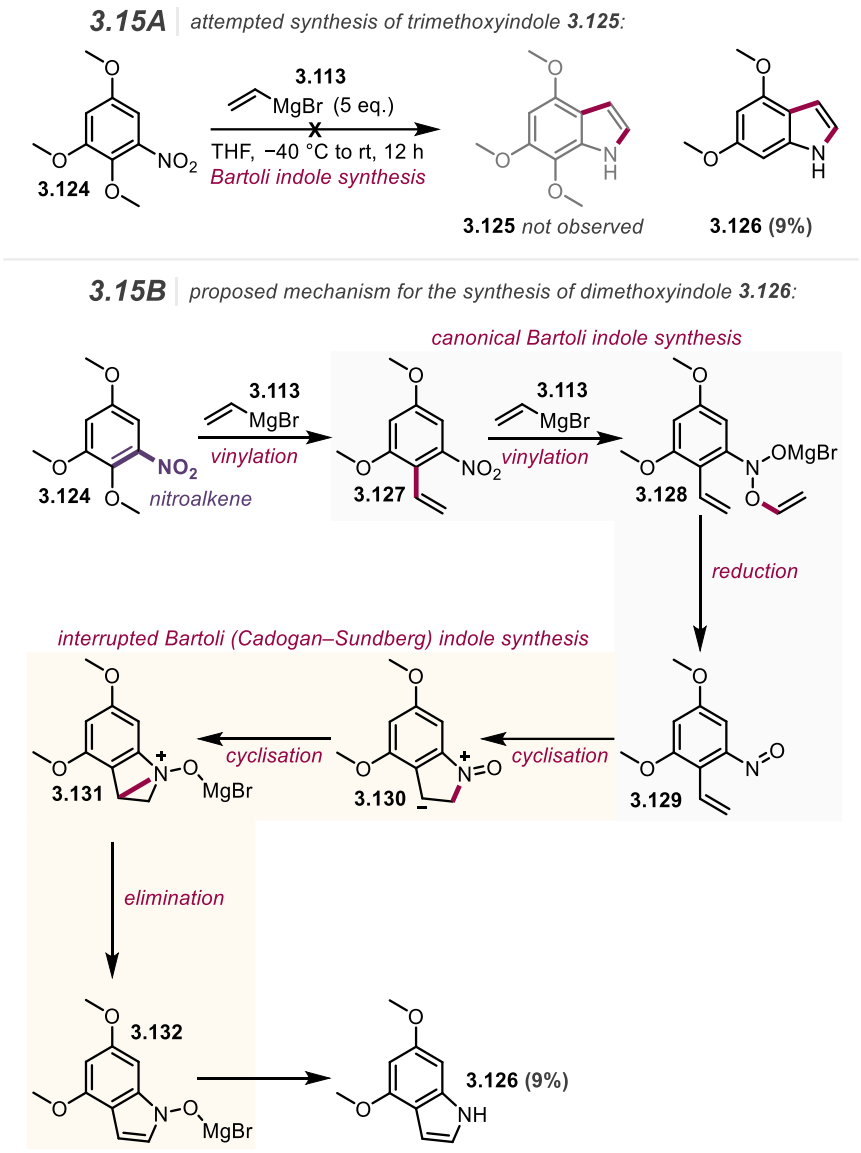

Scheme 3.15. (A) *Attempted synthesis of trimethoxyindole* ***3.125****. (B) Proposed mechanism for the generation of dimethoxyindole* ***3.126****. An abnormal Bartoli indole synthesis mechanism is also possible.*

Although an abnormal Fischer indole synthesis has been reported for *ortho*-methoxy substrates (refer back to **Scheme 3.4B**), in which cyclisation preferentially occurs at the *ipso*-position, an analogous abnormal Bartoli indole synthesis has not been realised. While this could be the mechanism, an alternative pathway has been proposed (**Scheme 3.15B**). Menéndez *et al.* observed that, in certain *ortho*-methoxynitrobenzene systems, vinylation occurred preferentially to afford *ortho*-nitrostyrenes, rather than proceed through to indole formation.[107] It is hypothesised that trimethoxynitrobenzene **3.124** behaves more like a nitroalkene, with vinylmagnesium bromide **3.113** undergoing 1,4-conjugate addition to form *ortho*-nitrostyrene

3.127. As with the canonical Bartoli indole synthesis, vinylmagnesium bromide **3.113** attacks the nitro group, forming intermediate **3.128**.[108] Subsequent elimination of ethenolate leads to partial reduction of the nitro group to nitroso **3.129**, which is believed to be the end-point of the Bartoli reaction. Further transformation can proceed via the Cadogan–Sundberg reaction, a known method for converting *ortho*-nitrostyrenes to indoles using a reductant, typically trialkyl phosphites, to generate a nitroso species *in situ*.[109] The lone pair on the *N*-atom adds across the olefin, forming benzyl anion **3.130**, which undergoes intramolecular cyclisation to afford bicyclo[2.1.0]pentane **3.131**. Final proton elimination affords indole **3.132**. While the exact mechanism for N–O bond cleavage to dimethoxyindole **3.126** remains uncertain, there is evidence that Grignard reagents can serve as single-electron reductants.[110,111]

3.5.4.2. Continued synthesis of trimethoxytryptamine 3.135

Following the unsuccessful synthesis of a model substrate, we redirected our efforts again toward the preparation of trimethoxytryptamine **3.135** (**Scheme 3.16A**). Iodination of trimethoxynitrobenzene **3.124** with iodine and silver nitrate proceeded smoothly and with complete regioselectivity, affording *ortho*-iodonitrobenzene **3.133** in an excellent 94% yield. Subsequent Béchamp reduction of the nitro group using iron and ammonium chloride furnished the corresponding *ortho*-iodoaniline **3.134** in 92% yield, ready for the Larock indole synthesis. Due to the instability of *ortho*-iodoaniline **3.134**, this compound was always synthesised, purified and used as a reagent the same day, and was kept in the dark. Additionally, compared to its dimethoxy analogue, **3.70**, *ortho*-iodoaniline **3.134** exhibited increased susceptibility towards protodeiodination. When the reaction was conducted under stringent anhydrous conditions – including azeotropic drying of *ortho*-iodoaniline **3.134** and alkyne **3.84**, extended drying of DMF over activated 3 Å molecular sieves, and drying of lithium chloride and sodium carbonate under vacuum while heating – the desired trimethoxytryptamine **3.135** was obtained in an excellent 84% yield. The regioisomer arising from carbopalladation at the other site was not detected by

^{1}H NMR analysis of the crude mixture prior to FCC. Neglecting stringent drying conditions, however, led to a marked reduction in yield, achieving a mere 28% yield.

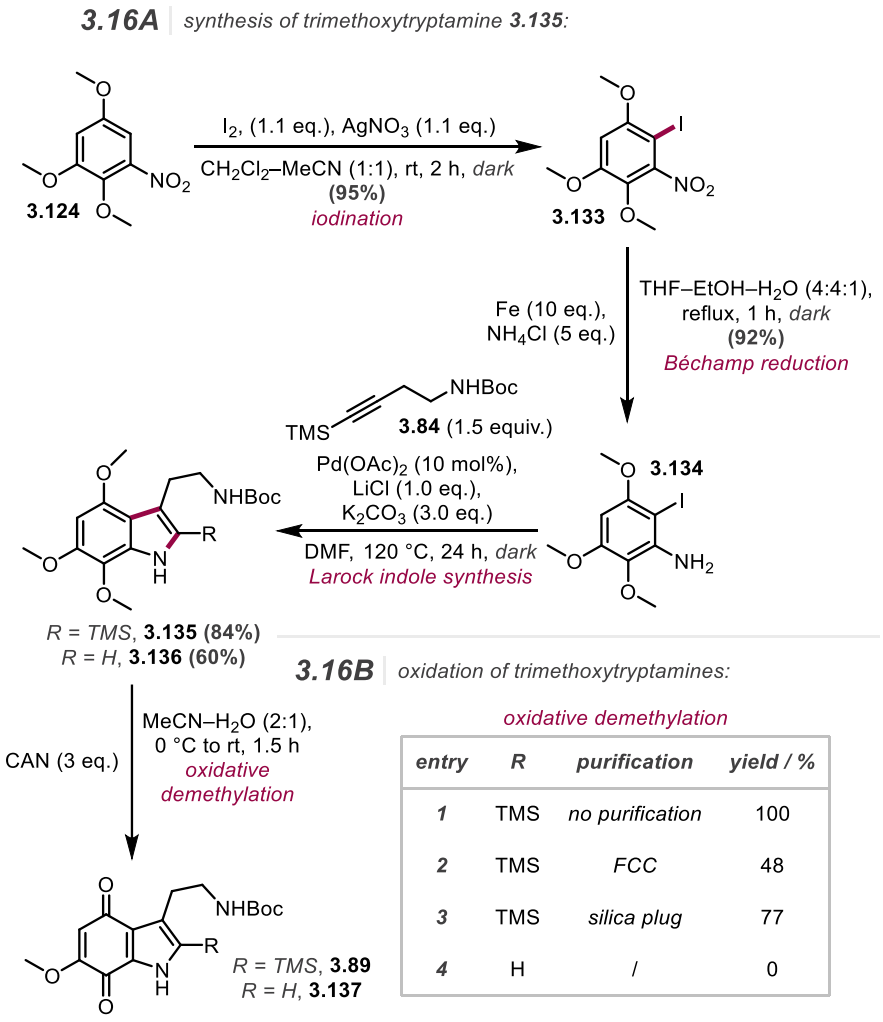

Scheme 3.16. (A) *Synthesis of trimethoxytryptamine* ***3.135****.* ***(B)*** *Oxidation of trimethoxytryptamine* ***3.135****.*

3.5.5. Oxidation of trimethoxytryptamine 3.135 to indolequinone 3.89

Oxidation of trimethoxytryptamine **3.135** with CAN proceeded cleanly to afford the desired indolequinone **3.89** in quantitative yield and high purity without FCC (**Scheme 3.16B** table, entry 1). Notably, purification by FCC resulted in a significant reduction in isolated yield to 48% (entry 2). Modification of the purification protocol by employing a short silica plug and increasing eluent polarity improved the yield to 77% (**Scheme 3.16B** table, entry 3). Nonetheless, the crude product obtained directly from oxidation was of sufficient purity to be used in the next step without further purification.

The importance of the C2-TMS substituent for the oxidation step was highlighted after it was deliberately removed during work-up of the Larock indole synthesis. Vigorous shaking of the organic layer with 3 M HCl solution gave trimethoxytryptamine **3.136** in 60% yield (**Scheme 3.16A**).[112] However, exposure of **3.136** to CAN led to complete decomposition (**Scheme 3.16B** table, entry 4). It is well precedented that electron-rich aromatics can undergo competitive side-reactions reactions with CAN, such as nitration.[113,114] One could postulate that the C2-TMS group provides our system protection through: (1) electronic deactivation of the indole moiety through negative hyperconjugation of the σ^*_{C-Si} with the π-system (the α-effect), or (2) steric hinderance shielding the pyrrole core, thus limiting decomposition via undesirable reaction pathways.

In summary, *ortho*-iodoaniline **3.134**, the key precursor for the Larock indole synthesis, was efficiently prepared in four steps from commercially available 5-nitrovanillin **3.122**. During efforts to access this intermediate, the synthesis of a model trimethoxyindole system was explored via a Bartoli indole synthesis from trimethoxynitrobenzene **3.124**. Unexpectedly, novel reactivity was observed in which C–C bond formation occurred at the *ipso*-position of the *ortho*-methoxy group, forming dimethoxyindole **3.126**. For the Larock indole synthesis of *ortho*-iodoaniline **3.134**, under stringent anhydrous conditions, the desired trimethoxytryptamine

3.135 was obtained in excellent yield and clean oxidation to the corresponding indolequinone was achieved. However, in the absence of the C2-TMS group, CAN oxidation resulted in decomposition. With indolequinone **3.89** successfully in hand, attention turned to the construction of the thiazine 1,1-dioxide ring.

3.5.6. Thiazine 1,1-dioxide formation

The thiazine 1,1-dioxide motif is a recurring structural feature in several natural product families including the thiaplakortones (**Figure 3.3**, **1.12** & **3.1**),[84] ascidiathiazones (**3.138** & **3.139**),[115] aplidinones (**3.142** & **3.143**),[116] euthyroideones (**3.140** & **3.141**),[117] and conithiaquinones (**3.144** & **3.145**).[118] To date, hypotaurine **3.10** has been the sole reagent employed for the installation of this ring in reported total syntheses in peer-reviewed literature.[85,115,119–122] However, an alternative strategy, disclosed in a recent doctoral thesis, was developed during the total synthesis of ascidiathiazone B **3.139**.[123] Hypotaurine **3.10**, which is biosynthetically-derived from cysteine **3.6** and an enzymatic substrate for the synthesis of taurine, remains cost-prohibitive – being 300-fold more expensive than taurine. The high cost of hypotaurine **3.10** presents a significant limitation for the large-scale synthesis of natural products and impedes the exploration of analogues for biological evaluation.

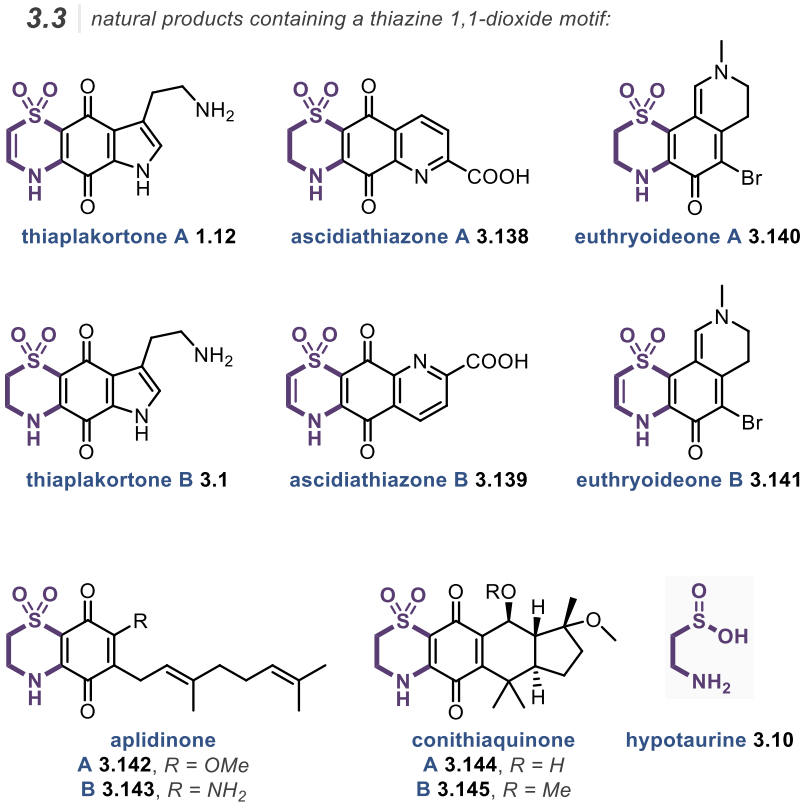

Figure 3.3. *Selected natural products containing the thiazine 1,1-dioxide motif – primarily constructed from hypotaurine **3.10**.*

Cystamine **3.153** (**Scheme 3.17**), also derived from cysteine, is a commercially available organic disulfide with a cost similar to taurine which thus presents an attractive alternative. Disulfide bonds have been shown to be readily cleaved under a range of conditions, including by oxidation and reduction,[124,125] but also by nucleophilic attack, and photochemical and electrochemical approaches.[126,127] While the use of cystamine **3.153** for thiazine 1,1-dioxide formation has not yet been demonstrated, Kohn *et al.* reported the reductive cleavage of disulfide **3.146** with Cleland's reagent **3.147** (dithiothreitol), which likely afforded putative sulfide **3.149** alongside cyclisation product **3.150** and **3.151** (detected by high resolution mass spectroscopy, HRMS) via intermediate **3.148**. [128] However, attempts to isolate these cyclisation products led to their convergence to dimer **3.152**.

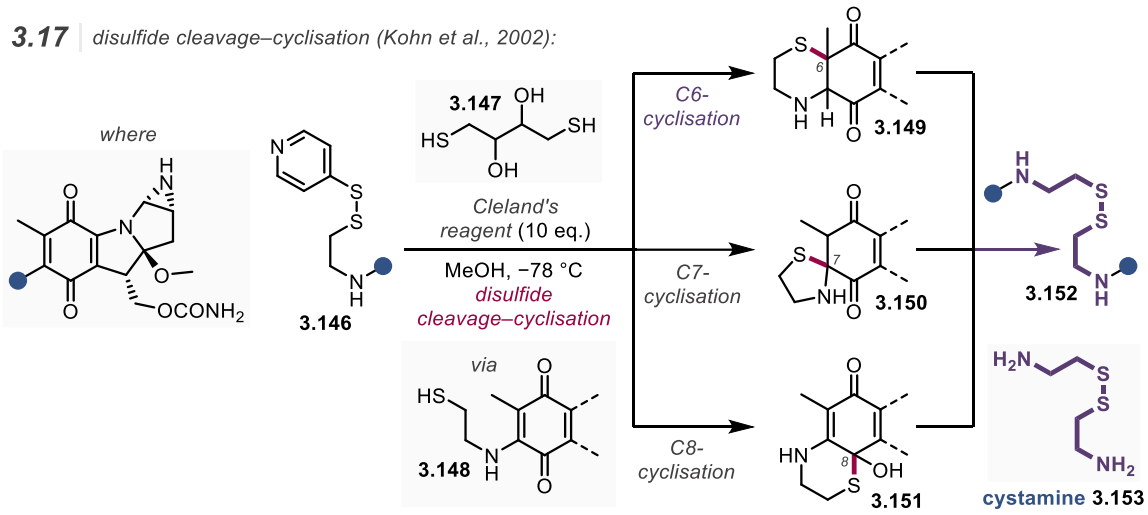

Scheme 3.17. *Disulfide cleavage–cyclisation (Kohn et al., 2002).*

3.5.6.1. Thiazine 1,1-dioxide formation on a model substrate

It was envisioned that cystamine **3.153** could serve as a novel alternative to hypotaurine **3.10** by enabling oxidative cleavage of the disulfide bond to access the sulfinic acid oxidation state. It was hoped that formation of an enamine intermediate via addition–elimination of a cystamine-derived nucleophile to indolequinone **3.89** would enable cyclisation to the requiste sulfone. The

feasibility of oxidative disulfide cleavage was demonstrated using cystamine **3.154**, prepared in quantitative yield from cystamine **3.153** dihydrochloride (**Scheme 3.18A**). Treatment with *N*-bromosuccinimide (NBS) in methanol cleanly afforded methyl sulfinate **3.155** in 98% yield.

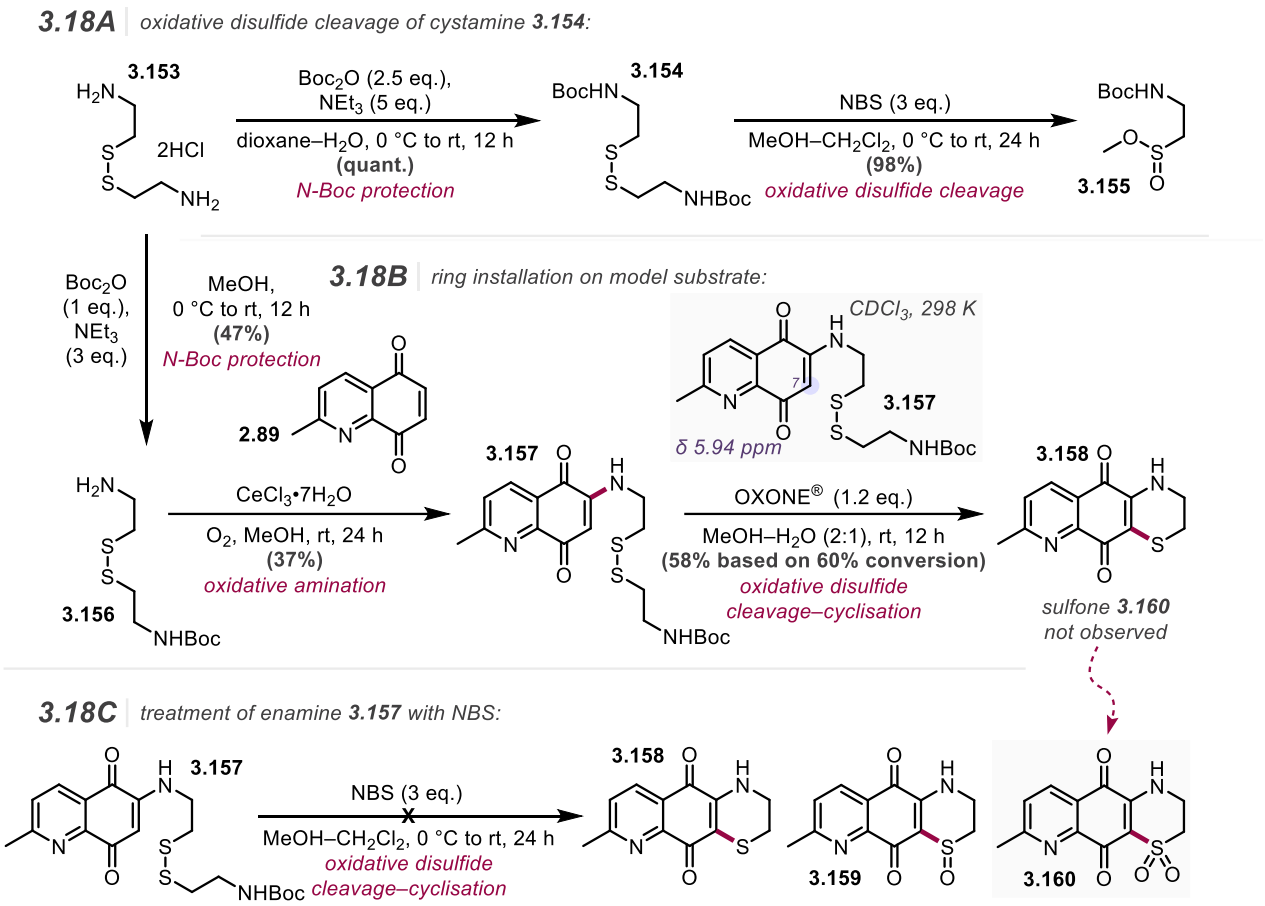

Scheme 3.18. (A) *Oxidative disulfide cleavage of cystamine **3.154**. **(B)** Installation of dihydrothiazine ring onto model quinone. **(C)** Treatment of enamine **3.157** with NBS. Unknown product obtained.*

Subsequent efforts focused on exploring conditions to install a thiazine 1,1-dioxide ring onto a model quinone system, **2.89** (**Scheme 3.18B**). Mono-protected cystamine **3.156** was prepared in 47% yield from cystamine dihydrochloride. Enamine **3.157** was obtained via oxidative amination of quinone **2.89** using cystamine **3.156** and cerium(III) chloride, affording the product in 37% yield. This yield was significantly lower than those previously observed with aniline nucleophiles (refer back to **Scheme 2.12B** & **2.16B**). It was postulated that the reduced nucleophilicity of cystamine **3.156** was due to the disulfide acting as a β-electron-withdrawing group – with the *N*-lone pair partially delocalising into the S–S σ* orbital.

When enamine **3.157** was treated with NBS in methanol this did not, however, afford desired sulfone **3.160** as hoped (**Scheme 3.18C**). A cyclisation event was believed to have occurred due to the disappearance of the H7 resonance of **3.157** at δ 5.94 ppm (**Scheme 3.18B**), but the identity of the product remains unconfirmed. The infrared spectroscopy (IR) did not show any characteristic absorptions for a S=O stretching vibration of a sulfone. Additionally, HRMS did not detect the presence of sulfone **3.160**. Diastereotopic proton signals were observed when the sample was analysed by ^{1}H NMR spectroscopy in dimethyl sulfoxide-d_6 suggesting the presence of a stereogenic centre. However, it was unlikely that the product was sulfoxide **3.159** since this would have required reduction of the *S*-oxidation state (additionally IR spectroscopy and HRMS disfavoured sulfoxide **3.159**). The presence of an additional signal in the ^{1}H NMR spectrum with an integration of three protons suggested the incorporation of a methoxy substituent (from the solvent) into the molecule. No further structural elucidation was undertaken.

Treatment of enamine **3.157** with potassium peroxymonosulfate (OXONE®) in a water–methanol mixture (**Scheme 3.18B**) led to formation of a cyclised product, as evidenced by the disappearance of the characteristic H7 resonance in the ^{1}H NMR spectrum. However, the isolated product was identified as sulfide **3.158** (35% yield, or 58% accounting for 60% conversion). A plausible mechanistic rationale involves initial oxidation by OXONE® of the *S*-atom that is eliminated during dihydrothiazine ring formation, thereby generating a better leaving group and promoting intramolecular cyclisation via attack by the enamine. However, it is likely the oxidation is not regioselective, and oxidation at the non-eliminating *S*-atom may account for the modest yield of sulfide **3.158**.

Although sulfide **3.158** was not the envisioned targeted product and would require further oxidation to access sulfone **3.160**, the significantly lower cost and greater availability of cystamine **3.153** relative to hypotaurine **3.10** rendered this approach more attractive. With proof-of-concept established for the use of cystamine **3.156** as a viable alternative to hypotaurine

3.10, attention was directed toward evaluating its applicability for dihydrothiazine ring installation on indolequinone **3.89**.

3.5.6.2. Addition–elimination with cystamine 3.156

To evaluate the addition–elimination propensity of indolequinone **3.89**, tyramine **3.163** was initially selected as a model nucleophile given its successful use with iminoquinone **3.161** in the synthesis of makaluvamine K **3.120** (**Scheme 3.19A**). Under identical conditions, enamine **3.164** was obtained as a single regioisomer in 24% yield after four days (**Scheme 3.19B** table, entry 1). In comparison, the same transformation with iminoquinone **3.161** afforded the product in 43% yield within 16 hours.[106] This disparity may suggest reduced electrophilicity of the indolequinone scaffold relative to its iminoquinone analogue.

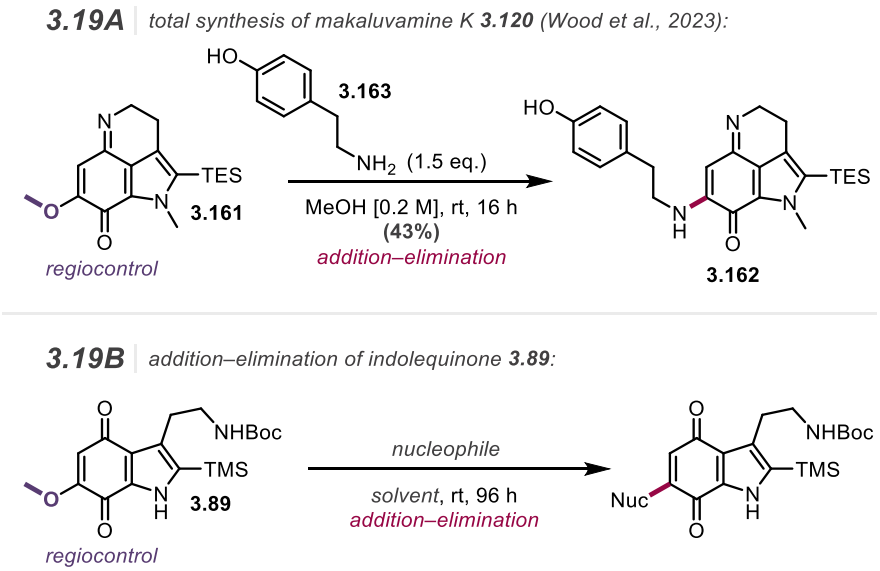

entry	nucleophile	solvent [concentration]	product	yield / %
1	HO, **3.163** (1.5 eq.), NH_2	MeOH [0.2 M]	**3.164**	23
2	BocHN, S, S, **3.156** (3 eq.), NH_2	EtOH [0.5 M]	**3.165**	48 *(brsm)*

Scheme 3.19. (A) *Addition–elimination of iminoquinone* ***3.161*** *using tyramine* ***3.163*** *during the total synthesis of makaluvamine K* ***3.120*** *(Wood et al., 2023).* ***(B)*** *Addition–elimination of indolequinone* ***3.89****.*

Encouraged by the feasibility of regioselective addition–elimination of indolequinone **3.89**, the use of cystamine **3.156** as a nucleophile was next investigated (**Scheme 3.19B** table, entry 2). Given that the nucleophilicity of the *N*-lone pair is likely reduced due to the β-electron-withdrawing nature of the disulfide, the reaction concentration was increased to 0.5 M to promote reactivity. Additionally, methanol was replaced with ethanol as a greener alternative. After three days at room temperature, TLC analysis indicated incomplete conversion, prompting the addition of a further 1.5 equivalents of the nucleophile (3 eq. in total), which furnished enamine **3.165** in 33% yield, or 48% based on recovered starting material (brsm). Increasing the reaction temperature to 35 °C improved the isolated yield to 47%, albeit without recovery of starting material, and additional products observed by TLC analysis.

Although the overall yields for the addition–elimination of indolequinone **3.89** were modest, the transformation of enamine **3.165** to the sulfide – the key step in the synthetic sequence for the synthesis of thiaplakortone A **1.12** – was next pursued.

3.5.6.3. Dihydrothiazine formation on indolequinone 3.89

Initial attempts to convert enamine **3.165** to sulfide **3.166** via thermal activation, with heating from room temperature to 100 °C in DMF, resulted in incomplete conversion and decomposition products (**Table 3.2**, entry 1). Given prior success using OXONE® to promote cyclisation with model enamine **3.157** (refer back to **Scheme 3.18B**), these conditions were applied to enamine **3.165** (**Table 3.2**, entry 2). While no reaction occurred at room temperature, raising the temperature to 50 °C led to partial consumption of starting material, accompanied by significant decomposition. Similarly, NBS in methanol resulted in degradation without formation of sulfide **3.166** (**Table 3.2**, entry 3).

3.2 | *conditions screened for dihydrothiazine ring formation:*

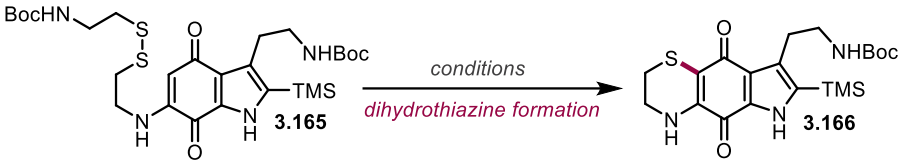

	entry	conditions	yield / %
oxidants	1	DMF [0.01 M], rt to 100 °C, 24 h	0
	2	OXONE® (1.2 eq.) MeOH–H_2O (2:1) [0.05 M], rt to 50 °C	0
	3	NBS (1.2 eq.) MeOH–CH_2Cl_2 (1:1) [0.02 M], 0 °C to rt, 12 h	0
	4	**[Ir]** (10 mol%) DCE, 455 nm, rt, 12 h	0
reductants	5	$NaBH_4$ (1.2 eq.) MeOH [0.5 M], 0 °C to rt, 3 h	0
	6	Mn (3 eq.), LiCl (1.5 eq.) DMF [0.02 M], rt to 50 °C, 24 h	0
	7	Rongalite® (4 eq.), K_2CO_3 (2 eq.) DMF, rt, 72 h	0
	8	*Cleland's reagent* (20 eq.) CH_2Cl_2, rt, 12 h	10
	9	(^{n}Bu)$_3$P (1.5 eq.), H_2O (1 eq.) CH_2Cl_2 [0.01 M], rt, 12 h	*trace*

Table 3.2. *Conditions screened to achieve the installation of the dihydrothiazine ring.*

Inspired by the photocatalytic disulfide cleavage–*thia*-Michael addition sequence reported by Glorius *et al.* using (Ir[dF(CF$_3$)ppy]$_2$(dtbpy))PF$_6$ under blue LED irradiation, this strategy was evaluated.[129] However, irradiation of enamine **3.165** under these conditions yielded an intractable mixture of products (**Table 3.2**, entry 4), with no sulfide **3.166** detected. It was postulated that the indolequinone moiety may act as a photosensitiser, absorbing light and engaging in higher-energy reaction pathways.[130]

Subsequent efforts focused on reductive disulfide cleavage to promote the desired transformation. Reductants such as sodium borohydride (**Table 3.2**, entry 5), manganese with lithium chloride (entry 6),[131] and Rongalite® (sodium hydroxymethanesulfinate, entry 7) proved ineffective.[132] In contrast, treatment of enamine **3.165** with Cleland's reagent **3.147** in methanol

produced sulfide **3.166** (**Table 3.2**, entry 8), albeit in a low yield of 10% with low conversion. This was proposed to proceed via thiol–disulfide exchange to form disulfide **3.168** (**Scheme 3.20**), which undergoes intramolecular cyclisation to afford the thermodynamically favoured six-membered ring **3.171**. The liberated thiol **3.167** engages in a 6-*endo-trig thia*-Michael addition to the tethered quinone, with oxidation of hydroquinone intermediate **3.172** completing the synthesis of sulfide **3.166**.

3.20 | *proposed mechanism for conversion of enamine **3.165** to sulfide **3.166** using Cleland's reagent **3.147**:*

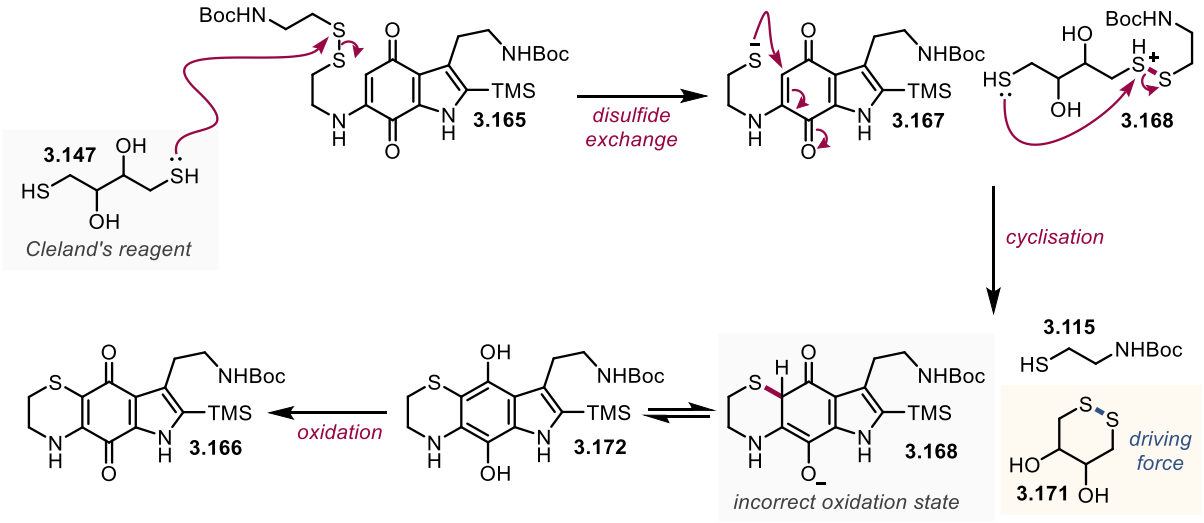

Scheme 3.20. *Proposed mechanism for the conversion of enamine **3.165** to sulfide **3.166** using Cleland's reagent **3.147**.*

Initially, it was assumed that aerobic oxidation during work-up was sufficient to complete this final step. However, efforts to reproduce the transformation under these conditions were unsuccessful. Various modifications were explored, including (1) oxygen sparging after enamine **3.165** consumption, (2) reaction dilution to suppress thiol recombination and favour intramolecular cyclisation, and (3) changing the solvent to dichloromethane. None restored the desired reactivity. Trace amounts of sulfide **3.166** were observed when tributylphosphine was used in wet DMF (**Table 3.2**, entry 9), though this pathway was not pursued further due to the same unresolved issue with the final hydroquinone oxidation state.

3.5.6.4. Other amine nucleophiles

As efforts to achieve a reproducible disulfide cleavage–intramolecular cyclisation–oxidation sequence proved unsuccessful, alternative amine nucleophiles were investigated for addition–elimination with indolequinone **3.89**. These nucleophiles were designed with embedded functionality incorporated to facilitate intramolecular cyclisation.

Given that the *thia*-Michael addition was believed to generate hydroquinone **3.172**, which required subsequent oxidation to afford desired sulfide **3.166**, it was reasoned that a *S*-protecting group amenable to oxidative removal would be advantageous. *S*-*para*-methoxybenzyl (PMB) cysteamine **3.174** was identified as a promising candidate, as oxidation with DDQ could both unmask the thiol and oxidise the hydroquinone intermediate. *S*-PMB cysteamine **3.174** was synthesised by treating cysteamine **3.173** hydrochloride with lithium hydroxide and PMB chloride, affording the product in 37% yield (**Scheme 3.21A**). Addition–elimination of indolequinone **3.89** with *S*-PMB cysteamine **3.173** afforded enamine **3.177** in 53% yield, and notably, the reaction tolerated elevated temperatures (**Scheme 3.21B**). However, subsequent treatment of enamine **3.177** with DDQ (3 eq.) failed to furnish sulfide **3.166**, with only *para*-anisaldehyde **3.179** observed in the ^{1}H NMR spectrum of the crude material (chloroform-d_1). This indicated the successful PMB-deprotection but no further progression to the desired product. The outcome suggested that the acidic nature of DDQ may have hindered oxidation, since a similar issue had previously been encountered during the conversion of C2-desilylated trimethoxytryptamine **3.136** to indolequinone **3.137** (refer back to **Scheme 3.16B**).

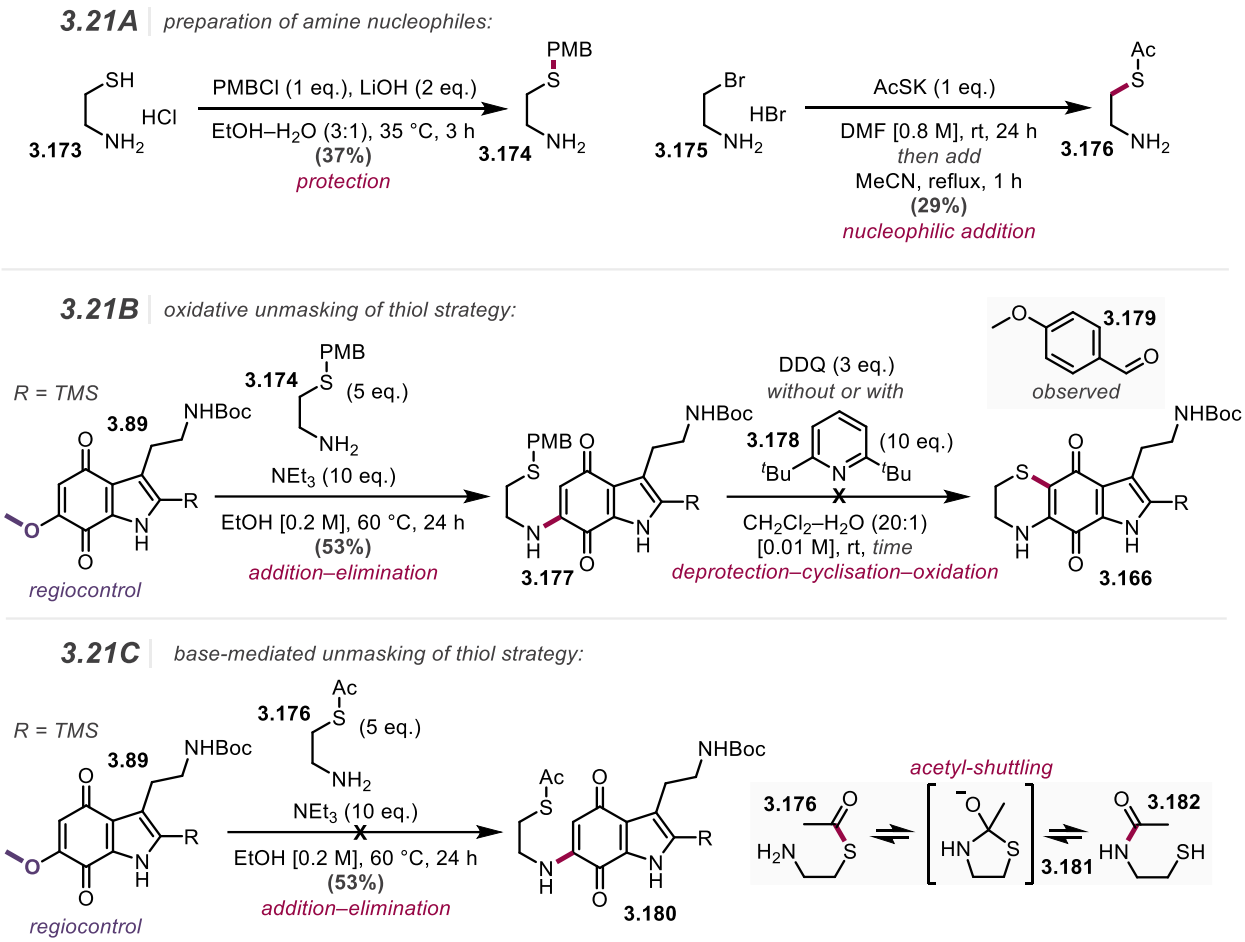

***Scheme 3.21**. **(A)** Preparation of other amine nucleophiles which were explored. **(B)** Alternative oxidative unmasking strategy of the thiol. Where time = 2 hours without base, or 24 hours with base. **(C)** Alternative base-mediated unmasking strategy. Failure to synthesise enamine **3.180** likely due to competing acetyl-shuttling.*

To address this, the oxidation protocol was modified to include 2,6-di-*tert*-butylpyridine **3.178** as a base (**Scheme 3.21B**), following the strategy reported by Danishefsky *et al.* for acid-sensitive systems.[133] However, this had a detrimental effect on the rate of reaction, with TLC analysis revealing minimal conversion.

As an alternative strategy, the disulfide was replaced with an *S*-acetyl group. While deprotection followed by *thia*-Michael addition was expected to produce the same hydroquinone intermediate (**3.172**), it remained unclear whether the initial reaction between the sulfide in enamine **3.165** and Cleland's reagent **3.147** was also a low yielding step. The *S*-acetyl protecting group was considered particularly appealing, as deprotection was envisioned to occur reliably under mildly basic conditions. *S*-Acetyl cysteamine **3.176** was selected for evaluation and was synthesised in 29% yield via nucleophilic substitution of 4-bromo-2-aminobutane **3.175** hydrobromide with

potassium thioacetate (**Scheme 3.21A**). But, addition–elimination with indolequinone **3.89** did not afford enamine **3.180** (**Scheme 3.21C**). The lack of reactivity was attributed to a competing acetyl-shuttling process (**3.182**), facilitated by a 5-*exo*-*trig* cyclisation (intermediate **3.181**).

3.5.6.5. Base-induced cyclisation

For the installation of the dihydrothiazine ring, thermal and oxidative activation had previously failed to promote intramolecular cyclisation via direct enamine attack (refer back to **Table 3.2**). It was hypothesised that base treatment of enamine **3.165** could unlock the desired reactivity and mechanism by generating a metalloenamine/enolate intermediate.

Enamine **3.165** contains four acidic protons. To assess their relative acidity, pK_a values were computationally calculated using Chemicalize [Chemicalize was used for prediction of pK_a properties, July, 2025, https://chemicalize.com/ developed by ChemAxon (http://www.chemaxon.com)], by comparison to known acidic scaffolds. The pK_a values for H1(10.93), H11 (15.50) and H20 (14.87) could be successfully calculated (**Scheme 3.22**), however, the value for the desired deprotonation site, H15, could not. It was postulated that H15 may be more acidic than H1 as deprotonation at this position would generate a malonate-like metalloenamine species capable of stabilising the resulting negative charge via resonance, analogous to classical enolate stabilisation. Moreover, initial deprotonation at H1 was not expected to pose a problem, as the resulting negative charge was thought to delocalise into non-productive enolate resonance structures. Consequently, it was anticipated that the reaction could be carried out under equilibrium conditions.

Gratifyingly, treatment of enamine **3.165** with KHMDS (1.2 eq.) in THF afforded desired sulfide **3.166** in 59% yield (**Scheme 3.22**). Substitution of THF with ethanol (thus generating potassium ethoxide *in situ*) resulted in only a modest decrease in yield to 42%, potentially enabling the development of a telescoped addition–elimination/base-induced cyclisation sequence.

3.22 | *base-induced intramolecular cyclisation of enamine **3.165** to sulfide **3.166**:*

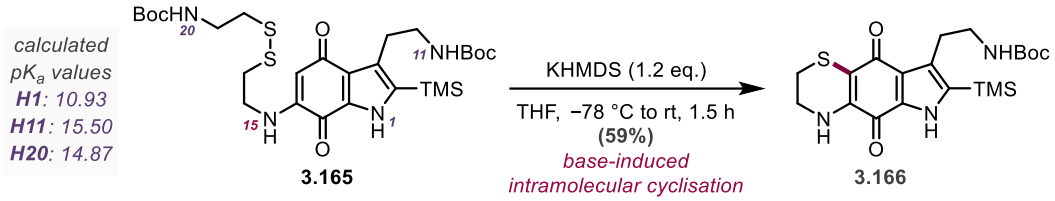

Scheme 3.22. *Base-induced cyclisation of enamine **3.165** to sulfide **3.166**.*

In summary, a range of conditions were evaluated for disulfide bond cleavage; however, the desired sulfide **3.166** was obtained only in trace amounts using Cleland's reagent **3.147** or tributyl phosphine. It was proposed that the inefficiency in forming sulfide **3.166** stemmed from progression through a hydroquinone intermediate following *thia*-Michael addition. To address this, the strategy was revised to promote direct intramolecular attack by the enamine, with the desired reactivity achieved via the potassium metalloenamine/enolate upon deprotonation. With a method established for the conversion of enamine **3.165** to sulfide **3.166** using KHMDS, efforts were refocused on optimising the synthesis of the enamine precursor for this transformation.

3.5.6.6. Optimising dihydrothiazine formation

3.5.6.6.1. Use of cystamine 3.153

To improve yields in the addition–elimination sequence, the use of strong bases was explored to accelerate the conversion of indolequinone **3.89** to enamine **3.165** and also promote cyclisation of **3.165** to sulfide **3.166**. However, stability studies revealed that cystamine **3.156** underwent disulfide scrambling under basic conditions, particularly with strong bases such as KHMDS (**Figure 3.4**) or sodium hydride. This led to mixtures of reactive, unprotected cystamine **3.153**, partially-protected cystamine **3.156**, and unreactive, fully-protected cystamine **3.154**. Evidence of scrambling was also observed for weaker bases, such as *N*,*N*-diisopropylethylamine (DIPEA), but at a reduced rate. It was postulated that scrambling was also temperature-dependent, with elevated temperatures exacerbating the issue (refer back to **Section 3.5.6.2.** Addition–elimination with cystamine **3.156**).

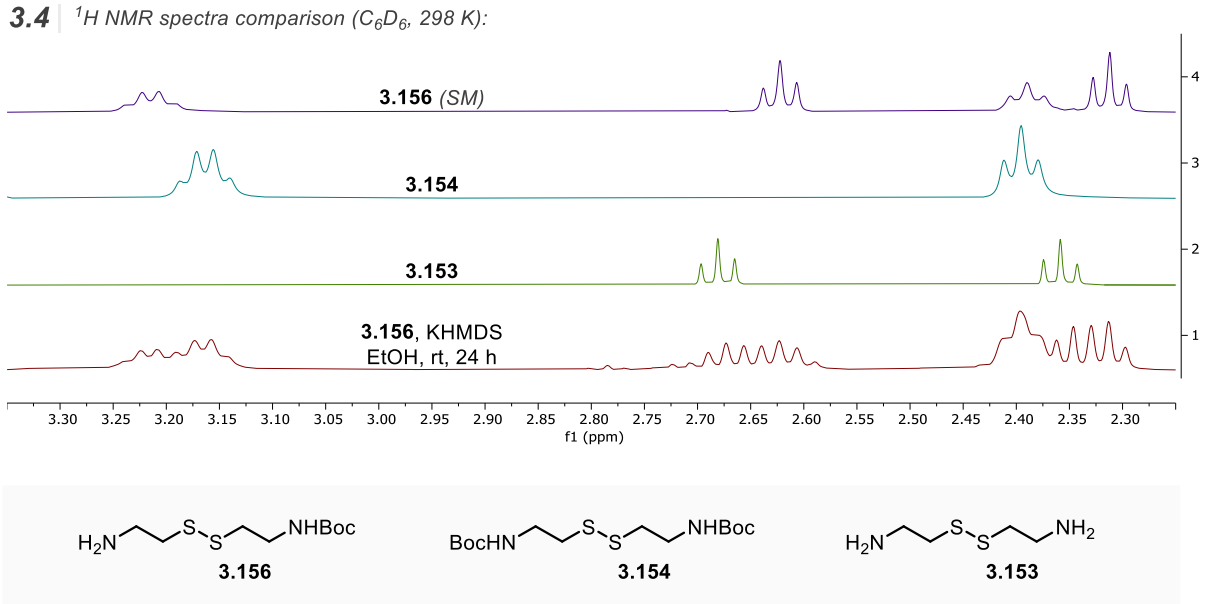

Figure 3.4. *Stability test of cystamine **3.156** in the presence of KHMDS in ethanol. Monitored by ¹H NMR spectroscopy (benzene-d6, 298 K) after 24 hours.*

These findings highlighted the advantage of using a symmetrical amine, such as cystamine **3.153**. It was believed this would enable the use of a base and elevated temperatures to improve the formation of enamine **3.183**, and possibly sulfide **3.166**.

Cystamine **3.153** was prepared in 81% yield by free-basing the dihydrochloride salt. Treatment of indolequinone **3.89** with cystamine **3.153** (10 eq.) and NEt_3 (10 eq.) in ethanol at room temperature afforded enamine **3.183** (**Scheme 3.23**) and, gratifyingly, sulfide **3.166**. Following a solvent swap to THF, the crude mixture was treated with KHMDS (1.5 eq.), furnishing sulfide **3.166** in 50% yield over two steps (**Scheme 3.23** table, entry 1). Alternatively, conducting the addition–elimination at 80 °C enabled a one-pot conversion of indolequinone **3.89** directly to sulfide **3.166** in a comparable 53% yield (**Scheme 3.23** table, entry 2).

3.23 *addition–elimination–cyclisation sequence of indolequinone **3.89** to sulfide **3.166**:*

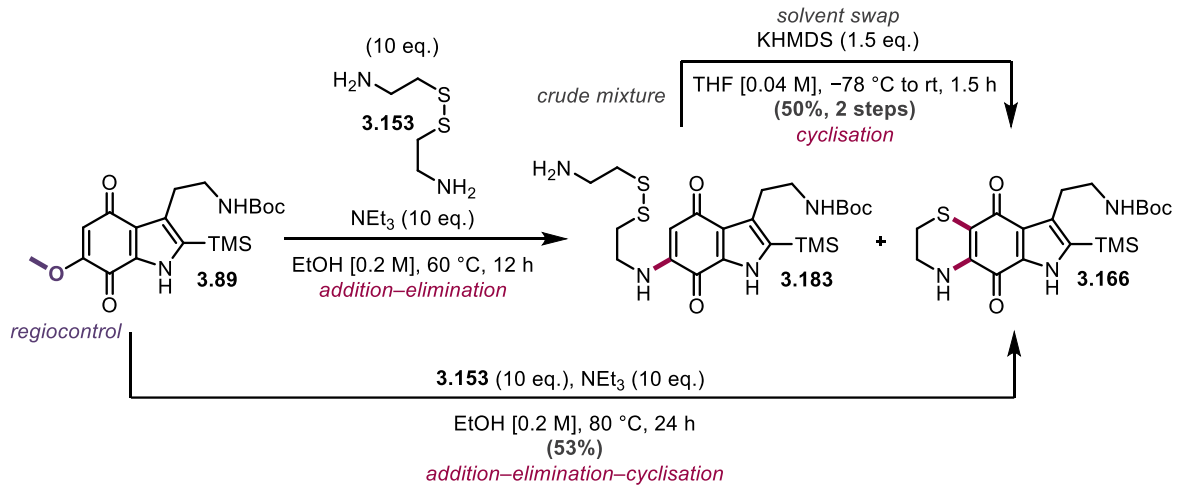

entry	*method*	*scale / mmol*	*yield of 3.166 / %*
1	*two-step*	0.01	50
2	*one-step*	0.01	53
3	*one-step*	0.05	39
4	*one-step*	0.150	23
5	*two-step*	0.500	31
6	*two-step*	4.000	14

Scheme 3.23. *Addition–elimination–cyclisation sequence of indolequinone **3.89** to sulfide **3.166**.*

While this one-pot process was initially promising, scale-up led to a decline in yield (**Scheme 3.23** table, entries 3 & 4). The stepwise approach was therefore adopted, but increasing the scale again resulted in diminished yields (**Scheme 3.23** table, entries 5 & 6). Rather than solely treating the crude mixture from *Step 1* to a solvent swap, sulfide **3.166** was isolated after the initial addition–elimination step in 21% yield; however, treatment of the remaining enamine **3.183** with KHMDS afforded sulfide **3.166** in only 15% yield.

Given that this sequence was the synthetic bottleneck, further optimisation was pursued. It was hoped that identifying optimal base–solvent conditions would enable the addition–elimination–cyclisation sequence to consistently afford sulfide **3.166** in good yield.

3.5.6.6.2. High-throughput experimentation

It was proposed that the problematic step during the formation of the dihydrothiazine ring was the base-induced cyclisation of unprotected enamine **3.183**. Alternative base–solvent combinations were sought to more efficiently convert indolequinone **3.89** to sulfide **3.166** (**Scheme 3.24**) – thus obviating the need of a second step for the base-induced cyclisation of enamine **3.183**. It was envisioned that high-throughput experimentation (HTE) could be used for this purpose, since it is a technique that leverages automation to rapidly test and analyse a large number of experiments simultaneously.

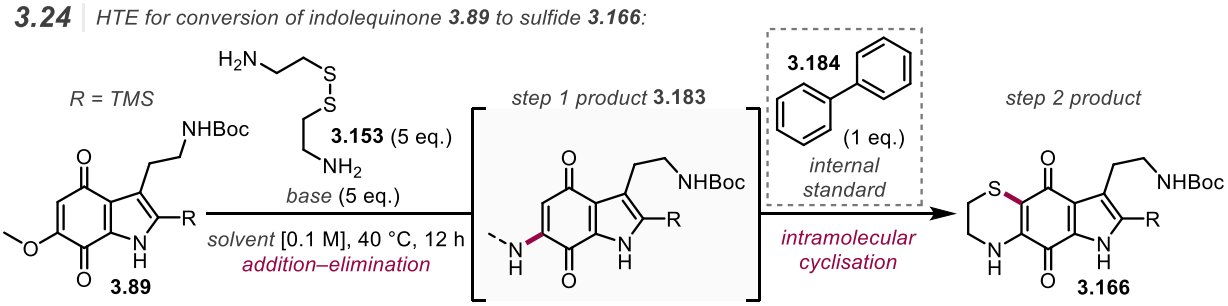

Scheme 3.24. *Use of HTE to explore base–solvent conditions for the conversion of indolequinone* ***3.89*** *to sulfide* ***3.166****.*

The initial screen focussed on the effect of different solvents and bases (**Figure 3.5**), with the original base–solvent combination (triethylamine in ethanol) included to enable direct comparison with alternative conditions. Based on prior reaction studies on the generation of enamines from quinones (refer back to **Scheme 2.12B** & **3.19B**), it was hypothesised that alcoholic solvents were beneficial, but it was unclear if they were required. Accordingly, four alcoholic solvents were selected for evaluation (ethanol, hexafluoroisopropanol (HFIP), isopropanol, methanol) along with four non-alcoholic solvents (dichloromethane, acetonitrile, toluene, THF) with a range of different polarities and dielectric constants. In combination with these solvents, three organic (1,8-diazabicyclo[5.4.0]undec-7-ene (DBU), DIPEA, triethylamine) and three inorganic bases (caesium carbonate, aqueous KOH, sodium bicarbonate) were screened. In all the HTE screens, the reactions were performed with fixed equivalents of

cystamine **3.153** (5 equivalents) and base (5 equivalents) at a fixed scale (0.005 mmol), concentration [0.1 M], temperature (40 °C), and duration (12 hours) (**Scheme 3.24**). After 12 hours, internal standard **3.184** (1 equivalent) was added and the crude reaction mixtures were analysed by UPLC. Each base–solvent combination was evaluated using three ratios calculated from the relative integrals between the three key species, sulfide **3.166**, enamine **3.183**, and indolequinone **3.89**, relative to internal standard **3.184**, respectively. The term 'mass balance' refers to the sum of all quantifiable components in a reaction mixture, and serves as a key metric for monitoring reaction conversion and material loss from decomposition. In the context of this work, mass balance will refer to the sum of the three calculated ratios relative to internal standard **3.184**.

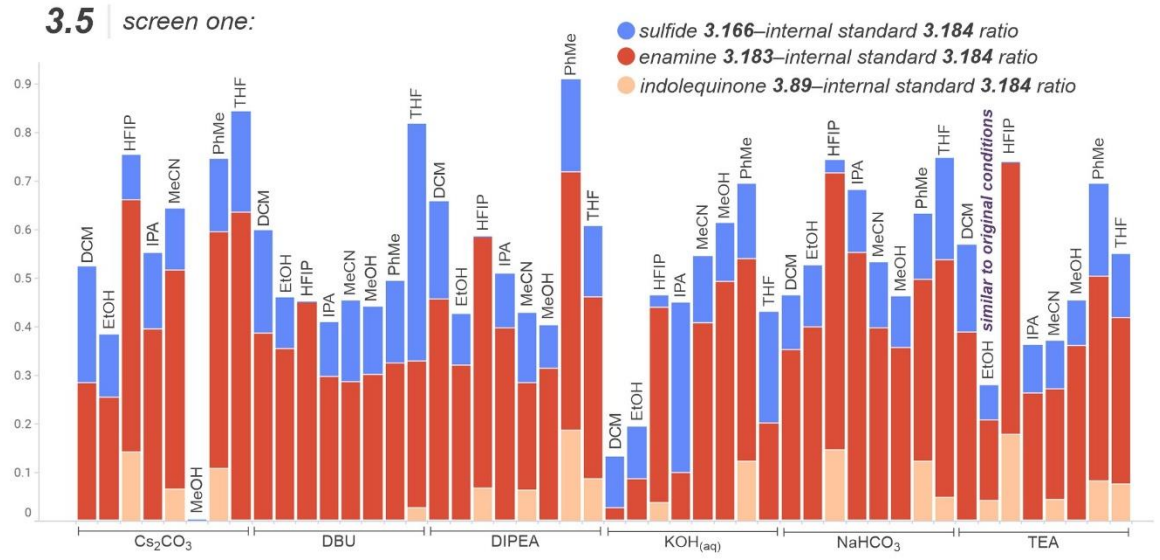

Figure 3.5. *HTE screen one. Three organic and three inorganic bases screened with four alcoholic and four non-alcoholic solvents. Cystamine* ***3.153*** *(5 eq.) and base (5 eq.) at a fixed scale (0.005 mmol), concentration [0.1 M], temperature (40 °C), and duration (12 hours). Where DBU = 1,8-diazabicyclo[5.4.0]undec-7-ene, DIPEA = N,N-diisopropylethylamine, TEA = triethylamine, DCM = dichloromethane, HFIP = hexafluoroisopropanol, IPA = isopropanol, THF = tetrahydrofuran.*

Based on the combined ratios of enamine **3.183** and sulfide **3.166** to the internal standard **3.184**, the non-alcoholic solvents were observed to perform better than alcoholic solvents across a greater range of bases, with base–solvent combination DBU in THF performing the best (0.79). Additionally, aqueous KOH in isopropanol, likely generating potassium isopropoxide *in situ*, performed well for the synthesis of desired sulfide **3.166** based on the sulfide **3.166**–internal standard **3.184** ratio (0.35). However, the mass balance was poor (0.45). In contrast, the previous

base–solvent combination of triethylamine in ethanol was one of the worst-performing. Although HFIP performed poorly for the synthesis of sulfide **3.166**, across a range of bases, based on the sulfide **3.166**–internal standard **3.184** ratios, it proved to be an excellent solvent for the synthesis of enamine **3.183**; for example, triethylamine in HFIP achieving a high enamine **3.183**–internal standard **3.184** ratio (0.56). Since HFIP is considered mildly acidic, owing to the negative inductive effect of the trifluoromethyl groups ($pK_{a(water)}$ = 9.3 versus for isopropanol: $pK_{a(water)}$ = 17.1),[134] this may suggest the addition–elimination step favours acid catalysis (or at least activation of the electrophile by hydrogen bonding). No apparent differences in the performance of organic versus inorganics bases was observed during this screen.

Given the first screen demonstrated that non-alcoholic solvents gave higher sulfide **3.166**–internal standard **3.184** ratios across a wide range of bases, for the second screen (**Figure 3.6**), primarily non-alcoholic solvents (2-methyltetrahydrofuran (2-MeTHF), 1,4-dioxane, dimethylacetamide (DMA), dimethyl sulfoxide (DMSO), ethyl acetate (EA), *N*-methyl-2-pyrrolidone (NMP), pyridine) were selected. Since THF was a high-performing solvent during the previous screen we wanted to evaluate the more sustainable alternative 2-MeTHF which boasts other advantages in its higher boiling point (78 versus 66 °C for THF; greater reaction temperature range) and immiscibility with water (providing a work-up advantage).[135] Highly polar aprotic solvents can provide enhanced basicity of ionic bases through cation coordination and the reduction of aggregation making the anion more 'naked' thus this was also explored by screening DMA, DMSO, and NMP.[136,137] For completion of the alcoholic solvents, the tertiary alcohol *tert*-amyl alcohol (TAA) was also screened as a more operationally convenient equivalent of *tert*-butanol since it is liquid at room temperature. Pyridine was selected as a solvent to investigate because it is also basic ($pK_{a(water)}$ of conjugate acid = 5.18).[138] Again, a mixture of two organic bases (DABCO, 4-dimethylaminopyridine (DMAP)) and three inorganic bases (monopotassium phosphate (MKP), aqueous NaOH, potassium carbonate), were screened with the aforementioned solvents. Both DABCO and DMAP were screened as bases since they could potentially also act as nucleophilic catalysts.[139,140] The acidic additive guanidinium chloride was

also evaluated to determine whether it performed similarly to HFIP in promoting the formation of enamine **3.183**.

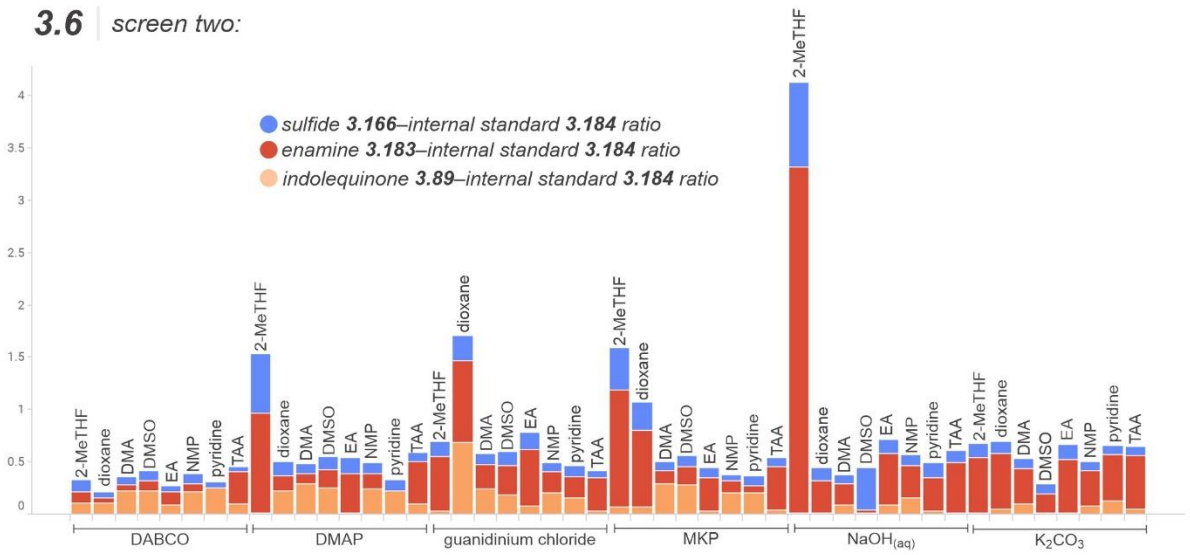

Figure 3.6. *HTE screen two. Three organic and three inorganic bases screened with solvents. Cystamine **3.153** (5 eq.) and base (5 eq.) at a fixed scale (0.005 mmol), concentration [0.1 M], temperature (40 °C), and duration (12 hours). Where DABCO = 1,4-diazabicyclo[2.2.2]octane, DMAP = 4-dimethylaminopyridine, MKP = monopotassium phosphate, 2-MeTHF = 2-methyltetrahydrofuran, dioxane = 1,4-dioxane, DMA = dimethylacetamide, DMSO = dimethyl sulfoxide, EA = ethyl acetate, NMP = N-methyl-2-pyrrolidone, TAA = tert-amyl alcohol.*

Based on the combined ratios of enamine **3.183**–internal standard **3.184** and sulfide **3.166**–internal standard **3.184**, the two ethereal solvents 2-MeTHF and 1,4-dioxane performed best across a greater range of bases/additives, such as: DMAP in 2-MeTHF, guanidinium chloride in 1,4-dioxane, and MKP in 2-MeTHF or 1,4-dioxane. To a lesser extent, EA also performed well as a solvent across a range of bases/additives. Although at first glance, the combination of aqueous NaOH in 2-MeTHF appeared to be superior, the unusually high combined value of the three ratios to internal standard **3.184** (4.11) raises concerns regarding validity; however, it has been included for completeness. Additionally aqueous NaOH in DMSO, a solvent known to enhance the basicity of metal hydroxide bases, performed well for the synthesis of sulfide **3.166** based on the sulfide **3.166**–internal standard **3.184** ratio (0.41). However, poor mass balance was suggested by the low combined total of the three ratios to internal standard **3.184** (0.44). Again, no apparent differences in the performance of organic versus inorganics bases was observed during this screen.

For screen three (**Figure 3.7**), bases and solvents were carefully selected based on previous findings. Based on the previous observation that ethereal solvents (THF, 2-MeTHF, 1,4-dioxane) performed the best across the range of bases used for each, for the third screen more ethereal solvents were investigated (cyclopentyl methyl ether (CPME), dimethoxyethane, methyl *tert*-butyl ether (MTBE), *N*-methylmorpholine (NMM)). Mixtures of THF with water as a co-solvent were also explored, as such mixtures were shown to have dramatically different solvent properties.[141,142] Additionally, due to the moderate performance of EA, isopropyl acetate was also evaluated as an alternative. Similarly to DMSO, DMF is a highly polar aprotic solvent known to enhance the basicity of bases,[136,137] accordingly, it was included in the evaluation for completeness. As in the previous two screens, it was ensured that more sustainable solvent alternatives were also considered, for example *N*-butylpyrrolidinone (NBP) as an alternative to NMP.[143] Since the amidine base DBU performed well in a previous screen, we opted to screen the five-membered ring analogue 1,5-diazabicyclo[4.3.0]non-5-ene (DBN) which possesses slightly greater nucleophilicity compared with its nine-membered counterpart.[144] Additionally, tetramethylguanidine (TMG, pK_a of the conjugate acid in acetonitrile = 24.3)[145] was selected since guanidine bases possess similar basicities to the amidine base series. The analogous inorganic base class to amidine bases is the non-ionic phosphazene superbases, it was proposed that the enhanced nucleophilicity and basicity of *tert*-butylimino-2-diethylamino-1,3-dimethylperhydro-1,3,2-diazaphosphorine (BEMP) and phosphazene base P_2-Et compared with DBU were worth exploring.[146] Due to the success of MKP (in 2-MeTHF or 1,4-dioxane) in the previous screen, the more basic tripotassium phosphate (TKP) was also evaluated. Since aqueous KOH in isopropanol performed well in synthesising sulfide **3.166**, *tert*-butoxide was screened as well.

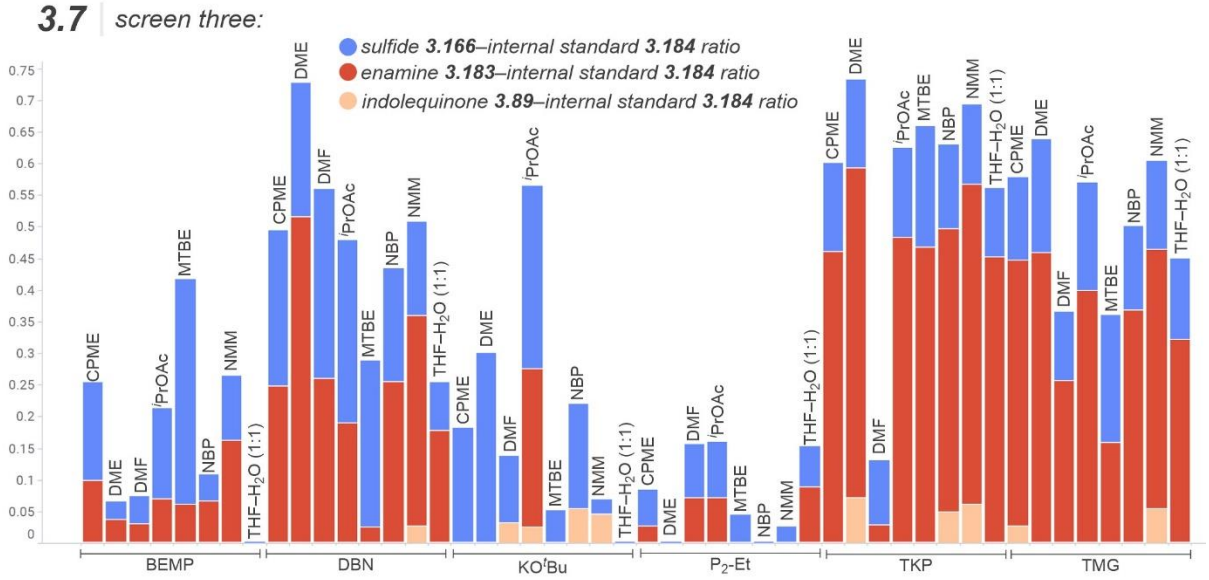

Figure 3.7. *HTE screen three. Cystamine* ***3.153*** *(5 eq.) and base (5 eq.) at a fixed scale (0.005 mmol), concentration [0.1 M], temperature (40 °C), and duration (12 hours). Where BEMP = tert-butylimino-2-diethylamino-1,3-dimethylperhydro-1,3,2-diazaphosphorine, DBN = 1,5-diazabicyclo[4.3.0]non-5-ene, TKP = tripotassium phosphate, TMG = tetramethylguanidine, CPME = cyclopentyl methyl ether, DME = dimethoxyethane, MTBE = methyl tert-butyl ether, NBP = N-butyl-2-pyrrolidone, NMM = N-methylmorpholine, THF = tetrahydrofuran.*

In terms of mass balance, the phosphazene superbases performed worse compared to other base classes across a larger range of solvents, with the more basic phosphazene base P$_2$-Et (pK_a of the conjugate acid in acetonitrile = 32.7) performing worse than BEMP (pK_a of the conjugate acid in acetonitrile = 27.6). It is worth noting, BEMP in MTBE performed well for the synthesis of sulfide **3.166** based on the sulfide **3.166**–internal standard **3.184** ratio (0.36), albeit with low overall mass balance (0.42). Overall mass balance was also poor for potassium *tert*-butoxide in a range of solvents, however in combination with dimethoxyethane or isopropyl acetate it performed well in synthesising sulfide **3.166** based on the sulfide **3.166**–internal standard **3.184** ratio (0.30 & 0.29, respectively). Both TKP and TMG performed the best in terms of overall mass balance over a greater range of solvents, but DBN performed the best in synthesising sulfide **3.166** based on the sulfide **3.166**–internal standard **3.184** ratio.

For the fourth and final screen (**Figure 3.8**), the best-performing bases and solvents from previous screens were combined. Bases/solvents which had a significantly higher sulfide **3.166**–internal standard **3.184** ratio and performed consistently well across a wide range of different combinations were selected. Additionally, those which had good mass balance based on the three

ratios combined, indicating minimal decomposition and/or the reaction was incomplete, were considered. Three organic (DBU, DMAP, TMG) and three inorganic bases (caesium carbonate, MKP, aqueous KOH) were selected to be screened with four ethereal (2-MeTHF, 1,4-dioxane, dimethoxyethane, THF) and four non-ethereal solvents (dichloromethane, DMSO, isopropyl acetate, toluene).

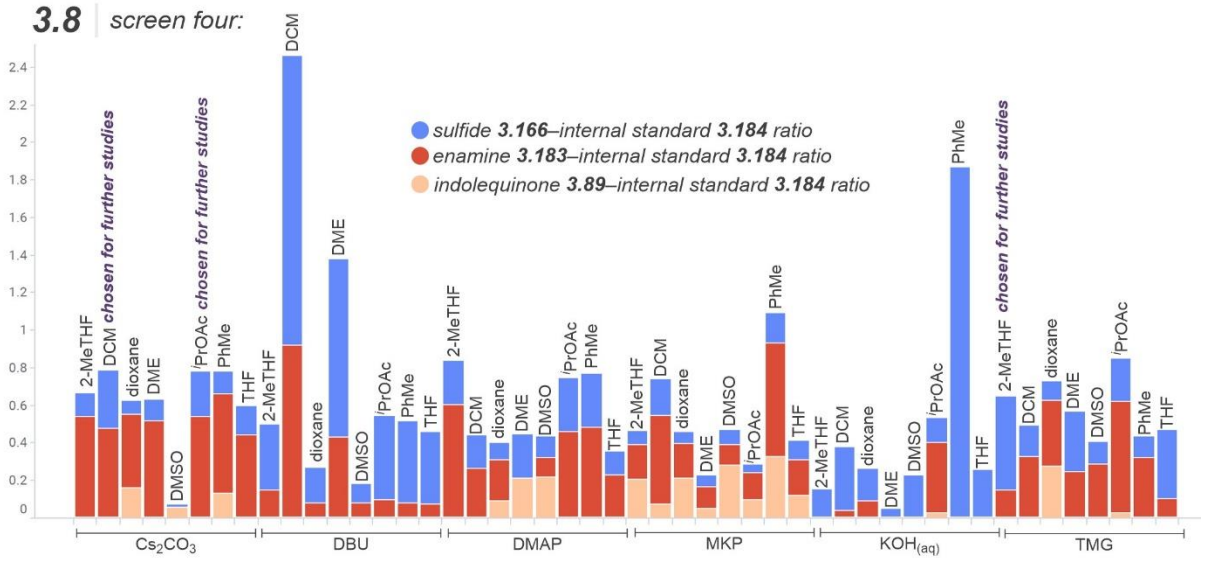

Figure 3.8. *HTE screen four – base bases in best solvents. Cystamine* ***3.153*** *(5 eq.) and base (5 eq.) at a fixed scale (0.005 mmol), concentration [0.1 M], temperature (40 °C), and duration (12 hours). Where DBU = 1,8-diazabicyclo[5.4.0]undec-7-ene, DMAP = 4-dimethylaminopyridine, MKP = monopotassium phosphate, TMG = tetramethylguanidine, 2-MeTHF = 2-methyltetrahydrofuran, DCM = dichloromethane, dioxane = 1,4-dioxane, DME = dimethoxyethane, DMSO = dimethyl sulfoxide, , THF = tetrahydrofuran.*

Several base–solvent combinations had previously been evaluated and some discrepancies were observed between the two set of results. For example, in screen one DBU in THF was one of the best-performing base–solvent combinations, out-performing DBU in dichloromethane. However, in screen four DBU performed significantly better in dichloromethane – the large value from the combination of all three ratios (2.46) suggests this may be due to operator error when dispensing the plate. Additionally, aqueous KOH in toluene had resulted in a mixture of enamine **3.183** and sulfide **3.166** with indolequinone **3.89** in screen one – with the former possessing the largest ratio versus internal standard **3.184**. However, in screen four solely sulfide **3.166** was observed and at a high ratio versus internal standard **3.184** (1.87). Due to the small scale of the reaction (0.005 mmol) a small volume of solvent was required for a concentration of 0.1 M. Additionally,

the reaction vials were not sealed with individual caps, rather the whole plate was sealed instead, and heating was not completely uniform across the plate, which may have led to evaporation and concentration differences. Collectively, this may have acted as a source of experimental error.

Reaction conditions that afforded both relatively high sulfide **3.166**–internal standard **3.184** ratios and clean UPLC spectra were prioritised for further study, as these criteria were suggestive of efficient conversion and minimal decomposition. On this basis, the following base–solvent combinations were selected: (1) caesium carbonate in dichloromethane, (2) caesium carbonate in isopropyl acetate, and (3) TMG in 2-MeTHF. To validate these results, each reaction was subsequently performed on a 10-fold greater scale (0.05 mmol) (**Scheme 3.25A**).

3.25A | *optimisation of the conversion of indolequinone **3.89** to sulfide **3.166**:*

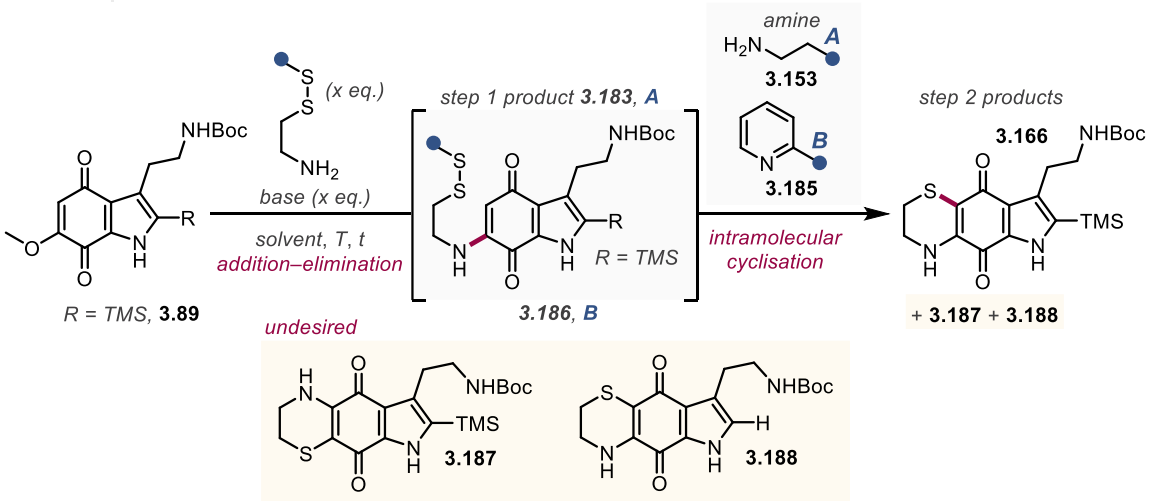

3.25B | *optimisation table:*

entry	*amine (eq.)*	*base (eq.)*	*solvent [concentration]*	*T / °C*	*t / h*	*combined yield / %*	*3.166–3.187 rr*	*yield of 3.166 / %*
1	A (5 eq.)	Cs_2CO_3 (5 eq.)	^{i}PrOAc [0.10 M]	40	48	21	6.7:1	18
2	A (5 eq.)	Cs_2CO_3 (5 eq.)	^{i}PrOAc–MeOH (9:1) [0.10 M]	40	48	13	1.6:1	8
3	A (5 eq.)	Cs_2CO_3 (5 eq.)	^{i}PrOAc [0.05 M]	90	2.5	19	1:1.6	7
4	A (5 eq.)	Cs_2CO_3 (10 eq.)	^{i}PrOAc [0.05 M]	90	4.5	19	1:2.6	5
5[a]	A (10 eq.)	Cs_2CO_3 (5 eq.)	^{i}PrOAc [0.05 M]	90	2	46	1:1.2	21
6[b]	A (10 eq.)	Cs_2CO_3 (5 eq.)	^{i}PrOAc [0.05 M]	90	2	46	1:1.1	22
7	B (10 eq.)	Cs_2CO_3 (5 eq.)	^{i}PrOAc [0.05 M]	90	12	2	50:1	2
8	A (10 eq.)	Cs_2CO_3 (2.5 eq.)	^{i}PrOAc [0.05 M]	90	12	13	6.5:1	11
9	A (10 eq.)	/	^{i}PrOAc [0.05 M]	90	12	1	200:1	1
10	A (20 eq.)	/	^{i}PrOAc [0.05 M]	90	12	6	200:1	6

***Scheme 3.25. (A)** Conversion of indolequinone **3.89** to sulfide **3.166** using base–solvent combinations identified by HTE. **(B)** Optimisation table. Where a = modified work-up passing through a pipette containing silica gel, b = modified work-up adding a solution of 1 M HCl, extracting with EA and passing the organic layers through a pipette containing anhydrous magnesium sulfate.*

For the base–solvent combination of caesium carbonate in dichloromethane the UPLC spectrum showed predominantly unreacted indolequinone **3.89** starting material and enamine **3.183** when monitoring the reaction after 24 hours at 40 °C, therefore this was not explored further (not shown in table). However, this discrepancy may be attributed to the low boiling point of the solvent, which likely led to increased reaction concentration via evaporation on small-scale.

Conversely, for caesium carbonate in isopropyl acetate (**Scheme 3.25B** table, entry 1), significant sulfide **3.166** was observed by UPLC after 24 hours. After 48 hours, the reaction was worked up and purified by column chromatography which enabled the discovery by ^{1}H NMR spectroscopy that sulfide **3.166** had been formed alongside undesired regioisomer **3.187** (**Scheme 3.25A**) in a 6.7:1.0 ratio (determined by quantitative ^{1}H NMR spectroscopy). Sulfide **3.166** and **3.187** possessed the same retention times by UPLC across multiple elution methods and columns – and were similarly inseparable by column chromatography – however they were found to be separable by analytical supercritical fluid chromatography (SFC). Consequently, undesired regioisomer **3.187** may have slightly inflated the sulfide **3.166**–internal standard **3.184** ratios obtained during screening. Although the UPLC spectrum appeared relatively clean for entry 1, the isolated 18% of sulfide **3.166** was relatively low. Two possible reasons for the low yield were hypothesised: (1) poor solubility of enamine **3.183** could result in precipitation out of the reaction mixture, or (2) lower stability of enamine **3.183** versus its reactivity – the rate of decomposition of enamine **3.183** could be greater than the rate of formation of sulfide **3.166**. Thus, to ensure enamine **3.183** remained in solution, the addition of a co-solvent or reduction of reaction concentration was considered. Furthermore, increasing the equivalents of cystamine **3.153** and caesium carbonate, along with elevating the reaction temperature, was expected to shift the equilibrium toward formation of sulfide **3.166**.

When methanol was included as a co-solvent with isopropyl acetate (isopropyl acetate–methanol 9:1) in an effort to prevent precipitation (**Scheme 3.25B** table, entry 2), both a decrease in yield and regioisomeric ratio (*rr*) (1.6:1.0 **3.166**–**3.187**, 8% yield of **3.166**) was observed compared to entry 1. When instead the concentration was decreased to 0.05 M and the temperature was increased to 90 °C, to increase the rate of conversion of enamine **3.183** to sulfide **3.166**, (**Scheme 3.25B** table, entry 3) the yield of sulfide **3.166** decreased from entry 1, with this time the undesired regioisomer being favoured (1.0:1.6 **3.166**–**3.187**, 7% yield of **3.166**). When the equivalents of caesium carbonate were increased to 10 (**Scheme 3.25B** table, entry 4) the undesired regioisomer **3.187** was further favoured (1.0:2.6 **3.166**–**3.187**; 5% yield of **3.187**),

although the reason for this is unknown. Increasing the equivalents of cystamine **3.153** to 10 was explored in entries 5 and 6, while the equivalents of caesium carbonate were maintained constant, as in entry 3. Additionally, instead of purifying by column chromatography the work-up procedure was modified either by passing the reaction mixture through a silica plug (**Scheme 3.25B** table, entry 5) or by acidic aqueous work-up (**Scheme 3.25B** table, entry 6), obviating the need for further purification. For both entries 5 and 6 this led to a comparable yield of sulfide **3.166** as entry 1 (21% and 22%, respectively), however the *rr* remained poor (1.0:1.2 and 1.0:1.1 **3.166**–**3.187**, respectively). To confirm that cystamine **3.513** was the best choice of nucleophile for the construction of the dihydrothiazine ring, the amine was changed from cystamine **3.153** to amine **3.185** (**Scheme 3.25B** table, entry 7). Interestingly, the *rr* improved (50:1 **3.166**–**3.187**), however, purification by column chromatography was required and the yield was low (2%). Amine **3.185** was observed to readily undergo disulfide exchange during storage, therefore the lower effective equivalents of nucleophile (refer back to **Figure 3.4**) could have contributed to the low isolated yield.

Returning to cystamine **3.153**, when the equivalents of caesium carbonate was further decreased to 2.5 (**Scheme 3.25B** table, entry 8) a similar *rr* (6.5:1.0 **3.166**–**3.187**) was observed, however the yield of sulfide **3.166** decreased to 11% yield – therefore no improvement from entry 1 was achieved. As cystamine **3.153** can itself act as a base, removing caesium carbonate from the reaction was also investigated (**Scheme 3.25B** table, entry 9). This resulted in almost complete shutdown of the desired reactivity, with sulfide **3.166** isolated in 1% yield alongside unknown by-products, although good *rr* was observed. Increasing the equivalents of cystamine **3.153** to 20 (**Scheme 3.25B** table, entry 10) in the absence of caesium carbonate did give a marginal improvement in yield, giving 6%, but not to a synthetically useful value.

With no improvement in the yield and *rr* observed for caesium carbonate in isopropyl acetate, we moved our attention to the other promising base–solvent combination, TMG in 2-MeTHF. Using the same conditions as entry 1 (**Scheme 3.26B** table, entry 11), the same, 18%, yield of sulfide

3.166 was obtained however thankfully a much higher *rr* was observed (17:1 **3.166–3.187**). When the reaction concentration was halved to 0.05 M to prevent precipitation, the equivalents of cystamine **3.153** and TMG were doubled, and the temperature was increased to 80 °C to favour conversion of enamine **3.183** to sulfide **3.166**, (**Scheme 3.26B** table, entry 12) no notable effect was observed on the yield (16% yield) or the *rr* (17:1 **3.166–3.187**) compared to entry 11. When only the equivalents of TMG were doubled (5 to 10 eq.), and both the temperature (40 to 70 °C) and the concentration [0.1 to 0.5 M] were increased (**Scheme 3.26B** table, entry 13), compared to entry 11, a marginal increase in the yield of sulfide **3.166** to 22% was observed, however this was off-set by a decrease in the *rr* (5.6:1.0 **3.166–3.187**). When the equivalents of TMG were halved to 5 versus entry 12 but other reaction conditions remained constant (**Scheme 3.26B** table, entry 14) a decrease in the yield of sulfide **3.166** to 10% was observed – while *rr* marginally increased (20:1 **3.166–3.187**). When the reaction temperature was decreased to 60 °C but the concentration was increased to 0.2 M (**Scheme 3.26B** table, entry 15) the same 18% yield of sulfide **3.166** was achieved, however a notable decrease in the *rr* was observed (11:1 **3.166–3.187**) compared to entry 11. A similar observation of decreasing *rr* with reaction concentration was observed with entry 13. It appeared that for the base–solvent combination of TMG in 2-MeTHF, base loading or reaction temperature had no observed effect on *rr*, however increasing the reaction concentration impacted it negatively.

3.26A | *optimisation of the conversion of indolequinone **3.89** to sulfide **3.166**:*

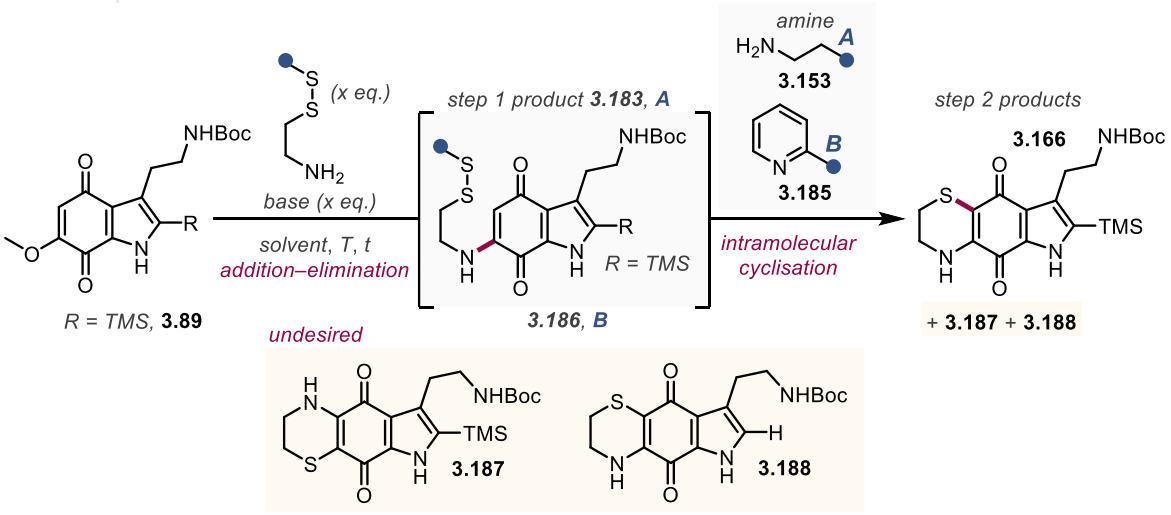

3.26B | *optimisation table:*

entry	*amine (eq.)*	*base (eq.)*	*solvent [concentration]*	*T / °C*	*t / h*	*combined yield / %*	*3.166–3.187 rr*	*yield of 3.166 / %*
11	A (5 eq.)	TMG (5 eq.)	2-MeTHF [0.10 M]	40	48	19	17:1	18
12	A (10 eq.)	TMG (10 eq.)	2-MeTHF [0.05 M]	80	12	17	17:1	16
13	A (5 eq.)	TMG (10 eq.)	2-MeTHF [0.50 M]	70	24	26	5.6:1	22
14	A (10 eq.)	TMG (5 eq.)	2-MeTHF [0.05 M]	80	24	11	20:1	10
15	A (10 eq.)	TMG (5 eq.)	2-MeTHF [0.20 M]	60	24	20	11:1	18
16	A (10 eq.)	TMG (5 eq.)	2-MeTHF–D_2O (9:1) [0.05 M]	80	12	5	2.9:1	4
17	A (10 eq.)	TMG (5 eq.)	2-MeTHF–CD_3OD (9:1) [0.05 M]	80	12	20	8.3:1	18
18[c]	A (10 eq.)	TMG (5 eq.)	2-MeTHF [0.05 M]	50	24	17	25:1	16
19[c]	A (10 eq.)	TMG (5 eq.)	2-MeTHF [0.05 M]	70	24	25	33:1	24
20[c]	A (10 eq.)	TMG (5 eq.)	THF [0.05 M]	70	24	18	20:1	17
21[c]	B (10 eq.)	TMG (5 eq.)	2-MeTHF [0.05 M]	70	48	0	*NA*	0
22[c,d]	A (10 eq.)	TMG (5 eq.)	2-MeTHF [0.05 M]	70	24	33	17:1	32

3.26C | *oxidation of sulfide **3.188** to sulfone **3.22**:*

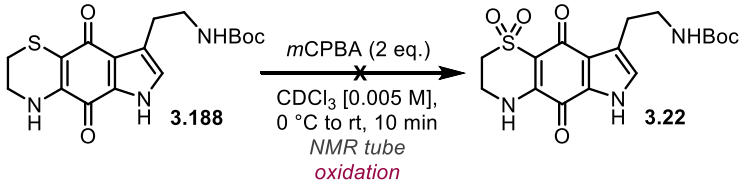

***Scheme 3.26. (A)** Conversion of indolequinone **3.89** to sulfide **3.166** using base–solvent combinations identified by HTE. **(B)** Optimisation table. Where c = with activated 4 Å molecular sieves, d = using purified indolequinone **3.89**. **(C)** Sulfide **3.188** was unable to be oxidised to sulfone **3.22** using mCPBA.*

For entries 1–15 C2-desilylated sulfide **3.188** was often isolated in trace quantities. It was speculated that **3.188** would be less soluble and more polar than sulfide **3.166** and more prone to be lost during aqueous work-up – likewise with enamine **3.183**. To evaluate whether C2-desilylated sulfide **3.188** was a useful compound for the synthesis of thiaplakortone A **1.12**, oxidation with *m*CPBA in chloroform-d_1 was trialled and the reaction monitored by ^{1}H NMR spectroscopy (**Scheme 3.26C**). However after 10 minutes at 0 °C, followed by warming to room temperature during the timescale of the NMR experiment, neither sulfone **3.22** or sulfide **3.188** were detected. Instead, decomposition was observed (see later **Table 3.3** for oxidation of sulfide **3.166**; 53% isolated yield). This highlighted the significance of ensuring minimal C2-desilylation, which presumably occurred due to the presence of a strong nucleophilic base. However, the exact reason is unknown since the C2-silyl group is more commonly recognised for its acid lability (refer back to **Scheme 3.16A** and see later **Scheme 3.32C**).

To maintain solubility of all components, co-solvents were introduced. Deuterated solvents, specifically deuterium oxide (**Scheme 3.26B** table, entry 16) and methanol-d_4 (**Scheme 3.26B** table, entry 17), were selected as their reduced acidity due to the kinetic isotope effect was expected to suppress the *in situ* generation of a strong base.[147] However, like with entry 2 with caesium carbonate in isopropyl acetate, a decrease in *rr* (2.9:1.0 and 8.3:1.0 **3.166–3.187**, respectively) was observed for entry 16 and 17 versus 14 – with the yield of sulfide **3.166** notably decreasing to 4% when deuterium oxide was used as a co-solvent (**Scheme 3.26B** table, entry 16), with more C2-desilylated sulfide **3.188** isolated. Given that the elimination reaction generates an equivalent of methoxide, the use of activated 4 Å molecular sieves was thus investigated to sequester the liberated nucleophilic base. Additionally, lower reaction temperatures were investigated in an effort to suppress the formation of undesired sulfide **3.187** and **3.188**. When the temperature was decreased to 50 °C (**Scheme 3.26B** table, entry 18) or 70 °C (**Scheme 3.26B** table, entry 19) with the inclusion of 4 Å molecular sieves, while the yield of sulfide **3.166** was not notably affected (16% & 22%, respectively), an increase in the *rr* was observed (25:1 and 33:1 **3.166–3.187**, respectively). When the solvent was changed from 2-

MeTHF to THF and 4 Å molecular sieves were included (**Scheme 3.26B** table, entry 20) a similar yield (18% yield) and *rr* (20:1 **3.166–3.187**) was observed. When the amine nucleophile was changed from cystamine **3.153** to amine **3.185** (**Scheme 3.26B** table, entry 21) none of sulfide **3.166** was isolated – instead only C2-desilylated sulfide **3.188** was obtained in 10% yield. In addition to using 4 Å molecular sieves, when indolequinone **3.89** was purified by column chromatography prior to the reaction (**Scheme 3.26B** table, entry 22), instead of crude material from the previous step (oxidative demethylation, refer back to **Scheme 3.16B**), although the highest *rr* was not obtained (17:1 **3.166–3.187**), an increase in the yield of sulfide **3.166** to 32% was achieved. However, this was off-set when considering the yield over three steps from trimethoxytryptamine **3.135** since it has already been shown that purifying indolequinone **3.89** by FCC led to a notable decrease in yield.

In summary, HTE was employed to identify effective base–solvent combinations for the one-pot conversion of indolequinone **3.89** to sulfide **3.166**. An initial screen of 144 conditions informed a focused evaluation of 48 combinations. From these, three base–solvent combinations were selected for a 10-fold scale-up, with two showing potential for further optimisation. Using ^{1}H NMR spectroscopy alongside UPLC analysis, the presence of undesired regioisomer sulfide **3.187** was detected in addition to **3.166**. For the combination of caesium carbonate in isopropyl acetate, the regioisomeric outcome was sensitive to the base loading; in some cases, regioselectivity could be reversed in favour of the undesired isomer. Despite efforts, the best *rr* achieved under these conditions was 6.5:1 **3.166–3.187**. In contrast, with TMG in 2-MeTHF, neither base equivalents nor temperature significantly influenced the *rr*, though higher reaction concentrations negatively impacted selectivity. Under optimised conditions, a *rr* of >20:1 **3.166–3.187** was achieved; however, overall improvements to selectivity and yield remained modest. Notably, C2-desilylation was observed in several conditions. This side reaction is detrimental, as the resulting C2-desilylated sulfide **3.188** was found to be unamenable to oxidation to sulfone **3.22** using *m*CPBA. Future work would explore an indolequinone bearing a more robust C2-TES protecting group to mitigate this issue. Further investigation is warranted to better understand the reaction.

Additional base–solvent combinations identified in screen four would be examined under optimised equivalents of cystamine **3.153** and base, and reaction temperature and concentration. To accelerate this process, HTE would be integrated with SFC to assess regioisomeric outcomes directly, without requiring product isolation and ^{1}H NMR analysis. Although isolated yields were not substantially improved throughout this optimisation process, a three-step overall yield of 24% for the synthesis of sulfide **3.166** (33:1 *rr*, **3.166**–**3.187**) from trimethoxytryptamine **3.135**, was deemed acceptable. However, as the original base–solvent combination of triethylamine in ethanol did not form undesired regioisomer sulfide **3.187** these conditions were used henceforth.

3.5.6.7. Oxidation of sulfide 3.166 to sulfone 3.190

With installation of the dihydrothiazine ring complete, a series of redox manipulations were required to convert sulfide **3.166** into thiaplakortone B **3.1** and thiaplakortone A **1.12**. The oxidation of sulfide **3.166** to sulfone **3.190** was initially pursued (**Table 3.3**). Peracids, such as *meta*-chloroperoxybenzoic acid (*m*CPBA), are among the most commonly employed oxidants for sulfur-oxidation, with oxidant stoichiometry and reaction temperature being key factors in determining the sulfoxide–sulfone ratio.[148]

3.3 *optimisation table for the oxidation of sulfide* ***3.166*** *to sulfone* ***3.190****:*

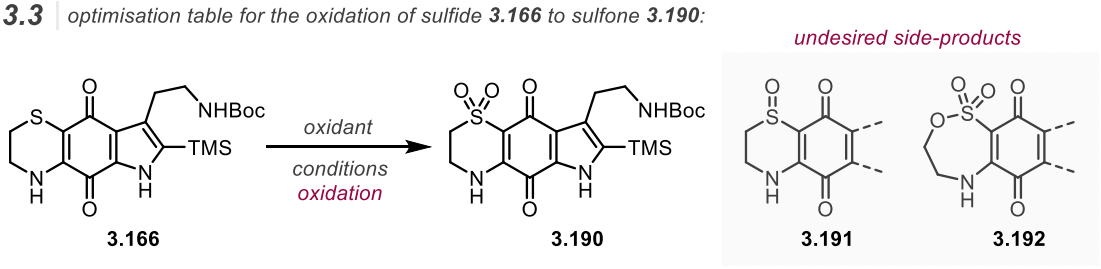

entry	*oxidant (eq.)*	*conditions*	*isolated yield of 3.190 / %*	*isolated yield of 3.191 / %*	*isolated yield of 3.192 / %*
1	*m*CPBA (2.5 eq.)	$CDCl_3$ [0.005 M], 0 °C to rt, 1.5 h	37	0	0
2	*m*CPBA (2.5 eq.)	CH_2Cl_2 [0.005 M], 0 °C to rt, 1.5 h	90	0	0
3	*m*CPBA (2.5 eq.)	CH_2Cl_2 [0.050 M], 0 °C to rt, 1.5 h	11	26	0
4	*m*CPBA (4.0 eq.)	CH_2Cl_2 [0.025 M], 40 °C, 24 h	33	0	0
5	*m*CPBA (4.0 eq.)	CH_2Cl_2 [0.005 M], 0 °C to rt, 4 h	38	0	0
6	*m*CPBA (8.0 eq.)	CH_2Cl_2–MeOH (4:1) [0.005 M], rt, 48 h	48	0	0
7	*m*CPBA (8.0 eq.)	CH_2Cl_2–MeOH (4:1) [0.100 M], rt, 48 h	15	0	0
8	*m*CPBA (4.0 eq.)	CH_2Cl_2–MeOH (20:1) [0.025 M], rt, 1 h	53	0	0
9	AcOOH (5.0 eq.)	CH_2Cl_2 [0.025 M], rt, 5 h	30	0	0
10	TFAA (5 eq.), $2Na_2CO_3{\bullet}3H_2O_2$ (5.0 eq.)	CH_2Cl_2 [0.010 M], rt, 5 h	0	0	0
11	OXONE® (3.0 eq.)	MeOH–H_2O (1:1) [0.050 M], rt, 24 h	20	0	2
12	$(NH_4)_2MoO_4$ (5 mol%), H_2O_2 (5.0 eq.)	MeOH [0.050 M], rt, 24 h	2	0	5

Table 3.3. *Optimisation table for the oxidation of sulfide* ***3.166*** *to sulfone* ***3.190****. Additionally, side-products, sulfoxide* ***3.191*** *and sulfonate ester* ***3.192****, observed under some conditions.*

Initially, the oxidation was trialled using *m*CPBA (97% purity) in chloroform-d_1, to enable reaction monitoring by ^{1}H NMR spectroscopy (**Table 3.3**, entry 1). Upon addition of *m*CPBA, an almost instantaneous colour change of the reaction mixture from blue to orange was observed. After 15 minutes at 0 °C (followed by warming to room temperature during the NMR experiment) the ^{1}H NMR spectrum indicated the complete consumption of sulfide **3.166** and the formation of a new product (**Figure 3.9**). The large deshielding observed in the ^{1}H NMR for the N*H* resonance of

the dihydrothiazine (H15, light blue; δ 5.69 ppm (SM) → 6.80 ppm (P), Δδ = +1.11 ppm) suggested a decrease in electron-density in the quinone core. Additionally, a smaller downfield change in chemical shift was observed for both the α-CH_2 (H17, pink; δ 2.92 ppm (SM) → 3.30 ppm (P), Δδ = +0.38 ppm) and β-CH_2 (H16, purple; δ 3.71 ppm (SM) → 4.07 ppm (P), Δδ = +0.36 ppm) resonances with respect to the *S*-atom, indicating a negative inductive effect. After aqueous work-up and purification by FCC, and confirmation of product identity by HRMS, the desired sulfone **3.190** was isolated in 37% yield.

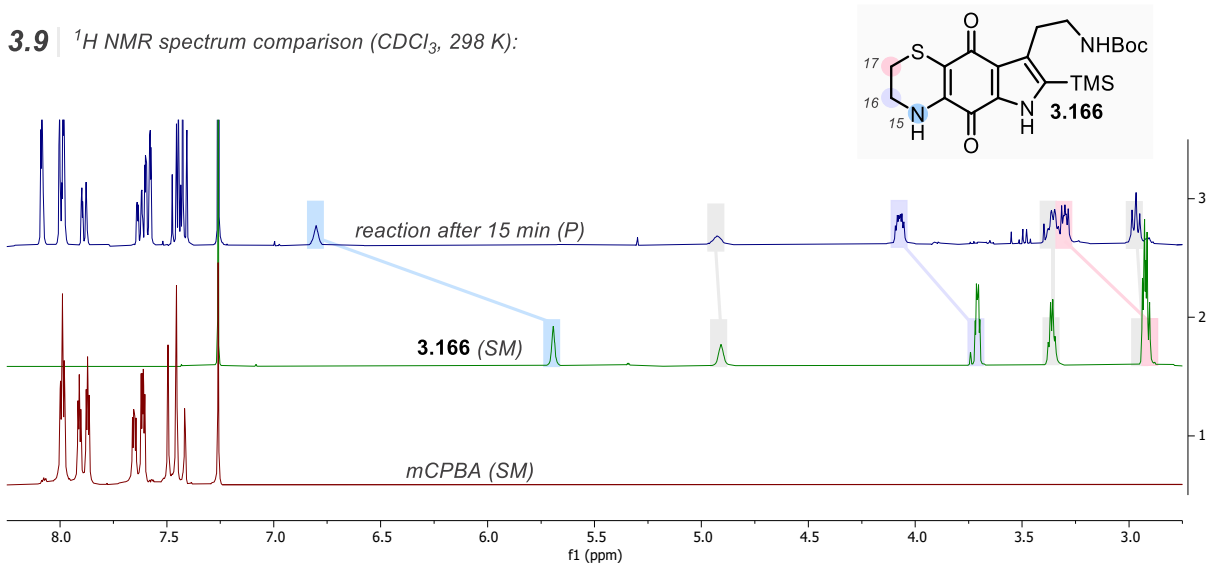

Figure 3.9. *^{1}H NMR spectrum (chloroform-d_1, 298 K) comparison for mCPBA and sulfide* ***3.166*** *starting material (SM) and the product (P) of the reaction between sulfide* ***3.166*** *and mCPBA after 15 minutes.*

As the yield was low, the reaction was retried using similar reaction conditions (swapping chloroform-d_1 for dichloromethane) and also employing a modified work-up procedure to quench any residual *m*CPBA and to wash-out the *meta*-chlorobenzoic acid by-product, obviating the need for FCC and hopefully limiting product loss (**Table 3.3**, entry 2). Initially this approach seemed successful, achieving an isolated yield of 90%. However, upon a ten-fold scale-up (**Table 3.3**, entry 3), accompanied by a 10-fold increase in reaction concentration, it became apparent that the previous yield of 90% was not correct. For entry 3, during the reaction an orange precipitate formed which was not observed during previous oxidation attempts. When the solvent used for ^{1}H NMR spectroscopic analysis of the crude reaction mixture was changed from chloroform-d_1 to

methanol-d_4 an additional compound was observed alongside sulfone **3.190**, which contained diastereoisotopic protons indicative of sulfoxide **3.191**. Following FCC, sulfone **3.190** was isolated in an 11% yield, alongside sulfoxide **3.191** (confirmed by HRMS) in 26% yield. Sulfoxide **3.191** displayed greater polarity during TLC analysis (5% methanol in dichloromethane: R_f = 0.29) compared to sulfone **3.190** (5% methanol in dichloromethane: R_f = 0.45), and exhibited poorer solubility.

To circumvent the under-oxidation of sulfide **3.166**, and limit the quantities of sulfoxide **3.191** isolated, reaction conditions were optimised by increasing the temperature (**Table 3.3**, entry 4; 33% yield of **3.190**), or by decreasing the reaction concentration (**Table 3.3**, entries 5 & 6; 38% and 48% yield of **3.190**, respectively). Methanol was also trialled as a co-solvent (**Table 3.3**, entries 6 & 7; 48% and 15% yield of **3.190**, respectively) to minimise the precipitation of sulfoxide **3.191** from the reaction mixture, while increasing the equivalents of *m*CPBA (4 eq.) to ensure complete oxidation of the sulfoxide **3.191** in solution to sulfone **3.190**. The inclusion of methanol as a co-solvent appeared to reduce the rate of oxidation, presumably since methanol is a polar protic solvent capable of hydrogen bonding, therefore reducing the reactivity of *m*CPBA.[149] To increase the reaction conversion, additional *m*CPBA (4 eq., 8 eq. in total) was added. A good balance was attained by employing a sufficient quantity of methanol to ensure complete solubility while avoiding suppression of the reaction rate, thereby affording the highest yield observed to date, 53%, within one hour at room temperature (**Table 3.3**, entry 8). In a hope to further improve the yield, the use of different peracids as an alternative to *m*CPBA was explored. Peracid reactivity is related to the strength of the parent acid.[150] Peracetic acid (39 weight% in acetic acid) performed slightly worse (**Table 3.3**, entry 9; 30% yield of **3.190**) to *m*CPBA. The stronger oxidant trifluoroperacetic acid, generated *in situ* from the addition of a solid hydrogen peroxide source ($2Na_2CO_3 \bullet 3H_2O_2$) to trifluoroacetic anhydride (TFAA), led to an intractable mixture with no desired sulfone **3.190** or sulfoxide **3.191** detected by TLC (**Table 3.3**, entry 10).[151]

3.5.6.7.1. The unexpected side-product

We then broadened our search for an oxidant that performed better than *m*CPBA. When using OXONE® (**Table 3.3**, entry 11; 20% yield of **3.190**)[152,153] and hydrogen peroxide with catalytic ammonium molybdate (**Table 3.3**, entry 12; 2% yield of **3.190**)[154] an additional product was observed (**3.192**; 2% and 5% isolated yield for entries 11 & 12, respectively) alongside sulfone **3.190**. Initial TLC analysis indicated the unknown product was less polar (5% methanol in dichloromethane: R_f = 0.50) than sulfone **3.190** (5% methanol in dichloromethane: R_f = 0.45) and the compound was pink in colour. Further analysis by ^{1}H NMR spectroscopy indicated a compound with the same total number of protons and number of different proton environments, but significant differences in chemical shifts of some resonances compared to sulfone **3.190** (**Figure 3.10**).

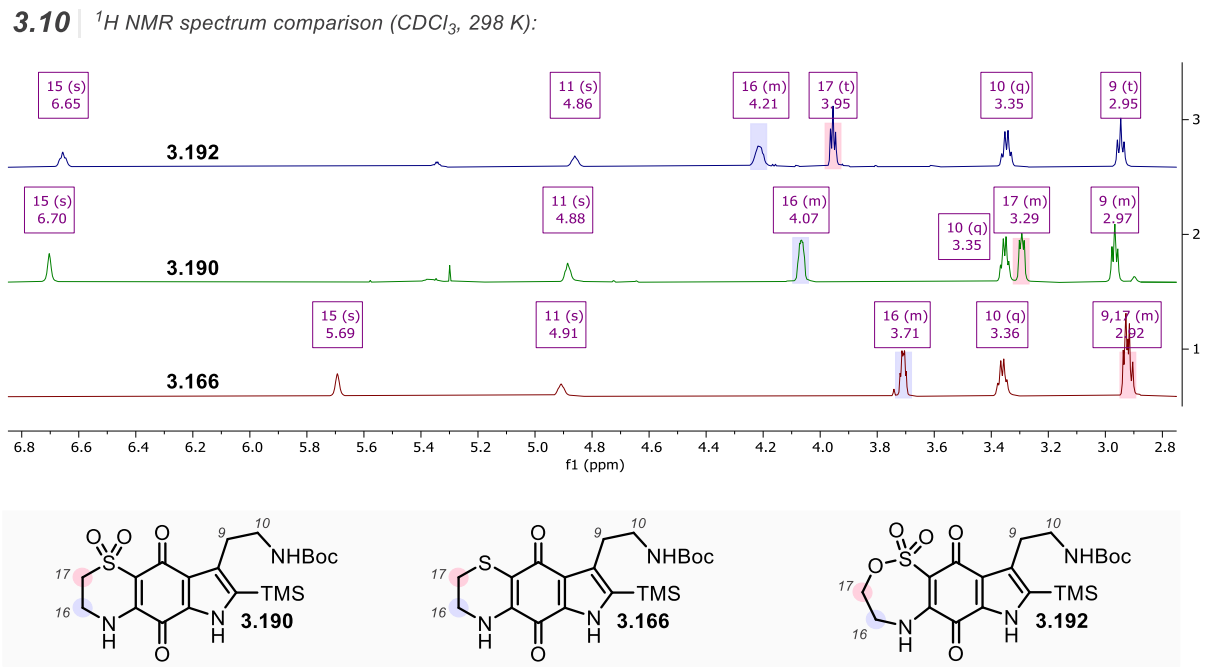

Figure 3.10. *^{1}H NMR spectrum (chloroform-d_1, 298 K) comparison of sulfide **3.166**, sulfone **3.190** and sulfonate ester **3.192**.*

A large downfield shift was observed for H16 (δ 3.71 ppm (**3.166**) → 4.21 ppm (**3.192**), Δδ = +0.50 ppm), which was a larger change than the previously observed change in the chemical shift of H16 upon conversion of sulfide **3.166** to sulfone **3.190** (Δδ = +0.36 ppm). An even greater

change in the chemical shift was observed for H17 (δ 2.92 ppm (**3.166**) → 3.95 ppm (**3.192**), Δδ = +1.03 ppm), compared to the change in the chemical shift of H17 upon converting sulfide **3.166** to sulfone **3.190** (Δδ = +0.37 ppm).

The change in the chemical shift for C17 of the unknown product was even more pronounced upon analysis of the ^{13}C NMR spectrum (**Figure 3.11**). A large downfield chemical shift was observed for C17 of the unknown product versus sulfide **3.166** (δ 23.9 ppm (**3.166**) → 70.0 ppm (**3.192**), Δδ = +46.1 ppm), which was approximately twice as large as the difference in chemical shift at C17 after converting sulfide **3.166** to sulfone **3.190** (δ 23.9 ppm (**3.166**) → 49.2 ppm (**3.192**), Δδ = +25.3 ppm). 2D NMR spectroscopy analysis coupled with mechanistic considerations identified sulfonate ester **3.192** as the putative undesired side-product.

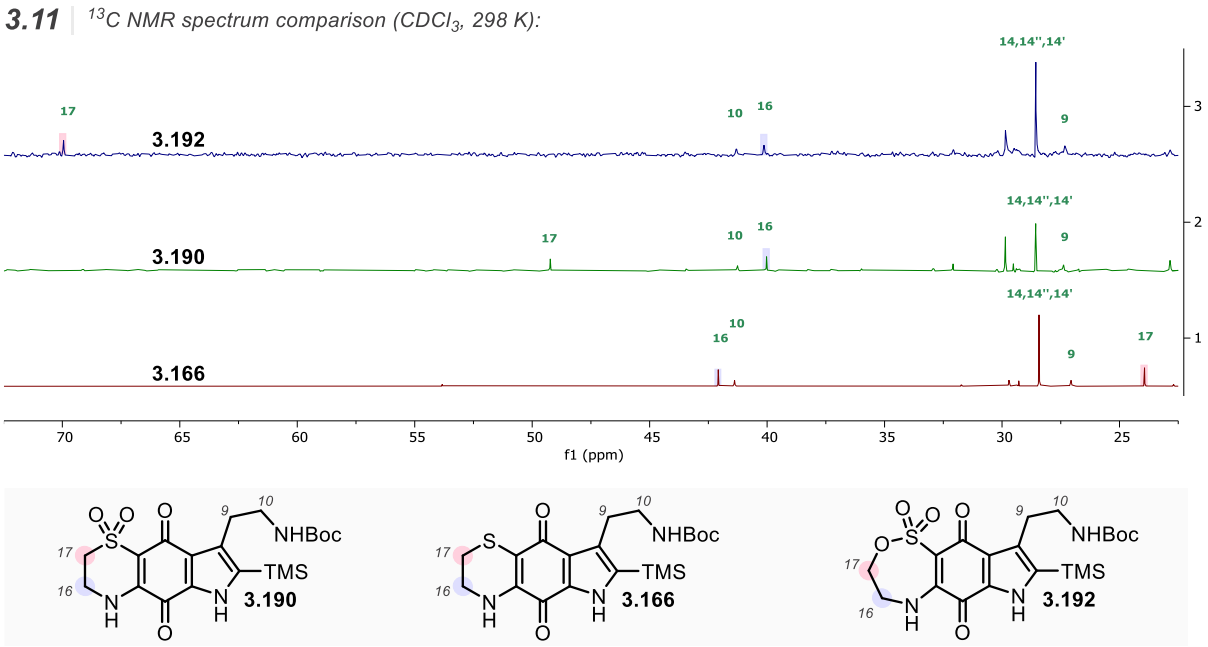

Figure 3.11. *^{13}C NMR spectrum (chloroform-d_1, 298 K) comparison of sulfide **3.166**, sulfone **3.190** and sulfonate ester **3.192**.*

We proposed sulfonate ester **3.192** could be formed by the over-oxidation of sulfone **3.190** through two possible pathways (**Scheme 3.27A**). In pathway (1), peroxide **3.193** attacks the electrophilic C–S σ* orbital of the C17-methylene α-to the sulfone, breaking the C–S σ-bond and delocalising the negative electron-density into the sulfinate (intermediate **3.194**). The newly formed sulfinate then bites back into the newly formed alkyl peroxide O–O σ* orbital, leading to

the elimination of an alkoxide (or hydroxide) and net ring-expansion. Alternatively, in pathway (2), peroxide **3.193** attacks the electrophilic sulfur-centre directly (intermediate **3.195**) followed by a Baeyer–Villiger-like migration of the C17-methylene onto the proximal oxygen atom of the newly added peroxide, leading to the elimination of an alkoxide (or hydroxide) and ring-expansion. However, sulfonate ester **3.192** was proposed to be a highly reactive species capable of undergoing alkylation reactions with even weak nucleophiles such as water (putative intermediate **3.196**), leading to decomposition, thus only trace quantities of sulfonate ester **3.192** could be isolated (**Table 3.3**, entries 11 & 12: 2% and 5% yield, respectively).

As sulfinate esters (**3.197**) have been reported to undergo rearrangements to sulfones (**3.198**) in certain cases (**Scheme 3.27A**),[155] it is believed unlikely that sulfonate ester **3.192** was formed by the (net) ring-expansion of sulfoxide **3.191** to the corresponding sulfinate ester, followed by oxidation to **3.192**.

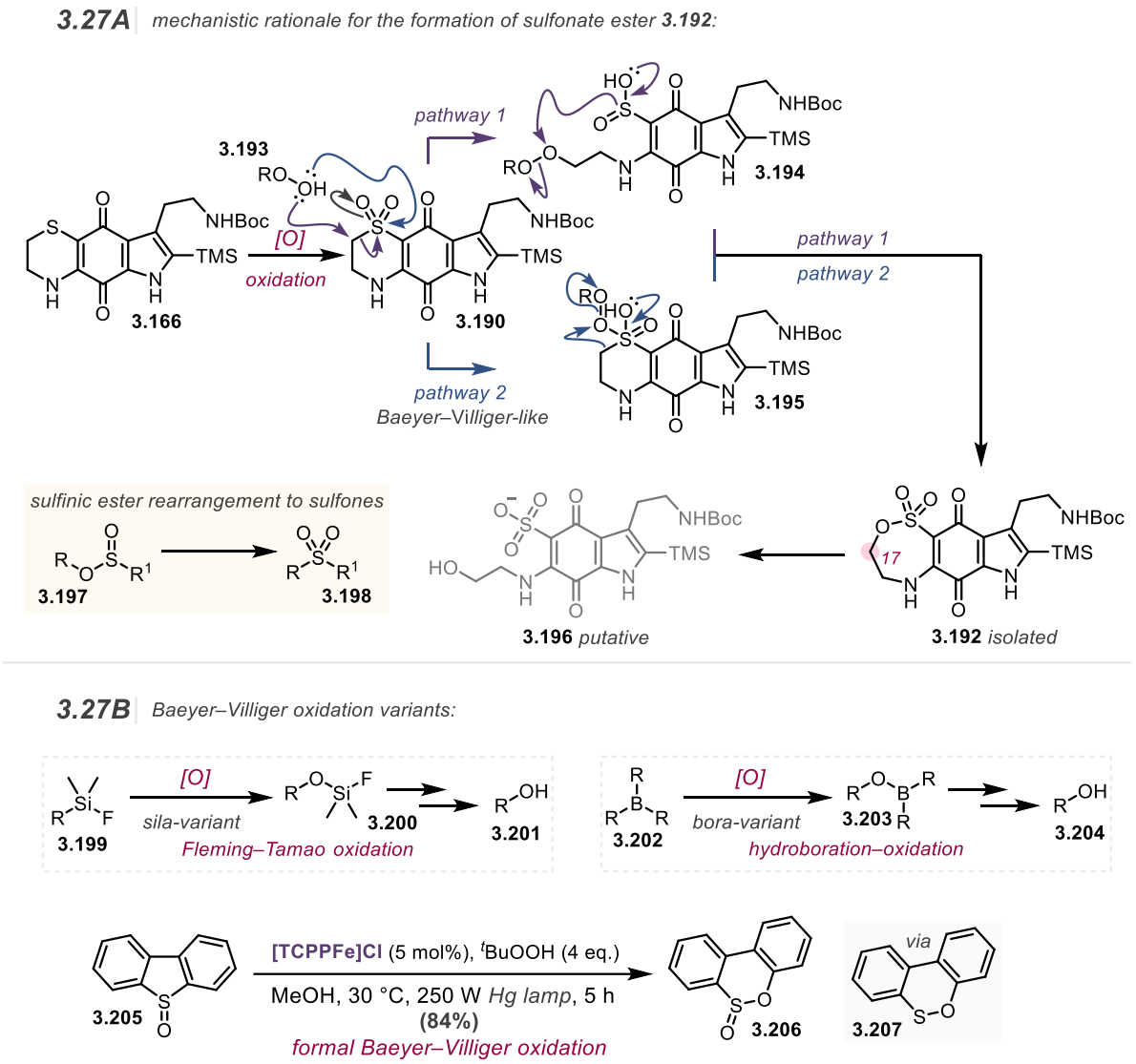

Scheme 3.27. (A) *Proposed mechanisms for the formation of sulfinate ester* ***3.192****.* ***(B)*** *Baeyer–Villiger oxidation variants.*

The identity of sulfonate ester **3.192** was further confirmed by comparison of the ^{13}C NMR chemical shift value for the α-methylene to the sulfur-functional group (δ 70.0 ppm) with that of known sulfonate ester **3.212** (δ 68.2 ppm) (**Figure 3.12**).[156–158]

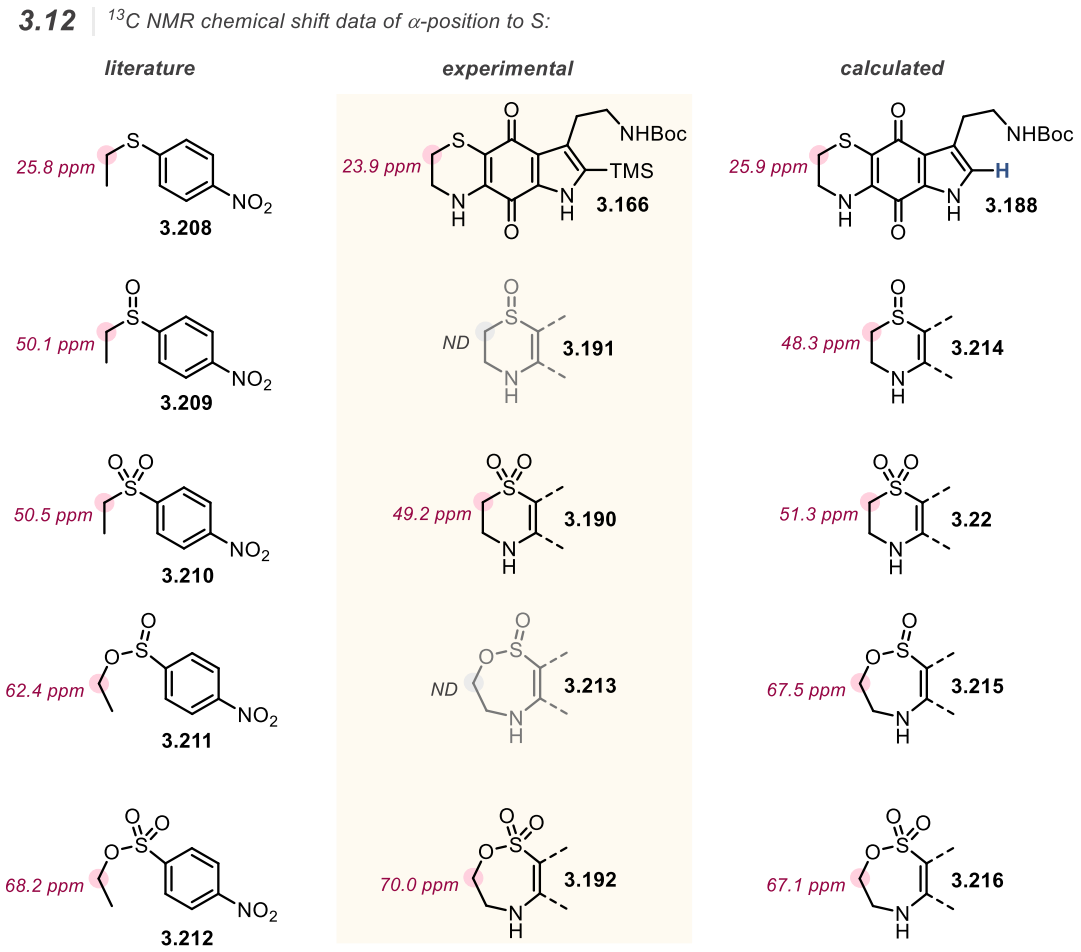

Figure 3.12. *Comparison of literature, experimental and calculated ^{13}C NMR chemical shift data of the α-position to the S-atom. Calculated values using CASCADE for the C2-desilylated compound as Si not tolerated. For completeness, the reported experimental ^{13}C NMR chemical shift values for sulfur containing functional groups, at different oxidation states, and calculated values for C2-deprotected analogues at different oxidation states with our observed experimental data have been included.*

Additionally, the C17 ^{13}C NMR chemical shift value of a close analogue was calculated using CASCADE (ChemicAl Shift CAlculation with DEep learning) developed by the Paton Group at Colorado State University, with the C2-desilylated sulfonate ester **3.216** having a calculated chemical shift for C17 of δ = 67.1 ppm. Sulfonate ester **3.192** could not be calculated due to the calculation not tolerating silicon atoms.[159]

Attempts were made to grow a single crystal to confirm the product identity using single crystal XRD, but they were unsuccessful. The use of ^{33}S NMR spectroscopy to confirm the identity of sulfonate ester **3.192** was briefly considered, however this technique suffers from extensive line

broadening caused by the rapid relaxation rates and low sensitivity due to the low natural abundance of the ^{33}S nucleus (0.76% abundance).[160,161] ^{18}O NMR spectroscopy was also considered, however, due to the prohibitively high cost of ^{18}O-labelled hydrogen peroxide and the low isolated yield of sulfonate ester **3.192** in entry 11 (**Table 3.3**; 5% yield) we did not pursue an isotope labelling strategy for compound identity validation. No IR spectroscopy absorptions could be conclusively assigned as those characteristic of a S=O stretching vibration of a sulfonate ester. Nonetheless, with good agreement between experimental and calculated ^{13}C NMR chemical shifts, we further supported the assignment of the by-product as sulfonate ester **3.192** by HRMS.

Uncertainties still remained regarding the mechanistic rationale for the formation of sulfonate ester **3.192**. Moreover, it was unknown if a *thia*-Baeyer–Villiger-like oxidation of sulfone **3.190** as proposed in pathway (2) is possible. Since the discovery of the Baeyer–Villiger oxidation several non-carbon versions have been identified (**Scheme 3.27B**) – such as the *sila*-variant observed when transforming silanes (**3.199**) to silyl ethers (**3.200**) in the Fleming–Tamao oxidation and the *bora*-variant observed when converting boranes (**3.202**) to borate esters (**3.203**) during the second step of hydroboration–oxidation; however, the *thia*-variant remains elusive. Despite the report by Markó *et al.* of a photoinduced iron porphyrin-catalysed *thia*-Baeyer–Villiger-like oxidation of sulfoxides (**3.205**) under ultraviolet light,[162] this is only a formal reaction since S^{IV} is initially reduced to S^{II} (**3.207**), before being oxidised back to S^{IV} (**3.206**). Additionally, an analogous transformation using sulfones has yet to be realised. Pathway (1) is also unusual and perhaps unlikely given the electrophilic nature of the oxidants used. Nevertheless, it is possible that the electronic properties of this specific quinonecore unlocked novel reactivity at the α-position of the sulfone, directly enabling a ring expansion from a 6-membered to a 7-membered ring – leading to a rather unique 7,6,5-fused tricyclic ring system.

3.5.6.7.2. Oxidation of sulfide 3.166 to sulfone 3.190 (continued)

Although the isolation of sulfonate ester **3.192** was academically interesting, it posed additional complications to the task of oxidising sulfide **3.166** to sulfone **3.190**. Not only was there a lack of understanding on the mechanism and on how to limit this undesired pathway, but issues with the solubility of sulfoxide **3.191**, generated after the first oxidation step, were also faced. Therefore, mild and selective oxidation conditions for the desired transformation were sought (**Table 3.4**), hoping to minimise the undesired pathway and improve on the yield previously obtained with *m*CPBA (refer back to **Table 3.3**, entry 8; 53%).

3.4 *optimisation table for the oxidation of sulfide **3.166** to sulfone **3.190**:*

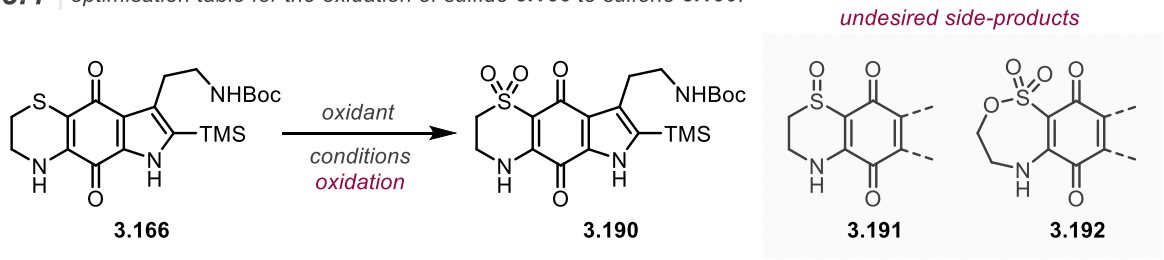

entry	*oxidant (eq.)*	*conditions*	*isolated yield of 3.190 / %*	*isolated yield of 3.191 / %*	*isolated yield of 3.192 / %*
13	$LiClO_4$ (10 eq.), Pt(+)–Pt(−) *undivided cell*	HFIP–AcOH (1:1) [0.002 M], rt, 0.5 mA, 2 h	0	20	0
14	$VO(acac)_2$ (0.25 eq.), ^tBuOOH (10 eq.)	CH_2Cl_2 [0.025 M], rt, 24 h	0	0	0
15	$KMnO_4$–MnO_2 (2.5 eq.)	CH_2Cl_2 [0.050 M], rt, 24 h	0	0	0
16	DMDO ([0.06 M in Me_2CO], 4.0 eq.)	CH_2Cl_2 [0.025 M], 0 °C, 10 min	55	0	0

Table 3.4. *Optimisation table for the oxidation of sulfide **3.166** to sulfone **3.190**, continued. Where, $KMnO_4$–MnO_2 = potassium permanganate supported on manganese oxide.*

Oxidation of sulfides by electrochemistry has recently emerged as an alternative approach to the use of chemical oxidants.[148] Xu *et al*. reported a chemoselective electrochemical oxidation of thioethers (**Scheme 3.28A**) facilitated by a strongly hydrogen bonding solvent system (HFIP–acetic acid, **3.223**). Modulation of the oxidation potential of the initial sulfoxide formed via

hydrogen bonding (**3.224**) prevents the overoxidation of sulfoxides to sulfones at low voltage (3 V). Further oxidation to the corresponding sulfone can only be achieved at high voltage (4 V).[163] It was hoped this would be an attractive alternative for the oxidation of sulfide **3.166**, and that the hydrogen bond network between sulfone **3.190** and the HFIP–acetic acid solvent system would prevent overoxidation to sulfonate ester **3.192** which has been observed with several chemical oxidants (refer back to **Table 3.3**, entries 4, 11 & 12).

Initially a model system was synthesised to trial both the electrochemistry set-up and conditions. Sulfide **3.226** was selected as a representative model substrate (**Scheme 3.28B**), as it was a substrate in the sulfoxide product scope reported by Xu *et al*. When using the reported constant voltage method (4 V) for the synthesis of sulfones from sulfides only trace quantities of sulfone **3.227** were detected by UPLC, primarily affording sulfoxide **3.228** instead. The voltage was increased gradually to 6 V but to no avail. Additionally, the isolated yield of sulfoxide **3.228** was significantly lower compared to that reported in the literature (9% versus 79% yield) likely as a consequence of using a higher voltage. Although the reaction was unsuccessful on sulfide **3.226**, it was believed that our system would behave differently due to conjugation of the sulfide with the quinone and would thus possess a different oxidation potential. Using the reported constant voltage method (4 V) on sulfide **3.166** (**Scheme 3.28C**) led to the formation of sulfoxide **3.191** (detected by UPLC). However, after just 1 hour, decomposition was observed and no sulfide **3.166**, sulfoxide **3.191**, or sulfone **3.190** was detected. The method was changed from constant voltage to constant current – initially beginning with 5 mA. The same observations were observed as with the constant voltage method but this time complete decomposition occurred after 2 hours. When the reaction was instead performed at 0.5 mA (Table **3.4**, entry 13), after 2 hours sulfide **3.166** had largely been consumed (monitored by UPLC), with sulfoxide **3.191** as the major product isolated in 20% yield (*c.f.* 55% when *m*CPBA was used, see later **Scheme 3.31B**).

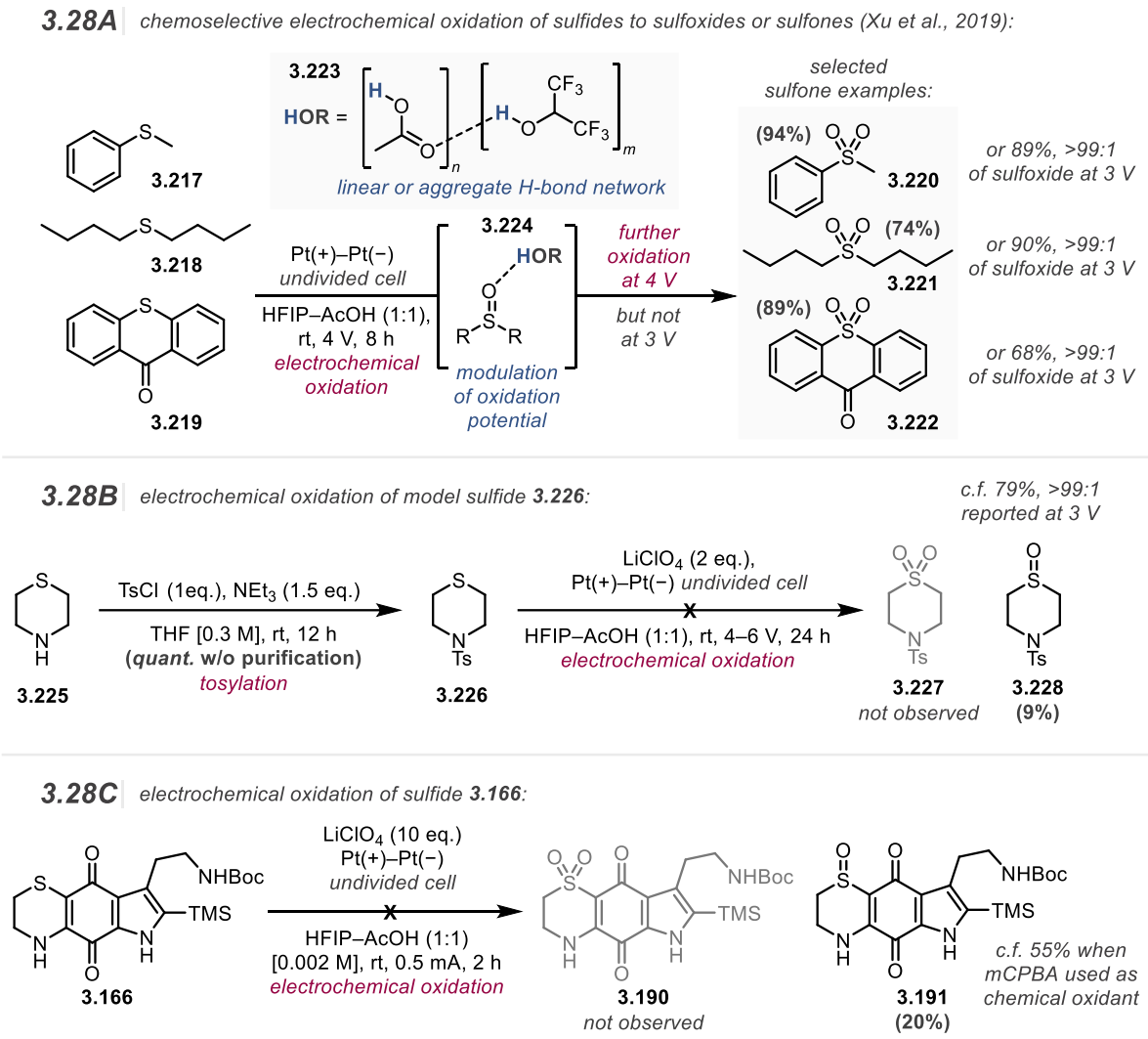

Scheme 3.28. (A) *Chemoselective electrochemistry oxidation of sulfides to sulfoxides or sulfones (Xu et al., 2019).* ***(B)*** *Electrochemical oxidation of model sulfide* ***3.226****.* ***(C)*** *Electrochemical oxidation of sulfide* ***3.166****.*

Our attention turned back to finding a mild chemical oxidant. No desired sulfone **3.190**, or sulfoxide **3.191** was observed using *tert*-butyl hydroperoxide with catalytic vanadyl acetylacetonate in dichloromethane (commonly used for directed epoxidations but shown in the literature to also oxidise sulfides) (**Table 3.4**, entry 14).[164] Potassium permanganate supported on manganese oxide (**Table 3.4**, entry 15)[165] gave only decomposition products. Dimethyldioxirane (DMDO) is considered a selective oxidant, as unlike the peracids, it reacts under neutral conditions generating acetone as a by-product.[166] A freshly prepared solution of DMDO in acetone was successfully employed to oxidise sulfide **3.166** in dichloromethane (**Table 3.4**, entry 16), affording sulfone **3.190** in 55% yield.[167] Although the highest yield obtained to

date, the modest improvement over *m*CPBA, coupled with the latter's greater operational simplicity, rendered *m*CPBA the more attractive oxidant.

In summary, sulfide **3.166** was successfully oxidised to sulfone **3.190**, with *m*CPBA and DMDO identified as the best-performing oxidants, affording the sulfone in a moderate 53–55% yield. During oxidant screening, an unexpected side-product, sulfonate ester **3.192**, was observed. The formation of this product is more plausibly attributed to a *thia*-Baeyer–Villiger-type oxidation of sulfone **3.190**, rather than nucleophilic attack at the α-position of the *S*-atom, since electrophilic oxidants were used. Notably, such a transformation, if confirmed, would represent the first example of its kind. Future studies would be necessary to confirm this mechanistic hypothesis. In addition, further investigation is warranted to evaluate the potential synthetic utility of this transformation.

3.5.6.8. Endgame

3.5.6.8.1. Oxidation strategies

With sulfone **3.190** successfully synthesised in 53% yield from sulfide **3.166** using *m*CPBA (refer back to **Table 3.3**), and in 55% yield employing freshly prepared DMDO (**Table 3.4**), installation of a C16–C17 olefin was required for the synthesis of thiaplakortone A **1.12** (**Scheme 3.29A**). Quinn and co-workers had previously reported the use of KOH and oxygen to effect this transformation on a related sulfide **3.22**, which lacks only the C2-TMS substituent.[85] Although no mechanistic rationale was disclosed within this publication, a plausible pathway may involve initial deprotonation at the C17-position (α to the sulfone) to generate α-carbanion **3.229**. Single-electron oxidation of this species could then afford α-*C*-centred radical **3.230**, which subsequently undergoes trapping by singlet oxygen to yield C17-peroxide adduct **2.231**. Under the basic reaction conditions, deprotonation at the C16-position (β to the sulfone) facilitates elimination of peroxide via an E2-type mechanism, yielding desired vinyl sulfone **3.23**.

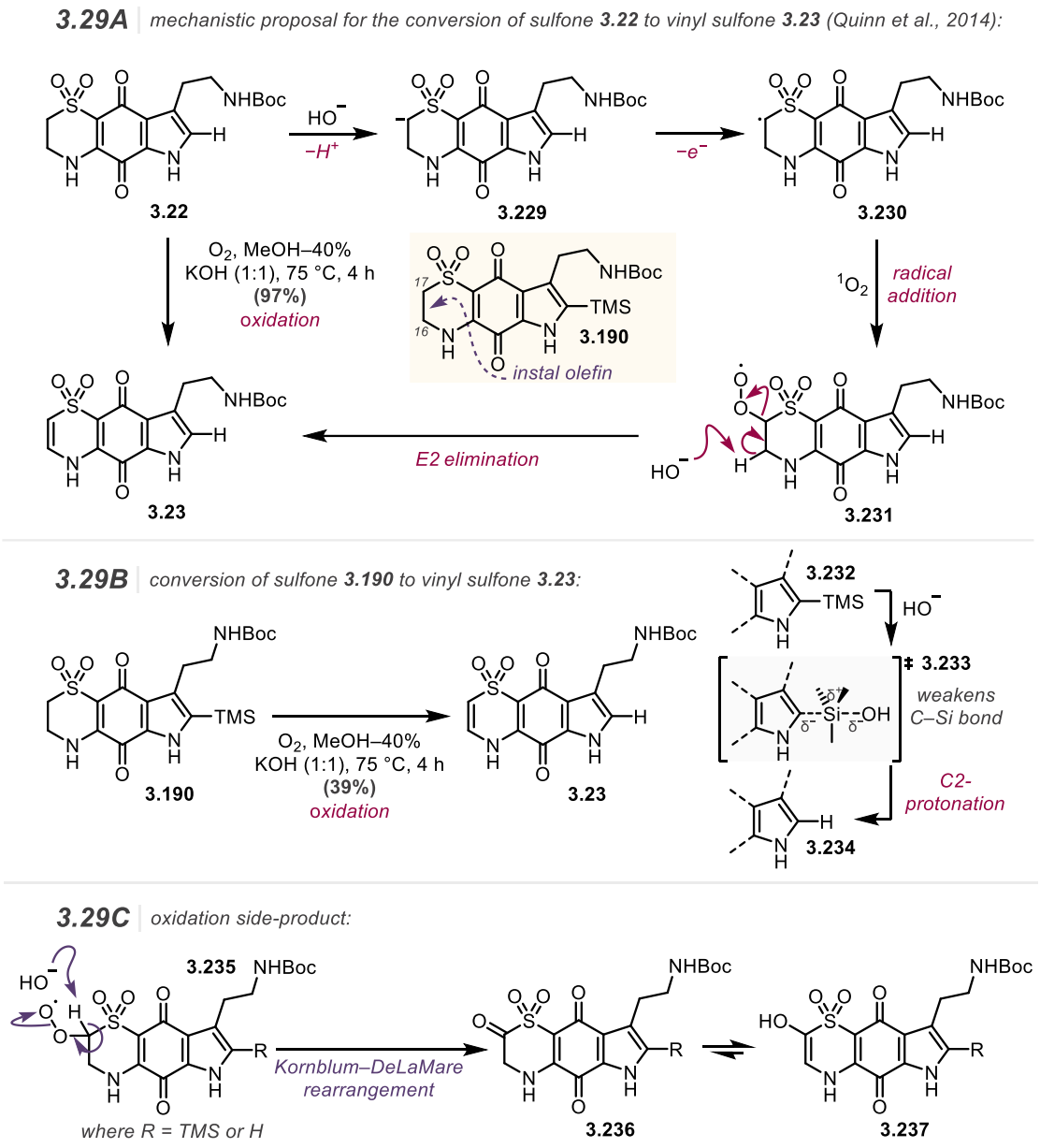

Scheme 3.29. (A) *Mechanistic proposal for the conversion of sulfone* ***3.22*** *to vinyl sulfone* ***3.23*** *using potassium hydroxide and oxygen.* ***(B)*** *Utilisation of conditions on sulfone* ***3.190*** *furnished vinyl sulfone* ***3.23****.* ***(C)*** *Putative side-products from a competing Kornblum–DeLaMare rearrangement.*

Treatment of sulfone **3.190** under the conditions reported by Quinn and co-workers furnished C2-desilylated vinyl sulfone **3.23** in 39% yield (**Scheme 3.29B**). Under these basic conditions, it is believed nucleophilic attack by hydroxide on the vacant 3d orbital of silicon (**3.232**/transition state **3.233**) generated a pentavalent -ate complex, which was more susceptible to C2-protonation, thereby facilitating removal of the TMS group (**3.234**). The yield obtained in our system of 39% was notably lower than the 97% yield reported in the original study.[85] A polar side-product was observed under the reaction conditions by TLC analysis; however, attempts to isolate

and characterise this product were unsuccessful. It was hypothesised that this side-product could have arose from a Kornblum–DeLaMare-type rearrangement (**3.235**), a transformation in which a secondary organic peroxide undergoes base-catalysed rearrangement to generate a ketone (**Scheme 3.29C**). The observed impurity may correspond to either putative ketone **3.236** or its tautomeric form, putative enol **3.237**.[168]

Due to the suboptimal yield obtained under the original conditions, which were assumed attributable to the formation of the putative ketone **3.236**/enol **3.237** side-product, alternative olefination strategies were investigated. The Ramberg–Bäcklund rearrangement is a reaction which converts α-halo sulfones (**Scheme 3.30A**, **3.238**) into olefins via deprotonation with a relatively strong base at the non-halogenated α-position, generating carbanion **3.239**. Subsequently, the proximal halide is eliminated to form episulfone intermediate **3.240**. Extrusion of SO_2 affords the corresponding olefin **3.241**, often with high *Z*-selectivity. A modified, one-pot variant employing dibromodifluoromethane (CBr_2F_2) and alumina-supported KOH (Al_2O_3–KOH) in *tert*-butanol has been developed by Chan and co-workers which enables a one-pot α-halogenation and rearrangement, which minimises over-halogenation and side reactions that can be caused by dibromocarbene generation.[169] It was envisioned that bromination at the C17-position of sulfone **3.190** would proceed under these conditions, and since no second α-proton is available SO_2 extrusion would be precluded (**Scheme 3.30B**). Instead, analogous to the reaction system with KOH and oxygen, it was anticipated that under basic conditions, proton abstraction at the β-position (intermediate **3.242**, C16-position) would enable the elimination of bromide via an E2 mechanism (interrupted Ramberg–Bäcklund rearrangement), thereby affording desired vinyl sulfone **3.23**. This strategy was attempted; however, the initial halogenation reaction was not observed upon treatment of sulfone **3.190** with CBr_2F_2 and Al_2O_3–KOH at room temperature,

and gradually increasing the reaction temperature up to 60 °C led to decomposition (**Scheme 3.30C**).

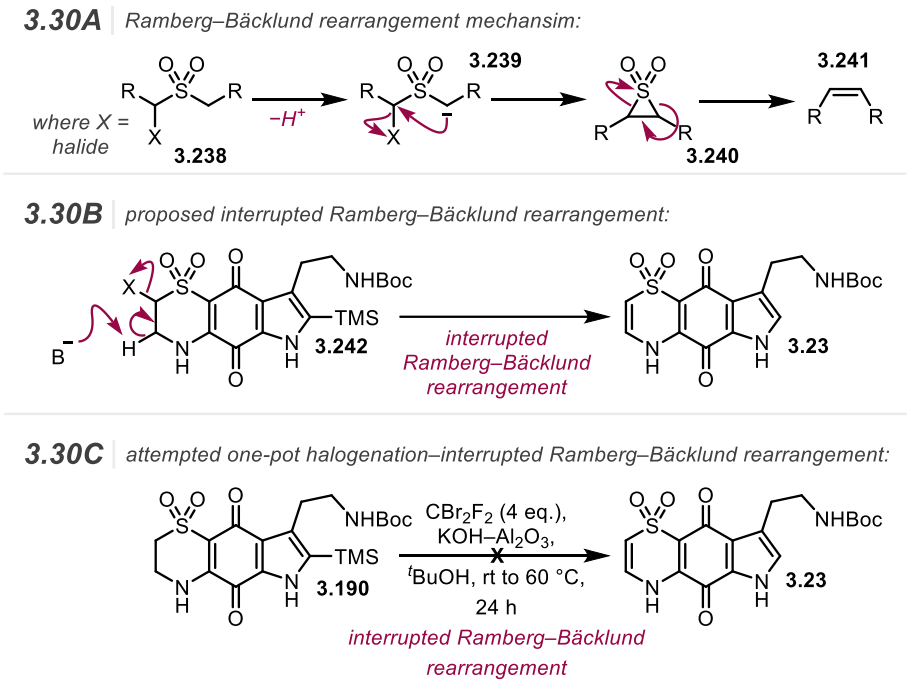

Scheme 3.30. (A) *Ramberg–Bäcklund rearrangement of an α-halosulfone to an alkene.* ***(B)*** *Envisioned interrupted Ramberg–Bäcklund rearrangement on α-halosulfone* ***3.242****.* ***(C)*** *Attempted one-pot α-halogenation–interrupted Ramberg–Bäcklund rearrangement.*

An alternative strategy was considered whereby the C16–C17 unsaturation would be introduced at an earlier stage of the synthesis (**Scheme 3.31A**). It was hypothesised that pre-installation of the olefin prior to sulfide **3.166** oxidation would preclude formation of the undesired putative ketone **3.236**/enol **3.237**. Additionally, this approach would prevent the formation of undesired sulfonate ester **3.192**, a side-product observed during oxidation of sulfide **3.166** to sulfone **3.190** (refer back to **Table 3.3**). The Pummerer rearrangement is a transformation in which sulfoxides are activated by an electrophile to form sulfonium intermediates, enabling α-functionalisation. Depending on the nature of the nucleophile, subsequent elimination can furnish the corresponding olefin. Sulfides may also serve as alternatives to sulfoxides in the oxidative Pummerer rearrangement, wherein activation, typically using NCS, enables the formation of the sulfonium intermediate. The liberated chloride may subsequently act as a nucleophile, affording the corresponding α-chloro sulfide. As envisioned in the interrupted Ramberg–Bäcklund

rearrangement (**3.242**, **Scheme 3.30B**), elimination of chloride can then furnish the olefin. It was anticipated that sulfide **3.166** may undergo an oxidative Pummerer rearrangement with NCS and sodium carbonate to afford vinyl sulfide **3.243** (**Scheme 3.31A**). However, treatment of sulfide **3.166** with these conditions resulted in decomposition (**Scheme 3.31B**). It was proposed that the *S*-lone pair was competing with multiple nucleophilic functional groups present within the substrate, thereby impeding the desired reactivity. Moving away from a one-pot synthesis and elimination of the α-chloro sulfide intermediate, a stepwise approach was attempted, with sulfide **3.166** oxidised using *m*CPBA to afford corresponding sulfoxide **3.191** in 55% yield. However, subsequent attempts to induce the Pummerer rearrangement using either acetic anhydride or trifluoroacetic anhydride were unsuccessful. TLC monitoring was conducted to investigate changes over the course of the reaction and indicated the formation of a new product, evidenced also by ^{1}H NMR spectroscopy. Nevertheless, characterisation was made difficult due to compound instability. Assuming formation of vinyl sulfide **3.243**, the instability of this intermediate was rationalised based on potential electronic effects. The predictive power of the Hückel's rule ($4n + 2$ for aromaticity and $4n$ for antiaromaticity) generally diminishes for polycyclic systems and when conjugation involves exocyclic atoms. Nevertheless, it was proposed that vinyl sulfide **3.243** may experience antiaromatic-like destabilisation due to the number of π-electrons in conjugation (**Scheme 3.31C**), which could contribute to its transient nature. Considering the possibility that the observed intermediate corresponded to the desired vinyl sulfide **3.243** but was prone to decomposition during isolation, *m*CPBA was added upon detection by TLC in an attempt to effect direct oxidation to vinyl sulfone **3.244** (**Scheme 3.31D**); however, this strategy did not yield the desired product.

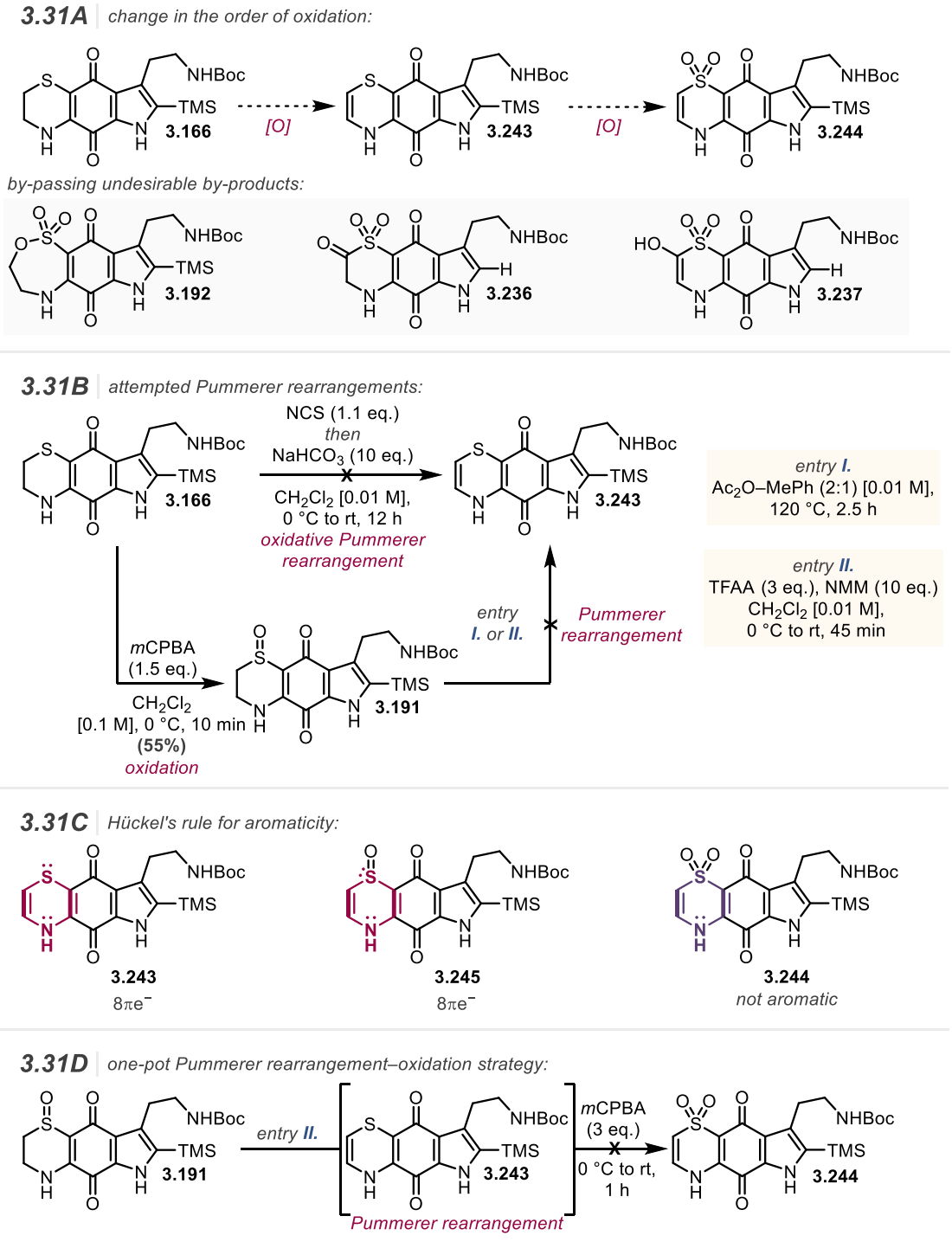

Scheme 3.31. ***(A)*** *Alternative strategy to change the order of oxidation steps.* ***(B)*** *Attempted oxidative Pummerer rearrangement of sulfide* ***3.166*** *and Pummerer rearrangement of sulfoxide* ***3.191****.* ***(C)*** *Proposed antiaromatic-like destabilisation for vinyl sulfide* ***3.243*** *and sulfoxide* ***3.245*** *based on Hückel's rule for aromaticity.* ***(D)*** *Attempted one-pot Pummerer rearrangement–oxidation of sulfoxide* ***3.191****.*

Revisiting the conditions reported by Quinn and co-workers, the reaction was conducted on a three-fold larger scale with a slight reduction in temperature, affording vinyl sulfone **3.23** in 59% yield from sulfone **3.190** (refer back to **Scheme 3.29B**); a 20% improvement over the previous

attempt, though still notably lower than the yield originally reported for sulfone **3.22** (refer back to **Scheme 3.29A**).

In summary, vinyl sulfone **3.23** was ultimately obtained under the conditions reported by Quinn and co-workers, although the yield that was achieved for sulfone **3.190** was notably lower. This reduction in yield was attributed to a possible competing Kornblum–DeLaMare rearrangement, giving rise to either putative ketone **3.236** or enol **3.237**. Alternative approaches to introduce the C16–C17 olefin, including an interrupted Ramberg–Bäcklund rearrangement and Pummerer rearrangement, were also explored but proved unsuccessful. In the future, a dehydrogenation strategy, such as with DDQ or palladium on carbon, may offer a more effective route to the C16–C17 olefin while avoiding formation of the undesired putative side-product. Nevertheless, with vinyl sulfone **3.23** successfully accessed, only a final deprotection step remained to complete the synthesis of thiaplakortone A **1.12**.

3.5.6.8.2. Deprotection to thiaplakortone B 3.1 and A 1.12

With both vinyl sulfone **3.23** and sulfone **3.190** in hand, deprotection to yield thiaplakortone A **1.12** and thiaplakortone B **3.1**, respectively, was pursued.

Treatment of vinyl sulfone **3.23** with aqueous HCl in a dichloromethane–methanol mixture effected clean removal of the *N*-Boc protecting group, affording thiaplakortone A **1.12** in quantitative yield (**Scheme 3.32A**). Notably, substitution of HCl to commonly employed trifluoroacetic acid resulted in significant decomposition of the substrate. In contrast, use of aqueous HCl on sulfone **3.190** in dichloromethane–methanol resulted only in *N*-Boc cleavage, with the C2-TMS group remaining intact, thereby affording sulfone **3.246** in 69% yield (**Scheme 3.32B**). However, exposure of sulfide **3.166** to the same deprotection conditions resulted in removal of both the *N*-Boc and C2-TMS groups, yielding sulfide **3.247** in 94% yield (**Scheme 3.32C**). This discrepancy was likely attributed to the increased electron deficiency of the ring system in sulfone **3.190**, relative to that in sulfide **3.166**, rendering direct C2-protonation less favourable. In the case of sulfone **3.190**, formation of a pentavalent silicon -ate complex was required to facilitate C2-protonation, consistent with observations made during the oxidation of sulfone **3.190** to vinyl sulfone **3.23** (refer back to **Scheme 3.29B**). To address this, sulfone **3.190** was first treated with tetrabutylammonium fluoride (TBAF), which successfully removed the C2-TMS group to afford C2-desilylated sulfone (**Scheme 3.32B**, intermediate **3.22**). Subsequent *N*-Boc deprotection using aqueous HCl in dichloromethane–methanol delivered thiaplakortone B **3.1** in 65% yield over two steps. Future efforts could examine alternative deprotection methods; for example, *in situ* generation of hydrofluoric acid may facilitate the removal of both protecting groups.

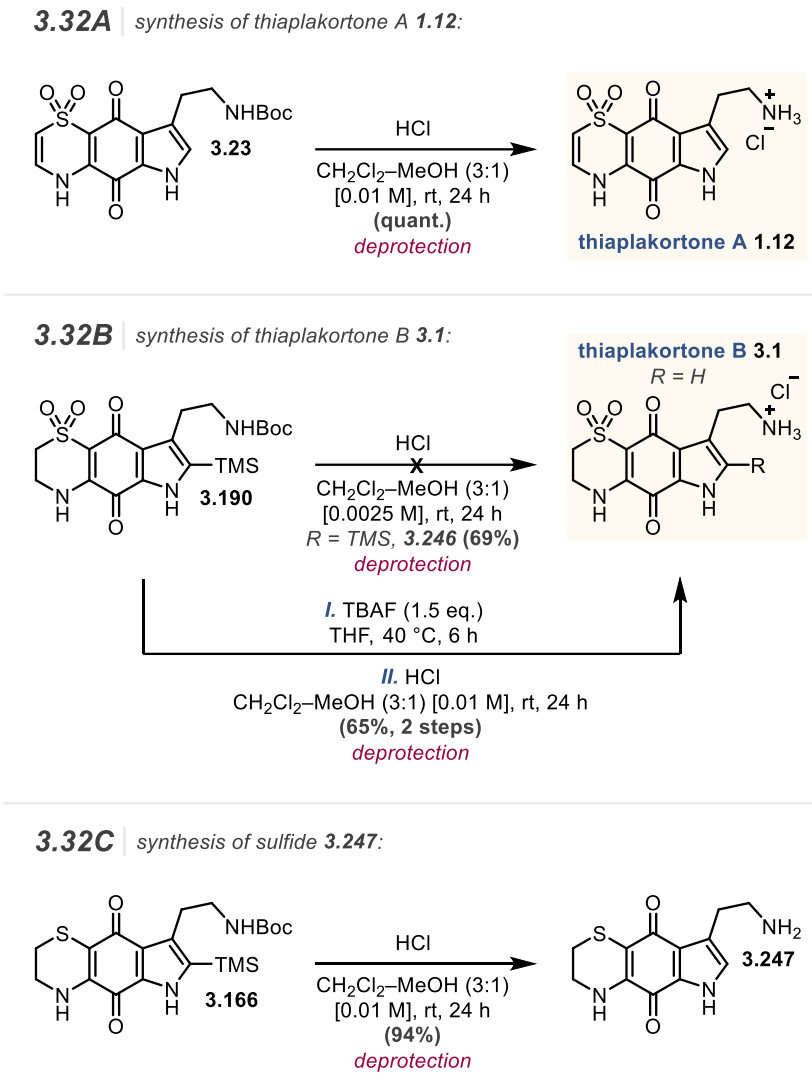

Scheme 3.32. (A) *Synthesis of thiaplakortone A* ***1.12****. (B) Synthesis of thiaplakortone B* ***3.1****. (C) Synthesis of sulfide* ***3.247****.*

Good agreement was observed between the ^{1}H and ^{13}C chemical shifts of synthesised thiaplakortone A **1.12** and those reported by Quinn and co-workers (see **Section 5.2.2.** Chapter 3, **Table 5.1** & **5.2**).[84,85] For consistency, both thiaplakortone A **1.12** and B **3.1** were synthesised as the HCl salt. Thiaplakortone B **3.1** was originally isolated as the trifluoroacetate salt, however good agreement was observed between the ^{1}H and ^{13}C chemical shifts of synthesised thiaplakortone B **3.1** and the isolated natural product (see **Section 5.2.2.** Chapter 3, **Table 5.3** & **5.4**).

3.5.6.9. Antiparasitic activity of thiaplakortone A 1.12, B 3.1 and sulfide 3.247

It was hypothesised that the highly potent antimalarial natural product thiaplakortone A **1.12** might also exhibit broader antiparasitic activity, as has been reported for other natural products, such as ascididemin **1.11** (refer back to **Table 2.4**). Unfortunately, thiaplakortone A **1.12** (IC_{50} = 8.95 ± 1.06 μM), as well as thiaplakortone B **3.1** (IC_{50} = 5.13 ± 3.82 μM) and sulfide **3.247** (IC_{50} = 2.84 ± 1.41 μM), demonstrated only moderate activity against extracellular *T. cruzi* trypomastigotes (**Table 3.5**), and were inactive against the intracellular amastigote stage of the parasite. Additionally, none of the compounds displayed activity against *L. infantum* promastigotes. However, notably, sulfide **3.247** was the most potent compound against *T. cruzi* trypomastigotes, exceeding the activity of both thiaplakortone A **1.12** and B **3.1**.

3.5 *antiparasitic activity of thiaplakortone A **1.12**, B **3.1** and sulfide **3.247**:*

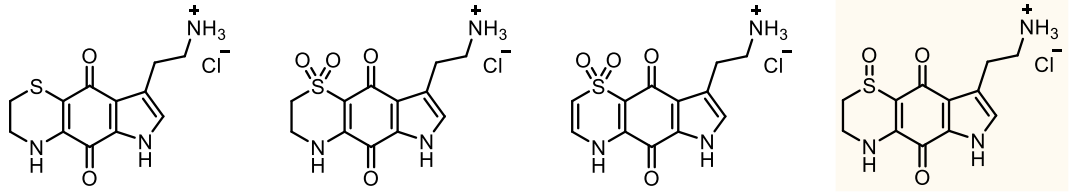

3.247 | **thiaplakortone B 3.1** | **thiaplakortone A 1.12** | **3.248** *future compound*

compound	*T. cruzi trypomastigotes / μM*	*T. cruzi amastigotes / μM*	*L. infantum promastigotes / μM*	*mammalian NCTC cells / μM*
3.247	2.84 ± 1.41	*not active*	*not active*	29.18 ±0.42
3.1	5.13 ± 3.82	*not active*	*not active*	10.43 ± 5.74
1.12	8.95 ± 1.06	*not active*	*not active*	1.57 ± 0.68

Table 3.5. *Antiparasitic activity of thiaplakortone A **1.12**, B **3.1** and sulfide **3.247**.*

All three compounds also exhibited cytotoxicity toward mammalian NCTC cells (**Table 3.5**). Although selectivity indexes (SI = CC_{50}/IC_{50}) are ideally determined using intracellular amastigote data, they were calculated here using *T. cruzi* trypomastigote values for comparative purposes. Sulfide **3.247** (CC_{50} = 29.18 ± 0.42 μM, SI = 10.3) demonstrated greater selectivity, compared with thiaplakortone A **1.12** (CC_{50} = 1.57 ± 0.68 μM, SI = 0.2) and B **3.1** (CC_{50} = 10.43

± 5.74 μM, SI = 2.0). The reduced cytotoxicity of sulfide **3.247** relative to thiaplakortone A **1.12**, combined with its greater antiparasitic activity and synthetic accessibility, identifies this analogue as a promising candidate for further investigation of antimalarial activity.

The presence of the quinone moiety in thiaplakortone A **1.12**, B **3.1**, and sulfide **3.247** suggests that antiparasitic activity, as well as cytotoxicity, may be partially mediated by reactive oxygen species generation; consistent with observations for other thiazine 1,1-dioxide fused quinone-natural products (thiazinoquinones).[87] Additionally, a similar mechanism has been proposed for ascididemin **1.11** as a result of the iminoquinone present (refer back to **Section 2.2.2.** Reactive oxygen species). The reduction potential of the quinone core, influenced by the attached substituents altering the electron-density, is potentially a key determinant of activity. Future studies would focus on the synthesis of sulfoxide **3.248** (**Table 3.5**) to assess whether it exhibits intermediate antiparasitic activity relative to sulfide **3.247** and thiaplakortones A **1.12**/B **3.1**, or if the altered electronic properties of the quinone afford improved potency and reduced cytotoxicity.

4. Attempted synthesis of related natural products

The synthetic route developed for the total synthesis of thiaplakortone B **3.1** and A **1.12** enabled access to thiaplakortone analogues at lower sulfur oxidation states – it was envisioned this could offer additional utility in addressing related target molecules.

4.1. Macrophilone F and G

Macrophilones F **4.2** and G **4.3** were first isolated in 2018 by Gustafson *et al.* (**Figure 4.1A**), alongside four related pyrroloiminoquinones, and feature a dihydrothiazine ring in the sulfide- and sulfoxide-oxidation state, respectively.[170] Several members of the macrophilone family exhibited anticancer activity, with a mechanism–of–action attributed to inhibition of small ubiquitin-like modifier (SUMO) protein conjugation.[171] In particular, treatment of cancer cells with macrophilone A **4.4** led to elevated intracellular reactive oxygen species levels. It was postulated that cysteine thiol sidechains (**4.6**) could be oxidised by these reactive oxygen species leading to cross-linking via disulfide bond formation (**4.7**), thus preventing SUMO protein conjugation (**Figure 4.1B**). It was hypothesised that macrophilones F **4.2** and G **4.3** could be accessed en route to thiaplakortones B **3.1** and A **1.12** via a common intermediate, sulfide **3.166**. Furthermore, given the close structural resemblance between the macrophilone and thiaplakortone families, it is plausible that the macrophilones may also exhibit antiparasitic activity.

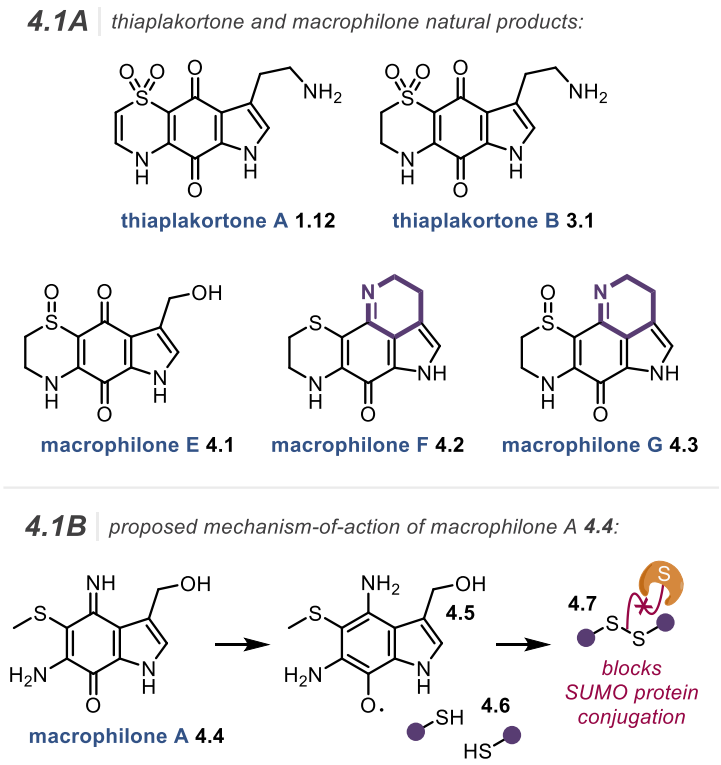

Figure 4.1. (A) *Thiaplakortone and macrophilone natural products.* ***(B)*** *Mechanism-of-action of macrophilone A* ***4.4****. Where S = SUMO protein.*

With the hypothesis that sulfide **3.166** might serve as a key intermediate to divergently access both the thiaplakortone and macrophilone families, the initial strategy focused on a cyclocondensation of its deprotected form, sulfide **3.247** (**Scheme 4.1A**).

4.1A | *failed intramolecular cyclisations to macrophilone F* ***4.2****:*

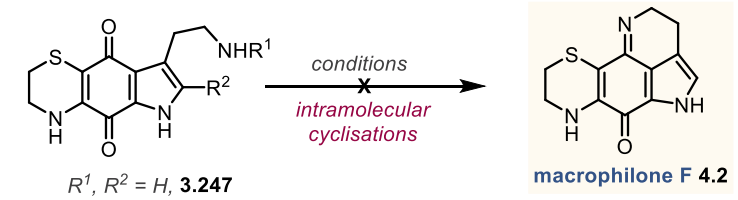

R^1, *R*^{2} = *H*, **3.247**
R^1 = *Boc and R*^{2} = *TMS*, **3.166**

entry	*R*^{1}	*R*^{2}	*conditions*
1	H	H	$NaHCO_3$ (6 eq.) EtOH [0.01 M], 80 °C, 12 h
2	H	H	PhMe [0.01 M], 140 °C, 4 h
3	H	H	$Fe_2(SO_4)_3$ (0.25 eq.) AcOH [0.01 M], 100 °C, 1.5 h
4	H	H	$ZnCl_2$ (3 eq.) EtOH–$HC(OMe_3)$ (10:1) [0.02 M], 70 °C, 12 h
5	H	H	$Ti(O^iPr)_4$ (3 eq.) DCE [0.01 M], 80 °C, 12 h
6	Boc	TMS	$Fe_2(SO_4)_3$ (0.25 eq.) AcOH [0.01 M], 100 °C, 1.5 h
7	Boc	TMS	*Eaton's reagent* [0.02 M], 100 °C, 1.5 h
8	H	H	$ImSO_2N_3$ (1.2 eq.), $CuSO_4$ (1.2 eq.), K_2CO_3 (5 eq.) H_2O–MeOH (8:1) [0.02 M] *then add* PPh_3 (eq.), THF [0.01 M]

4.1B | *future cyclocondensation to macrophilone G* ***4.3****:*

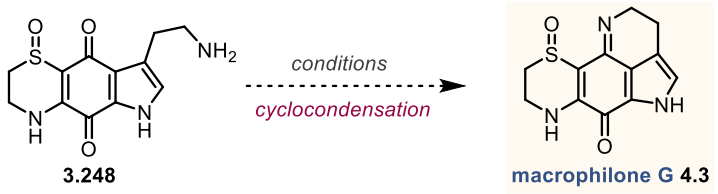

Scheme 4.1. (A) *Failed intramolecular cyclisation attempts to macrophilone F* ***4.2****. Table of conditions.* ***(B)*** *Future cyclocondensation of sulfoxide* ***3.248*** *to macrophilone G* ***4.3****.*

The conditions first examined were those reported by Heathcock and Aubart in their synthesis of discorhabdin natural products (**Scheme 4.2**).[172] However, treatment of sulfide **3.247** with sodium bicarbonate and activated 3 Å molecular sieves in distilled ethanol at 80 °C resulted in decomposition (**Scheme 4.1A** table, entry 1).

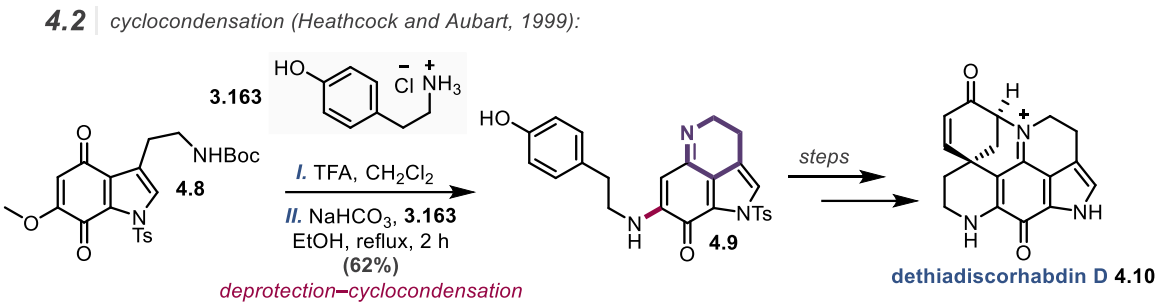

Scheme 4.2. *Cyclocondensation during the total synthesis of dethiadiscorhabdin D* ***4.10*** *(Heathcock and Aubart, 1999).*

Given this outcome in basic conditions, neutral conditions were next explored. Refluxing sulfide **3.247** in toluene with a Dean–Stark setup (**Scheme 4.1A** table, entry 2) led to formation of a new compound; however, the ^{1}H NMR spectrum in methanol-d_4 did not correspond to that reported for macrophilone F **4.2**, and the spectroscopic data was insufficient for structural identification. Since Schiff base formation is known to proceed more readily under acidic conditions,[173] a range of acidic catalysts and reagents were then investigated. Notably, when catalytic iron(III) sulfate in acetic acid was employed (**Scheme 4.1A** table, entry 3), the ^{1}H NMR spectrum of the product was similar to that obtained under the Dean–Stark conditions. Other attempts using zinc(II) chloride in ethanol–trimethyl orthoformate (**Scheme 4.1A** table, entry 4) or titanium isopropoxide in DCE (entry 5) led to decomposition. It is conceivable that the increased electrophilicity of sulfoxide **3.248** might facilitate cyclocondensation relative to sulfide **3.247** (**Scheme 4.1B**); however, this route toward macrophilone G **4.3** was not pursued.

Cyclisation conditions were also evaluated using protected sulfide **3.166**, bearing both *N*-Boc and C2-TMS groups, as both protecting groups were amenable to removal under acidic conditions. Treatment with catalytic iron(III) sulfate in acetic acid (**Scheme 4.1A** table, entry 6) again yielded a product whose ^{1}H NMR spectrum was similar to that obtained from sulfide **3.247** under a Dean–Stark set-up; however, the spectral data remained inconsistent with that of macrophilone F **4.2**. Exposure of sulfide **3.166** to Eaton's reagent (7.7% phosphorus pentoxide in methanesulfonic acid) led to decomposition (**Scheme 4.1A** table, entry 7). With efforts to access macrophilone F **4.2** via cyclocondensation of sulfide **3.166** and **3.247** proving unsuccessful, alternative synthetic approaches were next explored.

In the total synthesis of makaluvamine natural products, Wood *et al.* reported that an intramolecular cyclisation to afford indoleiminoquinone **3.161** in 65% yield could be achieved from azide **4.11** via an *aza*-Wittig reaction (**Scheme 4.3A**). It was envisioned that the primary amine in sulfide **3.247** could be converted to an azide (**4.12**) and subjected to a similar *aza*-Wittig reaction (intermediate **4.14**) to enable formation of macrophilone F **4.2** (**Scheme 4.3B**). Thus, sulfide **3.247** was treated with a diazo-transfer reagent, imidazole-1-sulfonyl azide **4.13** ($ImSO_2N_3$), copper(II) sulfate and potassium carbonate in a methanol–water solvent system (**Scheme 4.1A** table, entry 8). Upon consumption of the starting material, as suggested by TLC analysis, triphenylphosphine was added as a solution in THF. Although sulfide **3.247** was fully consumed, macrophilone F **4.2** was not observed by ^1H NMR analysis of the crude material. It was postulated that other nucleophilic sites present in the molecule (**Scheme 4.3B**), such as the *S*-lone pair, may have competed for the diazo-transfer reagent, preventing the synthesis of the desired azide (*cf.* oxidative Pummerer rearragenement of sulfide **3.166**, refer back to **Scheme 3.31B**).

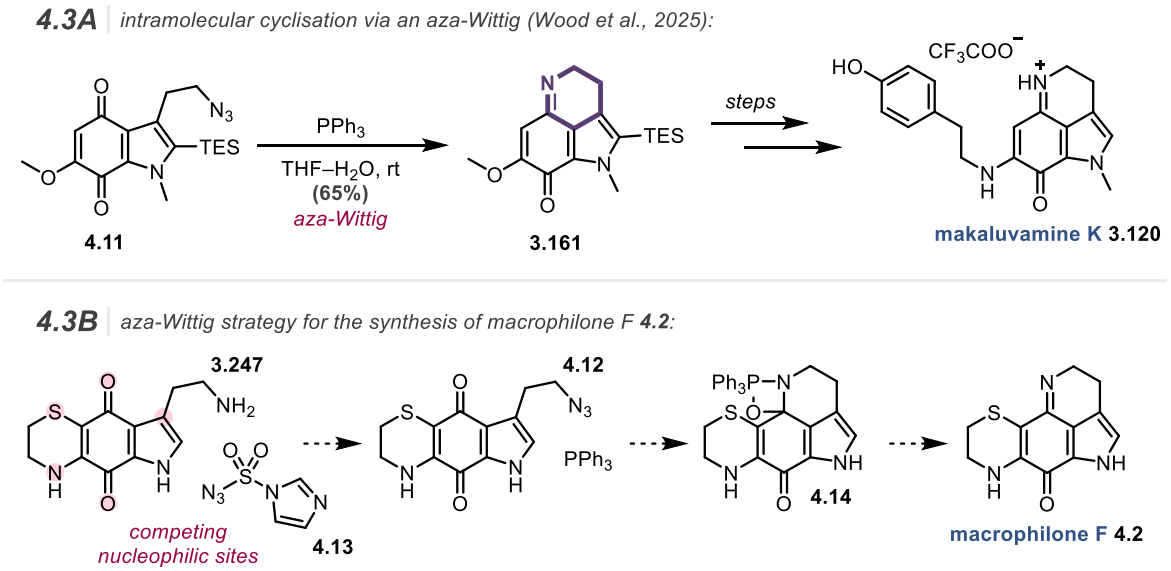

Scheme 4.3. (A) *aza-Wittig during the total synthesis of makaluvamine K* ***3.120*** *(Wood et al., 2025).* ***(B)*** *Proposed application of the aza-Wittig strategy for the synthesis of macrophilone F* ***4.2****.*

Recently, Wood and Tuccinardi encountered similar challenges in achieving intramolecular cyclisation to form imine **4.16** during their total synthesis of aleutianamine **4.17** (**Scheme**

4.4A).[174] They noted that "the viability of this cyclocondensation step is well-known to be highly dependent upon the substitution pattern of the pyrroloquinone", a conclusion also reached by Heathcock and Aubart in their studies on the discorhabdin natural product family (**Scheme 4.4B**).[172]

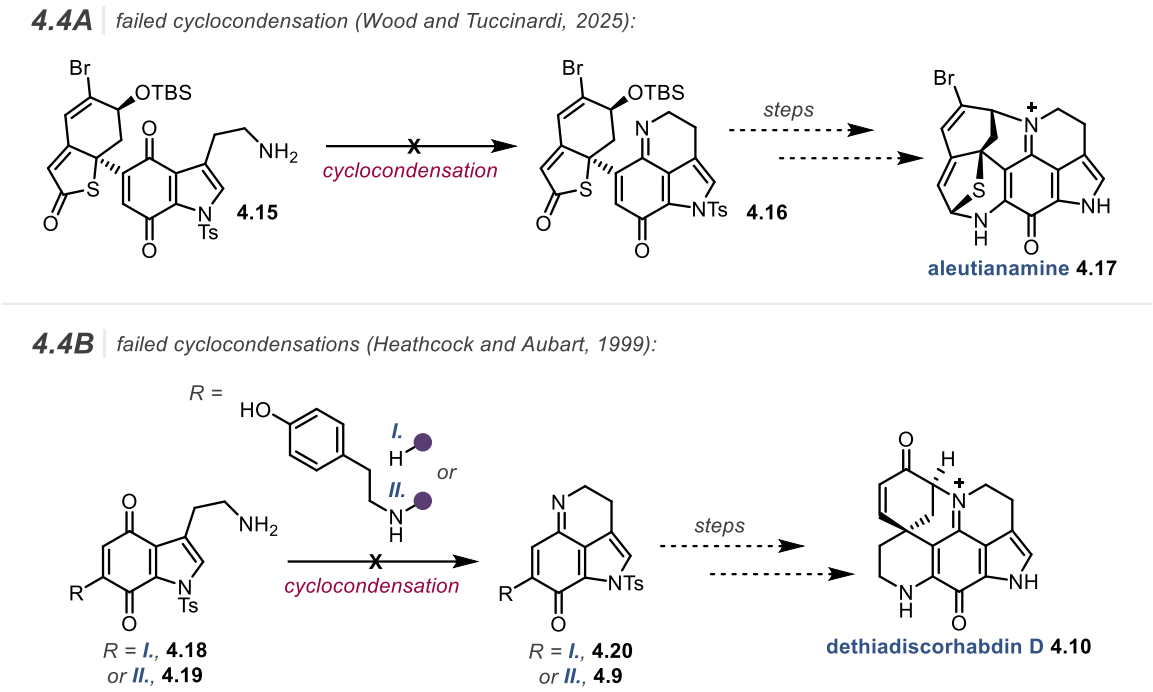

Scheme 4.4. (A) *Failed cyclocondensation attempt towards the total synthesis of aleutianamine* ***4.17*** *(Wood and Tuccinardi, 2025).* ***(B)*** *Failed cyclocondensation attempts towards the total synthesis of dethiadiscorhabdin D* ***4.10*** *(Heathcock and Aubart, 1999).*

An alternative strategy considered was the introduction of the *N*-atom prior to indole formation. Although intramolecular Larock indole syntheses have been reported (**Scheme 4.5A**),[175] their application to the construction of this particular [6.5.6] tricyclic framework for the synthesis of indoleiminoquinone natural products, such as macrophilone F **4.2**, remains unprecedented (**Scheme 4.5B**).

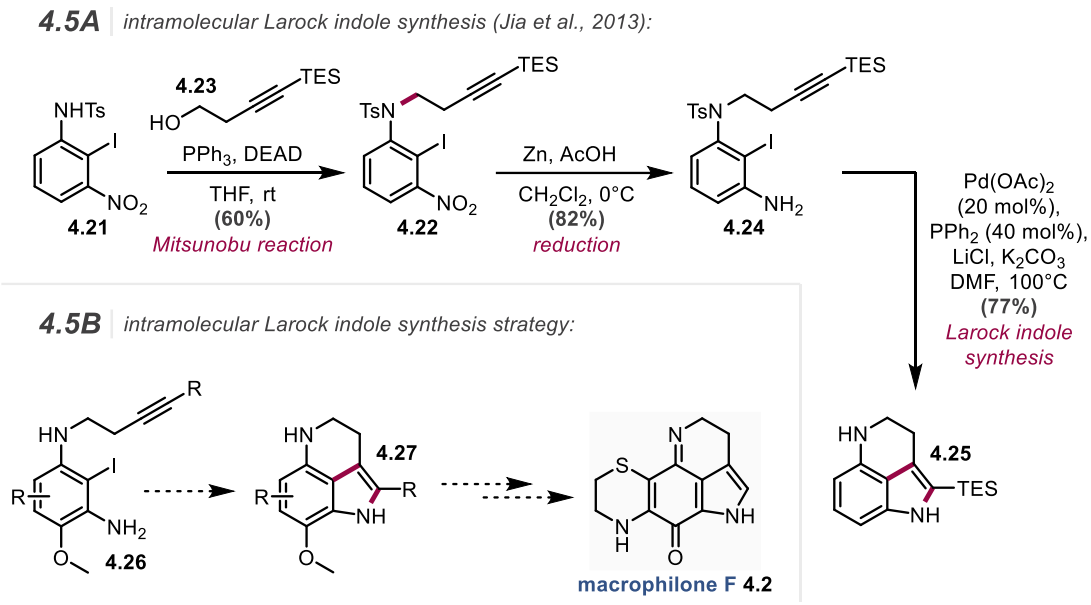

Scheme 4.5. (A) *Intramolecular Larock indole synthesis (Jia et al., 2013).* ***(B)*** *Intramolecular Larock indole synthesis strategy for the synthesis of macrophilone F* ***4.2****.*

To assess the viability of this approach, aminonitrobenzene **4.28** was selected as a model substrate (**Scheme 4.6A**). It was envisioned that alkylation of the aniline moiety would enable introduction of a suitable tethered alkyne for an intramolecular Larock indole synthesis. However, alkylation with homopropargyl bromide **4.30** resulted in an intractable mixture (**Scheme 4.6A** table, entry 1). It was hypothesised that with homopropargyl bromide **4.30** as the limiting reagent to avoid over-alkylation, aniline **4.28** preferentially reacted with itself via an S_NAr pathway. To circumvent this, the substrate was changed to aminonitrobenzene **4.29**, lacking the *para*-fluoride substituent. Nonetheless, attempts to alkylate this aniline using either homopropargyl bromide **4.30** or *O*-Ts homopropargyl alcohol **4.31** again proved unsuccessful (**Scheme 4.6A** table, entries 2 & 3, respectively). This may be attributed to competitive E2 elimination under basic conditions, producing enyne **4.34**, and thereby precluding S_N2 substitution with aniline **4.29**.

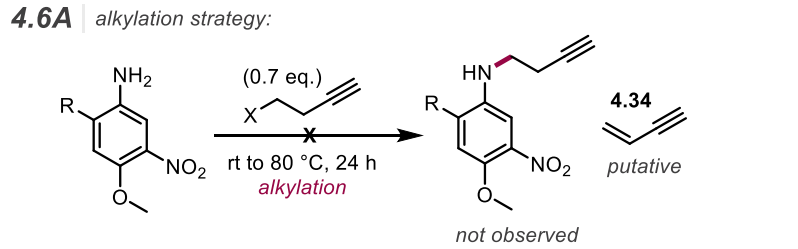

entry	R	X	product	conditions
1	F **4.28**	Br **4.30**	**4.32**	K_2CO_3 (1 eq.) MeCN [0.25 M]
2	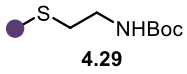 **4.29**	Br **4.30**	**4.33**	K_2CO_3 (1 eq.) MeCN [0.25 M]
3	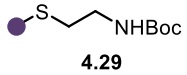 **4.29**	OTs **4.31**	**4.33**	K_2CO_3 (3 eq.), KI (0.1 eq.) MeCN [0.75 M]

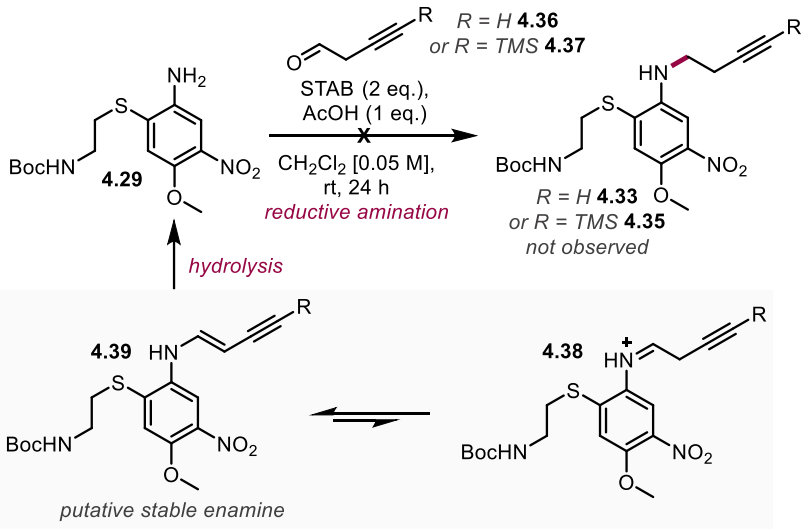

Scheme 4.6. (A) *Attempted synthesis of a homopropargyl amine via an alkylation strategy.* ***(B)*** *Attempted synthesis of a homopropargyl amine via a reductive amination strategy.*

Efforts were next directed toward the synthesis of a homopropargyl amine via reductive amination. Both aldehyde **4.36** and its TMS-protected analogue **4.37** were subjected to reaction with aminonitrobenzene **4.29** and sodium triacetoxyborohydride (STAB), but no desired product was observed (**Scheme 4.6B**). Analysis of the crude ^{1}H NMR spectra suggested the presence of only starting material. It is possible that after iminium **4.38** formation, tautomerisation to stable enamine **4.39** occurred instead of the desired reduction to aniline **4.33** or **4.35**. This intermediate could then have undergone hydrolysis to the starting material upon aqueous work-up.

Given the lack of success with the aniline-based approaches, attention turned to the introduction of homopropargyl amine **4.41** via a Buchwald–Hartwig cross-coupling with aryl bromide **4.40** (**Scheme 4.7**). HTE was employed to screen a range of catalyst systems using either caesium carbonate or P_2-Et as the base in 1,4-dioxane, both commonly used in Buchwald–Hartwig cross-couplings. For the catalyst, a collection of 33 'cutting-edge' catalysts were explored.[176] Each well contained a combination of two catalysts to increase the likelihood of identifying successful conditions. Reactions were conducted at 80 °C for 12 hours and then analysed by UPLC. Under most conditions, the reactions yielded intractable mixtures, and desired *N*-aryl homopropargyl amine **4.33** was not observed. The only identifiable species had a molecular weight consistent with the putative intramolecularly cyclised product **4.42**, which has therefore been tentatively assigned as such.

4.7 | *Buchwald–Hartwig cross-coupling screen using HTE:*

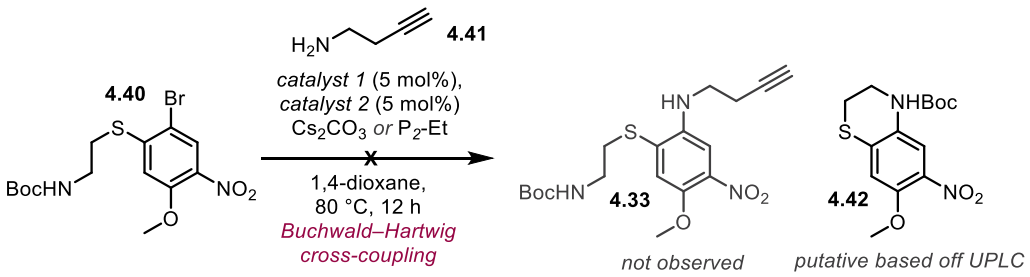

Scheme 4.7. *Buchwald–Hartwig cross-coupling strategy using HTE. Catalysts explored: BrettPhos Pd G4, GPhos Pd G6, JosiPhos Pd G3, [BippyPhos Pd(allyl]OTf , DPPF Pd G3, XantPhos Pd G3, RuPhos Pd G3, AdBrettPhos Pd G3, QPhos Pd G3, SPhos Pd G3, MorDalPhos Pd G3, P(tBu)3 Pd G3, AlPhos Pd G6-OTf, APhos Pd G3, JackiePhos Pd G3, CyJohnPhos Pd G3, CataCXiumA Pd G3, racBINAP Pd G3, tBuXPhos Pd G3, XPhos Pd G3, Me4tBuXPhos Pd G3, tBuDavePhos Pd G4, (tBu)PhCPhos Pd G3, Pd PEPPSI iHeptCl, BrettPhos Pd G3, CPhos Pd G3, DavePhos Pd G3, P(tBu)3 Pd G2, J009 Pd G3, RuPhos Pd G2, SPhos Pd G2, (tBu)XPhos Pd G3, XantPhos Pd G3.*

Attempts to divergently access macrophilone F **4.2** and G **4.3** from a common intermediate en route to thiaplakortone B **3.1** and A **1.12** were unsuccessful. Efforts to prepare a substrate suitable for intramolecular Larock indole synthesis, aimed at installing the six-membered ring prior to oxidation, also did not succeed. In future studies, cyclocondensation of sulfoxide **3.248** to afford macrophilone G **4.3** warrants investigation, as the reduced electron density of the quinone moity may facilitate this transformation. Finally, there is hope of the potential discovery of new

thiaplakortone natural products bearing sulfide or sulfoxide oxidation states, akin to macrophilones F **4.2** and G **4.3**, in the future.

4.2. Macrophilone E

It was anticipated that the Larock indole synthesis strategy could be adapted for the synthesis of macrophilone E **4.1** (**Scheme 4.8B**), another natural product isolated alongside macrophilone F **4.2** and G **4.3**,[170] by replacing the alkyne coupling partner with *O*-TBS propargyl alcohol **4.45**. The preparation of **4.45** was achieved in 45% yield over two steps from propargyl alcohol **4.43** (**Scheme 4.8A**). The same conditions previously employed for the Larock indole synthesis using homopropargyl amine **3.84** and *ortho*-iodoaniline **3.134** (refer back to **Scheme 3.16A**) were applied. While the starting material was fully consumed, no formation of the desired trimethoxyindole **4.46** was observed (**Scheme 4.8B**). It is likely that the C3-substituted benzylic-like *O*-TBS can be readily eliminated by the indole at high temperature (intermediate **4.47**) thus causing the product to be unstable.

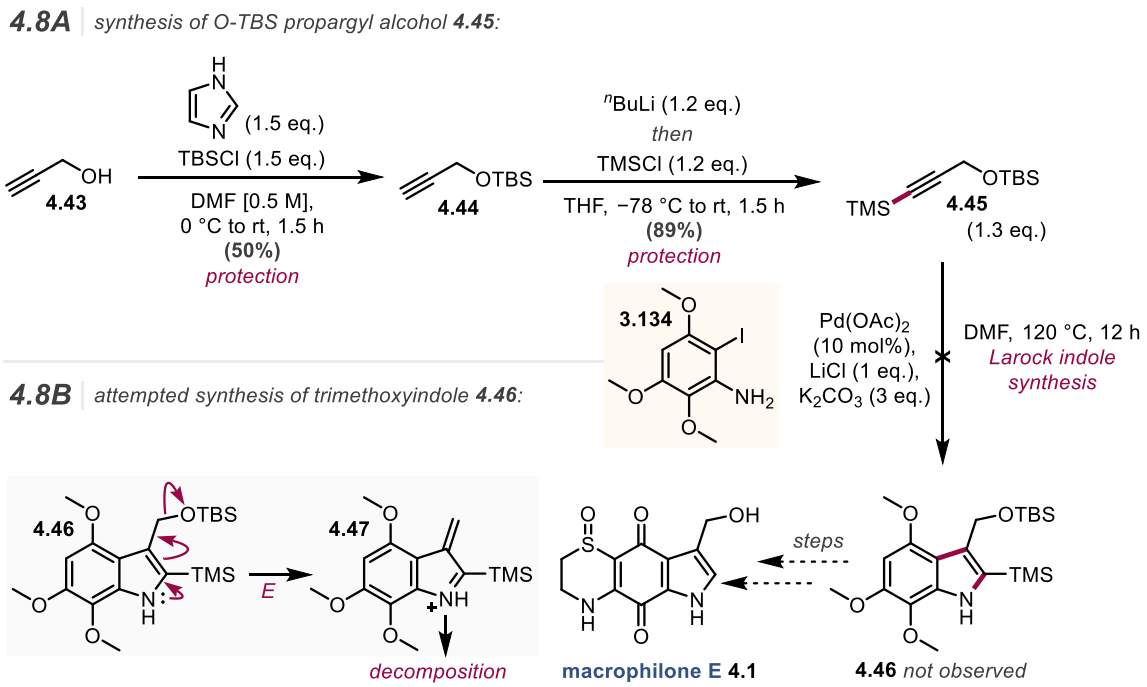

Scheme 4.8. (A) *Synthesis of O-TBS propargyl alcohol* ***4.45****. (B) Attempted synthesis of trimethoxyindole* ***4.46*** *using a Larock indole synthesis strategy for the synthesis of macrophilone E* ***4.1****.*

Given the lack of success with the Larock indole synthesis using *O*-TBS propargyl alcohol **4.45**, future efforts may employ methyl propiolate **4.49** as a masked alcohol (**Scheme 4.9A**), to be

revealed via reduction at a later stage.[171] A similar strategy has been employed for the total synthesis of macrophilone A **4.4** (**Scheme 4.9B**).

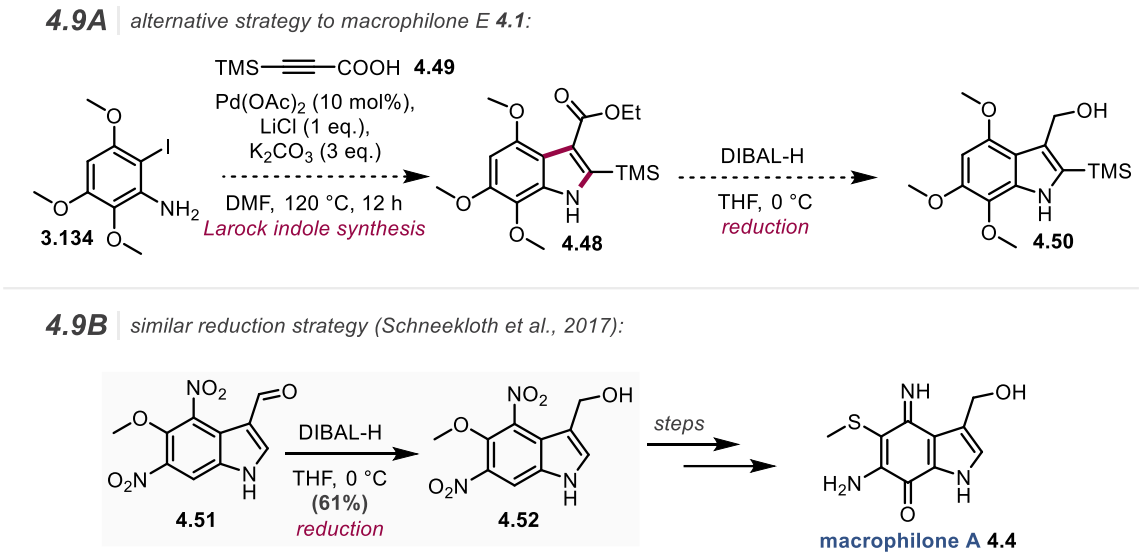

Scheme 4.9. (A) *Future strategy for the synthesis of trimethoxyindole* ***4.50****. (B) Reduction during the synthesis of macrophilone A* ***4.4*** *(Schneekloth et al., 2017).*

4.3. Ascidiathiazone B

Copp *et al.* first reported the isolation of the ascidian natural products ascidiathiazone A **3.138** and B **3.139** in 2007, alongside the total synthesis of ascidiathiazone A **3.138** (**Figure 4.2**).[115] Subsequent *in vitro* evaluation revealed that ascidiathiazone A **3.138** exhibited antiparasitic activity against *P. falciparum K1* strain (IC_{50} = 3.3 μM) and *T. b. rhodesiense* trypomastigotes (IC_{50} = 3.1 μM). Ascidiathiazone A **3.138** was effectively inactive against *T. cruzi* trypomastigotes and *L. donovani* promastigotes, however it also demonstrated minimal cytotoxicity against a mammalian cell-line. To date, no total synthesis of ascidiathiazone B **3.139** has been published in peer-reviewed literature, with the sole report appearing in a recent doctoral thesis.[123] Moreover, its antiparasitic activity has not been investigated. However, given previous findings that the regiochemistry and oxidation state of the thiazine 1,1-dioxide ring markedly influence activity of thiaplakortone analogues (refer back to **Table 3.1**), it is hypothesised that ascidiathiazone B **3.139** may exhibit enhanced potency. Thus, it was hoped to further demonstrate the synthetic utility of cystamine **3.153** as an alternative to hypotaurine **3.10** by targeting the synthesis of ascidiathiazone B **3.139**.

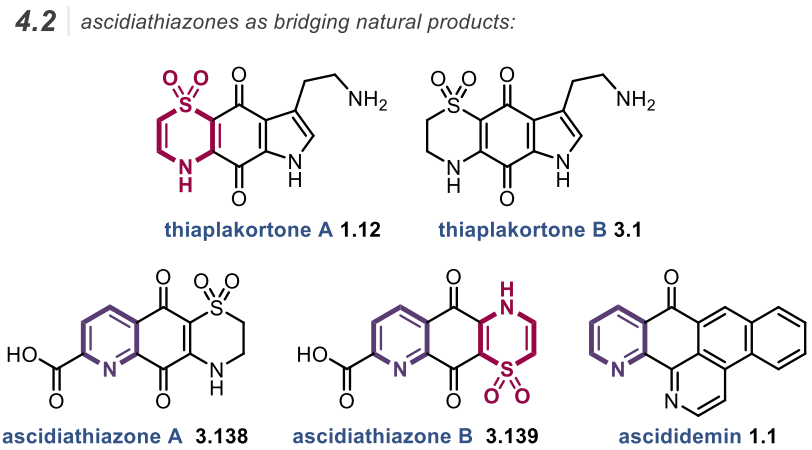

Figure 4.2. *Ascidiathiazone B **3.139** is a bridging natural product since it structural resembles both thiaplakortone A **1.12** and ascididemin **1.11**.*

For the synthesis of ascidiathiazone B **3.139**, the *de novo* synthesis of quinoline **4.56** was initially envisioned (**Scheme 4.10A**). Incorporation of an ester at the C2-position would have allowed the

carboxylic acid to be revealed at the end, while *para*-dimethoxy substitution of C5 and C8 was expected to facilitate oxidation to the corresponding quinone. However, this substitution pattern is synthetically challenging, as C2-functionalisation often results in concurrent functionalisation at the C3- or C4-positions.[177] Several literature-reported strategies were initially explored, beginning from 2,5-dimethoxyaniline **2.30**. A one-pot condensation of aniline **2.30** with aldehyde **4.57**, followed by a Povarov-style formal cycloaddition with enol ether **4.58**,[178] and subsequent elimination–aromatisation to afford quinoline **4.56**, was tested but proved unsuccessful (**Scheme 4.10B**); instead, an unknown product formed and therefore this was not pursued further.

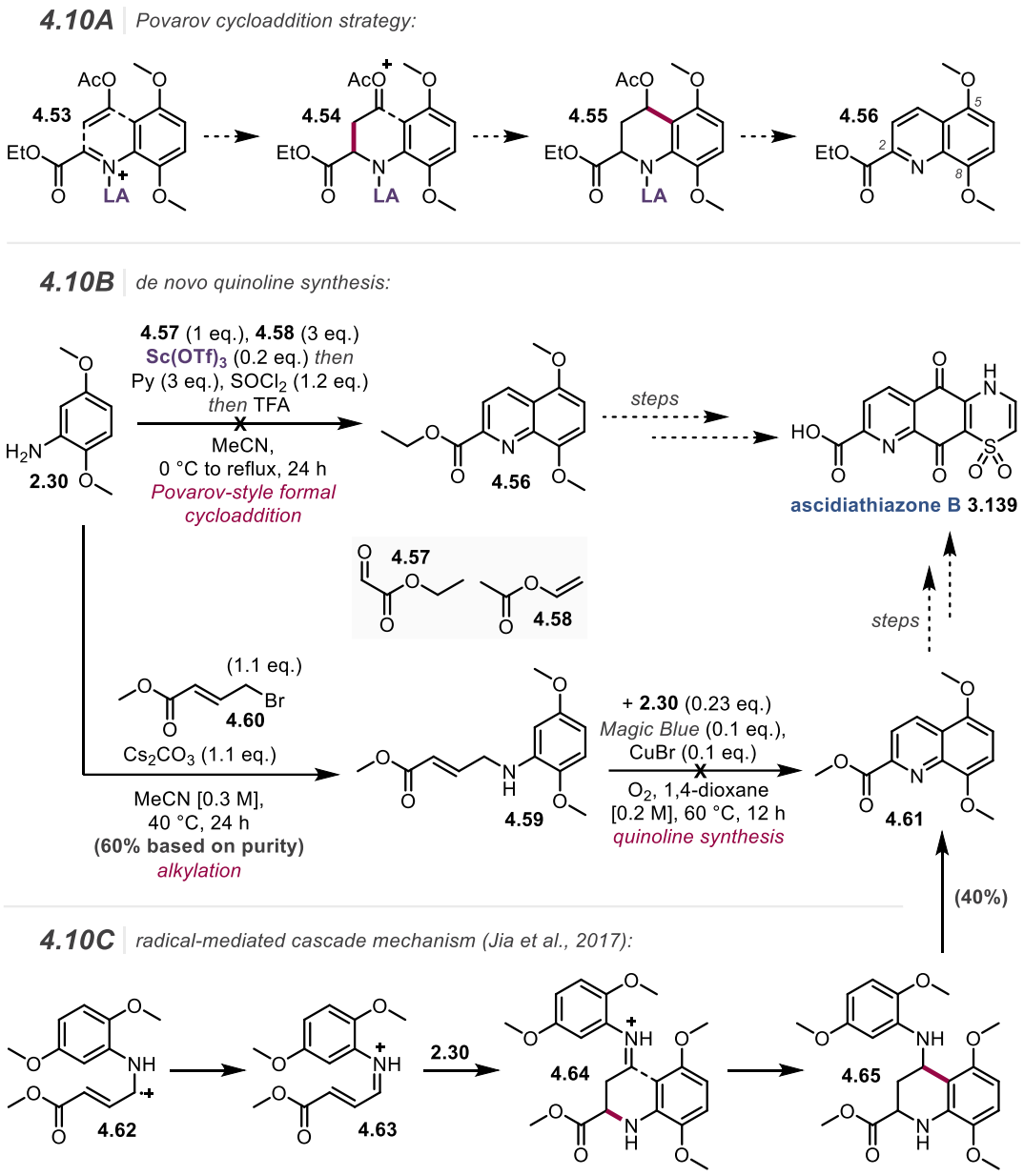

Scheme 4.10. (A) *Povarov cycloaddition strategy.* ***(B)*** *Attempted de novo quinoline synthesis.* ***(C)*** *Radical-mediated cascade mechanism (Jia et al., 2017).*

Quinoline **4.61** has previously been reported to arise from aniline **4.59** via a radical-mediated cascade (**Scheme 4.10B**). The proposed mechanism for this transformation involves single-electron oxidation of aniline **4.59** with tris(4-bromophenyl)ammoniumyl hexachloroantimonate (Magic Blue), generating a radical cation (**4.62**) at the α-position relative to the nitrogen atom (**Scheme 4.10C**). Subsequent oxidation furnishes an α,β-unsaturated iminium species **4.63**, which undergoes 1,4-conjugate addition with dimethoxyaniline **2.30**. Regeneration of the iminium intermediate (**4.64**) is followed by an intramolecular Friedel–Crafts reaction (**4.65**) and

final elimination–aromatisation delivers quinoline **4.61**. In our hands, 2,5-dimethoxyaniline **2.30** was converted to aniline **4.59** in 60% yield based on purity, though the crude material contained a 23% impurity of unreacted dimethoxyaniline **2.30** which could not be removed by FCC (**Scheme 4.10B**). As the subsequent transformation employed dimethoxyaniline **2.30** catalytically, this impurity was not expected to be detrimental. Nonetheless, despite reports of a 40% yield for quinoline **4.61** under the published conditions,[179] the desired product could not be obtained.

Given the challenges associated with the *de novo* synthesis of a quinoline bearing a C2-ester and C5- and C8-methoxy substituents, an alternative strategy was proposed wherein the C2-functionality would be introduced at a later stage. It was envisioned that Minisci-type chemistry on dimethoxy-5,8-quinoline **2.97** could enable selective C2-alkylation. Moschitto *et al.* reported a photocatalytic desulfinative C2-alkylation of heteroaromatic *N*-oxides using protected Rongalite® **4.68**.[180] Mechanistically, the *N*-oxide and protected Rongalite® **4.68** form an electrostatic electron donor–acceptor (EDA) complex, which, under visible light irradiation, enabled *in situ* extrusion of SO_2 and regioselective alkylation. Acidic work-up yielded C2-methylene alcohols, which could be oxidised to the corresponding carboxylic acids as needed. Towards this end, dimethoxy-5,8-quinoline **2.97** was converted to *N*-oxide **4.66** in 34% yield using *m*CPBA (**Scheme 4.11**). However, treatment of **4.66** with the conditions used by Moschitto *et al.* resulted in complete consumption of starting material without formation of quinoline **4.67**. ^{1}H NMR analysis revealed the presence of four aromatic-like protons and the absence of the methylene alcohol. Additionally, both methoxy substituents remained intact. Based on the observed chemical shifts, formation of benzo-4-pyridone **4.69** or benzo-2-pyridone **4.70** was considered (**Scheme 4.11**), although the data did not agree with literature values for either structure. As such, this route was not pursued further.

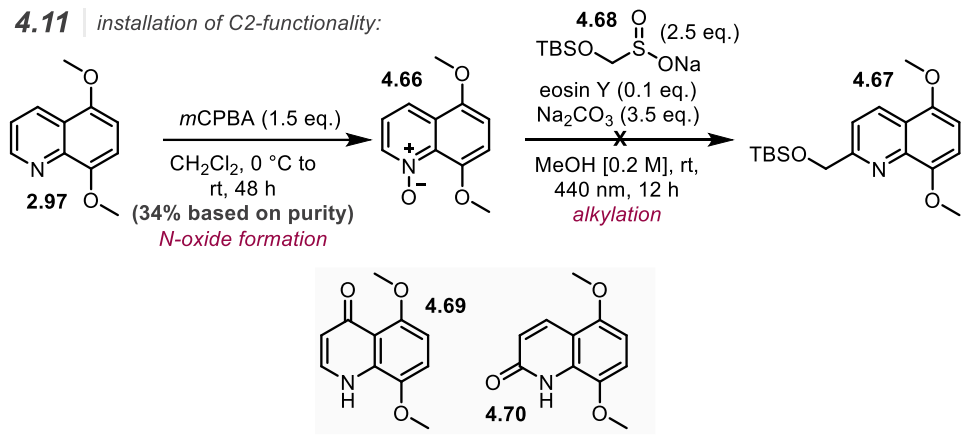

Scheme 4.11. *Attempted installation of C2-functionality.*

Owing to the lack of success with *de novo* quinoline synthesis, the strategy was revised to instead employ a commercially available 2-carboxylic acid-8-hydroxyquinoline **4.71** (**Scheme 4.12A**). The methyl ester **4.72** could be synthesised in 93% yield via Fischer–Speier esterification using thionyl chloride in methanol. Oxidation of methyl ester quinoline **4.72** with a large excess of Frémy's salt (10 eq.) resulted in incomplete conversion to desired 2-methyl ester quinoline-5,8-dione **4.73**, affording a 2:1 mixture of starting material to product. Due to the known instability of related quinones on silica gel (refer back to **Scheme 2.9B** & **3.13B**), the crude mixture was carried forward without purification. Treatment of the mixture with cerium(III) chloride in methanol under an oxygen atmosphere afforded enamine **4.76** in 10% yield over two steps (**Scheme 4.12B**). Alternatively, 2-methyl ester quinoline-5,8-dione **4.73** was accessed via electrochemical oxidation of 2-methyl ester quinoline **4.74** (**Scheme 4.12A**). This process proceeded through sequential hydroxylation to the corresponding hydroquinone **4.75**, which was subsequently oxidised with potassium persulfate to furnish the desired quinone in 38% yield.

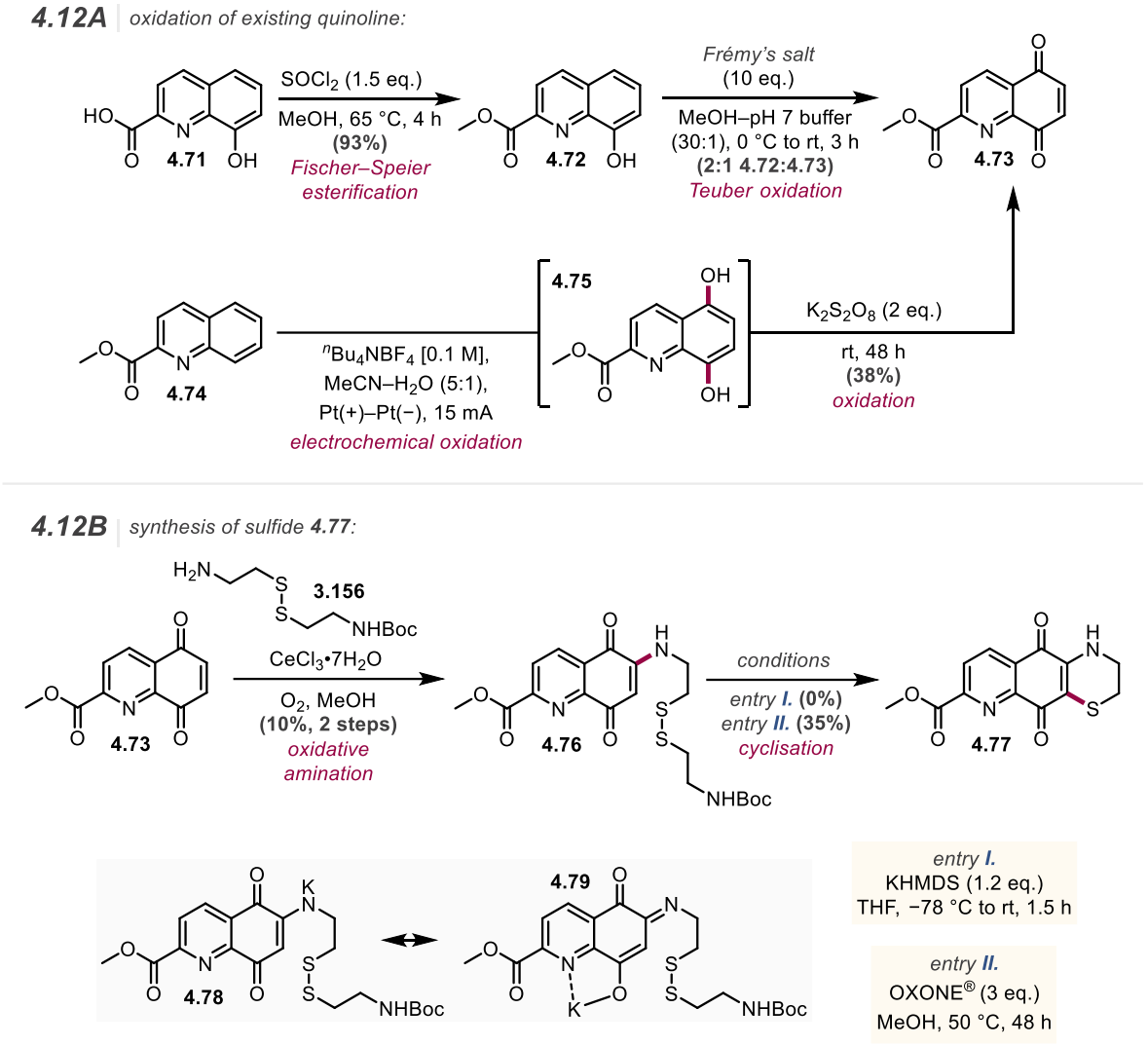

Scheme 4.12. (A) *Oxidation of pre-existing quinoline.* ***(B)*** *Installation of dihydrothiazine ring.*

Treatment of enamine **4.76** with KHMDS, previously effective in converting enamine **3.165** to sulfide **3.166** (refer back to **Scheme 3.22**), failed to yield desired sulfide **4.77**. A colour change upon addition of base was presumably indicative of deprotonation; however, the resulting potassium metalloenamine **4.78**/enolate **4.79** did not undergo nucleophilic attack at the electrophilic S–S σ* orbital. This lack of reactivity may be attributed to the potassium enolate **4.79** being the major resonance contributor, favouring the formation of a five-membered chelate ring with the potassium cation. As a result, intramolecular cyclisation was disfavoured, and the enolate was simply protonated upon aqueous work-up. Although not investigated, the use of 18-crown-6

to sequester the potassium cation may disrupt chelation and promote the desired base-induced cyclisation.

However, as observed for enamine **3.157** (formation of sulfide **3.158**, refer back to **Scheme 3.18B**), treatment with OXONE® in methanol afforded sulfide **4.77** in 35% yield. Furthermore, exposure of enamine **4.76** to NBS in methanol resulted in the formation of a similar, unidentified cyclised product, bearing an additional methoxy group (refer back to **Scheme 3.18C**). In contrast, conditions for dihydrothiazine formation previously identified via HTE for the formation of sulfide **3.166** (refer back to **Scheme 3.25B** & **3.26B**) were initially evaluated using a simpler substrate, quinoline-5,8-dione **2.4** (**Scheme 4.13**). In this case, a modified protocol was employed in which the base was added only after enamine **4.80** formation had been confirmed by UPLC analysis. Nevertheless, the desired sulfide **4.82** was isolated in 3% yield. When the same conditions were applied to 2-methyl ester quinoline-5,8-dione **4.73**, no formation of the target sulfide **4.77** was observed.

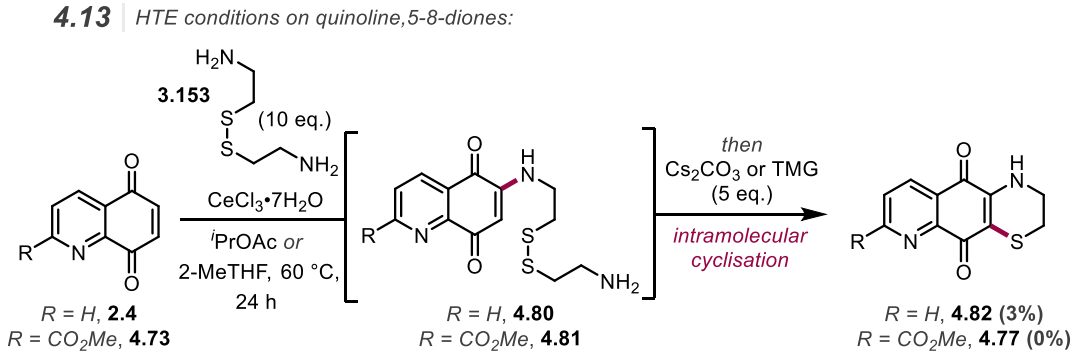

Scheme 4.13. *Employing conditions identified by HTE on quinoline-5,8-diones.*

In conclusion, initial efforts toward the *de novo* synthesis of the target trisubstituted quinoline, 2-ester-5,8-dimethoxyquinoline, as a precursor to 2-ester quinoline-5,8-dione, were unsuccessful. Attempts to introduce the C2-substituent following *de novo* construction of the disubstituted quinoline core were similarly unproductive. As an alternative strategy, 2-methyl ester quinoline-5,8-dione **4.73** was successfully prepared from pre-existing quinoline scaffolds. This was achieved either via chemical oxidation of 2-methyl ester-8-hydroxyquinoline **4.72** using Frémy's

salt, or through an electrochemical–chemical oxidation sequence of quinoline **4.74** employing platinum electrodes and potassium persulfate. Oxidative amination of 2-methyl ester quinoline **4.73** with cystamine **3.156** afforded enamine **4.76**; however, the base-induced cyclisation protocol that proved effective for enamine **3.165** failed in this case. Nevertheless, sulfide **4.77** could be accessed via treatment with OXONE® in methanol. Future efforts will focus on oxidation of sulfide **4.77** to the corresponding sulfone using *m*CPBA, followed by aqueous 1 M KOH treatment to deliver ascidiathiazone B **3.139**. In addition, the base-induced cyclisation of enamine **4.76** would be revisited in the presence of 18-crown-6 to potentially disrupt potassium chelation and facilitate ring closure.

4.4. Future work

In summary, a synthetic route has been developed for the synthesis of thiaplakortone A **1.12** and B **3.1** (**Scheme 4.14**). Central to this strategy was the use of cystamine **3.153** as a cost-effective alternative to hypotaurine **3.10**. This approach has additionally enabled access to analogues at a lower oxidation state. Such control over oxidation state is particularly significant, since the electronic density of the quinone core modulates its reduction potential. This is an important consideration given the proposed mechanism-of-action of thiaplakortone A **1.12** is related to the generation of reactive oxygen species. Furthermore, it is conceivable that additional members of the thiaplakortone family bearing a lower oxidation state may yet be discovered, as has already been observed within the structurally related macrophilone family.

4.14 | *total synthesis of thiaplakortone A* ***1.12*** *and B* ***3.1****:*

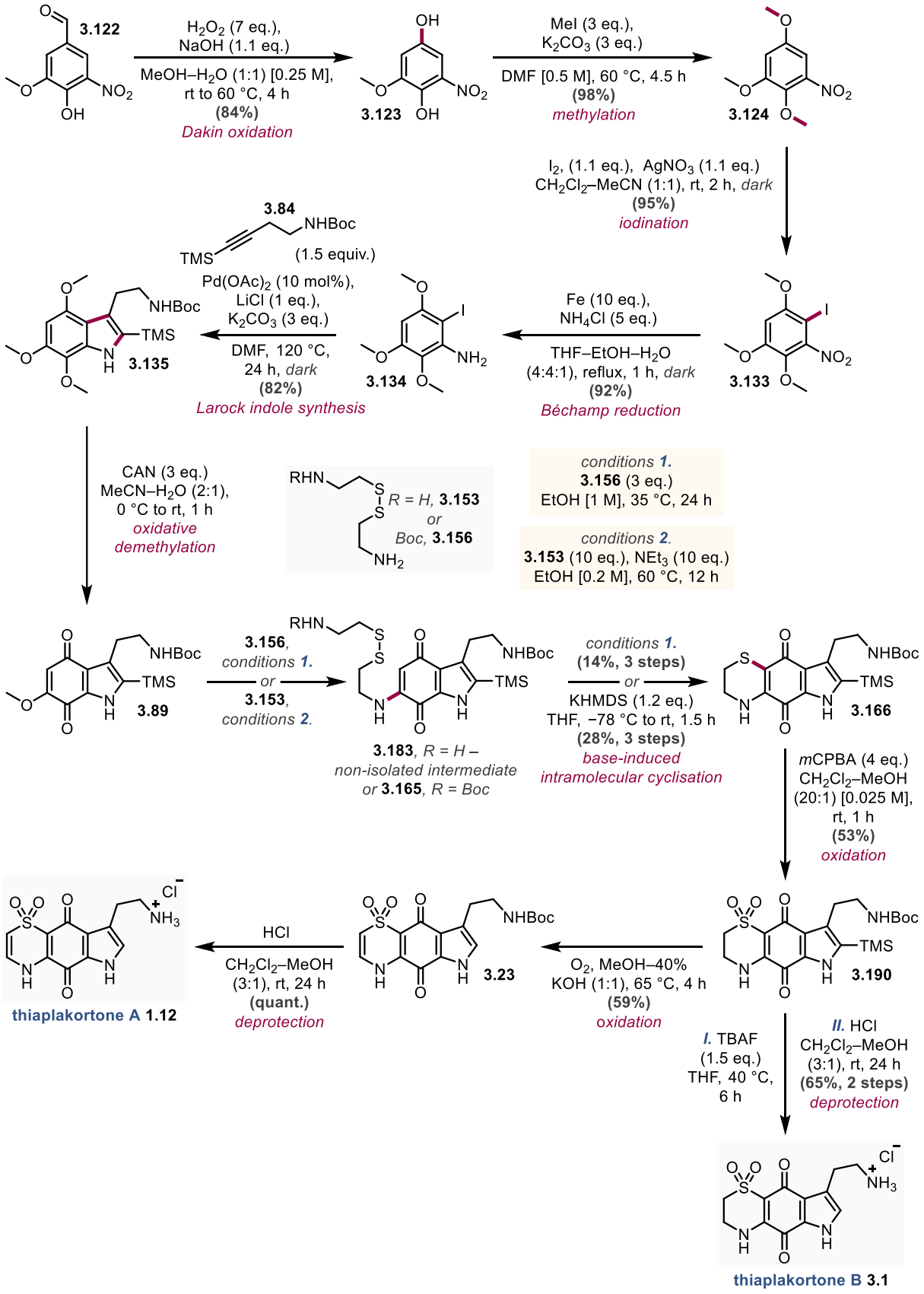

Scheme 4.14. *Total synthesis of thiaplakortone A* ***1.12*** *and B* ***3.1****.*

The designed total synthesis is anticipated to provide a route for the development of novel analogues by enabling access to structural variants that were previously inaccessible via earlier synthetic routes. Future analogue development should be guided by computationally predicted reduction potentials to prioritise structures with redox potentials that fall within the physiologically relevant window for *in vivo* bioreduction. Consequently, this route may facilitate the identification of analogues with enhanced potency relative to thiaplakortone A **1.12**, which has yet to be achieved. Additionally, this may reveal positions amenable to functionalisation without significant loss of activity, thereby enabling the incorporation of chemical probes for future mechanism-of-action studies.

Previously, Larock *et al.* have demonstrated that C2-silyl substituents (**4.84**) can serve as handles for Heck-type cross-coupling reactions (**Scheme 4.15A**, **4.83**). Building on this precedent, the incorporation of a boryl-homopropargyl amine (*N*-methyliminodiacetyl boronate, BMIDA) in the Larock indole synthesis would additionally enable subsequent Suzuki–Miyaura cross-coupling (**4.85**),[181] further expanding the scope of potential C2-functionalisation strategies. Both cross-coupling strategies facilitate the late-stage introduction of a variety of substituents at the C2-position (**4.86**). Functionalisation at the C11-position could likewise be achieved by employing substituted *N*-Boc homopropargyl amines in the Larock indole synthesis (**Scheme 4.15B**). These alkynes can be prepared via addition of TMS-acetylide to cyclic sulfamidate intermediates derived from ethanolamines. By utilising readily available chiral amino acids (**4.87**), enantioenriched *N*-Boc homopropargyl amines may be accessed (**4.89**), thereby enabling the synthesis of chiral thiaplakortone A **1.12** analogues (**4.90**). Further diversification of the side chain could be achieved through the use of non-homopropargyl amine coupling partners in the Larock indole synthesis, allowing for more significant structural deviations from the thiaplakortone A **1.12** scaffold (**4.94**). Finally, functionalisation at the C7-position could be accomplished using a cystine-derived nucleophile **4.96** (**Scheme 4.15C**), in place of cystamine **3.153**, for reaction with indolequinone **3.89** to install the dihydrothiazine ring. Pre-reduction of the carboxylic acid to the

primary alcohol prior to the addition–elimination sequence would allow for the synthesis of ether analogues (**4.98**), further expanding the accessible chemical space.

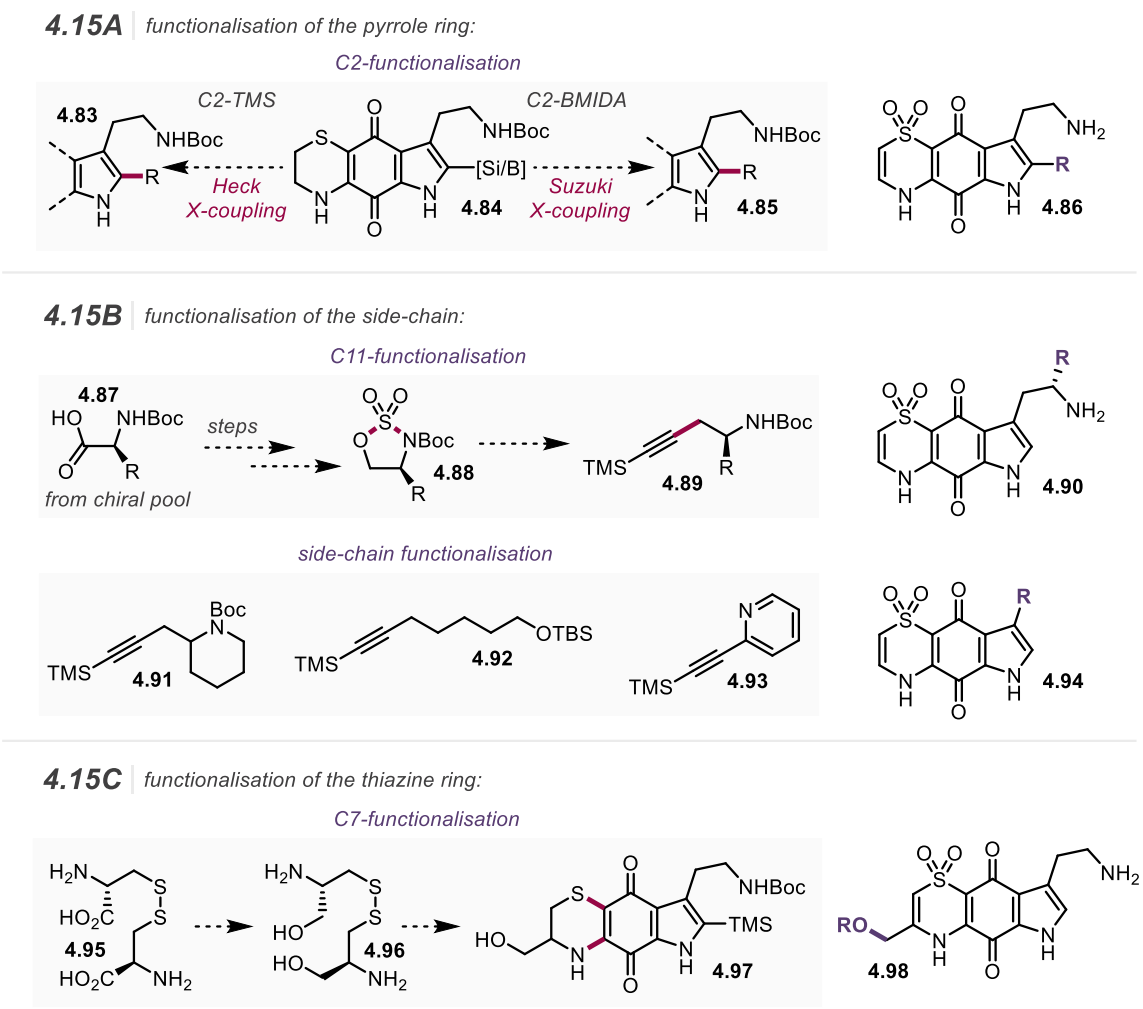

Scheme 4.15. *The developed route for the synthesis of thiaplakortone A* ***1.12*** *would enable novel analogues to be synthesised.* ***(A)*** *Functionalisation of the pyrrole ring.* ***(B)*** *Functionalisation of the side-chain.* ***(C)*** *Functionalisation of the thiazine ring.*

Additionally, the broader synthetic utility of the dihydrothiazine installation protocol will be explored through the synthesis of other natural products. As well as continuing with the macrophilone family and ascidiathiazone B **3.139**, the strategy would be extended to other targets, such as aplidinone A **3.142** (**Scheme 4.16**). This synthetic route would commence from phenol **4.99**. A Tsuji–Trost allylation with carbonate-protected geraniol **4.101**,[182] in the presence of the aryl bromide, is expected to afford ether **4.100**. Subsequent Claisen rearrangement would install the requisite geranyl side chain to furnish phenol **4.102**, which could then be oxidised to quinone **4.103**. Application of the dihydrothiazine installation protocol developed in this work

would enable regioselective construction of the ring system, yielding sulfide **4.104**. Final oxidation of the sulfide to the corresponding sulfone would deliver the natural product aplidinone A **3.142**.

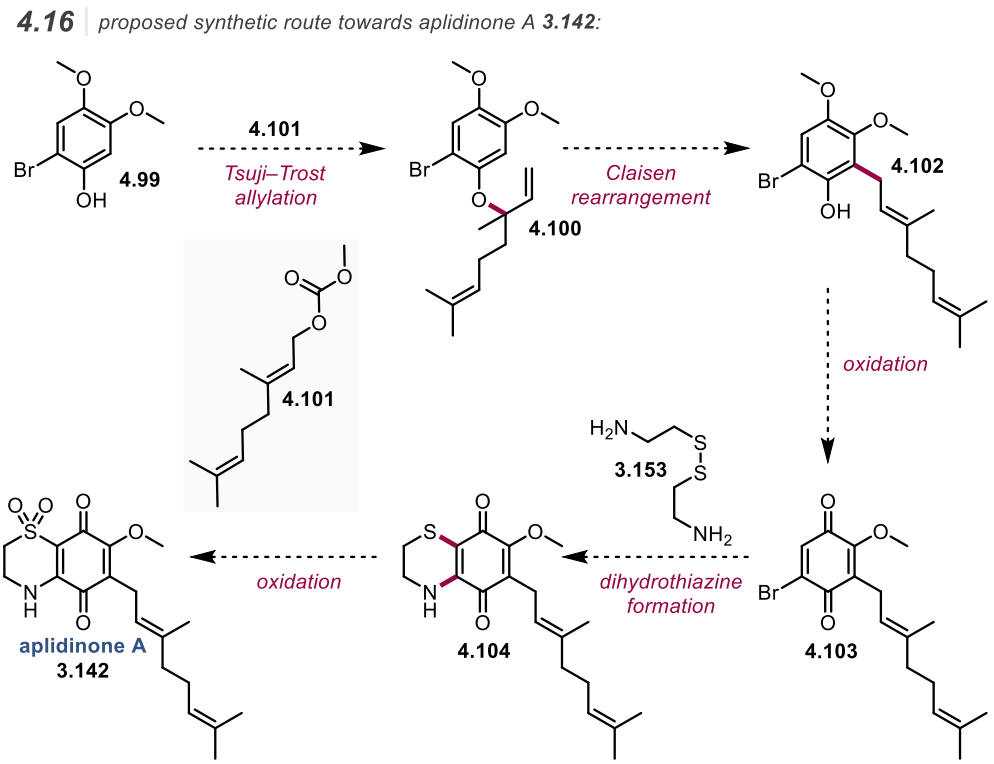

Scheme 4.16. *Proposed route towards the natural product aplidinone A* ***3.142****.*

5. Supporting information

5.1. Experimental details

5.1.1. Chemistry

Materials/procedures: All reactions were carried out with anhydrous solvents under air unless otherwise stated. Anhydrous solvents were passed through an activated alumina column under argon and collected fresh from an MBraun SPS-800 solvent purification system, stored over activated 3 Å molecular sieves, and were sparged for at least 30 minutes before use. Commercial reagents were obtained from Acros Organics, Alfa Aesar, Apollo Scientific, Fisher Scientific, Merck or Sigma Aldrich and were used without further purification unless otherwise stated. Heating was performed using DrySyn heating block inserts for vials or round-bottom flasks, and an oil bath for Schlenk tubes. Temperatures of 0 °C, −20 to −40 °C, and −40 to −78 °C were achieved using an ice-bath, acetonitrile–dry ice-bath, and acetone–dry ice-bath, respectively. Temperature was measured using a temperature probe in either the heating block inserts, oil bath or cooling bath. Lyophilisation was achieved by dissolving a sample in a vial in deionised water, freezing in liquid nitrogen and drying under vacuum.

Mass spectroscopy: Low-resolution mass spectra were recorded on a Micromass LCT Premier Open Access using electrospray ionisation (ESI). High-resolution mass spectra (HRMS) were recorded by the Departmental Mass Spectrometry Service, University of Oxford on a Thermo Scientific Exactive Mass Spectrometer (using a Waters Equity autosampler and pump) for electrospray ionisation (ESI). High resolution values are calculated to 4 decimal places from the molecular formula, and all values are within a tolerance of 5 ppm.

Infrared spectroscopy: Infrared spectra were obtained in $CDCl_3$, CH_2Cl_2, or CD_3OD as solvent on a Bruker Tensor 27 FT-IR spectrometer. The sample was prepared as a thin film on a diamond ATR

module. Wavelengths of maximum absorbance (ν_{max}) are quoted in cm^{-1}. Selected IR absorption data is provided for each compound.

Chromatography: Column chromatography refers to normal phase column chromatography and was performed manually on Geduran® Silicagel 60 (particle size 40–63 μm, pore diameter 60 Å) obtained from Merck®, under a positive pressure of nitrogen, using the stated solvent system. Analytical thin-layer chromatography (TLC) was performed on pre-coated aluminium-backed plates (Merck Kieselgel 60 F254 plates) with visualisation by ultraviolet light (254 nm) and/or by staining with potassium permanganate, vanillin, ninhydrin, *p*-anisaldehyde (*p*-Anis) or phosphomolybdic acid (PMA) followed by heating by using a heat gun. Retention factors (R_f) are reported with the solvent system in parentheses. Final compounds submitted for biological testing were purified using an Agilent Technologies 1200 Series HPLC system using the reported solvent system. For normal-phase, a Zorbax RX-SIL (particle size 5 μm, 9.4 x 250 mm) column was used. For reverse-phase, the column used was either: column (1) XBridge Prep C18 OBD (particle size 5 μm, 19 x 250 mm), or (2) XSelect CSH Prep Phenyl-Hexyl OBD (particle size 5 μm, 19 x 250 mm).

NMR spectroscopy: Proton (^1H) and carbon (^{13}C) NMR spectra were recorded on a Bruker AV200 (200 MHz), AVII HD 400 (400/101 MHz), AVII 500 (500/126 MHz) or NEO 600 (600/151 MHz) spectrometer. Proton and carbon chemical shifts (δ) are quoted in parts per million (ppm). Deuterated solvents used for analysis were chloroform-d_1, methanol-d_4, benzene-d_6 and dimethyl sulfoxide-d_6. Proton and carbon chemical shifts are referenced to residual protonated solvent. Assignments were determined on the basis of unambiguous chemical shifts, coupling patterns and 2D techniques: COSY, NOESY, HSQC and HMBC (8 Hz and 2 Hz optimised) experiments. Peak multiplicities are defined as app (apparent), s (singlet), d (doublet), t (triplet), q (quartet), quin (quintet), m (multiplet) and br (broad). Coupling constants (*J*) are reported to the nearest 0.1 Hz.

Melting points: A Gallenkamp Melting Point Apparatus (220/40 V, 50 Hz, 0.5 A) with a mercury thermometer was used to measure melting points. Crystalline compounds were recrystallised

from either dichloromethane or chloroform. Melting point capillaries were packed to a height of approximately 0.3 mm. Each melting point was only recorded once.

5.1.2. Biology

Cell culture: Promastigote *L. mexicana* expressing Cas9 and T7 polymerase, derived from WHO strain MNYC/BZ/62/M379 were grown in M199 medium with Earle's salts and *L*-glutamine supplemented with 26 mM $NaHCO_3$, 5 μg/ml haemin, 40 mM, HEPES-NaOH (pH 7.4) and 10% (*v*/*v*) heat-inactivated fetal calf serum (FCS) .[183] *L. mexicana* were grown at 28 °C and maintained at culture densities between 10^5 and 10^7 cells mL^{-1}.

Growth studies: Promastigotes (1×10^6 cells mL^{-1}) in 5 mL of M199 medium were treated with 5 μL of compound in DMSO (final carryover of DMSO 0.1%) and incubated at 28 °C for 24 h. Culture density was measured using an Improved Neubauer haemocytometer. Growth study experiments were performed twice.

Light microscopy: Microscopy was performed with a widefield fluorescence microscope (Axio Observer A1, Zeiss) using a 63× NA 1.4 Plan-Apochromat oil immersion objective lens and a 120 V metal halide fluorescence light source (Zeiss, HXP 120 V) with a Hamamatsu ORCA-Flash4.0 camera. Standard fluorescence microscopy was performed with a Purple (DAPI 49) filter cube. For microscopy of cells adhered to glass, log-phase promastigotes were harvested by centrifugation at 2500 min^{-1} for 3 min, washed once in Phosphate Buffered Saline (PBS, 1 mL) to improve adhesion to the glass slide and increase cell density. The cells were re-suspended in 50 to 80 μL PBS and 1 μL was placed on a microscope slide, a coverslip was applied and imaged immediately.

5.1.3. Analytical

Fluorescence spectroscopy: Fluorescence spectroscopic data were recorded using a Horiba Duetta fluorescence spectrophotometer, equipped with Peltier temperature controller and stirrer.

UV-Vis spectroscopy and titrations: UV-Vis spectra were recorded on a V-770 UV-Visible/NIR Spectrophotometer equipped with Peltier temperature controller and stirrer using quartz

cuvettes of 1 cm path length. Experiments were conducted at 25°C. A background measurement was initially recorded for methanol in the quartz cuvette. A run was then recorded for methanol in the quartz cuvette; this was subtracted from the baseline measurement to improve the baseline further. A 50 μM stock solution of ascididemin **1.11** in methanol (2 mL) was made: 1 mL was added to the quartz cuvette and used for the run for ascididemin **1.11** in the absence of metal(II) ions. The other 1 mL of the stock solution was used to make a 2.5 mM stock solution of zinc(II) or iron(II) chloride. A titration of the metal(II) stock solution was performed where 2 μL was added every run for 10 runs, 4 μL every run for 5 runs and 10 μL every run for 6 runs. For each titration, three repeats were measured.

5.1.4. Crystallography

Low temperature single crystal X-ray diffraction data for 9-methylascididemin **2.123** was collected using a Rigaku Oxford SuperNova diffractometer and processed by CrysAlisPro. Structure solution was carried out using SHELXT as implemented in Olex2, followed by refinement with SHELXL within Olex2. Crystallographic data has been deposited with the Cambridge Crystallographic Data Centre (CCDC 2480586) and can be obtained via www.ccdc.cam.ac.uk/data_request/cif.

5.2. Experimental procedures

5.2.1. Chapter 2

Propargylamine **2.20**:

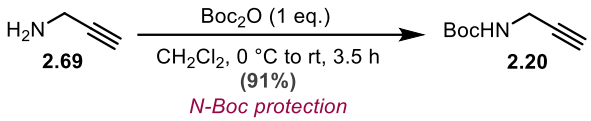

Adapted from the procedure of Wang et al.:[21] Di-*tert*-butyl dicarbonate (10.90 g, 50.0 mmol) in dichloromethane (30 mL) was added dropwise over 1 minute to a solution of propargylamine **2.69** (3.20 mL, 50.0 mmol) in dichloromethane (78 mL) at 0 °C. After 1 h, the ice-bath was removed and the reaction was allowed to warm to rt for 2.5 h. The pale-yellow solution was concentrated under reduced pressure. The yellow oil was purified using a silica plug (5% ethyl acetate in pentane) to yield propargylamine **2.20** (7.09 g, 45.7 mmol, 91%) as a pale-yellow crystalline solid.

R_f: 0.33 (5% ethyl acetate in pentane) – white spot (with vanillin)

^{1}H NMR (600 MHz, $CDCl_3$) δ 4.72 (br s, 1H), 3.92 (br s, 2H), 2.21 (t, *J* = 2.5 Hz, 1H), 1.45 (s, 9H)

^{13}C NMR (151 MHz, $CDCl_3$): δ 155.4, 80.2, 71.4, 30.5, 28.5

Data in agreement with literature.[21]

Aniline **2.21**:

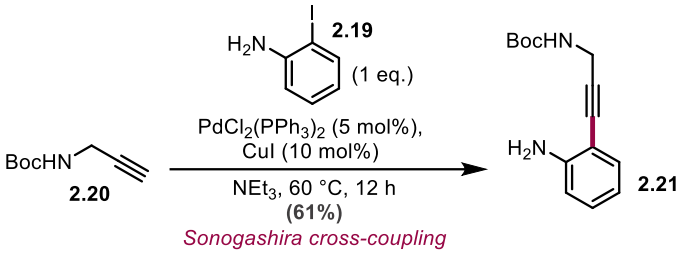

Adapted from the procedure of Wang et al.:[21] Under a nitrogen atmosphere, triethylamine (130 mL) was added to 2-iodoaniline **2.19** (1.41 g, 6.44 mmol), propargylamine **2.20** (1.00 g, 6.44 mmol), bis(triphenylphosphine)palladium(II) dichloride (0.22 g, 0.322 mmol, 5 mol%), and copper(I) iodide (0.12 g, 0.644 mmol, 10 mol%). The resulting solution was heated to 60 °C for 12 h. The reaction was cooled to rt and concentrated under reduced pressure. Water (20 mL) was added and the aqueous phase was extracted with dichloromethane (3 × 30 mL). The combined organic phases were washed with brine (30 mL), dried over anhydrous sodium sulfate, filtered, and concentrated under reduced pressure. The dark-brown oil was purified by silica column chromatography (5% to 40% ethyl acetate in pentane) to yield aniline **2.21** (0.97 g, 3.94 mmol, 61%) as a light-brown solid.

R_f: 0.29 (20% ethyl acetate in pentane) – yellow spot (with vanillin)

^{1}H NMR (400 MHz, $CDCl_3$): δ 7.24 (dd, *J* = 7.6, 1.6 Hz, 1H), 7.13 – 7.09 (m, 1H), 6.69 – 6.63 (m, 2H), 4.79 (br, 1H), 4.21 (s, 2H), 4.18 (d, *J* = 5.6 Hz, 2H), 1.47 (s, 9H)

^{13}C NMR (101 MHz, $CDCl_3$) δ 155.2, 148.0, 132.1, 129.6, 117.6, 114.1, 107.2, 90.7, 79.7, 77.1, 31.3, 28.2

Data in agreement with literature.[21]

Enamine **2.22**:

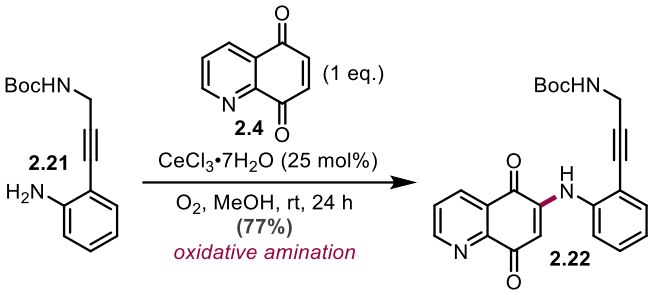

Adapted from the procedure of Wang et al.:[21] Under an oxygen atmosphere, cerium(III) chloride heptahydrate (0.12 g, 0.315 mmol, 25 mol%) and aniline **2.21** (0.34 g, 1.39 mmol) were successively added to a solution of quinoline-5,8-dione **2.4** (0.20 g, 1.26 mmol) in methanol (12.6 mL), and the resulting solution was stirred at rt for 24 h. The red solution was concentrated under reduced pressure and the dark-red residue was purified by silica column chromatography (silica deactivated by 1% triethylamine, 50% ethyl acetate in pentane to 100% ethyl acetate) to yield enamine **2.22** (0.39 g, 0.967 mmol, 77%) as a red solid.

R_f: 0.24 (100% ethyl acetate) – red spot (without stain)

^{1}H NMR (400 MHz, $CDCl_3$): δ 9.07 (dd, *J* = 4.7, 1.7 Hz, 1H), 8.46 (dd, *J* = 7.8, 1.7 Hz, 1H), 8.24 (s, 1H), 7.65 (dd, *J* = 7.9, 4.7 Hz, 1H), 7.53 – 7.45 (m, 2H), 7.43 – 7.37 (m, 1H), 7.17 – 7.12 (m, 1H), 6.74 (s, 1H), 4.94 (br, 1H), 4.26 (s, 2H), 1.46 (s, 9H)

^{13}C NMR (101 MHz, $CDCl_3$) δ 182.4, 181.8, 155.4, 148.7, 143.2, 138.6, 134.6, 133.1, 129.7, 127.4, 126.7, 124.9, 120.1, 116.1, 105.3, 94.3, 80.3, 78.2, 31.4, 28.5

Data in agreement with literature.[21]

Ascididemin **1.11**:

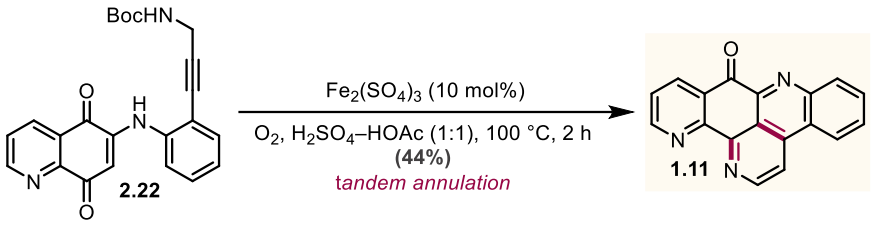

Adapted from the procedure of Wang et al.:[21] Under an oxygen atmosphere, $Fe_2(SO_4)_3$ (12 mg, 10 mol%, 30.0 µmol) and enamine **2.22** (0.12 g, 0.30 mmol) were successively added to a 1:1 solution of concentrated sulfuric acid–glacial acetic acid (3 mL), and the resulting solution was heated to 100 °C for 2 h. The black-green solution was then cooled to 0 °C and quenched by slow addition into a saturated aqueous sodium carbonate solution (30 mL) to achieve a pH of 9. The aqueous phase was extracted using dichloromethane (5 × 30 mL). The combined organic phases were washed sequentially with water (30 mL) and brine (30 mL), dried over anhydrous sodium sulfate, filtered and concentrated under reduced pressure. The yellow-brown solid was purified by silica column chromatography (silica deactivated by 1% triethylamine, 5% methanol in dichloromethane) to yield ascididemin **1.11** (37 mg, 0.131 mmol, 44%) as a yellow solid. Ascididemin **1.11** was further purified by normal-phase HPLC (5% methanol in chloroform) for biological testing.

R_f: 0.33 (5% methanol in dichloromethane)

^{1}H NMR (400 MHz, $CDCl_3$): δ 9.30 (d, *J* = 5.7 Hz, 1H), 9.20 (d, *J* = 4.6 Hz, 1H), 8.82 (dd, *J* = 7.9, 1.8 Hz, 1H), 8.72 (dd, *J* = 8.1, 1.4 Hz, 1H), 8.68 – 8.63 (m, 1H), 8.57 (d, *J* = 5.7 Hz, 1H), 8.04 (ddd, *J* = 8.3, 7.1, 1.5 Hz, 1H), 7.97 (ddd, *J* = 8.4, 7.0, 1.4 Hz, 1H), 7.69 (dd, *J* = 7.9, 4.6 Hz, 1H)

^{13}C NMR (126 MHz, $CDCl_3$): δ 182.0, 155.7, 152.5, 149.92, 149.86, 146.1, 145.9, 138.2, 136.8, 133.3, 132.1, 131.1, 129.2, 125.8, 123.6, 123.1, 118.3, 117.1

HRMS-ESI (m/z): Calculated for $C_{18}H_{10}N_3O$ [M+H]+, 284.0818; found 284.0823

Data in agreement with literature.[21]

Quinoline-5,8-dione **2.4**:

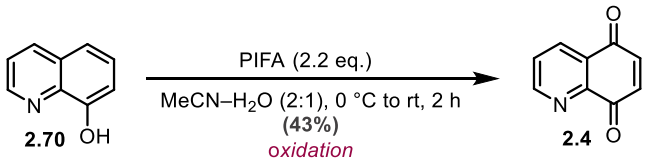

Adapted from the procedure of Barret et al.:[184] 8-Hydroxyquinoline **2.70** (0.50 g, 3.40 mmol) was added portion-wise to a solution of bis(trifluoroacetoxy)iodo benzene (PIFA) (2.44 g, 7.58 mmol) in 2:1 acetonitrile–water (18 mL) at 0 °C. The resulting solution was allowed to gradually warm to rt. After 2 h, the red-orange solution was concentrated under reduced pressure, and the aqueous phase was extracted with ethyl acetate (3 × 20 mL). The combined organic phases were washed with brine (20 mL), dried over anhydrous sodium sulfate, filtered and concentrated under reduced pressure. The dark-red oil was purified by silica column chromatography (80% ethyl acetate in pentane) to yield quinoline-5,8-dione **2.4** (0.24 g, 1.50 mmol, 43%) as a yellow-brown solid.

R_f: 0.31 (80% ethyl acetate in pentane) – yellow spot (with vanillin)

^{1}H NMR (400 MHz, $CDCl_3$): δ 9.06 (dd, *J* = 4.7, 1.7 Hz, 1H), 8.43 (dd, *J* = 7.9, 1.7 Hz, 1H), 7.71 (dd, *J* = 7.9, 4.7 Hz, 1H), 7.16 (d, *J* = 10.4 Hz, 1H), 7.07 (d, *J* = 10.4 Hz, 1H)

^{13}C NMR (101 MHz, $CDCl_3$): δ 184.6, 183.3, 154.9, 147.5, 139.2, 138.1, 134.7, 129.2, 128.0

Data in agreement with literature.[185]

Methylquinoline-5,8-dione **2.86**:

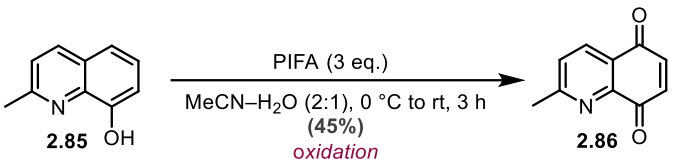

Adapted from the procedure of Barret et al.:[184] 2-Methyl 8-hydroxyquinoline **2.85** (0.50 g, 3.14 mmol) was added portion-wise to a solution of bis(trifluoroacetoxy)iodo benzene (3.92 g, 9.11 mmol) in 2:1 acetonitrile–water (9.6 mL) at 0 °C. The resulting solution was allowed to gradually warm to rt. After 3 h, the red-orange solution was concentrated under reduced pressure and the aqueous phase was extracted with ethyl acetate (5 × 20 mL). The combined organic phases were washed with brine (20 mL), dried over anhydrous sodium sulfate, filtered and concentrated under reduced pressure. The dark-red oil was purified by column chromatography (silica deactivated by 1% triethylamine, 10% to 60% ethyl acetate in pentane) to yield methylquinoline-5,8-dione **2.86** (0.24 g, 1.39 mmol, 45%) as a yellow-brown solid.

R_f: 0.29 (60% ethyl acetate in pentane) – dark-yellow spot (with vanillin)

^{1}H NMR (400 MHz, CD_3OD): δ 8.35 (d, *J* = 8.1 Hz, 1H), 7.71 (d, *J* = 8.1 Hz, 1H), 7.15 – 7.05 (m, 2H), 2.71 (s, 3H)

^{13}C NMR (151 MHz, CD_3OD) δ 184.4, 183.4, 164.6, 146.5, 138.4, 137.8, 134.6, 128.0, 127.1, 23.1

Methylquinoline **2.91**:

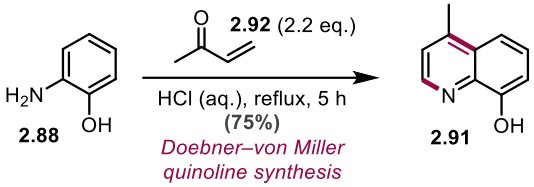

Adapted from the procedure of Choi et al.:[186] 2-Aminophenol **2.88** (5.00 g, 45.8 mmol) in 6 N hydrochloric acid (6 mL) was heated to reflux at 120 °C. Methyl vinyl ketone **2.92** (5.58 mL, 67.0 mmol) was added dropwise over 3 h using a dropping funnel and the solution was stirred for a further 2 h after complete addition. The reaction mixture was cooled to rt and 10 M aqueous NaOH solution (5 mL) was added slowly to achieve a pH of 9. The aqueous phase was extracted with ethyl acetate (3 × 30 mL). The combined organic phases were washed with brine (30 mL), dried over anhydrous sodium sulfate, filtered and concentrated under reduced pressure. The dark-brown residue was purified by silica column chromatography (100% dichloromethane to 5% acetone in dichloromethane) to yield methylquinoline **2.91** (4.98 g, 34.3 mmol, 75%) as an off-white solid.

R_f: 0.47 (2.5% acetone in dichloromethane) – white streak (with potassium permanganate)

^{1}H NMR (600 MHz, $CDCl_3$): δ 8.63 (d, *J* = 4.3 Hz, 1H), 7.47 (d, *J* = 4.3 Hz, 2H), 7.27 (dd, *J* = 4.4, 1.0 Hz, 1H), 7.17 (q, *J* = 4.6 Hz, 1H), 2.70 (d, *J* = 0.9 Hz, 3H)

^{13}C NMR (151 MHz, $CDCl_3$): δ 152.8, 147.6, 145.1, 138.2, 128.7, 127.5, 122.7, 114.3, 109.7, 18.9

Data in agreement with literature.[187]

Methylquinoline **2.94**:

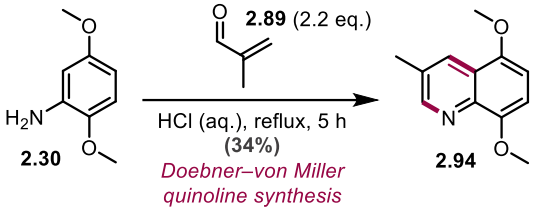

Adapted from the procedure of Choi et al.:[186] 2,5-Dimethoxyaniline **2.30** (1.50 g, 9.79 mmol) in 6 N hydrochloric acid (5 mL) was heated to reflux at 120 °C. Methacrolein **2.89** (1.80 mL, 21.8 mmol) was added dropwise over 3 h using a dropping funnel and the solution was stirred for a further 2 h after complete addition. The reaction mixture was cooled to rt and the solution was added to saturated aqueous sodium carbonate solution (30 mL) to achieve a pH of 7. The aqueous phase was extracted with ethyl acetate (3 × 50 mL). The combined organic phases were washed with brine (50 mL), dried over anhydrous sodium sulfate, filtered and concentrated under reduced pressure. The dark-brown residue was purified by silica column chromatography (5% acetone in dichloromethane) to yield methylquinoline **2.94** (0.67 g, 3.30 mmol, 34%) as an off-white solid.

R_f: 0.33 (5% acetone in dichloromethane) – yellow spot (with vanillin)

^{1}H NMR (400 MHz, $CDCl_3$): δ 8.78 (d, *J* = 2.3 Hz, 1H), 8.31 – 8.29 (m, 1H), 6.87 – 6.70 (m, 2H), 4.03 (s, 3H), 3.95 (s, 3H), 2.52 (s, 3H)

^{13}C NMR (101 MHz, $CDCl_3$): δ 151.5, 149.7, 148.4, 139.0, 130.6, 129.7, 121.6, 105.8, 103.8, 56.1, 55.9, 19.0

IR: 3000, 2951, 2836, 1606, 1479, 1380, 1269, 1162, 1102, 798, 728

Data in agreement with literature

Methylquinoline-5,8-dione **2.90**:

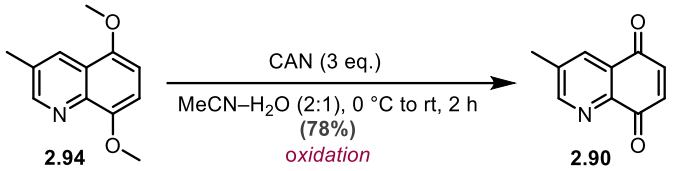

Adapted from the procedure of Callery et al.:[188] A solution of ceric ammonium nitrate (CAN) (2.43 g, 4.43 mmol) in water (5 mL) was added dropwise over 5 minutes to a solution of methylquinoline **2.94** (0.30 g, 1.48 mmol) in acetonitrile (10 mL) at 0 °C, and then the ice-water bath was removed. After 2 h, the reaction was diluted by the addition of water (10 mL) and the aqueous phase was extracted with chloroform (3 × 20 mL). The combined organic phases were washed with brine (20 mL), dried over anhydrous sodium sulfate, filtered and concentrated under reduced pressure to yield methylquinoline-5,8-dione **2.90** (0.20 g, 1.15 mmol, 78%) as a brown solid. Used in the next step without further purification.

R_f: 0.33 (5% acetone in CH_2Cl_2) – yellow spot (with vanillin)

^{1}H NMR (400 MHz, $CDCl_3$): δ 8.87 (d, *J* = 2.2 Hz, 1H), 8.20 – 8.18 (m, 1H), 7.14 – 7.01 (m, 2H), 2.53 (s, 3H)

^{13}C NMR (101 MHz, $CDCl_3$): δ 185.0, 183.4, 155.6, 145.4, 139.2, 139.1, 138.0, 134.3, 128.8, 19.1

HRMS-ESI (m/z): Calculated for $C_{10}H_8NO_2$ [M+H]+, 174.0550; found 174.0551

IR: 3056, 2927, 1675, 1592, 1308, 1266, 1063, 847, 736, 702

Methylquinoline **2.95**:

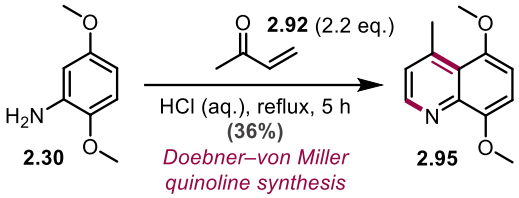

Adapted from the procedure of Choi et al.:[186] 2,5-Dimethoxyaniline **2.30** (1.50 g, 9.79 mmol) in 6 N hydrochloric acid (5 mL) was heated to reflux at 120 °C. Methyl vinyl ketone **2.92** (1.80 mL, 21.5 mmol) was added dropwise over 3 h using a dropping funnel and the solution was stirred for a further 2 h after complete addition. The reaction mixture was cooled to rt and the solution was slowly added to saturated aqueous sodium bicarbonate (30 mL) to achieve a pH of 9. The aqueous phase was extracted with ethyl acetate (3 × 50 mL). The combined organic phases were washed with brine (30 mL), dried over anhydrous sodium sulfate, filtered and concentrated under reduced pressure. The dark-brown residue was purified by silica column chromatography (5% acetone in dichloromethane) to yield methylquinoline **2.95** (0.71 g, mmol, 3.49 mmol, 36%) as an off-white solid.

R_f: 0.29 (5% acetone in dichloromethane) – yellow spot (with vanillin)

^{1}H NMR (400 MHz, $CDCl_3$): δ 8.71 (d, *J* = 4.4 Hz, 1H), 7.14 (dq, *J* = 4.4, 0.9 Hz, 1H), 6.91 (d, *J* = 8.6 Hz, 1H), 6.75 (d, *J* = 8.6 Hz, 1H), 4.02 (s, 3H), 3.88 (s, 3H), 2.87 (d, *J* = 0.9 Hz, 3H)

^{13}C NMR (101 MHz, $CDCl_3$): δ 151.3, 149.9, 149.2, 145.8, 141.6, 124.1, 122.0, 106.7, 104.8, 56.2, 55.8, 24.6

IR: 3461, 3366, 2996, 2937, 2835, 1709, 1623, 1517, 1359, 1206, 1044

Data in agreement with literature.[189]

Methylquinoline-5,8-dione **2.93**:

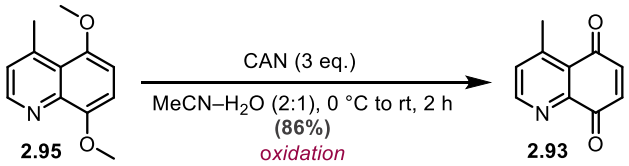

Adapted from the procedure of Callery et al.:[188] A solution of ceric ammonium nitrate (2.43 g, 4.43 mmol) in water (5 mL) was added dropwise over 5 minutes to a solution of methylquinoline **2.95** (0.30 g, 1.48 mmol) in acetonitrile (10 mL) at 0 °C, and then the ice-water bath was removed. After 2 h, the reaction was diluted by addition of water (10 mL) and the aqueous phase was extracted with chloroform (3 × 20 mL). The combined organic phases were washed with brine (20 mL), dried over anhydrous sodium sulfate, filtered and concentrated under reduced pressure to yield methylquinoline-5,8-dione **2.93** (0.22 g, 1.27 mmol, 86%) as a brown solid. Used in the next step without further purification.

R_f: 0.27 (60% ethyl acetate in pentane) – brown spot (with vanillin)

^{1}H NMR (400 MHz, $CDCl_3$): δ 8.86 (br s, 1H), 7.47 (d, *J* = 4.6 Hz, 1H), 7.09 (d, *J* = 10.3 Hz, 1H), 6.99 (d, *J* = 10.3 Hz, 1H), 2.80 (s, 3H)

^{13}C NMR (101 MHz, $CDCl_3$): δ 186.9, 183.6, 153.4, 150.8, 148.7, 139.8, 137.4, 131.2, 127.6, 22.2

HRMS-ESI (m/z): Calculated for $C_{10}H_8NO_2$ [M+H]+, 174.0550; found 174.0551

Data in agreement with literature.[190]

5,8-Dimethoxyquinoline **2.97**:

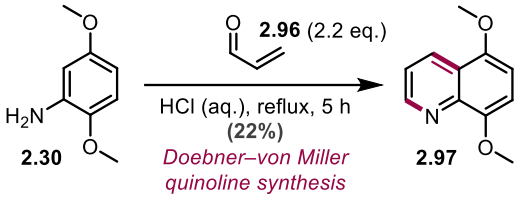

Adapted from the procedure of Choi et al.:[186] 2,5-Dimethoxyaniline **2.30** (3.00 g, 19.6 mmol) in 6 N hydrochloric acid (10 mL) was heated to reflux at 120 °C. Acrolein **2.96** (3.28 mL, 49.0 mmol) was added dropwise over 3 h using a dropping funnel and the solution was stirred for a further 2 h after complete addition. The reaction mixture was cooled to rt and the solution was slowly added to saturated aqueous sodium carbonate solution (50 mL) to achieve a pH of 9. The aqueous phase was extracted with ethyl acetate (3 × 100 mL). The combined organic phases were washed with brine (50 mL), dried over anhydrous sodium sulfate, filtered and concentrated under reduced pressure. The dark-brown residue was purified by silica column chromatography (5% acetone in dichloromethane) to yield 5,8-dimethoxyquinoline **2.97** (0.83 g, 4.39 mmol, 22%) as a light-brown solid.

R_f: 0.31 (5% acetone in dichloromethane) – yellow spot (with vanillin)

^{1}H NMR (400 MHz, $CDCl_3$): δ 8.94 (dd, *J* = 4.2, 1.8 Hz, 1H), 8.54 (dd, *J* = 8.5, 1.8 Hz, 1H), 7.42 (dd, *J* = 8.5, 4.2 Hz, 1H), 6.93 (d, *J* = 8.5 Hz, 1H), 6.75 (d, *J* = 8.5 Hz, 1H), 4.04 (s, 3H), 3.96 (s, 3H)

^{13}C NMR (101 MHz, $CDCl_3$): δ 149.8, 149.6, 148.8, 140.6, 130.9, 121.8, 121.0, 106.9, 103.7, 56.2, 55.9

Data in agreement with literature.[191]

Quinoline-5,8-dione **2.4**:

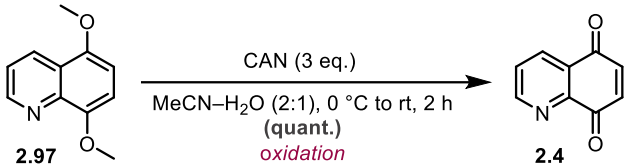

Adapted from the procedure of Callery et al.:[188] A solution of ceric ammonium nitrate (7.12 g, 13.0 mmol) in water (15 mL) was added dropwise over 5 minutes to a solution of 5,8-dimethoxyquinoline **2.97** (0.82 g, 4.33 mmol) in acetonitrile (30 mL) at 0 °C, and then the ice-water bath was removed. After 2 h, the reaction was diluted by addition of water (30 mL) and the aqueous phase was extracted with chloroform (3 × 50 mL). The combined organic phases were washed with brine (30 mL), dried over anhydrous sodium sulfate, filtered and concentrated under reduced pressure to yield quinoline-5,8-dione **2.4** (0.69 g, 4.33 mmol, quant.) as a brown solid. Used in the next step without further purification.

Refer back to page 200 for characterisation.

Aniline **2.105**:

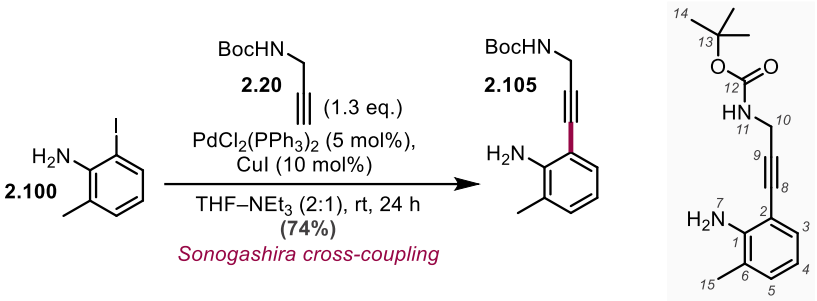

Adapted from the procedure of Wang et al.:[21] Under a nitrogen atmosphere, aniline **2.100** (77.2 mg, 0.331 mmol), bis(triphenylphosphine)palladium(II) dichloride (11.6 mg, 0.0166 mmol, 5 mol%) and copper(I) iodide (6.44 mg, 0.0331 mmol, 10 mol%) in triethylamine (0.75 mL) and tetrahydrofuran (0.75 mL) was pre-stirred for 30 minutes at rt. Then, a solution of propargylamine **2.20** (66.8 mg, 0.430 mmol) in tetrahydrofuran (0.75 mL) was added dropwise over 5 minutes. After 24 h, the black-brown suspension was filtered over Celite and washed with dichloromethane (40 mL). Water (70 mL) was added to the filtrate and the aqueous phase was extracted with dichloromethane (3 x 40 mL). The combined organic phases were washed with brine (100 mL), dried over anhydrous sodium sulfate, filtered and concentrated under reduced pressure. The crude material was purified by silica column chromatography (10% to 30% ethyl acetate in pentane) to yield aniline **2.105** (63.5 mg, 0.244 mmol, 74%) as a yellow oil.

R_f: 0.21 (25% ethyl acetate in pentane) – yellow-brown spot (with vanillin)

^{1}H NMR (400 MHz, $CDCl_3$): δ 7.13 – 7.11 (m, 1H, H5), 7.09 (dd, *J* = 8.1, 2.0 Hz, 1H, H4), 6.56 (d, *J* = 8.1 Hz, 1H, H3), 4.77 (br s, 1H, H11), 4.11 (d, *J* = 5.4 Hz, 1H, H10), 3.74 (br s, 2H, H7), 2.11 (s, 3H, H15), 1.46 (s, 9H, H14)

^{13}C NMR (101 MHz, $CDCl_3$): δ 155.5 (C, C12), 145.2 (C, C1), 134.0 (CH, C5), 130.8 (CH, C4), 122.1 (C, C6), 114.6 (CH, C3), 112.1 (C, C2), 84.0 (C, C8), 82.8 (C, C9), 79.9 (C, C13), 31.5 (CH_2, C10), 28.5 (CH_3, C14), 17.2 (CH_3, C15)

HRMS-ESI (m/z): Calculated for $C_{15}H_{20}N_2O_2Na$ [M+Na]+, 283.1417; found 283.1416

IR: 3369, 2978, 2972, 2849, 2225, 1701, 1506, 1169, 736.

Enamine **2.110**:

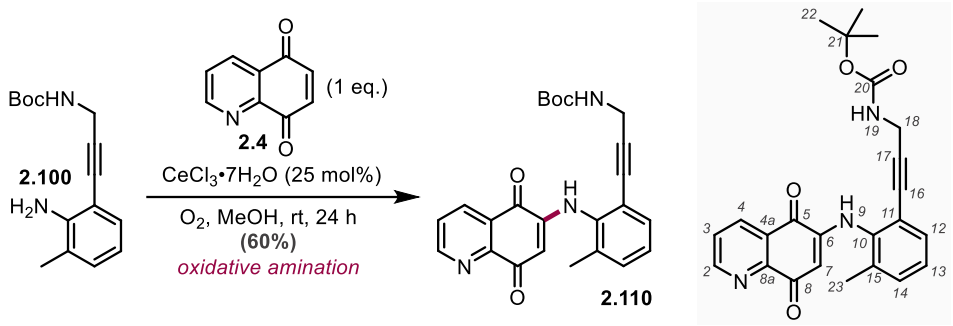

Adapted from the procedure of Wang et al.:[21] Under an oxygen atmosphere, cerium(III) chloride heptahydrate (28 mg, 75.9 µmol, 25 mol%) and aniline **2.100** (79 mg, 303 µmol) were successively added to a solution of quinoline-5,8-dione **2.4** (49 g, 308 µmol) in methanol (2.3 mL) at rt. After 24 h, the red solution was concentrated under reduced pressure and the dark-red residue was purified by silica column chromatography (100% dichloromethane to 20% acetone in dichloromethane) to yield enamine **2.110** (76 mg, 0.18 mmol, 60%) as a red solid.

R_f: 0.33 (10% acetone in dichloromethane) – red spot (without stain)

^{1}H NMR (500 MHz, $CDCl_3$): δ 9.05 (dd, *J* = 4.8, 1.7 Hz, 1H, H2), 8.45 (dd, *J* = 7.8, 1.7 Hz, 1H, H4), 7.63 (dd, *J* = 7.9, 4.7 Hz, 1H H3), 7.37 – 7.30 (m, 3H), 7.25 (d, *J* = 7.3 Hz, 1H), 6.26 (s, 1H, H7), 4.78 (s, 1H, H19), 4.19 – 4.14 (m, 2H, H18), 2.28 (s, 3H, H23), 1.48 (s, 9H, H22)

^{13}C NMR (126 MHz, $CDCl_3$): δ 182.1 (C, C8), 181.9 (C, C5), 155.48 (CH, C2), 155.43 (C, C20), 149.0 (C, C8a), 144.8 (C, C10), 135.3, 134.8 (CH), 134.5 (CH, C4), 132.7 (C), 130.7 (CH), 127.5 (C, C4a), 126.7 (CH, C3), 123.9 (CH), 121.3 (C), 104.8 (CH, C7), 86.4 (C), 82.4 (C, C16), 80.2 (C, C21), 31.2 (CH_2, C18), 28.5 (CH_3, C22), 17.7 (CH_3, C23)

HRMS-ESI (m/z): Calculated for $C_{24}H_{24}N_3O_4$ [M+H]+, 418.1761; found 418.1766

IR: 3345, 2976, 2930, 2860, 1702, 1685, 1639, 1613, 1595, 1569, 1510, 1454, 1392, 1366, 1327, 1271, 1250, 1168, 1129, 1102, 1048, 1021, 991, 913, 861, 828, 799, 732, 674, 649

Aniline **2.106**:

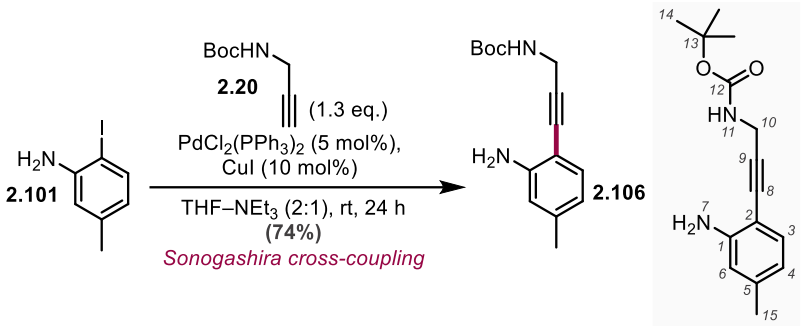

Adapted from the procedure of Wang et al.:[21] Under a nitrogen atmosphere, 2-iodo-5-methylaniline **2.101** (300 mg, 1.29 mmol), bis(triphenylphosphine)palladium(II) dichloride (45.2 mg, 0.0644 mmol, 5 mol%) and copper(I) iodide (24.5 mg, 0.129 mmol, 10 mol%) was pre-stirred for 30 minutes in triethylamine (3 mL) and tetrahydrofuran (3 mL) at rt. Then, a solution of propargylamine **2.20** (260 mg, 1.67 mmol) in tetrahydrofuran (3 mL) was added dropwise over 5 minutes. After 24 h, the black-brown suspension was filtered over Celite and washed with dichloromethane (60 mL). Water (70 mL) was added to the filtrate and the aqueous phase was extracted with dichloromethane (3 x 50 mL). The combined organic phases were washed with brine (100 mL), dried over anhydrous sodium sulfate, filtered and concentrated under reduced pressure. The crude material was purified by silica column chromatography (10 to 30% ethyl acetate in pentane) to yield aniline **2.106** (248 mg, 0.952 mmol, 74%) as a yellow oil.

R_f: 0.24 (20% ethyl acetate in pentane) – yellow spot (with vanillin)

^{1}H NMR (600 MHz, $CDCl_3$): δ 7.12 (d, *J* = 7.8 Hz, 1H, H3), 6.50 (s, 1H, H6), 6.48 (dd, *J* = 7.8, 1.6 Hz, 1H, H4), 4.79 (br s, 1H, H11), 4.17 (d, *J* = 5.5 Hz, 2H, H10), 2.24 (s, 3H, H15), 1.58 (s, 2H, H7), 1.46 (s, 9H, H14)

^{13}C NMR (151 MHz, $CDCl_3$): δ 155.5 (C, C12), 148.2 (C, C1), 140.2 (C, C5), 132.2 (CH, C3), 119.1 (CH, C4), 115.0 (CH, C6), 104.7 (C, C2), 90.2 (C, C9), 80.2 (C, C8 and C13), 31.6 (CH_2, C10), 28.5 (CH_3, C14), 21.7 (CH_3, C15)

HRMS-ESI (m/z): Calculated for $C_{15}H_{21}N_2O_2$ [M+H]+, 261.1598; found 261.1595

IR: 3352, 2980, 1759, 1522, 1171, 737

Enamine **2.111**:

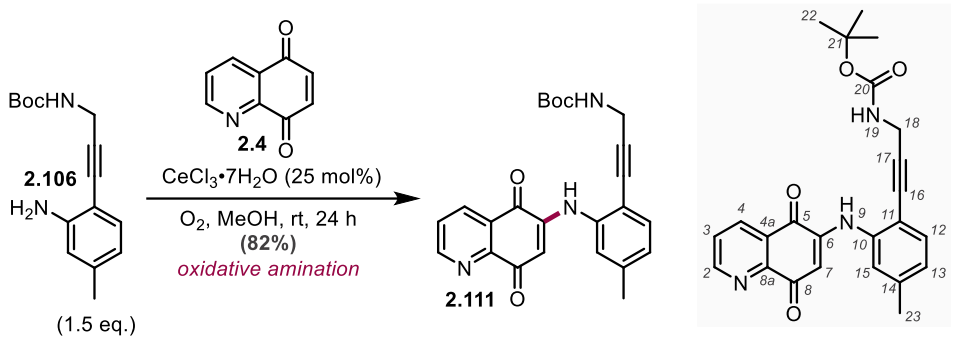

Adapted from the procedure of Wang et al.:[21] Under an oxygen atmosphere, cerium(III) chloride heptahydrate (34 mg, 91.3 µmol, 25 mol%) and aniline **2.106** (143 mg, 549 µmol) were successively added to a solution of quinoline-5,8-dione **2.4** (59 mg, 371 µmol) in methanol (3.6 mL) at rt. After 24 h, the red solution was concentrated under reduced pressure and the dark-red residue was purified by silica column chromatography (100% dichloromethane to 20% acetone in dichloromethane) to yield enamine **2.111** (0.10 mg, 0.30 mmol, 82%) as a red solid.

R_f: 0.31 (10% acetone in dichloromethane) – red spot (without stain)

^{1}H NMR (600 MHz, $CDCl_3$): δ 9.05 (dd, *J* = 4.7, 1.7 Hz, 1H, H2), 8.44 (dd, *J* = 7.8, 1.8 Hz, 1H, H4), 8.23 (br s, 1H, H9), 7.64 (dd, *J* = 7.8, 4.7 Hz, 1H, H3), 7.37 (d, *J* = 7.8 Hz, 1H, H12), 7.27 (br s, 1H, H15), 6.94 (app ddd, *J* = 7.9, 1.6, 0.8 Hz, 1H, H13), 6.75 (s, 1H, H7), 4.96 (br s, 1H, H19), 4.25 (d, *J* = 5.6 Hz, 2H, H18), 2.39 (s, 3H, H23), 1.45 (s, 9H, H22)

^{13}C NMR (151 MHz, $CDCl_3$): δ 182.5 (C, C8), 181.9 (C, C5), 155.46 (CH, C2), 155.41 (C, C20), 148.9 (C, C8a), 143.2 (C, C6), 140.4 (C, C14), 138.6 (C, C10), 134.7 (CH, C4), 132.8 (CH, C12), 127.5 (C, C4a), 126.7 (CH, C3), 125.8 (CH, C13), 120.6 (CH, C15), 113.1 (C, C11), 105.3 (CH, C7), 93.5 (C, C17), 80.2 (C, C21), 78.4 (C, C16), 31.4 (CH_2, C18), 28.5 (CH_3, C22), 22.0 (CH_3, C23)

HRMS-ESI (m/z): Calculated for $C_{24}H_{23}N_3O_4Na$ [M+Na]+, 440.1581; found 440.1578

IR: 3324, 2980, 2929, 2236, 1709, 1620, 1569, 1328, 1173, 913, 736

2-Methylascididemin **2.119**:

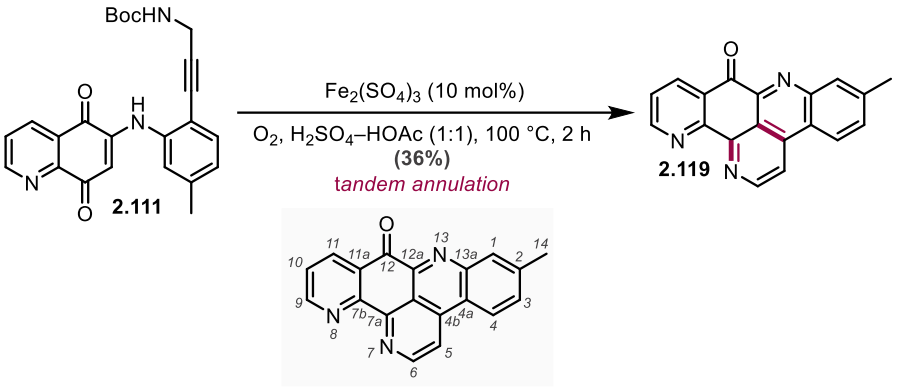

Adapted from the procedure of Wang et al.:[21] Under an oxygen atmosphere, $Fe_2(SO_4)_3$ (4.90 mg, 12.3 µmol, 10 mol%) and enamine **2.111** (51.2 mg, 0.123 mmol) in 1:1 concentrated sulfuric acid–glacial acetic acid (1.3 mL) was heated to 100 °C for 2 h. The black-green solution was cooled to 0 °C and quenched by slow addition to saturated aqueous sodium carbonate solution (20 mL) to achieve a pH of 9. The aqueous phase was extracted using dichloromethane (3 × 30 mL). The combined organic phases were washed sequentially with water (30 mL) and brine (30 mL), dried over anhydrous sodium sulfate, filtered and concentrated under reduced pressure. The yellow solid was purified by silica column chromatography (100% dichloromethane to 5% methanol in dichloromethane) to yield 2-methylascididemin **2.119** (13.0 mg, 43.7 µmol, 36%) as a yellow solid. 2-Methylascididemin **2.119** was further purified by reverse-phase HPLC (column (2), 5% to 50% acetonitrile in 0.005 M aqueous HCl) to afford 2-methylascididemin **2.119**•HCl for biological testing.

*2-Methylascididemin **2.119**:*

R_f: 0.35 (5% methanol in dichloromethane) – yellow spot (without stain)

^{1}H NMR (500 MHz, $CDCl_3$): δ 9.27 (d, *J* = 5.6 Hz, 1H, H6), 9.18 (dd, *J* = 4.6, 1.8 Hz, 1H, H9), 8.81 (dd, *J* = 7.9, 1.8 Hz, 1H, H11), 8.59 (d, *J* = 8.4 Hz, 1H, H4), 8.52 (d, *J* = 5.6 Hz, 1H, H5), 8.44 (s, 1H, H1), 7.79 (dd, *J* = 8.4, 1.8 Hz, 1H, H3), 7.68 (dd, *J* = 7.9, 4.6 Hz, 1H, H10), 2.70 (s, 3H, H14)

^{13}C NMR (126 MHz, $CDCl_3$): δ 181.9 (C, C12), 155.6 (CH, C9), 152.5 (C, C7b), 149.8 (C, C7a), 149.7 (CH, C6), 146.1 (C, C12a), 146.0 (C, C13a), 142.8 (C, C2), 138.0 (C, C4b), 136.6 (CH, C11), 132.8 (CH, C3), 132.6 (C, C1), 129.1 (C, C11a), 125.6 (CH, C10), 122.7 (CH, C4), 121.3 (C, C4a), 118.0 (C, C12b), 116.8 (CH, C5), 21.9 (CH_3, C14)

HRMS-ESI (m/z): Calculated for $C_{19}H_{12}N_3O$ [M+H]+, 298.0975; found 298.0974

IR: 3563, 2966, 2205, 1678, 1579, 1411, 1264, 1105, 871, 726

*2-Methylascididemin **2.119**•HCl:*

^{1}H NMR (600 MHz, CD_3OD): δ 9.20 (dd, *J* = 4.8, 1.6 Hz, 1H, H9), 9.13 (d, *J* = 6.2 Hz, 1H, H5 or H6), 9.11 (d, *J* = 6.2 Hz, 1H, H5 or H6), 8.96 (dd, *J* = 8.0, 1.6 Hz, 1H, H11), 8.86 (d, *J* = 8.4 Hz, 1H, H4), 8.28 (br s, 1H, H1), 8.09 (dd, *J* = 7.9, 4.9 Hz, 1H, H10), 7.94 (dd, *J* = 8.3, 1.7 Hz, 1H, H3), 2.71 (s, 3H, H14)

^{13}C NMR (151 MHz, CD_3OD): δ 180.3 (C, C12), 154.2 (CH, C9), 148.0 (C, C7b), 147.6 (C), 147.1 (C), 147.0 (C), 146.7 (C), 144.2 (CH, C5 or C6), 142.0 (C), 139.8 (CH, C11), 135.0 (CH, C3), 132.7 (CH, C1), 131.3 (C, C11a), 129.6 (C), 125.7 (CH, C4), 121.62, 121.56, 119.1 (C), 22.0 (CH_3, C14)

Aniline **2.107**:

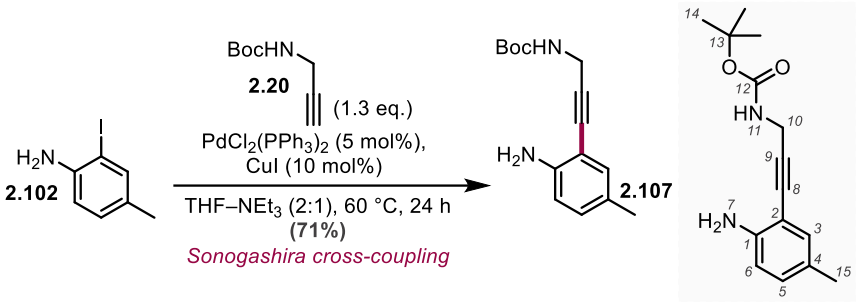

Adapted from the procedure of Wang et al.:[21] Under a nitrogen atmosphere, 2-iodo-4-methylaniline **2.102** (0.44 g, 1.89 mmol), bis(triphenylphosphine)palladium(II) dichloride (66 mg, 0.10 mmol, 5 mol%) and copper(I) iodide (36 mg, 0.19 mmol, 10 mol%) in triethylamine (2 mL) and tetrahydrofuran (2 mL) was pre-stirred for 30 minutes at rt. Then, a solution of propargylamine **2.20** (0.32 g, 2.46 mmol) in tetrahydrofuran (2 mL) was added dropwise over 5 minutes, and the resulting solution was heated to 60 °C. After 24 h, the black-brown suspension was filtered over Celite and washed with dichloromethane (50 mL). Water (50 mL) was added to the filtrate and the aqueous phase was extracted with dihloromethane (3 × 50 mL). The combined organic phases were washed with brine (50 mL), dried over anhydrous sodium sulfate, filtered and concentrated under reduced pressure. The dark-brown residue was purified by silica column chromatography (100% pentane to 20% ethyl acetate in pentane) to yield aniline **2.107** (0.35 g, 1.34 mmol, 71%) as an orange oil.

R_f: 0.35 (20% ethyl acetate in pentane) – yellow spot (with vanillin)

^{1}H NMR (600 MHz, $CDCl_3$): δ 7.07 – 7.04 (m, 1H, H3), 6.92 (dd, *J* = 8.2, 2.1 Hz, 1H, H5), 6.60 (d, *J* = 8.2 Hz, 1H, H6), 4.78 (br s, 1H, H11), 4.18 (d, *J* = 5.6 Hz, 2H, H10), 4.07 (s, 2H, H7), 2.19 (s, 3H, H15), 1.47 (s, 9H, H14)

^{13}C NMR (151 MHz, $CDCl_3$): δ 155.5 (C, C12), 145.9 (C, C1), 132.5 (CH, C3), 130.7 (CH, C5), 127.2 (C, C4), 114.6 (CH, C6), 107.5 (C, C2), 90.6 (C, C9), 80.2 (C, C8 and C13), 31.6 (CH_2, C10), 28.5 (CH_3, C14), 20.4 (CH_3, C15)

HRMS-ESI (m/z): Calculated for $C_{15}H_{21}N_2O_2$ [M+H]+ , 261.1598; found 261.1597

IR: 3358, 3022, 2924, 2856, 2222, 1699, 1624. 1504, 1366, 1277, 1250, 1167, 1047, 816

Enamine **2.112**:

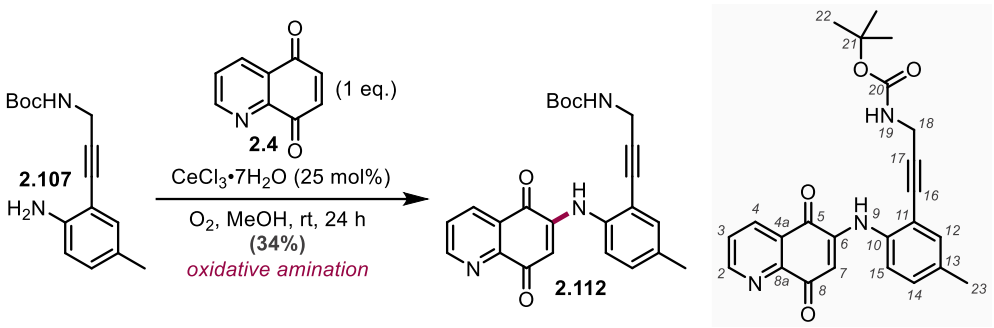

Adapted from the procedure of Wang et al.:[21] Under an oxygen atmosphere, cerium(III) chloride heptahydrate (68 mg, 0.183 mmol, 15 mol%) and aniline **2.107** (0.45 g, 1.73 mmol) were successively added to a solution of quinoline-5,8-dione **2.4** (0.19 g, 1.19 mmol) in methanol (7.3 mL) at rt. After 24 h, the red solution was concentrated under reduced pressure and the dark-red residue was purified by silica column chromatography (5 to 10% acetone in dichloromethane) to yield enamine **2.112** (0.17 g, 0.407 mmol, 34%) as a red crystalline solid.

R_f: 0.30 (10% acetone in dichloromethane) – red spot (without stain)

^{1}H NMR (600 MHz, $CDCl_3$): δ 9.03 (dt, *J* = 4.5, 1.9 Hz, 1H, H2), 8.42 (dq, *J* = 7.8, 1.5 Hz, 1H, H4), 8.13 (s, 1H, H9), 7.64 – 7.57 (m, 1H, H3), 7.32 (dd, *J* = 8.3, 2.1 Hz, 1H, H15), 7.28 (app t, *J* = 2.2 Hz, 1H, H12), 7.18 (dd, *J* = 8.4, 2.4 Hz, 1H, H14), 6.65 (s, 1H, H7), 4.96 (br s, 1H, H19), 4.23 (d, *J* = 5.5 Hz, 2H, H18), 2.31 (d, *J* = 2.1 Hz, 3H, H23), 1.46 – 1.44 (m, 9H, H22)

^{13}C NMR (151 MHz, $CDCl_3$): δ 182.3 (C, C8), 181.9 (C, C5), 155.4 (C and CH, C2 and C20), 148.9 (C, C8a), 143.4 (C), 136.1 (C), 135.0 (C), 134.6 (C), 133.5 (CH, C12), 130.4 (CH, C14), 127.5 (C, C4a), 126.6 (CH, C3), 120.3 (CH, C15), 116.1 (C, C11), 105.0 (CH, C7), 93.8 (C, C17), 80.2 (C, C21), 78.4 (C, C16), 31.4 (CH_2, C18), 28.5 (CH_3, C22), 20.9 (CH_3, C23)

HRMS-ESI (m/z): Calculated for $C_{24}H_{24}N_3O_4$ [M+H]+ , 418.1761; found 418.1757

IR: 3699, 2910, 1711, 1615, 1579, 1529, 1304, 1267, 745

MP: 159 – 160 °C

3-Methylascididemin **2.120**:

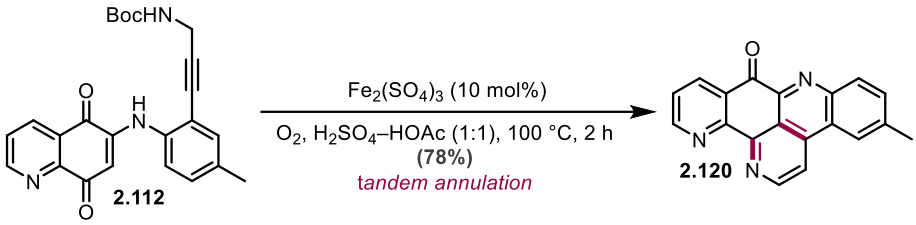

Adapted from the procedure of Wang et al.:[21] Under an oxygen atmosphere, $Fe_2(SO_4)_3$ (10 mg, 25.0 µmol, 10 mol%) and enamine **2.112** (0.10 g, 0.240 mmol) in 1:1 concentrated sulfuric acid–glacial acetic acid (2.4 mL) was heated to 100 °C for 2 h. The black-green solution was cooled to 0 °C and quenched by slow addition to saturated aqueous sodium carbonate solution (50 mL) to achieve a pH of 9. The aqueous phase was extracted using dichloromethane (3 × 50 mL). The combined organic phases were washed sequentially with water (50 mL) and brine (30 mL), dried over anhydrous sodium sulfate, filtered and concentrated under reduced pressure. The yellow-brown solid was purified by silica column chromatography (silica deactivated by 1% triethylamine, 100% dichloromethane to 5% methanol in dichloromethane) to yield 3-methylascididemin **2.120** (56 mg, 0.188 mmol, 78%) as a yellow solid. 3-Methylascididemin **2.120** was further purified by normal-phase HPLC (5% methanol in chloroform) for biological testing.

R_f: 0.30 (5% methanol in dichloromethane)

^{1}H NMR (600 MHz, $CDCl_3$): δ 9.25 (s, 1H), 9.18 (s, 1H), 8.81 – 8.78 (m, 1H), 8.54 – 8.48 (m, 2H), 8.45 (s, 1H), 7.85 – 7.81 (m, 1H), 7.70 – 7.65 (m, 1H), 2.72 (s, 3H)

^{13}C NMR (151 MHz, $CDCl_3$) δ 182.0, 155.6, 152.5, 149.8, 149.6, 145.3, 144.4, 142.1, 137.7, 136.7, 133.9, 133.1, 129.3, 125.7, 123.6, 122.6, 118.4, 117.0, 22.5

HRMS-ESI (m/z): Calculated for $C_{19}H_{12}N_3O$ [M+H]+ , 298.0975; found 298.0970

MP: 297 – 298 °C

Data in agreement with literature.[192]

Aniline **2.108**:

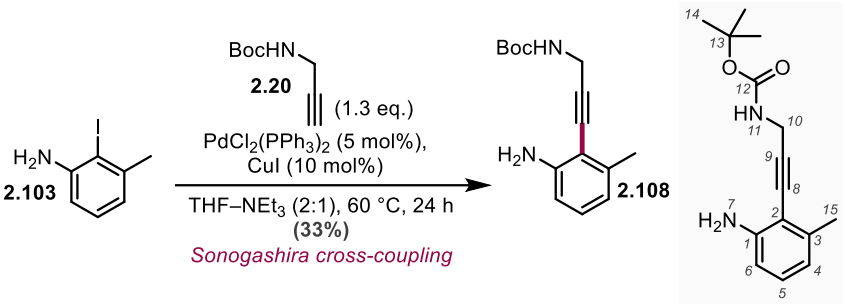

Adapted from the procedure of Wang et al.:[21] Under a nitrogen atmosphere, 2-iodo-3-methylaniline **2.103** (100 mg, 0.429 mmol), bis(triphenylphosphine)palladium(II) dichloride (15.1 mg, 0.0215 mmol, 5 mol%) and copper(I) iodide (8.17 mg, 0.0429 mmol, 10 mol%) in triethylamine (2.3 mL) and tetrahydrofuran (2.3 mL) was pre-stirred for 30 minutes at rt. Then, a solution of propargylamine **2.20** (107 mg, 0.558 mmol) in tetrahydrofuran (2.3 mL) was added dropwise over 5 minutes. After 24 h, the black-brown suspension was filtered over Celite and washed with dichloromethane (40 mL). Water (70 mL) was added to the filtrate and the aqueous phase was extracted with dichloromethane (3 x 40 mL). The combined organic phases were washed with brine (100 mL), dried over anhydrous sodium sulfate, filtered and concentrated under reduced pressure. The crude material was purified by silica column chromatography (10 to 30% ethyl acetate in pentane) to yield aniline **2.108** (36.9 mg, 0.142 mmol, 33%) as a yellow oil.

R_f: 0.32 (20% ethyl acetate in pentane) – brown spot (with vanillin)

^{1}H NMR (600 MHz, $CDCl_3$): δ 6.99 (t, *J* = 7.8 Hz, 1H, H5), 6.56 (d, *J* = 7.5 Hz, 1H, H4), 6.52 (d, *J* = 8.0 Hz, 1H, H6), 4.80 (s, 1H, H11), 4.21 (d, *J* = 5.6 Hz, 2H, H10), 2.35 (s, 3H, H15), 1.55 (d, *J* = 2.4 Hz, 2H, H7), 1.47 (s, 9H, H14)

^{13}C NMR (151 MHz, $CDCl_3$): δ 155.6 (C, C12), 148.5 (C, C1), 141.2 (C, C3), 129.1 (CH, C5), 119.0 (CH, C4), 111.7 (CH, C6), 107.7 (C, C2), 94.9 (C, C9), 80.2 (C, C13), 78.9 (C, C8), 31.8 (CH_2, C10), 28.5 (CH_3, C14), 21.1 (CH_3, C15)

HRMS-ESI (m/z): Calculated for $C_{15}H_{21}N_2O_2$ [M+H]+, 261.1598; found 261.1591

IR: 3360, 2980, 1699, 1507, 1170, 736.

Enamine **2.113**:

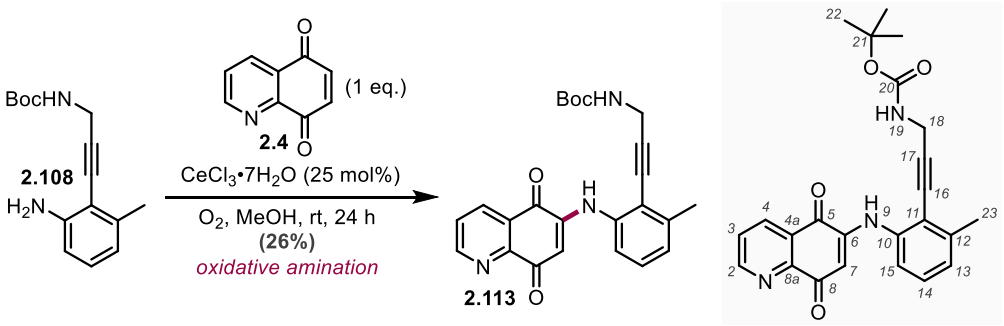

Adapted from the procedure of Wang et al.:[21] Under an oxygen atmosphere, cerium(III) chloride heptahydrate (10 mg, 26.8 µmol, 25 mol%) and aniline **2.108** (28 mg, 108 µmol) were successively added to a solution of quinoline-5,8-dione **2.4** (17 mg, 107 µmol) in methanol (1.1 mL) at rt. After 24 h, the red solution was concentrated under reduced pressure and the dark-red residue was purified by silica column chromatography (100% dichloromethane to 20% acetone in dichloromethane) to yield enamine **2.113** (11.6 mg, 27.8 µmol, 26%) as a red foam.

R_f: 0.31 (10% acetone in dichloromethane) – red spot (without stain)

^{1}H NMR (500 MHz, $CDCl_3$): δ 9.05 (dd, *J* = 4.8, 1.8 Hz, 1H, H2), 8.44 (dd, *J* = 7.9, 1.7 Hz, 1H, H4), 8.29 (s, 1H, H9), 7.63 (dd, *J* = 7.8, 4.7 Hz, 1H, H3), 7.31 – 7.27 (m, 1H, H14 or H15), 7.27 – 7.24 (m, 1H, H14 or H15), 7.03 (d, *J* = 7.1 Hz, 1H, H4), 6.73 (s, 1H, H7), 5.01 (s, 1H, H19), 4.30 (d, *J* = 5.7 Hz, 2H, H18), 2.45 (s, 3H, H23), 1.46 (s, 9H, H22)

^{13}C NMR (126 MHz, $CDCl_3$): δ 182.4 (C, C5 or C8), 182.0 (C, C5 or C8), 155.48 (C, C20), 155.45 (CH, C2), 148.9 (C, C8a), 143.3 (C, C6), 142.3 (C, C12), 138.7 (C, C10), 134.6 (CH, C4), 128.9 (CH, C14 or C15), 127.5 (C, C4a), 126.7 (CH, C3), 126.1 (CH, C13), 117.4 (CH, C14 or C15), 116.0 (C, C11), 105.4 (CH, C7), 98.3 (C, C17), 80.2 (C, C21), 77.3 (C, C16), 31.6 (CH_2, C18), 28.5 (CH_3, C22), 21.1 (CH_3, C23)

HRMS-ESI (m/z): Calculated for $C_{24}H_{24}N_3O_4$ [M+H]+, 418.1761; found 418.1752

IR: 3324, 2980, 2349, 1703, 1613, 1572, 1502, 1250, 1173, 913, 737

4-Methylascididemin **2.121**:

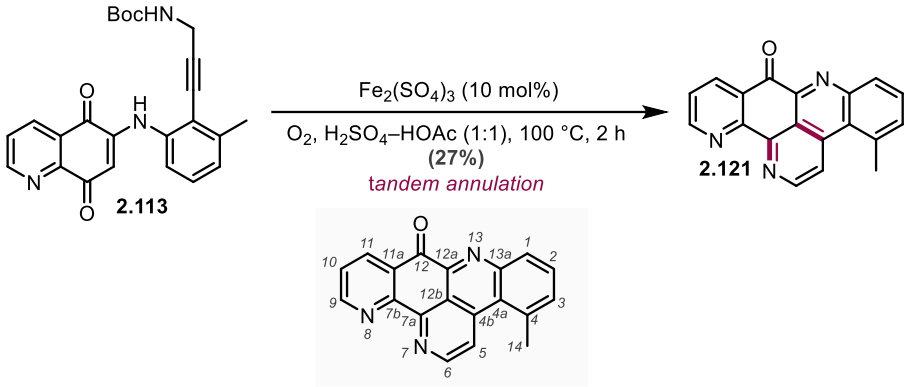

Adapted from the procedure of Wang et al.:[21] Under an oxygen atmosphere, $Fe_2(SO_4)_3$ (1.33 mg, 3.33 µmol, 10 mol%) and enamine **2.113** (13.9 mg, 33.3 µmol) in 1:1 concentrated sulfuric acid–glacial acetic acid (0.26 mL) was heated to 100 °C for 2 h. The black-green solution was cooled to 0 °C and quenched by slow addition to saturated aqueous sodium carbonate solution (4 mL) to achieve a pH of 9. The aqueous phase was extracted using dichloromethane (3 × 10 mL). The combined organic phases were washed sequentially with water (20 mL) and brine (20 mL), dried over anhydrous sodium sulfate, filtered and concentrated under reduced pressure. The yellow-brown solid was purified by silica column chromatography (100% dichloromethane to 5% methanol in dichloromethane) to yield 4-methylascididemin **2.121** (2.66 mg, 8.95 µmol, 27%) as an amorphous yellow solid. 4-Methylascididemin **2.121** was further purified by reverse-phase HPLC (column (2), 5% to 50% acetonitrile in 0.005 M aqueous HCl) to afford 4-methylascididemin **2.121**•HCl for biological testing.

*4-Methylascididemin **2.121**:*

R_f: 0.32 (5% methanol in dichloromethane) – yellow spot (without stain)

^{1}H NMR (400 MHz, $CDCl_3$): δ 9.30 (d, *J* = 6.0 Hz, 1H, H6), 9.20 (dd, *J* = 4.6, 1.9 Hz, 1H, H9), 8.87 (d, *J* = 6.0 Hz, 1H, H5), 8.80 (dd, *J* = 7.9, 1.8 Hz, 1H, H11), 8.56 (dd, *J* = 8.2, 1.4 Hz, 1H, H1), 7.91 (dd, *J* = 8.2, 7.3 Hz, 1H, H2), 7.79 (app d, *J* = 7.3 Hz, 1H, H3), 7.70 – 7.67 (m, 1H, H10), 3.23 (s, 3H, H14)

HRMS-ESI (m/z): Calculated for $C_{19}H_{12}N_3O$ [M+H]+, 298.0975; found 298.0974

IR: 3557, 2965, 1679, 1581, 1411, 1264, 1104, 804, 739.

*4-Methylascididemin **2.121**•HCl:*

^{1}H NMR (600 MHz, CD_3OD): δ 9.29 (d, *J* = 6.4 Hz, 1H, H6), 9.22 – 9.19 (m, 2H, H5 and H9), 8.98 (dd, *J* = 7.9, 1.7 Hz, 1H, H11), 8.46 (d, J = 8.0 Hz, 1H, H1), 8.08 – 8.04 (m, 2H, H2 and H10), 7.97 (d, *J* = 7.3 Hz, 1H, H3), 3.27 (s, 3H, H14)

^{13}C NMR (151 MHz, CD_3OD): δ 180.8 (C, C12), 154.2 (CH, C9), 149.5 (C), 148.6 (C), 146.9 (C), 146.6 (C), 145.7 (CH, C5), 142.1 (C), 139.74 (CH or C, C11 or Ar), 139.71 (CH or C, C11 or Ar), 137.1 (CH, C3), 133.8 (CH, C2 or C10), 132.7 (CH, C1), 130.8 (C), 129.0 (CH, C2 or C10), 124.8 (CH, C6), 123.6 (C, C4), 120.2 (C), 26.1 (CH_3, C14)

Aniline **2.109**:

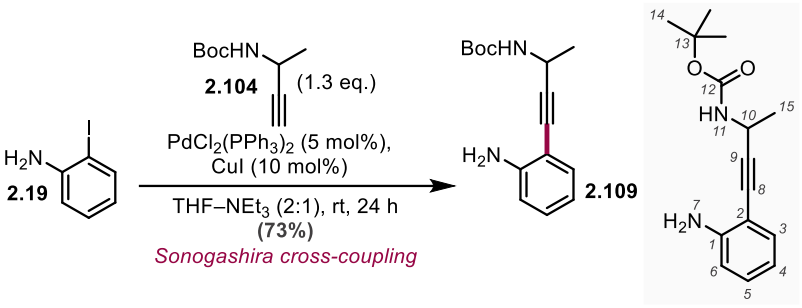

Adapted from the procedure of Wang et al.:[21] Under a nitrogen atmosphere, 2-iodoaniline **2.19** (50 mg, 228 µmol), bis(triphenylphosphine)palladium(II) dichloride (8 mg, 11.4 µmol, 5 mol%) and copper(I) iodide (4 mg, 21.0 µmol, 10 mol%) in triethylamine (0.5 mL) and tetrahydrofuran (0.5 mL) was pre-stirred for 30 minutes at rt. Then, a solution of propargylamine **2.104** (50 mg, 295 µmol) in tetrahydrofuran (0.5 mL) was added dropwise over 5 minutes. After 24 h, the black-brown suspension was filtered over Celite and washed with dichloromethane (30 mL). Water (30 mL) was added to the filtrate and the aqueous phase was extracted with dichloromethane (3 x 40 mL). The combined organic phases were washed with brine (30 mL), dried over anhydrous sodium sulfate, filtered and concentrated under reduced pressure. The dark-brown residue was purified by silica column chromatography (100% pentane to 20% ethyl acetate in pentane) to yield aniline **2.109** (43 mg, 0.165 mmol, 73%) as an orange semi-solid.

R_f: 0.26 (10% ethyl acetate in pentane)

^{1}H NMR (400 MHz, $CDCl_3$): δ 7.22 (dd, *J* = 7.7, 1.6 Hz, 1H, H6), 7.13 – 7.07 (m, 1H, ArH), 6.69 – 6.62 (m, 2H, ArH), 4.87 (br s, 1H, H11), 4.77 – 4.67 (m, 1H, H10), 4.24 (s, 2H, H7), 1.49 (d, *J* = 6.8 Hz, 3H, H15), 1.46 (s, 9H, H14)

^{13}C NMR (101 MHz, $CDCl_3$): δ 154.9 (C, C12), 148.2 (C, C1), 132.1 (CH, C6), 129.7 (CH, Ar), 117.8 (CH, Ar), 114.3 (CH, Ar), 107.4 (C, Ar), 95.4 (C, C9), 80.0 (C, C8), 78.9 (C, C13), 39.4 (CH, C10), 28.5 (CH_3, C14), 22.8 (CH_3, C15)

HRMS-ESI (m/z): Calculated for $C_{15}H_{21}N_2O_2$ [M+H]+ , 261.1598; found 261.1598

IR: 3466, 3357, 2978, 2933, 1692, 1616, 1493, 1456, 1367, 1247, 749

Enamine **2.114**:

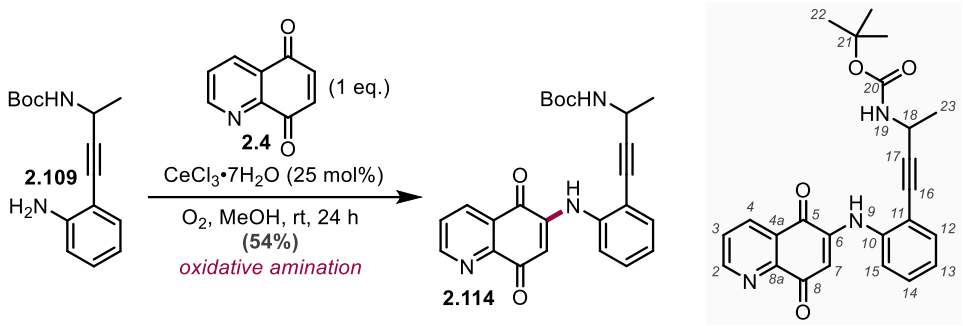

Adapted from the procedure of Wang et al.:[21] Under an oxygen atmosphere, cerium(III) chloride heptahydrate (15 mg, 40.3 µmol, 25 mol%) and aniline **2.109** (43 mg, 0.165 mmol) were successively added to a solution of quinoline-5,8-dione **2.4** (26 mg, 0.163 mmol) in methanol (1.6 mL) at rt. After 24 h, the red solution was concentrated under reduced pressure and the dark-red residue was purified by silica column chromatography (100% dichloromethane to 10% acetone in dichloromethane) to yield enamine **2.114** (37 mg, 88.6 µmol, 54%) as a red crystalline solid.

R_f: 0.33 (10% acetone in dichloromethane) – red spot (without stain)

^{1}H NMR (400 MHz, $CDCl_3$): δ 9.03 (dd, *J* = 4.3, 0.9 Hz, 1H, H2), 8.42 (dd, *J* = 7.7, 1.3 Hz, 1H, H4), 8.26 (s, 1H, H9), 7.62 (dd, *J* = 7.9, 4.8 Hz, 1H, H3), 7.47 – 7.41 (m, 2H, ArH), 7.36 (app t, *J* = 7.5 Hz, 1H, ArH), 7.10 (app t, *J* = 7.7 Hz, 1H, ArH), 6.72 (s, 1H, H7), 4.98 (br s, 1H, H19), 4.80 (br s, 1H, H18), 1.55 (d, *J* = 6.9 Hz, 3H, H23), 1.43 (s, 9H, H22)

^{13}C NMR (101 MHz, $CDCl_3$): δ 182.4 (C, C5 or C8), 181.8 (C, C5 or C8), 155.4 (CH, C2), 154.7 (C, C20), 148.8 (C), 143.0 (C), 138.6 (C), 134.6 (CH, C4), 132.9 (CH, Ar), 129.6 (CH, Ar), 127.4 (C), 126.7 (CH, C3), 124.7 (CH, Ar), 119.8 (CH, Ar), 115.9 (C, C17), 105.4 (CH, C7), 98.8 (C, C16), 80.1 (C, C21), 39.2 (CH, C18), 28.5 (CH_3, C22), 22.9 (CH_3, C23)

HRMS-ESI (m/z): Calculated for $C_{24}H_{24}N_3O_4$ [M+H]+, 418.1761; found 418.1758

IR: 3307, 2977, 2925, 2851, 1705, 1681, 1614, 1571, 1525, 1455, 1331, 1304, 1246, 1165, 992, 753, 671

MP: 168 – 169 °C

6-Methylascididemin **2.122**:

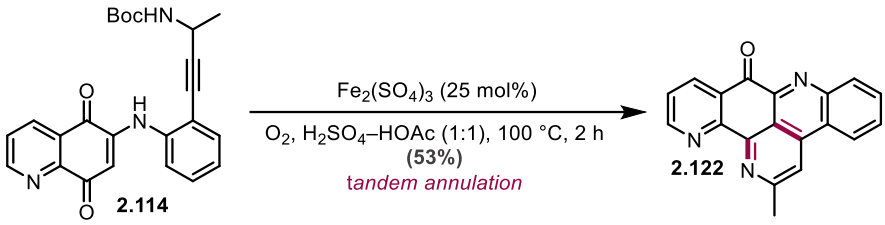

Adapted from the procedure of Wang et al.:[21] Under an oxygen atmosphere, (10 mg, 25.0 µmol, 25 mol%) and enamine **2.114** (40 mg, 95.8 µmol) in 1:1 concentrated sulfuric acid–glacial acetic acid (1 mL) was heated to 100 °C for 2 h. The black-green solution was cooled to 0 °C and quenched by slow addition to saturated aqueous sodium carbonate solution (15 mL) to achieve a pH of 9. The aqueous phase was extracted using dichloromethane (3 × 15 mL). The combined organic phases were washed sequentially with water (15 mL) and brine (15 mL), dried over anhydrous sodium sulfate, filtered and concentrated under reduced pressure. The yellow-brown solid was purified by silica column chromatography (100% dichloromethane to 5% methanol in dichloromethane) to yield 6-methylascididemin **2.122** (15 mg, 50.5 µmol, 53%) as a yellow solid. 6-Methylascididemin **2.122** was further purified by normal-phase HPLC (5% methanol in chloroform) for biological testing.

R_f: 0.28 (5% methanol in dichloromethane) – yellow spot (without stain)

^{1}H NMR (400 MHz, $CDCl_3$) δ 9.21 (dd, *J* = 4.6, 1.9 Hz, 1H), 8.80 (dd, *J* = 7.9, 1.9 Hz, 1H), 8.67 (dd, *J* = 8.1, 1.3 Hz, 1H), 8.61 (dd, *J* = 8.3, 1.1 Hz, 1H), 8.41 (br s, 1H), 7.99 (ddd, *J* = 8.3, 7.0, 1.4 Hz, 1H), 7.92 (ddd, *J* = 8.3, 7.0, 1.4 Hz, 1H), 7.66 (dd, *J* = 7.9, 4.6 Hz, 1H), 3.08 (br s, 3H)

^{13}C NMR (126 MHz, $CDCl_3$): δ 182.2, 160.0, 155.8, 152.7, 149.5, 146.2, 145.9, 138.7, 136.9, 133.3, 131.8, 130.7, 129.2, 125.6, 123.6, 123.0, 116.6, 115.9, 26.1

Data in agreement with literature.[33]

Enamine **2.115**:

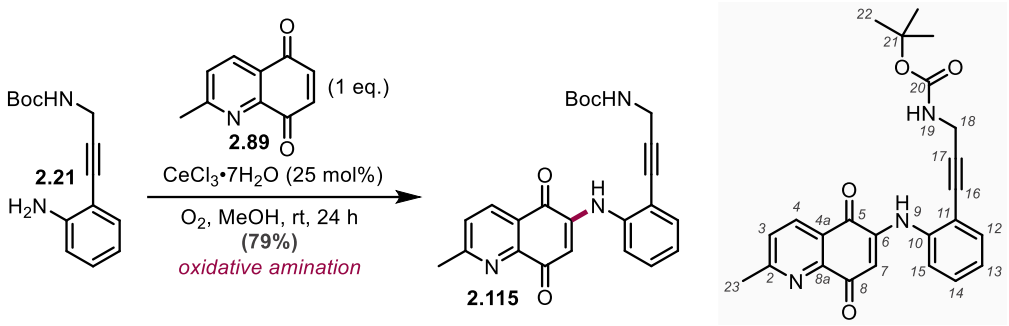

Adapted from the procedure of Wang et al.:[21] Under an oxygen atmosphere, cerium(III) chloride heptahydrate (60 mg, 0.173 mmol, 25 mol%) and aniline **2.21** (0.17 g, 0.692 mmol) were successively added to a solution of methylquinoline-5,8-dione **2.89** (0.12 g, 0.692 mmol) in methanol (6.9 mL) at rt. After 24 h, the red solution was concentrated under reduced pressure and the dark-red residue was purified by silica column chromatography (50% ethyl acetate in pentane to 100% ethyl acetate) to yield enamine **2.115** (0.21 g, 0.503 mmol, 79%) as a red crystalline solid.

R_f: 0.27 (80% ethyl acetate in pentane) – red spot (without stain)

^{1}H NMR (400 MHz, $CDCl_3$): δ 8.32 (d, *J* = 8.0 Hz, 1H, H4), 8.25 (s, 1H, H9), 7.51 – 7.44 (m, 3H, H3/H12/ArH), 7.41 – 7.35 (m, 1H, ArH), 7.15 – 7.10 (m, 1H, ArH), 6.71 (s, 1H, H7), 4.96 (br s, 1H, H19), 4.26 (d, *J* = 5.6 Hz, 2H, H18), 2.79 (s, 3H, H23), 1.46 (s, 9H, H22)

^{13}C NMR (151 MHz, $CDCl_3$): δ 182.8 (C, C8), 181.8 (C, C5), 166.1 (C, C2), 155.4 (C, C20), 148.5 (C, C6), 143.1 (C), 138.8 (C), 134.8 (CH, C4), 133.0 (CH, C3 or C12 or Ar), 129.7 (CH, Ar), 126.6 (CH, C3 or C12 or Ar), 125.3, 124.7 (CH, Ar), 120.1 (CH, C3 or C12 or Ar), 115.9 (C), 105.2 (CH, C7), 94.2 (C, C17), 80.3 (C, C21), 78.4 (C, C16), 31.4 (CH_2, C18), 28.5 (CH_3, C22), 25.7 (CH_3, C23)

IR: 3319, 2926, 2849, 1710, 1578, 1523, 1303, 1170, 756

HRMS-ESI (m/z): Calculated for $C_{24}H_{24}N_3O_4$ [M+H]+ , 418.1761; found 418.1754

MP: 116 – 117 °C (decomp.)

9-Methylascididemin **2.123**:

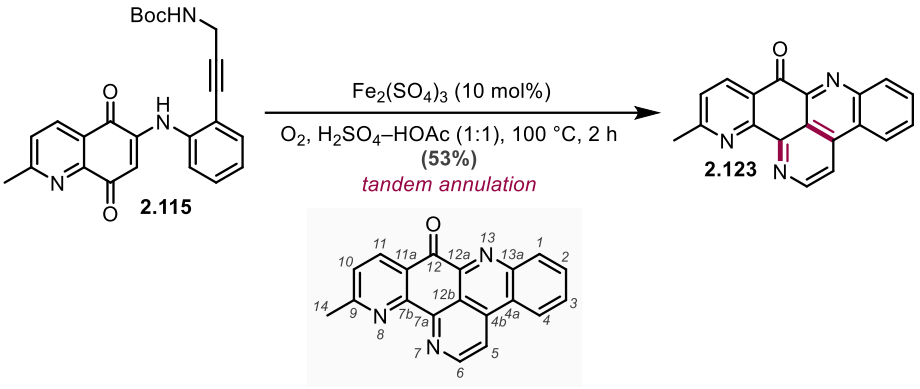

Adapted from the procedure of Wang et al.:[21] Under an oxygen atmosphere, $Fe_2(SO_4)_3$ (20 mg, 50.0 µmol, 10 mol%) and enamine **2.115** (0.20 g, 0.479 mmol) in 1:1 concentrated sulfuric acid–glacial acetic acid (4.8 mL) was heated to 100 °C for 2 h. The black-green solution was cooled to 0 °C and quenched by slow addition to saturated aqueous sodium carbonate solution (50 mL) to achieve a pH of 9. The aqueous phase was extracted using dichloromethane (3 × 50 mL). The combined organic phases were washed sequentially with water (30 mL) and brine (30 mL), dried over anhydrous sodium sulfate, filtered and concentrated under reduced pressure. The yellow-brown solid was purified by silica column chromatography (100% dichloromethane to 5% methanol in dichloromethane) to yield 9-methylascididemin **2.123** (76 mg, 0.256 mmol, 53%) as a yellow crystalline solid. 9-Methylascididemin **2.123** was further purified by normal-phase HPLC (5% methanol in chloroform) for biological testing.

R_f: 0.28 (5% methanol in dichloromethane) – yellow spot (without stain)

^{1}H NMR (600 MHz, $CDCl_3$): δ 9.33 (d, *J* = 5.6 Hz, 1H, H6), 8.71 – 8.69 (m, 2H, H4/H11), 8.65 (dd, *J* = 8.3, 1.2 Hz, 1H, H1), 8.56 (d, *J* = 5.7 Hz, 1H, H5), 8.05 – 8.01 (m, 1H, H2), 7.98 – 7.94 (m, 1H, H3), 7.54 (d, *J* = 8.0 Hz, 1H, H10), 2.92 (s, 3H, H14)

^{13}C NMR (151 MHz, $CDCl_3$): δ 181.8 (C, C12), 166.2 (C, C9), 151.9 (C, C7b), 150.0 (C), 149.8 (CH, C6), 146.3 (C), 146.0 (C, C13a), 138.3 (C), 137.0 (CH, C11), 133.3 (CH, C1), 132.1 (CH, C2), 130.9 (CH, C3), 127.2 (C, C11a), 126.0 (CH, C10), 123.6 (C, C4a), 123.1 (CH, C4), 118.3 (C), 116.9 (CH, C5), 26.0 (CH_3, C14)

HRMS-ESI (m/z): Calculated for $C_{19}H_{12}N_3O$ [M+H]+ , 298.0975; found 298.0974

IR: 3066, 2923, 1674, 1585, 1025

MP: >300 °C

Enamine **2.116**:

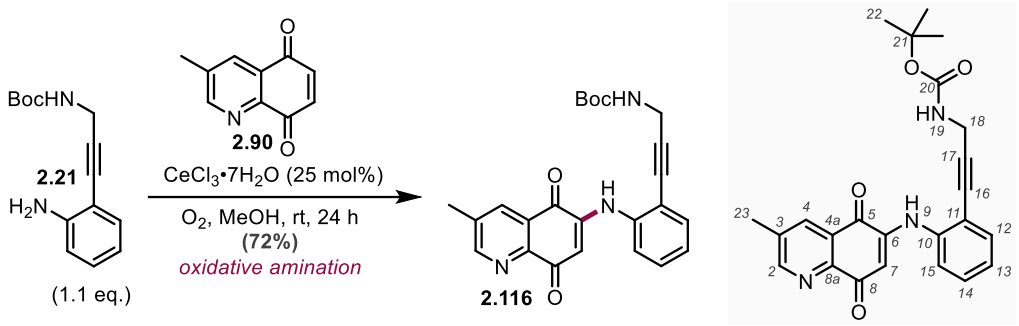

Adapted from the procedure of Wang et al.:[21] Under an oxygen atmosphere, cerium(III) chloride heptahydrate (53 mg, 0.142 mmol, 25 mol%) and aniline **2.21** (0.17 g, 0.693 mmol) were successively added to a solution of methylquinoline-5,8-dione **2.90** (0.11 g, 0.635 mmol) in methanol (5.7 mL) at rt. After 24 h, the red solution was concentrated under reduced pressure and the dark-red residue was purified by silica column chromatography (100% dichloromethane to 10% acetone in dichloromethane) to yield enamine **2.116** (0.19 g, 0.455 mmol, 72%) as a red crystalline solid.

R_f: 0.28 (10% acetone in dichloromethane) – red spot (without stain)

^{1}H NMR (600 MHz, $CDCl_3$): δ 8.89 (d, *J* = 2.2 Hz, 1H, H2), 8.26 – 8.22 (m, 2H, H4 and H9), 7.51 (dd, *J* = 7.7, 1.5 Hz, 1H, H12), 7.48 (d, *J* = 8.2 Hz, 1H, H15), 7.41 (td, *J* = 7.8, 1.6 Hz, 1H, H14), 7.15 (td, *J* = 7.6, 1.1 Hz, 1H, H13), 6.72 (s, 1H, H7), 4.99 (br s, 1H, H19), 4.29 (d, *J* = 5.6 Hz, 2H, H18), 2.55 (s, 3H, H23), 1.49 (s, 9H, H22)

^{13}C NMR (151 MHz, $CDCl_3$): δ 182.7 (C, C8), 182.2 (C, C5), 156.1 (CH, C2), 155.4 (C, C20), 146.7 (C), 143.2 (C), 138.8 (C), 137.5 (C), 134.5 (CH, C2), 133.0 (CH, C12), 129.7 (CH, C14), 127.1 (C), 124.7 (CH, C13), 120.1 (CH, C15), 116.0 (C), 105.3 (CH, C7), 94.2 (C, C17), 80.3 (C, C21), 78.4 (C, C16), 31.4 (CH_2, C18), 28.5 (CH_3, C21), 18.9 (CH_3, C23)

HRMS-ESI (m/z): Calculated for $C_{24}H_{24}N_3O_4$ [M+H]+, 418.1761; found 418.1758

IR: 3314, 3059, 2979, 2925, 2851, 1709, 1681, 1644, 1614, 1563, 1523, 1455, 1366, 1301, 1249, 1169, 1109, 1045, 757, 739

MP: 166 – 168 °C

10-Methylascididemin **2.124**:

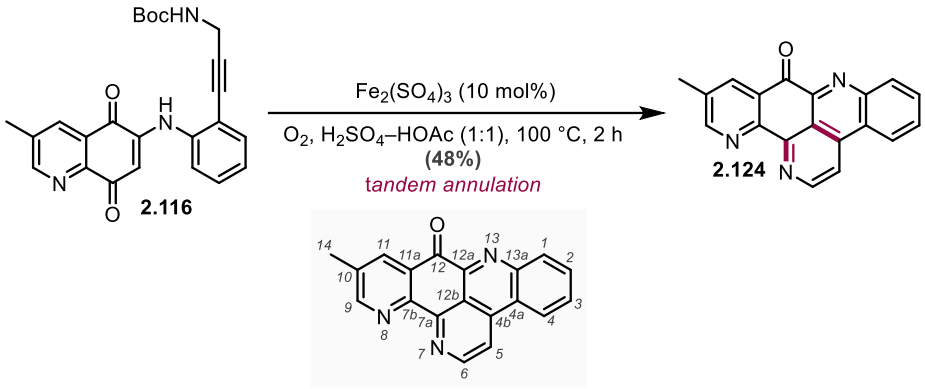

Adapted from the procedure of Wang et al.:[21] Under an oxygen atmosphere, $Fe_2(SO_4)_3$ (10 mg, 25.0 µmol, 10 mol%) and enamine **2.116** (0.10 g, 0.240 mmol) in 1:1 concentrated sulfuric acid–glacial acetic acid (2.4 mL) was heated to 100 °C for 2 h. The black-green solution was cooled to 0 °C and quenched by slow addition to saturated aqueous sodium carbonate solution (25 mL) to achieve a pH of 9. The aqueous phase was extracted using dichloromethane (3 × 50 mL). The combined organic phases were washed sequentially with water (30 mL) and brine (30 mL), dried over anhydrous sodium sulfate, filtered and concentrated under reduced pressure. The yellow-brown solid was purified by silica column chromatography (100% dichloromethane to 5% methanol in dichloromethane) to yield 10-methylascididemin **2.124** (34 mg, 0.115 mmol, 48%) as a yellow crystalline solid. 10-Methylascididemin **2.124** was further purified by normal-phase HPLC (5% methanol in chloroform) for biological testing.

R_f: 0.30 (5% methanol in dichloromethane) – yellow spot (without stain)

^{1}H NMR (400 MHz, $CDCl_3$): δ 9.26 (d, *J* = 5.7 Hz, 1H, H6), 9.00 (app d, *J* = 1.9 Hz, 1H, H9), 8.70 (d, *J* = 8.2 Hz, 1H, H4), 8.64 (d, *J* = 8.2 Hz, 1H, H1), 8.59 (app d, *J* = 2.3 Hz, 1H, H11), 8.52 (d, *J* = 5.7 Hz, 1H, H5), 8.05 – 7.99 (m, 1H, H2), 7.98 – 7.92 (m, 1H, H3), 2.59 (s, 3H, H14)

^{13}C NMR (126 MHz, $CDCl_3$): δ 182.3 (C, C12), 156.5 (CH, C9), 150.29 (C), 150.23 (C), 149.9 (CH, C6), 146.4 (C), 145.9 (C, C13a), 138.2 (C, C4b), 136.5 (CH, C11), 136.3 (C, C10), 133.3 (CH, C1), 132.0 (CH, C2), 130.9 (CH, C3), 128.7 (C), 123.7 (C, C4a), 123.1 (CH, C4), 118.0 (C), 116.6 (CH, C5), 18.7 (CH_3, C14)

HRMS-ESI (m/z): Calculated for $C_{19}H_{12}N_3O$ [M+H]+, 298.0975; found 298.0970

IR: 2974, 2920, 2847, 1681, 1595, 1477, 1421, 1339, 1306, 1265, 1197, 1175, 1103, 1069, 1038, 852, 830, 807

MP: 295 – 296 °C

Enamine **2.117**:

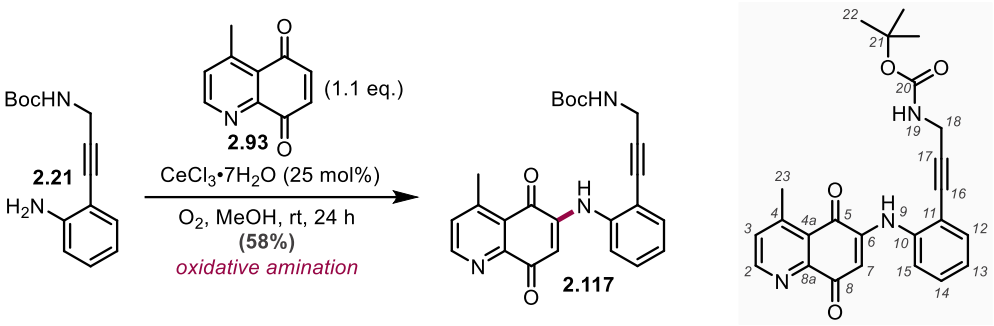

Adapted from the procedure of Wang et al.:[21] Under an oxygen atmosphere, cerium(III) chloride heptahydrate (53 mg, 0.142 mmol, 25 mol%) and aniline **2.21** (0.14 g, 0.577 mmol) were successively added to a solution of methylquinoline-5,8-dione **2.93** (0.11 g, 0.635 mmol) in methanol (5.7 mL) at rt. After 24 h, the red solution was concentrated under reduced pressure and the dark-red residue was purified by silica column chromatography (100% dichloromethane to 10% acetone in dichloromethane) to yield enamine **2.117** (0.14 g, 0.335 mmol, 58%) as a red crystalline solid.

R_f: 0.26 (10% acetone in dichloromethane) – red spot (without stain)

^{1}H NMR (400 MHz, $CDCl_3$): δ 8.84 (d, *J* = 4.9 Hz, 1H, H2), 8.34 (br s, 1H, H9), 7.48 (dd, *J* = 7.7, 1.5 Hz, 1H, H12), 7.46 – 7.44 (m, 1H, ArH), 7.41 – 7.39 (m, 1H, H3), 7.37 (dd, *J* = 8.1, 1.5 Hz, 1H, ArH), 7.12 (td, *J* = 7.6, 1.1 Hz, 1H, ArH), 6.70 (s, 1H, H7), 5.06 (br s, 1H, H19), 4.28 (d, *J* = 5.4 Hz, 2H, H18), 2.85 (s, 3H, H23), 1.46 (s, 9H, H21)

^{13}C NMR (151 MHz, $CDCl_3$): δ 183.2 (C, C5), 182.3 (C, C8), 155.3 (C, C20), 153.8 (CH, C2), 150.9 (C), 149.9 (C), 143.7 (C), 138.8 (C), 132.8 (CH, C12), 129.9 (CH, C3 or Ar), 129.6 (CH, C3 or Ar), 125.8 (C, Ar), 124.6 (CH, Ar), 119.9 (CH, Ar), 115.8 (C), 104.2 (CH, C7), 94.0 (C, C17), 80.1 (C, C21), 78.4 (C, C16), 31.4 (CH_2, C18), 28.4 (CH_3, C22), 22.6 (CH_3, C23)

HRMS-ESI (m/z): Calculated for $C_{24}H_{24}N_3O_4$ [M+H]+ , 418.1761; found 418.1757

IR: 3314, 2929, 2230, 1708, 1618, 1578, 1523, 1303, 1181, 732

MP: 127 – 129 °C

11-Methylascididemin **2.125**:

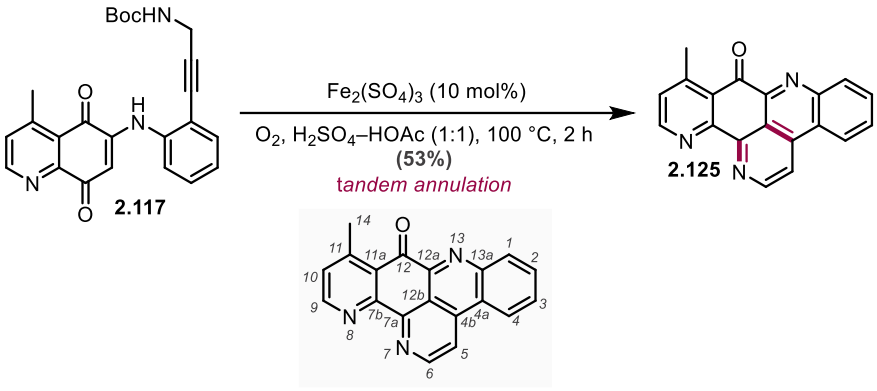

Adapted from the procedure of Wang et al.:[21] Under an oxygen atmosphere, $Fe_2(SO_4)_3$ (13 mg, 32.5 µmol, 10 mol%) and enamine **2.117** (0.13 g, 0.311 mmol) in 1:1 concentrated sulfuric acid–glacial acetic acid (3.2 mL) was heated to 100 °C for 2 h. The black-green solution was cooled to 0 °C and quenched by slow addition to saturated aqueous sodium carbonate solution (25 mL) to achieve a pH of 9. The aqueous phase was extracted using dichloromethane (3 × 50 mL). The combined organic phases were washed sequentially with water (30 mL) and brine (30 mL), dried over anhydrous sodium sulfate, filtered and concentrated under reduced pressure. The yellow-brown solid was purified by silica column chromatography (100% dichloromethane to 5% methanol in dichloromethane) to yield 11-methylascididemin **2.125** (49 mg, 0.165 mmol, 53%) as a yellow crystalline solid. 11-Methylascididemin **2.125** was further purified by normal-phase HPLC (5% methanol in chloroform) for biological testing.

R_f: 0.30 (5% methanol in dichloromethane) – yellow spot (without stain)

^{1}H NMR (500 MHz, $CDCl_3$) δ 9.29 (d, *J* = 5.7 Hz, 1H, H6), 8.96 (d, *J* = 4.8 Hz, 1H, H9), 8.69 (dd, *J* = 8.2, 1.4 Hz, 1H, H1 or H4), 8.62 – 8.60 (m, 1H, H1 or H4), 8.53 (d, *J* = 5.7 Hz, 1H, H5), 8.01 (ddd, *J* = 8.3, 7.0, 1.4 Hz, 1H, H2 or H3), 7.94 (ddd, *J* = 8.3, 7.1, 1.3 Hz, 1H, H2 or H3), 7.45 (dd, *J* = 4.8, 0.8 Hz, 1H, H10) 3.00 (d, *J* = 0.8 Hz, 3H, H14)

^{13}C NMR (126 MHz, $CDCl_3$): δ 183.7 (C, C12), 154.0 (CH, C9), 153.6 (C, Ar), 153.1 (C, C11), 150.5 (C, Ar), 150.1 (CH, C6), 146.9 (C, Ar), 146.0 (C, Ar), 138.0 (C, Ar), 133.2 (CH, C1 or C4), 132.0 (CH, C2 or C3), 130.7 (CH, C2 or C3), 129.3 (CH, C10), 128.2 (C, Ar), 123.6 (C, Ar), 123.1 (CH, C1 or C4), 117.6 (C, Ar), 116.8 (CH, C5), 23.5 (CH_3, C14)

HRMS-ESI (m/z): Calculated for $C_{19}H_{12}N_3O$ $[M+H]^+$, 298.0975; found 298.0969

IR: 2980, 1680, 1578, 1275, 1262, 764, 750, 725

MP: 274 – 275 °C

Aniline **2.103**:

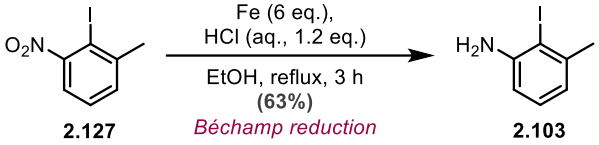

2.127 **2.103**

Adapted from the procedure of Bell et al.:[181] Concentrated aqueous hydrochloric acid (37%, 0.11 mL, 1.33 mmol) was added dropwise over 1 minute to a vigorously stirring suspension of 2-iodo-3-nitrotoluene **2.127** (0.30 g, 1.11 mmol) and iron powder (0.38 g, 6.86 mmol) in ethanol (3.3 mL) at rt. The resulting reaction mixture was then heated to reflux at 70 °C for 3 h. The reaction was then cooled to rt, diluted with ethyl acetate (15 mL), filtered through Celite and washed with ethyl acetate (25 mL). Water (25 mL) was added to the filtrate and the phases were separated. The organic phase was washed with brine (15 mL), dried over anhydrous sodium sulfate, filtered and concentrated under reduced pressure. The crude material was purified by silica column chromatography (100% pentane to 10% diethyl ether in pentane) to yield aniline **2.103** (0.16 g, 0.70 mmol, 63%) as a yellow solid.

R_f: 0.35 (7.5% diethyl ether in pentane) – yellow spot (with vanillin)

^{1}H NMR (700 MHz, $CDCl_3$): δ 7.02 (app t, *J* = 7.6 Hz, 1H), 6.68 – 6.64 (m, 1H), 6.61 – 6.57 (m, 1H) 4.18 (br s, 2H), 2.44 (s, 3H)

^{13}C NMR (176 MHz, $CDCl_3$): δ 147.2, 142.5, 128.6, 119.7, 112.0, 91.7, 29.4

Data in agreement with literature.[181]

Aniline **2.101**:

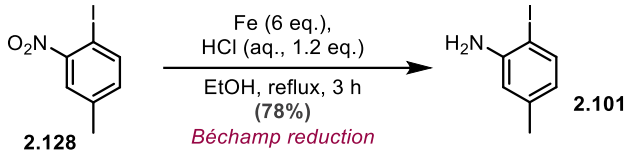

Adapted from the procedure of Bell et al.:[181] Concentrated aqueous hydrochloric acid (37%, 0.22 mL, 2.66 mmol) was added dropwise over 1 minute to a vigorously stirring suspension of 4-iodo-3-nitrotoluene **2.128** (0.60 g, 2.21 mmol) and iron powder (0.77 g, 13.7 mmol) in ethanol (6.6 mL) at rt. The resulting reaction mixture was then heated to reflux at 70 °C for 3 h. The reaction was then cooled to rt, diluted with ethyl acetate (30 mL), filtered through Celite and washed with ethyl acetate (50 mL). Water (50 mL) was added to the filtrate and the phases were separated. The organic phase was washed with brine (30 mL), dried over anhydrous sodium sulfate, filtered and concentrated under reduced pressure. The crude material was purified by silica column chromatography (100% pentane to 10% diethyl ether in pentane) to yield aniline **2.101** (0.40 g, 1.72 mmol, 78%) as a yellow solid.

R_f: 0.69 (10% diethyl ether in pentane) – yellow spot (with vanillin)

^{1}H NMR (500 MHz, $CDCl_3$): δ 7.49 (d, *J* = 8.0 Hz, 1H), 6.59 – 6.58 (m, 1H), 6.35 – 6.29 (m, 1H), 4.01 (s, 2H), 2.23 (s, 3H)

^{13}C NMR (126 MHz, $CDCl_3$): δ 146.7, 139.6, 138.7, 121.4, 115.7, 80.4, 21.2

Data in agreement with literature.[193]

Aniline **2.100**:

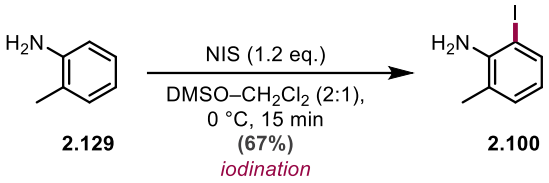

Adapted from the procedure of Tymann et al.:[194] Under a nitrogen atmosphere, *N*-iodosuccinimide (0.76 g, 3.38 mmol) was added portion-wise over 1 minute to a solution of *ortho*-toluidine **2.129** (0.30 g, 2.80 mmol) in a 2:1 dimethylsulfoxide–dichloromethane mixture (18 mL) at 0 °C. After 15 minutes, the reaction was quenched by addition of saturated aqueous sodium thiosulfate (30 mL), and the aqueous phase was extracted with dichloromethane (3 x 30 mL). The combined organic phases were washed with water (5 x 10 mL), brine (100 mL), dried over anhydrous sodium sulfate, filtered and concentrated under reduced pressure. The crude brown solid was purified by silica column chromatograph (100% pentane to 10% ethyl acetate in pentane) to yield aniline **2.100** (0.44 g, 1.87 mmol, 67%) as a brown solid.

R_f: 0.36 (15% ethyl acetate in pentane) – yellow spot (with vanillin)

^{1}H NMR (600 MHz, CDCl3): δ 7.36 – 7.33 (m, 1H), 7.29 (dd, *J* = 8.3, 1.5 Hz, 1H), 6.45 (d, *J* = 8.3 Hz, 1H) 3.61 (br s, 2H), 2.11 (s, 3H)

^{13}C NMR (151 MHz, $CDCl_3$): δ 144.5, 138.8, 135.7, 125.1, 117.0, 79.7, 17.2

Data in agreement with literature.[194]

Propargylamine **2.132**:

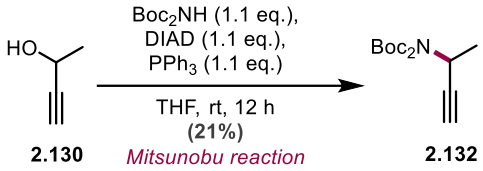

Adapted from the procedure of Guissart et al.:[195] Under nitrogen, diisopropyl azodicarboxylate (3.90 mL, 19.8 mmol) was added dropwise over 5 minutes to a solution of 3-butyn-2-ol **2.130** (1.40 mL, 17.9 mmol), triphenylphosphine (5.15 g, 19.6 mmol) and di-*tert*-butyl-iminodicarboxylate (4.27 g, 19.6 mmol) in tetrahydrofuran (60 mL) at 0 °C. After complete addition, the ice-bath was removed and the resulting mixture was allowed to warm to rt. After 12 h, the reaction mixture was concentrated under reduced pressure. The residue was purified by silica column chromatography (5% diethyl ether in pentane) to yield propargylamine **2.132** (1.00 g, 3.71 mmol, 21%) as a colourless oil.

R_f: 0.27 (5% diethyl ether in pentane)

^{1}H NMR (400 MHz, $CDCl_3$): δ 5.18 (qd, *J* = 7.0, 2.5 Hz, 1H), 2.28 (d, *J* = 2.5 Hz, 1H), 1.54 (d, *J* = 7.0 Hz, 3H), 1.52 (s, 18H)

^{13}C NMR (101 MHz, $CDCl_3$): δ 152.1, 83.2, 83.0, 70.6, 43.6, 28.2, 20.7

Data in agreement with literature.[195]

Propargylamine **2.104**:

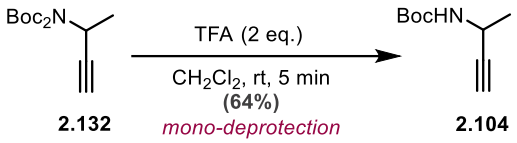

Adapted from the procedure of Boyle et al.:[196] Trifluoroacetic acid (0.06 mL, 0.784 mmol) was added dropwise over 1 minute to a solution of propargylamine **2.132** (0.11 g, 0.408 mmol) in dichloromethane (3.4 mL) and the resulting solution was stirred at rt for 5 minutes. The reaction was quenched by addition of 2 M sodium hydroxide (5 mL). The aqueous phase was extracted using dichloromethane (3 × 20 mL) and the combined organic phases were dried over anhydrous sodium sulfate, filtered, and concentrated under reduced pressure to yield propargylamine **2.104** (44 mg, 0.260 mmol, 64%) as a white solid. Used in the next step without further purification.

R_f: 0.21 (5% diethyl ether in pentane)

^{1}H NMR (400 MHz, $CDCl_3$) δ 4.75 (br s, 1H), 4.46 (br s, 1H), 2.25 – 2.23 (m, 1H), 1.43 (s, 9H), 1.40 – 1.36 (m, 3H)

^{13}C NMR (101 MHz, $CDCl_3$): δ 154.8, 84.7, 80.0, 70.2, 38.4, 28.5, 22.7

Data in agreement with literature.[197]

Aniline **2.137**:

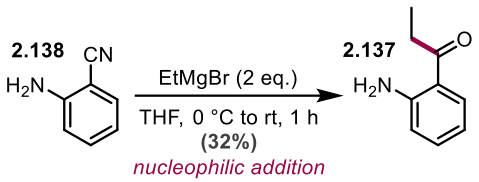

Adapted from the procedure of Li et al.:[198] Under a nitrogen atmosphere, ethylmagnesium bromide (34 mL, 1.0 M in tetrahydrofuran, 34.0 mmol) was added dropwise over 5 minutes to a solution of 2-aminobenzonitrile **2.138** (2.00 g, 16.9 mmol) in tetrahydrofuran (16 mL) at 0 °C. The ice-bath was removed and the resulting solution was allowed to warm to rt. After 1 h, the reaction was quenched by slow addition of saturated aqueous ammonium chloride solution (8 mL) and the aqueous phase was extracted with ethyl acetate (3 × 50 mL). The combined organic phases were washed with brine (50 mL), dried over anhydrous magnesium sulfate, filtered and concentrated under reduced pressure. The yellow oil was purified by silica column chromatography (5% ethyl acetate in pentane) to yield aniline **2.137** (0.82 g, 5.50 mmol, 32%) as a white solid.

R_f: 0.40 (5% ethyl acetate in pentane)

^{1}H NMR (400 MHz, $CDCl_3$): δ 7.76 (dd, *J* = 8.6, 1.5 Hz, 1H), 7.30 – 7.21 (m, 1H), 6.70 – 6.61 (m, 2H), 6.30 (br s, 2H), 2.98 (q, *J* = 7.3 Hz, 2H), 1.22 (t, *J* = 7.3 Hz, 3H)

^{13}C NMR (101 MHz, $CDCl_3$): δ 203.4, 150.4, 134.2, 131.1, 117.9, 117.4, 115.8, 32.4, 8.8

Data in agreement with literature.[198]

Aniline **2.139**:

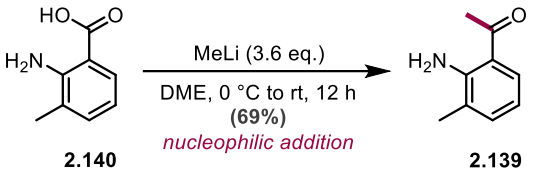

Adapted from the procedure of Mangas-Sánchez et al.:[199] Under a nitrogen atmosphere, methyllithium (10 mL, 1.2 M in tetrahydrofuran, 11.8 mmol) was added dropwise over 5 minutes to a solution of 2-amino-3-methylbenzoic acid **2.140** (0.50 g, 3.30 mmol) in dimethoxyethane (23.5 mL) at 0 °C. The ice-bath was removed and the resulting solution was allowed to warm to rt. After 12 h, the reaction was quenched by slow addition of saturated aqueous ammonium chloride solution (12 mL), the crude mixture was concentrated under reduced pressure to remove the organic layer and the aqueous phase was extracted with dichloromethane (3 × 20 mL). The combined organic phases were washed with brine (20 mL), dried over anhydrous magnesium sulfate, filtered and concentrated under reduced pressure. The yellow oil was purified by silica column chromatography (5% ethyl acetate in pentane) to yield aniline **2.139** (0.34 g, 2.30 mmol, 69%) as a white solid.

R_f: 0.35 (5% ethyl acetate in pentane) – white spot (with potassium permanganate)

^{1}H NMR (600 MHz, $CDCl_3$): δ 7.66 – 7.62 (m, 1H), 7.22 – 7.19 (m, 1H), 6.63 – 6.59 (m, 1H), 2.59 (s, 3H), 2.18 (s, 3H)

^{13}C NMR (151 MHz, $CDCl_3$): δ 201.3, 148.7, 135.3, 130.3, 123.7, 118.0, 115.4, 28.3, 17.4

Data in agreement with literature.[199]

Enamine **2.141**:

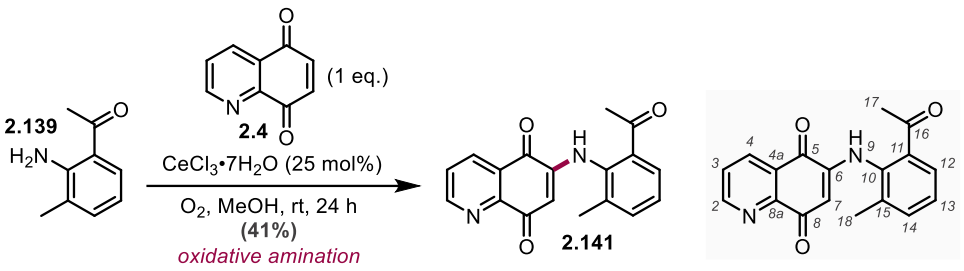

Adapted from the procedure of Bracher:[18] Under an oxygen atmosphere, cerium(III) chloride heptahydrate (29 mg, 77.8 µmol, 25 mol%) and aniline **2.139** (47.0 mg, 0.315 mmol) were successively added to a solution of quinoline-5,8-dione **2.4** (50 mg, 0.314 mmol) in methanol (3 mL) at rt. After 24 h, the red solution was concentrated under reduced pressure and the dark-red residue was purified by silica column chromatography (100% dichloromethane to 30% acetone in dichloromethane) to yield enamine **2.141** (39 mg, 0.130 mmol, 41%) as a red amorphous solid.

R_f: 0.23 (10% acetone in dichloromethane) – red spot (without stain)

^{1}H NMR (700 MHz, $CDCl_3$): δ 9.12 (s, 1H, H9), 9.02 – 9.00 (m, 1H, H2), 8.48 – 8.43 (m, 1H, H4), 7.75 (app d, *J* = 7.8 Hz, 1H, H12), 7.63 – 7.60 (m, 1H, H3), 7.47 (app d, *J* = 7.6 Hz, 1H, H14), 7.34 (t, *J* = 7.8 Hz, 1H, H13), 5.56 – 5.54 (m, 1H, H7), 2.61 – 2.59 (m, 3H, H17), 2.26 (s, 3H, H18)

^{13}C NMR (176 MHz, $CDCl_3$): δ 200.8 (C, C16), 182.2 (C, C8), 181.3 (C, C5), 155.1 (CH, C2), 149.0 (C, C8a), 145.5 (C, C6), 136.0 (CH, C14), 135.9 (C, C11), 135.4 (C, C15), 134.6 (CH, C4), 132.7 (C, C10), 129.0 (CH, C12), 127.8 (C, C4a), 127.0 (CH, C13), 126.6 (CH, C3), 106.3 (CH, C7), 29.0 (CH_3, C17), 18.8 (CH_3, C18)

HRMS-ESI (m/z): Calculated for $C_{18}H_{15}N_2O_3$ [M+H]+ , 307.1077; found 307.1080

IR: 3295, 2923, 2233, 1680, 1643, 1608, 1579, 1568, 1504, 1462, 1426, 1382, 1355, 1329, 1294, 1271, 1246, 1189, 1128, 1105, 1058, 1026, 991, 912, 861, 800, 733, 676, 647, 605

Tetracycle **2.143**:

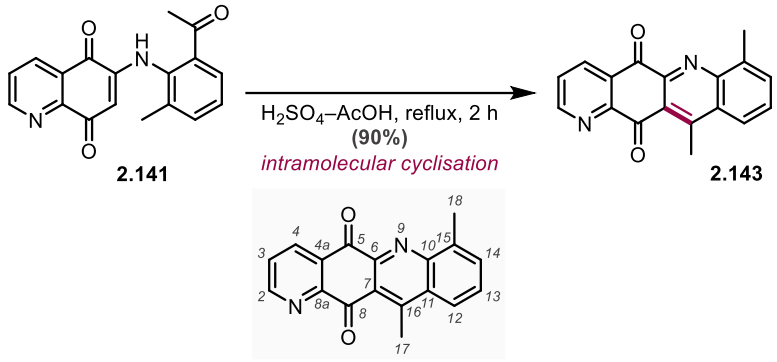

Adapted from the procedure of Bracher:[18] Enamine **2.141** (19 mg, 62.0 µmol) in glacial acetic acid (1.0 mL) and concentrated sulfuric acid (0.1 mL) was heated to 120 °C for 2 h. The black-green solution was cooled to 0 °C and quenched by slow addition to saturated aqueous sodium bicarbonate solution (30 mL) to achieve a pH of 7. The aqueous phase was extracted using dichloromethane (3 × 30 mL). The combined organic phases were washed with brine (30 mL), dried over anhydrous sodium sulfate, filtered and concentrated under reduced pressure to yield tetracycle **2.143** (16 mg, 55.5 µmol, 90%) as a yellow-green amorphous solid. Used in the next step without further purification.

R_f: 0.44 (10% acetone in dichloromethane) – yellow spot (without stain)

^{1}H NMR (700 MHz, $CDCl_3$): δ 9.09 (dd, *J* = 4.5, 1.7 Hz, 1H, H2), 8.65 (dd, *J* = 7.8, 1.8 Hz, 1H, H4), 8.19 – 8.16 (m, 1H, H12), 7.72 (dt, *J* = 6.9, 1.2 Hz, 1H, H14), 7.70 (dd, *J* = 7.8, 4.5 Hz, 1H, H3), 7.62 (dd, *J* = 8.6, 6.9 Hz, 1H, H13), 3.26 (s, 3H, H17), 2.93 (s, 3H, H18)

^{13}C NMR (176 MHz, $CDCl_3$): δ 184.0 (C, C8), 182.1 (C, C5), 155.7 (CH, C2), 152.7 (C), 150.5 (C, C8a), 148.0 (C), 146.6 (C), 140.9 (C), 135.8 (CH, C4), 133.1 (CH, C14), 130.5 (C, C4a), 130.2 (C), 129.9 (CH, C13), 128.0 (CH, C3), 125.5 (C), 123.6 (CH, C12), 18.4 (CH_3, C18), 17.0 (CH_3, C17)

HRMS-ESI (m/z): Calculated for $C_{18}H_{13}N_2O_2$ [M+H]+ , 289.0972; found 289.0964

IR: 2955, 2921, 2850, 1734, 1687, 1607, 1584, 1541, 1464, 1378, 1334, 1322, 1269, 1192, 1109, 1079, 1009, 913, 807, 784, 766, 739, 728, 668, 649, 630

1-Methylascididemin **2.118**:

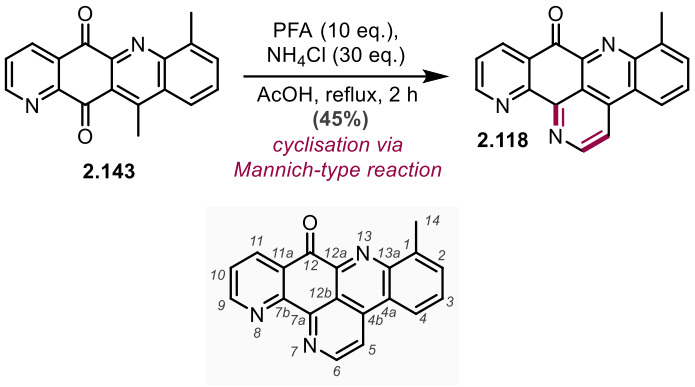

Adapted from the procedure of Lindsay et al.:[72] Under a nitrogen atmosphere, a solution of tetracycle **2.143** (8 mg, 27.7 µmol) and ammonium chloride (43 mg, 805 µmol) in glacial acetic acid (1.9 mL) was heated to 70 °C. Paraformaldehyde (PFA) (10 mg, 333 µmol) in glacial acetic acid (0.7 mL) was added dropwise over 1 minute and the resulting brown solution was heated to 120 °C for 2 h. The black-green solution was cooled to 0 °C and quenched by slow addition to saturated aqueous sodium bicarbonate solution (40 mL) to achieve a pH of 9. The aqueous phase was extracted using dichloromethane (3 × 30 mL). The combined organic phases were washed with brine (30 mL), dried over anhydrous sodium sulfate, filtered and concentrated under reduced pressure. The brown residue was purified using silica column chromatography (5% methanol in dichloromethane) to yield 1-methylascididemin **2.118** (3.7 mg, 12.4 µmol, 45%) as a yellow solid. 1-Methylascididemin **2.118** was further purified by reverse-phase HPLC (column (2), 5% to 50% acetonitrile in 0.005 M aqueous HCl) to afford 1-methylascididemin **2.118**•HCl for biological testing.

*1-Methylascididemin **2.118**:*

R_f: 0.28 (5% methanol in dichloromethane) – yellow spot (without stain)

^{1}H NMR (600 MHz, $CDCl_3$): δ 9.27 (d, *J* = 5.6 Hz, 1H, H6), 9.19 (dd, *J* = 4.5, 1.8 Hz, 1H, H9), 8.79 (dd, *J* = 7.9, 1.8 Hz, 1H, H11), 8.57 – 8.56 (m, 2H, H5 and ArH), 7.90 – 7.81 (m, 2H, ArH), 7.68 (dd, *J* = 7.8, 4.5 Hz, 1H, Hf10), 3.08 (s, 3H, H14)

HRMS-ESI (m/z): Calculated for $C_{19}H_{12}N_3O$ [M+H]+ , 298.0975; found 298.0979

*1-Methylascididemin **2.118**•HCl:*

^{1}H NMR (600 MHz, CD_3OD): δ 9.13 (dd, *J* = 4.7, 1.7 Hz, 1H, H9), 9.11 (d, *J* = 5.9 Hz, 1H, H6), 8.93 (d, *J* = 5.9 Hz, 1H, H5), 8.85 (dd, *J* = 7.9, 1.7 Hz, 1H, H4), 8.74 (d, *J* = 8.0 Hz, 1H, ArH), 7.94 (d, *J* = 7.2 Hz, 1H, H2 or ArH), 7.92 (dd, *J* = 7.3, 4.2 Hz, 1H, H10), 7.90 (app t, *J* = 7.1 Hz, 1H, H2 or ArH), 2.98 (s, 3H, H14)

^{13}C NMR (151 MHz, CD_3OD): δ 181.9 (C, C12), 155.1 (CH, C9), 151.0 (C), 148.8 (C), 147.4 (CH, C6), 146.0 (C), 145.8 (C), 142.8 (C), 140.7 (C), 138.6 (CH, C4), 134.6 (CH, C2 or Ar), 132.5 (CH, C2 or Ar), 131.0 (C), 128.2 (CH, C10), 124.4 (C), 122.9 (CH, Ar), 120.3 (CH, C5), 119.1 (C), 18.4 (CH_3, C14)

Enamine **2.142**:

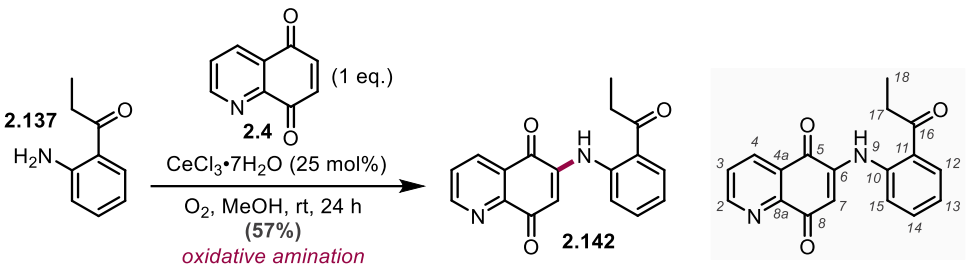

Adapted from the procedure of Bracher:[18] Under an oxygen atmosphere, cerium(III) chloride heptahydrate (0.22 g, 0.628 mmol, 25 mol%) and aniline **2.137** (0.37 g, 2.51 mmol) were successively added to a solution of quinoline-5,8-dione **2.4** (0.40 g, 2.51 mmol) in methanol (25 mL) at rt. After 24 h, the red solution was concentrated under reduced pressure and the dark-red residue was purified by silica column chromatography (5% acetone in dichloromethane) to yield enamine **2.142** (0.44 g, 1.44 mmol, 57%) as a red amorphous solid.

R_f: 0.25 (5% acetone in dichloromethane)

^{1}H NMR (400 MHz, $CDCl_3$): δ 11.37 (s, 1H, H9), 9.04 (dd, *J* = 4.7, 1.8 Hz, 1H, H2), 8.49 (dd, *J* = 7.9, 1.8 Hz, 1H, H4), 8.00 (dd, *J* = 8.0, 1.5 Hz, 1H, ArH), 7.67 – 7.62 (m, 2H, H3 and ArH), 7.60 – 7.56 (m, 1H, ArH), 7.23 – 7.18 (m, 1H, ArH), 6.92 (s, 1H, H7), 3.09 (q, *J* = 7.2 Hz, 2H, H17), 1.26 (t, *J* = 7.2 Hz, 3H, H18)

^{13}C NMR (101 MHz, $CDCl_3$): δ 204.2 (C, C16), 182.9 (C, C5 or C8), 181.7 (C, C5 or C8), 155.3 (CH, Ar), 148.7 (C), 143.8 (C), 139.9 (C), 134.9 (CH, Ar), 134.1 (CH, Ar), 131.6 (CH, Ar), 127.7 (C), 126.9 (CH, H3), 125.8 (C), 123.6 (CH, Ar), 121.1 (CH, Ar), 107.0 (CH, C7), 33.5 (CH_2, C17), 8.5 (CH_3, C18)

HRMS-ESI (m/z): Calculated for $C_{18}H_{15}N_2O_3$ [M+H]+ , 307.1077; found 307.1078

IR: 3728, 3628, 2915, 2226, 1570, 1536, 1303, 668

Tetracycle **2.144**:

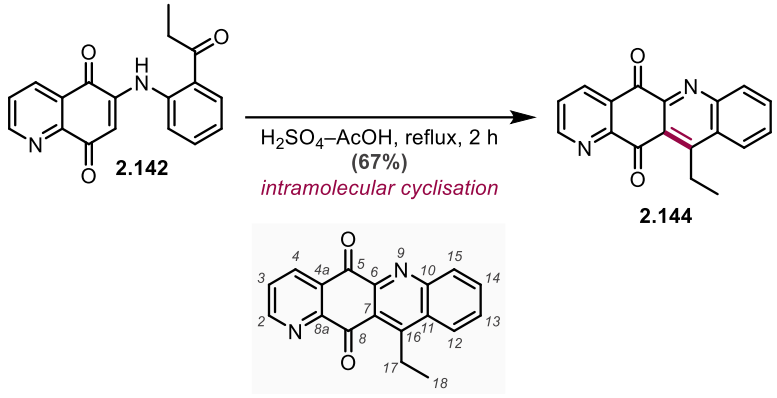

Adapted from the procedure of Bracher:[18] Enamine **2.142** (0.20 g, 0.653 mmol) in glacial acetic acid (10.7 mL) and concentrated sulfuric acid (1.0 mL) was heated to 120 °C for 2 h. The black-green solution was cooled to 0 °C and quenched by slow addition to saturated aqueous sodium bicarbonate solution (180 mL) to achieve a pH of 7. The aqueous phase was extracted using dichloromethane (4 × 50 mL). The combined organic phases were washed with brine (50 mL), dried over anhydrous magnesium sulfate, filtered and concentrated under reduced pressure. The brown residue was purified using silica column chromatography (100% dichloromethane to 5% acetone in dichloromethane) to yield tetracycle **2.144** (0.14 g, 0.486 mmol, 74%) as a blue-green crystalline solid.

R_f: 0.31 (5% acetone in dichloromethane)

^{1}H NMR (400 MHz, $CDCl_3$): δ 9.15 (dd, *J* = 4.7, 1.7 Hz, 1H, H2), 8.72 (dd, *J* = 7.9, 1.8 Hz, 1H, H4), 8.45 (dd, *J* = 8.5, 1.3 Hz, 1H, H12 or H15), 8.37 (dd, *J* = 8.6, 1.3 Hz, 1H, H12 or H15), 7.93 (ddd, *J* = 8.3, 6.8, 1.3 Hz, 1H, H13 or H14), 7.82 – 7.77 (m, 1H, H13 or H14), 7.76 (dd, *J* = 7.8, 4.5 Hz, 1H, H3), 3.81 (q, *J* = 7.5 Hz, 2H, H17), 1.51 (t, *J* = 7.5 Hz, 3H, H18)

^{13}C NMR (101 MHz, $CDCl_3$): δ 183.0 (C, C5 or C8), 182.0 (C, C5 or C8), 158.5 (C), 155.8 (CH, C2), 150.3 (C), 149.1 (C), 148.0 (C), 135.9 (CH, C4), 132.9 (CH, C13 or C14), 132.7 (CH, C12 or C15), 129.1 (C), 128.0 (CH, C3), 125.5 (CH, C12 or C15), 124.8 (C), 77.4 (C), 23.0 (CH_2, C17), 15.0 (CH_3, C18)

HRMS-ESI (m/z): Calculated for $C_{18}H_{13}N_2O_2$ $[M+H]^+$, 289.0972; found 289.0970

IR: 3069, 2929, 1687, 1580, 1334, 1281, 978, 765

MP: 215 – 217 °C

5-Methylascididemin **2.136**:

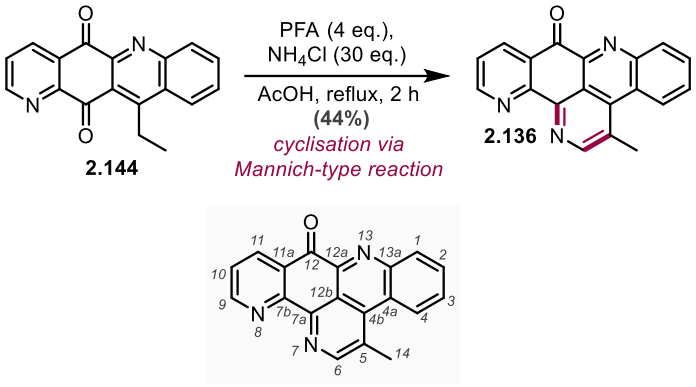

Adapted from the procedure of Lindsay et al.:[72] Under a nitrogen atmosphere, a solution of tetracycle **2.144** (22 mg, 76.3 µmol) and ammonium chloride (0.12 g, 2.24 mmol) in glacial acetic acid (5.4 mL) was heated to 70 °C. Paraformaldehyde (28 mg, 0.311 mmol) in glacial acetic acid (1.9 mL) was added dropwise over 1 minute and the resulting brown solution was heated to 120 °C for 2 h. The black-green solution was cooled to 0 °C and quenched by slow addition to saturated aqueous sodium carbonate solution (50 mL) to achieve a pH of 9. The aqueous phase was extracted using dichloromethane (3 × 30 mL). The combined organic phases were washed with brine (30 mL), dried over anhydrous sodium sulfate, filtered and concentrated under reduced pressure. The brown residue was purified using silica column chromatography (5% methanol in dichloromethane) to yield 5-methylascididemin **2.136** (10 mg, 33.6 µmol, 44%) as a yellow solid. 5-Methylascididemin **2.136** was further purified by normal-phase HPLC (5% methanol in chloroform) for biological testing.

R_f: 0.27 (5% methanol in dichloromethane) – yellow spot (without stain)

^{1}H NMR (600 MHz, $CDCl_3$) δ 9.21 (br s, 1H, H9), 9.16 (br s, 1H, H6), 9.01 (d, *J* = 8.4 Hz, 1H, H4), 8.80 (dd, *J* = 7.8, 1.0 Hz, 1H, H11), 8.71 (dd, *J* = 8.2, 1.0 Hz, 1H, H1), 8.07 – 8.02 (m, 1H, H2), 8.00 – 7.95 (m, 1H, H3), 7.71 – 7.64 (m, 1H, H10), 3.25 (s, 3H, H14)

^{13}C NMR (151 MHz, $CDCl_3$): δ 182.2 (C, C12), 155.8 (CH, C9), 152.7, 152.6 (CH, C6), 147.8 (C), 146.8 (C), 146.4 (C), 137.6 (C), 136.6 (CH, C11), 134.1 (CH, C1), 131.3 (CH, C2), 130.9 (C), 130.7 (CH, C3), 128.4 (C), 127.2 (CH, C4), 125.6 (C), 125.3 (CH, C10), 118.8, 23.6 (CH_3, C14)

HRMS-ESI (m/z): Calculated for $C_{19}H_{12}N_3O$ [M+H]+ , 298.0975; found 298.0971

IR: 2957, 2925, 2853, 1682, 1569, 1463, 1419, 1379, 1265, 1073, 1040, 740

Enamine **2.6**:

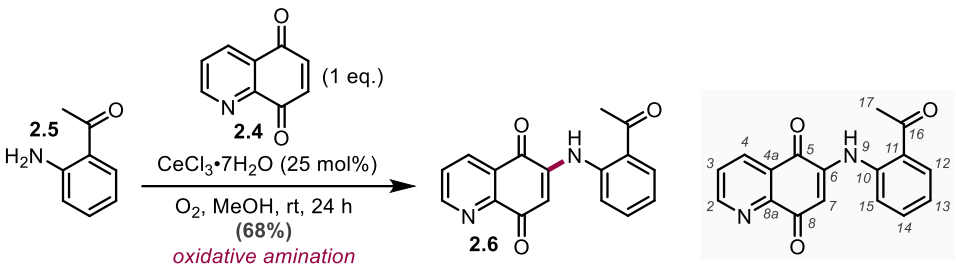

Adapted from the procedure of Bracher:[18] Under an oxygen atmosphere, cerium(III) chloride heptahydrate (0.58 g, 1.57 mmol, 25 mol%) and aniline **2.5** (0.76 mL, 6.28 mmol) were successively added to a solution of quinoline-5,8-dione **2.4** (1.00 g, 6.28 mmol) in methanol (63 mL) at rt. After 24 h, the red solution was concentrated under reduced pressure and the dark-red residue was purified by silica column chromatography (5% acetone in dichloromethane) to yield enamine **2.6** (1.25 g, 4.28 mmol, 68%) as a red amorphous solid.

R_f: 0.28 (10% acetone in pentane) – red spot (without stain)

^{1}H NMR (600 MHz, $CDCl_3$): δ 11.34 (s, 1H, H9), 9.05 (dd, *J* = 4.7, 1.7 Hz, 1H, H2), 8.49 (dd, *J* = 7.9, 1.7 Hz, 1H, H4), 7.98 (dd, *J* = 8.0, 1.5 Hz, 1H, H12), 7.66 (d, *J* = 8.2 Hz, 1H, H15), 7.65 – 7.63 (m, 1H, H3), 7.62 – 7.58 (m, 1H, H14), 7.24 – 7.20 (m, 1H, H13), 6.94 (s, 1H, H7), 2.70 (s, 3H, H17)

^{13}C NMR (151 MHz, $CDCl_3$): δ 201.7 (C, C16), 182.9 (C, C8), 181.7 (C, C5), 155.3 (CH, C2), 148.7 (C, C8a), 143.8 (C, C10), 140.0 (C, C6), 134.9 (C, C4), 134.4 (CH, C14), 132.6 (CH, C12), 127.8 (C, C4a), 126.9 (CH, C3), 126.0 (C, C11), 123.6 (CH, C13), 121.0 (CH, C15), 107.2 (CH, C7), 28.7 (CH_3, C17)

Data in agreement with literature.[18]

Tetracycle **2.7**:

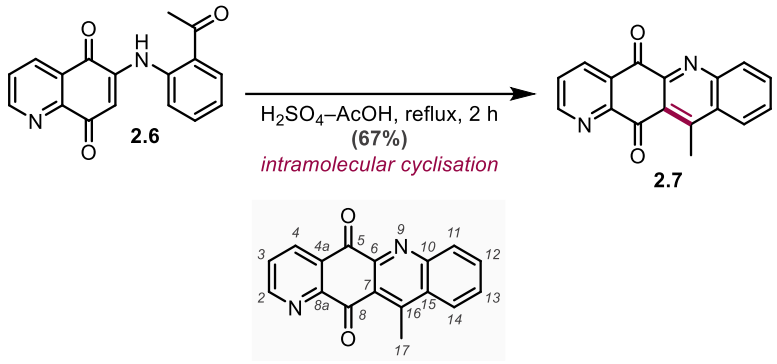

Adapted from the procedure of Bracher:[18] Enamine **2.6** (0.59 g, 2.0 mmol) in glacial acetic acid (27 mL) and concentrated sulfuric acid (3 mL) was heated to 120 °C for 2 h. The black-green solution was cooled to 0 °C and quenched by slow addition to saturated aqueous sodium carbonate solution (90 mL) to achieve a pH of 7. The aqueous phase was extracted using dichloromethane (3 × 50 mL). The combined organic phases were washed with brine (50 mL), dried over anhydrous sodium sulfate, filtered and concentrated under reduced pressure to yield tetracycle **2.7** (0.37 g, 1.3 mmol, 67%) as a light-brown solid. Used in the next step without further purification.

R_f: 0.16 (5% acetone in dichloromethane)

^{1}H NMR (600 MHz, $CDCl_3$): δ 9.17 (dd, *J* = 4.5, 1.7 Hz, 1H), 8.75 (dd, *J* = 7.9, 1.7 Hz, 1H), 8.49 (d, *J* = 8.4 Hz, 1H), 8.42 (d, *J* = 8.6 Hz, 1H), 7.96 (ddd, *J* = 8.3, 6.8, 1.3 Hz, 1H), 7.82 (ddd, *J* = 8.3, 6.7, 1.3 Hz, 1H), 7.77 (dd, *J* = 7.9, 4.5 Hz, 1H), 3.36 (s, 3H)

^{13}C NMR (151 MHz, $CDCl_3$): δ 183.6, 182.1, 155.9, 153.0, 150.5, 148.9, 147.8, 136.0, 133.0, 132.6, 130.3, 130.1, 128.1, 125.8, 125.8, 125.8, 16.9

Data in agreement with literature.[18]

6-Methylascididemin **2.122**:

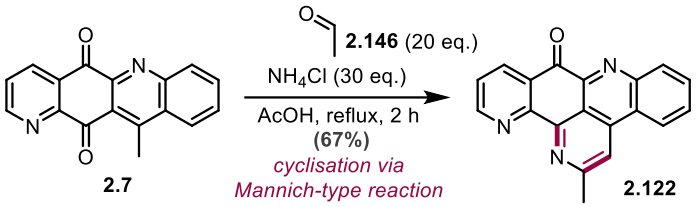

Adapted from the procedure of Lindsay et al.:[72] Under a nitrogen atmosphere, a solution of tetracycle **2.7** (0.37 g, 1.3 μmol) and ammonium chloride (2.2 g, 4.0 mmol) in glacial acetic acid (27 mL) was heated to 70 °C. Acetaldehyde **2.146** (1.5 mL, 27 mmol) was added dropwise over 1 minute and the resulting brown solution was heated to 120 °C for 2 h. The black-green solution was cooled to 0 °C and quenched by slow addition to saturated aqueous sodium bicarbonate solution (50 mL) to achieve a pH of 9. The aqueous phase was extracted using dichloromethane (3 × 50 mL). The combined organic phases were washed with brine (30 mL), dried over anhydrous sodium sulfate, filtered and concentrated under reduced pressure. The brown residue was purified using silica column chromatography (5% methanol in dichloromethane) to yield 6-methylascididemin **2.122** (0.27 g, 0.91 mmol, 67%) as a yellow solid.

Refer back to page 224 for characterisation.

Aldehyde **2.164**:

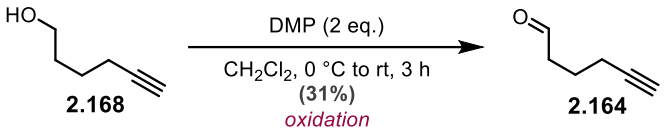

Adapted from the procedure of Lim et al.:[200] Alcohol **2.168** (0.11 mL, 1.0 mmol) was added dropwise over 1 minute to a solution of Dess–Martin periodinane (DMP) in dichloromethane (4.1 mL) at 0 °C. The reaction was removed from the ice-bath and allowed to gradually warm to rt. After 3 h, the reaction was cooled to 0 °C and quenched with a 1:1 saturated aqueous sodium bicarbonate–thiosulfate solution (80 mL) and the aqueous phase extracted with diethyl ether (3 × 30 mL). The combined organic phases were partially evaporated under reduced pressure at 0 °C to yield aldehyde **2.164** (0.10 g, 0.31 mmol, 31% based on purity) as a colourless oil. Used in the next step without further purification.

R_f: 0.30 (5% diethyl ether in pentane) – yellow spot (with potassium permanganate)

^{1}H NMR (600 MHz, $CDCl_3$): δ 9.80 (q, *J* = 1.1 Hz, 1H), 2.60 (app t, *J* = 1.0 Hz, 2H), 2.26 (td, *J* = 7.1, 3.0 Hz, 2H), 1.97 (t, *J* = 2.7 Hz, 1H), 1.85 (quint, *J* = 7.1 Hz, 2H)

^{13}C NMR (151 MHz, $CDCl_3$): δ 201.9, 83.3, 69.5, 42.7, 20.9, 17.9

Data in agreement with literature.[200]

Alkyne-ascididemin **2.165**:

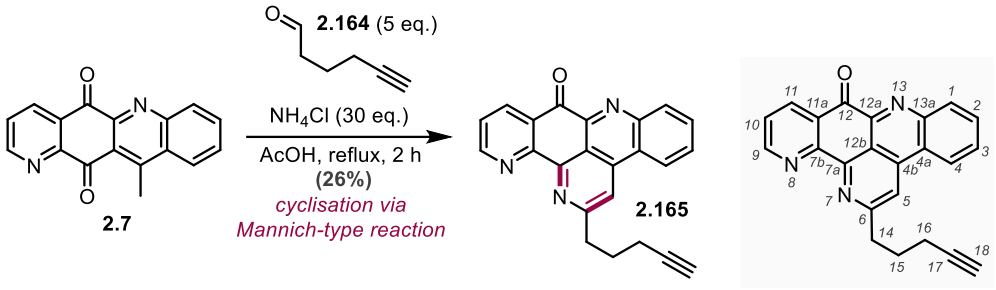

Adapted from the procedure of Lindsay et al.:[72] Under a nitrogen atmosphere, a solution of tetracycle **2.7** (8.4 mg, 30.6 µmol) and ammonium chloride (47 mg, 879 µmol) in glacial acetic acid (2.2 mL) was heated to 70 °C. Aldehyde **2.164** (30% purity, 50 mg, 156 µmol) in glacial acetic acid (0.8 mL) was added dropwise over 1 minute and the resulting brown solution was heated to 120 °C for 4 h. The black-green solution was cooled to 0 °C and quenched by slow addition to saturated aqueous sodium bicarbonate solution (60 mL) to achieve a pH of 9. The aqueous phase was extracted using dichloromethane (3 × 30 mL). The combined organic phases were washed with brine (30 mL), dried over anhydrous sodium sulfate, filtered and concentrated under reduced pressure. The brown residue was purified using silica column chromatography (100% dichloromethane to 5% acetone in dichloromethane) to yield alkyne-ascididemin **2.165** (2.8 mg, 8.01 µmol, 26%) as a yellow solid. Alkyne-ascididemin **2.165** was further purified by reverse-phase HPLC (column (2), 5% to 40% acetonitrile in 0.005 M aqueous HCl) to yield alkyne-ascididemin **2.165**•HCl for biological testing.

*Alkyne-ascididemin **2.165**:*

R_f: 0.13 (5% acetone in dichloromethane) – yellow spot (without stain)

HRMS-ESI (m/z): Calculated for $C_{23}H_{16}N_3O$ [M+H]+, 350.1288; found 350.1287

IR: 3307, 2955, 2925, 2856, 2361, 1805, 1738, 1703, 1605, 1580, 1555, 1510, 1503, 1461, 1453, 1402, 1377, 1349, 1333, 1276, 1261, 1190, 1160, 1101, 1070, 1038, 948, 913, 838, 814, 770, 736, 684, 649, 631, 614

*Alkyne-ascididemin **2.165**•HCl:*

^{1}H NMR (600 MHz, CD_3OD): δ 9.15 (dd, *J* = 4.9, 1.7 Hz, 1H, H9), 8.95 (dd, *J* = 7.9, 1.7 Hz, 1H, H11), 8.93 (dd, *J* = 8.2, 1.4 Hz, 1H, H4), 8.82 (s, 1H, H5), 8.46 (dd, *J* = 8.2, 1.3 Hz, 1H, H1), 8.08 (ddd, *J* = 8.3, 7.0, 1.4 Hz, 1H, H2), 8.04 – 8.01 (m, 1H, H3), 7.99 (dd, *J* = 8.0, 5.0 Hz, 1H, H10), 3.42 – 3.38 (m, 2H, H14), 2.40 (td, *J* = 7.0, 2.7 Hz, 2H, H16), 2.33 (t, *J* = 2.6 Hz, 1H, H18), 2.27 – 2.21 (m, 2H, H15)

^{13}C NMR (151 MHz, CD_3OD): δ 181.5 (C, C12), 163.3 (C, C6), 153.9 (CH, C9), 151.0 (C, C7b), 148.1 (C, C4b), 147.0 (C, C7a or C12a), 146.8 (C, C13a), 140.6 (C, C7a or C12a), 139.9 (CH, C11), 133.7 (CH, C2), 133.0 (CH, C1), 132.4 (CH, C3), 131.0 (C, C11a), 128.2 (CH, C10), 125.2 (CH, C4), 124.7 (C, C4a), 118.7 (CH, C5), 118.0 (C, C12b), 84.4 (C, C17), 70.5 (CH, C18), 38.1 (CH_2, C14), 29.9 (CH_2, C15), 18.9 (CH_2, C16)

5.2.2. Chapter 3

Phenylhydrazine **3.43**:

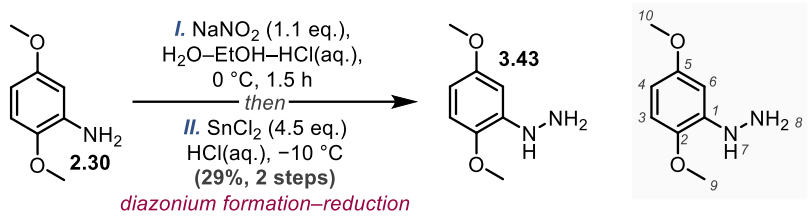

Adapted from the patent of Uniroyal Chem Co Inc:[201] Sodium nitrite (0.25 g, 3.59 mmol) in water (1.5 mL) was added dropwise over 1 minute to a solution of 2,5-dimethoxyaniline **2.30** (0.50 g, 3.26 mmol) in a mixture of water (7 mL), ethanol (5 mL), and concentrated hydrochloric acid (3.5 mL) at 0 °C, and the resulting solution was stirred at 0 °C for 1.5 h. The reaction mixture was cooled to −10 °C using a dry ice–brine bath. Stannous chloride (2.79 g, 14.7 mmol) was dissolved in concentrated hydrochloric acid (3.5 mL) at −10 °C and added dropwise over 1 minute to the reaction mixture. The reaction mixture was then stirred at −10 °C for 1 h. The light-purple precipitate was then collected via filtration. The precipitate was then dissolved in an ice-cold solution of sodium hydroxide (4.87 g, 122 mmol) in water (35 mL), and the reaction mixture was stirred at 0 °C for 30 minutes. The aqueous phase of the resultant light-peach solution was extracted with diethyl ether (3 × 30 mL). The combined organic phases were dried over anhydrous sodium sulfate, filtered and evaporated under a flow of nitrogen overnight to yield phenylhydrazine **3.43** (0.16 g, 0.951 mmol, 29%) as a brown semi-solid. Used in the next step without further purification.

R_f: 0.49 (10% dichloromethane in pentane)

^{1}H NMR (400 MHz, $CDCl_3$): δ 6.68 (d, *J* = 8.6 Hz, 1H, H3), 6.60 (d, *J* = 2.9 Hz, 1H, H6), 6.26 (dd, *J* = 8.7, 2.9 Hz, 1H, H4), 5.65 (s, 1H, H7), 3.79 (br s, 3H, H9), 3.78 (s, 3H, H10), 3.48 (br s, 2H, H8)

^{13}C NMR (151 MHz, $CDCl_3$): δ 155.0 (C, C5), 142.2 (C, C1), 141.2 (C, C2), 110.6 (CH, C3), 101.4 (CH, C4), 98.8 (CH, C6), 56.2 (CH_3, C9), 55.8 (CH_3, C10)

HRMS-ESI (m/z): Calculated for $C_8H_{13}N_2O_2$ [M+H]+ , 169.0972; found 169.0970

IR: 3371, 3350, 3012, 2942, 2918, 2834, 2360, 2333, 1615, 1603, 1513, 1465, 1454, 1423, 1287, 1259, 1220, 1178, 1047, 1025, 917, 836, 786, 716

Latent aldehyde **3.45**:

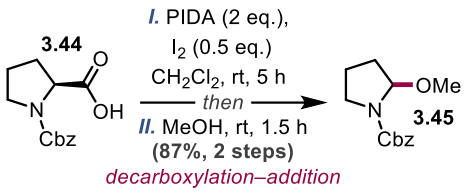

Adapted from the patent of Chia Tai Tianqing Pharmaceutical Group Co LTD:[202] (Diacetoxy)iodobenzene (1.29 g, 4.01 mmol) and iodine (0.26 g, 6.02 mmol) were successively added to a stirred solution of ((benzyloxy)carbonyl)-*L*-proline **3.44** (0.50 g, 2.01 mmol) in dichloromethane (25 mL) at rt. After 5 h, methanol (1 mL) was added and the reaction mixture was stirred for a further 1.5 h. The reaction was quenched by addition of saturated aqueous sodium thiosulfate (2 mL) and the aqueous phase was extracted with dichloromethane (3 × 20 mL). The combined organic phases were washed successively with saturated aqueous sodium thiosulfate (10 mL) and brine (10 mL), filtered and concentrated under reduced pressure. The colourless oil was purified by silica column chromatography (10% ethyl acetate in pentane) to yield latent aldehyde **3.45** (0.41 g, 1.74 mmol, 87%) as a colourless oil.

R_f: 0.35 (10% ethyl acetate in pentane)

^{1}H NMR (400 MHz, $CDCl_3$): δ 7.42 – 7.27 (m, 5H), 5.26 – 5.11 (m, 3H), 3.57 – 3.24 (m, 5H), 2.15 – 1.69 (m, 4H)

^{13}C NMR (151 MHz, $CDCl_3$): δ 156.0, 155.1, 136.8, 136.7, 128.6, 128.2, 128.0, 89.3, 88.7, 67.3, 67.0, 56.1, 55.5, 46.1, 45.9, 32.7, 32.1, 22.8, 21.9

Data in agreement with literature.[203]

ortho-Iodoaniline **3.70**:

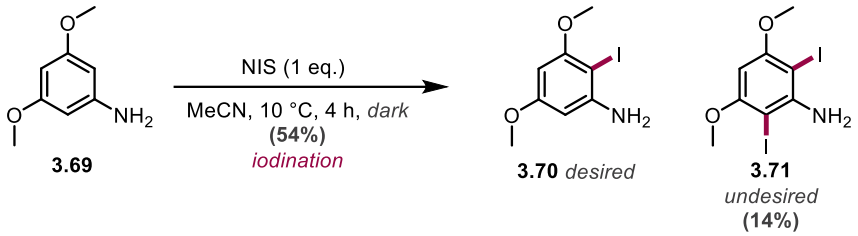

Adapted from the procedure of Murayama et al.:[204] Under a nitrogen atmosphere in the dark, *N*-iodosuccinimide (0.88 g, 3.9 mmol) was added portion-wise over 1 minute to a solution of 3,5-dimethoxyaniline **3.69** (0.50 g, 3.3 mmol) in acetonitrile (16 mL) at rt. After 1.5 h, the reaction was quenched by addition of a 5:1 saturated aqueous sodium bicarbonate–thiosulfate solution (30 mL) and the aqueous phase was extracted with ethyl acetate (3 × 40 mL). The combined organic phases were washed sequentially with saturated aqueous sodium bicarbonate solution (25 mL) then brine (25 mL), dried over anhydrous sodium sulfate, filtered, then concentrated under reduced pressure. The light-brown solid was purified by silica column chromatography (15% ethyl acetate in pentane to 25% ethyl acetate in pentane) to yield *ortho*-iodoaniline **3.70** (0.49 g, 1.8 mmol, 54%) as a yellow solid and *ortho*-iodoaniline **3.71** (0.19 g, 0.46 mmol, 14%) as a yellow solid.

Note: ortho-Iodoaniline **3.70** is unstable and must be used directly or stored in the freezer under an inert atmosphere.

*ortho-Iodoaniline **3.70**:*

R_f: 0.36 (20% ethyl acetate in pentane) – yellow spot (with vanillin)

^{1}H NMR (400 MHz, $CDCl_3$): δ 6.00 (d, *J* = 2.5 Hz, 1H), 5.89 (d, *J* = 2.5 Hz, 1H), 4.23 (s, 2H), 3.81 (s, 3H), 3.74 (s, 3H)

^{13}C NMR (101 MHz, $CDCl_3$): δ 161.8, 159.4, 148.5, 92.5, 89.5, 65.5, 56.3, 55.4

Data in agreement with literature.[205]

*Putative ortho-iodoaniline **3.71**:*

R_f: 0.59 (20% ethyl acetate in pentane) – yellow spot (with vanillin)

^{1}H NMR (400 MHz, $CDCl_3$): δ 5.92 (s, 1H), 4.87 (s, 2H), 3.88 (s, 6H)

Homopropargyl amine **3.73**:

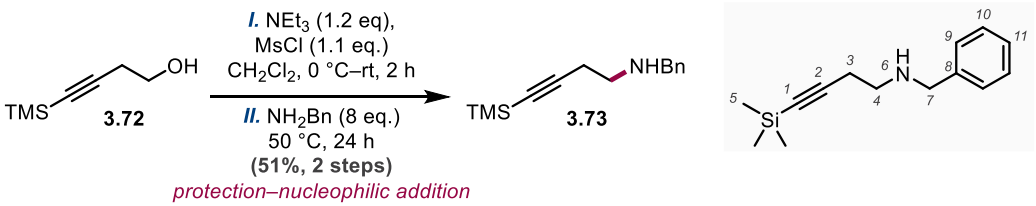

Adapted from the procedure of Zhdanko and Maier:[206] Under a nitrogen atmosphere, methanesulfonyl chloride (0.18 mL, 2.33 mmol) and triethylamine (0.59 mL, 4.23 mmol) were sequentially added to a solution of homopropargyl alcohol **3.72** (0.35 mL, 2.10 mmol) in dichloromethane (3.5 mL) at 0 °C. After 1.5 h the colourless solution became cloudy white. The reaction mixture was concentrated under reduced pressure. Benzylamine (3.5 mL, 32.0 mmol) was added and the reaction mixture was heated to 50 °C. After 24 h, the yellow-orange solution was cooled to rt and saturated aqueous sodium carbonate solution (5 mL) was added. The organic phase was separated and the aqueous phase was extracted with diethyl ether (2 × 20 mL). The combined organic phases were dried over anhydrous sodium sulfate, filtered and concentrated under reduced pressure. The orange oil was purified by silica column chromatography (40% ethyl acetate in pentane) to yield homopropargyl amine **3.73** (0.25 g, 1.08 mmol, 51% over two steps) as a colourless oil.

R_f: 0.36 (40% ethyl acetate in pentane) – black spot (with vanillin)

^{1}H NMR (400 MHz, $CDCl_3$): δ 7.27 (app d, *J* = 4.5 Hz, 3H, ArH) 7.19 (s, 2H, ArH), 3.76 (s, 2H, H7), 2.72 (t, *J* = 6.6 Hz, 2H, H4), 2.39 (t, *J* = 6.6 Hz, 2H, H3), 1.54 (s, 1H, H6), 0.09 (s, 9H, H5)

^{13}C NMR (101 MHz, $CDCl_3$): δ 140.4, 128.6, 128.2, 127.1, 105.2, 86.2, 53.4, 47.5, 21.1, 0.3 (CH_3, C5)

HRMS-ESI (m/z): Calculated for $C_{14}H_{22}NSi$ $[M+H]^+$, 232.1516; found 232.1516

IR: 3086, 3064, 3029, 2958, 2902, 2835, 2825, 2360, 2175, 1496, 1455, 1250, 1122, 1039, 843, 760, 736, 699, 639

Dimethoxytryptamine **3.74**:

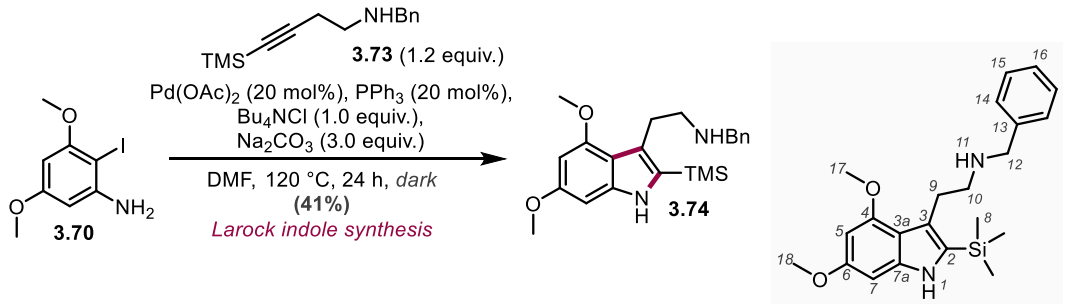

Adapted from the procedure of Danner et al.:[207] Under a nitrogen atmosphere in the dark, *ortho*-iodoaniline **3.70** (33 mg, 118 µmol), homopropargyl amine **3.73** (33 mg, 143 µmol), tetrabutylammonium chloride (33 mg, 359 µmol), sodium carbonate (38 mg, 359 µmol), triphenyl phosphine (7 g, 26.7 µmol, 20 mol%) and palladium(II) acetate trimer (5.8 mg, 25.8 µmol, 20 mol%) in *N*,*N*-dimethylformamide (2.5 mL) was stirred and heated to 120 °C. After 24 h, the reaction was cooled to rt and quenched by addition of saturated aqueous ammonium chloride (5 mL), diluted with water (5 mL) and the aqueous phase extracted with ethyl acetate (25 mL). The organic phase was washed sequentially with 5% lithium chloride aqueous solution (3 × 5 mL) and brine (5 mL), dried over anhydrous sodium sulfate, filtered and concentrated under reduced pressure. The dark-brown oil was purified by silica column chromatography (50% ethyl acetate in pentane) to yield dimethoxytryptamine **3.74** (18.3 mg, 47.8 µmol, 41%) as a brown oil.

R_f: 0.30 (50% ethyl acetate in pentane) – purple spot (with vanillin)

^{1}H NMR (600 MHz, $CDCl_3$): δ 7.73 (s, 1H, H1), 7.34 – 7.28 (m, 4H, H14 and H15), 7.24 – 7.21 (m, 1H, H16), 6.43 (d, *J* = 1.8 Hz, 1H, H7), 6.13 (d, *J* = 1.7 Hz, 1H, H5), 3.86 (s, 2H, H12), 3.82 (s, 3H, H17), 3.80 (s, 3H, H18), 3.11 – 3.06 (m, 2H, H10), 2.95 – 2.91 (m, 2H, H9), 0.36 – 0.32 (m, 9H, H8)

Note: Exchangeable proton H11 not observed

^{13}C NMR (151 MHz, $CDCl_3$): δ 158.1 (C, C6), 155.0 (C, C4), 141.0 (C, C13), 140.2 (C, C7a), 130.5 (C, C2), 128.4 (CH, C14 or C15), 128.2 (CH, C14 or C15), 126.8 (CH, C16), 123.7 (C, C3), 113.7 (C, C3a), 91.5 (CH, C5), 86.4 (CH, C7), 55.7 (CH_3, C17), 55.2 (CH_3, C18), 54.1 (CH_2, C12), 52.2 (CH_2, C9), 28.7 (CH_2, C10), -0.2 (CH_3, C8)

HRMS-ESI (m/z): Calculated for $C_{22}H_{31}N_2O_2Si$ [M+H]+, 383.2149; found 383.2161

IR: 3428, 3025, 3007, 2952, 2839, 1622, 1587, 1513, 1454, 1341, 1319, 1251, 1219, 1201, 1153, 1134, 1045, 999, 937, 911, 871, 839, 807, 757, 736, 699, 650, 631

Cyclic sulfamidate **3.81**:

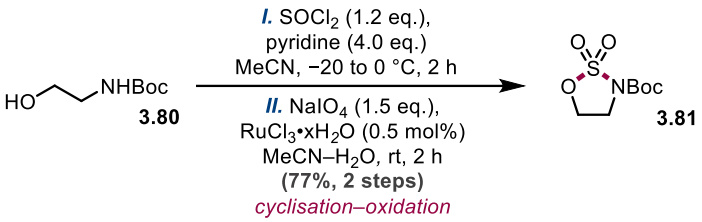

Adapted from the procedure of Moss et al.:[208] Under a nitrogen atmosphere, aminoalcohol **3.80** (1.55 mL, 10.0 mmol) in acetonitrile (5 mL) was added dropwise over 1 minute to a solution of thionyl chloride (0.91 mL, 12 mmol) in acetonitrile (50 mL) at −20 °C. After 10 minutes, pyridine (3.24 mL) was added dropwise over 1 minute and the resulting solution was maintained at this temperature. After 1 h, the reaction mixture was warmed to 0 °C. After 1 h, a colour change from colourless to cloudy-yellow was observed and the reaction was diluted with water (25 mL). The aqueous phase was extracted with ethyl acetate (25 mL) and the organic phase was washed with 1 N HCl solution (25 mL). The combined aqueous phases were extracted with ethyl acetate (25 mL). The combined organic phases were washed sequentially with saturated aqueous sodium bicarbonate (25 mL) and brine (25 mL), dried over anhydrous sodium sulfate, filtered and concentrated under reduced pressure. The orange-brown oil was dissolved in acetonitrile (40 mL) and ruthenium(III) chloride hydrate (10 mg, 48.2 μmol, 0.5 mol%), sodium periodate (3.21 g, 15 mmol) and water (40 mL) were successively added at rt. The resulting mixture was stirred vigorously. After 2 h, a colour change from dark-orange to cloudy dark-brown was observed and the reaction was diluted with water (40 mL). The aqueous phase was extracted with diethyl ether (5 × 20 mL). The combined organic phase was washed with water (4 × 50 mL), dried over anhydrous sodium sulfate, filtered and concentrated under reduced pressure to yield cyclic sulfamidate **3.81** (1.71 g, 7.66 mmol, 77%) as a white crystalline-solid. Used in the next step without further purification.

R_f: 0.19 (40% diethyl ether in pentane) – white streak (potassium permanganate)

^{1}H NMR (600 MHz, $CDCl_3$): δ 4.61 (t, *J* = 6.4 Hz, 2H), 4.04 (t, *J* = 6.4 Hz, 2H), 1.56 (s, 9H)

^{13}C NMR (151 MHz, $CDCl_3$): δ 148.8, 85.7, 65.7, 45.4, 28.1

Data in agreement with literature.[208]

Homopropargyl amine **3.84**:



Adapted from the procedure of Moss et al.:[209] Under a nitrogen atmosphere, *n*-butyllithium (2.70 mL, 3.59 mmol, 1.33 M in hexane) was added dropwise over 1 minute to a solution of ethynyltrimethylsilane **3.82** (0.44 mL, 3.40 mmol) in tetrahydrofuran (10 mL) at −78 °C. After 15 minutes, the reaction was removed from the acetone–dry ice bath for 10 minutes and then cooled back to −78 °C. Ground cyclic sulfamidate **3.81** (0.50 g, 2.24 mmol) in tetrahydrofuran (15 mL) was added dropwise over 3 minutes, and the reaction was maintained at −78 °C for 30 minutes, then removed from the acetone–dry ice bath and allowed to warm to rt gradually. After 2 h, the reaction was quenched by addition of 1 M citric acid aqueous solution (10 mL) and stirred for 10 minutes. The aqueous phase was extracted with ethyl acetate (3 × 30 mL). The combined organic phases were washed with brine (30 mL), dried over anhydrous sodium sulfate, filtered and concentrated under reduced pressure. The yellow oil was purified by silica column chromatography (100% pentane to 20% diethyl ether in pentane) to yield homopropargyl amine **3.84** (0.33 g, 2.24 mmol, 61%) as an off-white amorphous solid.

R_f: 0.28 (10% diethyl ether in pentane) – brown spot (with vanillin)

^{1}H NMR (600 MHz, $CDCl_3$): δ 4.79 (br s, 1H, H6), 3.31 – 3.23 (m, 2H, H4), 2.41 (t, *J* = 6.5 Hz, 2H, H3), 1.45 (s, 9H, H9), 0.15 (s, 9H, H5)

^{13}C NMR (151 MHz, $CDCl_3$): δ 155.9 (C, C7), 104.3 (C, C2), 86.5 (C, C1), 79.6 (C, C8), 39.5 (CH_2, C4), 28.5 (CH_3, C9), 21.5 (CH_2, C3), 0.2 (CH_3, C5)

HRMS-ESI (m/z): Calculated for $C_{12}H_{23}NO_2SiNa$ [M+Na]+, 264.1390; found 264.1398

IR: 3366, 3344, 2980, 2961, 2906, 2778, 1702, 1516, 1455, 1426, 1393, 1367, 1332, 1251, 1175, 1073, 1048, 1007, 973, 910, 845,761, 737, 700, 638

Homopropargyl amine **3.85**:

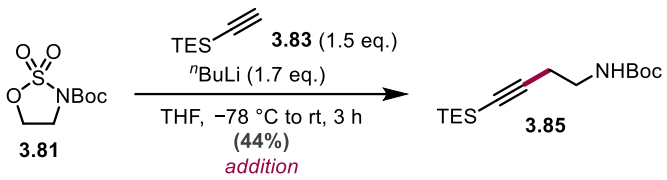

Adapted from the procedure of Moss et al.:[209] Under a nitrogen atmosphere, *n*-butyllithium (2.70 mL, 3.59 mmol, 1.33 M in hexane) was added dropwise over 1 minute to a solution of (triethylsilyl)acetylene **3.83** (0.60 mL, 3.36 mmol) in tetrahydrofuran (10 mL) at −78 °C. After 15 minutes, the reaction was removed from the acetone–dry ice bath for 10 minutes and then cooled back to −78 °C. Ground cyclic sulfamidate **3.81** (0.50 g, 2.24 mmol) in tetrahydrofuran (15 mL) was added dropwise over 3 minutes, and the reaction was maintained at −78 °C for 30 minutes, then removed from the acetone–dry ice bath and allowed to warm to rt gradually. After 2 h, the reaction was quenched by addition of 1 M citric acid aqueous solution (10 mL) and stirred for 10 minutes. The aqueous phase was extracted with ethyl acetate (3 × 30 mL). The combined organic phases were washed with brine (30 mL), dried over anhydrous sodium sulfate, filtered and concentrated under reduced pressure. The yellow oil was purified by silica column chromatography (100% pentane to 10% diethyl ether in pentane) to yield homopropargyl amine **3.85** (0.28 g, 0.99 mmol, 44%) as a yellow oil.

R_f: 0.32 (5% diethyl ether in pentane) –brown spot (with vanillin)

^{1}H NMR (600 MHz, $CDCl_3$): δ 4.81 (br s, 1H), 3.30 – 3.24 (m, 2H), 2.43 (t, *J* = 6.6 Hz, 2H), 1.44 (s, 9H), 0.98 (t, *J* = 7.9 Hz, 9H), 0.58 (q, *J* = 7.9 Hz, 6H)

^{13}C NMR (151 MHz, $CDCl_3$): δ 155.9, 105.3, 83.8, 79.5, 39.6, 28.5, 21.4, 7.6, 4.6

HRMS-ESI (m/z): Calculated for $C_{15}H_{29}NO_2SiK$ [M+K]+, 322.1599; found 322.1599

IR: 3365, 3350, 3008, 2956, 2936, 2913, 2876, 2175, 1704, 1521, 1459, 1416, 1393, 1367, 1330, 1268, 1253, 1175, 1096, 1074, 1042, 1018, 1008, 975, 963, 902, 870, 852, 805, 781, 739, 729, 672, 661, 652, 641, 627, 617

Data in agreement with literature.[210]

Homopropargyl amine **3.84**:

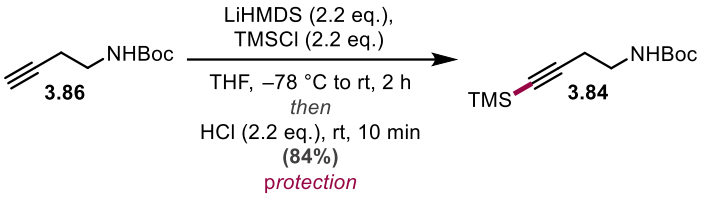

Under a nitrogen atmosphere, lithium bis(trimethylsilyl)amide (6.2 mL, 6.2 mmol, 1 M in toluene) was added dropwise over 1 minute to a solution of homopropargyl amine **3.86** (0.50 g, 3.0 mmol) in tetrahydrofuran (30 mL) at −78 °C. The reaction was removed from the acetone–dry ice bath for 5 minutes and then cooled back to −78 °C. Trimethylchlorosilane (0.78 mL, 6.1 mmol) was added dropwise over 1 minute, and the reaction was removed from the acetone–dry ice bath and allowed to warm to rt gradually. After 2 h, the reaction was quenched by addition of saturated aqueous ammonium chloride solution (15 mL). The aqueous phase was extracted with diethyl ether (3 × 30 mL) and the combined organic phases were concentrated under reduced pressure. The crude material was redissolved in diethyl ether (20 mL) and treated with hydrochloric acid (3.1 mL, 6.2 mmol, 2 M in diethyl ether). After 10 minutes, the reaction was diluted with water (10 mL) and the aqueous phase was extracted with ethyl acetate (3 × 20 mL). The combined organic phases were washed with brine (20 mL), dried over anhydrous sodium sulfate, filtered and concentrated under reduced pressure. The yellow oil was purified by silica column chromatography (100% pentane to 20% diethyl ether in pentane) to yield homopropargyl amine **3.84** (0.60 g, 2.5 mmol, 84%) as an off-white amorphous solid.

Refer back to page 257 for characterisation.

Dimethoxytryptamine **3.87**:

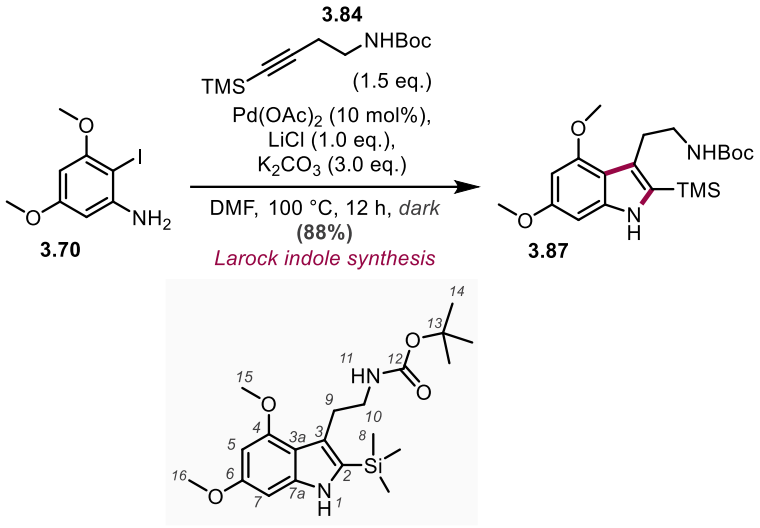

Adapted from the procedure of Danner et al.:[207] Under a nitrogen atmosphere in the dark, *ortho*-iodoaniline **3.70** (145 mg, 520 µmol) in *N*,*N*-dimethylformamide (9 mL) was added to lithium chloride (22 mg, 520 µmol), potassium carbonate (0.22 g, 1.59 mmol) and palladium(II) acetate trimer (12 mg, 53.4 µmol, 10 mol%) in a Schlenk tube at rt. After 10 minutes, homopropargyl amine **3.84** (0.19 g, 787 µmol) in *N*,*N*-dimethylformamide (2 mL) was added dropwise over 5 minutes, and reaction was stirred and heated to 100 °C. After 12 h, the reaction was cooled to rt, quenched by addition of saturated aqueous ammonium chloride (15 mL) and the aqueous phase extracted with ethyl acetate (3 × 40 mL). The combined organic phases were washed sequentially with 5% lithium chloride aqueous solution (3 × 30 mL) and brine (30 mL), dried over anhydrous sodium sulfate, filtered and concentrated under reduced pressure. The dark-brown oil was purified by silica column chromatography (100% pentane to 50% diethyl ether in pentane) to yield dimethoxytryptamine **3.87** (0.18 g, 0.46 mmol, 88%) as an off-white amorphous solid.

Note: Rigorous anhydrous conditions required – azeotropic drying of *ortho*-iodoaniline **3.70** and homopropargyl amine **3.84**, extended drying of dimethylformamide from solvent purification stills over activated 3 Å molecular sieves, and drying of lithium chloride, potassium carbonate (400 °C) and palladium(II) acetate trimer (120 °C) under vacuum while heating.

R_f: 0.35 (20% diethyl ether in pentane) – purple spot (with vanillin)

^{1}H NMR (600 MHz, $CDCl_3$): δ 7.76 (s, 1H, H1), 6.44 (d, *J* = 1.9 Hz, 1H, H7), 6.15 (d, *J* = 1.9 Hz, 1H, H5), 4.84 (br s, 1H, H11), 3.89 (s, 3H, H15), 3.82 (s, 3H, H16), 3.45 (app q, *J* = 6.5 Hz, 2H, H10), 3.02 (t, *J* = 6.6 Hz, 2H, H9), 1.40 (s, 9H, H14), 0.36 (s, 9H, H8)

^{13}C NMR (151 MHz, $CDCl_3$): δ 158.1 (C, C6), 156.0 (C, C12), 154.8 (C, C4), 140.4 (C, C7a), 131.3 (C, C2), 122.6 (C, C3), 113.6 (C, C3a), 91.6 (CH, C5), 86.4 (CH, C7), 78.7 (C, C13), 55.8 (CH_3, C16), 55.2 (CH_3, C15), 42.4 (CH_2, C10), 28.6 (CH_3, C14), 27.9 (CH_2, C9), -0.2 (CH_3, C8)

HRMS-ESI (m/z): Calculated for $C_{20}H_{33}N_2O_4Si$ [M+H]+, 393.2204; found 393.2200

IR: 3418, 3392, 3355, 2977, 2953, 2934, 2839, 1691, 1619, 1585, 1523, 1466, 1392, 1366, 1331, 1277, 1252, 1176, 1156, 1136, 1108, 1070, 1046, 995, 962, 939, 873, 839, 814, 759, 740, 634

Dimethoxytryptamine **3.88**:

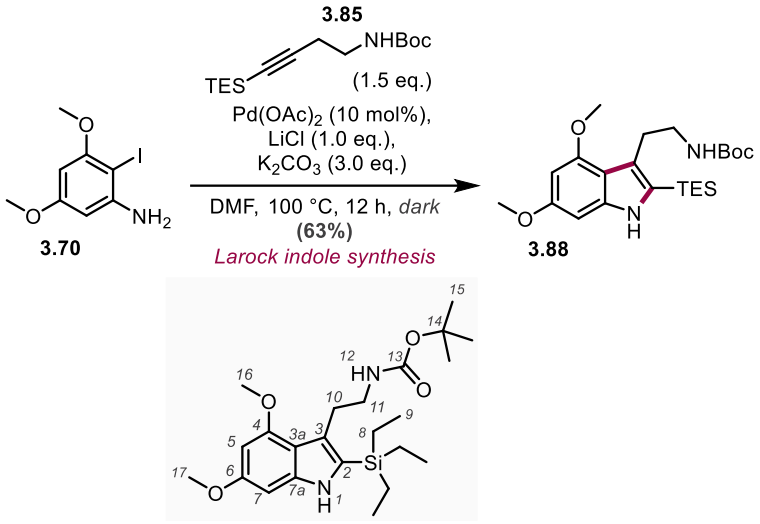

Adapted from the procedure of Danner et al.:[207] Under a nitrogen atmosphere in the dark, *ortho*-iodoaniline **3.70** (63 mg, 0.226 mmol) in *N*,*N*-dimethylformamide (3 mL) was added to lithium chloride (10 mg, 236 µmol), potassium carbonate (94 mg, 0.680 mmol) and palladium(II) acetate trimer (5 mg, 22.3 µmol, 10 mol%) in a Schlenk tube at rt. After 10 minutes, homopropargyl amine **3.85** (96 mg, 0.339 mmol) in *N*,*N*-dimethylformamide (2 mL) was added dropwise over 5 minutes, and reaction was heated to 100 °C. After 12 h, the reaction was cooled to rt, quenched by addition of saturated aqueous ammonium chloride (5 mL), diluted with water (10 mL) and the aqueous phase extracted with ethyl acetate (3 × 30 mL). The combined organic phases were washed sequentially with 5% lithium chloride aqueous solution (3 × 5 mL) and brine (5 mL), dried over anhydrous sodium sulfate, filtered and concentrated under reduced pressure. The dark-brown oil was purified by silica column chromatography (100% pentane to 30% diethyl ether in pentane) to yield dimethoxytryptamine **3.88** 62 mg, 143 µmol, 63%) as an off-white amorphous solid.

R_f: 0.29 (30% diethyl ether in pentane) – purple spot (with vanillin)

^{1}H NMR (600 MHz, $CDCl_3$): δ 7.80 (br s, 1H, H1), 6.45 (d, *J* = 1.9 Hz, 1H, H7), 6.16 (d, *J* = 1.9 Hz, 1H, H5), 4.82 (br s, 1H, H12), 3.89 (s, 3H, H16), 3.82 (s, 3H, H17), 3.49 – 3.42 (m, 2H, H11), 3.00 (t, *J* = 6.6 Hz, 2H, H10), 1.41 (s, 9H, H15), 1.03 – 0.96 (m, 9H, H9), 0.90 – 0.84 (m, 6H, H8)

^{13}C NMR (151 MHz, $CDCl_3$): δ 158.0 (C, C4), 156.0 (C, C13), 154.7 (C, C6), 140.7 (C, C7a), 128.9 (C, C2), 123.2 (C, C3), 113.5 (C, C3a) 91.5 (CH, C5), 86.4 (CH, C7), 78.6 (C, C14), 55.7 (CH_3, C17), 55.2 (CH_3, C16), 42.4 (CH_2, C10), 28.6 (CH_2, C11), 28.0 (CH_3, C15), 7.6 (CH_3, C9), 4.0 (CH_2, C8)

HRMS-ESI (m/z): Calculated for $C_{23}H_{38}N_2O_4SiK$ [M+K]+, 473.2232; found 473.2235

IR: 3375, 2955, 2875, 1698, 1622, 1587, 1512, 1392, 1155, 1135, 737

Aniline **3.99**:

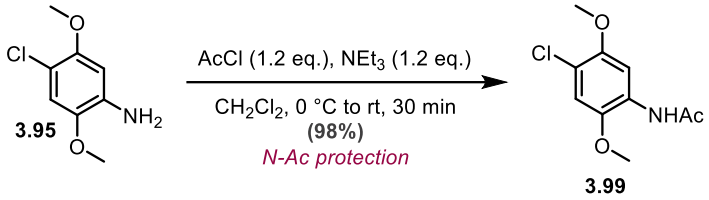

Adapted from the procedure of Nawrat et al.:[211] Acetyl chloride (0.23 mL, 3.20 mmol) was added to a solution of 4-chloro-2,5-dimethoxyaniline **3.95** (0.50 g, 2.70 mmol) and triethylamine (0.45 mL, 3.20 mmol) in dichloromethane (20 mL) at 0 °C. The reaction was then allowed to warm to rt. After 30 minutes, the reaction mixture was washed sequentially with water (3 × 20 mL), saturated aqueous sodium bicarbonate solution (20 mL) and brine (20 mL). The organic phases were dried over anhydrous sodium sulfate, filtered and concentrated under reduced pressure to yield aniline **3.99** (0.60 g, 2.60 mmol, 98%) as an off-white solid. Used in the next step without further purification.

R_f: 0.23 (40% ethyl acetate in pentane) – yellow spot (with vanillin)

^{1}H NMR (700 MHz, $CDCl_3$): δ 8.24 – 8.22 (m, 1H), 7.72 (br s, 1H), 6.88 – 6.85 (m, 1H), 3.86 (d, *J* = 1.9 Hz, 3H), 3.82 (d, *J* = 2.2 Hz, 3H), 2.20 – 2.19 (m, 3H)

^{13}C NMR (176 MHz, $CDCl_3$): δ 168.3, 149.1, 141.7, 127.1, 115.5, 112.2, 104.9, 56.7, 56.3, 25.0

Data in agreement with literature.[211]

Aniline **3.100**:

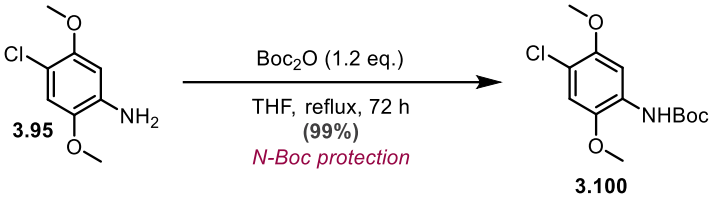

Adapted from the procedure of Nawrat et al.:[211] Di-*tert*-butyl dicarbonate (1.40 g, 6.40 mmol) was added to a solution of 4-chloro-2,5-dimethoxyaniline **3.95** (1.00 g, 5.33 mmol) in tetrahydrofuran (10 mL) and the resulting reaction mixture was heated to reflux for 3 days. The reaction was concentrated under reduced pressure and the crude material was purified by silica column chromatography (100% pentane to 15% diethyl ether in pentane) to yield aniline **3.100** (1.51 g, 5.25 mmol, 99%) as a white crystalline solid.

R_f: 0.31 (5% diethyl ether in pentane) –yellow spot (with vanillin)

^{1}H NMR (600 MHz, $CDCl_3$): δ 7.92 (br s, 1H), 7.05 (br s, 1H), 6.86 (s, 1H), 3.89 (s, 3H), 3.82 (s, 3H), 1.53 (s, 9H)

^{13}C NMR (151 MHz, $CDCl_3$): δ 152.7, 149.4, 141.6, 127.7, 114.3, 112.5, 103.5, 80.8, 56.9, 56.5, 28.5

Data in agreement with literature.[211]

Aniline **3.103**:

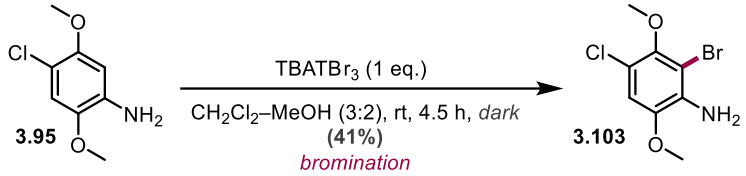

Adapted from the procedure of Watanabe et al.:[212] Under a nitrogen atmosphere in the dark, tetrabutylammonium tribromide (2.57 g, 5.33 mmol) in 3:2 dichloromethane–methanol (10 mL) was added dropwise over 1 minute to 4-chloro-2,5-dimethoxyaniline **3.95** (1.00 g, 5.33 mmol) in 3:2 dichloromethane–methanol (40 mL) at rt. After 4.5 h, the reaction was concentrated under reduced pressure. The crude material was partitioned between water (20 mL) and diethyl ether (20 mL), the organic phase was removed and the aqueous phase was extracted with diethyl ether (4 × 20 mL). The combined organic phases were washed with brine (30 mL), dried over anhydrous sodium sulfate, filtered and concentrated under reduced pressure. The dark-red residue was purified by passing through a plug of silica (20% ethyl acetate in pentane) to aniline **3.103** (0.58 g, 2.20 mmol, 41%) as a brown oil.

Best attempt: 79% yield (266 µmol)

R_f: 0.46 (20% ethyl acetate in pentane) – yellow spot (with vanillin)

^{1}H NMR ^{1}H NMR (600 MHz, $CDCl_3$): δ 6.74 (s, 1H), 4.26 (br s, 2H), 3.834 (s, 3H), 3.827 (s, 3H)

^{13}C NMR (151 MHz, $CDCl_3$): δ 147.3, 143.7, 135.1, 115.2, 110.6, 104.6, 60.8, 56.4

Data in agreement with literature.[212]

Nitrobenzene **3.109**:

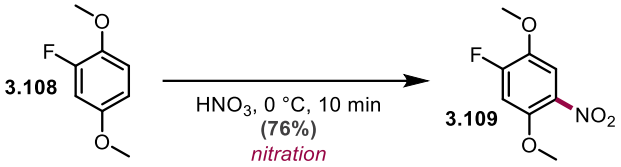

Following the procedure of Sweeney et al.:[104] 2-Fluoro-1,4-dimethoxybenzene **3.108** (3.52 mL, 25.6 mmol) was added dropwise over 5 minutes to a concentrated aqueous solution of nitric acid (64–66%, 35 mL) at 0 °C. A cloudy yellow solution with precipitation formed. After 10 minutes, the reaction mixture was poured onto ice-water (150 mL) and stirred for 30 minutes. The yellow precipitate was collected by vacuum filtration and washed with water (3 × 100 mL) and dried under high vacuum to yield nitrobenzene **3.109** (3.91 g, 19.4 mmol, 76%) as a yellow solid. Used in the next step without further purification.

Note: 2-Fluoro-1,4-dimethoxybenzene **3.108** is a liquid which solidifies at ambient temperature, therefore the syringe requires warming to transfer.

R_f: 0.13 (5% diethyl ether in pentane)

^{1}H NMR (600 MHz, $CDCl_3$): δ 7.63 (d, *J* = 8.7 Hz, 1H), 6.88 (d, *J* = 12.1 Hz, 1H), 3.93 (s, 3H), 3.91 (s, 3H)

^{13}C NMR (151 MHz, $CDCl_3$): δ 155.9 (d, *J* = 257.8 Hz), 149.1 (d, *J* = 9.3 Hz), 141.2 (d, *J* = 12.0 Hz), 111.6 (d, *J* = 4.4 Hz), 103.1 (d, *J* = 23.5 Hz), 57.4, 57.2

Data in agreement with literature.[104]

Aniline **3.110**:

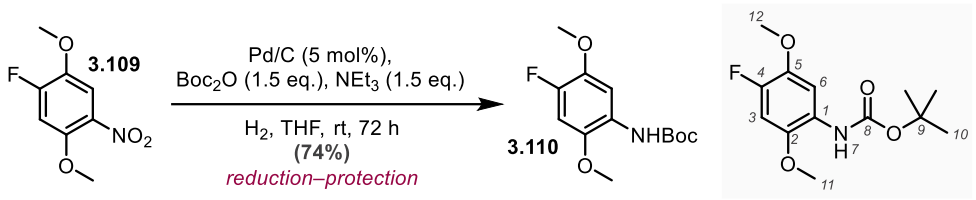

Adapted from the procedure of Kato et al.:[213] Under a nitrogen atmosphere, palladium on carbon (10 w%, 53 mg, 49.7 µmol, 5 mol%), di-tert-butyl dicarbonate (0.33 g, 1.51 mmol) and triethylamine (0.21 mL, 1.5 mmol) were added to nitrobenzene **3.109** (0.20 g, 0.994 mmol) in tetrahydrofuran (10 mL). The reaction mixture was sparged with a balloon of hydrogen and the reaction mixture was stirred under an atmosphere of hydrogen for 3 days. The reaction mixture was then sparged with nitrogen, prior to being filtered over Celite and washed with ethyl acetate (50 mL). The filtrate was concentrated under reduced pressure. The crude material was purified by silica column chromatography (100% pentane to 10% ether in pentane) to yield aniline **3.110** (0.20 g, 0.74 mmol, 74%) as an amorphous white solid.

R_f: 0.29 (5% diethyl ether in pentane) – yellow spot (with vanillin)

^{1}H NMR (600 MHz, $CDCl_3$): δ 7.91 (s, 1H, H6), 6.95 (br s, 1H, H7), 6.67 (d, *J* = 12.2 Hz, 1H, H3), 3.88 (s, 3H, H12), 3.81 (s, 3H, H11), 1.52 (s, 9H, H10)

^{13}C NMR (151 MHz, $CDCl_3$): δ 152.7 (C, C8), 147.3 (d, *J* = 240.7 Hz, C, C4), 141.2 (d, *J* = 8.0 Hz, C, C2), 141.0 (d, *J* = 11.1 Hz, C, C5), 124.0 (d, *J* = 3.3 Hz, C, C1), 105.2 (CH, C6), 100.2 (d, *J* = 23.4 Hz, CH, C3), 80.5 (C, C9), 57.0 (CH_3, C12), 56.4 (CH_3, C11), 28.4 (CH_3, C10)

^{19}F NMR (565 MHz, $CDCl_3$): δ -140.92 (t, *J* = 10.6 Hz)

HRMS-ESI (m/z): Calculated for $C_{13}H_{18}FNO_4Na$ [M+Na]+, 294.1112; found 294.1121

IR: 3440, 3005, 2979, 2940, 2872, 2841, 1808, 1727, 1613, 1537, 1491, 1466, 1412, 1368, 1243, 1214, 1162, 1041, 986, 918, 853, 779, 739, 675, 646

Nitrobenzene **3.114**:

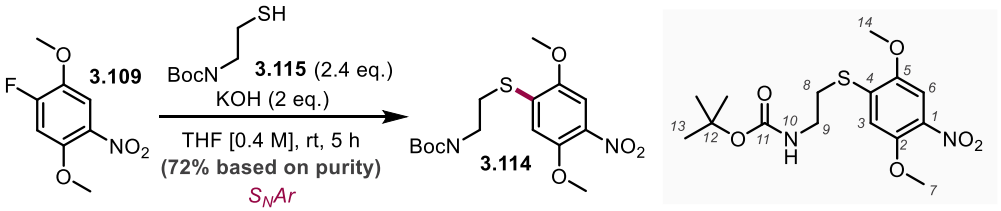

Adapted from the procedure of de Vicente et al.:[214] A 1 M aqueous potassium hydroxide solution (1 mL, 1.0 mmol) was added dropwise over 1 minute to a solution of nitrobenzene **3.109** (50 mg, 249 µmol) and aminothiol **3.115** (0.1 mL, 0.59 mmol) in tetrahydrofuran (0.62 mL) at rt. A yellow precipitate formed. After 5 h, the aqueous phase was extracted with ethyl acetate (3 × 5 mL). The combined organic phases were dried over anhydrous sulfate, filtered and concentrated under reduced pressure. The yellow solid was purified by silica column chromatography (100% pentane to 40% diethyl ether in pentane) to yield nitrobenzene **3.114** (97 mg, 0.18 mmol, 72% based on purity) as a yellow amorphous solid.

R_f: 0.20 (30% diethyl ether in pentane) – yellow spot (without stain)

^{1}H NMR (600 MHz, $CDCl_3$): δ 7.44 (s, 1H, H3 or H6), 7.21 (s, 1H, H3 or H6), 4.92 (br s, 1H, H10), 4.03 (s, 3H, H7 or H14), 3.90 (s, 3H, H7 or H14), 3.37 (dt, *J* = 7.7, 6.3 Hz, 2H, H9), 3.12 (t, *J* = 7.2 Hz, 2H, H8), 1.43 (s, 9H, H13)

^{13}C NMR (151 MHz, $CDCl_3$): δ 155.9 (C, C11), 149.4 (C, C2 or C5), 149.0 (C, C2 or C5), 135.8 (C, C1), 135.3 (C, C4), 112.1 (CH, C3 or C6), 107.4 (CH, C3 or C6), 80.0 (C, C12), 57.7 (CH_3, C7 or C14), 56.8 (CH_3, C7 or C14), 39.9 (CH_2, C9), 30.7 (CH_2, C8), 28.5 (CH_3, C13)

HRMS-ESI (m/z): Calculated for $C_{15}H_{22}N_2O_6SNa$ [M+Na]+, 381.1091; found 381.1086

IR: 3650, 2980, 2889, 1706, 1575, 1507, 1499, 1461, 1382, 1252, 1155, 1073, 954, 866, 815, 737

Hydroquinone **3.123**:

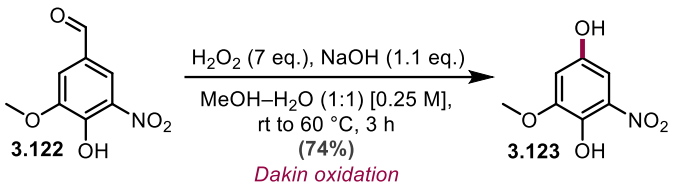

Adapted from the procedure of An et al.:[106] Under a nitrogen atmosphere, aqueous sodium hydroxide solution (1 M, 55.8 mL, 55.8 mmol) and hydrogen peroxide (35%, 32 mL, 372 mmol) were added sequentially to a solution of 5-nitrovanillin **3.122** (10 g, 50.7 mmol) in 1:1 methanol–water (200 mL) at rt and the resulting solution was heated to 60 °C. After 3 h, the dark-red reaction mixture was cooled to rt and concentrated under a stream of nitrogen to remove methanol; an orange precipitate formed. The reaction mixture was cooled to 0 °C to promote further precipitation. The precipitate was collected by vacuum filtration and washed with water (3 × 40 mL) to yield hydroquinone **3.123** (6.91 g, 37.3 mmol, 74%) as a bright orange amorphous solid. Used in the next step without further purification.

Best attempt: 84% yield (12.7 mmol)

R_f: 0.30 (30% ethyl acetate in pentane) – brown spot (with vanillin)

^{1}H NMR (600 MHz, $CDCl_3$): δ 10.45 (d, *J* = 0.6 Hz, 1H), 7.09 (d, *J* = 2.9 Hz, 1H), 6.76 (d, *J* = 2.9 Hz, 1H), 4.96 (d, *J* = 1.5 Hz, 1H), 3.93 (s, 3H)

^{13}C NMR (151 MHz, $CDCl_3$): δ 151.1, 147.8, 141.6, 133.3, 108.3, 99.8, 56.9

Data in agreement with literature.[106]

Nitrobenzene **3.124**:

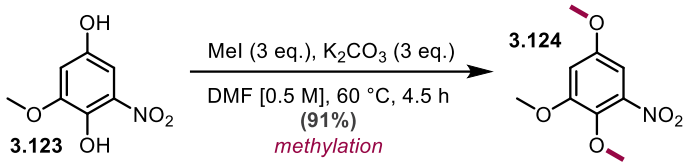

Adapted from the procedure of An et al.:[106] Methyl iodide (7 mL, 112 mmol) was added to a solution of hydroquinone **3.123** (6.91 g, 37.3 mmol) and potassium carbonate (15.5 g, 112 mmol) in dimethylformamide (75 mL) at rt and the resulting solution was heated to 60 °C. After 4.5 h, the reaction was cooled to rt, diluted with water (100 mL) and the aqueous phase extracted with ethyl acetate (3 × 80 mL). The combined organic phases were washed with water (40 mL), dried over anhydrous sodium sulfate, filtered and concentrated under reduced pressure to yield nitrobenzene **3.124** (7.23 g, 33.9 mmol, 91%) as a yellow-brown amorphous solid. Used in the next step without further purification.

Best attempt: 98% yield (17.1 mmol)

R_f: 0.69 (30% ethyl acetate in pentane)

^{1}H NMR (700 MHz, $CDCl_3$) δ 6.80 (d, *J* = 2.9 Hz, 1H), 6.67 (d, *J* = 2.9 Hz, 1H), 3.91 – 3.90 (m, 3H), 3.88 – 3.88 (m, 3H), 3.81 – 3.80 (m, 3H)

^{13}C NMR (176 MHz, $CDCl_3$): δ 155.6, 155.0, 144.8, 137.4, 104.8, 98.8, 62.2, 56.5, 56.1

Data in agreement with literature.[106]

Dimethoxyindole **3.126**:

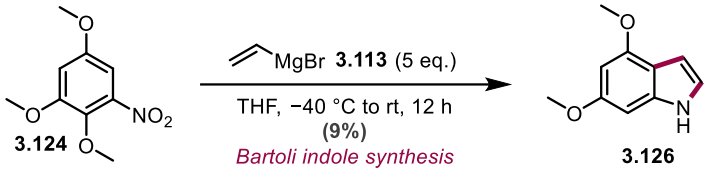

Adapted from the procedure of Meuser et al.:[215] Under a nitrogen atmosphere, vinylmagnesium bromide **3.113** (1.17 mL, 1.17 mmol, 1 M in tetrahydrofuran) was added dropwise over 1 minute to a solution of nitrobenzene **3.124** (50 mg, 235 µmol) in tetrahydrofuran (1.9 mL) at **−**40 °C. The reaction was allowed to gradually warm to rt. After 12 h, the reaction was quenched by addition of saturated aqueous ammonium chloride solution (2.5 mL). After 10 minutes, the aqueous phase was extracted with ethyl acetate (3 × 10 mL). The combined organic phases were washed with brine (5 mL), dried over anhydrous sodium sulfate, filtered and concentrated under reduced pressure. The crude material was purified by silica column chromatography (100% pentane to 30% diethyl ether in pentane) to yield dimethoxyindole **3.126** (3.1 mg, 22.0 µmol, 9%) as a brown amorphous solid.

R_f: 0.33 (30% diethyl ether in pentane) – purple spot (with vanillin)

^{1}H NMR (500 MHz, $CDCl_3$): δ 8.05 (s, 1H), 7.02 – 6.98 (m, 1H), 6.58 – 6.55 (m, 1H), 6.50 (s, 1H), 6.23 (d, *J* = 1.8 Hz, 1H), 3.92 (s, 3H), 3.84 (s, 3H)

^{13}C NMR (126 MHz, $CDCl_3$): δ 157.8, 153.8, 137.3, 121.3, 113.2, 99.9, 91.8, 86.9, 55.8, 55.5

Data in agreement with literature.[216]

Nitrobenzene **3.133**:

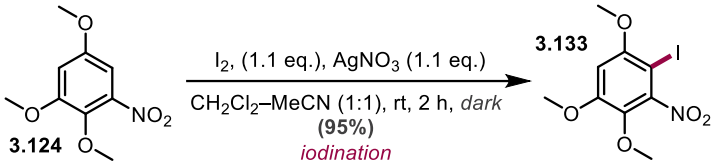

Adapted from the procedure of An et al.:[106] Under a nitrogen atmosphere in the dark, silver nitrate (1.75 g, 10.3 mmol) and iodine (2.62 g, 10.3 mmol) were sequentially added to a solution of nitrobenzene **3.124** (2.00 g, 9.38 mmol) in 1:1 dichloromethane–acetonitrile (86 mL) at rt. After 2 h, the reaction was filtered over Celite and washed with dichloromethane (300 mL). Saturated aqueous sodium thiosulfate solution (300 mL) was added, the phases separated and the aqueous phase was extracted with dichloromethane (2 × 100 mL). The combined organic phases were washed with brine (100 mL), dried over anhydrous sodium sulfate, filtered and concentrated under reduced pressure. The yellow-brown solid was triturated with hexane (3 × 20 mL) to yield nitrobenzene **3.133** (3.03 g, 8.94 mmol, 95%) as a yellow amorphous solid.

R_f: 0.48 (20% ethyl acetate in pentane)

^{1}H NMR ^{1}H NMR (700 MHz, $CDCl_3$) δ 6.56 (s, 1H), 3.94 (d, *J* = 0.9 Hz, 3H), 3.90 (d, *J* = 0.9 Hz, 3H), 3.85 (d, *J* = 0.9 Hz, 3H)

^{13}C NMR (176 MHz, $CDCl_3$): δ 155.7, 154.5, 151.6, 135.7, 98.0, 65.9, 62.6, 57.5, 56.7

Data in agreement with literature.[106]

ortho-Iodoaniline **3.134**:

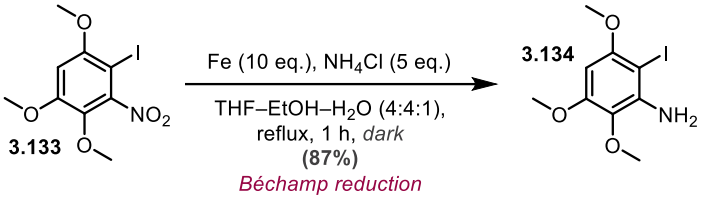

Adapted from the procedure of An et al.:[106] Under a nitrogen atmosphere in the dark, iron powder (5.00 g, 89.5 mmol) and ammonium chloride (2.39 g, 44.7 mmol) were added to a solution of nitrobenzene **3.133** (3.03 g, 8.94 mmol) in 4:4:1 tetrahydrofuran–ethanol–water (60 mL) and the resulting solution was stirred vigorously and heated to 95 °C. After 1 h, the reaction was cooled to rt, filtered over Celite and washed with dichloromethane (4 × 50 mL). The filtrate was dried over anhydrous sodium sulfate, filtered and concentrated under reduced pressure. The crude material was purified by silica column chromatography (100% pentane to 30% ethyl acetate in pentane) to yield *ortho*-iodoaniline **3.134** (2.40 g, 7.76 mmol, 87%) as a white amorphous solid.

Best attempt: 92% yield (4.39 mmol)

Note: ortho-Iodoaniline **3.134** is unstable therefore was always used directly.

R_f: 0.48 (20% ethyl acetate in pentane) – yellow spot (with vanillin)

^{1}H NMR (400 MHz, $CDCl_3$): δ 6.00 (s, 1H), 4.40 (s, 2H), 3.87 (s, 3H), 3.84 (s, 3H), 3.78 (s, 3H)

^{13}C NMR (126 MHz, $CDCl_3$): δ 155.2, 153.2, 142.3, 129.9, 87.1, 65.6, 60.3, 56.7, 56.1

Data in agreement with literature.[106]

Trimethoxytryptamine **3.135**:

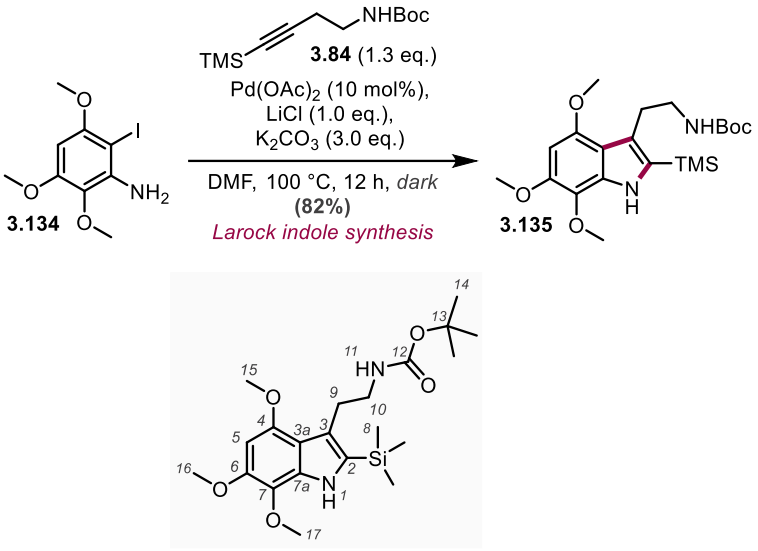

Adapted from the procedure of Danner et al.:[207] Under a nitrogen atmosphere in the dark, *ortho*-iodoaniline **3.134** (2.00 g, 6.47 mmol) in *N*,*N*-dimethylformamide (40 mL) was added to lithium chloride (0.30 g, 7.08 mmol), potassium carbonate (2.92 g, 21.1 mmol) and palladium(II) acetate trimer (0.16 g, 0.712 mmol, 10 mol%) in a Schlenk tube at rt. After 10 minutes, homopropargyl amine **3.84** (2.03 g, 8.41 mmol) in *N*,*N*-dimethylformamide (25 mL) was added dropwise over 5 minutes, and reaction was stirred and heated to 120 °C. After 12 h, the reaction was cooled to rt, quenched by addition of saturated aqueous ammonium chloride (70 mL) and the aqueous phase extracted with ethyl acetate (3 × 100 mL). The combined organic phases were washed sequentially with 5% lithium chloride aqueous solution (5 × 75 mL) and brine (75 mL), dried over anhydrous sodium sulfate, filtered and concentrated under reduced pressure. The dark-brown oil was purified by silica column chromatography (100% pentane to 40% diethyl ether in pentane) to yield trimethoxytryptamine **3.135** (2.24 g, 5.30 mmol, 82%) as an off-white foam.

Note: Rigorously anhydrous conditions required – azeotropic drying of *ortho*-iodoaniline **3.134** and homopropargyl amine **3.84**, extended drying of dimethylformamide from solvent purification stills over activated 3 Å molecular sieves, and drying of lithium chloride, potassium carbonate (400 °C) and palladium(II) acetate trimer (120 °C) under vacuum while heating.

Best attempt: 84% yield (2.6 mmol)

R_f: 0.35 (20% diethyl ether in pentane) – purple spot (with vanillin)

^{1}H NMR (600 MHz, $CDCl_3$): δ 7.88 (s, 1H, H1), 6.21 (s, 1H, H5), 4.85 (br s, 1H, H11), 3.94 (s, 3H, H15, H16 or H17), 3.92 (s, 3H, H15, H16 or H17), 3.89 (s, 3H, H15, H16 or H17), 3.45 (app q, *J* = 6.5 Hz, 2H, H10), 3.01 (t, *J* = 6.6 Hz, 2H, H9), 1.39 (s, 9H, H14), 0.37 (s, 9H, H8)

^{13}C NMR (151 MHz, $CDCl_3$): δ 155.8 (C, C12), 149.8 (C, C4 or C6 or C7), 147.1 (C, C4 or C6 or C7), 134.1 (C, C3a), 132.6 (C, C2), 128.9 (C, C4 or C6 or C7), 122.8 (C, C7a), 115.1 (C, C3), 90.2 (CH, C5), 78.6 (C, C13), 61.0 (CH_3, C15 or C16 or C17), 58.0 (CH_3, C15 or C16 or C17), 55.4 (CH_3, C15 or C16 or C17), 42.3 (CH_2, C10), 28.4 (CH_3, C14), 27.7 (CH_2, C9), -0.3 (CH_3, C8)

HRMS-ESI (m/z): Calculated for $C_{21}H_{34}N_2O_5SiNa$ [M+Na]+, 445.2129; found 445.2127

IR: 3418, 3392, 3355, 2977, 2953, 2934, 2839, 1691, 1619, 1585, 1523, 1466, 1392, 1366, 1331, 1277, 1252, 1176, 1156, 1136, 1108, 1070, 1046, 995, 962, 939, 873, 839, 814, 759, 740, 634

Trimethoxytryptamine **3.136**:

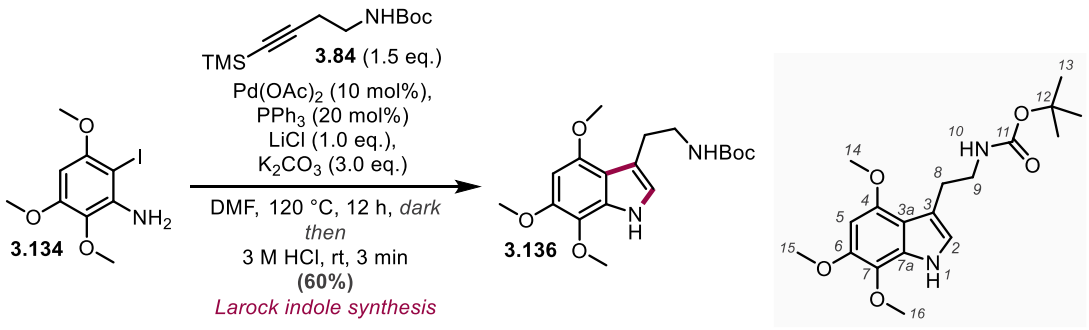

Adapted from the procedure of Foo et al.:[112] Under a nitrogen atmosphere in the dark, *ortho*-iodoaniline **3.134** (56 mg, 181 µmol) in *N*,*N*-dimethylformamide (2.0 mL) was added to lithium chloride (8 mg, 189 µmol), potassium carbonate (75 mg, 544 µmol), triphenylphosphine (10 mg, 38.1 µmol, 20 mol%) and palladium(II) acetate trimer (4 mg, 18.1 µmol, 10 mol%) in a Schlenk tube at rt. After 10 minutes, homopropargyl amine **3.84** (65 mg, 269 µmol) in *N*,*N*-dimethylformamide (1.3 mL) was added dropwise over 5 minutes, and reaction was stirred and heated to 120 °C. After 12 h, the reaction was cooled to rt and quenched by addition of saturated aqueous ammonium chloride (5 mL), then extracted with ethyl acetate (3 × 20 mL). The combined organic phases were vigorously shaken for 3 minutes with 3 M hydrochloric acid solution (20 mL), washed with brine (20 mL), dried over anhydrous sodium sulfate, filtered and concentrated under reduced pressure. The dark-brown oil was purified by silica column chromatography (100% dichloromethane to 7.5% acetone in dichloromethane) to yield trimethoxytryptamine **3.136** (37.8 mg, 108 µmol, 60%) as a brown oil.

R_f: 0.46 (2.5% acetone in dichloromethane) – purple spot (with vanillin)

^{1}H NMR (600 MHz, $CDCl_3$): δ 8.12 (s, 1H, H1), 6.82 (s, 1H, H2), 6.24 (s, 1H, H5), 4.82 (s, 1H, H10), 3.93 (s, 3H, H14 or H15), 3.91 (s, 3H, H16), 3.89 (s, 3H, H14 or H15), 3.43 (q, *J* = 6.3 Hz, 2H, H9), 2.97 (t, *J* = 6.3 Hz, 2H, H8), 1.40 (s, 9H, H13)

^{13}C NMR (151 MHz, $CDCl_3$): δ 156.2 (C, C11), 150.2 (C, C4 or C6), 147.1 (C, C4 or C6), 132.2 (C, C7a), 129.4 (C, C7), 120.8 (CH, C2), 114.3 (C, C3), 113.6 (C, C3a), 90.5 (CH, C5), 78.9 (C, C12), 61.1 (CH_3, C16), 58.1 (CH_3, C14 or C15), 55.5 (CH_3, C14 or C15), 41.9 (CH_2, C9), 28.6 (CH_3, C13), 27.0 (CH_2, C8)

HRMS-ESI (m/z): Calculated for $C_{18}H_{26}N_2O_5Na$ [M+Na]+, 373.1734; found 373.1748

IR: 3348, 2978, 2935, 2840, 2250, 1699, 1631, 1595, 1525, 1453, 1425, 1393, 1367, 1344, 1274, 1251, 1233, 1205, 1174, 1144, 1092, 1052, 1030, 990, 973, 911, 890, 868, 845, 788, 736, 660, 652, 634, 619, 609

Indolequinone **3.89**:

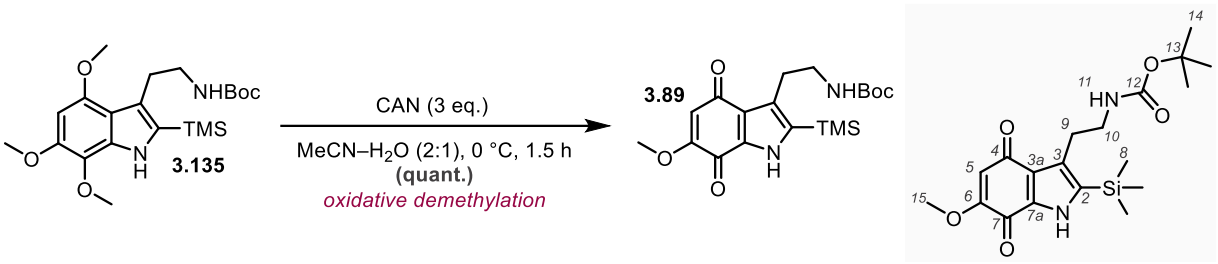

Adapted from the procedure of An et al.:[106] Ceric ammonium nitrate (3.89 g, 7.10 mmol) in water (11.5 mL) was added dropwise over 1 minute to a solution of trimethoxytryptamine **3.135** (1.00 g, 2.37 mmol) in acetonitrile (23 mL) at 0 °C. After 1.5 h, the reaction was diluted with water (30 mL), and the aqueous phase is extracted with ethyl acetate (3 × 80 mL). The combined organic phases were washed with brine (50 mL), dried over anhydrous sodium sulfate, filtered and concentrated under reduced pressure to yield indolequinone **3.89** (0.93 g, 2.37 mmol, quant.) as an orange foam. Used in the next step without further purification.

R_f: 0.24 (2.5% acetone in dichloromethane) – orange spot (without stain)

^{1}H NMR (600 MHz, $CDCl_3$): δ 9.10 (br s, 1H, H1), 5.70 (s, 1H, H5), 4.87 (t, *J* = 6.0 Hz, 1H, H11), 3.83 (s, 3H, H15), 3.37 (app q, *J* = 6.5 Hz, 2H, H10), 2.94 (t, *J* = 6.9 Hz, 2H, H9), 1.40 (s, 9H, H14), 0.38 (s, 9H, H8)

^{13}C NMR (151 MHz, $CDCl_3$): δ 184.8 (C, C4 or C7), 171.4 (C, C4 or C7), 159.9 (C, C6), 156.0 (C, C1), 139.9 (C, C2), 132.3 (C, C3 or C3a or C7a), 132.2 (C, C3 or C3a or C7a), 124.8 (C, C3 or C3a or C7a), 108.4 (CH, C5), 79.0 (C, C13), 56.8 (CH_3, C15), 41.4 (CH_2, C10), 28.6 (CH_3, C14), 27.1 (CH_2, C9), -0.7 (CH_3, C8)

HRMS-ESI (m/z): Calculated for $C_{14}H_{21}N_2O_3Si$ *[Boc-group removed in situ]* [M+H]+, 293.1316; found 293.1304

IR: 3339, 3324, 3011, 2952, 2932, 2850, 2252, 1700, 1690, 1672, 1643, 1602, 1542, 1514, 1473, 1459, 1442, 1422, 1394, 1367, 1329, 1253, 1175, 1122, 1098, 1070, 1022, 985, 962, 916, 848, 809, 796, 764, 736, 701, 655, 646, 626, 610

Cystamine **3.154**:

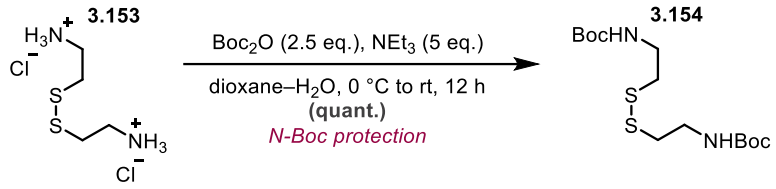

Adapted from the procedure of Zeisel et al.:[217] Triethylamine (10 mL, 71.7 mmol) and di-*tert*-butyl dicarbonate (8.14 g, 37.3 mmol) were successively added to a solution of cystamine **3.153** dihydrochloride (3.5 g, 15.5 mmol) in 1:1 1,4-dioxane–water (30 mL) at 0 °C. The resulting solution was allowed to gradually warm to rt. After 12 h, the reaction was treated with 1 M hydrochloric acid (25 mL) to achieve a pH of 2/3 and the aqueous phase was extracted with ethyl acetate (3 × 30 mL). The combined organic phases were washed with brine (30 mL), dried over anhydrous sodium sulfate, filtered and concentrate under reduced pressure to yield cystamine **3.154** (5.46 g, 15.5 mmol, quant.) as a white amorphous solid. Used in the next step without further purification.

R_f: 0.39 (20% ethyl acetate in pentane) – blue spot (with PMA)

^{1}H NMR (400 MHz, $CDCl_3$) δ 5.04 (s, 1H), 3.44 (q, *J* = 6.3 Hz, 4H), 2.79 (t, *J* = 6.3 Hz, 4H), 1.44 (s, 18H)

^{13}C NMR (101 MHz, $CDCl_3$): δ 156.0, 79.7, 39.4, 38.6, 28.5, 27.6

Data in agreement with literature.[217]

Sulfinate ester **3.155**:

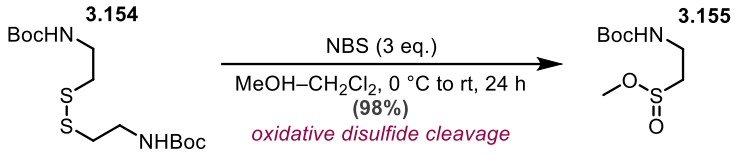

Adapted from the procedure of Xue et al.:[218] *N*-Bromosuccinimide (3.79 g, 21.3 mmol) was added portion-wise over 3 minutes to a solution of cystamine **3.154** (2.48 g, 7.04 mmol) in 1:1 methanol–dichloromethane (50 mL) at 0 °C. The resulting solution was allowed to gradually warm to rt. After 24 h, saturated aqueous sodium bicarbonate solution (10 mL) was added and then the solution was stirred for a further 10 minutes. Water (30 mL) was added, the organic phase was separated and the aqueous phase was further extracted with dichloromethane (3 × 30 mL). The combined organic phases were washed with saturated aqueous sodium bicarbonate solution (30 mL), dried over anhydrous sodium sulfate, filtered and concentrated under reduced pressure to yield sulfinate ester **3.155** (1.54 g, 6.90 mmol, 98%) as a colourless oil.

R_f: 0.35 (50% ethyl acetate in pentane) – blue spot (with PMA)

^{1}H NMR (400 MHz, $CDCl_3$) δ 5.15 – 4.98 (m, 1H), 3.83 – 3.76 (m, 3H), 3.64 – 3.50 (m, 2H), 3.03 – 2.83 (m, 2H), 1.47 – 1.39 (m, 9H)

^{13}C NMR (101 MHz, $CDCl_3$): δ 155.9, 79.9, 56.3, 55.2, 33.7, 28.5

Data in agreement with literature.[218]

Cystamine **3.156**:

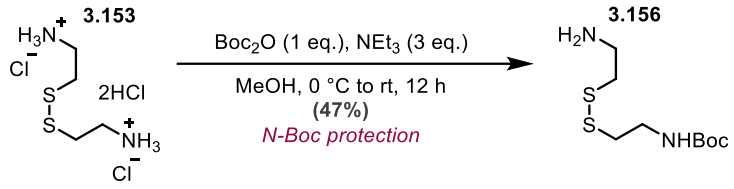

Adapted from the procedure of Fisher et al.:[219] Triethylamine (17.5mL, 126 mmol) was added to a solution of cystamine **3.153** dihydrochloride (10.00 g, 44.4 mmol) in methanol (400 mL) at 0 °C. After 30 minutes, di-*tert*-butyl dicarbonate (9.69 g, 44.4 mmol) in methanol (100 mL) was added dropwise over 45 minutes. The resulting solution was allowed to gradually warm to rt. After 12 h, the reaction was concentrated under reduced pressure and the white solids were washed with diethyl ether (3 × 20 mL). The residual solids were dissolved in 1 M sodium hydroxide solution (25 mL) and the aqueous phase was extracted with dichloromethane (3 × 30 mL). The combined organic phases were washed with water (2 × 20 mL), dried over anhydrous sodium sulfate, filtered, concentrated under reduced pressure and triturated with ice-cold hexane (3 × 20 mL) to yield cystamine **3.156** (5.31 g, 21.0 mmol, 47%) as a white amorphous solid.

R_f: 0.15 (4% methanol in dichloromethane) – blue spot (with PMA)

^{1}H NMR (600 MHz, $CDCl_3$): δ 4.96 (s, 1H), 3.44 (q, *J* = 6.5 Hz, 2H), 3.00 (td, *J* = 6.3, 4.7 Hz, 2H), 2.81 – 2.73 (m, 4H), 1.43 (s, 9H)

^{13}C NMR (151 MHz, $CDCl_3$): δ 155.9, 79.6, 42.6, 40.7, 39.4, 38.5, 28.5

Data in agreement with literature.[219]

Enamine **3.157**:

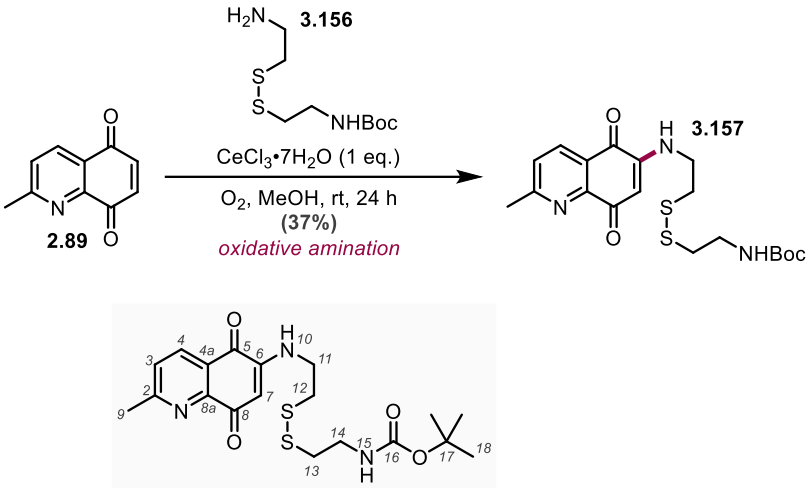

Adapted from the procedure of Wang et al.:[21] Under an oxygen atmosphere, cerium(III) chloride heptahydrate (120 mg, 0.318 mmol) and cystamine **3.156** (80 mg, 0.318 mmol) were successively added to a solution of methylquinoline-5,8-dione **2.89** (55 mg, 0.318 mmol) in methanol (1.6 mL) at rt. After 3 days, the red solution was concentrated under reduced pressure and the dark-red residue was purified by column chromatography (20% acetone in dichloromethane) to yield enamine **3.157** (49 mg, 0.12 mmol, 37%) as a red foam.

R_f: 0.26 (20% acetone in dichloromethane) – black spot (with ninhydrin)

^{1}H NMR (600 MHz, $CDCl_3$): δ 8.22 (d, *J* = 8.0 Hz, 1H, H4), 7.41 (d, *J* = 8.0 Hz, 1H, H3), 6.23 (t, *J* = 6.1 Hz, 1H, H10), 5.94 (s, 1H, H7), 4.90 (br s, 1H, H15), 3.57 (app q, *J* = 6.3 Hz, 2H, H11), 3.44 (q, *J* = 6.4 Hz, 2H, H14), 2.94 (t, *J* = 6.4 Hz, 2H, H12), 2.81 (t, *J* = 6.4 Hz, 2H, H13), 2.75 (s, 3H, H9), 1.42 (s, 9H, H18)

^{13}C NMR (151 MHz, $CDCl_3$): δ 181.8 (C, C5 or C8), 181.4 (C, C5 or C8), 165.8 (C, C2), 155.9 (C, C16), 148.9 (C, C8a), 147.2 (C, C6), 134.6 (CH, C4), 126.2 (CH, C3), 125.3 (C, C4a), 102.1 (CH, C7), 79.7 (C, C17), 41.3 (CH_2, C11), 39.5 (CH_2, C14), 38.6 (CH_2, C13), 35.8 (CH_2, C12), 28.5 (CH_3, C18), 25.6 (CH_3, C9)

HRMS-ESI (m/z): Calculated for $C_{19}H_{26}N_3O_4S_2$ [M+H]+, 424.1359; found 424.1357

IR: 3341, 2925, 2851, 2242, 1702, 1685, 1635, 1609, 1583, 1515, 1457, 1407, 1393, 1366, 1332, 1282, 1253, 1222, 1175, 1138, 1121, 1039, 948, 911, 866, 850, 804, 779, 736, 670, 649, 639, 626, 607

Sulfide **3.158**:

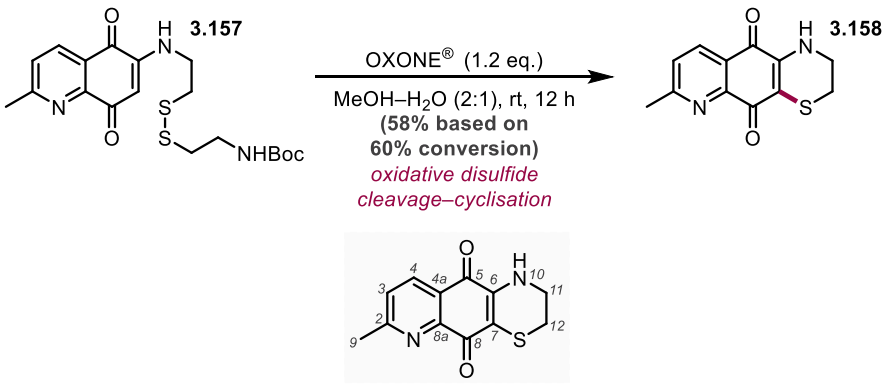

OXONE® (9 mg, 29.3 μmol) was added to a solution of enamine **3.157** (10.3 mg, 24.4 μmol) in a 2:1 mixture of methanol (0.6 mL) at rt and the reaction was heated to 90 °C. After 24 h, a colour change from a red-yellow solution to dark-brown was observed. The reaction mixture was cooled to rt, diluted with water (10 mL) and the aqueous phase was extracted with ethyl acetate (3 × 10 mL). The combined organic phases were washed with brine (10 mL), dried over anhydrous sodium sulfate, filtered and concentrated under reduced pressure. The purple-grey solid was purified by silica chromatography (10% acetone in dichloromethane) to yield sulfide **3.158** (2.1 mg, 8.5 μmol, 58% based on 60% conversion) as a purple solid.

R_f: 0.47 (10% acetone in dichloromethane)

^{1}H NMR (600 MHz, $CDCl_3$) δ 8.18 (d, *J* = 7.9 Hz, 1H, H4), 7.37 (d, *J* = 7.9 Hz, 1H, H3), 5.97 (br s, 1H, H10), 3.80 – 3.77 (m, 2H, H11), 3.05 – 3.01 (m, 2H, H12), 2.73 (s, 3H, H9)

^{13}C NMR (151 MHz, $CDCl_3$): δ 178.0 (C, C8), 177.8 (C, C5), 165.0 (C, C2), 148.9 (C, C8a), 140.4 (C, C6 or C7), 134.4 (CH, C4), 126.3 (CH, C3), 125.3 (C, C4a), 113.1 (C, C6 or C7), 41.8 (CH_2, C11), 25.5 (CH_3, C9), 24.2 (CH_2, C12)

HRMS-ESI (m/z): Calculated for $C_{12}H_{10}N_2O_2SNa$ [M+Na]+ , 269.0355; found 269.0349

IR: 2961, 2927, 2853, 1734, 1667, 1632, 1572, 1509, 1457, 1422, 1377, 1329, 1302, 1261, 1248, 1207, 1174, 1148, 1124, 1091, 1059, 1036, 912, 853, 832, 807, 775, 749, 735, 704, 676, 665, 650, 639, 629, 619

Enamine **3.164**:

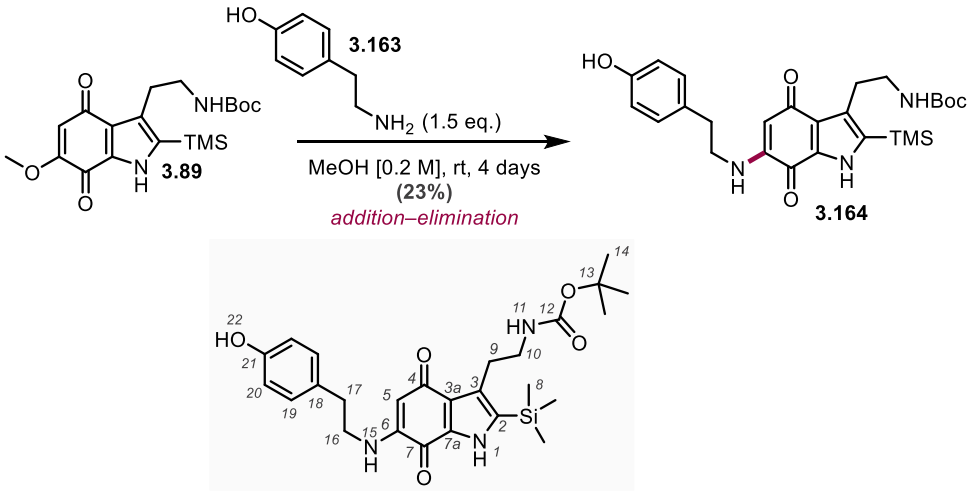

Adapted from the procedure of An et al.:[106] Tyramine **3.163** (2.6 mg, 19.0 μmol) was added to a solution of indolequinone **3.89** (5 mg, 12.7 μmol) in methanol (0.06 mL) at rt. After 4 days, the red solution was concentrated under reduced pressure and the dark-red residue was purified by silica column chromatography (100% dichloromethane to 5% acetone in dichloromethane) to yield enamine **3.164** (1.5 mg, 3.01 μmol, 24%) as a red foam.

R_f: 0.26 (5% acetone in dichloromethane) – red (without stain) or purple spot (with vanillin)

^{1}H NMR (600 MHz, $CDCl_3$): δ 8.93 (s, 1H, H1), 7.06 (d, *J* = 8.5 Hz, 2H, H19), 6.79 (d, *J* = 8.5 Hz, 2H, H20), 5.71 (t, *J* = 5.9 Hz, 1H, H15), 5.26 (s, 1H, H5), 5.14 (s, 1H, H11), 3.38 (app q, *J* = 6.2 Hz, 1H, H10), 3.34 (q, *J* = 6.8 Hz, 2H, H16), 2.96 (t, *J* = 6.7 Hz, 2H, H9), 2.86 (t, *J* = 7.2 Hz, 2H, H17), 1.40 (s, 9H, H14), 0.37 (s, 9H, H8)

^{13}C NMR (151 MHz, $CDCl_3$): δ 184.9 (C, C4), 172.0 (C, C7), 156.3 (C, C12), 154.8 (C, C21), 147.8 (C, C6), 140.6 (C, C2), 132.4 (C, C3), 131.0 (C, C7a), 130.2 (C, C18), 130.0 (CH, C19), 126.5 (C, C3a), 115.9 (CH, C20), 98.7 (CH, C5), 78.9 (C, C13), 44.3 (CH_2, C16), 41.9 (CH_2, C10), 33.6 (CH_2, C17), 28.6 (CH_3, C14), 25.5 (CH_2, C9), -0.8 (CH_3, C8)

HRMS-ESI (m/z): Calculated for $C_{26}H_{35}N_3O_5SiNa$ [M+Na]+, 520.2238; found 520.2235

IR: 3316, 3025, 2928, 2854, 2248, 1686, 1666, 1598, 1535, 1516, 1467, 1440, 1422, 1366, 1325, 1257, 1177, 1133, 1108, 1067, 1025, 993, 911, 848, 795, 736, 691, 678, 658, 639, 629, 607

Enamine **3.165**:

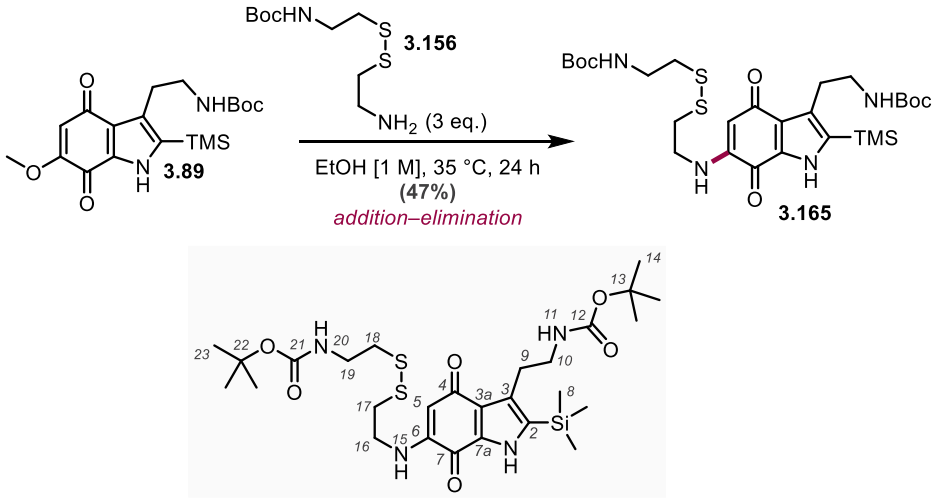

Cystamine **3.156** (58 mg, 230 µmol) was added to a solution of indolequinone **3.89** (30 mg, 76.4 µmol) in distilled ethanol (80 µL) at rt and the resulting reaction mixture was heated to 35 °C. After 24 h, water (1 mL) was added and the aqueous phase was extracted with ethyl acetate (3 × 2 mL). The combined organic phases were washed with brine (2 mL), dried over anhydrous sodium sulfate, filtered and concentrated under reduced pressure. The dark-red oil was purified by silica column chromatography (100% dichloromethane to 20% acetone in dichloromethane) to yield enamine **3.165** (21.9 mg, 35.7 µmol, 47%) as a red foam.

R_f: 0.27 (5% acetone in dichloromethane) – red (without stain) or purple spot (with vanillin)

^{1}H NMR (600 MHz, $CDCl_3$): δ 9.05 (s, 1H, H1), 5.98 (s, 1H, H15), 5.31 (s, 1H, H5), 5.12 (s, 1H, H11), 4.94 (s, 1H, H20), 3.51 (q, *J* = 6.4 Hz, 2H, H16), 3.49 – 3.44 (app q, *J* = 6.3 Hz 2H, H19), 3.40 (q, *J* = 6.5 Hz, 2H, H10), 2.97 (t, *J* = 6.8 Hz, 2H, H9), 2.93 (t, *J* = 6.5 Hz, 2H, H17), 2.82 (t, *J* = 6.3 Hz, 2H, H18), 1.46 (s, 9H, H14 or H23), 1.42 (s, 9H, H14 or H23), 0.40 (s, 9H, H8)

^{13}C NMR (151 MHz, $CDCl_3$): δ 184.8 (C, C4 or C7), 171.8 (C, C4 or C7), 156.2 (C, C12 or C21), 155.9 (C, C12 or C21), 147.5 (C, C6), 140.7 (C, C2), 132.4 (C, C3a or C7a), 131.1 (C, C3a or C7a), 126.3 (C, C3), 99.1 (CH, C5), 79.8 (C, C13 or C22), 78.8 (C, C13 or C22), 41.8 (CH_2, C10), 41.5 (CH_2, C16), 39.4 (CH_2, C19), 38.6 (CH_2, C18), 35.9 (CH_2, C17), 28.6 (CH_3, C14 or C23), 28.5 (CH_3, C14 or C23), 26.8 (CH_2, C9), -0.8 (CH_3, C8)

HRMS-ESI (m/z): Calculated for $C_{27}H_{45}N_4O_6S_2Si$ [M+H]+, 613.2544; found 613.2558

IR: 3363, 2978, 2933, 2856, 1699, 1599, 1512, 1458, 1420, 1394, 1367, 1255, 1177, 1132, 1108, 1068, 1050, 1028, 970, 912, 847, 794, 764, 737, 697, 652, 629, 614

Amine **3.174**:

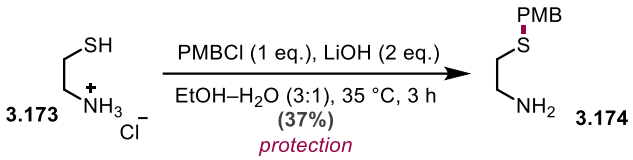

Adapted from the procedure of Ghosh et al.:[220] *para*-Methoxy benzyl chloride (0.69 mL, 5.1 mmol) was added dropwise over 1 minute to a solution of cysteamine **3.173** hydrochloride (0.58 g, 5.1 mmol) and lithium hydroxide (0.24 g, 10.0 mmol) in a 3:1 ethanol–water (20 mL) mixture at rt and the resulting reaction was heated to 35 °C. After 3 h, the reaction was concentrated under reduced pressure to remove ethanol. Water (20 mL) was added and the aqueous phase was extracted with dichloromethane (3 × 30 mL). The combined organic phases were dried over anhydrous sodium sulfate, filtered and concentrated under reduced pressure. The crude material was purified by silica column chromatography (100% dichloromethane to 20% methanol in dichloromethane) to yield amine **3.174** (0.37 g, 1.9 mmol, 37%) as a colourless oil.

R_f: 0.19 (20% methanol in dichloromethane) – purple-brown spot (with vanillin)

^{1}H NMR (600 MHz, $CDCl_3$): δ 7.24 – 7.21 (m, 2H), 6.87 – 6.82 (m, 2H), 3.79 (s, 3H), 3.67 (s, 2H), 2.83 (t, *J* = 6.4 Hz, 2H), 2.52 (t, *J* = 6.3 Hz, 2H), 1.70 (d, *J* = 10.8 Hz, 2H)

^{13}C NMR (151 MHz, $CDCl_3$): δ 158.8, 130.4, 130.0, 114.1, 55.4, 40.9, 35.5, 35.4

Data in agreement with literature.[220]

Amine **3.176**:

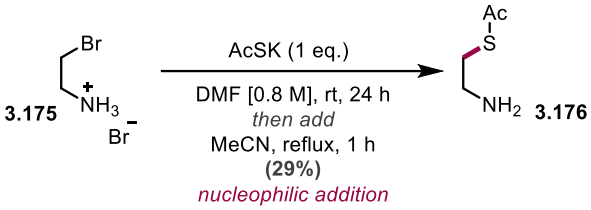

Adapted from the procedure of Krisani Biosciences P Ltd:[221] Under a nitrogen atmosphere, potassium thioacetate (0.35 mL, 4.84 mmol) was added dropwise over 30 seconds to alkyl bromide **3.175** hydrobromide (1.00 g, 4.88 mmol) in dimethylformamide (6 mL) at rt. After 24 h, the reaction was concentrated under reduced pressure, treated with acetonitrile (10 mL) and refluxed. After 1 h, the reaction was cooled to 0 °C and the precipitate was collected via vacuum filtration and washed sequentially with acetonitrile (20 mL) and dichloromethane (20 mL) to yield amine **3.176** (0.17 g, 1.4 mmol, 29%) as a white amorphous solid. Used directly in the next step without further purification.

R_f: 0.23 (20% methanol in dichloromethane) – purple-brown spot (with vanillin)

^{1}H NMR (600 MHz, DMSO): δ 7.92 (s, 2H, H1), 3.07 (t, *J* = 7.2 Hz, 2H, H3), 2.99 – 2.92 (m, 2H, H2), 2.37 (s, 3H, H5)

^{13}C NMR (151 MHz, DMSO): δ 194.8 (C, C4), 38.5 (CH_2, C2) 30.5 (CH_3, C5), 25.7 (CH_3, C3)

Data in agreement with literature.[221]

Enamine **3.177**:

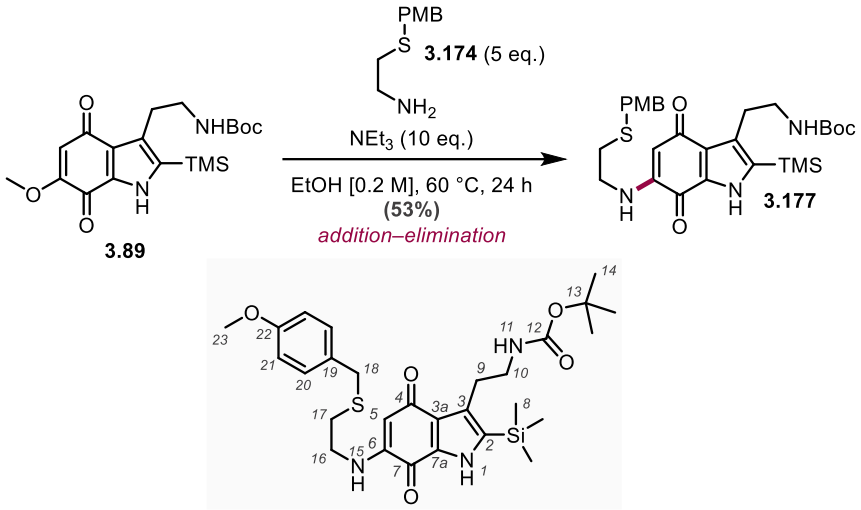

Amine **3.174** (43 mg, 218 µmol) was added to a solution of indolequinone **3.89** (17 mg, 43.3 µmol) and triethylamine (0.1 mL, 0.72 mmol) in ethanol (0.2 mL) at rt and the resulting solution was heated to 60 °C. After 24 h, the red solution was concentrated under reduced pressure, water (1 mL) was added and the aqueous phase was extracted with ethyl acetate (3 × 1 mL). The combined organic phases were washed with brine (1 mL), dried over anhydrous sodium sulfate, filtered and concentrated under reduced pressure. The dark-red residue was purified by silica column chromatography (100% dichloromethane to 5% acetone in dichloromethane) to yield enamine **3.177** (12.7 mg, 22.8 µmol, 53%) as a red foam.

R_f: 0.29 (5% acetone in dichloromethane) – red spot (without stain)

^{1}H NMR (600 MHz, $CDCl_3$) δ 9.01 (s, 1H, H1), 7.25 – 7.21 (m, 2H, H20), 6.87 – 6.83 (m, 2H, H21), 5.88 (t, *J* = 5.9 Hz, 1H, H15), 5.16 (s, 1H, H5), 5.12 (app t, *J* = 5.8 Hz, 1H, H11), 3.78 (s, 3H, H23), 3.69 (s, 2H, H18), 3.38 (q, *J* = 6.3 Hz, 3H, H10), 3.22 (q, *J* = 6.4 Hz, 2H, H16), 2.95 (t, *J* = 6.8 Hz, 2H, H9), 2.67 (t, *J* = 6.6 Hz, 2H, H17), 1.40 (s, 9H, H14), 0.37 (s, 9H, H8)

^{13}C NMR (151 MHz, $CDCl_3$) δ 184.8 (C, C4), 171.9 (C, C7), 159.0 (C, C22), 156.2 (C, C12), 147.5 (C, C6), 140.5 (C, C2), 132.4 (C, C3), 131.1 (C, C7a), 130.1 (CH, C20), 129.7 (C, C19), 126.3 (C, C3a), 114.3 (CH, C21), 98.9 (CH, C5), 78.8 (C, C13), 55.4 (CH_3, C23), 41.9 (CH_2, C10), 41.8 (CH_2, C16), 35.7 (CH_2, C18), 29.4 (CH_2, C17), 28.6 (CH_3, C14), 26.8 (CH_2, C9), -0.7 (CH_3, C8)

HRMS-ESI (m/z): Calculated for $C_{28}H_{40}N_3O_5SSi$ [M+H]+, 558.2452; found 558.2437

IR: 3330, 2925, 2850, 1686, 1663, 1596, 1511, 1421, 1365, 1302, 1251, 1176, 1129, 1107, 1034, 911, 845, 793, 763, 735, 699, 663, 649

Sulfide **3.166**:

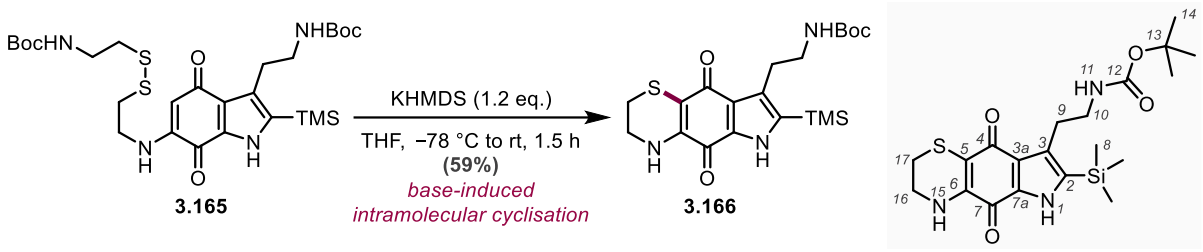

Under a nitrogen atmosphere, a stock solution of potassium bis(trimethylsilyl)amide (0.013 mL, 9.1 µmol, 0.7 M in toluene) in tetrahydrofuran (0.14 mL) was added to a solution of enamine **3.165** (4.8 mg, 7.83 µmol) in tetrahydrofuran (0.06 mL) at −78 °C. After 1 h, the reaction was warmed to 0 °C. After 30 minutes, the ice-bath was removed. After 5 minutes, saturated aqueous ammonium chloride (0.4 mL) was added and the aqueous phase was extracted with ethyl acetate (4 × 0.4 mL). The combined organic phases were passed through a pipette containing magnesium sulfate and concentrated under reduced pressure. The blue solid was purified by silica column chromatography (100% pentane to 20% acetone in pentane) to yield sulfide **3.166** (2.0 mg, 4.59 µmol, 59%) as a blue foam.

R_f: 0.30 (20% acetone in pentane) – blue spot (without stain)

^{1}H NMR (600 MHz, $CDCl_3$): δ 8.86 (s, 1H, H1), 5.69 (s, 1H, H15), 4.91 (s, 1H, H11), 3.73 – 3.68 (m, 2H, H16), 3.36 (q, *J* = 6.7 Hz, 2H, H10), 2.94 – 2.90 (m, 4H, H9 and H17), 1.40 (s, 9H, H14), 0.36 (s, 9H, H8)

^{13}C NMR (151 MHz, $CDCl_3$): δ 180.5 (C, C4 or C7), 169.5 (C, C4 or C7), 156.0 (C, C12), 139.7 (C, C6), 139.0 (C, C2), 132.7 (C, C3), 130.9 (C, C7a), 125.3 (C, C3a), 107.3 (C, C5), 78.7 (C, C13), 42.1 (CH_2, C16), 41.4 (CH_2, C10), 28.4 (CH_3, C14), 27.1 (CH_2, C9), 23.9 (CH_2, C17), -0.9 (CH_3, C8)

^{1}H NMR (600 MHz, CD_3OD): δ 3.68 – 3.56 (m, 2H, H16 or H17), 3.25 (t, *J* = 7.0 Hz, 2H, H10), 2.93 – 2.87 (m, 4H, H9 and H16 or H17), 1.40 (s, 9H, H14), 0.36 (s, 9H, H8)

^{13}C NMR (151 MHz, CD_3OD): δ 182.6 (C, C4 or C7), 170.7 (C, C4 or C7), 158.3 (C, C12), 142.6, 140.4, 133.4, 132.8, 126.1, 105.8, 79.8, 43.4 (CH_2, C16 or C17), 42.6 (CH_2, C10), 28.8 (CH_3, C14), 27.8 (CH_2, C9 or C16 or C17), 24.4 (CH_2, C9 or C16 or C17), -0.4 (CH_3, C8)

HRMS-ESI (m/z): Calculated for $C_{20}H_{30}N_3O_4SSi$ [M+H]+, 436.1721; found 436.1706

IR: 3743, 3326, 2958, 1696, 1686, 1648, 1621, 1583, 1537, 1506, 1457, 1417, 1366, 1340, 1271, 1255, 1179, 1140, 1075, 1050, 911, 862, 844, 810, 764, 738, 701, 669, 647, 631, 613

Cystamine **3.153**:

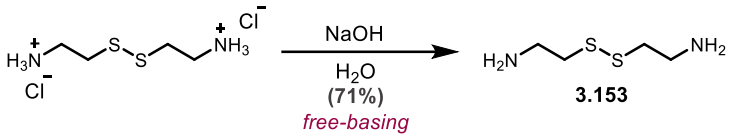

Adapted from the procedure of Monisha et al.: [222] 10 M NaOH solution (15 mL) was added over 30 minutes to cystamine **3.153** dihydrochloride (8.70 g, 38.6 mmol) in water (30 mL) at 0 ° C. Once added, the solution was stirred for a further 2 h at 0 ° C. The aqueous layer was extracted with dichloromethane (100 mL). The organic layer was dried over anhydrous sodium sulfate, filtered and concentrated under reduced pressure to yield cystamine **3.153** (4.18 g, 27.5 mmol, 71%) as a colourless oil.

R_f: 0.45 (20% methanol in dichloromethane) – blue spot (with PMA)

^{1}H NMR (400 MHz, $CDCl_3$): δ 3.02 – 2.97 (m, 4H), 2.77 – 2.72 (m, 4H), 1.25 (s, 4H)

^{13}C NMR (101 MHz, $CDCl_3$): δ 42.7, 40.7

Data in agreement with literature.[222]

Sulfide **3.166**:

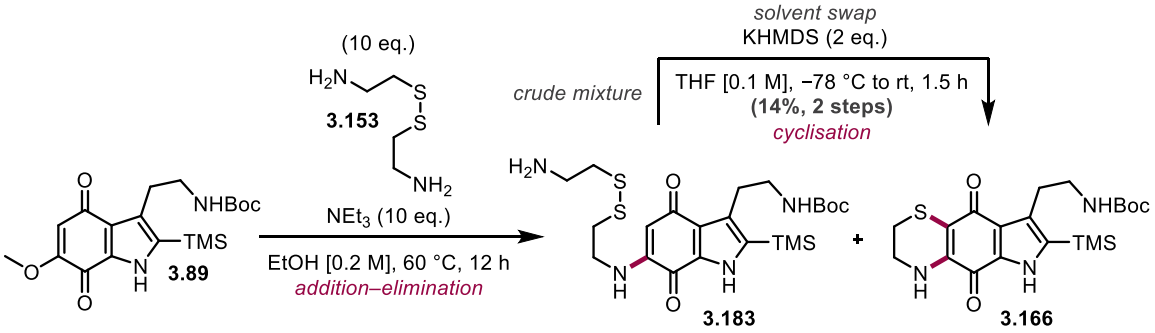

Cystamine **3.153** (3.61 mg, 23.7 mmol) was added to a solution of indolequinone **3.89** (0.93 g, 2.37 mmol) and triethylamine (3.3 mL, 23.7 mmol) in distilled ethanol (11.8 mL) at rt and the resulting reaction mixture was heated to 60 °C. After 24 h, the red solution was concentrated under reduced pressure. The dark-residue was azeotropically dried with toluene (3 × 10 mL), redissolved in tetrahydrofuran (20.1 mL) and cooled to −78 °C. Under a nitrogen atmosphere, bis(trimethylsilyl)amide (4 mL, 4.0 mmol, 1 M in tetrahydrofuran) was added dropwise over 1 minute. After 1 h, the reaction was warmed to 0 °C. After 30 minutes, the ice-bath was removed. After 5 minutes, saturated aqueous ammonium chloride (10 mL) was added and the aqueous phase was extracted with ethyl acetate (3 × 30 mL). The combined organic phases were washed with brine (20 mL), dried over anhydrous sodium sulfate, filtered and concentrated under reduced pressure. The brown residue was purified by silica column chromatography (100% pentane to 20% acetone in pentane) to yield sulfide **3.166** (0.12 g, 0.28 mmol, 14% over two steps) as a blue foam.

Refer back to page 290 for characterisation.

Sulfide **3.166**:

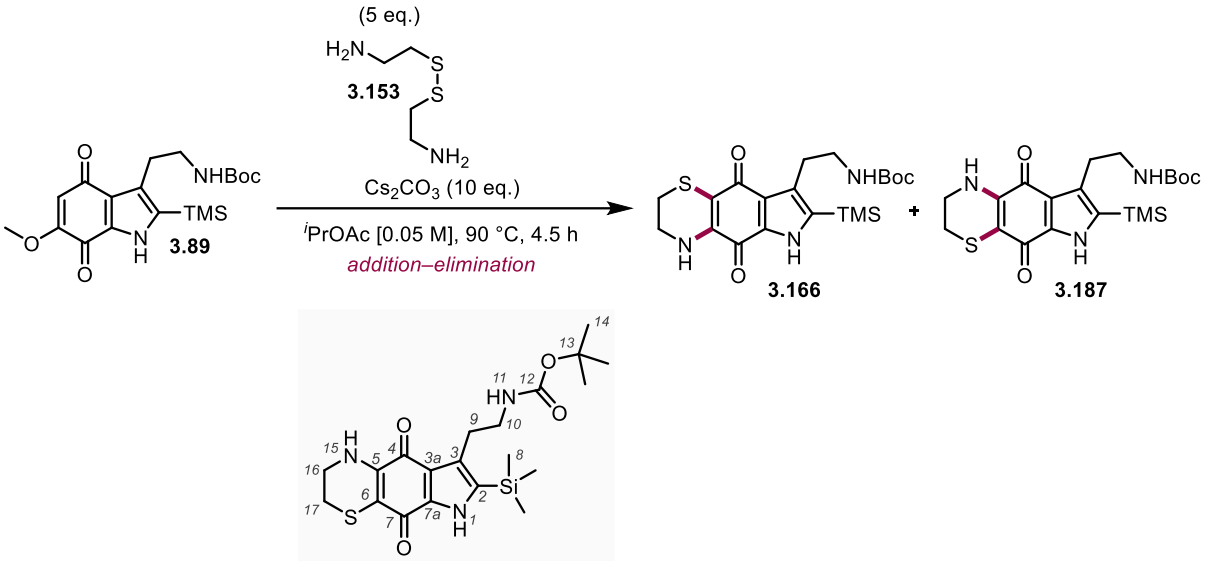

Cystamine **3.153** (40 mg, 263 µmol) and caesium carbonate (0.17 g, 522 µmol) were sequentially added to indolequinone **3.89** (20 mg, 51.0 µmol) in isopropyl acetate (1 mL) at rt and the resulting mixture was heated to 90 °C. After, 4.5 h the dark-purple solution was cooled to rt, diluted by the addition of water (1 mL) and the aqueous phase was extracted with ethyl acetate (3 × 2 mL). The combined organic phases were washed with brine (2 mL), dried over anhydrous sodium sulfate, filtered and concentrated under reduced pressure. The dark purple residue was purified by silica column chromatography (100% pentane to 20% acetone in pentane) to yield sulfide **3.187** and sulfide **3.166** (4.2 mg, 9.7 µmol, 19% combined yield) as a blue residue, as an inseparable mixture. The regioisomeric ratio of the sulfides was determined by ^{1}H NMR resonances (δ 3.73 – 3.68 ppm (**3.166**) and 3.79 – 3.75 ppm (**3.187**), CH_2) to be 1.0:2.6 (**3.166**:**3.187**). Additionally, sulfide **3.188** (0.7 mg, 1.9 µmol, 4%) isolated as a blue residue.

*Sulfide **3.187**:*

R_f: 0.30 (20% acetone in pentane) – blue spot (without stain)

^{1}H NMR (500 MHz, $CDCl_3$): δ 9.38 (s, 1H), 4.73 (s, 1H), 3.79 – 3.75 (m, 2H), 3.36 (t, *J* = 5.8 Hz, 3H*), 2.96 – 2.91 (m, 3H*), 2.88 (t, *J* = 6.8 Hz, 2H), 1.41 (s, 9H), 0.35 (s, 9H)

overlaps with signals of sulfide **3.166*

^{13}C NMR (151 MHz, $CDCl_3$) *[signals of the non-quaternary carbons]*:* 42.7, 41.2, 28.6 (C, C14), 27.4, 23.6, -0.5 (CH_3, C8)

**sample too weak to observe and assign quaternary carbons*

IR:* 3341, 2977, 2956, 2917, 2849, 1692, 1680, 1658, 1650, 1613, 1581, 1536, 1502, 1469, 1453, 1415, 1391, 1366, 1337, 1272, 1252, 1170, 1141, 1101, 1076, 910, 845, 761, 733, 698, 663, 644, 618

of the mixture with sulfide **3.166*

*Sulfide **3.188**:*

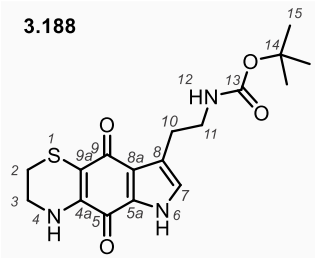

R_f: 0.24 (10% acetone in dichloromethane) – blue spot (without stain)

^{1}H NMR (500 MHz, $CDCl_3$): δ 9.87 (br s, 1H, H6), 6.78 (d, *J* = 2.4 Hz, 1H, H7), 3.74 – 3.67 (m, 2H, H2 or H3), 3.39 (t, *J* = 7.0 Hz, 2H, H11), 2.93 – 2.88 (m, 4H, H10 and H2 or H3), 1.42 (s, 9H, H15)

^{13}C NMR (126 MHz, $CDCl_3$): δ 180.3 (C, C5 or C9), 169.8 (C, C5 or C9), 156.4 (C, C13), 139.8, 128.7, 125.3 (CH, C7), 124.8, 124.7, 106.8, 79.5 (C, C14), 42.2 (CH_2, C2 or C3), 41.0 (CH_2, C11), 28.6 (CH_3, C15), 26.1 (CH_2, C10 and C2 or C3), 24.0 (CH_2, C10 and C2 or C3)

HRMS-ESI (m/z): Calculated for $C_{12}H_{14}N_3O_2S$ *[Boc-group removed in situ]* [M+H]+, 264.0801; found 264.0808

IR: 3339, 2977, 2929, 2884, 2870, 1658, 1625, 1580, 1548, 1504, 1453, 1402, 1366, 1339, 1273, 1254, 1169, 1145, 1103, 1018, 966, 911, 847, 828, 787, 736, 658, 619

Sulfone **3.190**:

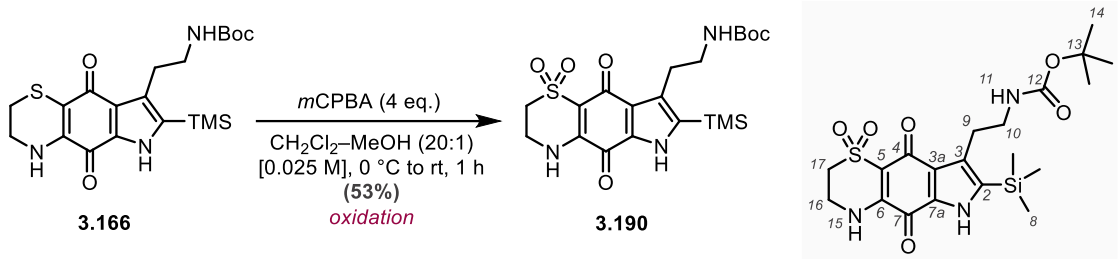

meta-Chloroperoxybenzoic acid (97% purity, 114 mg, 0.643 mmol) was added portion-wise over 1 minute to a solution of sulfide **3.166** (70 mg, 0.161 mmol) in a 20:1 dichloromethane–methanol (6.41 mL) [0.025 M] at 0 °C. After 1 minute, a colour change from blue to orange was observed. The ice-bath was removed and the reaction allowed to warm to rt. The reaction was monitored by TLC to ensure that intermediate sulfoxide **3.191** was consumed (R_f = 0.29, 5% methanol in dichloromethane). After 1 hour, the reaction was quenched by addition of 1:1 saturated aqueous thiosulfate–bicarbonate solution (30 mL). The aqueous phase was extracted with dichloromethane (3 × 30 mL). The combined organic phases were washed with brine (20 mL), dried over anhydrous sodium sulfate, filtered and concentrated under reduced pressure. The red-orange solid was dry loaded onto Celite and purified by silica column chromatography (multiplication factor = 100, CV = 15, 100% dichloromethane to 5% methanol in dichloromethane, increasing by 1% methanol every 2CV) to yield sulfone **3.190** (40 mg, 85.5 µmol, 53%) as a red-orange amorphous solid.

R_f: 0.45 (5% methanol in dichloromethane)

^{1}H NMR (700 MHz, $CDCl_3$): δ 9.09 (s, 1H, H1), 6.70 (s, 1H, H15), 4.88 (s, 1H, H11), 4.08 – 4.05 (m, 2H, H16), 3.35 (q, *J* = 6.8 Hz, 2H, H10), 3.31 – 3.28 (m, 2H, H17), 2.99 – 2.94 (m, 2H, H9), 1.41 (s, 9H, H14), 0.41 (s, 9H, H8)

^{1}H NMR (600 MHz, CD_3OD): δ 3.99 – 3.93 (m, 2H, H16), 3.32 (app d *[partly obscured by NMR solvent reference peak]*, *J* = 4.3 Hz, 2H, H17), 3.26 (t, *J* = 7.1 Hz, 2H, H10), 2.96 (t, *J* = 7.1 Hz, 2H, H9), 1.40 (s, 9H, H14), 0.39 (s, 9H, H8)

^{13}C NMR (151 MHz, CD_3OD): δ 179.1 (C, C4), 168.4 (C, C7), 158.3 (C, C12), 149.5 (C), 144.6 (C, C2), 134.2 (C, C3), 132.1 (C), 126.3 (C), 109.9 (C, C5), 79.8 (C, C13), 50.0 (CH_2, C17), 42.3 (CH_2, C10), 40.6 (CH_2, C16), 28.8 (CH_3, C14), 27.9 (CH_2, C9), -0.5 (CH_3, C8)

HRMS-ESI (m/z): Calculated for $C_{20}H_{29}N_3O_6SSiNa$ [M+Na]+, 490.1439; found 490.1437

IR: 3299, 2924, 2853, 1686, 1620, 1583, 1513, 1430, 1415, 1350, 1315, 1285, 1252, 1190, 1133, 1116, 1074, 1028, 913, 842, 771, 742, 710, 645

Sulfone **3.190**:

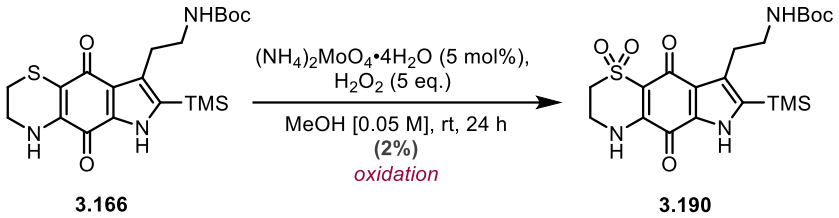

3.166 **3.190**

Hydrogen peroxide (10 µL, 97.9 µmol) was added to a solution of sulfide **3.166** (8.7 mg, 20.0 µmol) and ammonium molybdate tetrahydrate (1.2 mg, 0.971 µmol) in methanol (0.4 mL) at rt. After 24 h, the reaction was diluted by the addition of water (1 mL) and the aqueous phase was extracted with dichloromethane (3 × 2 mL). The combined organic phases were dried over anhydrous sodium sulfate, filtered and concentrated under reduced pressure. The brown residue was purified by silica column chromatography (100% dichloromethane to 5% methanol in dichloromethane) to yield sulfone **3.190** (0.2 mg, 0.43 µmol, 2%) as a red-orange residue, and sulfonate ester **3.192** (0.5 mg, 1.0 µmol, 5%) as a pink residue.

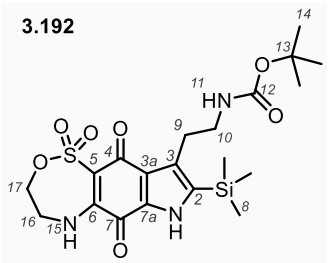

R_f: 0.50 (5% methanol in dichloromethane)

^{1}H NMR (600 MHz, $CDCl_3$): δ 9.03 (s, 1H, H1), 6.65 (t, *J* = 6.5 Hz, 1H, H15), 4.86 (s, 1H, H11), 4.24 – 4.18 (m, 2H, H16), 3.95 (t, *J* = 5.4 Hz, 2H, H17), 3.35 (app q, *J* = 6.8 Hz, 2H, H10), 2.95 (t, *J* = 7.0 Hz, 2H, H9), 1.41 (s, 9H, H14), 0.39 (s, 9H, H8)

^{13}C NMR (151 MHz, $CDCl_3$): δ 179.9 (C, C4 or C7), 166.8 (C, C4 or C7), 156.1 (C, C12), 147.8 (C), 142.9 (C, C2), 138.8 (C), 133.8 (C, C3), 130.4 (C), 126.1 (C, C3a), 79.0 (C, C13), 70.0 (CH_2, C17), 41.3 (CH_2, C10), 40.1 (CH_2, C16), 28.6 (CH_3, C14), 27.3 (CH_2, C9), -0.9 (C, C8)

^{1}H NMR (600 MHz, CD_3OD): δ 4.20 (br s, 2H, H16), 4.01 (t, *J* = 5.4 Hz, 2H, H17), 3.26 (app t, *J* = 6.8 Hz, 2H, H10 *[partly hidden by NMR solvent reference signal]*), 2.95 (t, *J* = 7.1 Hz, 2H, H9), 1.40 (s, 9H, H14), 0.38 (s, 9H, H8)

^{13}C NMR (151 MHz, CD_3OD) *[signals of the non-quaternary carbons]*:* δ 71.41 (CH_2, C17), 42.30 (CH_2, C10), 41.12 (CH_2, C16), 28.79 (CH_3, C14), 27.88 (CH_2, C9), -0.48 (CH_3, C8)

**sample too weak to observe and assign quaternary carbons*

HRMS-ESI (m/z): Calculated for (1) $C_{20}H_{29}N_3O_7SSiNa$ [M+Na]+, 506.1388; found 506.1380**,** (2) $C_{20}H_{29}N_3O_7SSiK$ [M+K]+, 522.1127; found 522.1149

IR: 2961, 2926, 2854, 1712, 1444, 1262 (strong, sharp), 1101 (strong, broad), 1031, 846, 808, 700, 652

Sulfide **3.226**:

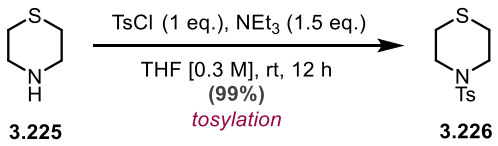

Adapted from the procedure of Gao et al.:[223] Tosyl chloride (0.93 g, 4.86 mmol) was added to a solution of sulfide **3.225** (0.46 mL, 4.85 mmol) and triethylamine (1 mL, 7.17 mmol) in tetrahydrofuran (32 mL) at 0 °C. The ice-bath was removed and the reaction was allowed to warm to rt. After 12 h, the reaction mixture was filtered through filter paper and the filtrate was concentrated under reduced pressure to yield sulfide **3.226** (1.24 g, 4.82 mmol, 99%) as an off-white amorphous solid.

R_f: 0.31 (20% diethyl ether in pentane) – white spot (with potassium permanganate)

^{1}H NMR (400 MHz, $CDCl_3$): δ 7.64 – 7.60 (m, 2H), 7.35 – 7.31 (m, 2H), 3.32 (dd, *J* = 6.7, 3.6 Hz, 4H), 2.73 – 2.68 (m, 4H), 2.44 (s, 3H)

^{13}C NMR (126 MHz, $CDCl_3$): δ 143.9, 133.9, 129.9, 127.6, 48.0, 27.4, 21.7

Data in agreement with literature.[224]

Vinyl sulfone **3.23**:

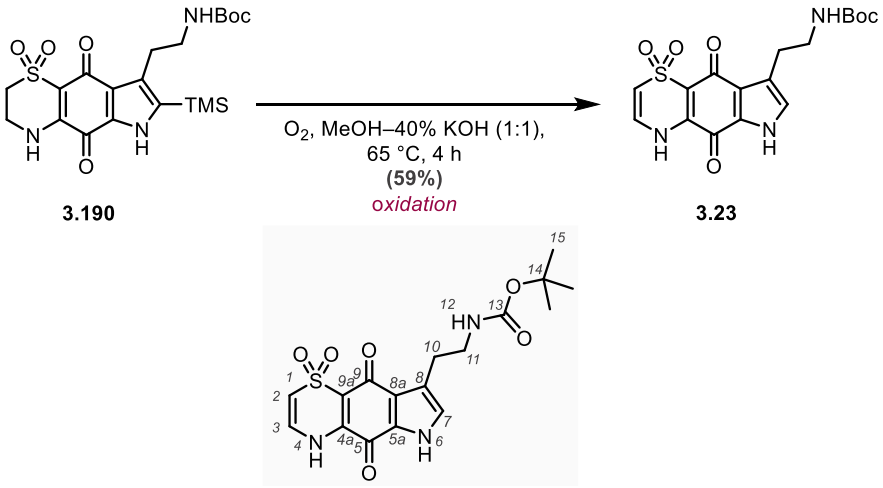

3.190 **3.23**

Adapted from the procedure of Pouwer et al.:[85] A freshly prepared 1 M KOH aqueous solution (1.92 mL, 1.92 mmol) was added dropwise over 1 minute to a solution of sulfone **3.190** (18 mg, 38.5 µmol) in methanol (1.92 mL) in a vial at rt. The resulting solution was sparged with an oxygen balloon, then kept under an oxygen atmosphere using an additional oxygen balloon and heated to 65 °C. After 4 h, the reaction mixture was cooled to rt and added to a 1 M solution of HCl (20 mL); a colour change from dark orange to yellow was observed. The aqueous phase was extracted with a 5% methanol in dichloromethane solution (3 × 30 mL). The combined organic phases were washed with brine (10 mL), dried over anhydrous sodium sulfate, filtered and concentrated under reduced pressure. The yellow-brown solid was purified by silica column chromatography (multiplication factor = 200, CV = 6, 100% dichloromethane to 5% methanol in dichloromethane, increasing by 1% methanol every 2CV) to yield vinyl sulfone **3.23** (9 mg, 22.9 µmol, 59%) as a yellow-orange solid.

R_f: 0.20 (5% methanol in dichloromethane) –yellow spot (without stain)

^{1}H NMR (600 MHz, CD_3OD): δ 7.19 (s, 1H, H7), 7.13 (d, *J* = 8.8 Hz, 1H, H3), 6.34 (d, *J* = 8.8 Hz, 1H, H2), *[~3.33 (2D NMR spectroscopic analysis identifies H11 underneath CD_3OD reference peak),]* 2.95 (t, *J* = 6.9 Hz, 2H, H10), 1.42 (s, 9H, H15)

^{13}C NMR (151 MHz, CD_3OD): δ 180.4 (C, C9), 168.6 (C, C5), 158.5 (C, C13), 141.6 (C, C4a), 131.5 (CH, C3), 129.8 (CH, C7), 129.5 (C, C5a), 126.5 (C, C8), 125.2 (C, C8a), 115.8 (C, C9a), 111.8 (CH, C2), 79.9 (C, C14), 41.4 (CH_2, C11), 28.7 (CH_3, C15), 27.1 (CH_2, C10)

HRMS-ESI (m/z): Calculated for $C_{17}H_{19}N_3O_6SNa$ [M+Na]+, 411.1333; found 411.1279

Characterised in a different solvent to literature.

Sulfoxide **3.191**:

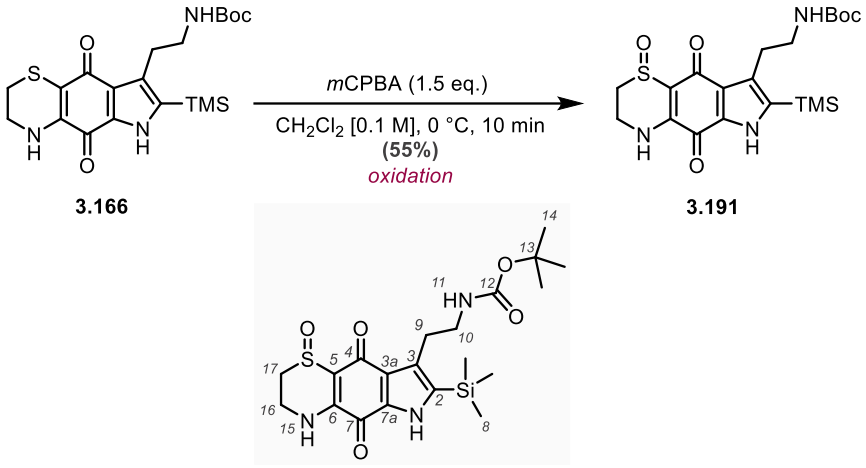

meta-Chloroperoxybenzoic acid (97% purity, 12.3 mg, 68.9 µmol) was added portion-wise over 1 minute to a solution of sulfide **3.166** (20 mg, 45.9 µmol) in dichloromethane (0.46 mL) at 0 °C; a colour change from blue to orange was observed. After 10 minutes, the reaction was quenched by addition of 1:1 saturated aqueous thiosulfate–bicarbonate solution (30 mL). The aqueous phase was extracted with ethyl acetate (3 × 30 mL). The combined organic phases were washed with brine (20 mL), dried over anhydrous sodium sulfate, filtered and concentrated under reduced pressure. The red-orange solid was dry loaded onto Celite and purified by silica column chromatography (multiplication factor = 100, CV = 5, 100% dichloromethane to 5% methanol in dichloromethane, increasing by 1% methanol every 2CV) to yield sulfoxide **3.191** (40 mg, 85.5 µmol, 53%) as a red-orange amorphous solid.

R_f: 0.29 (5% methanol in dichloromethane)

^{1}H NMR (600 MHz, CD_3OD): δ 3.93 (ddd, *J* = 14.7, 3.9, 2.7 Hz, 1H, H16), 3.72 (td, *J* = 14.6, 2.8 Hz, 1H, H16'), 3.31 – 3.26 (m, 1H, H10), 3.19 (dt, *J* = 14.1, 2.7 Hz, 1H, H17), 2.99 (dq, *J* = 22.3, 6.5 Hz, 2H, H9), 2.50 (td, *J* = 14.3, 3.9 Hz, 1H, H17'), 1.40 (s, 9H, H14), 0.40 (s, 9H, H8)

^{13}C NMR (151 MHz, CD_3OD): δ 181.0 (C, C7), 169.3 (C, C4), 158.3 (C, C12), 148.4 (C, C6), 144.2 (C, C2), 134.2 (C, C3), 132.9 (C, C7a), 126.4 (C, C3a), 108.6 (C, C5), 79.8 (C, C13), 42.3 (CH_2, C10), 41.3 (CH_2, C17), 31.7 (CH_2, C16), 28.8 (CH_3, C14), 27.9 (CH_2, C9), -0.5 (CH_3, C8)

HRMS-ESI (m/z): Calculated for $C_{20}H_{29}N_3O_5SSiNa$ [M+Na]+, 474.1489; found 474.1500

IR: 2957, 2926, 1580, 1548, 1535, 1513, 1493, 1442, 1424, 1410, 1367, 1335, 1267, 1177, 1105, 1067, 1026, 989, 928, 891, 850, 814, 737, 705, 640

Thiaplakortone A **1.12**:

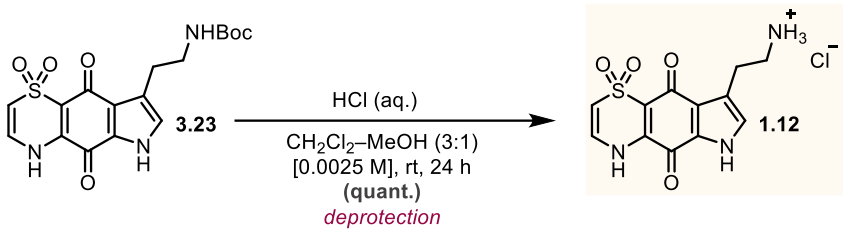

Adapted from the procedure of Pouwer et al.:[85] Concentrated hydrochloride solution (aqueous, 37 wt%, 0.06 mL, 0.7 mmol) in methanol (0.5 mL) was added dropwise over 1 minute to a solution vinyl sulfone **3.23** (2 mg, 5.08 µmol) in dichloromethane (1.5 mL) at rt. After 24 h, the reaction was concentrated under a stream of nitrogen to yield thiaplakortone A **1.12**•HCl (1.7 mg, 5.08 µmol, quant.) as a yellow-orange amorphous solid. Thiaplakortone A **1.12**•HCl was further purified by reverse-phase HPLC (column (1), 100% 0.005 M aqueous HCl) for biological testing.

R_f: 0.15 (7.5% (7 M NH_3 in methanol) in dichloromethane) – orange spot (without stain)

^{1}H NMR (600 MHz, DMSO-d_6): δ 13.07 (s, 1H), 11.08 (s, 1H), 7.80 (s, 3H), 7.38 (s, 1H), 7.07 (d, J = 8.8 Hz, 1H), 6.45 (d, J = 8.8 Hz, 1H), 3.06 (t, J = 7.6 Hz, 2H), 2.98 (t, J = 7.6 Hz, 2H)

^{13}C NMR (151 MHz, DMSO-d_6): δ 178.6, 167.8, 140.0, 130.2, 129.2, 128.1, 123.3, 121.7, 114.1, 111.7, 38.4, 23.5

HRMS-ESI (m/z): Calculated for $C_{12}H_{12}N_3O_4S$ [M+H]+, 294.0543; found 294.0536

Data in agreement with literature.[85]

Table 5.1. ^{1}H NMR chemical shift comparison between isolated and synthesised thiaplakortone A **1.12** (600 MHz, DMSO-d_6)**.**

thiaplakortone numbering system

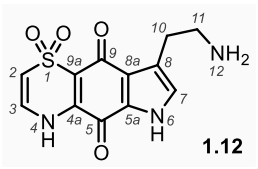

1.12

	^{1}H NMR (600 MHz, DMSO-d_6): δ		
position	***isolated 1.12•TFA (Quinn et al., 2013)***	***synthetic 1.12•HCl (Quinn et al., 2014)***	***synthetic 1.12•HCl (Anderson et al., 2025)***
2	6.43 (d, *J* = 9.0 Hz)	6.46 (d, *J* = 8.8 Hz)	6.45 (d, *J* = 8.8 Hz)
3	7.06 (dd, *J* = 9.0, 5.4 Hz)	7.07 (dd, *J* = 8.8, 5.7 Hz)	7.07 (d, *J* = 8.8 Hz)
4	11.07 (d, *J* = 5.4 Hz)	11.11 (d, *J* = 5.1 Hz)	11.08 (br s)
6	13.09 (s)	13.11 (br s)	13.07 (br s)
7	7.36, (d, *J* = 2.4 Hz)	7.40, (d, *J* = 2.6 Hz)	7.38, (s)
10	2.97 (t, *J* = 7.8 Hz)	3.01–2.95 (m)	2.98 (t, *J* = 7.6 Hz)
11	3.05 (m)	3.09–3.01 (m)	3.06 (t, *J* = 7.6 Hz)
12	7.84 (br s)	7.92 (br s)	7.80 (br s)

Table 5.2. ^{13}C NMR chemical shift comparison between isolated and synthesised thiaplakortone A **1.12** (151 MHz, DMSO-d_6).

	^{13}C NMR (151 MHz, DMSO-d_6): δ		
position	*isolated 1.12•TFA (Quinn et al., 2013)*	*synthetic 1.12•HCl (Quinn et al., 2014)*	*synthetic 1.12•HCl (Anderson et al., 2025)*
2	111.7 (CH)	111.6	111.7
3	130.2 (CH)	130.2	130.2
4a	139.9 (C)	139.9	140.0
5	167.8 (C)	167.7	167.8
5a	128.0 (C)	128.0	128.1
7	129.2 (CH)	129.2	129.2
8	121.7 (C)	121.8	121.7
8a	123.3 (C)	123.3	123.3
9	178.5 (C)	178.5	178.6
9a	114.1 (C)	114.1	114.1
10	23.4 (CH_2)	23.4	23.5
11	38.4 (CH_2)	38.2	38.4

Thiaplakortone B **3.1**:

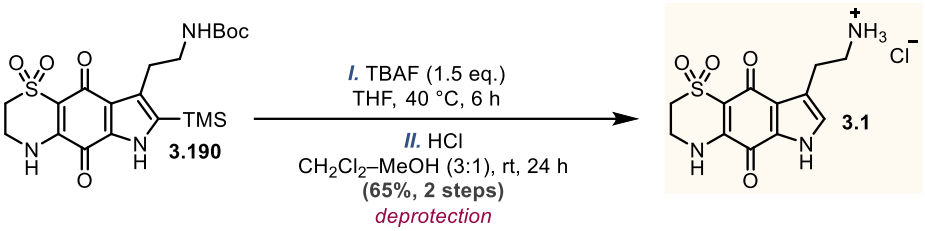

Tetrabutylammonium fluoride (0.025 mL, 25 µmol, 1 M in tetrahydrofuran) was added to sulfone **3.190** (7.3 mg, 15.6 µmol) in tetrahydrofuran (0.5 mL) at rt and the resulting solution was heated to 60 °C. After 6 h, the reaction was cooled to rt, quenched by addition of saturated aqueous sodium bicarbonate solution (2 mL) and the aqueous phase was extracted with ethyl acetate (3 × 5 mL). The combined organic phases were washed with brine (2 mL), dried over anhydrous sodium sulfate, filtered, concentrated under reduced pressure. The crude material was redissolved in dichloromethane (1.5 mL). Concentrated hydrochloride solution (aqueous, 37 w%, 0.06 mL, 0.7 mmol) in methanol (0.5 mL) was added dropwise over 1 minute at rt. After 24 h, the reaction was concentrated under a stream of nitrogen to yield thiaplakortone B **3.1**•HCl (4.0 mg, 10.1 µmol, 65% over two steps) as a yellow-orange amorphous solid. Thiaplakortone B **3.1**•HCl was further purified by reverse-phase HPLC (column (1), 100% 0.005 M aqueous HCl) for biological testing.

R_f: 0.16 (7.5% (7 M NH_3 in methanol) in dichloromethane) – orange spot (without stain)

^{1}H NMR (600 MHz, DMSO-d_6): δ 12.90 (s, 1H), 8.93 (d, *J* = 3.7 Hz, 1H), 7.82 (s, 3H), 7.34 (d, *J* = 2.9 Hz, 1H), 3.83 – 3.77 (m, 2H), 3.28 (d, *J* = 5.3 Hz, 1H), 3.04 (dq, *J* = 11.6, 6.3 Hz, 2H), 2.96 (t, *J* = 7.6 Hz, 2H).

^{13}C NMR (151 MHz, DMSO-d_6):* δ 176.1, 167.9, 147.3, 129.6, 127.7, 124.2, 121.4, 108.6, 48.4, 38.6, 23.4

C3 (Table 5.4**) hidden under DMSO-d_6*

HRMS-ESI (m/z): Calculated for $C_{12}H_{14}N_3O_4S$ [M+H]+, 296.0700; found 296.0685

Data in agreement with literature.

Table 5.3. ^{1}H NMR chemical shift comparison between isolated and synthesised thiaplakortone B **3.1** (600 MHz, DMSO-d_6)**.**

thiaplakortone numbering system

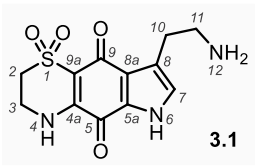

3.1

	^{1}H NMR (600 MHz, DMSO-d_6): δ	
position	***isolated 3.1•TFA (Quinn et al., 2013)***	***synthetic 3.1•HCl (Anderson et al., 2025)***
2	3.28 (m)	3.28 (m)
3	3.81 (m)	3.80 (m)
4	8.92 (s)	8.93 (s)
6	12.89 (s)	12.90 (s)
7	7.32 (d, *J* = 2.4 Hz)	7.34 (d, *J* = 2.9 Hz)
10	2.94 (t, *J* = 7.2 Hz)	2.96 (t, *J* = 7.6 Hz)
11	3.04 (m)	3.04 (dq, *J* = 11.6, 6.3 Hz)
12	7.76 (br s)	7.82 (br s)

Table 5.4. ^{13}C NMR chemical shift comparison between isolated and synthesised thiaplakortone B **3.1** (151 MHz, DMSO-d_6)**.**

	^{13}C NMR (151MHz, DMSO-d_6): δ	
position	***isolated 3.1•TFA (Quinn et al., 2013)***	***synthetic 3.1•HCl (Anderson et al., 2025)***
2	48.4 (CH_2)	48.4
3	39.0 (CH_2)	*under DMSO-d_6 signal*
4a	147.3 (C)	147.3
5	167.9 (C)	167.9
5a	127.6 (C)	127.7
7	129.6 (CH)	129.6
8	121.4 (C)	121.4
8a	124.2 (C)	124.2
9	176.1 (C)	176.1
9a	108.6 (C)	108.6
10	23.4 (CH_2)	23.4
11	38.6 (CH_2)	38.6

Sulfide **3.247**:

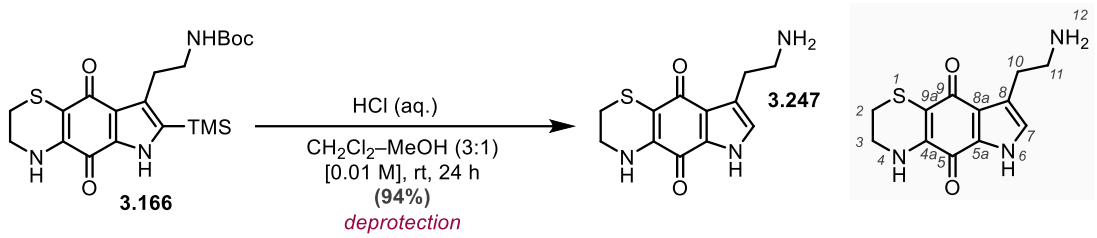

Concentrated hydrochloride solution (aqueous, 37 w%, 0.06 mL, 0.7 mmol) in methanol (0.5 mL) was added dropwise over 1 minute to a solution sulfide **3.166** (8.3 mg, 20.0 µmol) in dichloromethane (1.5 mL) at rt. After 24 h, the reaction was concentrated under a stream of nitrogen and the crude material was redissolved in ammonium hydroxide (30 w%, 2 mL) to achieve a pH of 11. The aqueous phase was extracted with ethyl acetate (3 × 10 mL). The combined organic phases were washed with brine (5 mL), dried over anhydrous sodium sulfate, filtered and concentrated under reduced pressure to yield sulfide **3.247** (4.7 mg, 17.8 µmol, 94%) as a blue amorphous solid. Sulfide **3.247** was further purified by reverse-phase HPLC (column (1), 0% to 50% acetonitrile in 0.005 M aqueous HCl) to yield sulfide **3.247•HCl** for biological testing.

*Sulfide **3.247**:*

R_f: 0.17 (7.5% (7 M NH_3 in methanol) in dichloromethane) – blue spot (without stain)

HRMS-ESI (m/z): Calculated for $C_{12}H_{13}N_3O_2SNa$ [M+Na]+, 286.0621; found 286.0620

IR: 3085, 2923, 2853, 2508, 2349, 2295, 2284, 2241, 2074, 1680, 1667, 1578, 1547, 1507, 1452, 1430, 1399, 1356, 1336, 1268, 1213, 1180, 1125, 1034, 1008, 983, 942, 927, 903, 830, 756, 694, 664, 614

*Sulfide **3.247•HCl**:*

^{1}H NMR (600 MHz, CD_3OD): δ 6.98 (s, 1H, H7), 3.67 (t, *J* = 4.7 Hz, 2H, H2 or H3), 3.19 (t, *J* = 7.3 Hz, 2H, H11), 3.01 (t, *J* = 7.3 Hz, 2H, H10), 2.90 (t, *J* = 4.7 Hz, 2H, H2 or H3)

^{13}C NMR (151 MHz, CD_3OD): δ 182.1 (C, C5 or C9), 171.0 (C, C5 or C9), 142.7 (C, C4a or C9a), 130.5 (C, C5a), 127.1 (CH, C7), 125.5 (C, C8a), 121.6 (C, C8), 105.1 (C, C4a or C9a), 43.5 (CH_2, C2 or C3), 41.0 (CH_2, C11), 24.9 (CH_2, C10), 24.3 (CH_2, C2 or C3)

5.2.3. Chapter 4

Nitrobenzene **4.28**:

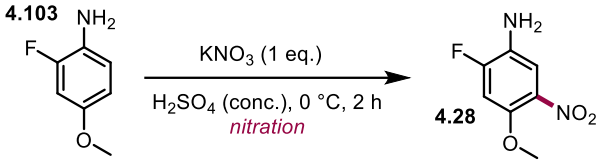

Adapted from the procedure of J2h Biotech Inc:[225] Potassium nitrate (2.15 g, 21.3 mmol) was added portion-wise over 1 minute to a solution of 2-fluoro-4-methoxyaniline **4.103** (3.00 g, 21.3 mmol) in concentrated sulfuric acid (15.6 mL) at 0 °C. After 2 h, the reaction mixture was poured onto ice-water (150 mL) and treated with a 10 M NaOH solution (30 mL) to achieve a pH of 7. The aqueous phase was extracted with ethyl acetate (3 × 100 mL). The combined organic phases were dried over sodium sulfate, filtered and concentrated under reduced pressure to yield nitrobenzene **4.28** as a yellow amorphous solid. Used in the next step without further purification.

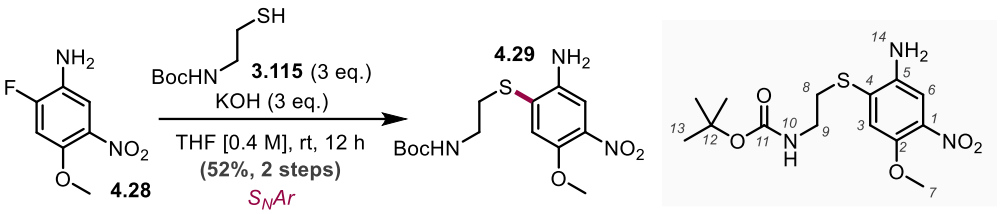

Adapted from the procedure of de Vicente et al.:[214] A 1 M aqueous potassium hydroxide solution (10 mL, 5.50 mmol) was added dropwise over 1 minute to a solution of nitrobenzene **4.28** (0.55 g, 2.95 mmol) and aminothiol **3.115** (1.51 mL, 8.86 mmol) in tetrahydrofuran (7.4 mL) at rt. After 12 h, the crude mixture was concentrated under reduced pressure to remove the organic layer and the aqueous phase was extracted with ethyl acetate (3 × 30 mL). The combined organic phases were washed with brine (20 mL), dried over anhydrous sulfate, filtered and concentrated under reduced pressure. The crude material was purified by silica column chromatography (100% pentane to 50% diethyl ether in pentane) to yield nitrobenzene **4.29** (0.53 g, 1.5 mmol, 52% over two steps) as a dark-orange oil.

R_f: 0.27 (50% diethyl ether in pentane) – orange spot (without stain)

^{1}H NMR (600 MHz, $CDCl_3$):* δ 7.28 (s, 1H, H6), 7.18 (s, 1H, H3), 4.92 (br s, 1H, H10), 3.92 (s, 3H, H7), 3.31 (app q, *J* = 6.6 Hz, 2H, H9), 3.01 (t, *J* = 6.5 Hz, 2H, H8), 1.42 (s, 9H, H13)

**exchangeable H14 not observed*

^{13}C NMR (151 MHz, $CDCl_3$): δ 155.9 (C, C11), 146.0 (C, C2), 140.3 (C, C1 or C5), 139.4 (C, C1 or C5), 126.5 (C, C4), 119.1 (CH, C3), 111.7 (CH, C6), 79.9 (C, C12), 57.6 (CH_3, C7), 40.3 (CH_2, C9), 34.3 (CH_2, C8), 28.5 (CH_3, C13)

HRMS-ESI (m/z): Calculated for $C_{14}H_{22}N_3O_5S$ [M+H]+, 344.1275; found 344.1271

IR: 656, 3432, 3349, 2980, 2889, 1702, 1605, 1567, 1518, 1461, 1393, 1317, 1253, 1163, 1073, 954, 914, 870, 831, 797, 736, 644

Nitrobenzene **4.40**:

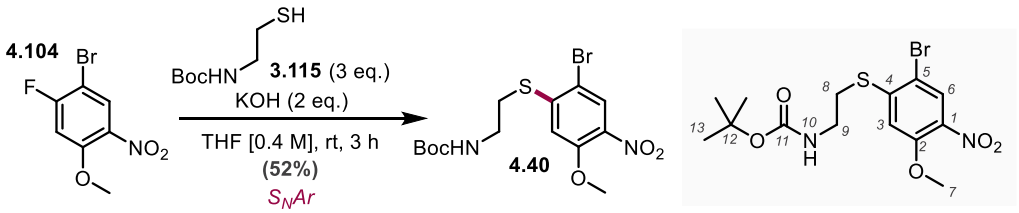

Adapted from the procedure of de Vicente et al.:[214] A 1 M aqueous potassium hydroxide solution (3.7 mL, 3.70 mmol) was added dropwise over 1 minute to a solution of nitrobenzene **4.104** (0.50 g, 2.00 mmol) and aminothiol **3.115** (1.02 mL, 6.00 mmol) in tetrahydrofuran (5 mL) at rt. After 3 h, the crude mixture was concentrated under reduced pressure to remove the organic layer and the aqueous phase was extracted with ethyl acetate (3 × 30 mL). The combined organic phases were washed with brine (20 mL), dried over anhydrous sulfate, filtered and concentrated under reduced pressure. The crude material was purified by silica column chromatography (100% pentane to 20% ethyl acetate in pentane) to yield nitrobenzene **4.40** (0.67 g, 1.6 mmol, 82%) as a pale-yellow amorphous solid.

R_f: 0.23 (20% ethyl acetate in pentane)

^{1}H NMR (600 MHz, $CDCl_3$): δ 8.10 (d, *J* = 1.8 Hz, 1H, H3 or H6), 7.26 (s, 3H, H3 or H6), 4.96 – 4.92 (m, 1H, H10), 4.09 (s, 3H, H7), 3.42 – 3.36 (m, 2H, H9), 3.16 (dd, *J* = 9.1, 6.1 Hz, 2H, H8), 1.44 (s, 9H, H13)

^{13}C NMR (151 MHz, $CDCl_3$): δ 156.0 (C, C11), 153.5 (C, C2), 147.1 (C, C4), 136.4 (C, Ar), 129.8 (CH, C3 or C6), 110.8 (C, Ar), 110.7 (CH, C3 or C6), 80.2 (C, C12), 57.6 (CH_3, C7), 39.8 (CH_2, C9), 31.6 (CH_2, C8), 28.5 (CH_3, C13)

HRMS-ESI (m/z): Calculated for $C_9H_{12}BrN_2O_3S$ *[Boc-group removed in situ]* [M+H]+, 306.9747; found 306.9741

IR: 3650, 2980, 2889, 1701, 1592, 1559, 1507, 1473, 1462, 1382, 1252, 1154, 1073, 954, 817, 736, 656

Propargyl alcohol **4.45**:

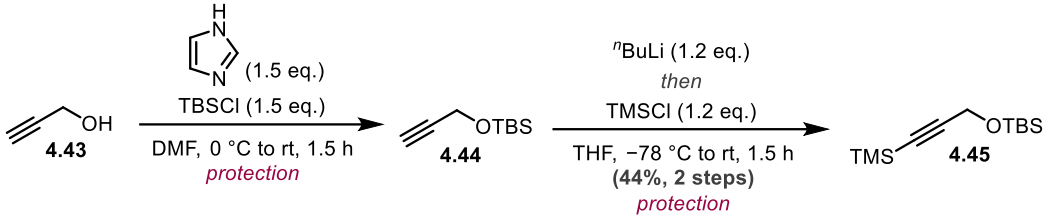

Adapted from the procedure of Higashino et al.:[226] *tert*-Butylchlorodimethylsilane (2.00 g, 13.3 mmol) was added portion-wise over 1 minute a solution of propargyl alcohol **4.43** (0.52 mL, 8.92 mmol) and imidazole (0.90 g, 13.3 mmol) in dichloromethane (17 mL) at 0 °C. The reaction was allowed to warm gradually to rt. After 1.5 h, the reaction was quenched by addition of saturated aqueous ammonium chloride solution (20 mL) and the aqueous phase extracted with diethyl ether (3 × 100 mL). The combined organic phases were washed with brine (20 mL), dried over anhydrous sodium sulfate, filtered and concentrated under reduced pressure to yield propargyl alcohol **4.44** as a colourless oil. Used in the next step without further purification.

^{1}H NMR (200 MHz, $CDCl_3$): δ 4.31 (d, *J* = 2.4 Hz, 2H), 2.39 (t, *J* = 2.4 Hz, 1H), 0.91 (s, 9H), 0.12 (s, 6H)

Under a nitrogen atmosphere, *n*-butyllithium (3.4 mL, 5.4 mmol, 1.58 M in tetrahydrofuran) was added dropwise over 1 minute to a solution of propargyl alcohol **4.44** (0.76 g, 4.5 mmol) in tetrahydrofuran (45 mL) at −78 °C. The reaction was removed from the acetone–dry ice bath for 5 minutes and then cooled back to −78 °C. Trimethylchlorosilane (0.68 mL, 5.4 mmol) was added dropwise over 1 minute, and the reaction was removed from the acetone–dry ice bath and allowed to warm to rt. After 2 h, the reaction was quenched by addition of saturated aqueous ammonium chloride solution (20 mL). The aqueous phase was extracted with diethyl ether (3 × 30 mL). The combined organic phases were washed with brine (20 mL), dried over anhydrous sodium sulfate, filtered and concentrated under reduced pressure to yield propargyl alcohol **4.45** (0.96 g, 4.0 mmol, 44% over two steps) as a colourless oil.

R_f: 0.70 (100% pentane) – white streak (with potassium permanganate)

^{1}H NMR (600 MHz, $CDCl_3$): δ 4.31 (s, 2H), 0.91 (s, 9H), 0.16 (s, 9H), 0.13 (s, 6H)

^{13}C NMR (151 MHz, $CDCl_3$): δ 104.7, 89.8, 52.4, 26.0, 18.5, -0.1, -4.9

Data in agreement with literature.[227]

Aniline **4.59**:

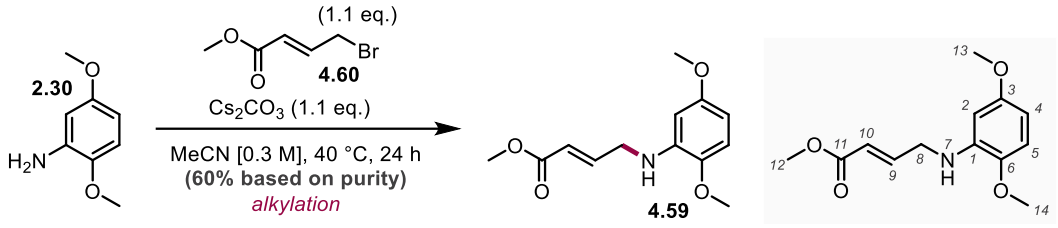

Adapted from the procedure of Yamagata et al.:[228] Under a nitrogen atmosphere, 4-bromocrotonate **4.60** (0.10 mL, 0.84 mmol) was added dropwise over 1 minute to a solution of 2,5-dimethoxyaniline **2.30** (0.12 g, 0.76 mmol) and caesium carbonate (0.27 g, 0.84 mmol) in acetonitrile (2.8 mL) at rt. The reaction mixture was heated to 40 °C. After 24 h, the reaction was diluted by addition of water (5 mL) and the aqueous phase was extracted with ethyl acetate (3 × 20 mL). The combined organic phases were washed with brine (10 mL), dried over anhydrous sodium sulfate, filtered and concentrated under reduced pressure. The dark brown oil was purified by silica column chromatography (100% pentane to 40% ethyl acetate in pentane) to yield aniline **4.59** (0.15 g, 0.46 mmol, 60% based on purity) as a brown oil.

Note: 23% 2,5-dimethoxyaniline **2.30** impurity present.

R_f: 0.26 (10% ethyl acetate in pentane) – red spot (with vanillin)

^{1}H NMR (600 MHz, $CDCl_3$): δ 7.06 (dt, *J* = 15.7, 4.6 Hz, 1H, H9), 6.70 (d, *J* = 8.6 Hz, 1H, H5), 6.20 (dd, *J* = 8.6, 2.9 Hz, 1H, H4), 6.15 (d, *J* = 2.8 Hz, 1H, H2), 6.06 (dt, *J* = 15.7, 2.0 Hz, 1H, H10), 4.56 (br s, 1H, H7), 3.98 (br s, 2H, H8), 3.84 (s, 3H, H14), 3.76 (s, 3H, H13), 3.75 (s, 3H, H12)

^{13}C NMR (151 MHz, $CDCl_3$): δ 166.9 (C, C11), 154.9 (C, C3 or C6), 145.8 (CH, C9), 141.7 (C, C3 or C6), 138.4 (C, C1), 121.5 (CH, C10), 110.2 (CH, C5), 99.5 (CH, C4), 98.6 (CH, C2), 56.2 (CH_3, C14), 55.7 (CH_3, C13), 51.7 (CH_3, C12), 44.6 (CH_2, C8)

HRMS-ESI (m/z): Calculated for $C_{13}H_{17}NO_4Na$ [M+Na]+, 274.1050; found 274.1052

IR:* 3426, 3383, 2998, 2950, 2913, 2834, 1721, 1660, 1616, 1522, 1461, 1435, 1357, 1277, 1220, 1170, 1142, 1099, 1048, 1025, 970, 923, 908, 831, 781, 712, 653, 633, 621

of the mixture with aniline **2.30*

N-oxide **4.66**:

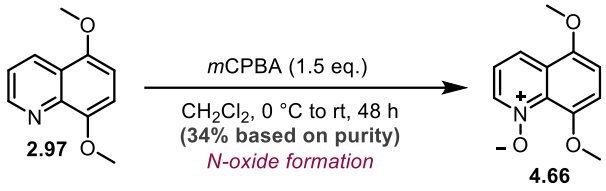

Adapted from the procedure of Laha et al.:[180] *meta*-Chloroperoxybenzoic acid (97% purity, 42 mg, 236 μmol) was added portion-wise over 1 minute to a solution of 5,8-dimethoxyquinoline **2.97** (30 mg, 159 μmol) in dichloromethane (1.6 mL) at rt. After 48 h, water (10 mL) was added and the aqueous phase was extracted with dichloromethane (3 × 20 mL). The combined organic phases were washed with brine (20 mL), dried over anhydrous sodium sulfate, filtered and concentrated under reduced pressure to yield *N*-oxide **4.66** (14 mg, 53 μmol, 34% based on purity) as a brown oil.

Note: 5,8-Dimethoxyquinoline **2.97** and *N*-oxide **4.66** have the same R_f.

R_f: 0.31 (5% acetone in dichloromethane) – yellow spot (with vanillin)

^{1}H NMR (400 MHz, $CDCl_3$): δ 8.43 (d, *J* = 6.1 Hz, 1H), 8.07 (d, *J* = 8.6 Hz, 1H), 7.19 (dd, *J* = 8.6, 6.2 Hz, 1H), 7.03 (d, *J* = 8.7 Hz, 1H), 6.82 (d, *J* = 8.7 Hz, 1H), 3.97 (s, 3H), 3.96 (s, 3H)

Data in agreement with literature.[191]

Note: N-oxide **4.66** converted into an unknown product whilst awaiting characterisation by NMR spectroscopy:

^{1}H NMR (600 MHz, $CDCl_3$): δ 9.23 (d, *J* = 7.9 Hz, 1H), 8.84 (dd, *J* = 4.7, 1.7 Hz, 1H), 7.79 (dd, *J* = 7.8, 1.6 Hz, 1H), 7.56 (dd, *J* = 7.7, 4.8 Hz, 1H), 5.76 (d, *J* = 7.9 Hz, 1H), 3.97 (s, 3H), 3.89 (s, 3H)

^{13}C NMR (151 MHz, $CDCl_3$): δ 189.7, 174.2, 163.8, 149.8, 146.8, 138.5, 129.5, 124.6, 105.9, 56.4, 52.1

Quinoline **4.72**:

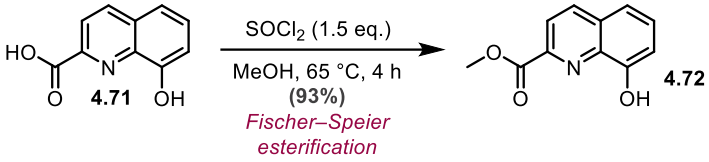

Adapted from the procedure of Vu et al.:[229] Thionyl chloride (0.29 mL, 4.0 mmol) was added dropwise over 1 minute to a suspension of quinoline **4.71** (0.50 g, 2.6 mmol) in methanol (13 mL) at rt, and the resulting mixture was heated to 65 °C. After 4 h, the reaction was cooled to rt and water (25 mL) was added dropwise resulting in the formation of a yellow precipitate which was filtered under vacuum to yield quinoline **4.72** (0.50, 2.6 mmol, 93%) as a pale-yellow solid. Used in the next step without further purification.

R_f: 0.40 (5% acetone in pentane) – yellow spot (with vanillin)

^{1}H NMR (500 MHz, $CDCl_3$): δ 8.41 (br s, 1H), 8.29 (d, *J* = 8.5 Hz, 1H), 8.18 (d, *J* = 8.5 Hz, 1H), 7.57 (dd, *J* = 8.3, 7.7 Hz, 1H), 7.39 (dd, *J* = 8.3, 1.2 Hz, 1H), 7.24 (dd, *J* = 7.6, 1.2 Hz, 1H), 4.06 (s, 3H)

^{13}C NMR (126 MHz, $CDCl_3$): δ 165.6, 153.4, 145.5, 137.9, 137.4, 130.4, 129.9, 121.8, 117.8, 111.2, 53.1

Data in agreement with literature.[230]

Enamine **4.76**:

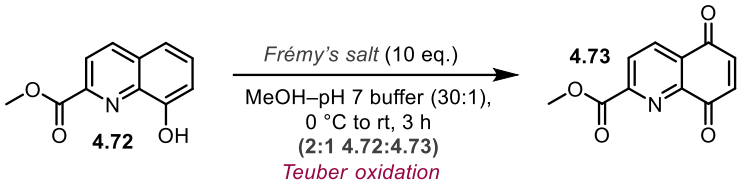

Adapted from the procedure of Pearce et al.:[115] Quinoline **4.72** (0.10 g, 0.49 mmol) in methanol (14 mL) was added dropwise over 1 minute to a solution Frémy's salt (0.65 g, 2.4 mmol) in 30:1 water–1 M potassium phosphate buffer (pH 7, 31 mL) at 0 °C. After 10 minutes, a colour change from purple to brown occurred and the ice-bath was removed and the reaction was allowed to warm to rt. After 1 h, Frémy's salt (0.65 g, 2.4 mmol) in 30:1 water–1 M potassium phosphate buffer (pH 7, 31 mL) was added at rt. After 2 h, the aqueous phase was extracted with dichloromethane (3 × 30 mL) and the combined organic phases were concentrated under reduced pressure to yield quinoline-5,8-dione **4.73**. Used in the next step without further purification.

^{1}H NMR (500 MHz, $CDCl_3$): δ 8.59 (d, *J* = 8.0 Hz, 1H), 8.49 (d, *J* = 8.1 Hz, 1H), 7.24 (d, *J* = 10.4 Hz, 1H), 7.13 (d, *J* = 10.4 Hz, 1H), 4.07 (s, 3H)

^{13}C NMR (126 MHz, $CDCl_3$): δ 183.8, 182.1, 164.7, 152.5, 147.2, 139.8, 138.3, 136.4, 130.8, 128.7, 53.6

Data in agreement with literature.[115]

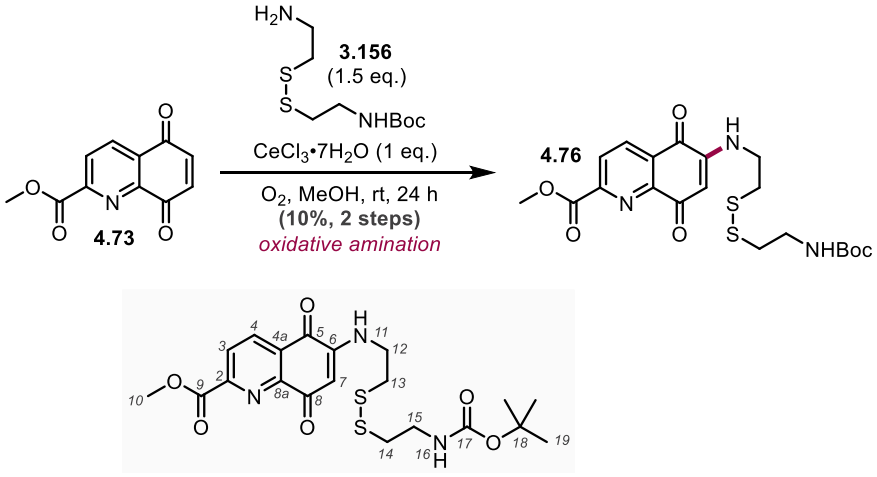

Quinoline-5,8-dione **4.73** was dissolved in methanol (4.9 mL) under an oxygen atmosphere. Cerium(III) chloride heptahydrate (0.18 g, 0.49 mmol) and cystamine **3.156** (0.19 g, 0.74 mmol) were then added sequentially at rt. After 24 h, the reaction mixture was concentrated under reduced pressure. Water (10 mL) was added and the organic phase was extracted with

dichloromethane (3 × 20 mL). The combined organic phases were washed sequentially with 1 M aqueous hydrochloric acid (15 mL), water (15 mL) and brine (15 mL), dried over anhydrous sodium sulfate, filtered and concentrated under reduced pressure. The brown residue was purified by silica column chromatography (100% dichloromethane to 20% acetone in dichloromethane) to yield enamine **4.76** (21.8 mg, 46.6 µmol, 10% over two steps) as a red amorphous solid.

R_f: 0.13 (10% acetone in pentane) – red spot (without stain)

^{1}H NMR (600 MHz, $CDCl_3$): δ 8.51 (d, *J* = 8.0 Hz, 1H, H4), 8.35 (d, *J* = 8.0 Hz, 1H, H3), 6.31 (t, *J* = 6.0 Hz, 1H, H11), 6.07 (s, 1H, H7), 4.89 (br s, 1H, H16), 4.03 (s, 3H, H10), 3.60 (q, *J* = 6.3 Hz, 2H, H12), 3.45 (q, *J* = 6.5 Hz, 3H, H15), 2.96 (t, *J* = 6.4 Hz, 2H, H13), 2.82 (t, *J* = 6.5 Hz, 2H, H14), 1.42 (s, 9H, H19)

^{13}C NMR (151 MHz, $CDCl_3$): δ 180.8 (C, C5 or C8), 180.1 (C, C5 or C8), 165.0 (C, C9), 155.9 (C, C17), 152.6 (C, C2), 148.9 (C, C8a), 147.4 (C, C6), 135.8 (CH, C4), 129.2 (C, C4a), 127.2 (CH, C3), 103.2 (CH, C7), 79.8 (C, C18), 53.5 (CH_3, C10), 41.4 (CH_2, C12), 39.5 (CH_2, C15), 38.6 (CH_2, C14), 35.8 (CH_2, C13), 28.5 (CH_3, C19)

HRMS-ESI (m/z): Calculated for $C_{20}H_{26}N_3O_6S_2$ [M+H]+, 468.1258; found 468.1273

IR: 3347, 2979, 2929, 2873, 2245, 1700, 1636, 1606, 1580, 1518, 1456, 1392, 1366, 1343, 1305, 1256, 1175, 1142, 1116, 1043, 949, 912, 867, 842, 820, 802, 779, 736, 673, 646, 612

Sulfide **4.77**:

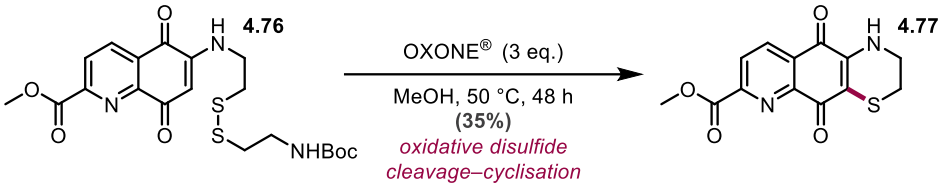

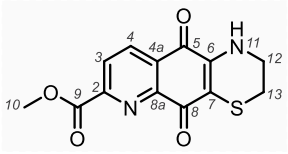

OXONE® (12.6 mg, 41.1 µmol) was added to a solution of enamine **4.76** (6 mg, 12.8 µmol) in methanol (1.0 mL) at rt and the reaction was heated to 50 °C. After 48 h, a colour change from a red-yellow solution to dark brown was observed. The reaction mixture was cooled to rt, diluted with water (10 mL) and the aqueous phase was extracted with ethyl acetate (3 × 10 mL). The combined organic phases were washed with brine (10 mL), dried over anhydrous sodium sulfate, filtered and concentrated under reduced pressure. The brown solid was purified by silica chromatography (100% dichloromethane to 10% acetone in dichloromethane) to yield sulfide **4.77** (1.3 mg, 4.5 µmol, 35%) as a purple solid.

R_f: 0.27 (10% acetone in pentane) – purple spot (without stain)

^{1}H NMR (600 MHz, $CDCl_3$): δ 8.47 (d, *J* = 8.0 Hz, 1H, H4), 8.34 (d, *J* = 7.9 Hz, 1H, H3), 6.03 (br s, 1H, H11), 4.06 (s, 3H, H10), 3.85 – 3.81 (m, 2H, H12), 3.10 – 3.07 (m, 2H, H13)

^{13}C NMR (151 MHz, $CDCl_3$): δ 176.6 (C, C5 or C8), 176.5 (C, C5 or C8), 165.0 (C, C9), 151.9 (C, C2 or C8a), 148.9 (C, C2 or C8a), 140.7 (C, C6), 135.5 (CH, C4), 129.5 (C, C4a), 127.5 (CH, C3), 115.4 (C, C7), 41.7 (CH_2, C12), 24.2 (CH_2, C13)

HRMS-ESI (m/z): Calculated for $C_{13}H_{10}N_2O_4SK$ [M+K]+, 328.9993; found 328.9999

IR: 2925, 2853, 1718, 1593, 1560, 1509, 1457, 1393, 1366, 1339, 1269, 1170, 1125, 1043, 913, 869, 800, 743, 650, 632, 607

5.3. Spectroscopic data

Figure 5.1. ^{1}H NMR spectrum of ascididemin **1.11** (400 MHz, $CDCl_3$):

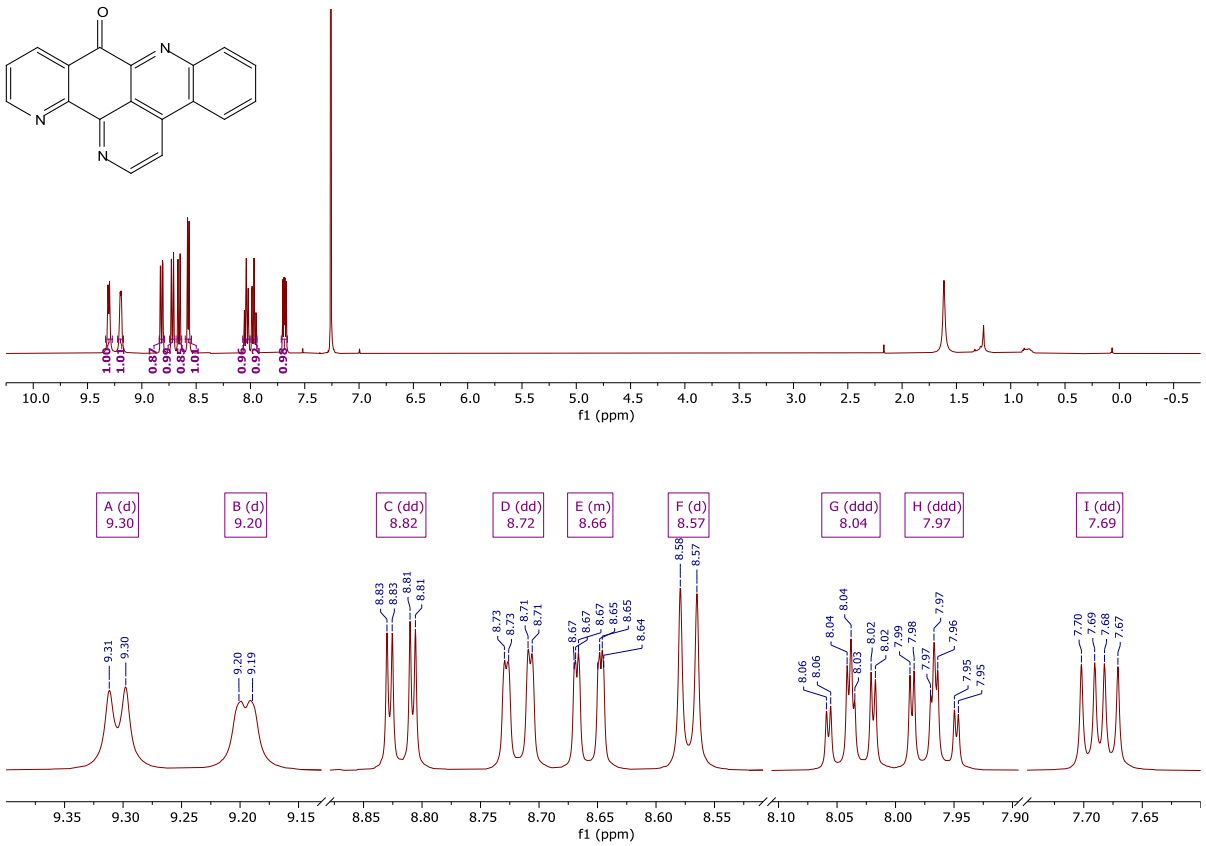

Figure 5.2. ^{13}C NMR spectrum of ascididemin **1.11** (126 MHz, $CDCl_3$):

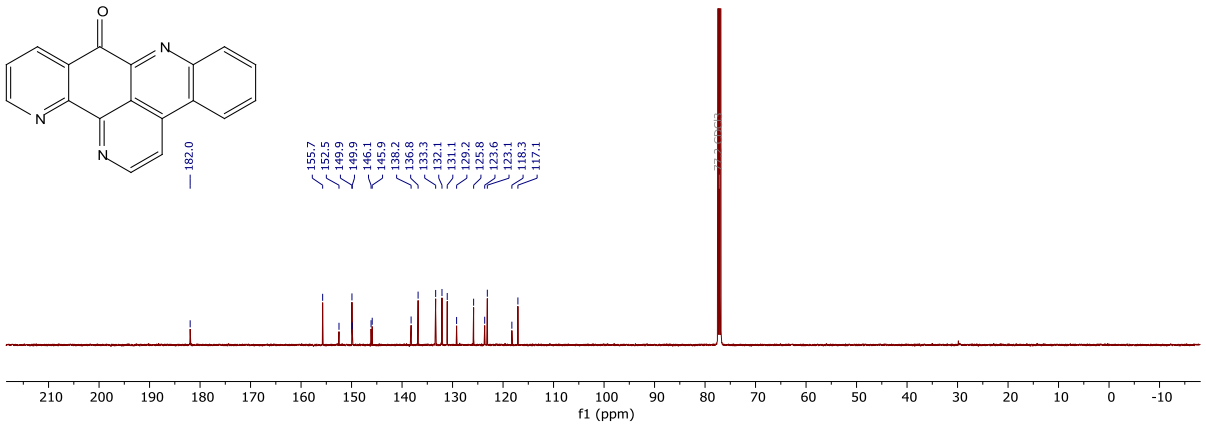

Figure 5.3. ^{1}H NMR spectrum of thiaplakortone A **1.12**•HCl (600 MHz, DMSO-d_6):

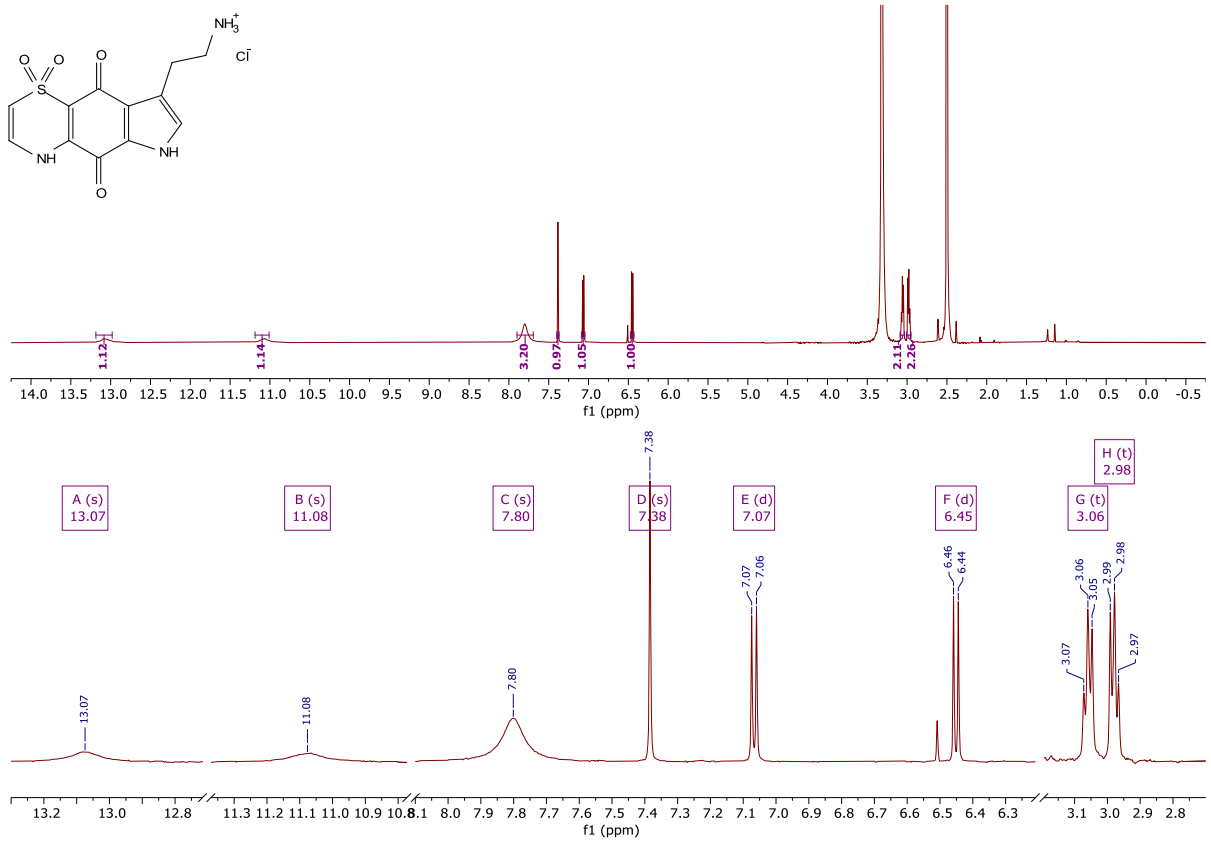

Figure 5.4. ^{13}C NMR spectrum of thiaplakortone A **1.12**•HCl (151 MHz, DMSO-d_6):

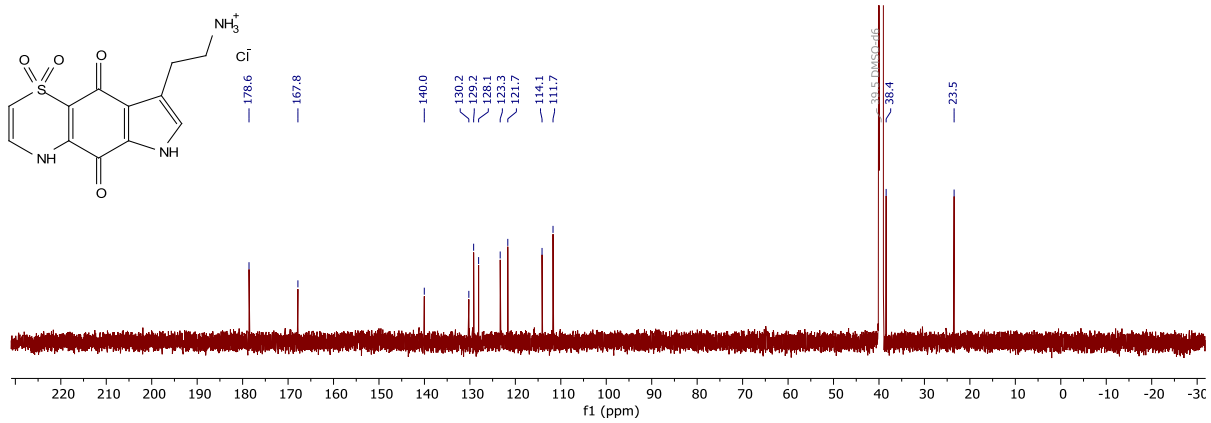

Figure 5.5. ^{1}H NMR spectrum of thiaplakortone B **3.1**•HCl (600 MHz, DMSO-d_6):

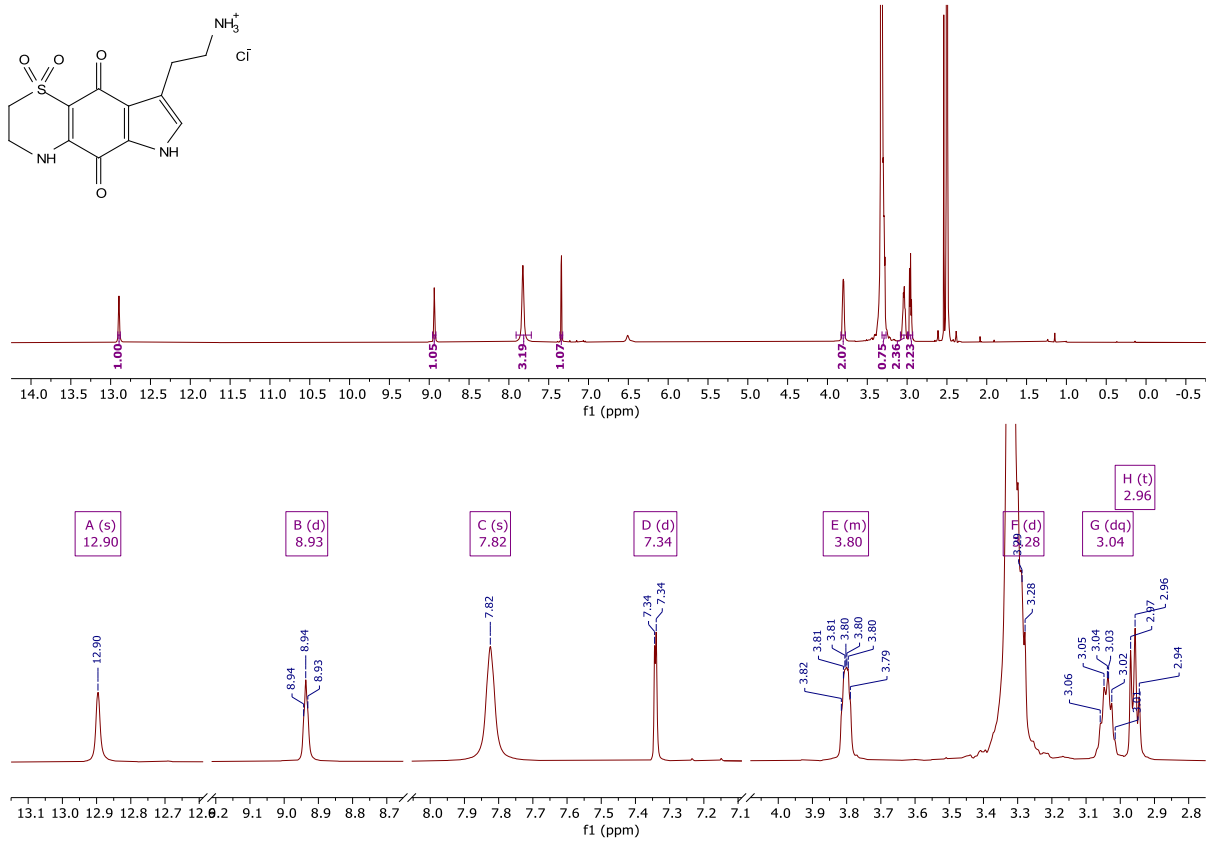

Figure 5.6. ^{13}C NMR spectrum of thiaplakortone B **3.1**•HCl (151 MHz, DMSO-d_6):

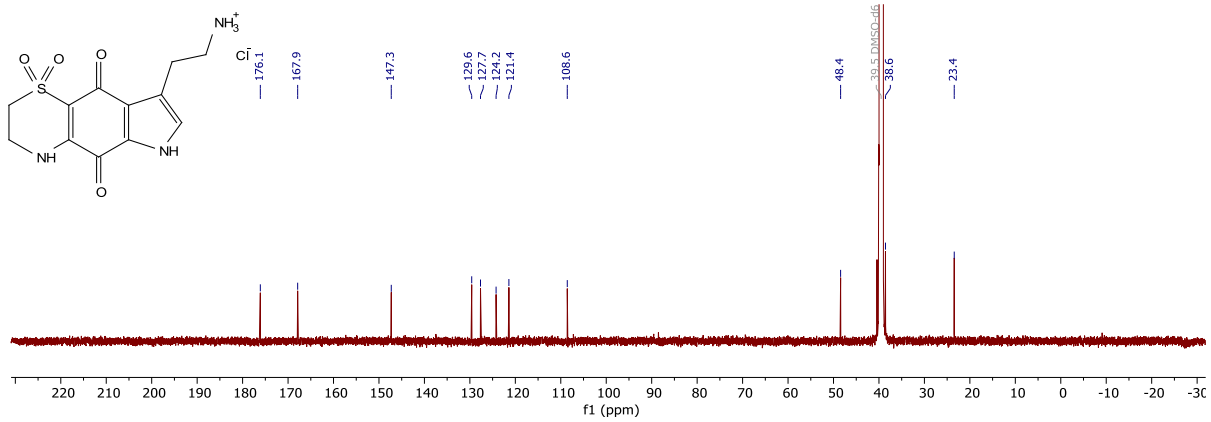

5.4. Crystallographic data

Table 5.5. Crystal data and structure refinement for 9-methylascididemin **2.123**.

CCDC identification code	2408040	
Empirical formula	C21.50 H11 D2.50 Cl7.50 N3 O	
Formula weight	598.24	
Crystal system	Monoclinic	
Space group	C 1 2/c 1	
Unit cell dimensions	a = 18.58434(19)	α = 90°
	b = 20.20036(19)	β = 106.4631(11)
	c = 13.56984(14)	γ = 90°
Volume	4885.41(9) $Å^3$	
Z	8	
Temperature	150 K	
Wavelength	1.54184	
Reflections collected	41461	
Independent reflections	5105 [R(int) = 0.0337]	
Completeness to theta = 67.684°	100%	
Refinement method	Full-matrix least-squares on F^2	
Data / restraints / parameters	5105 / 583 / 466	
Goodness-of-fit on F^2	1.028	
Final R indices [I>2σ(I)]	R1 = 0.0366, wR2 = 0.1058	
R indices (all data) R1 =	R1 = 0.0406, wR2 = 0.1103	

6. References

(1) Adams, A. M.; Vuckovic, M.; Birch, E.; Brant, T. A.; Bialek, S.; Yoon, D.; Koroma, J.; Direny, A.; Shott, J.; Lemoine, J. F.; Dembele, M.; Baker, M. C., Eliminating Neglected Tropical Diseases in Urban Areas: A Review of Challenges, Strategies and Research Directions for Successful Mass Drug Administration. *Trop. Med. Infect. Dis.* **2018**, *3*, 122.

(2) Crampton, J. M.; Beard, C. B.; Louis, C., *The Molecular Biology of Insect Disease Vectors : A Methods Manual*, 1st ed.; Chapman & Hall: London, UK 1997.

(3) Bates, P. A., Leishmania Sand Fly Interaction: Progress and Challenges. *Curr. Opin. Microbiol.* **2008**, *11*, 340–344.

(4) Stuart, K.; Brun, R.; Croft, S.; Fairlamb, A.; Gürtler, R. E.; McKerrow, J.; Reed, S.; Tarleton, R., Kinetoplastids: Related Protozoan Pathogens, Different Diseases. *J. Clin. Invest.* **2008**, *118* (4), 1301–1310.

(5) Pradhan, S.; Schwartz, R. A.; Patil, A.; Grabbe, S.; Goldust, M., Treatment Options for Leishmaniasis. *Clin. Exp. Dermatol.* **2022**, *47*, 516–521.

(6) Achan, J.; Talisuna, A. O.; Erhart, A.; Yeka, A.; Tibenderana, J. K.; Baliraine, F. N.; Rosenthal, P. J.; D'Alessandro, U., Quinine, an Old Anti-Malarial Drug in a Modern World: Role in the Treatment of Malaria. *Malar. J*. **2011**, *10*, 144.

(7) Saritha, C.; Rajana, V. K.; Choudhary, K.; Vairagar, A.; Mishra, A.; Penumaka, S. M.; Jain, S.; Dande, A.; Naresh, P.; Kumar, N.; Ramalingam, P.; Mandal, D., Highly Selective Ergosterol Binding and Impaired Redox Balance Leads to Improved Antileishmanial Efficacy for Amphotericin b Synthesized Silver Nanoparticles with Reduced Toxicity– In Vitro and in Vivo Studies. *Free Radic. Biol. Med.* **2025**, *235*, 405–425.

(8) Pou, S.; Winter, R. W.; Nilsen, A.; Kelly, J. X.; Li, Y.; Doggett, J. S.; Riscoe, E. W.; Wegmann, K. W.; Hinrichs, D. J.; Riscoe, M. K., Sontochin as a Guide to the Development of Drugs against Chloroquine-Resistant Malaria. *Antimicrob. Agents Chemother.* **2012**, *56* (7), 3475–3480.

(9) Wang, J.; Xu, C.; Wong, Y. K.; Li, Y.; Liao, F.; Jiang, T.; Tu, Y., Artemisinin, the Magic Drug Discovered from Traditional Chinese Medicine. *Engineering* **2019**, *5* (1), 32–39.

(10) Makanga, M.; Krudsood, S., The Clinical Efficacy of Artemether/Lumefantrine (Coartem®). *Malar. J* **2009**, *8*, S5.

(11) Rao, K. V.; Kasanah, N.; Wahyuono, S.; Tekwani, B. L.; Schinazi, R. F.; Hamann, M. T., Three New Manzamine Alkaloids from a Common Indonesian Sponge and Their Activity against Infectious and Tropical Parasitic Diseases. *J. Nat. Prod.* **2004**, *67* (8), 1314–1318.

(12) Jakubec, P.; Hawkins, A.; Felzmann, W.; Dixon, D. J., Total Synthesis of Manzamine A and Related Alkaloids. *J. Am. Chem. Soc.* **2012**, *134* (42), 17482–17485.

(13) Tempone, A. G.; Pieper, P.; Borborema, S. E. T.; Thevenard, F.; Lago, J. H. G.; Croft, S. L.; Anderson, E. A., Marine Alkaloids as Bioactive Agents against Protozoal Neglected Tropical Diseases and Malaria. *Nat. Prod. Rep*. **2021**, *38*, 2214–2235.

(14) Van den Kerkhof, M.; Sterckx, Y. G. J.; Leprohon, P.; Maes, L.; Caljon, G., Experimental Strategies to Explore Drug Action and Resistance in Kinetoplastid Parasites. *Microorganisms* **2020**, *8*, 950.

(15) Kobayash, J.; Cheng, J.; Nakamura, H.; Ohizumi, Y.; Hirata, Y.; Sasaki, T.; Ohta, T.; Nozoe, S., Ascididemin, a novel pentacyclic aromatic alkaloid with potent antileukemic activity from the okinawan tunicate didemnum sp. *Tetrahedron Lett.* **1988**, *29*(10), 1177–1180.

(16) Plodek, A.; Bracher, F., Marine Drugs New Perspectives in the Chemistry of Marine Pyridoacridine Alkaloids. *Mar. Drugs* **2016**, *14*, 26.

(17) Schmitz, F. J.; DeGuzman, F. S.; Hossain, M. B.; van der Helm, D., Cytotoxic aromatic alkaloids from the ascidian *Amphicarpa meridiana* and *Leptoclinides* sp.: meridine and 11-hydroxyascididemin. *J. Org. Chem.* **1991**, *56*(2), 804–808.

(18) Bracher, F., Total Synthesis of the Pentacyclic Alkaloid Ascididemin. *Heterocycles* **1989**, *29* (11), 2093–2095.

(19) Gellerman, G.; Rudi, A.; Kashman, Y., The biomimetic synthesis of marine alkaloid related pyrido- and pyrrolo[2,3,4-kl]acridines. *Tetrahedron* **1994**, *50* (45), 12959–12972.

(20) Cuerva, J. M.; Cárdenas, D. J.; Echavarren, A. M., Intramolecular Michael-Type Addition of Azadienes to 1,4-Naphthoquinones Instead of Aza-Diels–Alder Cycloaddition: A Synthesis of Ascididemin. *J. Chem. Soc. Perkin Trans. 1* **2002**, *2* (11), 1360–1365.

(21) Yin, H.; Shan, N.; Wang, S.; Yao, Z. J., Total Synthesis of Ascididemin-Type Alkaloids Using Alkyne Building Blocks. *J. Org. Chem.* **2014**, *79* (20), 9748–9753.

(22) Moody, C. J.; Rea, C. W.; Thomas, R., Synthesis of the marine alkaloid ascididemin. *Tetrahedron Lett.* **1990**, *31* (30), 4375–4376.

(23) Álvarez, M.; Feliu, L.; Ajana, W.; Joule, J. A.; Fernández-Puentes, J. L., Synthesis of Ascididemine and an Isomer. *Eur. J. Org. Chem.* **2000**, *2000* (55, 849–855.

(24) Petersen, I. N.; Crestey, F.; Kristensen, J. L., Total Synthesis of Ascididemin *via* Anionic Cascade Ring Closure. *Chem. Commun.* **2012**, *48* (72), 9092–9094.

(25) McDonald, L. A.; Eldredge, G. S.; Barrows, L. R.; Ireland, C. M., Inhibition of Topoisomerase II Catalytic Activity by Pyridoacridine Alkaloids from a *Cystodytes* sp. Ascidian: A Mechanism for the Apparent Intercalator-Induced Inhibition of Topoisomerase II. *J. Med. Chem.* **1994**, *37*, 3819–3827.

(26) Bonnard, I.; Bontemps, N.; Lahmy, S.; Banaigs, B.; Combaut, G.; Francisco, C.; Colson, P.; Houssier, C.; Waring, M. J.; Bailly, C. Binding to DNA and Cytotoxic Evaluation of Ascididemin,

the Major Alkaloid from the Mediterranean Ascidian *Cystodytes dellechiajei*. *Anticancer Drug Des.* **1995**, *10* (4), 333–346.

(27) Matsumoto, S. S.; Biggs, J.; Copp, B. R.; Holden, J. A.; Barrows, L. R., Mechanism of Ascididemin-Induced Cytotoxicity. *Chem. Res. Toxicol.* **2003**, *16* (2), 113–122.

(28) Matsumoto, S. S.; Sidford, M. H.; Holden, J. A.; Barrows, L. R.; Copp, B. R., Mechanism of Action Studies of Cytotoxic Marine Alkaloids: Ascididemin Exhibits Thiol-Dependent Oxidative DNA Cleavage. *Tetrahedron Lett.* **2000**, *41* (10), 1667–1670.

(29) Guittat, L.; De Cian, A.; Rosu, F.; Gabelica, V.; De Pauw, E.; Delfourne, E.; Mergny, J. L., Ascididemin and Meridine Stabilise G-Quadruplexes and Inhibit Telomerase *in vitro*. *Biochim. Biophys. Acta.* **2005**, *1724* (3), 375–384.

(30) Goulle, V.; Lehn, J. -M; Schoentjes, B.; Schmitz, F. J., Ruthenium(II) Complex of the Alkaloid 2-Bromoleptoclinidinone. Preparation and Interaction with Double-Stranded DNA. *Helv. Chim. Acta*. **1991**, *74* (7), 1471–1476.

(31) Dassonneville, L.; Wattez, N.; Baldeyrou, B.; Mahieu, C.; Lansiaux, A.; Banaigs, B.; Bonnard, I.; Bailly, C.; De, L.; Antitumorale, P., Inhibition of Topoisomerase II by the Marine Alkaloid Ascididemin and Induction of Apoptosis in Leukemia Cells. *Biochem. Pharmacol.* **2000**, *60* (4), 527–537

(32) Appleton, D. R.; Pearce, A. N.; Copp, B. R., Anti-Tuberculosis Natural Products: Synthesis and Biological Evaluation of Pyridoacridine Alkaloids Related to Ascididemin. *Tetrahedron* **2010**, *66* (27–28), 4977–4986.

(33) Lindsay, B. S.; Christiansen, H. C.; Copp, B. R., Structural Studies of Cytotoxic Marine Alkaloids: Synthesis of Novel Ring-E Analogues of Ascididemin and Their *in vitro* and *in vivo* Biological Evaluation. *Tetrahedron* **2000**, *56* (3), 497–505.

(34) Copp, B. R.; Kayser, O.; Brun, R.; Kiderlen, A. F., Antiparasitic Activity of Marine Pyridoacridone Alkaloids Related to the Ascididemins. *Planta. Med.* **2003**, *69* (6), 527–531.

(35) Feng, Y.; Davis, R. A.; Sykes, M. L.; Avery, V. M.; Carroll, A. R.; Camp, D.; Quinn, R. J., Antitrypanosomal Pyridoacridine Alkaloids from the Australian Ascidian *Polysyncraton echinatum*. *Tetrahedron Lett.* **2010**, *51* (18), 2477–2479.

(36) Kumari, A.; Singh, K. P.; Mandal, A.; Paswan, R. K.; Sinha, P.; Das, P.; Ali, V.; Bimal, S.; Lal, C. S., Intracellular Zinc Flux Causes Reactive Oxygen Species Mediated Mitochondrial Dysfunction Leading to Cell Death in *Leishmania donovani*. *PLoS One* **2017**, *12* (6), e0178800.

(37) Santos, A. L. S.; Sodre, C. L.; Valle, R. S.; Silva, B. A.; Abi-Chacra, E. A.; Silva, L. V.; Souza-Gonçalves, A. L.; Sangenito, L. S.; Gonçalves, D. S.; Souza, L. O. P.; Palmeira, V. F.; d'Avila-Levy, C. M.; Kneipp, L. F.; Kellett, A.; McCann, M.; Branquinha, M. H., Antimicrobial Action of Chelating Agents: Repercussions on the Microorganism Development, Virulence and Pathogenesis. *Curr. Med. Chem*. **2012**, *19* (17), 2715–2737.

(38) Hübner, C.; Haase, H., Interactions of Zinc- and Redox-Signaling Pathways. *Redox Biol.* **2021**, *41*, 101916.

(39) Taylor, M. C.; Kelly, J. M., Iron Metabolism in Trypanosomatids, and Its Crucial Role in Infection. *Parasitology* **2010**, *137* (6), 899–917.

(40) Zaidi, A.; Singh, K. P.; Ali, V., *Leishmania* and Its Quest for Iron: An Update and Overview. *Mol. Biochem. Parasitol.* **2017**, *211*, 15–25.

(41) Das, N. K.; Biswas, S.; Solanki, S.; Mukhopadhyay, C. K., *Leishmania donovani* Depletes Labile Iron Pool to Exploit Iron Uptake Capacity of Macrophage for Its Intracellular Growth. *Cell. Microbiol.* **2009**, *11* (1), 83–94.

(42) Michael, J. P.; Pattenden, G., Marine Metabolites and Metal Ion Chelation: The Facts and the Fantasies. *Angew. Chem. Int. Ed.* **1993**, *32* (1), 1–23.

(43) Bloor, S. J.; Schmitz, F. J., A Novel Pentacyclic Aromatic Alkaloid from an Ascidian. *J. Am. Chem. Soc.* **1987**, *109* (20), 6134–6136.

(44) de Guzman, F. S.; Schmitz, F. J., Chemistry of 2-Bromoleptoclinidinone, Structure Revision. *Tetrahedron Lett.* **1989**, *30* (9), 1069–1070.

(45) Wall, R. J.; Moniz, S.; Thomas, M. G.; Norval, S.; Ko, E.-J.; Marco, M.; Miles, T. J.; Gilbert, I. H.; Horn, D.; Fairlamb, A. H.; Wyllie, S., Antitrypanosomal 8-Hydroxy-Naphthyridines Are Chelators of Divalent Transition Metals. *Antrimicrob. Agents Chemother.* **2018**, *62* (8), e00235-18.

(46) Wheeler, R. J.; Gluenz, E.; Gull, K., The Cell Cycle of *Leishmania*: Morphogenetic Events and Their Implications for Parasite Biology. *Mol. Microbiol.* **2011**, *79* (3), 647–662.

(47) Halliday, C.; de Liz, L. V.; Vaughan, S.; Sunter, J. D., Disruption of *Leishmania* Flagellum Attachment Zone Architecture Causes Flagellum Loss. *Mol. Microbiol.* **2024**, *121* (1), 53–68.

(48) Asiki, H., DPhil Thesis: Target Discovery and Mode of Action Studies of Dehydrodieugenol B Analogues in *Leishmania*. University of Oxford, 2024.

(49) Thordarson, P., Determining Association Constants from Titration Experiments in Supramolecular Chemistry. *Chem. Soc. Rev.* **2011**, *40* (3), 1305–1323.

(50) Docker, A.; Shang, X.; Yuan, D.; Kuhn, H.; Zhang, Z.; Davis, J. J.; Beer, P. D.; Langton, M. J. Halogen Bonding Tetraphenylethene Anion Receptors: Anion-Induced Emissive Aggregates and Photoswitchable Recognition. *Angew. Chem. Int. Ed.* **2021**, *60* (35), 19442–19450.

(51) Filippova, G.; Simonov, Y. A.; Gdanets, M.; Stavila, V.; Filippova, I. G., Crystal structure of tris(1,10-phenan-throline)iron(ii) dinitrate dihydrate. *J. Struct. Chem.* **2005**, *46* (6), 1095–1098.

(52) Li, Y. M.; Shi, J.; Wu, X.; Luo, Z. F.; Wang, F. L.; Guo, Q. X., Tracing of Intracellular Zinc(II) Fluorescence Flux to Monitor Cell Apoptosis by Using FluoZin-3AM. *Cell Biochem. Funct.* **2009**, *27* (7), 417–423.

(53) Carvalho, S.; Barreira da Silva, R.; Shawki, A.; Castro, H.; Lamy, M.; Eide, D.; Costa, V.; Mackenzie, B.; Tomás, A. M., LiZIP3 Is a Cellular Zinc Transporter That Mediates the Tightly Regulated Import of Zinc in *Leishmania infantum* Parasites. *Mol. Microbiol.* **2015**, *96* (3), 581–595.

(54) Zalewski, P. D.; Forbes, I. J.; Seamark, R. F.; Borlinghaus, R.; Betts, W. H.; Lincoln, S. F.; Ward, A. D. Flux of Intracellular Labile Zinc during Apoptosis (Gene-Directed Cell Death) Revealed by a Specific Chemical Probe, Zinquin. *Chem. Biol.* **1994**, *1* (3), 153–161.

(55) Simpson, L., The Mitochondrial Genome of Kinetoplastid Protozoa: Genomic Organization, Transcription, Replication, and Evolution. *Annu. Rev. Microbiol.* **1987**, *41* (1), 363–380.

(56) Lindsay, B. S.; Barrows, L. R.; Copp, B. R., Structural Requirements for Biological Activity of the Marine Alkaloid Ascididemin. *Bioorg. Med. Chem. Lett.* **1995**, *5* (7), 739–742.

(57) Alsford, S.; Eckert, S.; Baker, N.; Glover, L.; Sanchez-Flores, A.; Leung, K. F.; Turner, D. J.; Field, M. C.; Berriman, M.; Horn, D., High-Throughput Decoding of Antitrypanosomal Drug Efficacy and Resistance. *Nature* **2012**, *482* (7384), 232–236.

(58) Shanmugasundram, A.; Starns, D.; Böhme, U.; Amos, B.; Wilkinson, P. A.; Harb, O. S.; Warrenfeltz, S.; Kissinger, J. C.; McDowell, M. A.; Roos, D. S.; Crouch, K.; Jones, A. R., TriTrypDB: An Integrated Functional Genomics Resource for Kinetoplastida. *PLoS Negl. Trop. Dis.* **2023**, *17* (1), e0011058.

(59) Dattani, A.; Drammeh, I.; Mahmood, A.; Rahman, M.; Szular, J.; Wilkinson, S. R., Unraveling the Antitrypanosomal Mechanism of Benznidazole and Related 2-Nitroimidazoles: From Prodrug Activation to DNA Damage. *Mol. Microbiol.* **2021**, *116* (2), 674–689.

(60) Hall, B. S.; Meredith, E. L.; Wilkinson, S. R., Targeting the Substrate Preference of a Type I Nitroreductase to Develop Antitrypanosomal Quinone-Based Prodrugs. *Antimicrob. Agents Chemother.* **2012**, *56* (11), 5821–5830.

(61) Wyllie, S.; Roberts, A. J.; Norval, S.; Patterson, S.; Foth, B. J.; Berriman, M.; Read, K. D.; Fairlamb, A. H., Activation of Bicyclic Nitro-Drugs by a Novel Nitroreductase (NTR2) in *Leishmania*. *PLoS Pathog.* **2016**, *12* (11), e1005971.

(62) Shang, B.; Yu, Z.; Wang, Z., Recent Advances and Applications of Nitroreductase Activable Agents for Tumor Theranostic. *Front. Pharmacol*. **2024**, *15.*

(63) Mahdi, F.; Morgan, J. B.; Liu, W.; Agarwal, A. K.; Jekabsons, M. B.; Liu, Y.; Zhou, Y. D.; Nagle, D. G., Sampangine (a Copyrine Alkaloid) Exerts Biological Activities through Cellular Redox Cycling of Its Quinone and Semiquinone Intermediates. *J. Nat. Prod.* **2015**, *78* (12), 3018–3023.

(64) Valiauga, B.; Williams, E. M.; Ackerley, D. F.; Čėnas, N. Reduction of Quinones and Nitroaromatic Compounds by *Escherichia coli* Nitroreductase A (NfsA): Characterization of Kinetics and Substrate Specificity. *Arch. Biochem. Biophys.* **2017**, *614*, 14–22.

(65) Nasiri, H. R.; Hohmann, K.; Hatemler, M. G.; Plodek, A.; Bracher, F.; Schwalbe, H., *In vitro* Production of Reactive Oxygen Species (ROS) by Sampangine. *Med. Chem. Res.* **2017**, *26* (6), 1170–1175.

(66) Tiano, M.; Courdurié, C.; Colinet, P., Predicting the Modulation of UV–Vis Absorption and Emission of Mono-Substituted Pyrido[2,3,4-Kl]Acridines by Electronic Density Variations Analysis. *Comput. Theor. Chem.* **2022**, *1213*, 113733.

(67) Ibrahim, S. R. M.; Mohamed, G. A., Pyridoacridine Alkaloids from Deep-Water Marine Organisms: Structural Elucidation. *Bull. Fac. Pharm. Cairo Univ.* **2016**, *54* (2), 107–135.

(68) Gunawardana, G. P.; Koehn, F. E.; Lee, A. Y.; Clardy, J.; He, H.; Faulkner, D. J., Pyridoacridine Alkaloids from Deep-Water Marine Sponges of the Family: Pachastrellidae: Structure Revision of Dercitin and Related Compounds and Correlation with the Kuanoniamines. *J. Org. Chem.* **1992**, *57* (5), 1523–1526.

(69) Aynetdinova, D.; Callens, M. C.; Hicks, H. B.; Poh, C. Y. X.; Shennan, B. D. A.; Boyd, A. M.; Lim, Z. H.; Leitch, J. A.; Dixon, D. J., Installing the "Magic Methyl"-C-H Methylation in Synthesis. *Chem. Soc. Rev*. **2021**, *50* (9), 5517–5563.

(70) Jacob III, P.; Callery, P. S., A Convenient Synthesis of Quinones from Hydroquinone Dimethyl Ethers. Oxidative Demethylation with Ceric Ammonium Nitrate. *J. Org. Chem.* **1976**, *41* (22), 3627–3629.

(71) Guissart, C.; Dolbois, A.; Tresse, C.; Saint-Auret, S.; Evano, G.; Blanchard, N., A Straightforward Entry to γ-Trifluoromethylated Allenamides and Their Synthetic Applications. *Synlett* **2016**, *27* (18), 2575–2580.

(72) Lindsay, B. S.; Pearce, A. N.; Copp, B. R., Efficient and Convenient Pyridine Ring-E Formation of the Cytotoxic Marine Alkaloid Asciddemin and Related Analogues. *Synth. Commun.* **1997**, *27* (15), 2587–2592.

(73) Jiang, Z.; Liu, N.; Dong, G.; Jiang, Y.; Liu, Y.; He, X.; Huang, Y.; He, S.; Chen, W.; Li, Z.; Yao, J.; Miao, Z.; Zhang, W.; Sheng, C., Scaffold Hopping of Sampangine: Discovery of Potent Antifungal Lead Compound against Aspergillus Fumigatus and Cryptococcus Neoformans. *Bioorg. Med. Chem. Lett*. **2014**, *24* (17), 4090–4094.

(74) Delfourne, E.; Kiss, R.; Le Corre, L.; Dujols, F.; Bastide, J.; Collignon, F.; Lesur, B.; Frydman, A.; Darro, F., Synthesis and *in vitro* Antitumor Activity of Ring C and D-Substituted Phenanthrolin-7-One Derivatives, Analogues of the Marine Pyridoacridine Alkaloids Asciddemin and Meridine. *Bioorg. Med. Chem.* **2004**, *12* (15), 3987–3994.

(75) Sozanschi, A.; Asiki, H.; Amaral, M.; de Castro Levatti, E. V.; Tempone, A. G.; Wheeler, R. J.; Anderson, E. A., Synthesis and Evaluation of (Bis)Benzyltetrahydroisoquinoline Alkaloids as Antiparasitic Agents. *JACS Au* **2024**, *4* (2), 847–854.

(76) St. George, S.; Bishop, J. V.; Titus, R. G.; Selitrennikoff, C. P., Novel Compounds Active against Leishmania Major. *Antimicrob. Agents Chemother.* **2006**, *50* (2), 474–479.

(77) Szatylowicz, H.; Stasyuk, O. A.; Krygowski, T. M., Substituent Effects in Heterocyclic Systems. *Adv. Heterocycl. Chem* **2015**, *116*, 137–192.

(78) Montefiori, M.; Jørgensen, F. S.; Olsen, L., Aldehyde Oxidase: Reaction Mechanism and Prediction of Site of Metabolism. *ACS Omega* **2017**, *2* (8), 4237–4244.

(79) Montoli, A.; Dimasi, A.; Citarella, A.; Ronchi, P.; Passarella, D.; Fasano, V., Metal-free, Selective *ortho*-Deuteration of *N*-Heterocyclic Oxides. *Adv. Synth. Catal.* **2025**, *367* (6), e202401585.

(80) Cui, H.-B.; Ma, T.; Zhang, R.-Y.; Shan, J.; Wang, Z.-Q.; Bai, M.; Chen, Y.-Z., Biocatalytic Synthesis of Chiral Benzylic Alcohols via Enantioselective Hydroxylation by a Self-Sufficient Cytochrome P450 from *Deinococcus gobiensis*. *Synthesis* **2024**, *56* (04), 567–572.

(81) Morais, T. R.; Conserva, G. A. A.; Varela, M. T.; Costa-Silva, T. A.; Thevenard, F.; Ponci, V.; Fortuna, A.; Falcão, A. C.; Tempone, A. G.; Fernandes, J. P. S.; Lago, J. H. G., Improving the Drug-Likeness of Inspiring Natural Products - Evaluation of the Antiparasitic Activity against *Trypanosoma cruzi* through Semi-Synthetic and Simplified Analogues of Licarin A. *Sci. Rep.* **2020**, *10*, 5467.

(82) Zhong, W.; Sun, B.; Lu, C.; Yu, H.; Wang, C.; He, L.; Gu, J.; Chen, S.; Liu, Y.; Jing, X.; Bi, Z.; Yang, G.; Zhou, H.; Sun, T.; Yang, C., Problems and Solutions in Click Chemistry Applied to Drug Probes. *Sci Rep* **2016**, *6*, 35579.

(83) Králová, J.; Jurášek, M.; Mikšátková, L.; Marešová, A.; Fähnrich, J.; Cihlářová, P.; Drašar, P.; Bartůněk, P.; Král, V., Influence of Fluorophore and Linker Length on the Localization and Trafficking of Fluorescent Sterol Probes. *Sci. Rep.* **2020**, *10*, 22053.

(84) Davis, R. A.; Duffy, S.; Fletcher, S.; Avery, V. M.; Quinn, R. J., Thiaplakortones A-D: Antimalarial Thiazine Alkaloids from the Australian Marine Sponge *Plakortis lita*. *J. Org. Chem.* **2013**, *78* (19), 9608–9613.

(85) Pouwer, R. H.; Deydier, S. M.; Le, P. Van; Schwartz, B. D.; Franken, N. C.; Davis, R. A.; Coster, M. J.; Charman, S. A.; Edstein, M. D.; Skinner-Adams, T. S.; Andrews, K. T.; Jenkins, I. D.; Quinn, R. J., Total Synthesis of Thiaplakortone A: Derivatives as Metabolically Stable Leads for the Treatment of Malaria. *ACS Med. Chem. Lett.* **2014**, *5* (2), 178–182.

(86) Schwartz, B. D.; Coster, M. J.; Skinner-Adams, T. S.; Andrews, K. T.; White, J. M.; Davis, R. A., Synthesis and Antiplasmodial Evaluation of Analogues Based on the Tricyclic Core of Thiaplakortones A-D. *Mar. Drugs* **2015**, *13* (9), 5784–5795.

(87) Imperatore, C.; Cimino, P.; Cebrián-Torrejón, G.; Persico, M.; Aiello, A.; Senese, M.; Fattorusso, C.; Menna, M.; Doménech-Carbó, A., Insight into the Mechanism of Action of Marine Cytotoxic Thiazinoquinones. *Mar. Drugs* **2017**, *15* (11), 335.

(88) Schwartz, B. D.; Skinner-Adams, T. S.; Andrews, K. T.; Coster, M. J.; Edstein, M. D.; MacKenzie, D.; Charman, S. A.; Koltun, M.; Blundell, S.; Campbell, A.; Pouwer, R. H.; Quinn, R. J.; Beattie, K. D.; Healy, P. C.; Davis, R. A., Synthesis and Antimalarial Evaluation of Amide and Urea Derivatives Based on the Thiaplakortone A Natural Product Scaffold. *Org. Biomol. Chem.* **2015**, *13* (5), 1558–1570.

(89) Egbewande, F. A.; Schwartz, B. D.; Duffy, S.; Avery, V. M.; Davis, R. A., Synthesis and Antimalarial Evaluation of Halogenated Analogues of Thiaplakortone A. *Mar. Drugs* **2023**, *21* (5), 317.

(90) Barnes, G. L.; Magann, N. L.; Perrotta, D.; Hörmann, F. M.; Fernandez, S.; Vydyam, P.; Choi, J. Y.; Prudhomme, J.; Neal, A.; Le Roch, K. G.; Ben Mamoun, C.; Vanderwal, C. D., A Divergent Synthesis of Numerous Pyrroloiminoquinone Alkaloids Identifies Promising Antiprotozoal Agents. *J. Am. Chem. Soc.* **2024**, *146* (43), 29883–29894.

(91) Przheval´skii, N. M.; Laipanov, R. K.; Tokmakov, G. P.; Nam, N. L., The Grandberg Reaction in the Synthesis of Biologically Active Compounds. *Russ. Chem. Bull. Int. Ed.* **2016**, *65* (7), 1709–1715.

(92) Murakami, Y., Peculiarity of Methoxy Group-Substituted Phenylhydrazones in Fischer Indole Synthesis. *Proc. Jpn. Acad. Ser. B.* **2012**, *88* (1), 1–17.

(93) Ishii, H., Nucleophilic Displacement of the Methoxy Group in Abnormal Fischer Indolization of 2-Methoxyphenylhydrazones. *Acc. Chem. Res.* **1981**, *14* (9), 275–283.

(94) Larock, R. C.; Yum, E. K.; Refvik, M. D., Synthesis of 2,3-Disubstituted Indoles via Palladium-Catalyzed Annulation of Internal Alkynes. *J. Org. Chem.* **1998**, *63* (22), 7652–7662.

(95) Takikawa, H.; Hashimoto, T.; Matsuura, M.; Tashiro, T.; Kitahara, T.; Mori, K.; Sasaki, M., Synthetic Studies on Basidifferquinones: The First Synthesis of (±)-Basidifferquinone C. *Tetrahedron Lett.* **2008**, *49* (14), 2258–2261.

(96) Mohri, K; Isobe, K.;Maeda, M.;Takeda, T.; Ohkubo, R.; Tsuda, Y., Studies Toward Total Synthesis of Non-Aromatic Erythrinan Alkaloids. Synthesis of Cocculolidine Skeleton. *Chem. Pharm. Bull.* **1998**, *46* (12), 1872–1877.

(97) Holland, H. L.; Qi, J.; Manoharan, T. S., Synthesis of (S)-4-Hydroxy-a-Lapachone and Biotransformation of Some 4-Chromanones by *Mortierella isabellina* ATCC 42613. *Can. J. Chem.* **1995**, *73* (9), 1399–1405.

(98) Kimachi, T.; Tamura, Y.; Bessho, K.; Yoneda, F., Synthesis and Catalytic Properties of 5-Deazaflavo-6,9-Quinones. *J. Chem. Soc. Perkin Trans. 1* **1993**, *6*, 697–700.

(99) Nawrat, C. C.; Kitson, R. R. A.; Moody, C. J., Toward the Total Synthesis of Hygrocin B and Divergolide C: Construction of the Naphthoquinone-Azepinone Core. *Org. Lett.* **2014**, *16* (7), 1896–1899.

(100) Radeke, H. S.; Digits, C. A.; Bruner, S. D.; Snapper, M. L. New Tools for Studying Vesicular-Mediated Protein Trafficking: Synthesis and Evaluation of Ilimaquinone Analogs in a Non-Radioisotope-Based Antisecretory Assay. *J. Org. Chem.* **1997**, *62* (9), 2823–2831.

(101) Mithani, S.; Weeratunga, G.; Taylor, N. J.; Dmitrienko, G. I., The Kinamycins Are Diazofluorenes and Not Cyanocarbazoles. *J. Am. Chem. Soc.* **1994**, *116* (5), 2209–2210.

(102) Appleton, D. R.; Pearce, A. N.; Copp, B. R., Anti-Tuberculosis Natural Products: Synthesis and Biological Evaluation of Pyridoacridine Alkaloids Related to Ascididemin. *Tetrahedron* **2010**, *66* (27–28), 4977–4986.

(103) Shen, M.; Li, G.; Lu, B. Z.; Hossain, A.; Roschangar, F.; Farina, V.; Senanayake, C. H., The First Regioselective Palladium-Catalyzed Indolization of 2-Bromo- or 2-Chloroanilines with Internal Alkynes: A New Approach to 2,3-Disubstituted Indoles. *Org. Lett.* **2004**, *6* (22), 4129–4132.

(104) Sweeney, M.; McArdle, P.; Aldabbagh, F. 1-Fluoro-2,5-Dimethoxy-4-Nitrobenzene. *Molbank* **2018**, *2018* (1), M984.

(105) Argyle, M. D.; Bartholomew, C. H., Heterogeneous Catalyst Deactivation and Regeneration: A Review. *Catalysts*. **2015**, *5* (1), 145–269.

(106) An, J.; Jackson, R. K.; Tuccinardi, J. P.; Wood, J. L., Pyrroloiminoquinone Alkaloids: Total Synthesis of Makaluvamines A and K. *Org. Lett*. **2023**, *25* (11), 1868–1871.

(107) Egris, R.; Villacampa, M.; Carlos Menéndez, J., Vinylation of Nitro-Substituted Indoles, Quinolinones, and Anilides with Grignard Reagents. *Chem. Eur. J.* **2009**, *15* (41), 10930–10939.

(108) Bartoli, G.; Dalpozzo, R.; Nardi, M., Applications of Bartoli Indole Synthesis. *Chem. Soc. Rev.* **2014**, *43* (13), 4728–4750.

(109) Majgier-Baranowska, H.; Williams, J. D.; Li, B.; Peet, N. P., Studies on the Mechanism of the Cadogan–Sundberg Indole Synthesis. *Tetrahedron Lett.* **2012**, *53* (35), 4785–4788.

(110) Peltzer, R. M.; Gauss, J.; Eisenstein, O.; Cascella, M., The Grignard Reaction-Unraveling a Chemical Puzzle. *J. Am. Chem. Soc.* **2020**, *142* (6), 2984–2994.

(111) Ashby, E. C.; Goel, A. B., Direct Evidence Supporting a Single-Electron Transfer Pathway in the Reduction of Ketones by Primary, Secondary, and Tertiary Grignard Reagents. *J. Am. Chem. Soc.* **1981**, *103* (16), 4983–4985.

(112) Foo, K.; Newhouse, T.; Mori, I.; Takayama, H.; Baran, P. S., Total Synthesis Guided Structure Elucidation of (+)-Psychotetramine. *Angew. Chem. Int. Ed.* **2011**, *50* (12), 2716–2719.

(113) Grenier, J. L.; Catteau, J. P.; Cotelle, P., Nitration of Electron-Rich Aromatic Compounds by Cerium Ammonium Nitrate Coated on Silica. *Synth. Commun*. **1999**, *29* (7), 1201–1208.

(114) Dinçtürk, S.; Ridd, J. H., Reactions of Cerium(IV) Ammonium Nitrate with Aromatic Compounds in Acetonitrile. Part 2. Nitration; Comparison with Reactions of Nitric Acid. *J. Chem. Soc. Perkin Trans. 2* **1982**, 965–969.

(115) Pearce, A. N.; Chia, E. W.; Berridge, M. V.; Clark, G. R.; Harper, J. L.; Larsen, L.; Maas, E. W.; Page, M. J.; Perry, N. B.; Webb, V. L.; Copp, B. R., Anti-Inflammatory Thiazine Alkaloids Isolated from the New Zealand Ascidian *Aplidium* sp.: Inhibitors of the Neutrophil Respiratory Burst in a Model of Gouty Arthritis. *J. Nat. Prod.* **2007**, *70* (6), 936–940.

(116) Aiello, A.; Fattorusso, E.; Luciano, P.; Mangoni, A.; Menna, M., Isolation and Structure Determination of Aplidinones A-C from the Mediterranean Ascidian *Aplidium conicum*: A Successful Regiochemistry Assignment by Quantum Mechanical ^{13}C NMR Chemical Shift Calculations. *Eur. J. Org. Chem.* **2005**, *23*, 5024–5030.

(117) Morris, B. D.; Prinsep, M. R., Euthyroideones, Novel Brominated Quinone Methides from the Bryozoan *Euthyroides episcopalis*. *J. Org. Chem.* **1998**, *63* (25), 9545–9547.

(118) Menna, M.; Aiello, A.; D'Aniello, F.; Imperatore, C.; Luciano, P.; Vitalone, R.; Irace, C.; Santamaria, R., Conithiaquinones A and B, Tetracyclic Cytotoxic Meroterpenes from the Mediterranean Ascidian Aplidium Conicum. *Eur. J. Org. Chem.* **2013**, *16*, 3241–3246.

(119) Carbone, A.; Lucas, C. L.; Moody, C. J., Biomimetic Synthesis of the Apoptosis-Inducing Thiazinoquinone Thiaplidiaquinone A. *J. Org. Chem.* **2012**, *77* (20), 9179–9189.

(120) Manzo, E., Synthesis of Marine Natural Products and Molecules Inspired by Marine Substances. *Mar. Drugs* **2021**, *19* (4), 208.

(121) Harada, N.; Sugioka, T.; Soutome, T.; Hiyoshi, N.; Uda, H.; Kuriki, T., Synthesis and Absolute Stereoehemistry of (+)-Adociaquinones A and B. *Tetrahedron Asymmetry* **1995**, *6* (2), 375–376.

(122) Harper, J. L.; Khalil, I. M.; Shaw, L.; Bourguet-Kondracki, M. L.; Dubois, J.; Valentin, A.; Barker, D.; Copp, B. R., Structure-Activity Relationships of the Bioactive Thiazinoquinone Marine Natural Products Thiaplidiaquinones A and B. *Mar. Drugs* **2015**, *13* (8), 5102–5110.

(123) Santoso, K. T., PhD Thesis: The Synthesis and Evaluation of Heterocycles as Anti-Tuberculosis Agents. University of Wellington, 2019.

(124) Mthembu, S. N.; Sharma, A.; Albericio, F.; de la Torre, B. G., Breaking a Couple: Disulfide Reducing Agents. *ChemBioChem* **2020**, *21* (14), 1947–1954.

(125) Liang, G.; Liu, M.; Chen, J.; Ding, J.; Gao, W.; Wu, H., NBS-Promoted Sulfenylation of Sulfinates with Disulfides Leading to Unsymmetrical or Symmetrical Thiosulfonates. *Chin. J. Chem.* **2012**, *30* (7), 1611–1616.

(126) Malviya, B. K.; Hansen, E. C.; Kong, C. J.; Imbrogno, J.; Verghese, J.; Guinness, S. M.; Salazar, C. A.; Desrosiers, J. N.; Kappe, C. O.; Cantillo, D., Metal-Free Electrochemical Reduction of

Disulfides in an Undivided Cell under Mass Transfer Control. *Chem. Eur. J.* **2023**, *29* (66), e202302664.

(127) Ochmann, M.; Harich, J.; Ma, R.; Freibert, A.; Kim, Y.; Gopannagari, M.; Hong, D. H.; Nam, D.; Kim, S.; Kim, M.; Eom, I.; Lee, J. H.; Yorke, B. A.; Kim, T. K.; Huse, N., UV Photochemistry of the *L*-Cystine Disulfide Bridge in Aqueous Solution Investigated by Femtosecond X-Ray Absorption Spectroscopy. *Nat. Commun.* **2024**, *15*, 8838.

(128) Na, Y.; Wang, S.; Kohn, H., 7-*N*-(Mercaptoalkyl)Mitomycins: Implications of Cyclization for Drug Function. *J. Am. Chem. Soc.* **2002**, *124* (17), 4666–4677.

(129) Teders, M.; Henkel, C.; Anhäuser, L.; Strieth-Kalthoff, F.; Gómez-Suárez, A.; Kleinmans, R.; Kahnt, A.; Rentmeister, A.; Guldi, D.; Glorius, F., The Energy-Transfer-Enabled Biocompatible Disulfide–Ene Reaction. *Nat. Chem.* **2018**, *10* (9), 981–988.

(130) Zhang, Z.; Haruna, K. I.; Ito, T.; Hatta, H.; Nishimoto, S. I., Development of Novel Oxygen-Independent Photosensitizers. *Nucleic Acids Symp. Ser.* **2007**, *51* (1), 229–230.

(131) Zhang, C. P.; Wang, T. Z.; Liang, Y. F., Manganese-Promoted Reductive Cross-Coupling of Disulfides with Dialkyl Carbonates. *Chem. Commun.* **2023**, *59* (97), 14439–14442.

(132) Guo, W.; Lv, G.; Chen, J.; Gao, W.; Ding, J.; Wu, H., Rongalite® and Base-Promoted Cleavage of Disulfides and Subsequent Michael Addition to α,β-Unsaturated Ketones/Esters: An Odorless Synthesis of β-Sulfido Carbonyl Compounds. *Tetrahedron* **2010**, *66* (13), 2297–2300.

(133) Kim, H. M.; Kim, I. J.; Danishefsky, S. J., Total Syntheses of Tumor-Related Antigens N3: Probing the Feasibility Limits of the Glycal Assembly Method. *J. Am. Chem. Soc.* **2001**, *123* (1), 35–48.

(134) Colomer, I.; Chamberlain, A. E. R.; Haughey, M. B.; Donohoe, T. J., Hexafluoroisopropanol as a Highly Solvent. *Nat. Rev. Chem.* **2017**, *1*, 0088.

(135) Pace, V.; Hoyos, P.; Castoldi, L.; Domínguez De María, P.; Alcántara, A. R., 2-Methyltetrahydrofuran (2-MeTHF): A Biomass-Derived Solvent with Broad Application in Organic Chemistry. *ChemSusChem* **2012**, *5* (8), 1369–1379.

(136) Trofimov, B. A.; Vasil'tsov, A. M.; Amosova, S. V., Physical Chemistry Basicity of Saturated Solutions of Alkali Metal Hydroxides in Dimethylsulfoxide. *Bull Acad. Sci. USSR Div. Chem. Sci.* **1986**, *35* (4), 682–686.

(137) Seebach, D., Structure and Reactivity of Lithium Enolates. From Pinacolone to Selective C-Alkylations of Peptides. Difficulties and Opportunities Afforded by Complex Structures. *Angew. Chem. Int. Ed. Engl*. **1988**, *27*, 1624–1654.

(138) Mech, P.; Bogunia, M.; Nowacki, A.; Makowski, M., Calculations of pKa Values of Selected Pyridinium and Its N-Oxide Ions in Water and Acetonitrile. *J. Phys. Chem. A* **2020**, *124* (3), 538–551.

(139) Baidya, M.; Kobayashi, S.; Brotzel, F.; Schmidhammer, U.; Riedle, E.; Mayr, H. DABCO and DMAP - Why Are They Different in Organocatalysis? *Angew. Chem. Int. Ed.* **2007**, *46* (32), 6176–6179.

(140) Chakraborty, N.; Mitra, A. K., The Versatility of DABCO as a Reagent in Organic Synthesis: A Review. *Org. Biomol. Chem*. **2023**, *21* (34), 6830–6880.

(141) Cortes-Clerget, M.; Yu, J.; Kincaid, J. R. A.; Walde, P.; Gallou, F.; Lipshutz, B. H., Water as the Reaction Medium in Organic Chemistry: From Our Worst Enemy to Our Best Friend. *Chem. Sci.* **2021**, *12* (12), 4237–4266.

(142) Smith, M. D.; Mostofian, B.; Petridis, L.; Cheng, X.; Smith, J. C., Molecular Driving Forces behind the Tetrahydrofuran-Water Miscibility Gap. *J. Phys. Chem. B* **2016**, *120* (4), 740–747.

(143) Sherwood, J.; Parker, H. L.; Moonen, K.; Farmer, T. J.; Hunt, A. J., *N* -Butylpyrrolidinone as a Dipolar Aprotic Solvent for Organic Synthesis. *Green Chem.* **2016**, *18* (14), 3990–3996.

(144) Baidya, M.; Mayr, H., Nucleophilicities and Carbon Basicities of DBU and DBN. *Chem. Commun.* **2008**, *15*, 1792–1794.

(145) Barton, D. H. R.; Elliott, J. D.; Géro, S. D., Synthesis and Properties of a Series of Sterically Hindered Guanidine Bases. *J. Chem. Soc. Perkin Trans. 1* **1982**, 2085–2090.

(146) Zhang, L.; Nederberg, F.; Pratt, R. C.; Waymouth, R. M.; Hedrick, J. L.; Wade, C. G., Phosphazene Bases: A New Category of Organocatalysts for the Living Ring-Opening Polymerization of Cyclic Esters. *Macromolecules* **2007**, *40* (12), 4154–4158.

(147) Backstrom, N.; Burton, N. A.; Turega, S.; Watt, C. I. F., The Primary Kinetic Hydrogen Isotope Effect in the Deprotonation of a Nitroalkane by an Intramolecular Carboxylate Group. *J. Phys. Org. Chem.* **2008**, *21* (7–8), 603–613.

(148) Liang, S.; Hofman, K.; Friedrich, M.; Keller, J.; Manolikakes, G., Recent Progress and Emerging Technologies towards a Sustainable Synthesis of Sulfones. *ChemSusChem*. **2021**, *14* (22), 4878–4902.

(149) Maciuk, S.; Wood, S. H.; Patel, V. K.; Shapland, P. D. P.; Tomkinson, N. C. O., Peracid Oxidation of Unactivated Sp^3 C–H Bonds: An Important Solvent Effect. *Chem. Eur. J.* **2023**, *29* (31), e202204007.

(150) Kaur, N.; Kishore, D., Peroxy Acids: Role in Organic Synthesis. *Synth. Commun*. **2014**, *44* (6), 721–747.

(151) Balicki, R., A Mild and Efficient Procedure for the Oxidation of Organic Sulfides to Sulfones by Use of Urea-Hydrogen Peroxide/Trifluoroacetic Anhydride System. *Synth. Commun.* **1999**, *29* (13), 2235–2239.

(152) Yu, B.; Liu, A. H.; He, L. N.; Li, B.; Diao, Z. F.; Li, Y. N., Catalyst-Free Approach for Solvent-Dependent Selective Oxidation of Organic Sulfides with Oxone. *Green Chem.* **2012**, *14* (4), 957–962.

(153) Trost, B. M.; Curran, D. P., Chemoselective Oxidation of Sulfides to Sulfones with Potassium Hydrogen Persulfate. *Tetrahedron Lett.* **1981**, *22* (14), 1287–1290.

(154) Jeyakumar, K.; Chakravarthy, R. D.; Chand, D. K., Simple and Efficient Method for the Oxidation of Sulfides to Sulfones Using Hydrogen Peroxide and a Mo(VI) Based Catalyst. *Catal. Commun.* **2009**, *10* (14), 1948–1951.

(155) Yoshida, S., Recent Advances in the Synthesis and Transformations of Sulfinate Esters. *Chem. Commun.* **2025**, *61* (27), 5084-5093.

(156) Santhoshkumar, P.; Kanagaraj, T.; Suresh, P., Iron-Catalysed Synthesis of Sulfonamides and Sulfonic Esters: Greener Sulfonation of Amines and Alcohols under Mechanical Grinding Conditions. *Tetrahedron* **2025**, *171*, 134410.

(157) Pasto, D. J.; Cottard, F.; Jumelle, L., Photooxidation of Alkyl 4-Nitrophenyl Sulfides and Sulfoxides. Observation of Oxidative C-S Bond Cleavage and Rearrangement Reactions. *J. Am. Chem. Soc.* **1994**, *116* (20), 8978–8984.

(158) Shengrong, G. U. O.; Yanqin, Y., Method for Preparation of Sulfinic Acid Ester from Thiophenol or Thiol. CN 106518734 A, March 22 2017.

(159) Guan, Y.; Shree Sowndarya, S. V.; Gallegos, L. C.; St. John, P. C.; Paton, R. S., Real-Time Prediction Of ^{1}H and ^{13}C Chemical Shifts with DFT Accuracy Using a 3D Graph Neural Network. *Chem. Sci.* **2021**, *12* (36), 12012–12026.

(160) Hinton, J. F., Sulphur-33 NMR Spectroscopy. *Annu. Rep. NMR Spectrosc.* **1987**, *19*, 1–34.

(161) Rosman, K.; Taylor, P., Report of the IUPAC Subcommittee for Isotopic Abundance Measurements. *Pure Appl. Chem.* **1999**, *71*, 1593–1607.

(162) Ma, X.; Liu, Y.; Du, L.; Zhou, J.; Markó, I. E., Post-Functionalization of Dibenzothiophene to Functionalized Biphenyls via a Photoinduced Thia-Baeyer-Villiger Oxidation. *Nat. Commun.* **2020**, *11*, 914.

(163) Liu, S.; Chen, B.; Yang, Y.; Yang, Y.; Chen, Q.; Zeng, X.; Xu, B., Electrochemical Oxidations of Thioethers: Modulation of Oxidation Potential Using a Hydrogen Bonding Network. *Electrochem. Commun.* **2019**, *109*, 106583

(164) Kantam, M. L.; Neelima, B.; Reddy, C. V.; Chaudhuri, M. K.; Dehury, S. K., $VO(acac)_2$ Supported on Titania: A Heterogeneous Protocol for the Selective Oxidation of Sulfides Using TBHP. *Catal. Lett.* **2004**, *95*, 19–22.

(165) Shaabani, A.; Mirzaei, P.; Naderi, S.; Lee, D. G., Green Oxidations. The Use of Potassium Permanganate Supported on Manganese Dioxide. *Tetrahedron* **2004**, *60* (50), 11415–11420.

(166) González-Núñez, M. E.; Mello, R.; Royo, J.; Ríos, J. V.; Asensio, G., Mechanism of the Oxidation of Sulfides by Dioxiranes. 1. Intermediacy of a 10-S-4 Hypervalent Sulfur Adduct. *J. Am. Chem. Soc.* **2002**, *124* (31), 9154–9163.

(167) Taber, D. G.; DeMatteo, P. W.; Hassan, R. A., Simplified Preparation of Dimethyldioxirane (DMDO). *Org. Synth.* **2013**, *90*, 350–357.

(168) Yu, J. Q.; Wu, H. C.; Corey, E. J., $Pd(OH)_2$/C-Mediated Selective Oxidation of Silyl Enol Ethers by *tert*-Butylhydroperoxide, a Useful Method for the Conversion of Ketones to α,β-Enones or β-Silyloxy-α,β-Enones. *Org. Lett.* **2005**, *7* (7), 1415–1417.

(169) Chan, T.-L.; Fong, S.; Li, Y.; Man, T.-O.; Poon, C.-D., A New One-Flask Ramberg-Backlund Reaction. *J. Chem. Soc., Chem. Commun.* **1994**, *15*, 1771–1772.

(170) Yan, P.; Ritt, D. A.; Zlotkowski, K.; Bokesch, H. R.; Reinhold, W. C.; Schneekloth, J. S.; Morrison, D. K.; Gustafson, K. R., Macrophilones from the Marine Hydroid *Macrorhynchia philippina* Can Inhibit ERK Cascade Signaling. *J. Nat. Prod.* **2018**, *81* (7), 1666–1672.

(171) Zlotkowski, K.; Hewitt, W. M.; Yan, P.; Bokesch, H. R.; Peach, M. L.; Nicklaus, M. C.; O'Keefe, B. R.; McMahon, J. B.; Gustafson, K. R.; Schneekloth, J. S., Macrophilone A: Structure Elucidation, Total Synthesis, and Functional Evaluation of a Biologically Active Iminoquinone from the Marine Hydroid *Macrorhynchia philippina*. *Org. Lett.* **2017**, *19* (7), 1726–1729.

(172) Aubart, K. M.; Heathcock, C. H., A Biomimetic Approach to the Discorhabdin Alkaloids: Total Syntheses of Discorhabdins C and E and Dethiadiscorhabdin D. *J. Org. Chem.* **1999**, *64* (1), 16–22.

(173) Cordes, E. H.; Jencks, W. P.; Cordes, E. H.; Jencks, W. P., On the Mechanism of Schiff Base Formation and Hydrolysis. *J. Am. Chem. Soc.* **1962**, *84* (5), 832–837.

(174) Tuccinardi, J. P.; Wood, J. L., Convergent Total Synthesis of Aleutianamine. *J. Am. Chem. Soc.* **2025**, *147* (7), 5736–5742.

(175) Shan, D.; Gao, Y.; Jia, Y. Intramolecular Larock Indole Synthesis: Preparation of 3,4-Fused Tricyclic Indoles and Total Synthesis of Fargesine. *Angew. Chem.* **2013**, *125* (18), 5002–5005.

(176) Ruiz-Castillo, P.; Buchwald, S. L., Applications of Palladium-Catalyzed C-N Cross-Coupling Reactions. *Chem. Rev.* **2016**, *116* (19), 12564–12649.

(177) Elebiju, O. F.; Ajani, O. O.; Oduselu, G. O.; Ogunnupebi, T. A.; Adebiyi, E., Recent Advances in Functionalized Quinoline Scaffolds and Hybrids—Exceptional Pharmacophore in Therapeutic Medicine. *Front. Chem*. **2023**, *10,* 2022.

(178) Isambert, N.; Cruz, M.; Arévalo, M. J.; Gómez, E.; Lavilla, R., Enol Esters: Versatile Substrates for Mannich-Type Multicomponent Reactions. *Org. Lett.* **2007**, *9* (21), 4199–4202.

(179) Jia, X.; Li, P.; Shao, Y.; Yuan, Y.; Hou, W.; Liu, X.; Zhang, X.; Ji, H., Facile Construction of Quinoline-2-Carboxylate Esters through Aerobic Oxidation of Alkyl 4-Anilinocrotonates Induced by a Radical Cation Salt. *Chem. Asian J.* **2017**, *12* (14), 1719–1723.

(180) Laha, R.; Patel, T. I.; Moschitto, M. J., Desulfinative Alkylation of Heteroarenes via an Electrostatic Electron Donor-Acceptor Complex. *Org. Lett.* **2022**, *24* (40), 7394–7399.

(181) Bell, G. E.; Fyfe, J. W. B.; Israel, E. M.; Slawin, A. M. Z.; Campbell, M.; Watson, A. J. B. Synthesis of 2-BMIDA Indoles via Heteroannulation: Applications in Drug Scaffold and Natural Product Synthesis. *Org Lett* **2022**, *24* (16), 3024–3027.

(182) Trost, B. M.; Toste, F. D., A Catalytic Enantioselective Approach to Chromans and Chromanols. A Total Synthesis of (−)-Calanolides A and B and the Vitamin E Nucleus. *J. Am. Chem. Soc.* **1998**, *120* (36), 9074–9075.

(183) Beneke, T.; Madden, R.; Makin, L.; Valli, J.; Sunter, J.; Gluenz, E., A CRISPR Cas9 High-Throughput Genome Editing Toolkit for Kinetoplastids. *R. Soc. Open Sci.* **2017**, *4* (5), 1–16.

(184) Barret, R.; Daudon, M., Oxidation of Phenols to Quinones by Bis(Trifluoroacetoxy)Iodobenzene. *Tetrahedron Lett.* **1990**, *31* (34), 4871–4872.

(185) Wellauer, J.; Miladinov, D.; Buchholz, T.; Schütz, J.; Stemmler, R. T.; Medlock, J. A.; Bonrath, W.; Sparr, C., Organophotocatalytic Aerobic Oxygenation of Phenols in a Visible-Light Continuous-Flow Photoreactor. *Chem. Eur. J.* **2021**, *27* (38), 9748–9752.

(186) Kim, C. S.; Kim, J. H.; Lee, Y. S., Synthesis of Praziquantel via *N*-Acyliminium Ion Cyclization of Amido Acetals through Several Synthetic Routes. *Heterocycles* **1998**, *48* (11), 2279–2285.

(187) Belser, P.; Bernhard, S.; Guerig, U., Synthesis of Mono-and Dialkylsubstituted 1,10-Phenanthrolines. *Tetrahedron* **1996**, *52* (8), 2937–2944.

(188) Jacob III, P.; Callery, P. S., A Convenient Synthesis of Quinones from Hydroquinone Dimethyl Ethers. Oxidative Demethylation with Ceric Ammonium Nitrate. *J. Org. Chem.* **1976**, *41* (22), 3627–3629.

(189) Jang, K. S.; Shin, D. S.; Srisook, E.; Song, H. C.; Chi, D. Y., Versatile Functionalization of Electron Rich-Fused Heterocyclic Arenes via Electrophilic Aromatic Addition Reaction and Their Applications. *Tetrahedron* **2016**, *72* (33), 5106–5114.

(190) Zjawionyl, J. K.; Srivastava, A. R.; Hufford, C. D.; Clark, A. M., Chemistry of Sampangines. *Heterocycles* **1994**, *39* (2), 779–800.

(191) Sachin, K.; Jeong, H. J.; Lim, S. T.; Sohn, M. H.; Chi, D. Y.; Kim, D. W., An Efficient Synthesis of ([^{18}F]Fluoropropyl)Quinoline-5,8-Diones by Rapid Radiofluorination-Oxidative Demethylation. *Tetrahedron* **2011**, *67* (10), 1763–1767.

(192) Delfourne, E.; Darro, F.; Portefaix, P.; Galaup, C.; Bayssade, S.; Bouteillé, A.; Le Corre, L.; Bastide, J.; Collignon, F.; Lesur, B.; Frydman, A.; Kiss, R., Synthesis and *in vitro* Antitumor Activity of Novel Ring D Analogues of the Marine Pyridoacridine Ascididemin: Structure-Activity Relationship. *J. Med. Chem.* **2002**, *45* (17), 3765–3771.

(193) Wetzel, A.; Gagosz, F., Gold-Catalyzed Transformation of 2-Alkynyl Arylazides: Efficient Access to the Valuable Pseudoindoxyl and Indolyl Frameworks. *Angew. Chem. Int. Ed.* **2011**, *50* (32), 7354–7358.

(194) Tymann, D. C.; Benedix, L.; Iovkova, L.; Pallach, R.; Henke, S.; Tymann, D.; Hiersemann, M., Photochemical Approach to the Cyclohepta[b]Indole Scaffold by Annulative Two-Carbon Ring-Expansion. *Chem. Eur. J.* **2020**, *26* (52), 11974–11978.

(195) Guissart, C.; Dolbois, A.; Tresse, C.; Saint-Auret, S.; Evano, G.; Blanchard, N., A Straightforward Entry to γ-Trifluoromethylated Allenamides and Their Synthetic Applications. *Synlett.* **2016**, *27* (18), 2575–2580.

(196) Boyle, T. P.; Bremner, J. B.; Coates, J. A.; Keller, P. A.; Pyne, S. G., A Convenient and Efficient Synthesis of (*S*)-Lysine and (*S*)-Arginine Homologues via Olefin Cross-Metathesis. *Tetrahedron* **2005**, *61* (30), 7271–7276.

(197) Majhail, M. K.; Ylioja, P. M.; Willis, M. C., Direct Synthesis of Highly Substituted Pyrroles and Dihydropyrroles Using Linear Selective Hydroacylation Reactions. *Chem. Eur. J.* **2016**, *22* (23), 7879–7884.

(198) Li, X.; Li, H.; Song, W.; Tseng, P.; Liu, L.; Guzei, I. A.; Tang, W., Divergent Reactivity of Rhodium(I) Carbenes Derived from Indole Annulations. *Angew. Chem.* **2015**, *127* (44), 13097–13100.

(199) Mangas-Sánchez, J.; Busto, E.; Gotor-Fernández, V.; Gotor, V., Highly Stereoselective Chemoenzymatic Synthesis of the 3H-Isobenzofuran Skeleton. Access to Enantiopure 3-Methylphthalides. *Org. Lett.* **2012**, *14* (6), 1444–1447.

(200) Lim, J.; Chintalapudi, V.; Gudmundsson, H. G.; Tran, M.; Bernasconi, A.; Blanco, A.; Song, L.; Challis, G. L.; Anderson, E. A., Synthesis of the C1-C27 Fragment of Stambomycin D Validates Modular Polyketide Synthase-Based Stereochemical Assignments. *Org. Lett.* **2021**, *23* (19), 7439–7444.

(201) Dekeyser, M. A.; McDonald, P. T., Insecticidal Phenylhydrazine Derivatives. US 5367093 A, November 22 1994.

(202) Yinsheng, Z.; Yong, G.; Yuan, Y.; Wei, S..; Chengqi, W., Fused Bicyclic Compound Containing Pyrrolinone. WO 2023/160577 A1, August 31 2023.

(203) Walęcka-Kurczyk, A.; Adamek, J.; Walczak, K.; Michalak, M.; Październiok-Holewa, A. Non-Kolbe Electrolysis Of N-protected-a-aminoacids: a standardized method for the synthesis of *N*-protected (1-methoxyalkyl)amines. *RSC Adv.* **2022**, *12* (4), 2107–2114.

(204) Murayama, T.; Shibuya, M.; Yamamoto, Y. Divergent Synthesis of Polymethoxylated 4-Aryl-2-Quinolones. *J. Org. Chem.* **2016**, *81* (23), 11940–11949.

(205) Batail, N.; Bendjeriou, A.; Lomberget, T.; Barrett, R.; Dufaud, V.; Djakovitch, L., First Heterogeneous Ligand- and Salt-Free Larock Indole Synthesis. *Adv. Synth. Catal.* **2009**, *351* (13), 2055–2062.

(206) Zhdanko, A.; Maier, M. E. Mechanistic Study of Gold(I)-Catalyzed Hydroamination of Alkynes: Outer or Inner Sphere Mechanism? *Angew. Chem. Int. Ed.* **2014**, *53* (30), 7760–7764.

(207) Danner, P.; Morkunas, M.; Maier, M. E., Synthesis of *D*-Abrines by Palladium-Catalyzed Reaction of *ortho*-Iodoanilines with *N*-Boc-*N*-Methylalanyl-Substituted Acetaldehyde and Acetylene. *Org. Lett.* **2013**, *15* (10), 2474–2477.

(208) Moss, T. A.; Barber, D. M.; Kyle, A. F.; Dixon, D. J., Catalytic Asymmetric Alkylation Reactions for the Construction of Protected Ethylene-Amino and Propylene-Amino Motifs Attached to Quaternary Stereocentres. *Chem. Eur. J.* **2013**, *19* (9), 3071–3081.

(209) Moss, T. A.; Lister, A. S.; Wang, J., A Larock Indolization Approach to Substituted Tryptamines. *Tetrahedron Lett.* **2017**, *58* (32), 3136–3138.

(210) Kamakolanu, U. G.; Meyer, M. E.; Yasuda, D.; Polgar, W. E.; Marti, M.; Mercatelli, D.; Pisanò, C. A.; Brugnoli, A.; Morari, M.; Zaveri, N. T., Discovery and Structure-Activity Relationships of Nociceptin Receptor Partial Agonists That Afford Symptom Ablation in Parkinson's Disease Models. *J. Med. Chem.* **2020**, *63* (5), 2688–2704.

(211) Nawrat, C. C.; Lewis, W.; Moody, C. J., Synthesis of Amino-1,4-Benzoquinones and Their Use in Diels–Alder Approaches to the Aminonaphthoquinone Antibiotics. *J. Org. Chem.* **2011**, *76* (19), 7872–7881.

(212) Watanabe, K.; Iwata, Y.; Adachi, S.; Nishikawa, T.; Yoshida, Y.; Kameda, S.; Ide, M.; Saikawa, Y.; Nakata, M., Synthetic Studies on Lactonamycins: Synthesis of the Model BCDEF Aglycon. *J. Org. Chem.***2010**, *75* (16), 5573–5579.

(213) Kato, E.; Tsuji, H.; Kawabata, J., Selective Purification of Intestinal Maltase Complex by Affinity Chromatography Employing an Uncompetitive Inhibitor as the Ligand. *Tetrahedron* **2015**, *71* (9), 1419–1424.

(214) de Vicente, J.; Hendricks, R. T.; Smith, D. B.; Fell, J. B.; Fischer, J.; Spencer, S. R.; Stengel, P. J.; Mohr, P.; Robinson, J. E.; Blake, J. F.; Hilgenkamp, R. K.; Yee, C.; Zhao, J.; Elworthy, T. R.; Tracy, J.; Chin, E.; Li, J.; Lui, A.; Wang, B.; Oshiro, C.; Harris, S. F.; Ghate, M.; Leveque, V. J. P.; Najera, I.; Pogam, S. Le; Rajyaguru, S.; Ao-Ieong, G.; Alexandrova, L.; Fitch, B.; Brandl, M.; Masjedizadeh, M.; Wu, S. yong; Keczer, S. de; Voronin, T., Non-Nucleoside Inhibitors of HCV Polymerase NS5B. Part 3: Synthesis and Optimization Studies of Benzothiazine-Substituted Tetramic Acids. *Bioorg. Med. Chem. Lett.* **2009**, *19* (19), 5648–5651.

(215) Meuser, M. E.; Rashad, A. A.; Ozorowski, G.; Dick, A.; Ward, A. B.; Cocklin, S. Field-Based Affinity Optimization of a Novel Azabicyclohexane Scaffold HIV-1 Entry Inhibitor. *Molecules* **2019**, *24* (8), 1581.

(216) Nguyen, P.; Doan, P.; Rimpilainen, T.; Konda Mani, S.; Murugesan, A.; Yli-Harja, O.; Candeias, N. R.; Kandhavelu, M., Synthesis and Preclinical Validation of Novel Indole Derivatives as a GPR17 Agonist for Glioblastoma Treatment. *J. Med. Chem.* **2021**, *64* (15), 10908–10918.

(217) Zeisel, L.; Felber, J. G.; Scholzen, K. C.; Poczka, L.; Cheff, D.; Maier, M. S.; Cheng, Q.; Shen, M.; Hall, M. D.; Arnér, E. S. J.; Thorn-Seshold, J.; Thorn-Seshold, O., Selective Cellular Probes for

Mammalian Thioredoxin Reductase TrxR1: Rational Design of RX1, a Modular 1,2-Thiaselenane Redox Probe. *Chem* **2022**, *8* (5), 1493–1517.

(218) Xue, F.; Wang, F.; Liu, J.; Di, J.; Liao, Q.; Lu, H.; Zhu, M.; He, L.; He, H.; Zhang, D.; Song, H.; Liu, X.; Qin, Y., A Desulfurative Strategy for the Generation of Alkyl Radicals Enabled by Visible-Light Photoredox Catalysis. *Angew. Chem.* **2018**, *130* (22), 6777–6781.

(219) Fisher, K. J.; Turkett, J. A.; Corson, A. E.; Bicker, K. L., Peptoid Library Agar Diffusion (PLAD) Assay for the High-Throughput Identification of Antimicrobial Peptoids. *ACS Comb. Sci.* **2016**, *18* (6), 287–291.

(220) Ghosh, S.; Tochtrop, G. P. A New Strategy for the Synthesis of β-Benzylmercaptoethylamine Derivatives. *Tetrahedron Lett* **2009**, *50* (15), 1723–1726.

(221) Mahesh, K., Compound, Composition and Uses Thereof. US 8445707 B1, May 21 2013.

(222) Monisha, M.; Sahu, S.; Lochab, B., Self-Polymerization Promoting Monomers: In Situ Transformation of Disulfide-Linked Benzoxazines into the Thiazolidine Structure. *Biomacromolecules* **2021**, *22* (10), 4408–4421.

(223) Gao, D.; Tang, S.; Cen, Y.; Yuan, L.; Lan, X.; Li, Q. H.; Lin, G. Q.; Huang, M.; Tian, P., Discovery of Novel Drug-like PHGDH Inhibitors to Disrupt Serine Biosynthesis for Cancer Therapy. *J. Med. Chem.* **2023**, *66* (1), 285–305.

(224) Venkat Shivaji Ramarao, E. V.; Solanke, J. N.; Chatterjee, R.; Gat, S.; Dhayalan, V.; Dandela, R., Metal-Free Efficient Synthesis of Aryl Sulfonamides from *N*-Hydroxy Sulfonamide and Amines. *Org. Biomol. Chem.* **2024**, *22* (29), 5918–5923.

(225) Hyung-Chul, R.; Jae-Sun, K.; Jee-Woong, L.; Young, L. J.; Kwanghyun, C.; Sumi, L.; Guanghai, J.; Kang, H. J. Compounds Inhibiting Alk And/Or Egfr Mutation Kinases And Medical Use Thereof. WO 2023/063751 A1, April 20 2023.

(226) Higashino, M.; Ikeda, N.; Shinada, T.; Sakaguchi, K.; Ohfune, Y., Stereoselective Anti-S_N2' Mitsunobu Reaction of α-Hydroxy-α-Alkenylsilanes. *Tetrahedron Lett.* **2011**, *52* (3), 422–425.

(227) Ruan, H.; Zhu, D.; Zhao, J.; Zhu, S. Difluorocarbene-Mediated Trimethylsilylation of Nucleophiles with $HCF_2N(TMS)_2$ as a Silylation Reagent. *Org. Lett.* **2025**, *27* (7), 1741–1749.

(228) Gammack Yamagata, A. D.; Datta, S.; Jackson, K. E.; Stegbauer, L.; Paton, R. S.; Dixon, D. J., Enantioselective Desymmetrization of Prochiral Cyclohexanones by Organocatalytic Intramolecular Michael Additions to α,β-Unsaturated Esters. *Angew. Chem. Int. Ed.* **2015**, *54* (16), 4899–4903.

(229) Huyen Vu, T.; Serradji, N.; Seydou, M.; Brémond, É.; Ha-Duong, N.-T., Electronic Spectroscopic Characterization of the Formation of Iron(III) Metal Complexes: The 8-HydroxyQuinoline as Ligand Case Study. *J. Inorg. Biochem.* **2020**, *203*, 110864.

(230) Baskin, M.; Fridman, N.; Kosa, M.; Maayan, G., Heteroleptic Complexes *via* Solubility Control: Examples of Cu(II), Co(II), Ni(II) and Mn(II) Complexes Based on the Derivatives of Terpyridine and Hydroxyquinoline. *Dalton Trans.* **2017**, *46* (44), 15330–15339.